Induced-Fit Anion Sensing

ADAM NEIL SWINBURNE

Induced-Fit Anion Sensing

A thesis submitted for the fulfillment of the requirements for the degree of

Doctor of Philosophy

In the Faculty of Science at Durham University

by

Adam Neil Swinburne

Department of Chemistry

Durham University

South Road

Durham

2011

Abstract

Anions have many important roles in biological systems, as well as in the environment and as such there is significant interest in their binding and sensing. In induced-fit anion sensing, the binding of an anion causes a shift in the equilibrium of conformers of the molecule, which in turn may lead to a change in a physical property. In this thesis four experimental chapters describe the synthesis and anion sensing properties of a series of induced-fit anion sensors derived from a hexa-substituted triethylbenzene and diphenylacetylene motif.

Chapter one provides an introduction to anion recognition and sensing, whilst Chapter two describes a new synthetic method towards triethylbenzene receptors involving the solvent-drop grinding technique. Facile synthesis of known and novel anion receptors was achieved. Chapter three describes the use of the triethylbenzene motif, functionalised with quinolinium groups to sense anions. The receptor binds anions strongly, with complex binding observed, involving a host dimer, 2:1 host:guest and 1:1 host:guest stoichiometries. The receptor functions as a turn-off fluorescence sensor with selectivity for acetate. Chapter four describes the further functionalisation of the triethylbenzene core with the viologen moiety, leading to a series of tri- and tetrapodal anion receptors. These receptors show a colourimetic response to carboxylates through a charge transfer interaction. These receptors bind several different anions strongly. However a colourimetric response is only observed with carboxylates.

Chapter five describes the use of diphenylacetylene derivatives functionalised with urea groups which have also been investigated as induced-fit anion sensors. The receptors show a high degree of preorganisation, except for free rotation around the acetylene bond. The receptors bind a range of anions to varying extents, with strong binding observed with basic anions. Upon the addition of anions, several different fluorescent responses are observed depending on the receptor design. A turn-on fluorescent response is observed with diphenylacetylene and diphenylbutadiyne derivatives due to planarisation of the receptor. Fluorescent quenching is also observed with several receptors and can allow for the discrimination of several anions when the receptors are used as part of an array. The diphenylbutadiyne derivative can also be incorporated into a dipstick which shows a turn-off response in the presence of chloride.

Table of Contents

Acknowledgments

I would like to start by thanking my supervisors Prof. Jon Steed and Dr Andrew Beeby for their invaluable guidance, advice and patience during my time at Durham and for being open to ideas. I would also like to thank Drs Kirsty Anderson and Gareth Lloyd for their assistance in crystallography, Drs. Charlotte Willans for teaching me air sensitive techniques and Katharina Fucke for her advice on solid state analytical techniques. I also need to thank Kathrin Fischer, Sara Jane Dickson and Emma Wallace for their preliminary work on the viologen systems, as well as everyone in the Steed and Beeby labs, past and present.

I would like to thank the analytic staff in mass spectrometry and elemental analysis. Particular thanks go to Dr Alan Kenwright, Catherine Heffeman and Ian McKeag in NMR without whom I would never have completed my NMR experiments. I must also thank Dr. Ian Terry (Department of Physics, Durham University) for his assistance in ESR measurements. A great deal of thanks also goes to Dr. Martin Paterson at Heriot-Watt University, whose knowledge of DFT and calculations has been invaluable in helping understand my research.

Finally, I would like to thank my friends and family for keeping me going, particularly my parents and Ammie for their never ending support and encouragement over the years.

Abbreviations

AMP	Adenosine Monophosphate
API	Active Pharmaceutical Ingredient
Ar	Aryl
aq	Aqueous
ATP	Adenosine Triphosphate
ATR	Attenuated Total Reflection
br	Broad
Bpy	Bipyridine/Bipyridinium
Bu	Butyl
CASSCF	Complete Active-Space Self-Consistent Field
Cbz	Carbobenzyloxy
CCD	Charge Coupled Device
CFSE	Crystal Field Stabilisation Energy
CHEF	Chelation Enhanced Fluorescence
C_i	Co-efficient of Orbital Transition
CMC	Critical Micelle Concentration
Cp	Cyclopentyl
CT	Charge Transfer
-d	Deuterated
d (NMR)	Doublet
DABCO	1,4-diazabicyclo[2.2.2]octane
DCE	1, 2-Dichloroethane
DCM	Dichloromethane
dd (NMR)	Doublet of Doublets
ddd (NMR)	Doublet of Doublet of Doublets
DFT	Density Functional Theory
DMF	Dimethylformamide
DMSO	Dimethylsulfoxide
DOSY	Diffusion Ordered Spectroscopy
DPA	Diphenylacetylene
DPQ	Dipyrrolyl Quinoxalines
DPV	Differential Pulse Voltammogram

$E_{0,0}$	Singlet Excited State Energy
E	Electrochemical potential
eq	Equivalents
ES	Electrospray
ESR	Electron Spin Resonance
Et	Ethyl
F	Fluorophore
f	Oscillator Strength
Fc	Ferrocene
FT	Fourier Transform
FWHM	Full Width at Half Maximum
Glu	Glutamate
GTP	Guanidine Triphosphate
HOMO	Highest Occupied Molecular Orbital
ICT	Intramolecular Charge Transfer
IDA	Indicator Displacement Assay
IP_3	Inositol Triphosphate
IR	Infrared
IRF	Instrument Response Function
ITC	Isothermal Titration Calorimetry
J (NMR)	Coupling Constant
K or K_a	Association Constant
k_f	Rate Constant of Fluorescence
k_{nr}	Rate Constant of Non-radiative Decay
k_q	Rate Constant of Quenching
K_{sv}	Stern-Volmer Constant
LFER	Linear Free Energy Relationship
LUMO	Lowest Unoccupied Molecular Orbital
m (configuration)	Meta
m (IR)	Medium
m (NMR)	Multiplet
MALDI	Matrix Assisted Laser Desorption Ionisation
Me	Methyl
MeCN	Acetonitrile

MeOH	Methanol
MS	Mass Spectrometry
MV	Methyl Viologen
n	Aliphatic Chain
NMR	Nuclear Magnetic Resonance
NOESY	Nuclear Overhauser Effect Spectroscopy
o (configuration)	Ortho
OAc	Acetate
OMe	Methoxide
p (configuration)	Para
PCA	Principal Component Analysis
PET	Photo-induced Electron Transfer
Ph	Phenyl
PHA	Pulse Height Analyser
PL	Photoluminescent
PLQY	Photoluminescent Quantum Yield
Py	Pyridinium
Q	Quencher
q (NMR)	Quintet
Quin	Quinolinium
R	Any Functional Group (unless defined)
s (IR)	Strong
s (NMR)	Singlet
S_1	First Excited State
S_2	Second Excited State
SCE	Saturated Calomel Electrode
t (configuration)	Tertiary
t (NMR)	Triplet
TBA	Tetrabutylammonium
TCSPC	Time Correlated Single Photon Counting
TEA	Tetraethylammonium
TD-DFT	Time Dependant Density Functional Theory
td(NMR)	Triplet of Doublets
THF	Tetrahydrofuran

TLC	Thin Layer Chromotography
Ts	Tosyl
TTL	Transistor-Transistor Logic
UV	Ultraviolet
UV-vis	Ultraviolet-visible
vol	Volume
VT	Variable Temperature
v/v	Volume ratio
w (IR)	Weak
YAG	Yttrium Aluminium Garnate
β	Stepwise Binding Constant
δ	Chemical Shift
λ	Wavelength
ν	Wavenumber
τ	Fluorescence Lifetime

Glossary

Anionophore a lipophilic molecule capable of transporting an anion across a cell membrane.

Complementarity. For a host to be complementary to a guest, the host must have the correct topological arrangement of binding groups and have the correct electronic character (in terms of polarity, hydrogen bond donor/acceptor ability, hardness/softness).

Excimer emission is the emission of a photon from a excited state dimer formed from the association of an electronically excited and a ground state fluorophore.

Gallate is the conjugate base of gallic acid (3,4,5-trihydroxybenzoic acid).

Glucose-6-phosphate is the common name for D -Glucopyranose 6-phosphate.

Induced-Fit is a term used to describe the change in conformation of a host upon the binding of a guest. The guest induces a change in conformation of the host in order to bind the guest, with the extent of the conformational change dependent on the preorganisation of the receptor.

Inositol triphosphate

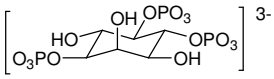

$\boldsymbol{K_a}$ is the association constant for a particular host-guest binding equilibrium. For a simple 1:1 host:guest stoichiometry K_a or K_{11} is used and is defined by the equation:-

$$K_{11} = \frac{[\mathrm{HG}]}{[\mathrm{H}][\mathrm{G}]}$$

Where H = host, G = guest

Alternative binding stoichiometries are denoted by K_{HG} where H and G are the stoichiometry of the host and guest respectively. For example K_{12} corresponds to a 1:2 host:guest stoichiometry and the equilibrium:-

$$H \overset{K_{11}}{\rightleftharpoons} HG \overset{K_{12}}{\rightleftharpoons} HG_2$$

$$K_{11} = \frac{[HG]}{[H][G]} \qquad K_{12} = \frac{[HG_2]}{[HG][G]}$$

Association constants are frequently reported as the $\log_{10}$ value.

Lucigenin is the common name for the fluorescent compound bis-*N*-methylacridinium nitrate.

POPOP is the abbreviation for the fluorophore 1,4-bis(5-phenyloxazol-2-yl) benzene.

Preorganisation. A preorganised receptor is one in which the design of the receptor means there is little conformational change upon binding of a guest and provides an enhancement to the overall free energy of the complexation process.

β is a stepwise binding constant and describes a series of binding equilibria. Frequently β_{HG} values are reported, for example β_{11}, which corresponds to 1:1 host:guest stoichiometry. For the case of β_{11} it is equal to:-

$$\beta_{11} = K_{11}$$

However, β_{12} corresponds to:-

$$\beta_{12} = K_{11} \,.\, K_{12}$$

1. Anion Binding Podands

1.1 Introduction

Anion binding has emerged over the last twenty years as a highly active research area. Anions are ubiquitous in biology with up to 75% of enzyme substrates and co-factors being anionic. They also play a role in disease with cystic fibrosis caused by a defective chloride transport protein.[1-2] Anions can also have a large environmental impact for example perchlorate pollution in the Colorado river and the radioactive anion $^{99}TcO_4^-$ which can leach from nuclear waste.[2] There is a wealth of literature on anion recognition with interest in both macrocyclic and podand systems.[1-4] Podands have a great deal of potential; the preorganisation of a podand for anion binding can be tuned quite readily by altering the rigidity, or tailoring steric or other non-covalent interactions to finely tune the system. Anion binding podand receptors are dominated by NH hydrogen bond acceptors such as amide[5-6], pyrrole[7], indole[8] and urea/thiourea[5] derivatives.[1] Charged systems containing guanidinium[9-10] and imidazolium[11] functional groups are also commonly used. Podands not only provide receptors which are often synthetically simpler than macrocyclic systems,[5] but the flexibility in binding group choice and variable level of preorganisation, which in turn allows a great deal of flexibility in receptor design to suit almost any application. Crucially, as in cation-binding podands, anion binding systems offer flexibility generally leading to rapid binding and decomplexation kinetics[2,12] coupled with binding constants that are suitable for analytical and sensing applications. It is perhaps fair to say that anion binding is the major focus of work in the podand field at present and the following sections give an overview of some representative anion binding podands that cover a range of structural and functional features, highlighting the wealth of variety that is possible by tuning the preorganisation of a receptor, changing the binding moiety and introducing reporter groups which can turn receptors into sensors. The initial focus will be on the cholopods, an unusual class of podands, as they are rigidly preorganised and as such can achieve binding constants to rival any macrocyclic receptor.

1.2 Cholapods – Preorganised Podands

1.2.1 Concept and Properties

Podand systems are intrinsically more flexible than macrocyclic systems, however this reduction in preorganisation can also lead to lower binding affinities for anions. Rigid, aryl end groups can increase binding affinity,[13] however to truly enhance binding strength, a rigid receptor design with a highly preorganised binding cavity is required. This concept is typified best in anion binding receptors by the cholapods, pioneered by Anthony Davis of Bristol University, UK. The cholapods are derivatives of the bile acid, cholic acid and are based on a steroidal, fused alicyclic ring system. This provides a highly rigid scaffold on which binding functionality can be added. The cholic acid core allows for variation in design by both *regio*- and *stereo*-control.[14]

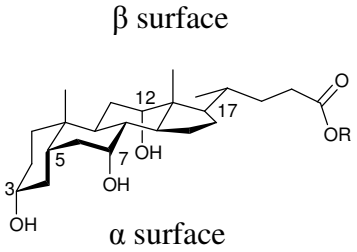

Figure 1.1 Basic structure of cholic acid derivatives

The conformation of the core cholic acid scaffold is curved with three hydroxyl groups on the α surface (Figure 1.1). The equatorial 3α-OH group is the least hindered, whilst the 12α-OH is less hindered than the 7α-OH due to unfavourable 1,3-diaxial interactions between the 7α-OH and CH_2 groups. The hydroxyl groups can themselves act as hydrogen bond donors to bind anions, however it is possible to convert all or individual hydroxyl functional groups to amine or amide moieties to further enhance the hydrogen bonding capabilities or to provide a versatile receptor design. The large extended structure, with separated functionality of the cholopods, is an advantage when trying to bind often large anions.[14]

Neutral anion receptors have many potential advantages over charged systems. Primarily they may provide more selective binding by ensuring directionality, as anisotropic hydrogen bonding is the primary binding interaction rather than non-

directional electrostatic attraction. Additionally, neutral systems do not have counter-ions which can compete to bind to the receptor. Binding constants measured are therefore absolute affinities and not relative to the counter-ion affinity. Neutral podand cholic acid derivatives have been studied extensively.[14-15] A range of neutral receptors has been produced, incorporating hydrogen bond donor NH functionality to the α surface of the cholic acid in the form of amides, sulfonamides, carbamates, ureas and thioureas. Examples of first generation receptors of this type are compounds **1** and **2**.[16] In **1** free rotation is possible around the C3-N bond, however further preorganisation (in addition to that provided by the core) is achieved by the restricted rotation of the carbamate-O/NH groups and the preferential *Z*,*Z*-conformation across the carbamate moieties. Binding affinity was measured by ^{1}H NMR spectroscopic titrations in $CDCl_3$, with **2** showing large affinity for chloride (92000 M^{-1} as the tetraethylammonium, TEA salt), two orders of magnitude higher than its closest rival bromide. Binding constants are smaller for **1,** with fluoride binding the strongest K_a = 15400 M^{-1} (fluoride was not measured for **2**).

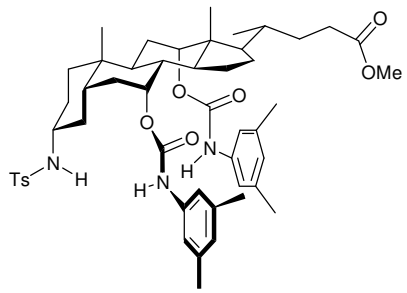

1

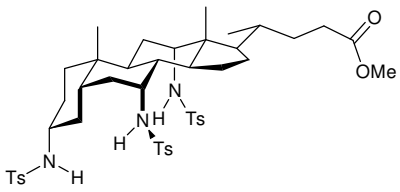

2

Further refinement of the receptor design has involved the addition of electron withdrawing substituents on the binding arms, increasing the acidity of the hydrogen bond donor and hence increasing the potential strength of the hydrogen bonds to guest anions. Receptors **3** and **4** exhibit a *p*-nitrophenylsulfonyl group and the use of nitro or trifluoromethyl groups on the carbamates leads to a ten-fold increase in the binding constant (*c.f.* 3.4 x 10^7 M^{-1} for chloride (as the TEA salt) for **4** compared to 92000 M^{-1} for **1**).[17]

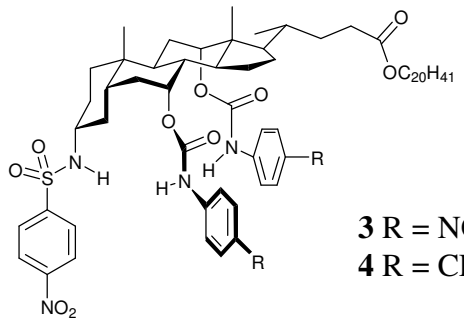

3 R = NO_2
4 R = CF_3

By increasing the number of hydrogen bond donors to five using urea or thiourea moieties, exceptionally high binding constants can be achieved. For example compound **5** shows a chloride (as the TEA salt) association constant of 1.03 x 10^{11} M^{-1}, the highest binding affinity measured for a neutral organic anion receptor and highlights the level of binding strength that can be achieved through highly preorganised receptors, with convergent binding cavities and multiple, strong hydrogen bond donors.[18]

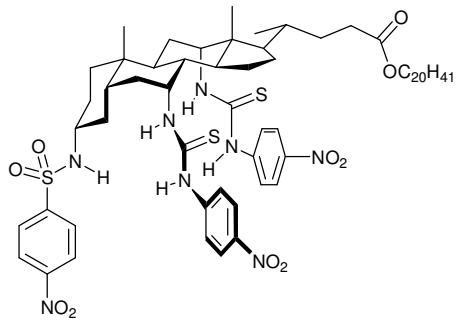

5

It is also possible to produce charged cholapods, typically using guanidinium or ammonium groups but also imidazolium[19] and triazolium[20] moieties. These charged systems have been employed as anion receptors, 'smart transfer agents' and membrane transport anionophores.

1.2.2 Membrane Transport by Cholapods

Trans-membrane transport of anions is a highly active area of research with many implications for biological and medicinal chemistry,[21] most notably in the case of the genetic disease cystic fibrosis which arises through mutations in the cystic fibrosis transmembrane conductance regulator protein, which acts both as a transmembrane chloride channel and as a regulator of other ion channels.[2]

Neutral cholapods have been shown to be effective anionophores, transporting nitrate, hydrogen carbonate and notably chloride, particularly in the case of compound **5**. The anion transport was measured using a dye technique in which the fluorescence of lucigenin encapsulated in a vesicle, is quenched by the inward flow of chloride ions.[22]

The charged guanidinium derivatives such as compound **6** proved capable of extracting *N*-acyl amino acids from an aqueous phosphate buffer into chloroform often with good efficiencies (measured using NMR spectroscopy) and good enantioselectivies.[23-24]

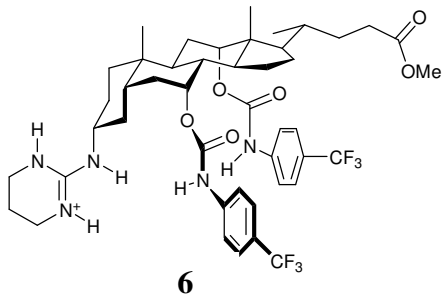

6

Membrane transport experiments using compound **6** and a U-tube apparatus showed that the compound can transport *N*-acetyl-DL-phenylaniline with 70% enantiomeric excess, with the anions bound by hydrogen bonds from the guanidinium and carbamate NH groups.

Ammonium based cholapods have also been investigated as 'smart transfer agents' as well as membrane transporters. The use of ammonium groups not only provides a positive charge but also hydrogen bonding groups. Receptors of type **7** transfer anions from the aqueous to organic phase.[25] The extent of anion transfer is dependent on the lipophilicity of the anion (given by the Hofmeister series, Table 1.1[2]). It was hoped that anion recognition would allow anti-Hofmeister behaviour in which less lipophilic anions are extracted more readily. However whilst the lipophilic anions were extracted less preferentially, the order of extraction in the Hofmeister series remained intact.

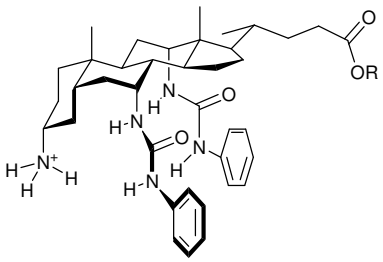

7 R = CH_3
8 R = $C_{20}H_{41}$

Table 1.1 The Hofmeister Series

Weakly hydrated (hydrophobic) Strongly hydrated (hydrophilic)

Anions: organic anions > ClO_4^- > I^- > SCN^- > NO_3^- > ClO_3^- > Br^- > Cl^- >> F^-, IO_3^- > $CH_3CO_2^-$, CO_3^{2-} > HPO_4^{2-}, SO_4^{2-} > citrate^{3-}

Cations: $N(CH_3)_4^+$ > NH_4^+ > Cs^+ > Rb^+ > K^+ > Na^+ > H^+ > Ca^{2+} > Mg^{2+}, Al^{3+}

Whilst compound **7** is ineffective at membrane transport of anions, the addition of a long alkyl chain as in **8** does result in the transport of anions through a chloroform liquid membrane (as part of a U-tube set-up) with a small selectivity for chloride.

A bicyclic guanidinium core has been utilised by de Mendoza and co-workers for transport of uronic acid salts. Receptors **9** and **10** contain a bicyclic guanidinium group connected to two modified deoxycholic acid motifs.[26] The binding of D-glucuronate, **11**, (as the TBA salt) was evaluated using ^{1}H NMR spectroscopic titrations in acetonitrile. The receptors with the most flexible linker group showed the lowest binding constants, consistent with reduced preorganisation. The glucoronate is bound to the guanidinium groups via the carboxylate moiety with the hydroxyl groups of the deoxycholic acid derivatives providing additional hydrogen bonds to the carbohydrate alcohol groups. The largest contribution to the binding strength is from the ion-pairing of the carboxylate and the guanidinium group.

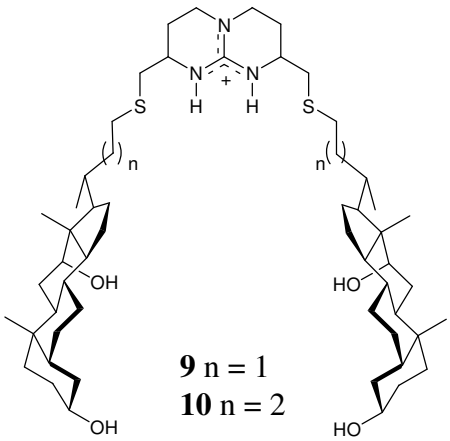

9 n = 1
10 n = 2

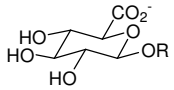

11

Regan and co-workers have synthesised a range of charged anion transporters. An interesting example is that of **12** known as a molecular umbrella.[27] This dicationic species containing ammonium and guanidinium functionality can bind adenosine triphosphate (ATP) through the interaction of the phosphate residues of the anion to the guanidinium moiety. The cholic acid groups can then encapsulate the anion by OH hydrogen bonds to the inner surface, presenting a lipophilic outer surface, allowing the complex to pass through the membrane.

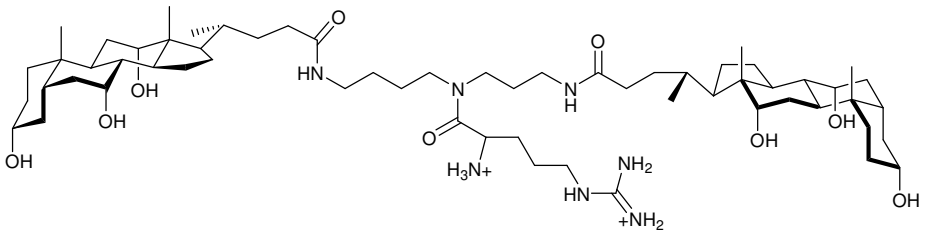

12

1.2.3 Anion Sensing by Cholapods

The addition of fluorescent moieties can provide a reporter group which, in principle, can result in a selective receptor with high anion binding that can signal this binding through changes in the fluorescence emission. The advantage of a podand-type receptor is that binding and release are generally fast in comparison to rigidly preorganised macrocyclic systems.

Fang and co-workers have developed cholopods functionalised at the C24 position which provides both additional hydrogen bonding functionality and an anthracenyl reporter group, compounds **13** and **14**.[28-29]

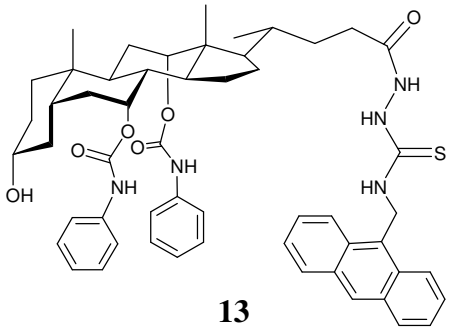

13

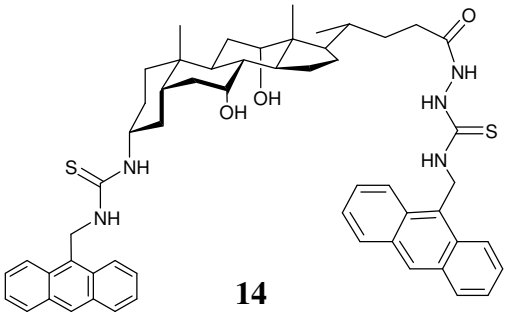

14

Compound **13** shows strong anion affinity in acetonitrile, particularly for carboxylates with an acetate binding constant of 7.7×10^4 M^{-1}. The compound functions as a photo-induced electron transfer (PET) sensor (see Section 1.4.3), with fluorescence quenching observed upon addition of anions. Compound **14** is also a PET sensor and shows remarkably strong anion binding to dicarboxylates in highly competitive solvents (1:1 *v/v* methanol:water), for example L-glutamate is bound with a binding constant of 5.6×10^6 M^{-1}. As with **13**, fluorescence quenching is observed on addition of anions however only a maximum of 20% reduction in intensity is achieved.

1.3 Induced-Fit Anion Binding

1.3.1 General Considerations

The principal advantage of highly preorganised receptors such as the cholapods, is their specific and strong anion binding. However this can also be a disadvantage in some circumstances, for example in sensing. The small changes in conformation resulting from anion binding means the communication of the binding event to the reporter group, such as a fluorophore or chromophore, must be done via a change in the electronic distribution of the receptor. This may prove inefficient in comparison to processes requiring significant structural or conformational rearrangement. An alternative approach is to use conformationally flexible receptors, which can change their shape or relative disposition of binding sites or chromophores upon anion binding

and in doing so, lead to a change in a physical property of the molecule. Flexible systems also have faster complexation/decomplexation kinetics which is also an advantage in sensing applications. Induced-fit binding can also lead to anion sensors capable of a significant degree of discrimination between anionic guests because the induced conformation of the host is dependent on the size and geometry of the anion bound, therefore each host/guest geometry is unique and can potentially affect a reporter group in a distinct way. The term discrimination in this context is distinct from binding selectivity (as measured by the magnitude of the binding constant) since it refers to the response of the receptor system to the guest binding event. The distinction is particularly well exemplified in colourimetric sensor arrays in which each individual receptor is only very poorly selective, but the array as a whole can be highly discriminating in its ability to recognise particular guests based on the pattern of their response.[30-31]

A possible disadvantage of an induced-fit receptor is the intrinsically lower binding constants compared to preorganised systems. Typically a negative entropic contribution is expected when binding an anion as the system becomes more ordered. In macrocyclic systems, with less conformational freedom, this entropy cost is paid during the synthesis of the molecule. However the situation can be complicated by the restrictions on small conformation motion imposed by the binding.[32] For flexible systems this is not the case, and the reorganizational energy represents an unfavourable contribution to the overall binding free energy. The conformational flexibility can potentially mean that a large range of anions are bound with similar binding constants, resulting in reduced thermodynamic binding selectivity. However, as the sensing method is dependent on conformation rather than binding strength, induced-fit sensors can still discriminate for particular anions, even though that anion may not have the highest affinity for the receptor.

By using well designed molecular architectures, it is also possible to increase the preorganisation of a receptor (and hence increase the binding constant) whilst still allowing a degree of flexibility. The trialkylbenzene motif has been used extensively for this purpose due to its ability to balance these two competing attributes and is discussed in the following section.

1.3.2 The Trialkylbenzene Motif

The hexa-substituted benzene moiety, typically consisting of ethyl substituents in the 1, 3 and 5 positions and binding arms in the 2, 4 and 6 positions has proved to be a highly versatile motif in both cation and anion binding. It has been combined with a wide range of binding groups to create both neutral and charged receptors and sensors.

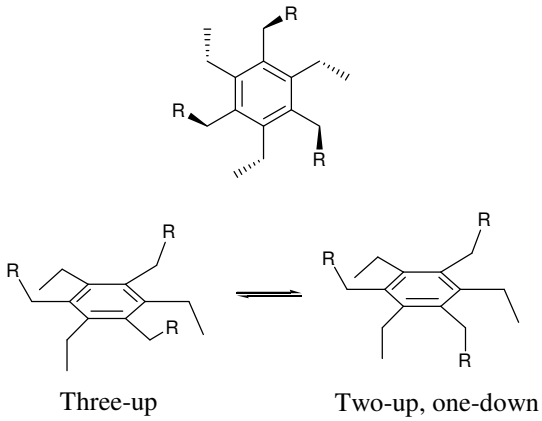

Figure 1.2 Trialkybenzene motif and its conformations

The moiety provides a balance between flexibility and preorganisation; steric interactions between adjacent substituents on the hexa-substituted benzene ring favours an alternating three-up, three-down arrangement of substituents by approximately 15 kJ mol^{-1} (so called 'steric gearing').[33-34] This arrangement creates a convergent binding cavity, although the stability of the three-up, three-down conformation can be influenced by both electrostatic repulsion and steric interactions between binding arms. In cationic receptors, the C_3 symmetric 'three-up' conformation is by no means the only conformation observed and can be in equilibrium with the 'two-up, one-down' conformation also present in solution (Figure 1.2).[35] In some cases additional conformational flexibility is also possible, involving the relative orientation of binding functional groups with respect to the cavity. Hence, *in* and *out* conformations of the binding groups are also possible, for example in the hypothetical molecule in Figure 1.3, conformation (a) has all binding arms (R) in the *in* conformation, forming a convergent binding cavity, whilst (b) has all R groups in the *out* conformation and has a divergent cavity. Both *in* and *out* conformations have been shown to be present at room temperature in solution.[35]

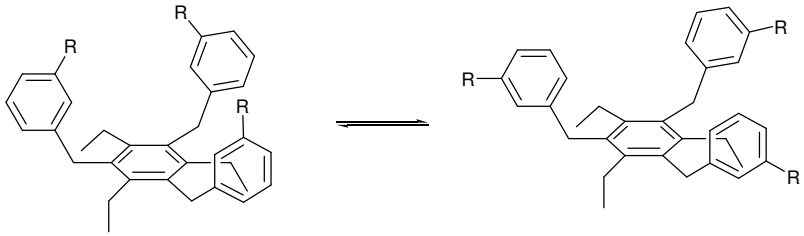

(a) *in* (b) *out*

Figure 1.3 *In* and *out* conformations of the trialkylbenzene motif

The trialkylbenzene motif in anion binding was pioneered by Ansyln and co-workers and proved to be a highly successful platform for a range of anion sensors incorporated into an indicator displacement assay (IDA).[36] An indicator displacement assay system consists of a receptor such as **15** and a fluorophore or chromophore guest molecule such as the fluorescent indicator **16**, which weakly binds to the receptor in solution. When an anion which has a higher affinity than the guest dye is added to the system, it displaces the indicator from the binding cavity. The change in the microenvironment of the fluorophore causes a change in the UV-vis absorption and/or fluorescence emission of the indicator. In the case of **15**, the receptor proved to be highly selective for the tricarboxylate citrate, above even other carboxylates, as well as other salts and sugars.[33,37] The molecular structure of the **15**.citrate complex determined by X-ray crystallography can be seen in Figure 1.4. The assay is able to detect the concentration of citrate in water (a highly competitive solvent) by increases in the absorbance and emission intensity. The concentration of citrate was also determined in orange juice and other soft drinks.

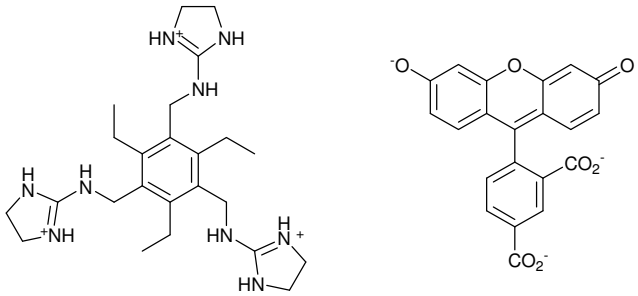

15 **16**

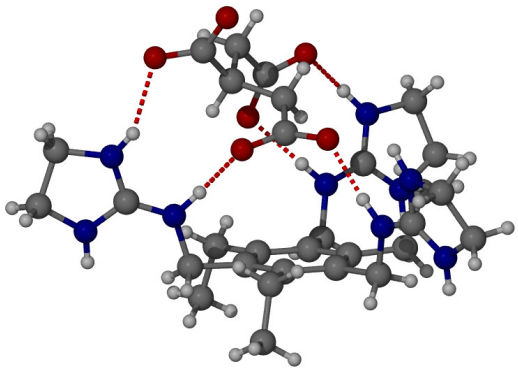

Figure 1.4 Molecular structure of **15**.citrate. Second complex in the asymmetric unit is omitted for clarity[33]

Several other sensing arrays have been developed by the Ansyln group, for example compound **17** with pyrocatechol violet (**18**). The binding of gallate–like anions (the conjugate base of gallic acid) can occur through the reaction of the alcohol group with the boronate ester and the binding of the carboxylate to the guanidinium group.[38] This results in the displacement of the indicator from the binding cavity, resulting in an observable colour change. This sensing system was used to accurately determine the age of Scotch whiskey, as gallate-like anions leach into the whiskey over time from the storage barrels. The same receptor with alizarin complexone (**19**) was able to determine the concentration of tartrate in wine and fruit juice.[39] Several other assays designed to sense the biologically important anions glucose-6-phosphate[40] and inositol triphosphate (IP_3) have also been developed.[41]

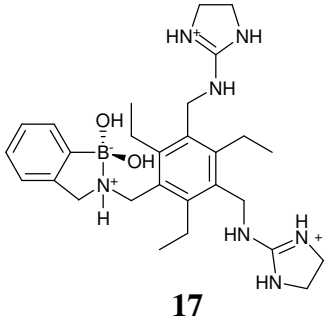

17

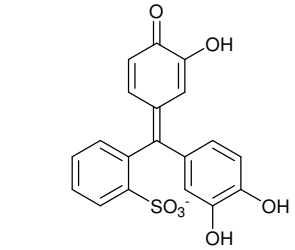

18

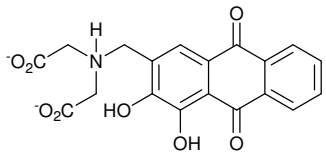

19

Combining several different anion receptors into a microarray can allow for the discrimination of anions present in a solution and are often known as electronic tongues or noses. Here, a series of receptors, each with often subtly different peak anion

selectivity, can discriminate between various anions through their differential colourimetric, fluorescence or electrochemical responses.

An example of this sensing array concept has been developed by Ansyln and co-workers who used a differential receptor system to discriminate between the nucleotides adenosine triphosphate (ATP), adenosine monophosphate (AMP) and guanidine triphosphate (GTP). The trialkylbenzene motif was used as the basis for the receptors with each receptor immobilised on to a polymer resin by attachment to one of the binding arms (for example **20** in Figure 1.5). The two remaining arms were functionalised with short peptides; synthesised using combinatorial synthesis. Thirty polymer beads were then used to generate the sensing array. The sensing method was based on an IDA, with fluoroscein used as the chromophore. Analyte solutions were allowed to flow over the beads and the change in absorbance of the fluoroscein as it is displaced from the receptor by the analyte, was monitored using a CCD camera. Principal component analysis (PCA) was then successfully used to determine which analytes were present in the mixture.[30-31]

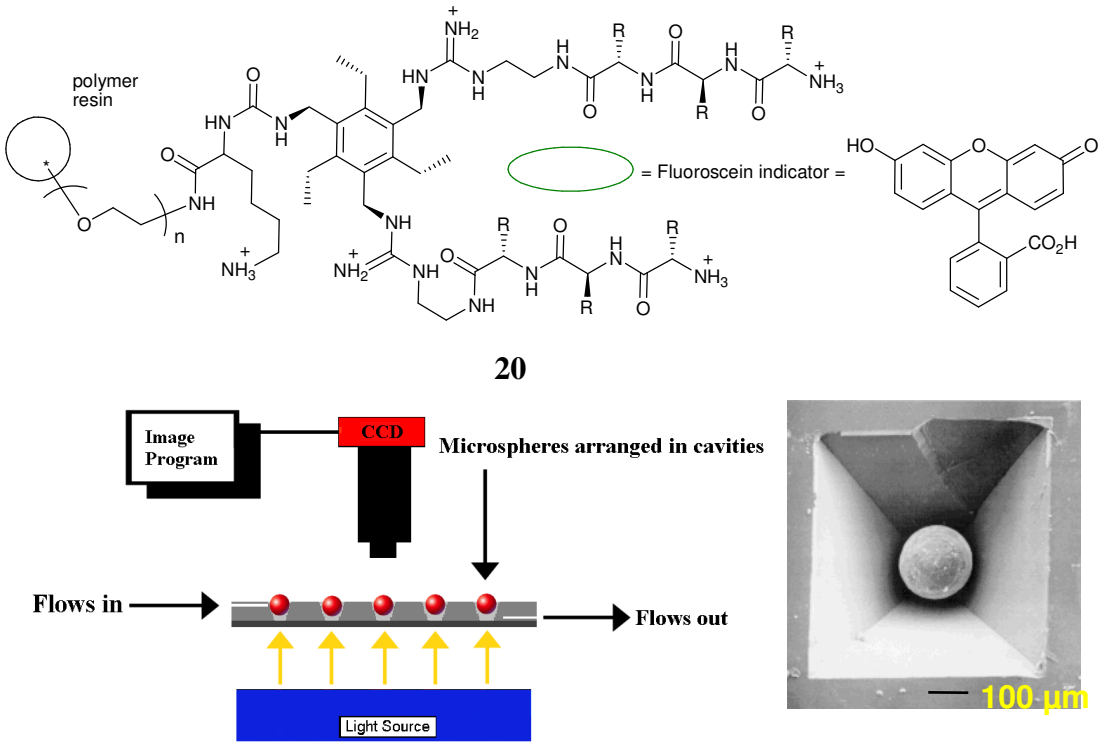

Figure 1.4 Diagram of an array sensing system, with receptor and indicator illustrated. Reproduced with permission from reference 30, 2001 © American Chemical Society

Steed and co-workers have used the trialkylbenzene motif in designing receptors such as **22** and **23** with pyridinium derivatives providing charge assisted CH···X^- hydrogen bonds and/or NH···X^- hydrogen bonds, as can be seen in the molecular structure (determined by X-ray crystallography, Figure 1.6) of the **23**·Br^- complex. This shows the host in the three-up conformation with both *in* and *out* conformations of the binding arms present. ^{1}H NMR spectroscopic titrations show that compound **22** binds chloride strongly with a binding constant of 82000 M^{-1} in CD_3CN/DMSO (*v/v* 95/5). The high affinity shows the complementarity between the binding cavity and the chloride.[35]

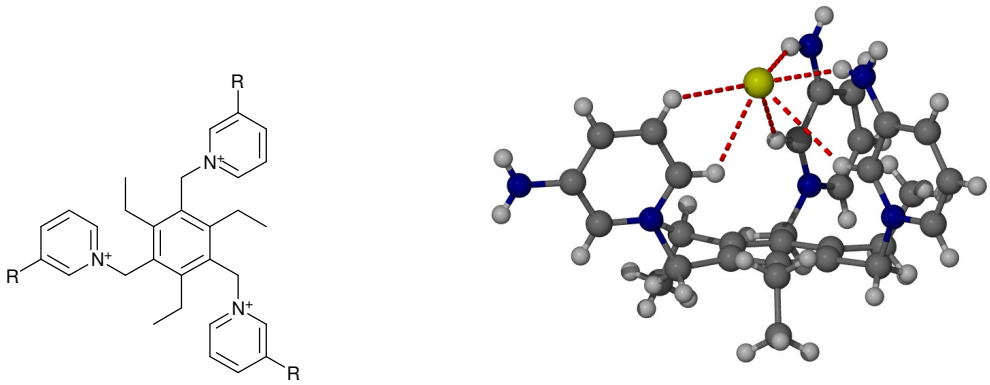

22 R = H
23 R = NH_2

Figure 1.6 Receptor design for **22** and **23** along with the **23**.Br^- complex molcular structure determined by X-ray diffraction[35]

Variable temperature (VT) NMR spectroscopy in acetone–d_6 revealed the presence of the two-up, one-down conformer, evidenced by the splitting and up-field shifting of the ethyl CH_3 resonance as the proton moves into the shielding area of the pyridinium groups for the 'down' ethyl group. *In* and *out* binding arm fluctuations were also observed. VT NMR spectroscopic experiments with varying amounts of added chloride revealed that binding to one equivalent of Cl^- switches the system to the symmetric 'three-up' conformation, while in the presence of substoichiometric amounts of Cl^- the Cl^-/PF_6^- exchange equilibrium can be observed on the NMR spectroscopic time scale. While such anion exchange equilibria are sometimes slow in macrocyclic systems,[42] they are generally fast in podands highlighting the degree of preorganisation afforded by the steric crowding in **23**.

A similar receptor (**24**) has been designed by Fabbrizzi and co-workers which also utilises NH and CH charge assisted hydrogen bonding and shows strong binding to chloride.[43]

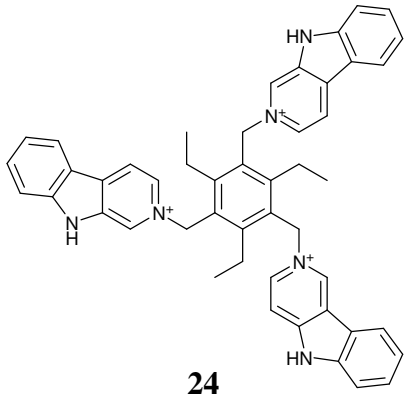

24

The incorporation of halogen atoms onto a pyridyl ring can also allow halogen bonding, for example compound **25**.[44] The halogen bonding occurs between the positive region of electrostatic potential of the halogen, which is enhanced by the electron-withdrawing cationic pyridinium motif, and the negatively charged anion. When in the three-up conformation, compound **25** is capable of forming a convergent binding cavity with very strong binding to phosphate, PO_4^{3-} (as the sodium salt) with a binding constant of log K_a 5.6 in water (at pH 12.1). A related receptor, compound **26**, derived from a *para*-iodotetrafluorophenyl binding group, also binds anions strongly using halogen bonds.[45] Interestingly, receptor **26** displays a different anion selectivity with chloride (K_a = 1.9 x 10^4 M^{-1} in acetone) having a larger binding constant than oxo-anions. It is likely that the smaller cavity size in **26**, is a poor match to oxo-anions and is more complementary to chloride.

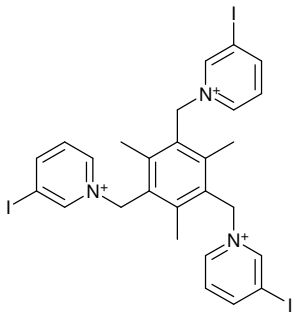

25

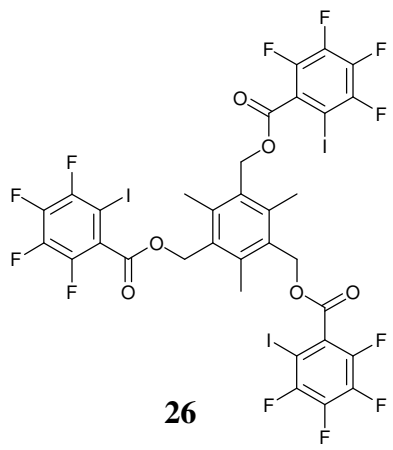

26

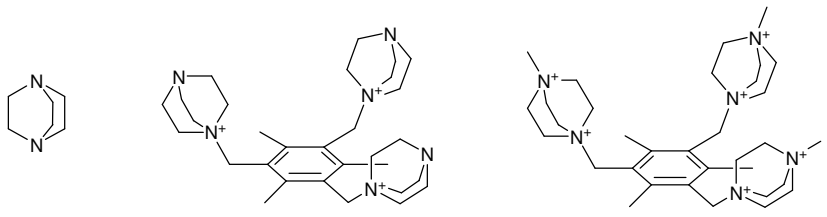

27 **28** **29**

The binding arm 1,4-diazabicyclo[2.2.2]octane (DABCO, **27**) is useful as its derivatives can be both mono- or di-cationic, leading to a tri- (**28**) or hexa-cationic (**29**) species and allows for the investigation of the effect of charge on the guest interaction. The strongest binding was found for complementary anions, for example, a tri-cationic host and a tri-anionic guest. An interesting example of this charge matching is in the selective binding and precipitation of ferricyanide, an Fe(III) species over ferrocyanide, an Fe(II) species with the tri-cationic host.[46]

Further development of the trialkylbenzene motif has lead to receptor **30** by Schmuck and co-workers which exhibit exceptionally high binding of tricarboxylates in water. The cationic guanidinium groups create a tri-cationic receptor which binds carboxylates in a 1:1 stoichiometry largely by electrostatic interactions. A binding constant of $> 10^5$ M^{-1} was measured for citrate, by UV-vis and fluorescence spectroscopy, with excellent selectivity over monoanionic species.[47]

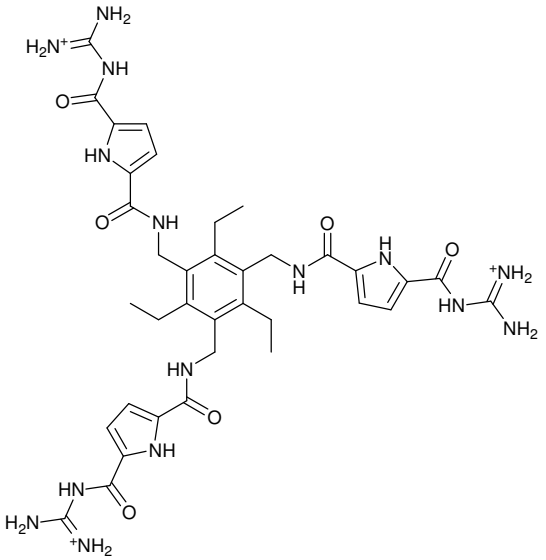

30

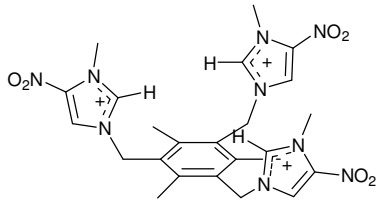

31

As an alternative to the more usual hydrogen bonding groups such as urea, amides, guanidinium etc, it is possible to use imidazolium groups to create $CH^{+}\ldots X^{-}$ hydrogen bonds as in receptor **31**.[48] The charged nature of this system means that the main interaction is electrostatic. To further enhance the strength of this form of hydrogen bond, a nitro group can be attached to the imidazolium ring at the C(4) position, enhanced by the electron withdrawing nature of the nitro group. *Ab initio* calculations and ^{1}H NMR spectroscopic titrations were used to determine the binding constant for halide anions, with both methods concurring to give a selectivity series of $Cl^{-} > Br^{-} > I^{-}$. The binding constant for Cl^{-} in DMSO-d_6 is 4800 M^{-1} with a tenfold selectivity over Br^{-}. Additionally, the compound also binds dihydrogen phosphate with a binding constant of 2500 M^{-1} due to the strong basicity of dihydrogen phosphate increasing its binding affinity.

The principle of using anion binding to shift the equilibrium of conformations of a host has been used by Duan and co-workers to synthesise the chloride selective sensor **32**.[49] In this system anions are bound by charge assisted hydrogen bonding to the benzimidazolium group with a binding constant of 3.9×10^{3} M^{-1} in DMSO. The **32**·3BPh_4 complex shows only monomer emission from the naphthyl reporter groups. However on addition of chloride an excimer band (emission from an excited state naphthyl dimer at longer wavelengths) is observed in the emission spectrum (Figure 1.7). The anion induced conformational change brings two naphthyl groups into close contact and allows for excimer formation. Only chloride is able to induce a conformation where this can occur.

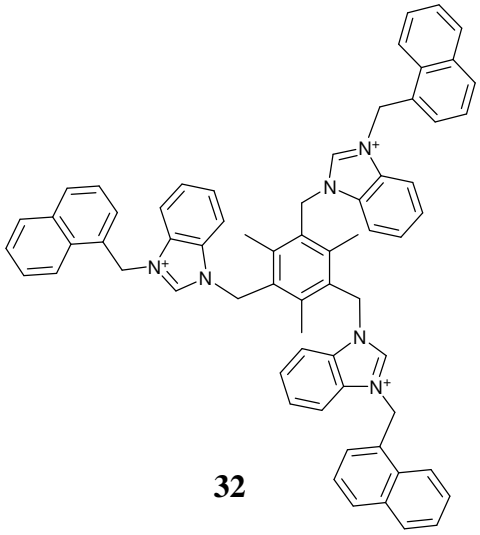

32

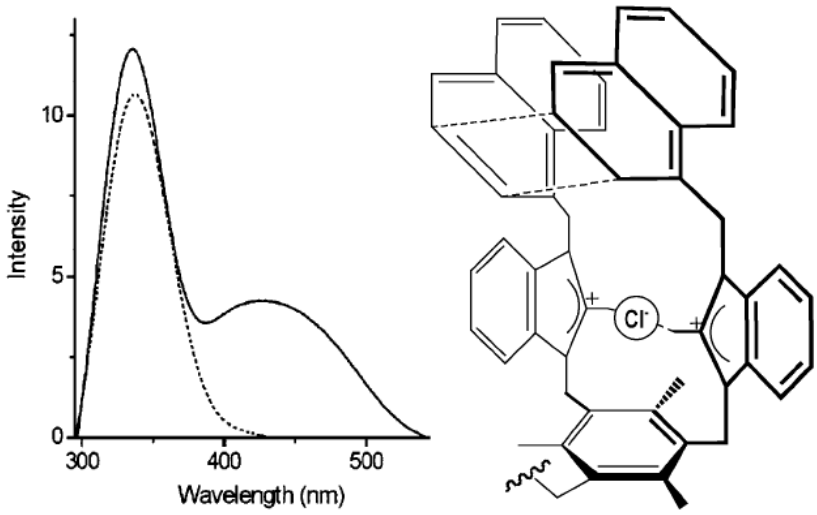

Figure 1.7 Emission spectrum of **32** in the absence (dotted line) and presence of TBA-Cl (solid line). Reproduced by permission from reference 49, 2005 © The Royal Society of Chemistry (RSC) for the Centre National de la Recherche Scientifique (CNRS) and the RSC

Building on previous work Duan and co-workers have developed the ditopic and the tripodal ferrocenyl derivatives **33** and **34**.[50] Of the anions tested, both receptors bind chloride strongly with moderate selectivity. Differential pulse voltammograms (DPV) show a cathodic shift of 50 mV in the $E_{1/2}$ value of **33**. Smaller cathodic shifts were observed for other anions. No response was observed with the tripodal derivative **34**, despite anion ^{1}H NMR spectroscopic titrations confirming the receptor does bind anions strongly, in the region of 10^3 M^{-1}.

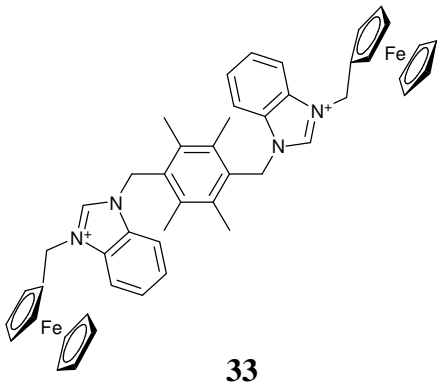

33

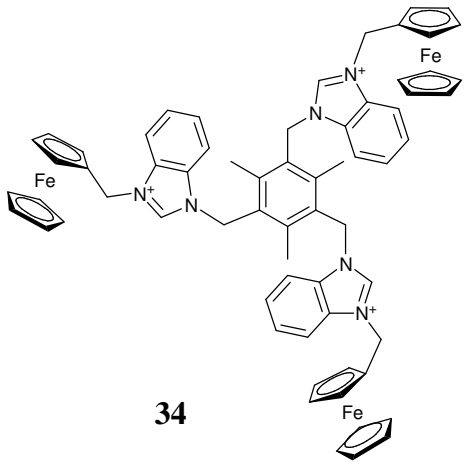

34

1.3.3 Anion Induced Excimer Formation in Calixarene-Based Podands

The design of induced-fit anion sensors in not limited to the trialkylbenzene motif. Calixarenes with pendent binding arms have also been explored with pyrene derivatives typically used as the fluorophore. Pyrene excimer emission has been used as a fluorescent reporter which requires close contact between adjacent pyrene molecules for its formation. They are an ideal candidate for induced-fit sensing as conformational changes can dramatically affect intramolecular pyrene-pyrene distances in both the ground and excited states.

Kim and co-workers have synthesised receptor **35**, with two pendent pyrenyl binding arms.[51] The system can shift from the dominance of a dynamic excimer (dimer formation in the excited state) in the free host to a static dimer (ground state dimer formation) on addition of fluoride. The binding of the fluoride in the receptor holds the pyrenyl groups in close proximity and allows a ground state dimer to form. This results in a 73 nm red-shift in the excitation spectrum and a 12 nm blue-shift in the excimer emission.

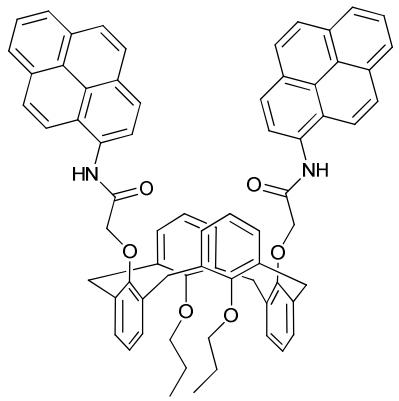

35

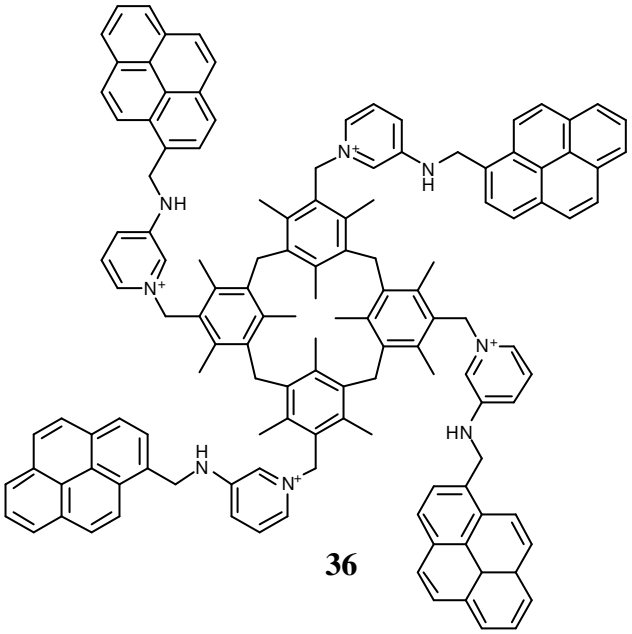

36

Steed and co-workers have also synthesised a calix[4]arene derived receptor **36**.[52] The compound is locked into a 1,3-alternate conformation through steric interactions between the mesitylene rings. This creates a ditopic receptor with pyridinium binding groups and a pyrenyl reporter. The receptor binds two equivalents of dicarboxylates strongly (K_{11} > 100000 M^{-1} in acetonitrile) with the dicarboxylate capable of spanning across the two binding arms. However no significant change in the fluorescence emission was observed for this anion. The binding of chloride is an order of magnitude lower than that of dicarboxylates. However chloride binding alters the conformation of the receptor in such a way as to allow ground state interactions between the pyrenyl groups and promote the formation of an excimer on excitation (Figure 1.8). Chloride binding also has an electronic effect in that it prevents fluorescence quenching by intramolecular charge transfer to the pyridinium moieties resulting in the observation of both pyrene excimer and monomer emission in the presence of excess chloride. This example shows the importance of conformation in this class of receptor. The sensor discriminates the anion which induces a conformation allowing excimer formation to occur and has the appropriate electronic effect on the system, rather than the one that is the most strongly bound.

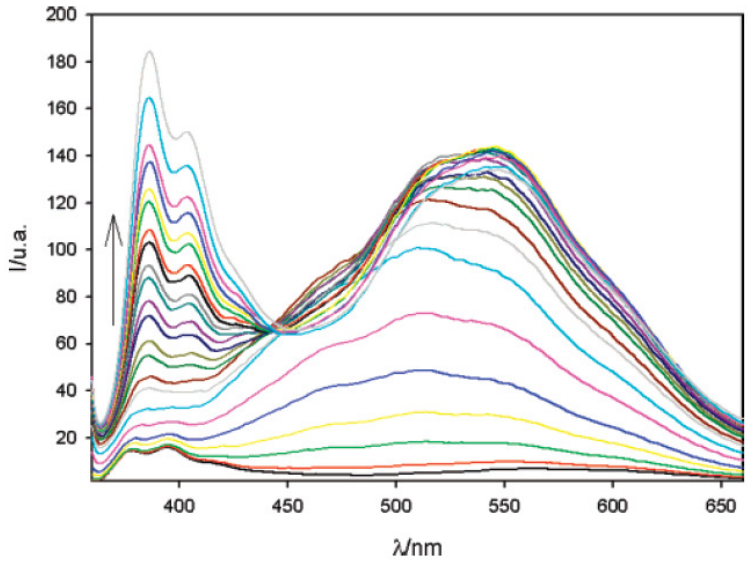

Figure 1.8 Emission spectrum of **36** upon increasing amounts of TBA-Cl. Reproduced with permission from reference 52, 2008 © American Chemical Society

1.3.4 Induced-Fit Molecular Clip Sensors

Molecular clips were first developed as hosts for molecular guests in the 1970s by Whitlock and co-workers.[53] The concept has been further developed by Zimmerman[54], Rebek[55] and Harmata.[56] Typically, molecular clips are simple receptors consisting of two binding domains, which when binding molecular guests, have generally consisted of aromatic groups tethered by a linker/spacer, which bind guests through π-π and ion-dipole interactions. Preorganisation can depend on the rigidity of the receptor and its ability to maintain a convergent binding site.

The use of molecular clip receptors in induced-fit anion sensing has been relatively unexplored, even though the design of these receptors appears to be well suited to the task. In general, these systems consist of biaryl units with the addition of anion binding groups. The relatively rigid nature of the coupled aromatic systems means that the conformational freedom is largely restricted to rotation about the inter-aryl bond. This provides a degree of preorganisation to the system.

Receptor **37** shows a 2.4 fold increase in emission intensity after the addition of 2.5 equivalents of fluoride which was attributed to a concept known as conformational

restriction, in which one fluoride anion is bound by both urea moieties, rigidifying the receptor and reducing non-radiative decay. Further addition of F^- resulted in a decrease in the intensity. The binding of a second fluoride (one F^- bound to each urea group) allows more conformational flexibility and hence increases non-radiative decay.[57]

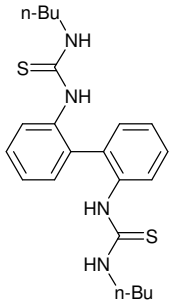

37

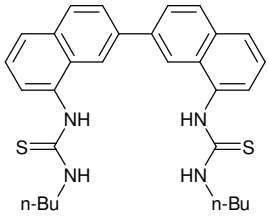

38

A similar receptor design based on a 2,2'-binaphthalene derivative (**38**) shows a red-shift in the UV-vis spectrum on addition of fluoride, consistent with planarisation of the binaphthyl groups and conformational restriction, although for this receptor, only small changes were observed in the fluorescence emission.[58]

Lin and co-workers have developed receptor **39** which consists of naphthyl groups at the end of urea binding moieties.[59] Upon binding *ortho*-phthalate there is a significant increase in emission at 460 nm, which is not observed with *meta* or *para* isomers of phthalate. The emission is from the excited state of the product of a photochemical reaction between the naphthyl groups and it is only *ortho*-phthalate which induced the conformation necessary for this photochemical reaction to occur.

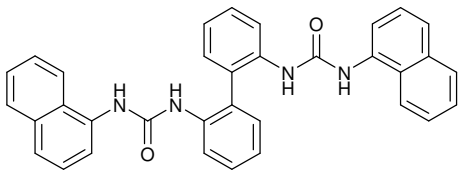

39

1.4 Prodigiosins and Small Molecule Anion Receptors and Sensors

1.4.1 Prodigiosins and their Analogues

Prodigiosins are a class of compounds isolated from microorganism of the *Serratia* and *Streptomyces* genus. These naturally occurring pigments are dark red and colonies of the gram-negative bacteria often resemble droplets of blood and have been put forward as the scientific explanation to many apparent miracles.[60] More recently it has been shown that prodigiosins have immunosuppressive and anti-cancer properties and the compounds are a promising lead in new drug therapies. The structure of prodigiosins consists of a tripyrrolic skeleton (**40**) as in prodigiosin 25-C (**41**) for example, which has been studied extensively for pharmaceutical use.[1]

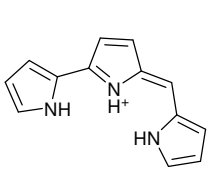

40

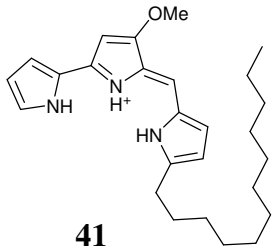

41

Two primary mechanisms have been suggested for the biological activity of prodigiosins. The first involves the ability of prodigiosins to mediate into-cell transport of HCl, whilst the alternative involves the coordination of copper and subsequent modification of DNA.[1,60] The transport of HCl into a cell is necessarily intimately linked with anion binding and transport and so efforts have been made to understand the anion recognition behaviour of prodigiosins.

Sessler and co-workers have investigated a series of prodigiosin analogue compounds **42** and **43 - 46**.[1, 61-62] Both types of compounds bind chloride strongly when protonated. Binding constants in the order of 10^6 M^{-1} were observed for **42** and 10^5 M^{-1} for **43** measured by isothermal titration calorimetry (ITC) in acetonitrile. This data shows that even very simple acyclic pyrrole-derived sensors can bind anions strongly due to the relatively rigid nature of the skeleton, creating a preorganised binding cavity with NH hydrogen bond donors and electrostatic attraction.

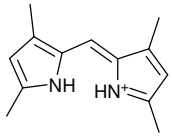

42

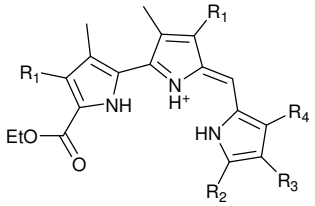

43 R_1 = Et, R_2 = R_4 = Me, R_3 =H
44 R_1 = Et, R_2 = R_3 = R_4 = H
45 R_1 = Et, R_2 = H, R_3 = R_4 = OMe
46 R_1 = R_2 = R_4 =Me, R_3 = H

The molecular structure of compound **42**.Cl^- was determined by X-ray crystallography and confirms the chloride is bound by two NH hydrogen bonds and electrostatic interactions in an essentially planar conformation (Figure 1.9). The molecular structure of **43**.Cl^- determined by X-ray crystallography shows the chloride bound by three NH hydrogen bonds with the receptor in a slightly twisted conformation (Figure 1.9). Further modification to the prodigiosin analogues **44 – 46** also proved to be effective at binding chloride with binding constants in the range of 10^4 - 10^5 M^{-1}. The synthesis of tetrapyrrolic receptors such as **47**, creating an additional hydrogen bond donor site also binds chloride effectively (*ca.* 10^5 M^{-1}). [1,62]

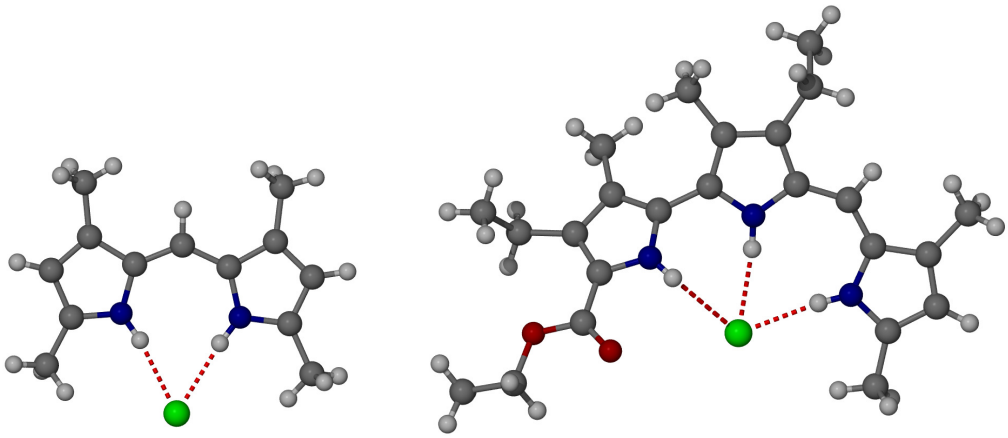

Figure 1.9 Molecular structure of **42**.Cl^- and **43**.Cl^- determined by X-ray diffraction[61]

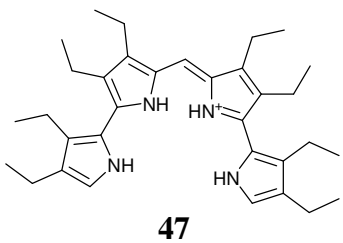

47

Membrane transport studies were also conducted on naturally occurring prodigiosins and analogous compounds **42** and **43** and suggest the anticancer properties of the receptors follow the trend for membrane transport efficiencies, rather than the anion binding strengths. This result supports the symport transport of H^+/Cl^- theory as the source of the anticancer properties of this class of compound and that large chloride binding constants impair the release of the chloride, i.e. the kinetics of the systems are more important than the thermodynamics.[61]

Prodigiosin minics based on amidopyrroles synthesised by Gale and co-workers also showed membrane transport of HCl.[63] The amidopyrrole derivative **48** with a pendant imidazole derivative proved to be the most effective membrane transporter. Interestingly compound **49** showed relatively weak anion binding even when protonated i.e. 397 M^{-1} in acetonitrile but proved effective at transporting HCl, highlighting the importance of kinetic lability in this process.

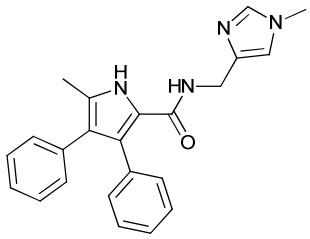

48

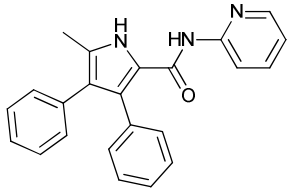

49

Prodigiosins have shown that small molecules consisting of a relatively rigid skeletal framework and convergent hydrogen bond donors can be highly effective at anion binding. Research in this area is highly active and there are a wide variety of structural motifs which are discussed in the following section.

1.4.2 Small Molecule Podand Receptors

Isophthalamide anion receptors were originally synthesised by Crabtree and co-workers e.g. compound **50**, as a binding motif with little rigidity or preorganisation. However reasonable binding affinities with halides were observed in the range of 10^3 - 10^4 M^{-1} in

dichloromethane. The molecular structure determined by X-ray diffraction shows a distinctly non-planar binding mode.[64-65]

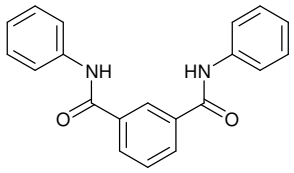

50

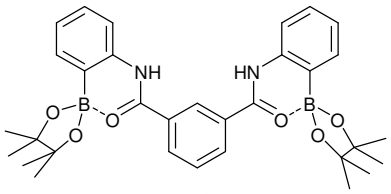

51

Smith and co-workers synthesised an isophthalamide derivatives functionalised with boronate esters, **51**.[66] The carbonyl group is able to coordinate to the boron atom and increases the preorganisation whilst also increasing the dipole moment, allowing stronger ion-dipole interactions. The NH residue has a greater positive charge and so has a stronger interaction with the acetate. Consequently, compound **51** has an order of magnitude higher binding constant than **50**.

Gale and co-workers have designed isophthalamide and 2,6-dicarboxyamidopyridine derivatives.[67] The addition of two indole motifs provides the molecule with a total of four NH hydrogen bond donors.[68] Compound **52** is highly selective for fluoride (K_a of 1360 M^{-1} in DMSO) even compared to other basic anions such as acetate (K_a of 250 M^{-1} in DMSO). It was postulated that the twisted binding conformation observed in the molecular structure (measured by X-ray diffraction, Figure 1.10) is also found in solution and is more stable than the binding modes possible with other anions.

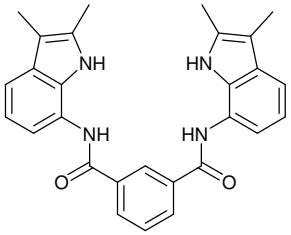

52

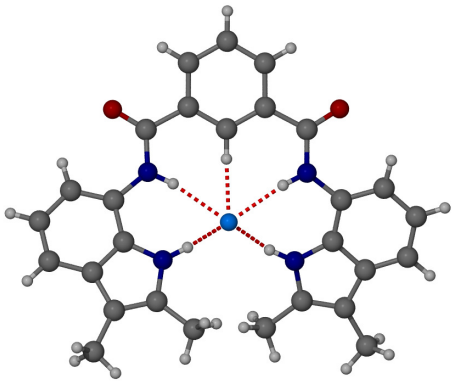

Figure 1.10 Compound **52** with the molecular structure of **52**.F^- determined by X-ray crystallography[68]

Modification of the core motif allows for 2,5-diamidopyrrole derivatives, **53**, having a additional NH hydrogen bond donor compared with isophthalamide receptors.[69] A binding constant for benzoate of 2500 M^{-1} in acetonitrile is observed with an asymmetric binding mode apparent in the molecular structure measured by X-ray crystallography.

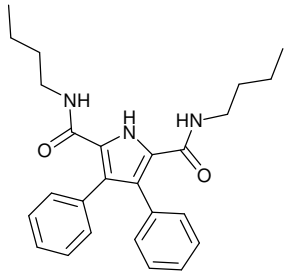

53

Ortho-phenylaminediamine derivatives have also been investigated as anion receptors containing four NH hydrogen bond donors in the form of urea groups or amide and pyrrole moieties.[70] Compounds **54** and **55** are selective for carboxylates with compound **54** showing significantly higher binding constants for carboxylates than **55**. It is suggested that the more open binding cleft in **54** is more structurally complementary to carboxylates than **55**. The presence of chloro groups in an analogous compound to **54** showed an increase in binding constant from 3210 M^{-1} for acetate to 8079 M^{-1}. It is suggested that the increased acidity of the hydrogen atoms in the central ring allows for CH...O hydrogen bonding, effectively preorganising the receptor into a planar conformation. Indeed using thiourea derivatives reduces the acetate binding constant by an order of magnitude, as the large size of the sulfur atom results in steric hindrance between the sulfur and phenyl hydrogen atoms, distorting the binding cleft.

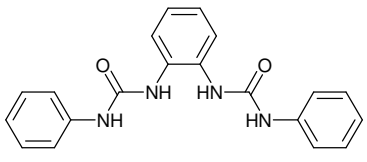

54

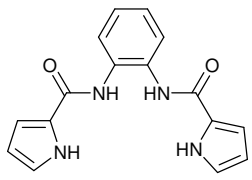

55

It has been shown above that intramolecular interactions can enhance the preorganisation of small molecule acyclic receptors.[71] As an alternative, increasing

structural rigidity using aryl rings can also provide preorganisation. This is typified well by the indolocarbazoles. The rigidity of compound **56** is provided by five fused aromatic rings and contains two convergent NH hydrogen bond donors. Compound **56** is an effective anion receptor with benzoate and dihydrogen phosphate bound strongly (log K_a of 5.3 and 4.9 respectively measured by UV-vis titration in acetone). The addition of bromine in the 3 and 8 positions (**57**) leads to a marked increase in binding strength through their electron withdrawing effect. Figure 1.11 shows the molecular structure of the **56**.Cl^- complex determined using X-ray crystallography.

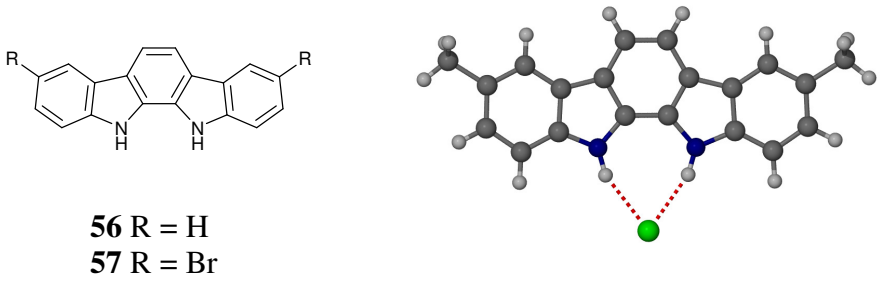

56 R = H
57 R = Br

Figure 1.11 Compounds **56**, **57** with the molecular **56**.Cl^- determined X-ray crystallography[71]

The indolocarbazole derivative **58** is able to bind anions in water in a helical conformation creating a tubular cavity in which multiple NH hydrogen bonds bind the anion. The binding conformation was confirmed using NOESY NMR experiments with chloride bound strongest (K_a of 65 M^{-1} in water). Whilst this binding constant is small, it is measured in a highly competitive medium. The use of less competitive solvents on related compounds show strong anion binding.[72]

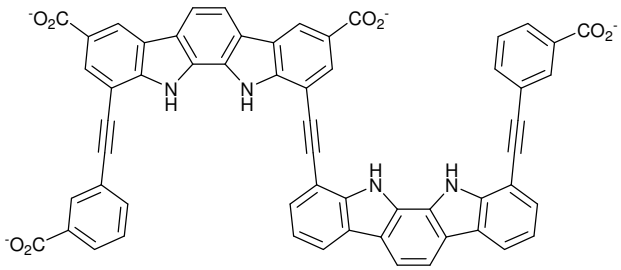

58

As final examples of acyclic receptors, compounds **59** and **60** are recently published examples of compounds with the potential to extract sulfate from solution through

crystallisation.[73] Sulfate is generally a difficult anion to bind due to its delocalised charge and low basicity. It has an important environmental impact, particularly as a component of nuclear waste. The receptors designed by Gale and co-workers are elegantly designed to provide NH hydrogen bonds from a variety of moieties such as ureas, amide and pyrrolic groups. The molecular structure of **59.**SO_4^{2-} determined by X-ray crystallography shows each SO_4^{2-} oxygen is bound by two NH hydrogen bonds, with a binding constant in DMSO/10% H_2O of > 10^4 measured by ^1H NMR spectroscopic titration (Figure 1.12). Crystallisation of **59**.SO_4^{2-} from DMSO/10% H_2O occurs in as little as twenty minutes.

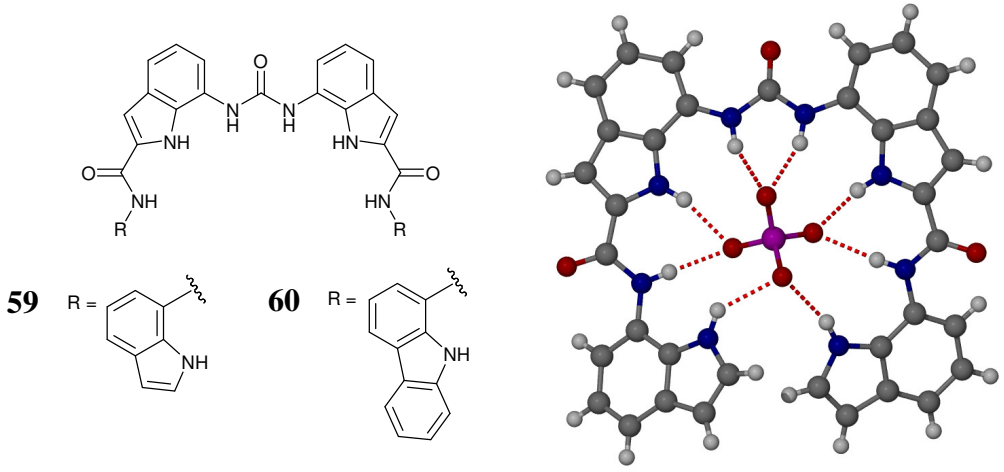

Figure 1.12 Compounds **59** and **60** and the molecular structure of **59**.SO_4^{2-} determined by X-ray diffraction[73]

1.4.3 Small Molecule Podand Anion Sensors

Small molecule anion sensors have been an active field of research for the last 20 years. Fluorescent sensors have received significant attention and have been reviewed extensively.[74-76] They offer advantages such as high sensitivity and simple instrumentation. The incorporation of a fluorophore such as the molecular clip, indolocarbazoles and indoles described previously not only provide a reporter group but can also provide a structural element to the receptor.

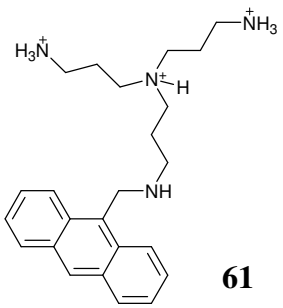

61

A luminescent sensor for anions (**61**) was synthesised by Czarnik and co-workers and is possibly the first example of its type.[77] In this system, an anthracenyl reporter and a tertiary amine receptor are linked by a methylene bridge. This sensor works via photo-induced electron transfer (PET). Under the conditions of the experiment – an aqueous solution at pH 6 – all amine groups except the benzylic amine (which is less basic) are protonated. The excitation of an electron to an excited state by a photon leaves an electron hole, into which the benzylic amine lone pair donates an electron. The excited electron cannot radiatively decay back down to the ground state, thereby giving fluorescence and must relax via a non-radiative method. The fluorescence is therefore quenched.[76] Addition of HPO_4^{2-} to **61** leads to complexation, forming three NH…O^- hydrogen bonds by the primary amines and one N…HO hydrogen bond to the benzylic hydrogen with a log K_a of 0.82. It is likely a partial or full proton transfer occurs leading to protonation of the nitrogen lone pair, preventing PET, and therefore luminescence is observed. Thermodynamically this can also be rationalised as the nitrogen lone pair energy is greater than that of the anthracenyl HOMO, therefore electron transfer is possible. The interaction with HPO_4^{2-} stabilizes the lone pair so its energy is less than the anthracenyl HOMO, therefore electron transfer is disfavoured. This effect is also given the name chelation enhanced fluorescence (CHEF).

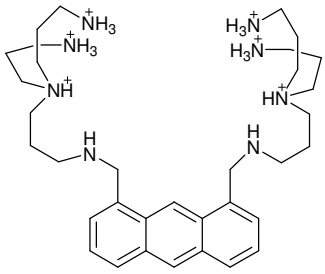

62

Citrate and sulfate can also give rise to the CHEF effect in **61**, although their binding constants are lower. Sulfate does not have any acidic hydrogens itself, but leads to water dissociation, thereby leading to amine protonation. Similarly, the receptor **62** binds pyrophosphate in an analogous way to the above, with a K_a sufficient to allow micromolar fluorescent sensing. The mechanism of sensing is again a CHEF effect, found upon pyrophosphate complexation.[78]

Gunnlaugsson and co-workers have synthesised a series of 4-amino-1,8-naphthalimide based receptors **63** and **64**.[79] These receptors are quenched by acetate, $H_2PO_4^-$ and F^- through PET with the greatest quenching observed with F^- in DMSO. Usually for 4-amino-1,8-naphthalimide receptors, PET quenching is only observed when binding

functionality is in the 4 position. However, in this instance the position of the binding groups does not affect the PET, with quenching found in both the 4-amino and the imide positions.

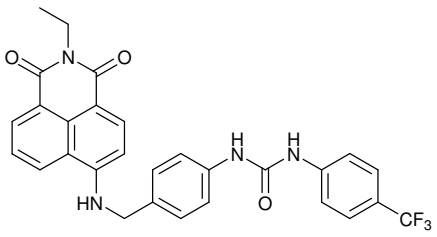

63

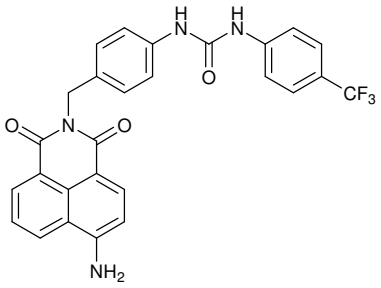

64

The Gunnlaugsson group have also synthesised the simple anion receptor **65** in which the addition of acetate, $H_2PO_4^-$ and F^- leads to fluorescence quenching by PET. Chloride however results in an increase in fluorescence emission. This was attributed to twisting of the molecule on binding chloride which reduces the efficiency of the pre-existing intramolecular PET process, hence emission is increased.[80]

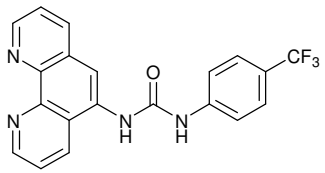

65

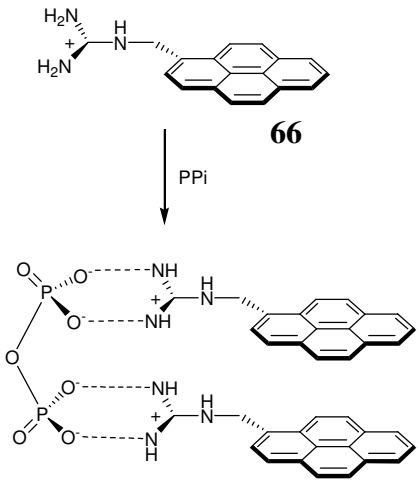

66

In addition to intramolecular excimer formation as a means of anion sensing, anion induced self-assembly systems can also be used to good effect. The pyrene functionalised guanidinium receptor **66** demonstrates a fluorescence emission at 376 nm in its monomeric state. Upon addition of pyrophosphate (PP_i), a 2:1 stoichiometry self-assembly system is formed between the receptor and pyrophosphate. A structure-less emission band at 475 nm is then

observed with quenching of the monomer emission. This is assigned to an excimer emission. Furthermore, significant excimer emission is only seen for pyrophosphate, showing good selectivity over other anions e.g. HPO_4^{2-}, $H_2PO_4^-$, Cl^- etc.[81]

Colourimetic sensors, are sensors in which binding of an anion results in a visible colour change. They are a particularly attractive form of anion sensor as qualitative results can be achieved through 'naked eye' sensing which does not require any equipment. There have been many examples of small molecule colourimetric sensors[75,82] with a selection discussed below to give a flavour of the concepts which can be used when designing receptors.

Hong and co-workers have combined two chormophores – azophenol and *p*-nitrophenyl into a receptor design, compound **67**.[83] Red-shifts were seen in the absorption bands of the receptor on addition of the highly basic anion dihydrogen phosphate in chloroform resulting in a visible colour change from light yellow to violet. Less basic anions such as Br^-, Cl^- and HSO_4^- do not cause significant colour changes, however significantly, anions of similar basicity to $H_2PO_4^-$, F^- and acetate do not cause red-shifts to the same extent due to their different binding geometries.

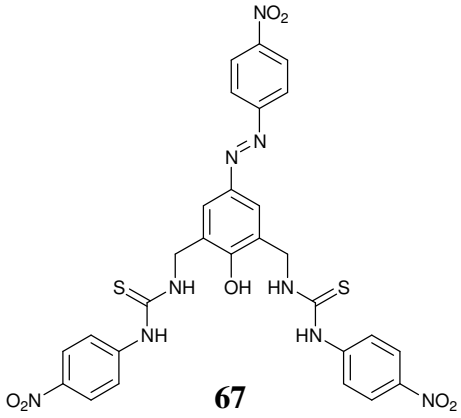

67

Gunnlaugsson and co-workers have synthesised a range of colourimetric and fluorescent anion sensors derived from a 1,8-naphthalimide chromophore.[84] For example, compound **68** proved to bind anions strongly in DMSO by UV-vis spectroscopic titrations ($H_2PO_4^-$, log β = 4.0, F^-, log β = 4.4 and acetate, log β = 4.95). A colour change from yellow to purple was observed on the addition of acetate, $H_2PO_4^-$

and F^- (Figure 1.13) due to the effect of hydrogen bonding of the anion to the thiourea group on the intramolecular charge transfer (ICT). Interestingly, this receptor is effective in aqueous solvent mixtures as well as buffered aqueous systems with similar colour changes observed.

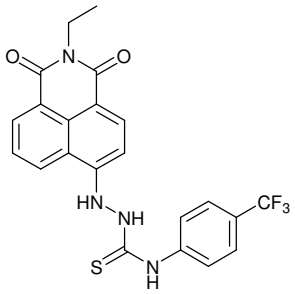

68

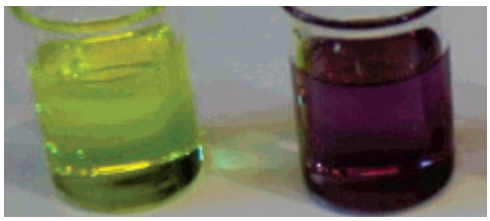

Figure 1.13 Compound **68** and **68** without acetate (left) and on the addition of acetate (right). Reproduced with permission from reference 84, 2005 © American Chemical Society

Dipyrrolyl quinoxalines (DPQ) derived receptors have been developed as colourimetric anion receptors.[85] The receptors proved effective at binding F^- (K_a = 118000 M^{-1} for F^- in $CHCl_3$ for **69**). A colour change from yellow to blue is observed on addition of F^- to the receptors in $CHCl_3$ and DMSO. It is suggested that the colour change is due to disrupting the conjugation of the molecule by puckering the pyrrole moieties on binding F^-. DPQ derivatives also have a dual function as fluorescent anion sensors with quenching of fluorescence observed with receptors **69 - 71**.

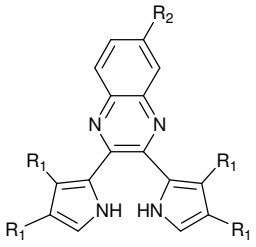

69 $R_1 = R_2 = H$
70 $R_1 = H$, $R_2 = NO_2$
71 $R_1 = F$, $R_2 = H$

Extended DPQ chromophores have been investigated by Anzenbacher and co-workers, compounds **72 - 74**.[86] The effect of using 5,8-aryl substituents on the fluorescence was two-fold with a red-shift in the emission maximum and in an increase in the quantum yield. These modifications of the DPQ design also lead to an increase in binding affinity towards anions. Fluoride is bound strongly by all hosts (e.g. **72**, K_a = 51300 M^{-1}

in acetonitrile) however, pyrophosphate was bound very strongly (K_a = 93700 M^{-1} in acetonitrile). The addition of fluoride or pyrophosphate leads to the appearance of a new absorbance band at 500 - 550 nm and a decrease in the band at 400 - 450 nm. As well as a colourimetric response, fluorescence quenching is also observed.

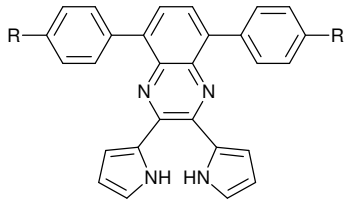

72 R = H
73 R = OMe
74 R = NMe_2

The phenomenon of urea deprotonation has been used extensively in the detection of fluoride and is one of the most common methods of producing a colourimetric sensor. The sensing of fluoride itself is a highly topical subject and has been recently reviewed.[87] The urea derivative **75** with two electron-withdrawing nitro-substituents deprotonates a single urea NH proton on the addition of fluoride leading to a colour change.[88] This deprotonation was confirmed by ^{1}H NMR and crystallographic methods. The drive for the deprotonation is ascribed to the intrinsic acidity of the urea NH, enhanced by electron withdrawing substituents and the high stability of the HF_2^- anion formed after deprotonation.

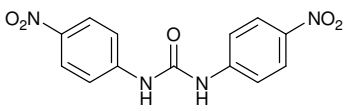

75

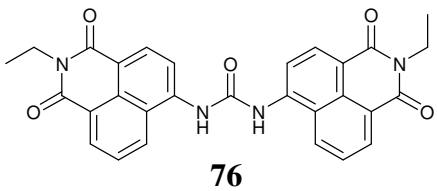

76

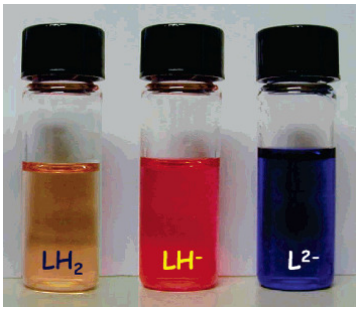

Figure 1.14 Compound **76** and **76** in presence of TBA-F (L = compound **76**)[88] Reproduced with permission from reference 88, 2005 © American Chemical Society

Fabbrizzi and co-workers have synthesised a naphthalimide substituted urea capable of double deprotonation.[88-89] The addition of TBA-F to **76** in DMSO leads to a yellow to red colour change after the addition of a few equivalents of anion and upon further addition, a second deprotonation step occurs leading to a blue colouration. This process can be monitored by UV-vis spectroscopy with the emergence of a new band at 540 nm for the single deprotonated species and a decrease in the free host band at 400 nm. With further addition of F^- a new band at 600 nm forms corresponding to the doubly deprotonated species, with a decrease in the band intensity at 540 nm (Figure 1.14). Isobestic points are observed for all new bands showing a clear transition between species. Carboxylates such as acetate also lead to a similar effect.

The use of electron withdrawing substituents on pyrrole 2,5-diamides, e.g. **77** synthesised by Gale and co-workers, also leads to deprotonation of a urea NH upon addition of F^- with a concurrent colour change from yellow to blue due to charge transfer from the deprotonated N and the nitrophenyl moiety.[90]

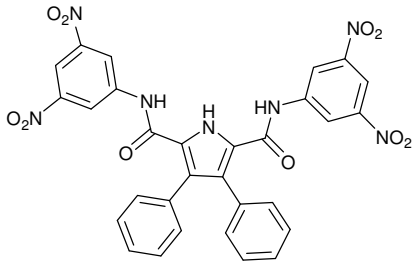

77

1.5 Metal and Lewis Acid Derived Podand Receptors

The use of metals as part of anion receptors is well established and the versatility of metal chemistry has lead to their varied used in receptor design. There are five major classes of metallic receptor:-[91]

1) a substitutionally inert metal is used in a structural role
2) a Lewis acidic metal ion forms part of the binding site
3) self-assembled complexes of substitutionally labile metals involving thermodynamic anion templation
4) anion-binding solid-state coordination polymers
5) metal based redox, colourimetic or luminescence reporter groups

There is often a large degree of overlap between classes, for example it is possible for a metal to perform both a structural role and a reporter group role in the same molecule.

1.5.1 Metals as Structural Elements

By using substitutionally inert metals such a Ru(II), as low spin d^6 metal which when bonded to hard donors results in a large crystal field stabilisation energy (CFSE), the metal can perform a structural role akin to that of the organic cholic acid or trialkylbenzene motifs.

The receptors **78 - 80** developed by Loeb and co-workers consist of a tetra-substituted Pt(II) complex.[92-94] Pyridyl amide derivatives are used as ligands to the metal and as anion binding groups. This type of receptor can exist in many conformations e.g. a cone, partial cone, 1,2-alternate and 1,3-alternate, analogous to that of calixarenes, with a 1,2-alternate conformation found in the solid state with PF_6^-.[92] The use of isoquinoline as a progression from pyridine resulted in an interesting anion selectivity. When bound to halides, complex **79** binds two anions strongly in DMSO measured using ^{1}H NMR spectroscopic titrations. A 1,3-alternate conformation is found in the solid state, with the receptor behaving in a ditopic manner. The anion is bound with NH and CH hydrogen bonds as well as an electrostatic contribution from the Pt(II). In contrast, with $H_2PO_4^-$ and SO_4^{2-}, a cone conformation is observed in the solid state with a 1:1 host:guest stoichiometry (Figure 1.15).[93]

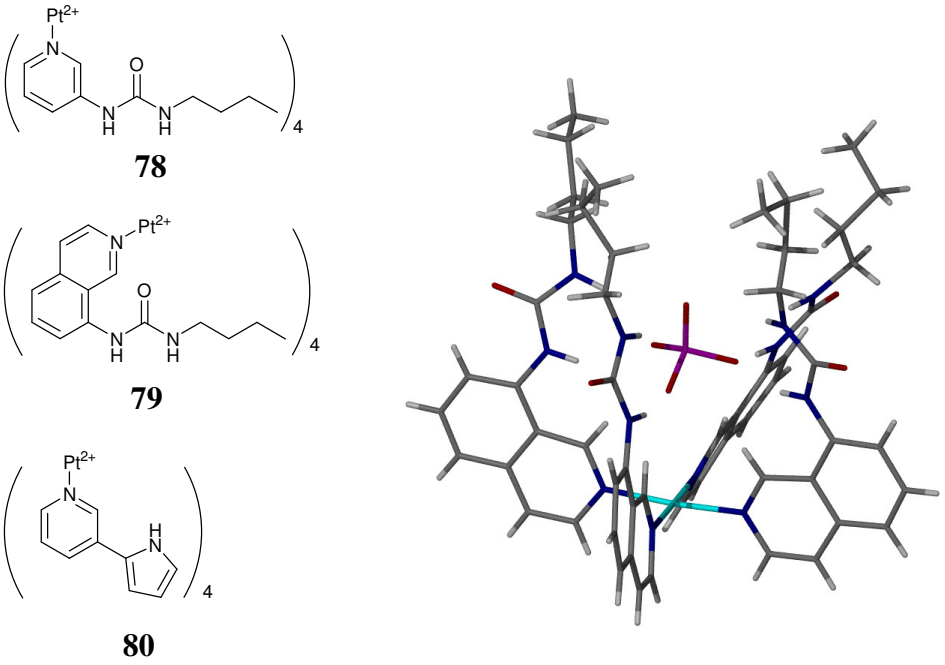

Figure 1.15 Compound **78**, **79** and **80** and the molecular stucture of **79**.SO_4^+ determined by X-ray crystallography[93]

The use of pyrrolylpyridine ligands in complex **80** allows for competition between binding groups by allowing a choice between NH or CH hydrogen bond donors. For **80** with anions such as Cl^-, HSO_4^- and NO_3^- predominant downfield shifts were observed for the CH proton in DMSO, whilst for more basic anions such as acetate, NH downfield shifts were observed with acetate binding in a 1:2 host:guest stoichiometry. Binding in nitromethane shows significant downfield shifts in the NH proton only. It is suggested that the strong hydrogen bond acceptor properties of the DMSO compete with the anion to bind with the NH, with only basic anions able to compete. The poor hydrogen bond acceptor ability of nitromethane means there is less competition and therefore the NH can interact with the anion.[94]

Steed and co-workers have synthesised a series of (arene)ruthenium(II) complexes such as complexes **81** and the analogous complex formed with the ligand **83**.[95] Receptors **81** and **82** have a low number of equivalent protons in the ^{1}H NMR spectrum suggestive of low symmetry in solution. Anions are bound strongly in acetonitrile with a 1:1 and 2:1 host:guest stoichiometry observed. Interestingly, on addition of strongly bound anions such as chloride, the methylene protons collapse into a singlet suggestive of a more

symmetric species and this is attributed to the loss of the ligated chloride to form a 16 electron species which would provide the required symmetry.

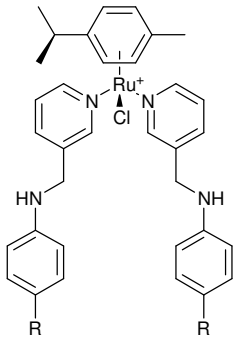

81 R = H
82 R = NO_2

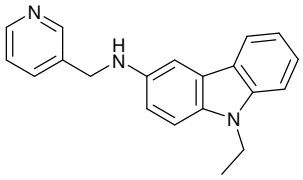

83

By including a carbazole fluorophore, as in the complex derived from ligand **83,** a fluorescent sensor can be created, whereby the binding of chloride results in charge transfer from the chloride to a Ru-pyridyl centred orbital which quenches the fluorescence emission.

Complexes **81 - 83** are on the border line of substitutionally stable and labile complexes with prolonged exposure to high equivalents of chloride leading to the displacement of a ligand and direct Ru-Cl complexation. This is on the timescale of hours to days and the ligand exchange is slow on an experimental timescale.

Gale and co-workers have designed receptor **84** which is an interesting example of tuning preorganisation, with Pt forming an integral structural role in preorganising the receptor. Receptor **84** binds anions weakly in a DMSO-d_6 - 0.5% water solution with $H_2PO_4^-$ having an affinity constant of 90 M^{-1} due to flexibility around the aryl-aryl bond of the bipyridine. However, when receptor **84** is reacted with $PtCl_2(DMSO)_2$, to form the Pt complex, **85**, the $H_2PO_4^-$ binding constant is increased to 3644 M^{-1} as the binding groups are forced into a *syn* arrangement forming a preorganised, convergent binding cavity. The receptor also proved effective as a colourimetric sensor for F^-, through deprotonation of a urea NH group. A colour change from yellow to purple is observed after deprotonation.[96]

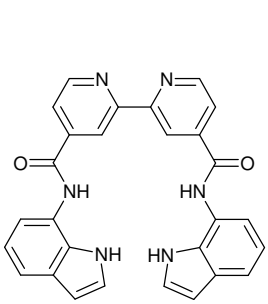

84

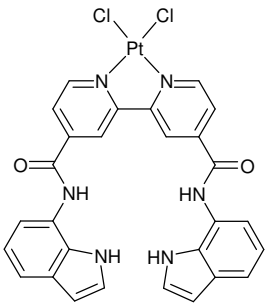

85

Beer and co-workers have developed $Ru(Bpy)_3^{2+}$ derivatives which are intrinsically chiral due to the helicity of the $Ru(Bpy)_3^{2+}$ but can also allow the incorporation of additional chiral functionality, for example **86** and **87**.[97] Each receptor was isolated in an enantiomerically pure form and binds chiral anions such as *N*-Cbz-Glu and lactate in DMSO determined via ^{1}H NMR spectroscopic titrations. However in all cases enatiomeric selectivity could not be achieved or was low.

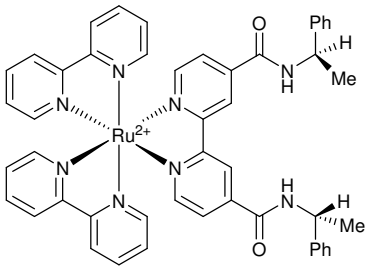

86

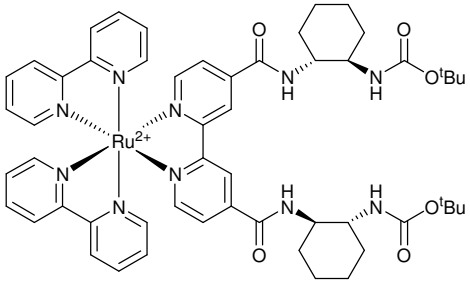

87

Stable transition metal pyrazole complexes using Mn (**88**), Re (**89**) and Mo (**90**) have been synthesised by Pérez and co-workers.[98-100] To create a convergent binding cavity, the metal fragment was functionalised with CO groups which prefer to adopt a *fac* arrangement of the CO groups to maximise back bonding. The rhenium complex proved to be substitutionally inert due to its d^6 configuration, however a pyrazole ligand was displaced from the Mn and Mo complexes in the presence of anions. Hydrogen bond formation between anions and the NH groups of the pyrazole is observed by ^{1}H NMR spectroscopic titrations as well as in the solid state. The solid state structures reveal an unfavourable deformation in the N-Re-N bond angles of **89** when binding anions when compared to the tetrahedral B and Zn derivatives. Interestingly, HSO_4^-

leads to protonation of the pyrazole unit and binding of a sulfate anion. Fluoride on the other hand, deprotonates a pyrazole NH groups.

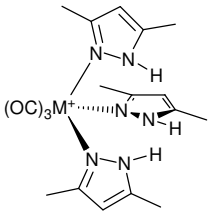

88 M = Mn
89 M = Re

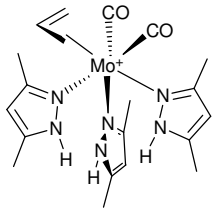

90

The Pérez group have also synthesised a range of d^6 transition metal derived anion receptors based on rhenium and ruthenium, for example complexes **91**[101] and **92**[102]. Compound **91** contains a bidentate pyrazoylamidino ligand which provides one NH hydrogen bond donor and an additional pyrazolyl NH donor. The complex binds chloride particularly strongly due to its rigid nature with a binding constant of 8725 M^{-1} in CD_3CN measured by ^1H NMR spectroscopic titrations.

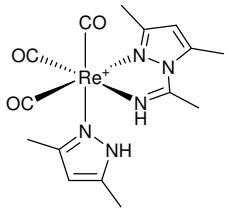

91

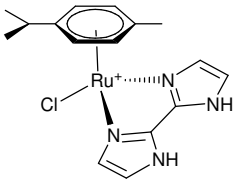

92

Receptor **92** utilised biimidazole as the anion binding groups. In this system the metal centre effectively preorganises the biimidazole to bind anions by preventing rotation around the aryl-aryl bond and by also preventing self-association (Figure 1.16). The receptor binds anions strongly in CD_3CN, for example K_a = 5920 M^{-1} for HSO_4^-.

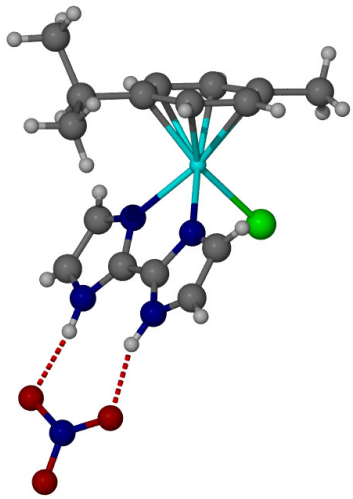

Figure 1.16 Molecular structure of **92**.NO_3^- determined by X-ray diffraction[102]

1.5.2 Labile Metal Derived Anion Receptors

The use of labile metal atoms, that is those in which ligand association and disassociation is fast on an experimental timescale, have also been investigated, where the receptor-anion complex is essentially self-assembled in solution as the thermodynamic product.

Halcrow has designed a receptor involving the d^{10} Zn^{2+} metal and a pyrazole derivative (**93**).[103] This receptor is analogous to the systems by Pérez described previously however the lability of these ligands with the Zn(II) metal means the complex, whilst being thermodynamically stable, is not kinetically stable in solution. The solid state structure shows the assembled complex with a tetrahedral Zn^{2+} and three 3{5}*t*-butylpyrazole groups (Figure 1.17). The pyrazole derivative hydrogen bonds to the chloride of an adjacent complex in the crystal, forming a hydrogen bonding polymer. Stable complexes of this type utilising covalent bonding can be synthesised using a triprotonated trispyrazolyborate dication and has been shown to bind chloride in the solid state.[104]

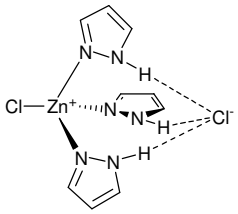

93

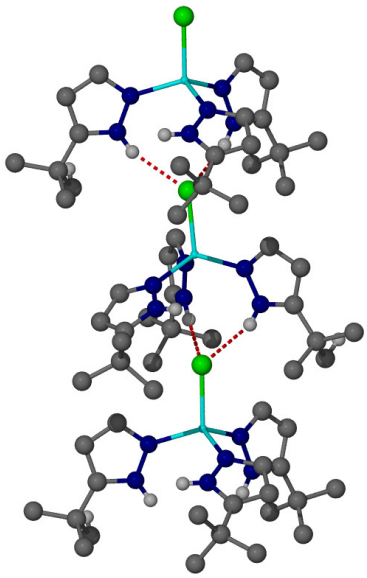

Figure 1.17 Compound **93** and the crystal structure of **93** determined by X-ray diffraction[103]

Metal complexes of pyridylurea ligands and silver salts have been investigated by Steed and co-workers.[105] In this work the ligand self-assembles with a Ag^+ cation to form an $[Ag(\mathbf{94})_2]^+$ species. This is able to bind anions such as nitrate strongly in a 1:1 and 1:2 host:guest stoichiometry, measured by ^{1}H NMR spectroscopic titration (K_{11} = 30200 M^{-1}, K_{12} = 2900 M^{-1} in CD_3CN), as well as a 1:3 stoichiometry due to ligation of nitrate to the silver centre (K_{13} = 550 M^{-1}). A solid state structure of the $[Ag(\mathbf{94})_2(NO_3)]$ was determined by X-ray crystallography and is shown in Figure 1.18. The structure shows a convergent binding site with the nitrate bound by NH and CH hydrogen bonds.

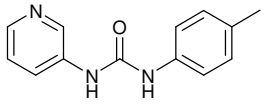

94

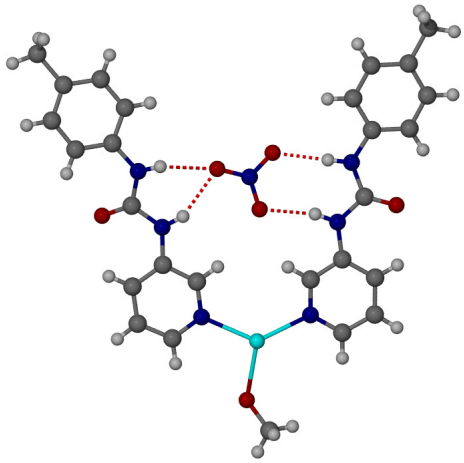

Figure 1.18 Compound **94** and molecular structure of $[Ag(\mathbf{94})_2(NO_3)(OMe)]$ complex. Only one complex in the asymmetric unit is shown for clarity[105]

1.5.3 Lewis Acid Metal Based Receptors

Metals which act as Lewis acids can increase the effectiveness of a receptor by directly interacting with an anion, polarising a hydrogen bond donor - hence increasing its acidity, providing a structural element, or more usually a combination of both.

Schiff bases are an important class of receptor design when coordinating metals. In the case of **95** the dicationic metal atom performs a structural and polarising rather than direct Lewis acid coordination to the anion. The uncomplexed ligand is able to extract $CuSO_4$ into organic solvent with 100% efficiency.[106]

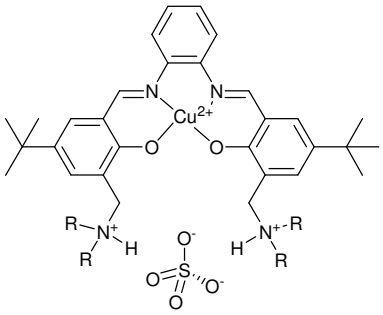

95

Rudkevich and co-workers have synthesised a range of anion receptors containing a uranyl fragment as a Lewis acid centre. Compounds such as **96** bind anions strongly, particularly $H_2PO_4^-$ measured via a conductance method ($K_a > 10^5\ M^{-1}$ in MeCN:DMSO *v/v* 99:1) and a selectivity over Cl^- of 10^2. The molecular structure of **96**.$2H_2PO_4^-$ shows bond formation between the dihydrogen phosphate O and the UO_2 centre, i.e. a Lewis acid interaction. ^{1}H NMR spectroscopic titrations and the molecular structure also confirm hydrogen bond formation between the amide functionality and the anion.[107]

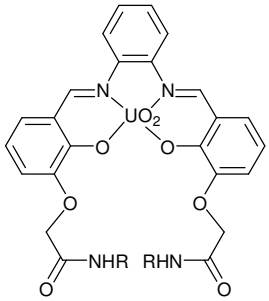

96 R = 4-MeC_6H_4

Receptor **97** is capable of self organising in the presence of NaX (where X is a halide) into dimeric structure held together by Lewis acid interactions between two crown ether moieties and the Na^+. This allows a binding cleft to be formed between the urea groups which is able to bind anions, for example chloride as shown in the crystal structure determined by X-ray crystallography (Figure 1.19).[108]

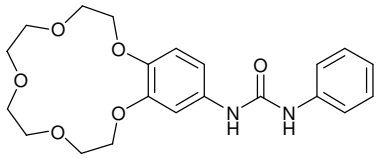

97

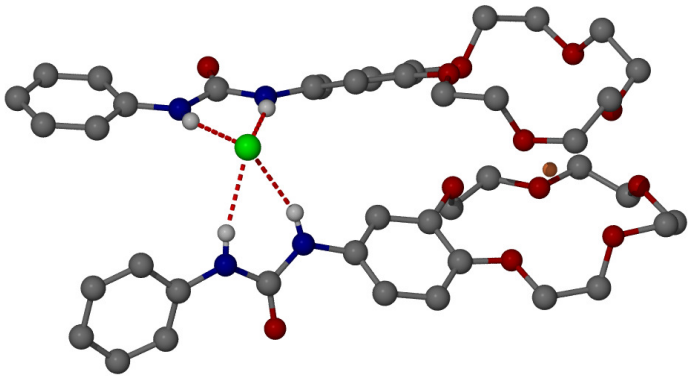

Figure 1.19 Compound **97** and the crystal structure of the **97**.NaCl complex, determined by X-ray crystallography[108]

Receptors **98** and **99** were developed by Ansyln and co-workers and rely on a tetrahedral Cu(II) cation to structurally hold the receptor into a convergent binding cavity.[109] Ammonium or guanidinium groups provide hydrogen bond donors to bind anions. Very strong binding is seen in a highly competitive aqueous environment at neutral pH. For example **98** binds hydrogen phosphate with a K_a of 2.5 x 10^4 M^{-1} in water, whilst **99** binds with a K_a of 1.5 x 10^4 M^{-1} in water measured by UV-vis spectroscopic titration. Interestingly despite the similarities in design, the thermodynamic driving force in binding anions for compound **98** is entropic due to desolvation upon binding. Binding to compound **99** is enthalpy driven and is due to the lower solvation of guanidinium groups compared to ammonium derivatives and the lower enthalpy of solvation of the guanidinium group.

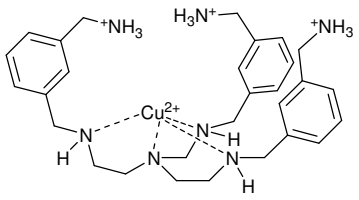

98

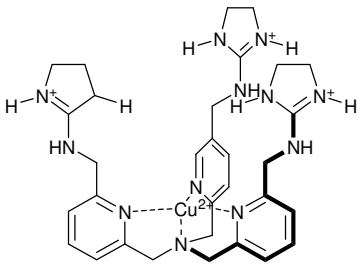

99

1.5.4 Metals as Sensing Units

Electrochemical based anion receptors have been a versatile means of sensing since the pioneering work of Beer and co-workers in the late 1980s, principally using cyclic voltammetry. A range of redox active moieties have been incorporated into these receptors including cobaltocenium, ferrocene and $Ru(bpy)_3^{2+}$ derivatives.

Beer and co-workers have also described five mechanisms of sensing using redox groups:-[110]

1. A through space interacting with the anion binding site in close proximity to the redox centre
2. Direct coordination of the anion to the redox centre
3. A through bond interaction through conjugation between binding site and redox centre
4. An anion-induced conformational change which leads to a perturbation in the redox centre
5. An interference mechanism whereby the interaction between several redox active centres is affected by anion binding

Beer and co-workers have synthesised a large library of electrochemical sensors.[110] The first cobaltocenium sensor devised was compound **100** and its binding properties were investigated using Br^-.[111] Binding is via electrostatic interactions and the cobaltocenium Cp_2Co^+/Cp_2Co redox couple displays a cathodic shift i.e. the anion increases the cobaltocenium reduction potential.

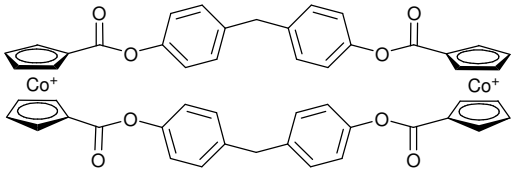

100

It is also possible to add hydrogen bonding functionality to this class of sensors, for example **101**[112] and **102**[113-114] ^{1}H NMR titrations of compounds **101** and **102** reveal the highest binding affinity of $H_2PO_4^-$. As would be expected, the formation of macrocyclic systems analogous to **101** increases the binding constants significantly, with a ten-fold increase.

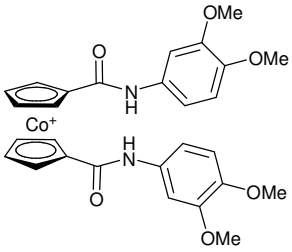

101

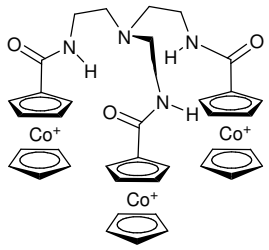

102

Calixarene-cobaltocene sensors have also been developed e.g. compounds **103 - 106**.[115-116] An interesting aspect of these sensors is that varying the topology of the receptor allows for the selective sensing of a specific anion. For example, the topology of **103** favours Cl^- determined via NMR spectroscopic titrations. Further functionalisation of the lower rim with tosylate allows tuning of the binding properties. For example, when the tosyl groups are *para* to the cobaltocenium (**104**), $H_2PO_4^-$ binding was favoured due to the tosyl groups forcing the cobaltocenium groups together. However, when *ortho*, **105**, the tosyl groups force the cobaltocenium groups slightly apart, favouring Cl^-. Finally, compound **106** is preorganised for carboxylate binding, due to the bridging cobaltocenium orientating the amide groups for carboxylate hydrogen bond formation.

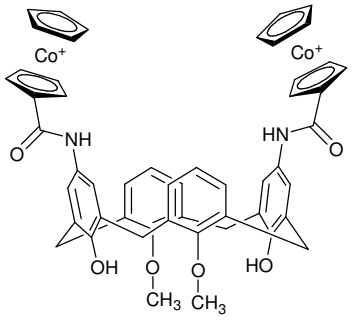

103

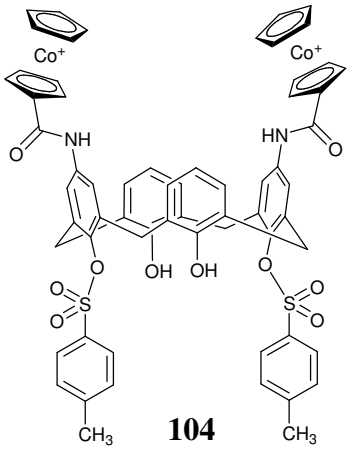

104

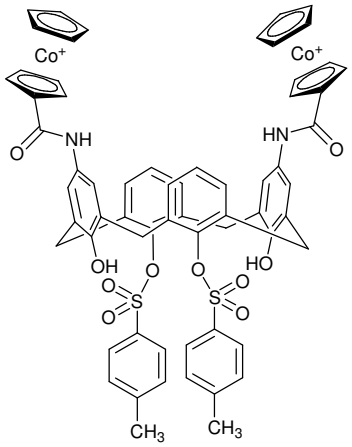

105

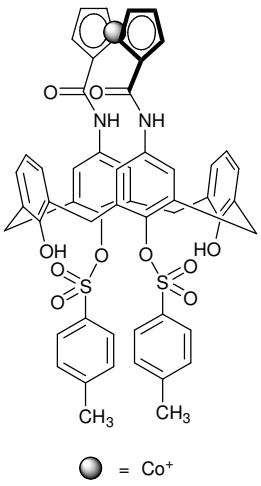

106

Ferrocene derivatives have also been studied for electrochemical sensing. However, as the sensor is neutral there is no intrinsic electrostatic interaction, unless the ferrocene is oxidized to ferrocenium, in which case the receptor becomes cationic and binding is increased.[1]

Receptors **107 - 108** contain a mixture of hydrogen bond acceptor and donor groups.[117] These receptors are able to selectively bind dihydrogen phosphate in acetonitrile due to its binding group complementarity and high basicity. Large cathodic shifts in the redox potential were observed in the presence of excess $H_2PO_4^-$ (**107**, 120 mV, **108**, 240 mV in acetonitrile), although **108** exhibits irreversible oxidation. Receptor **107** was able to sense $H_2PO_4^-$ even in the presence of competing anions such as Cl^- and HSO_4^-. Tripodal and calixarene derivatives have been synthesised. All display large cathodic shifts in the redox potentials.

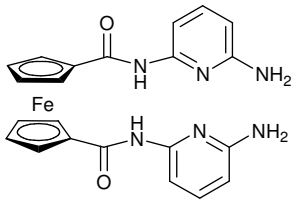

107

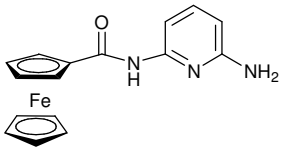

108

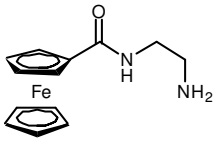

109

The receptor **109** is interesting as it is difunctional.[117] Typically in neutral hydrogen bonding receptors, $H_2PO_4^-$ binds more strongly than HSO_4^- as its higher basicity forms stronger hydrogen bonds. In this receptor however, two binding modes are possible; the first operates for non-acidic guests and the receptors act as the hydrogen bond donor from the amide. The second mode applies to acidic guests in which proton transfer occurs, allowing electrostatic and hydrogen bonding interactions with the guest. In the case of $H_2PO_4^-$ it does not fit well into either category and therefore is not bound strongly. HSO_4^- however, fits well into the second binding mode and is bound strongly, giving rise to this unusual selectivity. The electrochemical behaviour of the receptor on addition of HSO_4^- showed a new oxidation peak, cathodically shifted by 220 mV from the free receptor, showing anion binding greatly increases the ease of oxidation, although the receptor showed irreversible behaviour.

Gale and co-workers have appended the ferrocene moiety on to the 2,5-diamidopyrrole core described previously.[118] Receptor **110** showed a large cathodic shift in the redox potential of -130 mV with F^- in dichloromethane. This compares to only -75 mV for chloride and this selectivity corresponds well with binding constants measured by NMR techniques (K_a = 170 M^{-1} for F^- and < 20 for Cl^- in dichloromethane).

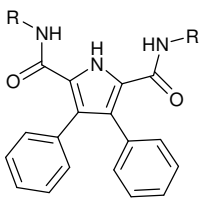

110

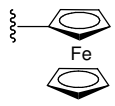

111

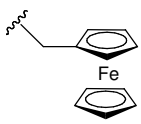

Receptor **111** also shows cathodic shifts in the redox potential, however upon the addition of F^- two redox waves are observed (ΔE = -125 and -255 mV in

dichloromethane) and is only observed with F^-. As with **110**, chloride shows a lower cathodic shift of -55 mV corresponding well with the binding affinity measured by NMR.

As well as iron and cobalt based receptors, ruthenium can also be used. This has the advantage of being both redox active and luminescent. A wide range of receptor designs have been synthesised, for example compounds **112 - 114**.[119] The molecular structure of **112** showing the bound Cl^- anion is shown in Figure 1.20 and shows two NH amide hydrogen bonds to the anion. All receptors show significant downfield shifts of NH resonance in the NMR spectrum on addition of anions with chloride binding constants in the region of 10^2 M^{-1} and $H_2PO_4^-$ in the region of 10^3 M^{-1} in DMSO.

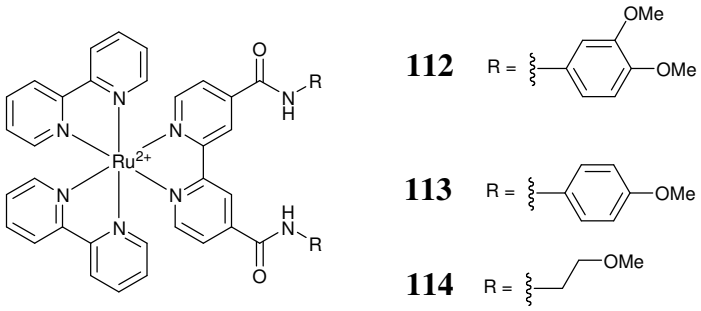

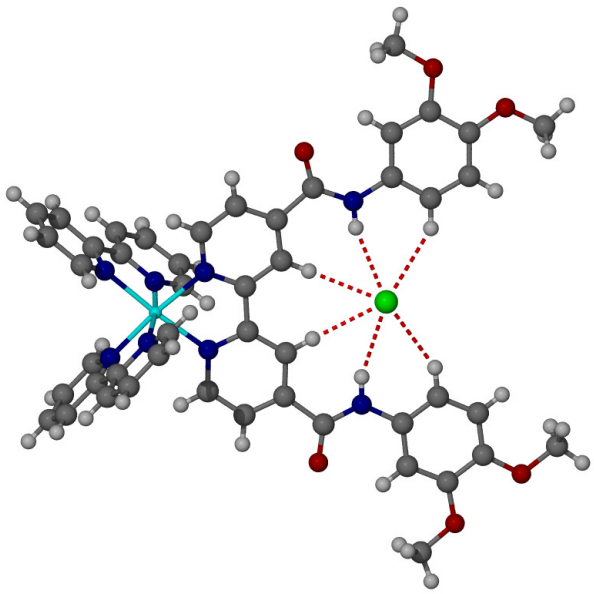

Figure 1.20 Molecular structure of **112**.Cl^- determined by X-ray diffraction[119]

It is also possible to incorporate other binding motifs such as imidazole groups in receptor **115**.[120] Neutral and anionic phosphodiesters are bound by the receptor with an increase in emission intensity observed.

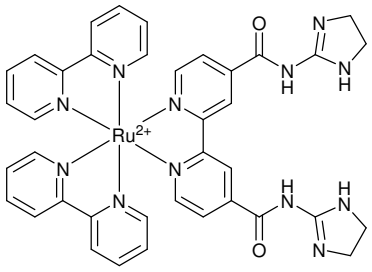

115

In addition to transition metal based receptors, lanthanides have been used as a means to sense anions by Parker and co-workers.[121] In these systems the anion directly coordinates to the metal, displacing existing ligands and changes the environment of the lanthanide. This is modulated as a change in the emission spectrum of the receptor. These receptors can be ratiometric in that there is an increase in the intensity of one band at the expense of another. This is an advantage as it means the sensor can work without knowing the absolute concentration of the host in solution. Receptors **116**[122] and **117**[123] were able to bind and sense a range of biologically important anions such as citrate, lactate and HCO_3^- under physiological conditions with citrate being bound particularly strongly.

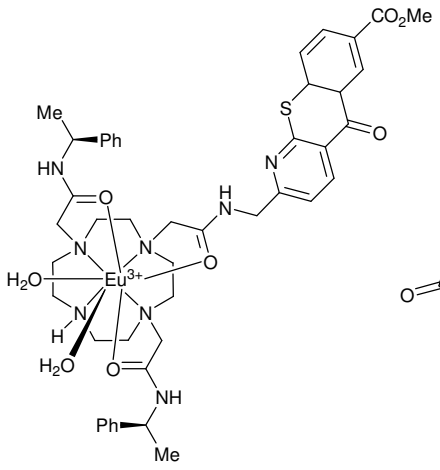

116

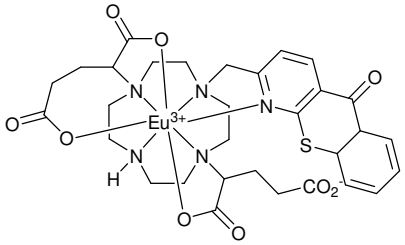

117

Receptor **116** has proved highly effective at binding citrate in biological fluid such as prostate fluid with high affinity (log K_a = 4.98 in saline solution).[123] Citrate levels in prostate fluid have been shown to be a reliable marker for prostate cancer. The system was able to accurately determine the citrate concentration in prostate fluid samples compared with the currently used enzyme based method, whilst proving to be experimentally simpler and quicker and may prove useful in the diagnosis of prostate cancer.

In conclusion, the field of anion binding podands has developed rapidly over the last twenty years, with the adaptability in design meaning receptors can be rigidly preorganised or flexible allowing induced-fit binding, or tuned for properties in between. Podands have also proved highly effective as molecular sensors with fluorescent, colourimetric and electrochemical sensors all being realised with many different sensing modes observed within each category, intimately linked to the receptor design. Many of these receptors also function in water with real world applications, for example prostate cancer diagnosis with increasing examples as the field matures.

1.6 Project Aims

The aim of this project is to synthesise anion receptors and sensors, with the focus on induced-fit binding and fluorimetric detection.

The initial focus will be on the use of the triethylbenzene motif to provide induced-fit recognition, including the use of the viologen motif, building on a promising preliminary study conducted by the Steed Group. However other induced-fit motifs will also be explored, such as molecular clip receptors with restricted conformational freedom, in the form of diphenylacetylene derivatives. New synthetic routes to the receptors will also be explored, such as mechanochemical synthesis.

All receptors will be fully characterised and their binding properties will be investigated using ^{1}H NMR spectroscopic titrations and where appropriate, UV-vis, fluorescent spectroscopic titrations and electrochemical titrations. When possible investigations will include the receptors' binding properties in competitive solvents, and possible

applications will be investigated. The results of the study will further the development of chemical sensors.

1.7 References

1. J. L. Sessler, P. A. Gale and W.-S. Cho, '*Anion Receptor Chemistry*', Royal Society of Chemistry, Cambridge, 2006.
2. J. W. Steed and J. L. Atwood, '*Supramolecular Chemistry*', J. Wiley & Sons, Chichester, 2009.
3. P. A. Gale, *Coord. Chem. Rev.*, 2006, **250**, 2917 preface to the special issue and subsequent reviews.
4. P. A. Gale, *Coord. Chem. Rev.*, 2003, **240**, 1.
5. E. Weber, in '*Encyclopedia of Supramolecular Chemistry*', eds. J. W. Steed and J. L. Atwood, Marcel Dekker, New York, 2004, pp. 1106.
6. S. O. Kang, R. A. Begum and K. Bowman-James, *Angew. Chem., Int. Ed.*, 2006, **45**, 7882.
7. J. L. Sessler, S. Camiolo and P. A. Gale, *Coord. Chem. Rev.*, 2003, **240**, 17.
8. P. A. Gale, *Chem. Commun.*, 2008, 4525.
9. M. D. Best, S. L. Tobey and E. V. Anslyn, *Coord. Chem. Rev.*, 2003, **240**, 3.
10. P. Blondeau, M. Segura, R. Perez-Fernandez and J. de Mendoza, *Chem. Soc. Rev.*, 2007, **36**, 198.
11. J. Yoon, S. K. Kim, N. J. Singh and K. S. Kim, *Chem. Soc. Rev.*, 2006, **35**, 355.
12. H.-J. Schneider and A. K. Yatsimirsky, *Chem. Soc. Rev.*, 2008, **37**, 263.
13. F. Vogtle and E. Weber, *Angew. Chem., Int. Ed.*, 1979, **18**, 753.
14. A. P. Davis and J. B. Joos, *Coord. Chem. Rev.*, 2003, **240**, 143.
15. A. P. Davis, *Coord. Chem. Rev.*, 2006, **250**, 2939.
16. A. P. Davis, J. J. Perry and R. P. Williams, *J. Am. Chem. Soc.*, 1997, **119**, 1793.
17. A. J. Ayling, S. Broderick, J. P. Clare, A. P. Davis, M. N. Perez-Payan, M. Lahtinen, M. J. Nissinen and K. Rissanen, *Chem.-Eur. J.*, 2002, **8**, 2197.
18. A. J. Ayling, M. N. Perez-Payan and A. P. Davis, *J. Am. Chem. Soc.*, 2001, **123**, 12716.
19. M. Chahar, S. Upreti and P. S. Pandey, *Tetrahedron*, 2007, **63**, 171.
20. A. Kumar and P. S. Pandey, *Org. Lett.*, 2008, **10**, 165.
21. A. P. Davis, D. N. Sheppard and B. D. Smith, *Chem. Soc. Rev.*, 2007, **36**, 348.
22. B. A. McNally, A. V. Koulov, B. D. Smith, J. B. Joos and A. P. Davis, *Chem. Commun.*, 2005, 1087.
23. A. P. Davis and L. J. Lawless, *Chem. Commun.*, 1999, 9.
24. L. J. Lawless, A. G. Blackburn, A. J. Ayling, M. N. Perez-Payan and A. P. Davis, *J. Chem. Soc.-Perkin Trans. 1*, 2001, 1329.
25. A. L. Sisson, J. P. Clare, L. H. Taylor, J. P. H. Charmant and A. P. Davis, *Chem. Commun.*, 2003, 2246.
26. M. Segura, V. Alcazar, P. Prados and J. de Mendoza, *Tetrahedron*, 1997, **53**, 13119.
27. V. Janout, B. W. Jing, I. V. Staina and S. L. Regen, *J. Am. Chem. Soc.*, 2003, **125**, 4436.

28. L. Fang, W. H. Chan, Y. B. He, D. W. J. Kwong and A. W. M. Lee, *J. Org. Chem.*, 2005, **70**, 7640.
29. S. Y. Liu, L. Fang, Y. B. He, W. H. Chan, K. T. Yeung, Y. K. Cheng and R. H. Yang, *Org. Lett.*, 2005, **7**, 5825.
30. A. Goodey, J. J. Lavigne, S. M. Savoy, M. D. Rodriguez, T. Curey, A. Tsao, G. Simmons, J. Wright, S. J. Yoo, Y. Sohn, E. V. Anslyn, J. B. Shear, D. P. Neikirk and J. T. McDevitt, *J. Am. Chem. Soc.*, 2001, **123**, 2559.
31. S. C. McCleskey, M. J. Griffin, S. E. Schneider, J. T. McDevitt and E. V. Anslyn, *J. Am. Chem. Soc.*, 2003, **125**, 1114.
32. F. P. Schmidtchen, *Coord. Chem. Rev.*, 2006, **250**, 2918.
33. A. Metzger, V. M. Lynch and E. V. Anslyn, *Angew. Chem., Int. Ed.*, 1997, **36**, 862.
34. D. J. Iverson, G. Hunter, J. F. Blount, J. R. Damewood and K. Mislow, *J. Am. Chem. Soc.*, 1981, **103**, 6073.
35. K. J. Wallace, W. J. Belcher, D. R. Turner, K. F. Syed and J. W. Steed, *J. Am. Chem. Soc.*, 2003, **125**, 9699.
36. S. L. Wiskur, H. Ait-Haddou, J. J. Lavigne and E. V. Anslyn, *Acc. Chem. Res.*, 2001, **34**, 963.
37. A. Metzger and E. V. Anslyn, *Angew. Chem., Int. Ed.*, 1998, **37**, 649.
38. S. L. Wiskur and E. V. Anslyn, *J. Am. Chem. Soc.*, 2001, **123**, 10109.
39. J. J. Lavigne and E. V. Anslyn, *Angew. Chem., Int. Ed.*, 1999, **38**, 3666.
40. L. A. Cabell, M. K. Monahan and E. V. Anslyn, *Tetrahedron Lett.*, 1999, **40**, 7753
41. K. Niikura, A. Metzger and E. V. Anslyn, *J. Am. Chem. Soc.*, 1998, **120**, 8533.
42. K. H. Choi and A. D. Hamilton, *J. Am. Chem. Soc.*, 2003, **125**, 10241.
43. V. Amendola, M. Boiocchi, L. Fabbrizzi and A. Palchetti, *Chem.-Eur. J.*, 2005, **11**, 5648.
44. A. Abate, E. Cariati, A. Forni, X. Xiaogian, S. Righetto, P. Metrangolo, T. Pilati, G. Resnati and G. Terraneo, *Angew. Chem., Int. Ed.*, 2010, *in press*.
45. M. G. Sarwar, B. Dragisic, S. Sagoo and M. S. Taylor, *Angew. Chem., Int. Ed.*, 2010, **49**, 1674.
46. P. J. Garratt, A. J. Ibbett, J. E. Ledbury, R. O'Brien, M. B. Hursthouse and K. M. A. Malik, *Tetrahedron*, 1998, **54**, 949.
47. C. Schmuck and M. Schwegmann, *J. Am. Chem. Soc.*, 2005, **127**, 3373.
48. H. Ihm, S. Yun, H. G. Kim, J. K. Kim and K. S. Kim, *Org. Lett.*, 2002, **4**, 2897.
49. Y. Bai, B. G. Zhang, J. Xu, C. Y. Duan, D. B. Dang, D. J. Liu and Q. J. Meng, *New J. Chem.*, 2005, **29**, 777.
50. Y. Bai, B.-G. Zhang, C. Y. Duan, D.-B. Dang and Q.-J. Meng, *New. J. Chem.*, 2006, **30**, 266.
51. S. K. Kim, J. H. Bok, R. A. Bartsch, J. Y. Lee and J. S. Kim, *Org. Lett.*, 2005, **7**, 4839.
52. M. H. Filby, S. J. Dickson, N. Zaccheroni, L. Prodi, S. Bonacchi, M. Montalti, C. Chiorboli, M. J. Paterson, T. D. Humphries and J. W. Steed, *J. Am. Chem. Soc.*, 2008, **130**, 4105.
53. C. W. Chen and H. W. Whitlock, *J. Am. Chem. Soc.*, 1978, **100**, 4921.
54. S. C. Zimmerman, *Top. Curr. Chem.*, 1993, **165**, 71.
55. J. Rebek, *Angew. Chem., Int. Ed.*, 1990, **29**, 245.
56. M. Hamata, *Acc. Chem. Res.*, 2004, **37**, 862.

57. D. H. Lee, J. H. Im, J. H. Lee and J. I. Hong, *Tetrahedron Lett.*, 2002, **43**, 9637.
58. S. Kondo and M. Sato, *Tetrahedron*, 2006, **62**, 4844.
59. Z. H. Lin, L. X. Xie, Y. G. Zhao, C. Y. Duan and J. P. Qu, *Org. Biomol. Chem.*, 2007, **5**, 3535.
60. A. Furstner, *Angew. Chem., Int. Ed.*, 2003, **42**, 3582.
61. J. L. Sessler, L. R. Eller, W. S. Cho, S. Nicolaou, A. Aguilar, J. T. Lee, V. M. Lynch and D. J. Magda, *Angew. Chem., Int. Ed.*, 2005, **44**, 5989.
62. W. S. Cho, J. L. Sessler, L. R. Eller, G. D. Pantos and B. R. Peterson, *Abstr. Pap. Am. Chem. Soc.*, 2003, **225**, 486.
63. P. A. Gale, M. E. Light, B. McNally, K. Navakhun, K. E. Sliwinski and B. D. Smith, *Chem. Commun.*, 2005, 3773.
64. K. Kavallieratos, S. R. deGala, D. J. Austin and R. H. Crabtree, *J. Am. Chem. Soc.*, 1997, **119**, 2325.
65. K. Kavallieratos, C. M. Bertao and R. H. Crabtree, *J. Org. Chem.*, 1999, **64**, 1675.
66. M. P. Hughes and B. D. Smith, *J. Org. Chem.*, 1997, **62**, 4492.
67. P. A. Gale, *Acc. Chem. Res.*, 2006, **39**, 465.
68. G. W. Bates, P. A. Gale and M. E. Light, *Chem. Commun.*, 2007, 2121.
69. S. Camiolo, P. A. Gale, M. B. Hursthouse and M. E. Light, *Tetrahedron Lett.*, 2002, **43**, 6995.
70. S. J. Brooks, P. R. Edwards, P. A. Gale and M. E. Light, *New J. Chem.*, 2006, **30**, 65.
71. D. Curiel, A. Cowley and P. D. Beer, *Chem. Commun.*, 2005, 236.
72. J. M. Suk and K. S. Jeong, *J. Am. Chem. Soc.*, 2008, **130**, 11868.
73. P. A. Gale, J. R. Hiscock, C. Z. Jie, M. B. Hursthouse and M. E. Light, *Chem. Sci.*, 2010, 215
74. A. P. de Silva, D. B. Fox, T. S. Moody and S. M. Weir, *Pure Appl. Chem.*, 2001, **73**, 503.
75. R. Martinez-Manez and F. Sancenon, *Chem. Rev.*, 2003, **103**, 4419.
76. L. Fabbrizzi, M. Licchelli, G. Rabaioli and A. Taglietti, *Coord. Chem. Rev.*, 2000, **205**, 85.
77. M. E. Huston, E. U. Akkaya and A. W. Czarnik, *J. Am. Chem. Soc.*, 1989, **111**, 8735.
78. D. H. Vance and A. W. Czarnik, *J. Am. Chem. Soc.*, 1994, **116**, 9397.
79. E. B. Veale, G. M. Tocci, F. M. Pfeffer, P. E. Kruger and T. Gunnlaugsson, *Org. Biomol. Chem.*, 2009, **7**, 3447.
80. C. M. G. Dos Santos, T. McCabe and T. Gunnlaugsson, *Tetrahedron Lett.*, 2007, **48**, 3135.
81. S. Nishizawa, Y. Kato and N. Teramae, *J. Am. Chem. Soc.*, 1999, **121**, 9463.
82. T. Gunnlaugsson, M. Glynn, G. M. Tocci, P. E. Kruger and F. M. Pfeffer, *Coord. Chem. Rev.*, 2006, **250**, 3094.
83. D. H. Lee, H. Y. Lee, K. H. Lee and J.-I. Hong, *Chem. Commun.*, 2001, 1188.
84. T. Gunnlaugsson, P. E. Kruger, P. Jensen, J. Tierney, H. D. P. Ali and G. M. Hussey, *J. Org. Chem.*, 2005, **70**, 10875.
85. C. B. Black, B. Andrioletti, A. C. Try, C. Ruiperez and J. L. Sessler, *J. Am. Chem. Soc.*, 1999, **121**, 10438.
86. D. Aldakov and P. Anzenbacher, *Chem. Commun.*, 2003, 1394.
87. M. Cametti and K. Rissanen, *Chem. Commun.*, 2009, 2809.
88. D. Esteban-Gomez, L. Fabbrizzi and M. Liechelli, *J. Org. Chem.*, 2005, **70**, 5717.

89. D. Esteban-Gomez, L. Fabbrizzi, M. Licchelli and D. Sacchi, *J. Mater. Chem.*, 2005, **15**, 2670.
90. S. Camiolo, P. A. Gale, M. B. Hursthouse and M. E. Light, *Org. Biomol. Chem.*, 2003, **1**, 741.
91. J. W. Steed, *Chem. Soc. Rev.*, 2009, **38**, 506.
92. C. R. Bondy, P. A. Gale and S. J. Loeb, *Chem. Commun.*, 2001, 729.
93. C. R. Bondy, P. A. Gale and S. J. Loeb, *J. Am. Chem. Soc.*, 2004, **126**, 5030.
94. I. E. Vega, P. A. Gale, M. E. Light and S. J. Loeb, *Chem. Commun.*, 2005, 4913.
95. S. J. Dickson, M. J. Paterson, C. E. Willans, K. M. Anderson and J. W. Steed, *Chem. -Eur. J.*, 2008, **14**, 7296.
96. C. Caltagirone, A. Mulas, F. Isaia, V. Lippolis, P. A. Gale and M. E. Light, *Chem. Commun.*, 2009, 6279.
97. L. H. Uppadine, F. R. Keene and P. D. Beer, *J. Chem. Soc., Dalton Trans.*, 2001, 2188.
98. S. Nieto, J. Pérez, V. Riera, D. Miguel and C. Alvarez, *Chem. Commun.*, 2005, 546.
99. J. Perez, D. Morales, S. Nieto, L. Riera, V. Riera and D. Miguel, *Dalton Trans.*, 2005, 884.
100. S. Nieto, J. Perez, L. Riera, V. Riera, D. Miguel, J. A. Golen, A. L. Rheingold and L. Rheingold, *Inorg. Chem.*, 2007, **46**, 3407.
101. M. Arroyo, D. Miguel, F. Villafane, S. Nieto, J. Perez and L. Riera, *Inorg. Chem.*, 2006, **45**, 7018.
102. L. Ion, D. Morales, J. Pérez, L. Riera, V. Riera, R. A. Kowenicki and M. McPartlin, *Chem. Commun.*, 2006, 91.
103. S. L. Renard, A. Franken, C. A. Kilner, J. D. Kennedy and M. A. Halcrow, *New J. Chem.*, 2002, **26**, 1634.
104. A. Looney, G. Parkin and A. L. Rheingold, *Inorg. Chem.*, 1991, **30**, 3099.
105. D. R. Turner, B. Smith, E. C. Spencer, A. E. Goeta, I. R. Evans, D. A. Tocher, J. A. K. Howard and J. W. Steed, *New J. Chem.*, 2005, **29**, 90.
106. P. G. Plieger, P. A. Tasker and S. G. Galbraith, *Dalton Trans.*, 2004, 313.
107. D. M. Rudkevich, W. Verboom, Z. Brzozka, M. J. Palys, W. Stauthamer, G. J. Vanhummel, S. M. Franken, S. Harkema, J. F. J. Engbersen and D. N. Reinhoudt, *J. Am. Chem. Soc.*, 1994, **116**, 4341.
108. M. Barboiu, G. Vaughan and A. van der Lee, *Org. Lett.*, 2003, **5**, 3073.
109. S. L. Tobey and E. V. Anslyn, *J. Am. Chem. Soc*, 2003, **125**, 14807.
110. P. D. Beer, *Acc. Chem. Res.*, 1998, **31**, 71.
111. P. D. Beer and A. D. Keefe, *J. Organomet. Chem.*, 1989, **375**, C40.
112. P. D. Beer, M. G. B. Drew, A. R. Graydon, D. K. Smith and S. E. Stokes, *J. Chem. Soc., Dalton Trans.*, 1995, 403.
113. P. D. Beer, D. Hesek, J. Hodacova and S. E. Stokes, *J. Chem. Soc.-Chem. Commun.*, 1992, 270.
114. P. D. Beer, C. Hazlewood, D. Hesek, J. Hodacova and S. E. Stokes, *J. Chem. Soc., Dalton Trans.*, 1993, 1327.
115. P. D. Beer, *Chem. Commun.*, 1996, 689.
116. P. D. Beer, D. Hesek, K. C. Nam and M. G. B. Drew, *Organometallics*, 1999, **18**, 3933.
117. P. D. Beer, A. R. Graydon, A. O. M. Johnson and D. K. Smith, *Inorg. Chem.*, 1997, **36**, 2112.
118. G. Denuault, P. A. Gale, M. B. Hursthouse, M. E. Light and C. N. Warriner, *New J. Chem.*, 2002, **26**, 811.

119. F. Szemes, D. Hesek, Z. Chen, S. W. Dent, M. G. B. Drew, A. J. Goulden, A. R. Graydon, A. Grieve, R. J. Mortimer, T. Wear, J. S. Weightman and P. D. Beer, *Inorg. Chem.*, 1996, **35**, 5868.
120. S. Watanabe, O. Onogawa, Y. Komatsu and K. Yoshida, *J. Am. Chem. Soc.*, 1998, **120**, 229.
121. C. P. Montgomery, B. S. Murray, E. J. New, R. Pal and D. Parker, *Acc. Chem. Res.*, 2009, **42**, 925.
122. B. S. Murray, E. J. New, R. Pal and D. Parker, *Org. Biomol. Chem.*, 2008, **6**, 2085.
123. R. Pal, D. Parker and L. C. Costello, *Org. Biomol. Chem.*, 2009, **7**, 1525.

2. The Mechanochemical Synthesis of Tripodal Anion Receptors

2.1 Introduction

Mechanochemical synthesis (i.e. chemical reaction arising from the grinding together of two or more solid reactants) has tremendous potential as a solvent-free alternative to conventional solution-based chemistry.[1-4] Work by Kaupp has shown that a wide range of organic reactions can proceed in the solid state[5-6] and Raston has applied mechanochemical synthetic methods to the preparation of supramolecular systems useful in self-assembly.[7-9] Mechanochemistry is also interesting in the preparation of new solid forms (polymorphs and co-crystals) of organic materials such as active pharmaceutical ingredients (APIs)[10-15] and in the preparation of coordination complexes and coordination polymer materials, e.g. for applications in gas storage and separation.[16-20] Extensive work by Braga and co-workers has also used mechanochemistry to form new materials via a crystal engineering approach.[21-33] Even in cases where purely solid state grinding is ineffective, the addition of a drop of solvent (so-called solvent drop grinding[18, 34-36]) can facilitate extremely smooth and high yielding transformations. The ideal mechanochemical reaction is one with high atom efficiency in which two reactants combine in a well-defined ratio to give a single product. The formation of by-products is problematic since the product must then be purified in some fashion that may entail the use of solution methods at some point during the process. High atom efficiency is a feature of the synthesis of a number of pyridinium and imidazolium-based podand hosts for anions studied by the Steed group and a number of other groups in recent years.[37-48] This chapter reports the results of investigations into the mechanochemical synthesis of pyridinium-based anion binding hosts and shows that the mechanochemical solvent drop grinding method is, in many cases, an efficient, high yielding alternative to solution-phase synthesis at every stage in the preparation of these hosts.

2.2 Synthesis of 1-(Pyridin-3-yl)-3-*p*-tolylurea

Ureas have been used extensively in supramolecular chemistry where their marked hydrogen bonding propensity has led to a range of diverse applications such as solid

state and solution anion binding, metallogels and sensors.[46,49-53] The urea derivative **118** binds anions in the solid and solution states both as an individual ligand and as part of a tripodal anion receptor.[44,54]

The simple synthesis of compound **118** is shown in Scheme 2.1. The compound can be readily synthesised using solution based methods (reflux in CH_2Cl_2 for 12 hours).[54] However the A + B → C nature of the reaction is ideally suited to solid state synthesis.

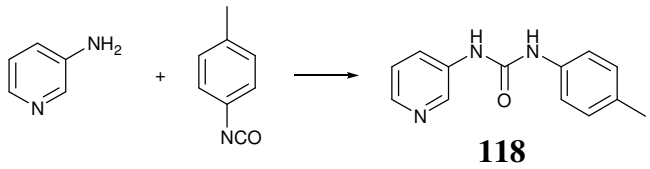

118

Scheme 2.1. Synthesis of 1-(pyridin-3-yl)-3-*p*-tolyl urea

The mechanochemical synthesis of compound **118** was achieved in high yield by grinding the two starting materials in a ball mill for one hour at a frequency of 18 Hz. The reaction was monitored by ^{1}H NMR spectroscopy using a sample of the powder taken every fifteen minutes. No purification of the powder was performed. Figure 2.1 shows a comparison of the ^{1}H NMR spectrum of the two starting materials, the mechanochemical product and the purified product obtained by solution methods.[54] Compound **118** synthesised by the mechanochemical method has the same ^{1}H NMR spectrum as the solution derived product. However, the as-synthesised mechanochemical product contains small traces of both starting materials, indicating the reaction has not gone to completion.

The integrals for one urea proton and the NH_2 peak at 5.27 ppm of the 3-aminopyridine in Figure 2.1c, indicate greater than 90% conversion to product. In the solution-based synthesis, purification is achieved by simple isolation of the precipitated product by filtration and washing with CH_2Cl_2. Purification of the mechanochemical product could also be achieved by washing with dichloromethane.

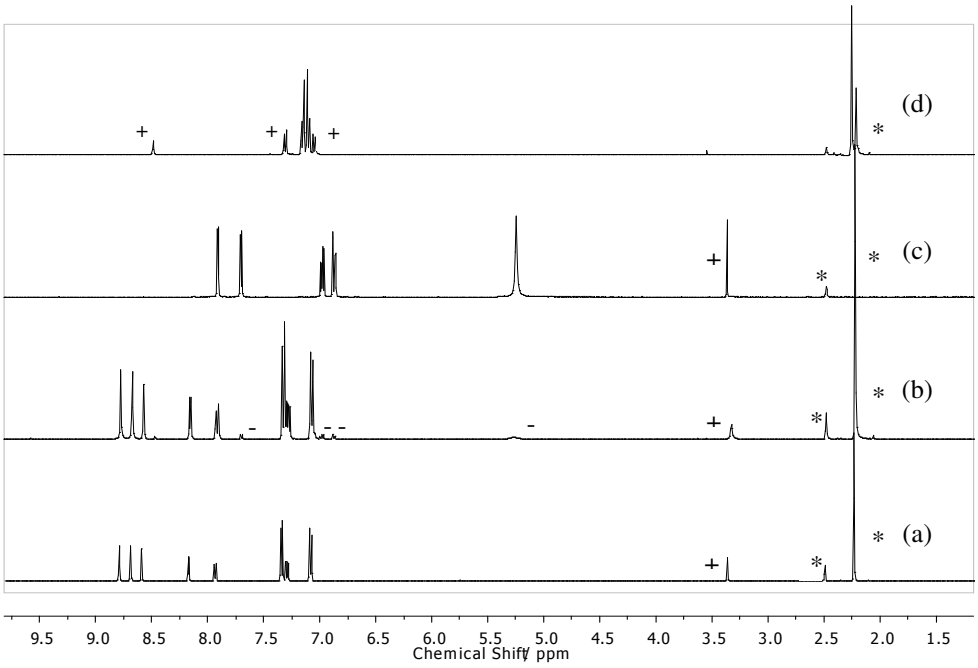

Figure 2.1 Comparison of the ^{1}H NMR spectra (DMSO-d_6) for (a) solution state synthesised **118** after purification, (b) the mechanochemically synthesised **118** without purification, (c) 3-aminopyridine and (d) *p*-tolyl isocyanate. * indicates residual solvent resonances, + indicates impurity resonances (DMSO and water), - indicates 3-aminopyridine impurities. ^{1}H NMR assignments can be found in Appendix I

The ^{1}H NMR spectrum of **118** recorded after 15 minutes shows significant formation of the product, even after this short time span. Comparison of the relative integrals of the urea and NH_2 peaks in the ^{1}H NMR spectra recorded after 30, 45 and 60 minutes, suggests the reaction does not proceed any further beyond 30 minutes of grinding. This reaction is significantly faster than the typical solution based procedure and demonstrates a high yielding, facile route to urea derivatives.

Powder X-ray diffraction was performed on samples of **118** synthesised via solid state and solution based methods. A comparison of the powder diffraction patterns is shown in Figure 2.2. As can be seen, both methods produce the same crystalline form and the mechanochemical product is relatively crystalline.

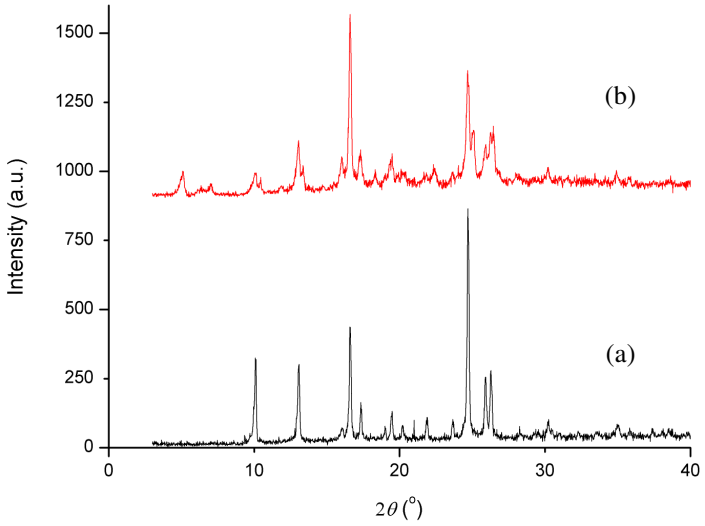

Figure 2.2 Powder diffraction pattern of (a) solid state synthesised and (b) purified solution state synthesised compound **118** (offset vertically for clarity)

2.3 Synthesis of Tripodal Anion Receptors

The synthesis of tripodal anion receptors based on pyridinium salts has been an area of active research by this group and others for several years.[37-48] The synthesis of these receptors has almost exclusively been based around solution state chemistry. However, as with urea derivatives, the simple S_N2 nature of these reactions, with no by-product, also lend themselves to solid state synthesis. The synthesis of several known and novel anion receptors, including those derived from **118**, by an alternative mechanochemical route, is summarised in Schemes 2.2 and 2.3.

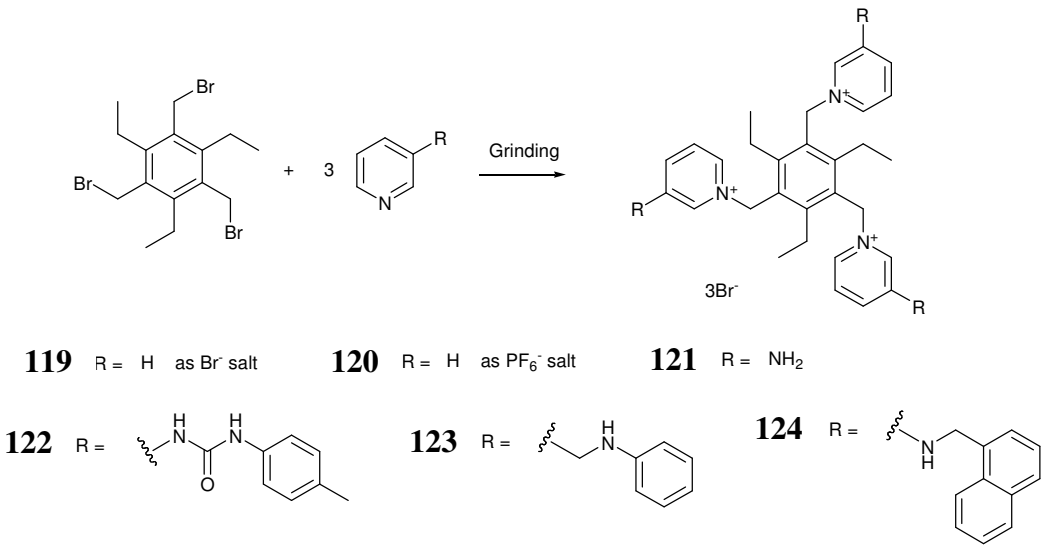

Scheme 2.2 Synthesis of tripodal anion receptors

In all cases the solid reactants consisting of a pyridine derivative such as **118** and a bromomethylated triethylbenzene derivative were ground for 1 hour at 18 Hz, except in the synthesis of compounds **125** and **126** where the solid was ground for 2 hours. The solvent-drop grinding technique was used exclusively in all cases, except for compound **119** where a liquid was used as a reagent. It has been shown that the addition of small quantities of solvent can greatly improve the yield obtained and therefore this technique was chosen for the syntheses outlined.[18,34,36]

Figure 2.3 shows a comparison between the starting materials, and the product (compound **119**) derived from solution and solid state synthesis. The ^{1}H NMR spectra of the metathesised PF_6^- salt (**120**) is also shown. These compounds are specifically designed to be sensitive to anions and hence there are significant chemical shift differences between the bromide salt (**119**) and hexafluorophosphate derivative (**120**). Figure 2.3 shows that very little unreacted pyridine is present in the mechanochemically derived product. This may arise from its evaporation. The solution based synthesis followed the literature procedure[42] and the ^{1}H NMR spectrum shows there is unreacted or partially reacted starting material remaining before purification, as indicated by resonances at approximately 4.75 ppm corresponding to CH_2-Br and an additional peak at 8.93 ppm in the aromatic region.

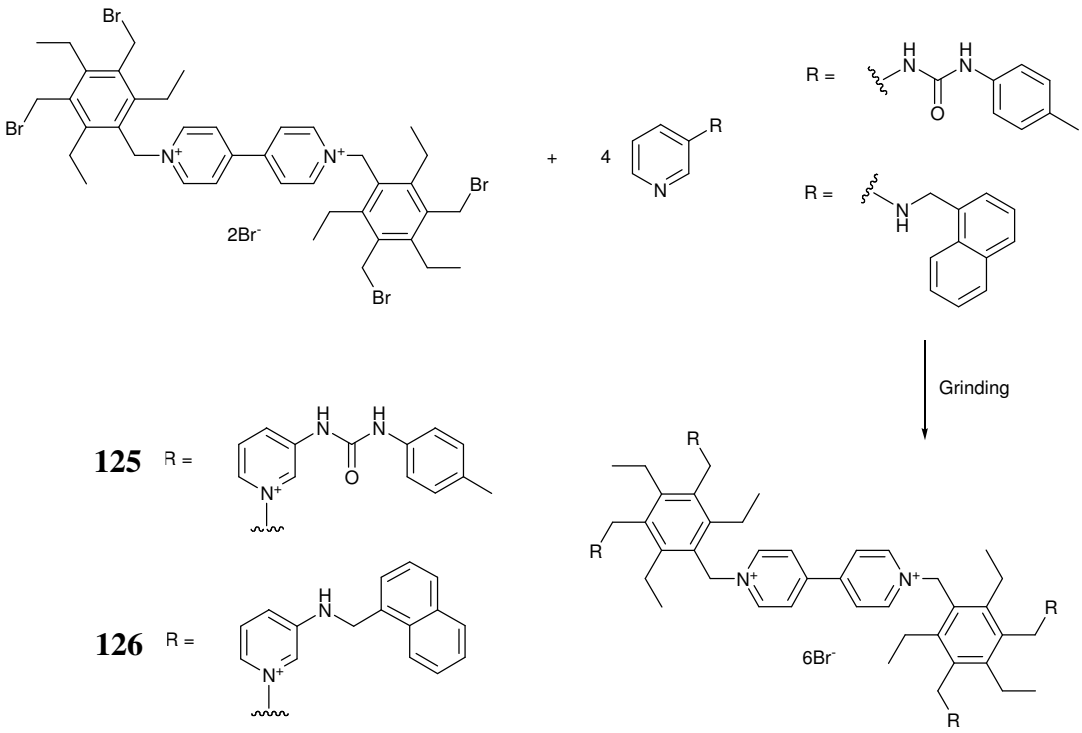

Scheme 2.3. Synthesis of tetrapodal anion receptors

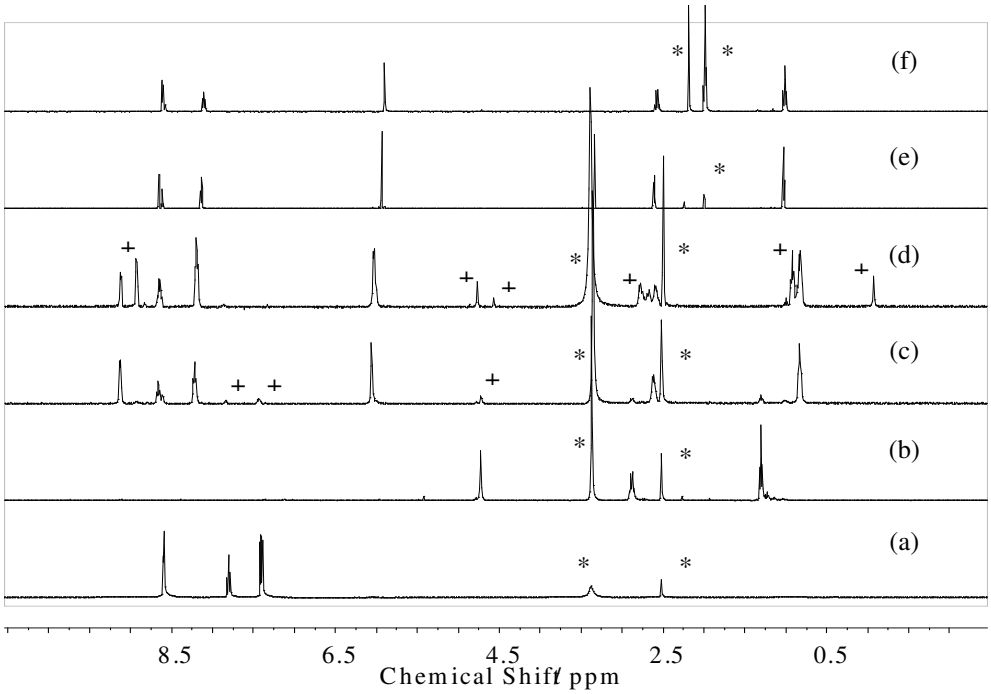

Figure 2.3 Comparison of the ^{1}H NMR spectra for (a) pyridine, (b) 1,3,5-tri(bromomethyl)-2,4,6-triethylbenzene, (c) the mechanochemically synthesised **119** without purification, (d) the solution state synthesis of **119** without purification, (e) **120** from solution state metathesis and (f) **120** from solid state metathesis. Spectra a-d in DMSO-d_6 and spectra e-f in CD_3CN. * indicates residual solvent resonances, + indicates impurity resonances. ^{1}H NMR assignments can be found in Appendix I

The solid state synthesis of compound **119** appears to be significantly cleaner than the solution state method with significantly less CH_2-Br impurity. This result was achieved in a twelfth of the time of the solution synthesis in a 93% yield and for this reaction, appears to be the most facile route to the tripodal anion host.

Figure 2.4 shows the appearance of compound **122** as a function of time. As with compound **119** the reaction is almost complete within the first 15 minutes and after that time only a small additional amount of product is formed. This result shows that as with compound **119**, increasing the grinding time does not have a significant effect on the yield of the desired product.

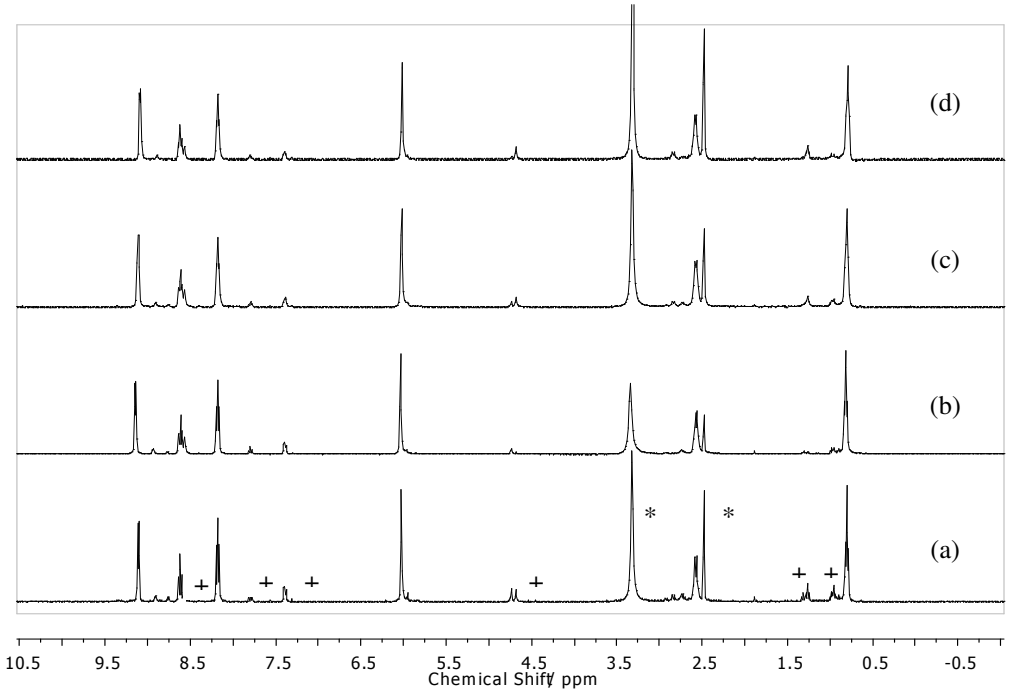

Figure 2.4 ^{1}H NMR spectra of compound **122** recorded after (a) 15 mins (b) 30 mins, (c) 45 mins and (d) 60 mins of grinding in DMSO-d_6. * indicates residual solvent resonances (DMSO and water), + indicates 3-aminopyridine resonances. ^{1}H NMR assignments can be found in Appendix I

In an attempt to drive the reaction to completion, an excess of pyridine was used. This was also done for the synthesis of compound **119** where an excess of *p*-tolyl isocyanate was used. In both cases the reactants seemed to react with the grinding jar, resulting in a metallic looking residue which could not be readily removed. It was envisioned that the use of an excess of reactant would improve the yield. However, in reality, it introduced unforeseen impurities which would require additional unwanted purification

steps. For this reason reactions involving an excess of reagent were not investigated further.

For many cationic anion sensors it is necessary to exchange the Br^- counter-ion for a non-interacting anion such as PF_6^-. This provides a simple means of purifying the impure bromide salts from the solid state synthesis. In the majority of cases the bromide salt is soluble in methanol. The addition of NH_4PF_6 results in the immediate precipitation of the product as the PF_6^- salt. The product can be isolated by filtration and the impurities remain in the filtrate. Figure 2.3 shows the ^1H NMR spectrum of purified **120** isolated by this method.

To try and remove a dissolution and precipitation step in the preparation of the final product **120**, a solid state anion metathesis was attempted. Bromide salt **119** was ground in the ball mill for one hour with ten equivalents of $NaPF_6$ to give **120** and NaCl. The excess $NaPF_6$ and NaCl by-product were removed by washing the residual powder with distilled water. A white solid remained which was dried under ambient conditions. The ^1H NMR (Figure 2.3f) spectrum along with bromide elemental analysis revealed the product to be the pure PF_6^- salt. The change in counter anion was confirmed by the anion sensitivity of the pyridyl CH proton chemical shifts in the ^1H NMR spectrum. As the Br^- salt, the protons are shifted downfield due to hydrogen bonding to Br^- (compare Figures 2.3c and 2.3f).

Powder X-ray diffraction patterns of the solution and solid state synthesised compound **119** are shown in Figure 2.5. The solids were sticky and not particularly crystalline. It appears that the bromide salts are hygroscopic, an observation supported by previously reported crystal structures which contained solvent molecules.[42] The resulting diffraction patterns are broadened and confirm the predominantly amorphous nature of the solids.

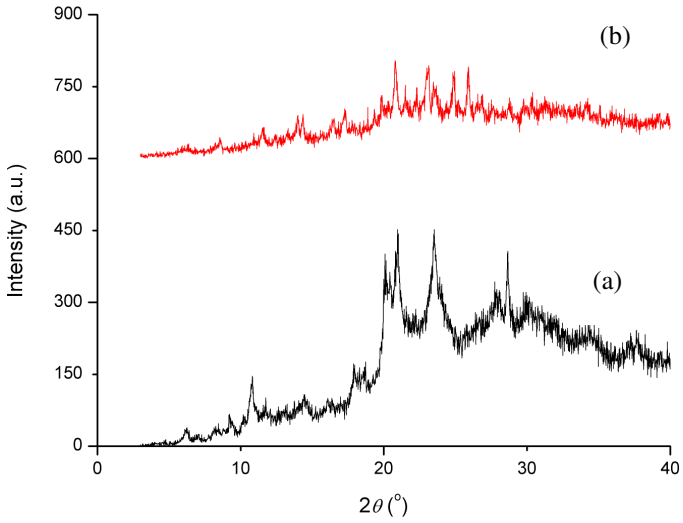

Figure 2.5 Powder X-ray diffractograms of (a) solid state and (b) solution state synthesised **119** (offset vertically for clarity)

The mechanochemical synthesis of several other tripodal and tetrapodal anion receptors was attempted, as summarised in Scheme 2.3. In order to compare the relative yields of each reaction it was necessary to metathesise the bromide salts to the PF_6^- salt. Unreacted starting material was then removed in the filtrate. The yields of the purified PF_6^- salts are compared to the literature in Table 2.1.

In most cases for the known compounds, the mechanochemical technique is able to compete with the solution based yield with gains in simplicity, time and removal of one solvent-based step. Compounds **124** and **126** represent novel compounds that have been prepared for the first time using the mechanochemical method. The yield of compound **121** is particularly low using mechanochemistry for reasons that are unclear, but may relate to the highly crystalline nature of the 3-aminopyridine starting material.

Table 2.1 Isolated percentage yields for the PF_6^- salts of the tripodal and tetrapodal anion receptors. * = synthesised as part of this work

Compound Number	Percentage Yield (%)	Literature Yield for Solution Synthesis[42,44] (%)
120	93	92
121	18	90
122	48	57
123	56	79
124	55	-*
125	27	31
126	39	-*

2.4 Conclusions

This work shows that the solid state mechanochemical synthesis of tripodal anion receptors based on pyridinium salts is a viable alternative to conventional methods. The synthetic procedure is simple and fast with purification of the reaction products achieved using traditional organic solvent based techniques or alternatively by using mechanochemical anion metathesis. It is also possible to efficiently prepare precursors such as compound **118** in this fashion. The yields for the various reactions are variable but are broadly similar to solution based preparations and demonstrate that mechanochemistry can provide a real alternative to solution based methods for the reaction types discussed.

2.5 Experimental

Materials were obtained from standard commercial sources. 1,3,5-Tri(bromomethyl)-2,4,6-triethylbenzene and 1,1'-bis(3,5-bis(bromomethyl)-2,4,6-triethylbenzyl)-4,4'-bipyridine-1,1'-diium bromide were prepared as previously reported.[46,55] Experimental data is given for the metathesised PF_6^- salts.

Instrumentation

All NMR spectra were performed on a Varian Mercury-400 (400 MHz for ^{1}H), Varian Inova-500 machine (500 MHz for ^{1}H, 126 Hz for ^{13}C) or a Varian DD-700 (700 MHz for ^{1}H, 176 MHz for ^{13}C) and were referenced to residual solvent. Electrospray (ES) mass spectrometry was recorded on a Thermo-Finnigan LTQ instrument, whilst Matrix Assisted Laser Desorption Ionisation (MALDI) experiments were recorded on an ABI Voyager-DC STR. Fourier transform infrared spectra were recorded with a Perkin Elmer Spectrum 100 ATR instrument (Perkin-Elmer). For each spectrum, 64 scans were conducted over a spectral range of 4000 to 600 cm^{-1} with a resolution of 4 cm^{-1}. Elemental analysis was performed using an Exeter Analytical inc. CE-400 Elemental Analyser.

Powder diffraction was performed on a Siemens D5000 X-Ray Diffractometer using CuKα radiation at a wavelength of 1.5406 Å.

General Proceedure for Mechanochemical Synthesis

All solid state reactions were carried out using a Retsch MM200 ball mill with 25 ml vessel. 1,3,5-Tri(bromomethyl)-2,4,6-triethylbenzene (0.50 g, 1.1 mmol) and 3 equivalents of the required binding arm were placed in a 25 ml grinding jar with 5 drops of acetonitrile (except when pyridine was used). The reactants were ground at 18 Hz for 60 minutes after which methanol was added and unreacted starting material removed by filtration. Excess NH_4PF_6 was added to the methanol solution and the product precipitated as the PF_6^- salt.

Synthesis of 118. 3-aminopyridine (0.50 g, 1.1 mmol) and *p*-tolyl isocyanate (0.15 g, 1.1 mmol) were placed in a 25 ml shaker grinding jar and ground for 1 hour at 18 Hz. No further purification was performed. Characterisation was consistent with the published literature.[56]

Solution-State Synthesis of 119. Literature procedure was followed. No purification was performed. Characterisation consistent with published literature.[42]

Solid-State Synthesis of 119. Followed general procedure with pyridine (0.27 g, 3.4 mmol). Yield = 0.93 g, 1.0 mmol, 93%. Characterisation consistent with published literature.[42]

Solid-State Anion Methathesis of 119. Compound **119** (0.20 g, 0.30 mmol) and $NaPF_6$ (0.50 g, 3.0 mmol) were placed in a 25 ml grinding jar and ground for 60 minutes at 18 Hz. The solid residue was washed with distilled water (30 ml) and the resulting white powder was allowed to dry under ambient conditions. Yield = 0.11 g, 0.13 mmol, 43%. Characterisation consistent with published literature.[42] Bromide analysis confirmed greater than 95% conversion.

Synthesis of 121. Followed general procedure with 3-aminopyridine (0.32 g, 3.4 mmol). Water was added to precipitate the PF_6^- salt in the final step. Yield = 0.19 g, 0.20 mmol, 18%. Characterisation consistent with published literature.[42]

Synthesis of 122. Followed general procedure with 1-(pyridin-3-yl)-3-*p*-tolylurea (0.77 g, 3.4 mmol). Yield = 0.72 g, 0.54 mmol, 48%. Characterisation consistent with published literature.[44]

Synthesis of 123. Followed general procedure with *N*-((pyridin-3-yl)methyl)benzenamine (0.62 g, 3.4 mmol).[57] Yield = 0.75 g, 0.63 mmol, 56%. Characterisation consistent with solution state product.[48]

Synthesis of *N*-(naphthalen-4-yl)methyl)pyridine-3-amine. 1-Naphthaldehyde (2.0 g, 13 mmol) and 3-aminopyridine (1.8 g, 19 mmol) were dissolved in dry 1,2-dichloroethane (DCE) under N_2 along with 4Å molecular sieves. The mixture was heated at reflux for 24 hours, allowed to cool and the molecular sieves removed by filtration. The solvent was removed from the filtrate *in vacuo* and 30 ml of diethyl ether added and any residue removed by filtration. The solvent was removed *in vacuo* resulting in the imine which was dissolved in 70 ml of methanol. $NaBH_4$ (1.9 g, 50 mmol) was added slowly. The reaction was stirred for 2 hours at room temperature. HCl (37%) was added until the pH was approximately 5, followed by 2M NaOH until the pH was approximately 8 and the solution turned from cloudy to clear. The solvent was removed *in vacuo* and the resulting oil was left to crystallise. The solid was

washed gently with water and diethyl ether. Yield = 1.85 g, 10 mmol, 79%. m.p. 118 - 122 °C; ^{1}H NMR (CD_3CN, 700 MHz /ppm) δ = 8.12 (1H, d, *J* = 2.4 Hz, PyH), 8.03 (1H, d, *J* = 8.0 Hz, ArH), 8.00 (1H, d, *J* = 4.7 Hz, PyH), 7.91 (1H, d, *J* = 7.4 Hz, ArH), 7.83 (1H, d, *J* = 8.0 Hz, ArH), 7.53 (3H, m, ArH), 7.44 (1H, m, ArH), 7.10 (1H, dd, *J* = 8.6 and 4.7 Hz, PyH), 6.93 (1H, d, *J* = 8.2 Hz, PyH), 4.75 (2H, d, *J* = 5.1 Hz, CH_2), 4.09 (1H, s, NH); ^{13}C-{^{1}H} NMR (CD_3CN, 176 MHz /ppm) δ = 144.2, 139.2, 136.2, 134.1, 133.6, 131.5, 129.0, 128.6, 126.6, 126.1, 126.0, 125.6, 123.8, 123.4, 118.5, 46.1; *m/z* (ES^+) 235.0 $[M+H]^+$; ν/cm^{-1} 3216 (N-H), 3027 (C-H), 2979 (C-H), 1578, 1420, 1295, 1094, 1009, 776; Found: C, 81.80; H, 6.07; N, 11.96; Calc. for C, 82.02; H, 6.02; N, 11.96.

Synthesis of 124. Followed general procedure with 1,3,5-tri(bromomethyl)-2,4,6-triethylbenzene (0.50 g, 1.1 mmol) and *N*-((naphthalene-1-yl)methyl)pyridine-3-amine (0.80 g, 3.4 mmol). Yield = 0.39 g, 0.28 mmol, 25 %. A portion of the product was recrystallised from acetonitrile/diethyl ether for analysis. m.p. melting under decomposition 236 - 248 °C; ^{1}H NMR (CD_3CN, 700 MHz /ppm) δ = 8.04 (3H, d, *J* = 8.2 Hz, PyH), 7.97 (3H, d, *J* = 7.8 Hz, Ar/PyH), 7.88 (3H, t, *J* = 5.0 Hz, Ar/PyH), 7.7-7.55 (6H, m, Ar/PyH), 7.45 (6H, m, Ar/PyH), 6.24 (3H, br s, NH), 5.49 (6H, s, CH_2-N^+), 4.86 (6H, d, *J* = 6.0 Hz, C*H*$_2$-NH_2), 2.42 (6H, q, *J* = 7.2 Hz, C*H*$_2$-CH_3), 0.77 (9H, br t, C*H*$_3$-CH_2); ^{13}C-{^{1}H} NMR (CD_3CN, 176 MHz /ppm) δ = 150.1, 148.1, 134.0, 131.5, 131.1, 130.4, 128.8, 128.4, 128.1, 127.8, 126.6, 126.2, 125.5, 125.0, 123.2, 65.3, 57.5, 44.5, 23.7, 14.6, 14.0; *m/z* (MALDI$^+$) 1193.6 $[M-PF_6]^+$; ν/cm^{-1} 3424 (N-H), 2972 (C-H), 1620, 1593, 1537, 1313, 1151, 822; Found: C, 55.80; H, 4.98; N, 6.75; Calc. for $C_{63}H_{63}N_6(PF_6)_3.0.4C_4H_{10}O/1.5H_2O/CH_3CN$: C, 55.67; H, 5.12; N, 6.82, residual solvent observed in ^{1}H NMR spectrum.

For synthesis of compounds **125** and **126** see Chapter 4.8

2.6 References

1. F. Toda, *Synlett*, 1993, 303.
2. F. Toda, H. Takumi and M. Akehi, *J. Chem. Soc.-Chem. Commun.*, 1990, 1270.
3. F. Toda, *J. Synth. Org. Chem. Jpn.*, 1994, **52**, 923.
4. P. T. Anastas, '*Green Chemistry*', Oxford University Press, New York, 2000.
5. G. Kaupp, *CrystEngComm*, 2003, **5**, 117.

6. G. Kaupp and M. R. Naimi-Jamal, *CrystEngComm*, 2005, **7**, 402.
7. G. Rothenberg, A. P. Downie, C. L. Raston and J. L. Scott, *J. Am. Chem. Soc.*, 2001, **123**, 8701.
8. J. L. Atwood, M. J. Hardie, C. L. Raston and C. A. Sandoval, *Org. Lett.*, 1999, **1**, 1523.
9. C. L. Raston and J. L. Scott, *Green Chemistry*, 2000, **2**, 49.
10. N. Shan, F. Toda and W. Jones, *Chem. Commun.*, 2002, 2372.
11. D. Cincic, T. Friscic and W. Jones, *J. Am. Chem. Soc.*, 2008, **130**, 7524.
12. K. L. Nguyen, T. Friscic, G. M. Day, L. F. Gladden and W. Jones, *Nature Materials*, 2007, **6**, 206.
13. W. Jones, S. Motherwell and A. V. Trask, *Mrs Bulletin*, 2006, **31**, 875.
14. A. V. Trask, D. A. Haynes, W. D. S. Motherwell and W. Jones, *Chem. Commun.*, 2006, 51.
15. A. V. Trask and W. Jones, in *Organic Solid State Reactions*, 2005, pp. 41.
16. W. J. Belcher, C. A. Longstaff, M. R. Neckenig and J. W. Steed, *Chem. Commun.*, 2002, 1602.
17. P. J. Nichols, C. L. Raston and J. W. Steed, *Chem. Commun.*, 2001, 1062.
18. A. L. Garay, A. Pichon and S. L. James, *Chem. Soc. Rev.*, 2007, 846.
19. A. Pichon and S. L. James, *CrystEngComm*, 2008, **10**, 1839.
20. A. Pichon, A. Lazuen-Garay and S. L. James, *CrystEngComm*, 2006, **8**, 211.
21. D. Braga, S. L. Giaffreda, F. Grepioni, A. Pettersen, L. Maini, M. Curzi and M. Polito, *Dalton Trans.*, 2006, 1249.
22. D. Braga, M. Curzi, A. Johansson, M. Polito, K. Rubini and F. Grepioni, *Angew. Chem. Int. Ed.*, 2006, **45**, 142.
23. D. Braga and F. Grepioni, *Angew. Chem. Int. Ed.*, 2004, **43**, 4002.
24. D. Braga, L. Maini, S. L. Giaffreda, F. Grepioni, M. R. Chierotti and R. Gobetto, *Chem.-Eur. J.*, 2004, **10**, 3261.
25. D. Braga, D. D'Addario, M. Polito and F. Grepioni, *Organometallics*, 2004, **23**, 2810.
26. D. Braga, L. Maini, M. Polito, L. Mirolo and F. Grepioni, *Chem.-Eur. J.*, 2003, **9**, 4362.
27. D. Braga, L. Maini, M. Polito and F. Grepioni, *Chem. Commun.*, 2002, 2302.
28. D. Braga, S. L. Giaffreda, F. Grepioni, G. Palladino and M. Polito, *New J. Chem.*, 2008, **32**, 820.
29. D. Braga, F. Grepioni, L. Maini, R. Brescello and L. Cotarca, *CrysEngComm*, 2008, **10**, 469.
30. D. Braga, S. L. Giaffreda, F. Grepioni, M. R. Chierotti, R. Gobetto, G. Palladino and M. Polito, *CrystEngComm*, 2007, **9**, 879.
31. D. Braga, M. Gandolfi, M. Lusi, D. Paolucci, M. Polito, K. Rubini and F. Grepioni, *Chem.-Eur. J.*, 2007, **13**, 5249.
32. D. Braga, M. Polito, E. Dichiarante, K. Rubini and F. Grepion, *Chem. Commun.*, 2007, 1594.
33. D. Braga, S. L. Giaffreda, K. Rubini, F. Grepioni, M. R. Chierotti and R. Gobetto, *CrystEngComm*, 2007, **9**, 39.
34. S. Karki, T. Friscic, W. Jones and W. D. S. Motherwell, *Molecular Pharmaceutics*, 2007, **4**, 347.
35. G. A. Bowmaker, N. Chaichit, C. Pakawatchai, B. W. Skelton and A. H. White, *Dalton Trans.*, 2008, 2926.
36. G. A. Bowmaker, J. V. Hanna, R. D. Hart, B. W. Skelton and A. H. White, *Dalton Trans.*, 2008, 5290.
37. V. Amendola, M. Boiocchi, L. Fabbrizzi and A. Palchetti, *Chem.-Eur. J.*, 2005, **11**, 5648.

38. B. G. Zhang, P. Cai, C. Y. Duan, R. Miao, L. G. Zhu, T. Niitsu and H. Inoue, *Chem. Commun.*, 2004, 2206.
39. Y. Bai, B.-G. Zhang, C. Y. Duan, D.-B. Dang and Q.-J. Meng, *New. J. Chem.*, 2006, **30**, 266.
40. Y. Bai, B. G. Zhang, J. Xu, C. Y. Duan, D. B. Dang, D. J. Liu and Q. J. Meng, *New J. Chem.*, 2005, **29**, 777.
41. L. O. Abouderbala, W. J. Belcher, M. G. Boutelle, P. J. Cragg, M. Fabre, J. Dhaliwal, J. W. Steed, D. R. Turner and K. J. Wallace, *Chem. Commun.*, 2002, 358.
42. K. J. Wallace, W. J. Belcher, D. R. Turner, K. F. Syed and J. W. Steed, *J. Am. Chem. Soc.*, 2003, **125**, 9699.
43. M. H. Filby, T. D. Humphries, D. R. Turner, R. Kataky, J. Kruusma and J. W. Steed, *Chem. Commun.*, 2006, 156.
44. D. R. Turner, M. J. Paterson and J. W. Steed, *J. Org. Chem.*, 2006, **71**, 1598.
45. D. R. Turner, M. J. Paterson and J. W. Steed, *Chem. Commun.*, 2008, 1395.
46. S. J. Dickson, E. V. B. Wallace, A. N. Swinburne, M. J. Paterson, G. O. Lloyd, A. Beeby and J. W. Steed, *New J. Chem.*, 2008, **32**, 786.
47. M. H. Filby, S. J. Dickson, N. Zaccheroni, L. Prodi, S. Bonacchi, M. Montalti, C. Chiorboli, M. J. Paterson, T. D. Humphries and J. W. Steed, *J. Am. Chem. Soc.*, 2008, **130**, 4105.
48. A. Barnard, S. J. Dickson, M. J. Paterson, A. M. Todd and J. W. Steed, *Org. Biomol. Chem.*, 2008, **7**, 1554.
49. D. R. Turner, A. Pastor, M. Alajarín and J. W. Steed, *Structure and Bonding*, 2004, **108**, 97.
50. M.-O. M. Piepenbrock, G. O. Lloyd, N. Clarke and J. W. Steed, *Chem. Commun.*, 2008, 2644.
51. V. Amendola, D. Esteban-Gomez, L. Fabbrizzi and M. Licchelli, *Acc. Chem. Res.*, 2006, **39**, 343.
52. R. Custelcean, *Chem. Commun.*, 2008, 295.
53. V. Arnendola, M. Bonizzoni, D. Esteban-Gomez, L. Fabbrizzi, M. Licchelli, F. Sancenon and A. Taglietti, *Coord. Chem. Rev.*, 2006, **250**, 1451.
54. D. R. Turner, E. C. Spencer, J. A. K. Howard, D. A. Tocher and J. W. Steed, *Chem. Commun.*, 2004, 1352.
55. K. J. Wallace, R. Hanes, E. Anslyn, J. Morey, K. V. Kilway and J. Siegel, *Synthesis-Stuttgart*, 2005, 2080.
56. D. R. Turner, B. Smith, A. E. Goeta, I. R. Evans, D. A. Tocher, J. A. K. Howard and J. W. Steed, *CrystEngComm*, 2004, **6**, 633.
57. S. J. Dickson, M. J. Paterson, C. E. Willans, K. M. Anderson and J. W. Steed, *Chem. -Eur. J.*, 2008, **14**, 7296.

3. A Quinolinium Derived Anion Receptor and Sensor

3.1 Introduction

The design of receptors capable of selectively binding and sensing anions is challenging and is a current area of active research.[1-4] The Steed group[5-9] and others[10-13] have used receptors derived from a hexa-substituted triethylbenzene scaffold as a means of creating conformationally flexible anion hosts exhibiting some degree of preorganisation. These hosts have proved effective anion receptors with the addition of redox active (ferrocenyl)[14] or luminescent (anthracenyl,[5] pyrenyl[9]) reporter groups, allowing electrochemical or 'turn-on' fluorescent sensing. Several recent examples of turn-off PET sensors for biologically relevant anions have also been reported.[15-19]

The use of quinolinium salts as anion sensors has been investigated due to their ease of synthesis, their water solubility and their known fluorescent quenching by anions.[20-23] Many studies have focused on halide detection, particularly chloride. Chloride is an anion of great importance in biological chemistry, as a component of extra-cellular fluids, in environmental science as well as consumer products and industrial processes.[20]

The quinolinium based sensors reported to date are invariably sensors based on dynamic quenching processes with no specific anion recognition built-in.[20] To the authors knowledge there have been no quinolinium based sensors derived from preorganised anion receptors capable of binding and discriminating between anions. This chapter investigates the synthesis of a receptor based on quinolinium functionalities that acts as both a binding and 'turn-off' fluorescent sensing unit appended to a hexa-substituted benzene core.

3.2 Synthesis

The synthesis of compound **127** follows the general procedure used for the synthesis of related compounds, outlined in Scheme 3.1. The synthesis of compound **127** involves the reaction of quinoline with 1,3,5-tribromomethyl-2,4,6-triethylbenzene in a manner analogous to related pyridinium-based receptors.[5] The reaction time

required is considerably longer than for pyridinium-derived compounds (*ca*. 48 hours as opposed to 6 hours) and reflects the added steric hinderance found in the quinolinium derivative. The (unoptimised) isolated yield is also lower (24%) compared to 92% for the pyridinium analogue. However, the low yield might be due in part to the repeated recrystallisations required to remove the incompletely reacted two arm substituted product.

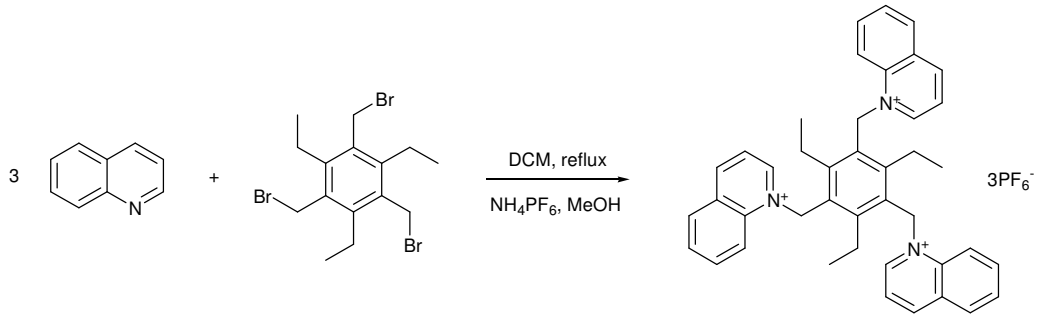

127

Scheme 3.1 Synthesis of compound **127**

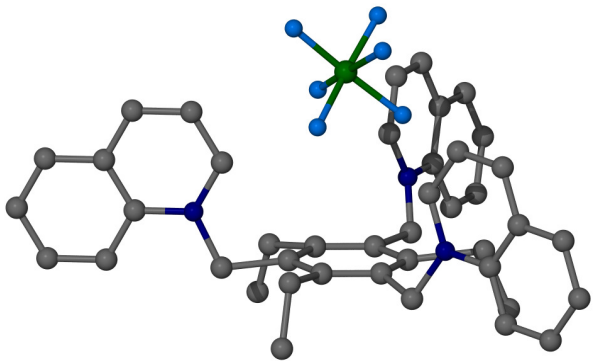

Figure 3.1 Molecular structure of compound **127**. Hydrogen atoms are emitted for clarity

Crystals of compound **127** of suitable quality for X-ray diffraction were grown and the data collected at I19 on the Diamond synchrotron by Prof. W. Clegg. Unfortunately the crystals proved to be of poor quality and hence the refinement has a very large *R* factor and as such, the determination can only be used to gain general, gross, structural insights. As can be seen in Figure 3.1, the data suggests that the host is in the three-up, three-down conformation with a PF_6^- counter-ion found in the binding cavity of the host.

The control compound **128** has also been prepared in an analogous manner (Scheme 3.2). This lacks the preorganised, multiply charged binding cavity found in compound **127** and allows a comparison to be made between preorganised multivalent[24] and non-preorganised, single binding site quinolinium based anion sensors.

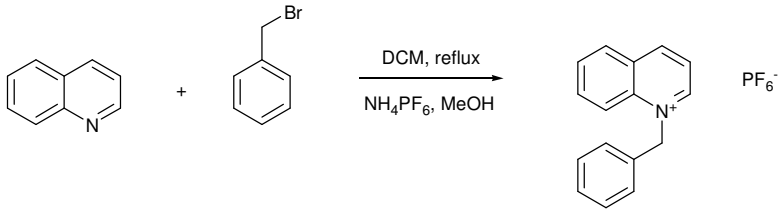

128

Scheme 3.2 Synthesis of compound **128**

The structure of compound **128** was confirmed by single crystal X-ray structural determination (Figure 3.2). The crystal packing exhibits π-π stacking of the aryl rings, with a plane to plane distance of 3.616(3) Å. The crystal also shows quinolinium to quinolinium π-π stacking with a plane to plane distance of 3.413(2) Å.

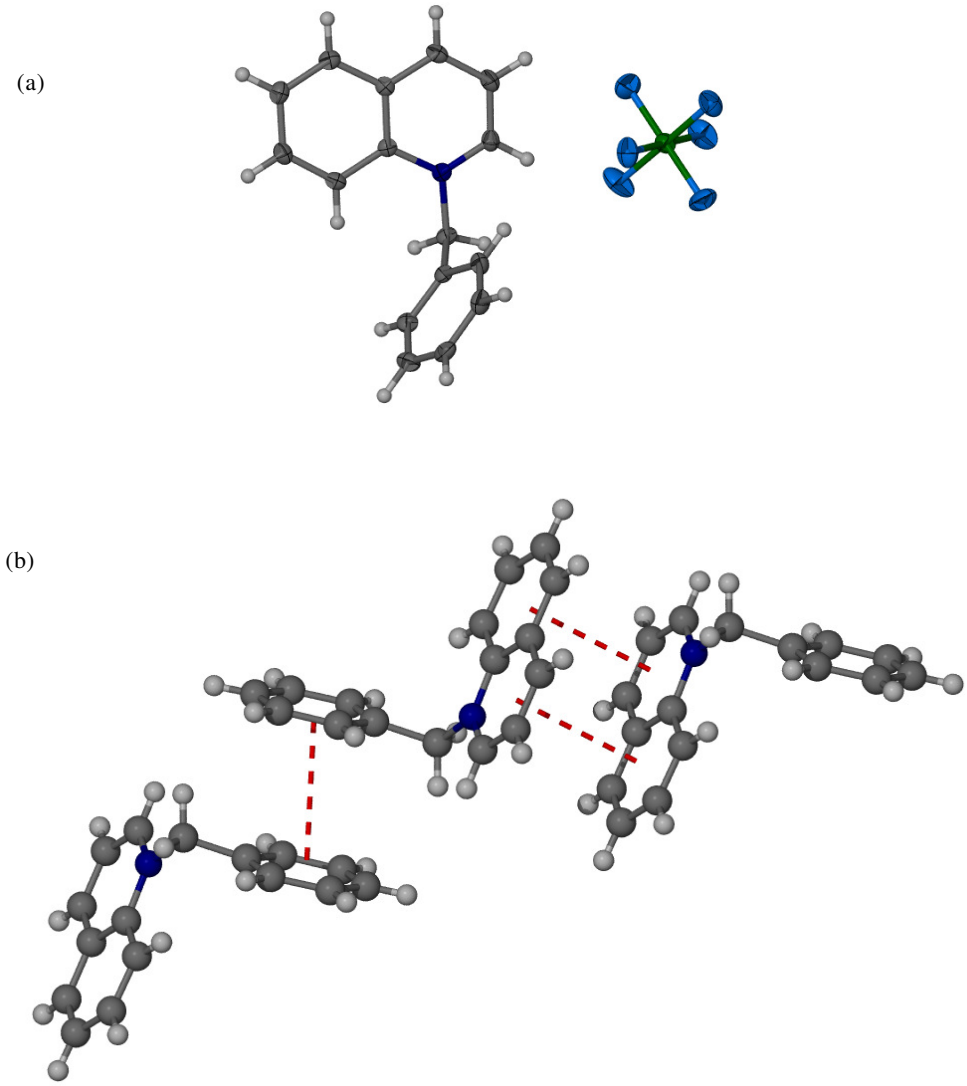

Figure 3.2 (a) Molecular structure of compound **128**, (b) packing diagram highlighting the π stacking interactions between phenyl-phenyl (plane to plane distance of 3.616(3) Å) and quinolinium-quinolinium rings (plane to plane distance of 3.413(2) Å)

3.3 Solution-State Binding Properties

The solution state binding properties of compound **127** were investigated using ^{1}H NMR spectroscopic titrations in CD_3CN solvent with a number of anionic guests. The binding isotherms are shown in Figure 3.3.

Significant chemical shift changes in the resonances assigned to the protons *ortho* (*o*) and *meta* (*m*) to the quinolinium nitrogen atom were observed, with very small shifts for the other signals. In several cases, inflections in the isotherms occur before the addition

of one equivalent of anion, suggesting a more complicated series of binding equilibria than a 1:1 host:guest stoichiometry.

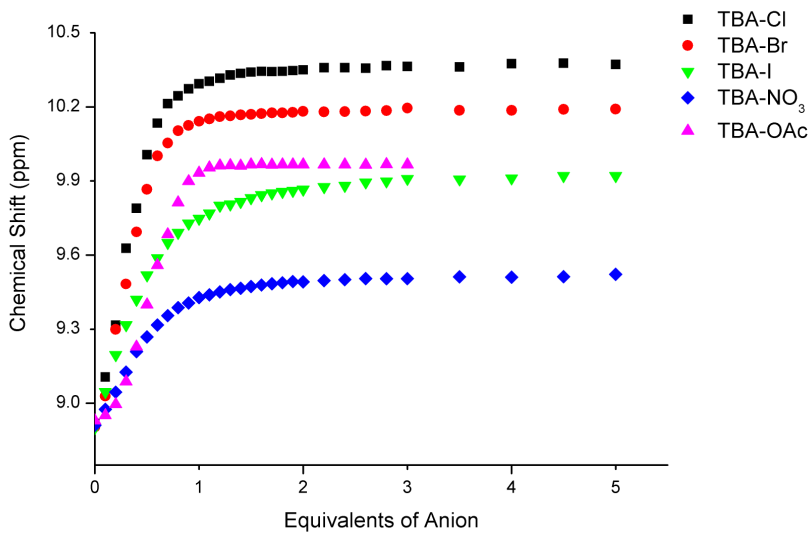

Figure 3.3 Binding isotherms for the *ortho*-quinolinium proton of compound **127** with various anions in CD_3CN. Precipitation occurred after 3 equivalents of acetate

In order to determine the appropriate binding model a Job plot with TBA-I was determined (Figure 3.4). Iodide was chosen due to the high solubility of the host-iodide complex. The data points appear skewed further to the right hand side of the plot than might be expected for a 1:1 host:guest stoichiometry. A 2:1 host:guest stoichiometry would give rise to a maximum at a mole fraction of 0.66, whereas a 1:1 host:guest stoichiometry would give a maximum at 0.5 mole fraction. It is possible that both of these species coexist, resulting in an intermediate value between the two. However, the method of continuous variation is also often inappropriate for systems with multiple exchanging species and as such a Job plot may provide inaccurate stoichiometric ratios at the concentration used.[25]

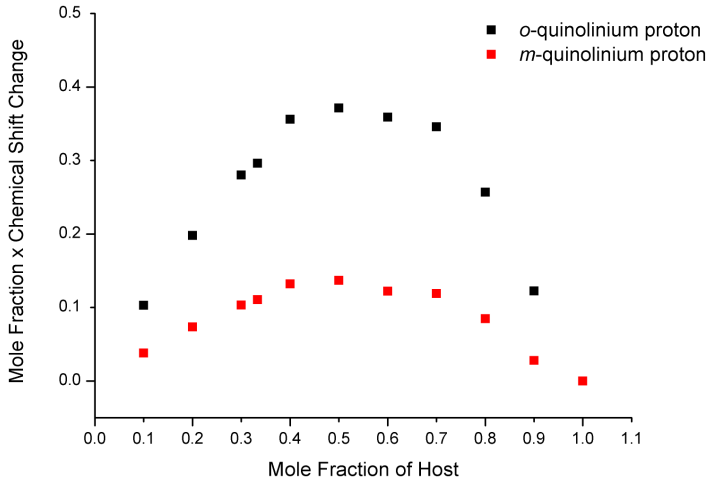

Figure 3.4 Job plot for compound **127** with TBA-I in CD_3CN

The presence of a host dimer can be established via a dilution study on compound **127** as the PF_6^- salt (Figure 3.5). The host shows modest chemical shift changes as a function of concentration, however a value of log K_{20} = 1.57(7) fits the data well. This dimerisation constant was included into the stoichiometry model incorporating both 1:1 and 2:1 host:anion complexes, to give an improved fit to the complexation data. The binding constants thus determined for compound **127** for various anions are summarised in Table 3.1 as determined by non-linear least squares fitting using *HypNMR* 2006.[26] DOSY NMR experiments were attempted to further confirm the presence of a host dimer. However as the dimer also forms in the presence of anions other than PF_6^-, with relatively small changes in the combined molecular mass of the complex, this technique was not able to distinguish a change in diffusion coefficient within the experimental error.

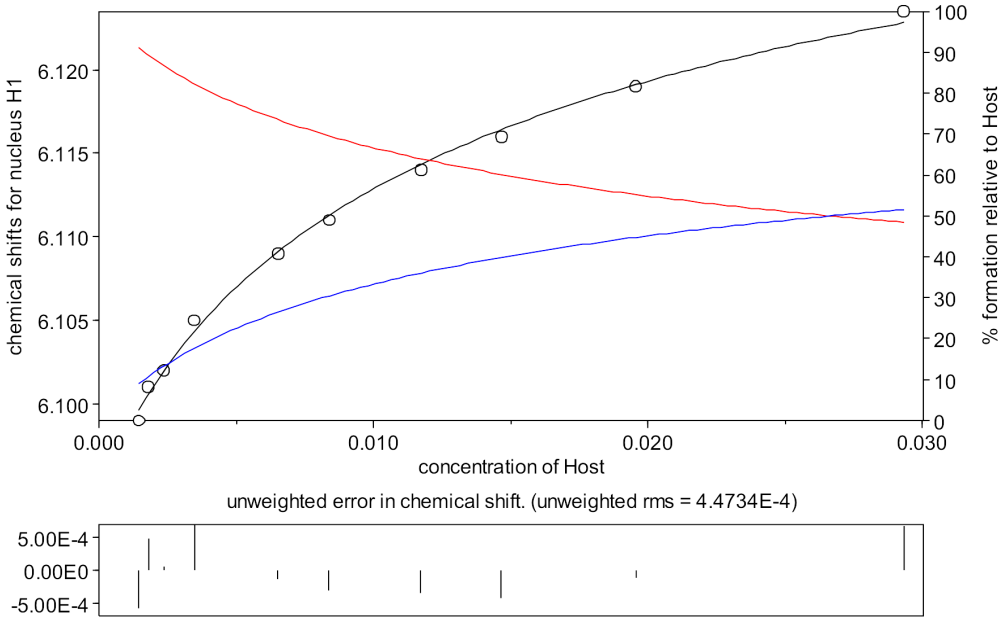

Figure 3.5 ^{1}H NMR dilution study for **127** in CD_3CN. The CH_2-quinolinium proton was followed. Circles – experimental data points, black line – refined data fit, blue line – speciation of H_2, red line – speciation of H.

Bromide was found to have the highest affinity to **127**, with chloride being similar. Iodide is bound significantly less strongly than the other anions tested, consistent with its larger size and its smaller charge to radius ratio. Interestingly, the compound shows strong binding to nitrate, a weakly basic anion, with binding constants in the same region as those to chloride. Binding constants could not be refined for acetate in this solvent due to very strong binding, as indicated by the steady chemical shift values above one equivalent in the binding isotherm. A ^{1}H NMR spectroscopic titration of compound **127** with acetate in DMSO-d_6 (a more competitive solvent) was carried out. Unfortunately small chemical shift changes were observed (*ca*. 0.2 ppm) for which a binding constant could not be determined due to a low binding constant.

The ^{1}H NMR spectrum of compound **128** was also recorded with the addition of 1, 2 and 3 equivalents of TBA-Cl. The major change is a shift of the peak at 9.17 ppm by up to 0.3 ppm, accompanied by broadening of the resonances and is in contrast to compound **127** in which a change of approximately 1.5 ppm is observed; all other chemical shift changes for compound **128** are less than 0.1 ppm. This is indicative of a binding constant less than 10 M^{-1}. This experiment implies that there is a markedly

weaker interaction between anions and **128** compared to the preorganised, multidentate compound **127**.

Table 3.1 Binding constants determined by ^{1}H NMR spectroscopic titrations in CD_3CN for compound **127**. All anions are used as TBA salts

Anion	**Log β_{HG}**
Host Dimer	Log β_{20} = 1.57(7)
Acetate	> 5
Chloride	Log β_{11} = 4.54(5) Log β_{21} = 8.01(8)
Bromide	Log β_{11} = 4.75(5) Log β_{21} = 8.10(7)
Iodide	Log β_{11} = 3.391(1) Log β_{21} = 6.120(8)
Nitrate	Log β_{11} = 4.55(2) Log β_{21} = 8.18(3)
Dihydrogen phosphate	Precipitate
Hydrogen sulfate	Precipitate

Where species are in the following equilibria:

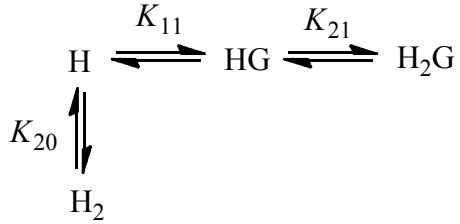

Binding constants are defined as:

$$K_{20} = \frac{[H_2]}{[H]} \qquad K_{11} = \frac{[HG]}{[H][G]} \qquad K_{21} = \frac{[H_2G]}{[H][HG]}$$

$$\text{Log}\,\beta_{20} = \text{Log}\,K_{20} \qquad \text{Log}\,\beta_{11} = \text{Log}\,K_{11}$$

$$\text{Log}\,\beta_{21} = \text{Log}\,K_{11} + \text{Log}\,K_{21}$$

H = Host, G = Guest

DFT calculations were used to further understand the binding mode of compound **127** and were performed in collaboration with Dr Martin Paterson at Heriot-Watt University. The complex geometry was optimised using a B3LYP/4-31G basis set on the host with the hydrogen atoms proximal to the anion augmented with additional s and p diffuse functions and a B3LYP/6-311+G* basis set on chloride and B3LYP/6-31+G* on acetate.[27]

The optimised 1:1 host:guest complex of **127** with chloride is shown in Figure 3.6. The complex shows C_{3v} symmetry with hydrogen bonding to the chloride by *o*- and *m*-quinolinium hydrogen atoms. The hydrogen bonding pattern suggested by the calculation matches the pattern of contact induced chemical shift changes observed using ^{1}H NMR spectroscopic titrations in solution. Acetate also binds strongly to the host. The non-spherical shape of the acetate means the optimised geometry consists of each of acetate's oxygen atoms hydrogen bonded to two quinolinium arms.

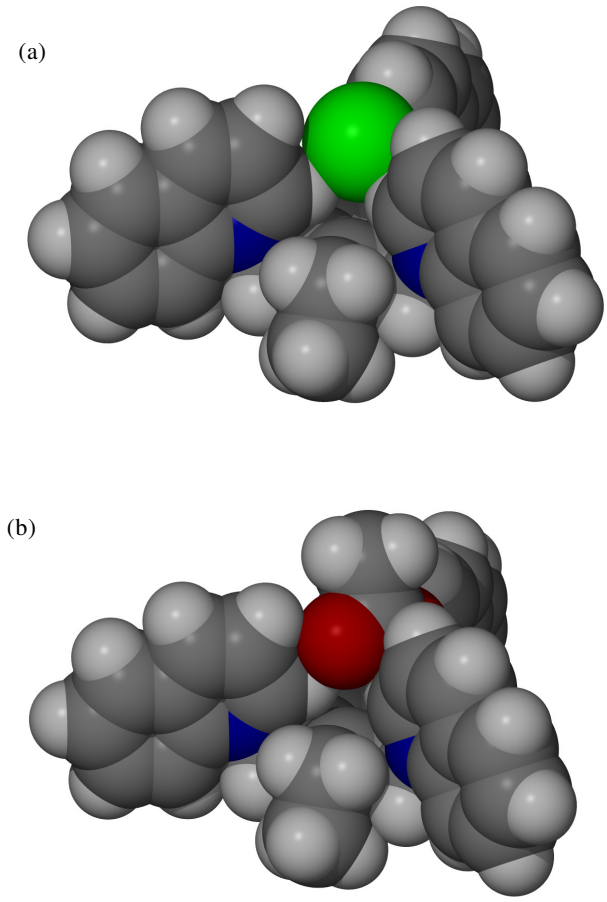

Figure 3.6 DFT optimised geometries for (a) **127** with chloride and (b) **127** with acetate

The binding equilibrium suggested by ^{1}H NMR titration data suggests a 2:1 host:guest complex. DFT calculations were used to further test the feasibility of this complex. Figure 3.7 shows the optimised geometry for the 2:1 host:chloride complex. The chloride is equidistant between the two cationic receptors and sits higher in the binding cavity than is observed for the 1:1 complex. At low basis sets the complex falls apart and is only stable using higher basis sets. This suggests that the interactions in the complex are weak, as would be expected given the electrostatic repulsion between the two hosts and the measured association may be enhanced by solvent interactions.

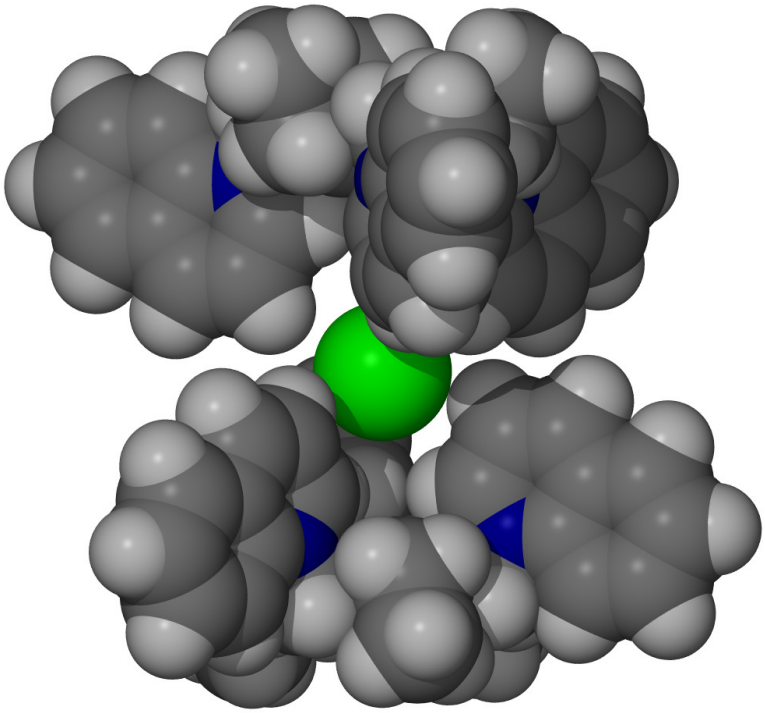

Figure 3.7 DFT optimised geometry for the 2:1 host:guest structure of **127** with chloride

3.4 Photophysical Properties

The absorbance and excitation spectra of **127** as the hexafluorophosphate salt are shown in Figure 3.8. Both spectra show the same λ_{max} of 317 nm (typical for compounds of this type) and the same overall band shape.[20,28-29] A broad featureless emission band is observed with a tail reaching to approximately 550 nm and a Stokes shift of 90 nm.

The fluorescent properties of compound **128**, used as a standard, were also investigated. The band shapes and λ_{max} of the absorbance, excitation and emission spectra, are identical to that of compound **127**.

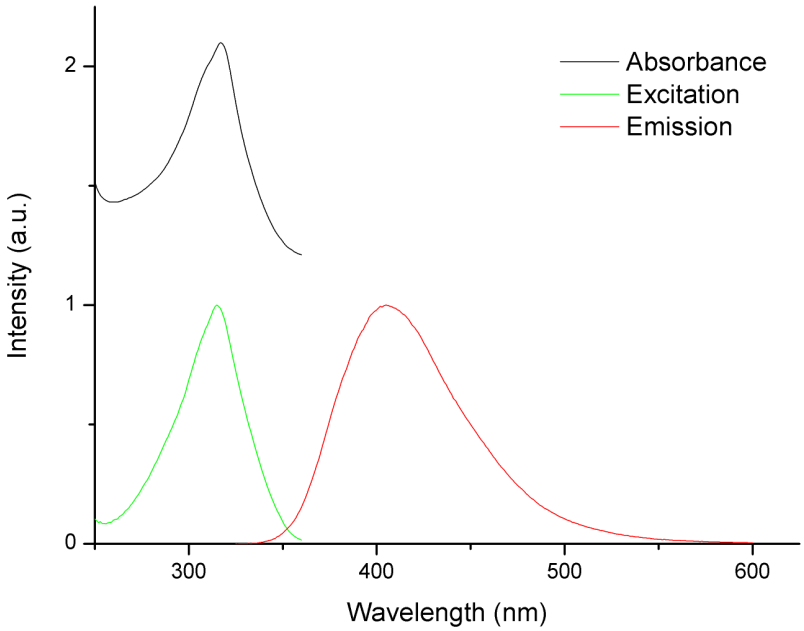

Figure 3.8 Absorbance, excitation and emission spectra of compound **127**. MeCN used as solvent, λ_{ex} = 317 nm, λ_{em} = 408 nm. Absorbance spectrum has been offset for clarity

Table 3.2 Summary of the photophysical data of **127** and **128** in MeCN

Compound	**127**	**128**
Absorbance λ_{max} /nm	317	317
Excitation λ_{max} /nm	317	317
Emission λ_{max} /nm	408	408
PLQY	0.21	0.09
Lifetime /ns	17.7 2.26	5.1 1.84
$E_{1/2}$ /V	-0.79	-0.84

The photoluminescent quantum yield (PLQY) of compounds **127** and **128** was calculated via an integration sphere methodology[30] to give a PLQY of 0.21 for compound **127** and a markedly lower value of 0.09 for compound **128**. Table 3.2 collates the important photophysical data of compound **127** and **128**. The effect of the addition of anions on the fluorescent emission of compound **127** was investigated using fluorescent spectroscopic titrations. Solutions of 2.33 x 10^{-6} mol dm^{-3} of host were titrated against the TBA-salts of chloride, bromide, iodide, nitrate and acetate. Figure

3.9 shows the quenching of the fluorescence emission observed with the addition of acetate and chloride.

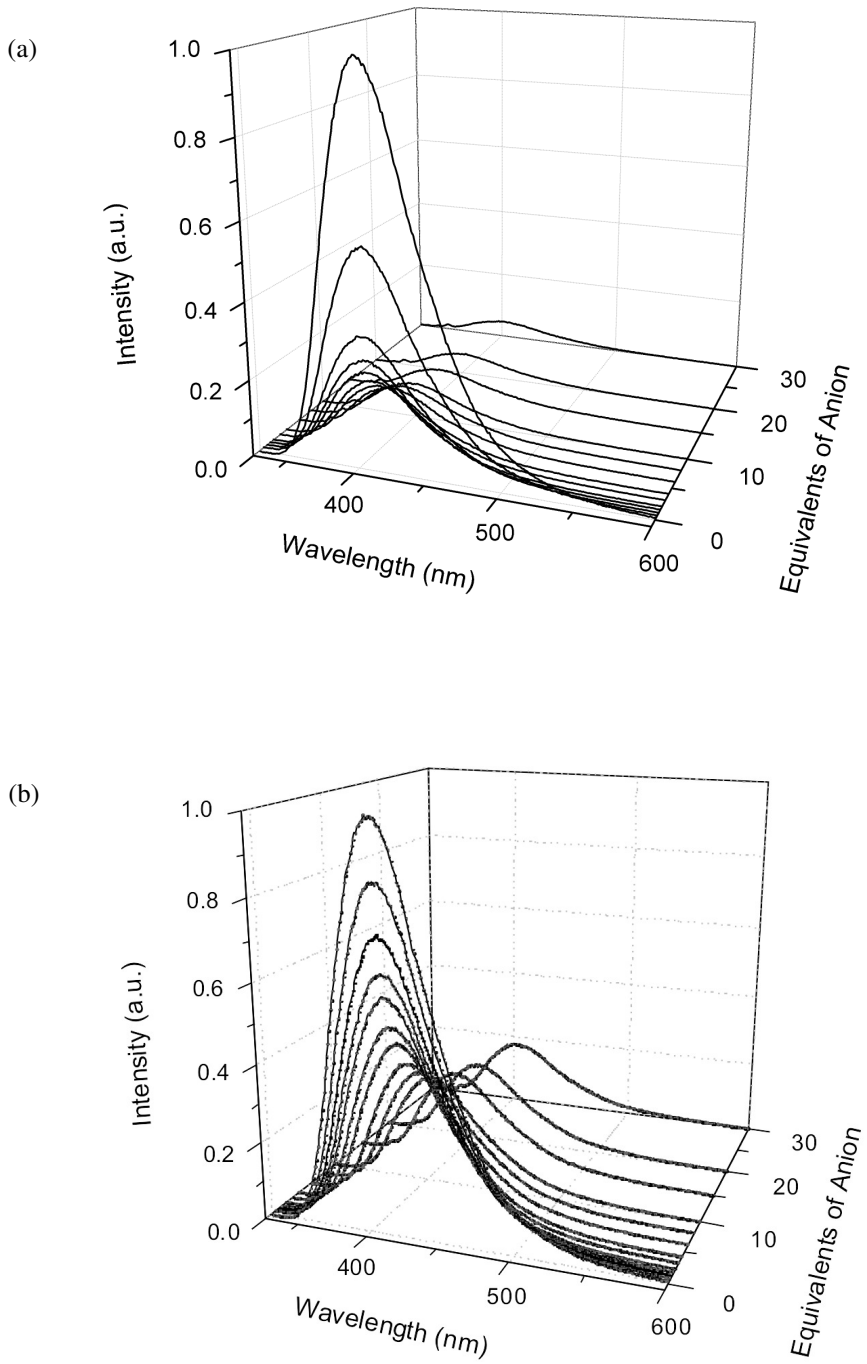

Figure 3.9 Fluorescence quenching of **127** (2.33 x 10^{-6} mol dm^{-3} in MeCN, λ_{ex} = 317 nm, λ_{em} = 408 nm) upon addition of (a) acetate, (b) chloride

This quenching is significant and can be observed with the naked eye, Figure 3.10.

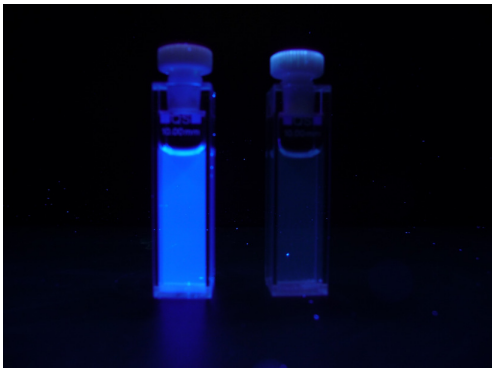

Figure 3.10 Compound **127** in MeCN in the absence (left) and presence of a large excess of acetate (right)

The quenching of fluorescence by a quencher is typically described by Stern-Volmer kinetics[20, 31] (Equation 3.1)

$$\frac{I_0}{I} = 1 + K_{SV}[Q]$$

$$K_{SV} = k_q \tau_0$$

Equation 3.1 Stern-Volmer equation. I_0 = initial intensity, I = intensity, K_{sv} = Stern-Volmer constant, Q = quencher, k_q = rate constant of quenching, τ_0 = initial fluorescence lifetime

The terms k_q and τ_0 are usually combined in the Stern-Volmer constant, K_{sv}. A plot of I_0/I against the concentration of quencher produces a Stern-Volmer plot with the gradient equal to K_{sv}. There are two basic forms of quenching mechanism, dynamic or collisional quenching, in which quenching occurs due to a collision between quencher and fluorophore, and static quenching in which an excited state fluorophore forms a non-fluorescent complex with the quencher (Figure 3.11). Both of these mechanisms can produce linear Stern-Volmer plots. Importantly static quenching does not lead to any change in the fluorescent lifetime in the presence of quencher. Conversely, dynamic quenching results in the reduction of the fluorescent intensity and the lifetime. The mechanisms can be differentiated by the use of UV-vis spectroscopy or lifetime measurements and will subsequently be discussed in more detail. More complicated

Stern-Volmer equations exist which allow for the modelling of both static and dynamic quenching together.

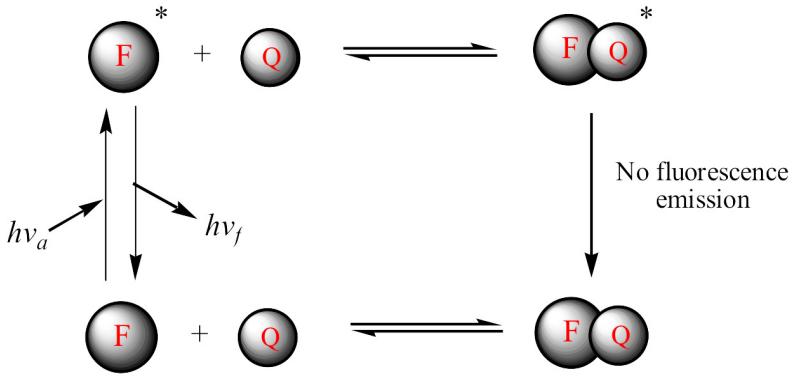

Figure 3.11 Summary of binding equilibria involved in static quenching. F = fluorophore, Q = quencher (figure concept from reference 20)

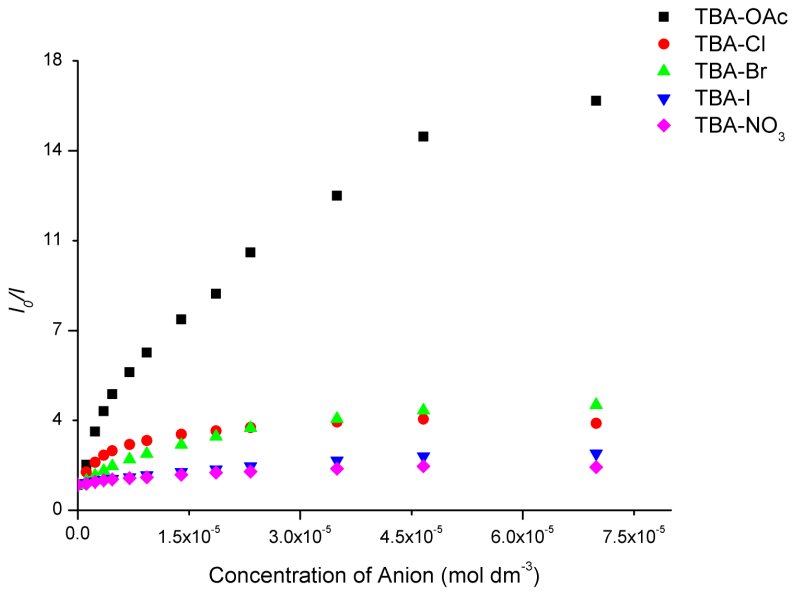

Figure 3.12 Stern-Volmer plot for compound **127** (2.33 x 10^{-6} mol dm^{-3} in MeCN, λ_{ex} = 317 nm, λ_{em} = 408 nm) with various anions

Stern-Volmer plots were created for the various anions titrated and have been corrected for dilution effects (Figure 3.12). Due to the complex nature of the binding equilibrium it is not possible to fit the data using standard Stern-Volmer equations, although the data is still useful in a qualitative sense. As can be seen from Figure 3.12, acetate is by far the best quencher at virtually all equivalents of guest, and it can therefore be concluded that the receptor is selective for acetate and discriminates this anion. This also

corresponds well to the strong binding of acetate by **127** shown by ^{1}H NMR spectroscopy. Interestingly, chloride is also a very good quencher, showing equal or better quenching than the heavier atom bromide (especially at low equivalents). Iodide on the other hand is much worse at quenching the fluorescence. This is the opposite selectivity observed for related published quinolinium based systems containing one fluorophore, which are dominated by the electron transfer properties of the anion in water.[32] A dynamic quenching mechanism has been suggested for these compounds that does not involve specific complex formation.[20] Thus the present preorganised anion receptor is apparently altering the ability of the quinolinium to discriminate particular anions by means of its fluorescence emission by specific binding effects, with strongly bound anions such as chloride quenching more than iodide.

The control compound **128** also shows quenching of its fluorescence upon addition of anions. A linear trend with anion concentration is observed in most cases (Figure 3.13). Table 3.3 contains the calculated K_{sv} values. Comparison of the K_{sv} values to the literature for similar systems shows compound **128** has much less variation in the K_{sv} than has previously been observed, although water was used in previous work instead of acetonitile.[20,28,33,29] This may be explained by binding processes of anions to **128,** supported by NMR experiments detailed previously, and which would not be as significant in water. The use of a less viscous solvent may, in part, also explain the observation.[32] Importantly, compound **127** shows significantly higher quenching and greater discrimination of anions than compound **128**.

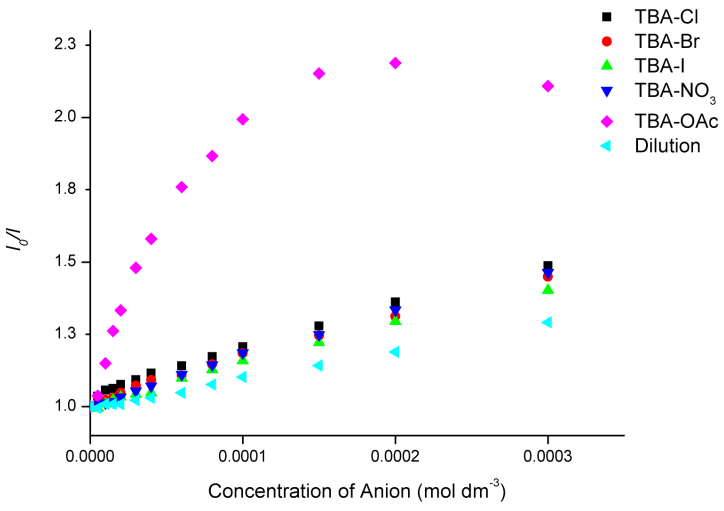

Figure 3.13 Stern-Volmer plot of compound **128** (1.0 x 10^{-5} mol dm^{-3} in MeCN) with various anions

Table 3.3 Stern-Volmer data for compound **128** in MeCN**.** Anions used as TBA salt

Anion	K_{SV} **/M^{-1}**
Chloride	570 ± 50
Bromide	490 ± 40
Iodide	410 ± 40
Nitrate	600 ± 40
Acetate	Non-linear

Stern-Volmer plots can be linear for static or dynamic quenching, showing deviations if mixtures of the two mechanisms are operating.[18,20] The Stern-Volmer plot for acetate quenching of **127** shows two principal regions – significant quenching up to 2 equivalents of anion followed by a shallower region which eventually begins to curve. Since the binding affinity is high, complexation is likely to be essentially complete after the addition of only a few equivalents of guest and hence the continued quenching up to a 30 fold excess of anion suggests that a collisional quenching mechanism is also operating. Fluorescence lifetime measurements and UV-vis spectroscopy were undertaken in order to determine the mechanism of quenching.

Figure 3.14 shows the UV absorbance spectrum of compound **127** with a λ_{max} of 317 nm in the absence of guest and in the presence of 10 equivalents of TBA-Cl with negligible dilution effects. There is an increase in the overall intensity of the band and a small shift in the λ_{max} (*ca.* 2 nm), suggesting the formation of a host-guest complex and static quenching, consistent with the ^{1}H NMR spectroscopic experiments. The same experiment was also performed on compound **128**. There is an overall decrease in the band intensity and no significant λ_{max} change, consistent with dilution effects only and dynamic quenching.

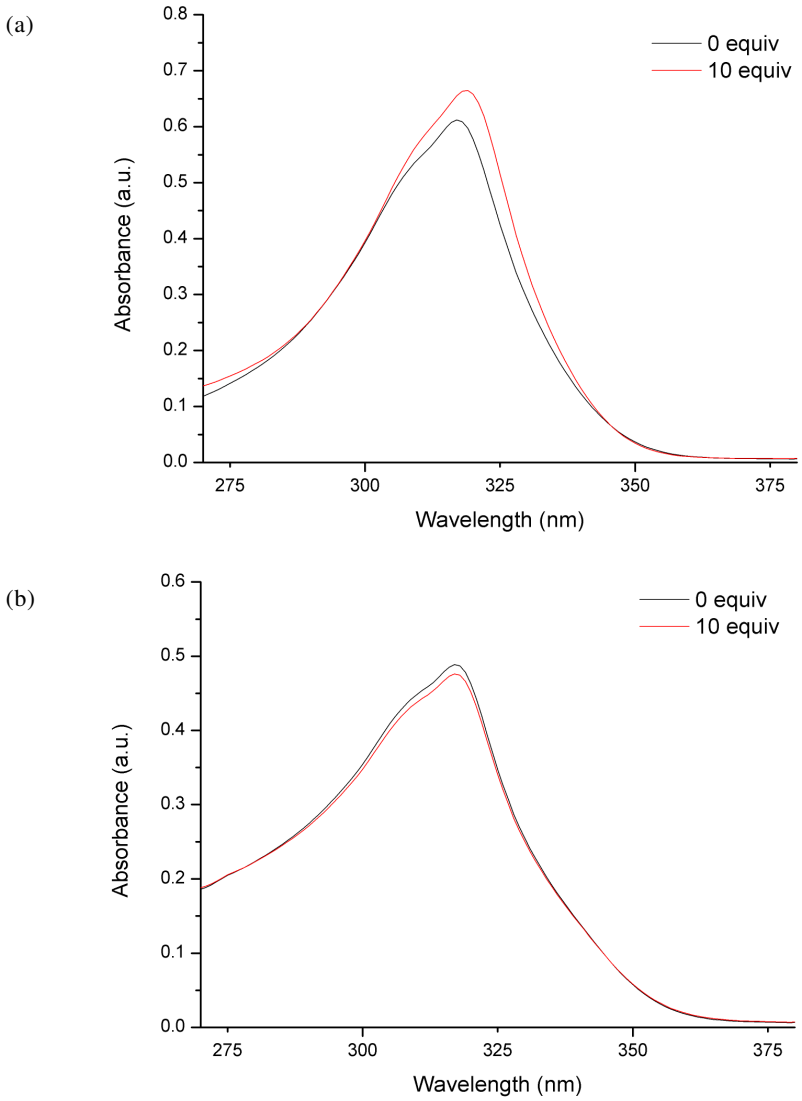

Figure 3.14 UV-vis spectra of (a) compound **127** and (b) compound **128** in the absence and presence of 10 equivalents of TBA-Cl in MeCN

A dilution study was also conducted on compound **127** in the absence of guest and is shown in Figure 3.15. The data shows a distinct non-linear trend and deviates from the Beer-Lambert law. The control compound **128** however shows a linear relationship between concentration and absorbance. This provides further evidence for the formation of a host dimer for **127**.

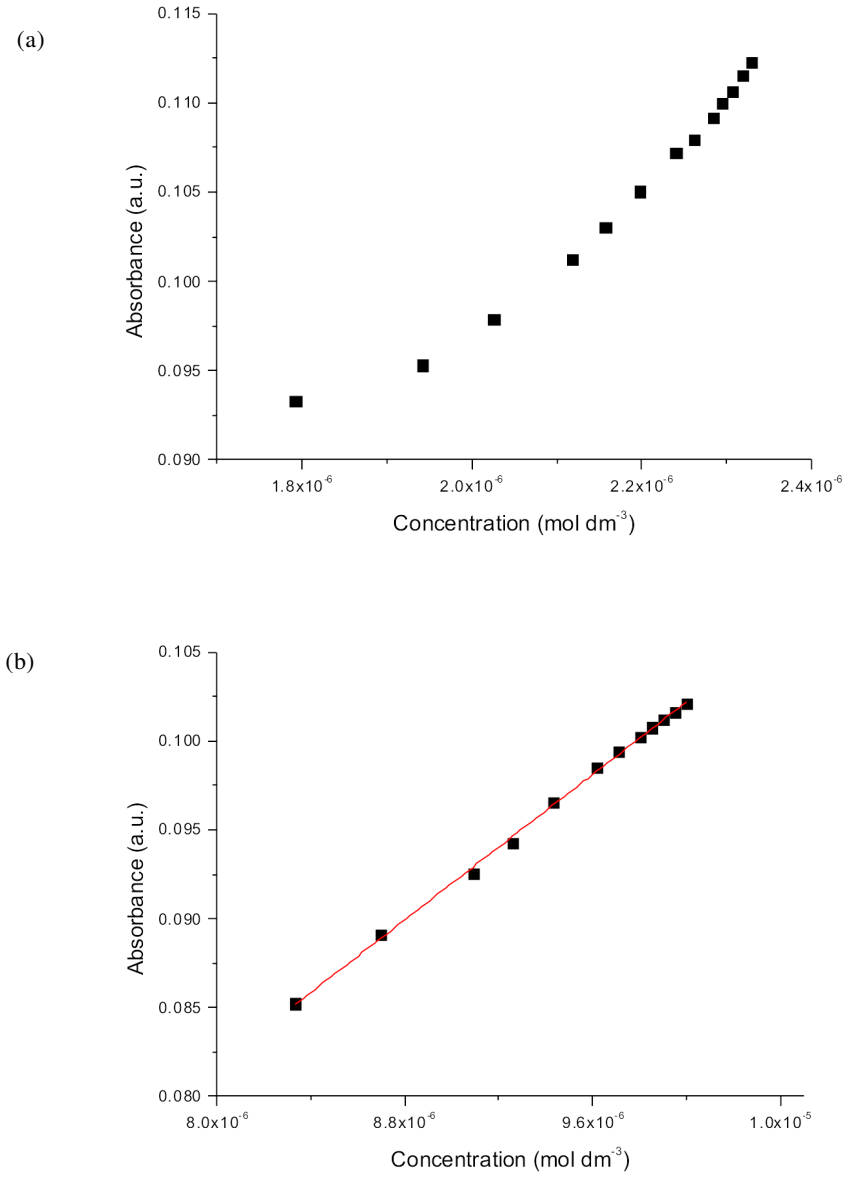

Figure. 3.15 UV-vis dilution study of (a) compound **127**, and (b) compound **128** in MeCN

A further method of distinguishing static from dynamic quenching is to investigate how the fluorescent lifetime of a species varies with added anion. In the case of static quenching the anion and the host form a non-fluorescent complex; it is therefore the unbound host which fluoresces and as it is not interacting with a quencher, its lifetime is unaffected. Dynamic quenching on the other hand involves the collisional quenching of the host's excited state.[20,31] As the concentration of quencher increases, the frequency of collisions between the host and the quencher increases. There is therefore less time between the formation of the host excited state and it being quenched by the anion.

Dynamic quenching therefore leads to a decrease in the fluorescent lifetime of the compound.

The emission from both compounds **127** and **128** show a bi-exponential decay, possibly suggesting complex emissive decay processes. Similar behaviour has been observed for related systems and is attributed to solvent relaxation processes that take place on the nanosecond timescale.[34,35-36] The fluorescent lifetimes of compound **127** were monitored at a range of anion concentrations for a range of anions. Figure 3.16 shows the logarithmic plot of the decay of the fluorescence at various equivalents of chloride. The decay becomes steeper, consistent with shorter lifetimes, and less linear as chloride concentration increases. In all cases a decrease in the excited state lifetime is observed and suggests that dynamic processes, in addition to static processes, contribute to the quenching of the fluorescence of compound **127**.

Similar experiments conducted on compound **128** also show a general decrease in the excited state lifetime of the compound in the presence of anion. It seems likely that, as with compound **127**, there is a mixture of dynamic and collisional quenching occurring for this system. ^{1}H NMR, UV-vis and fluorescence spectroscopic titrations suggest static quenching is the dominant process. The ^{1}H NMR data suggests static quenching may also play a role in the quenching of compound **128**, however dynamic quenching dominates.

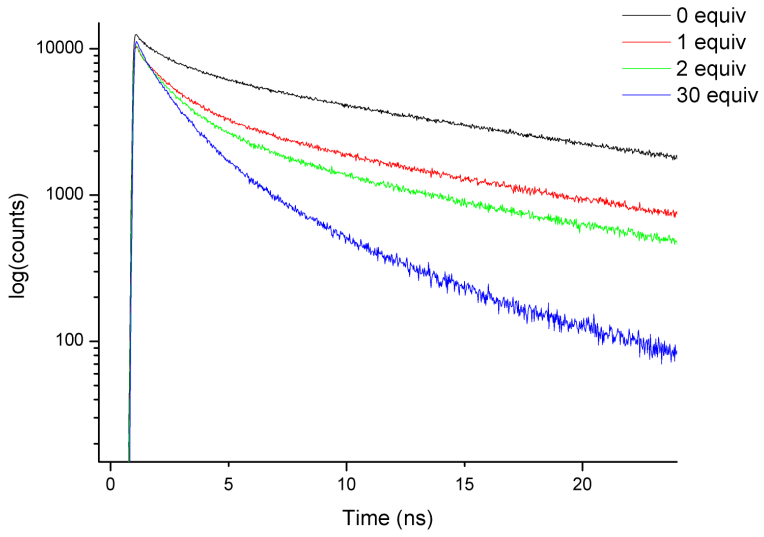

Figure 3.16 Logarithmic plot of the fluorescence decay of compound **127** at several equivalents of TBA-Cl (2.33 x 10^{-6} mol dm^{-3} in MeCN, λ_{ex} = 300 nm, λ_{em} = 408 nm)

3.5 Mechanism of Quenching

There are several possible quenching mechanisms for quinolinium based sensors including electron transfer from the anion,[37-39] charge-transfer complex or exciplex formation,[40-41] or heavy atom quenching.[42] Figure 3.17 shows a modified Jablonski diagram of the various photophysical processes which can occur for this system. Excited state relaxation can be achieved through either fluorescent emission, non-radiative decay or quenching by an anion. Electron transfer can occur from an anion, either by a static or collisional process, and fill the electron hole left in the HOMO. The excited state electron then relaxes by non-radiative means.

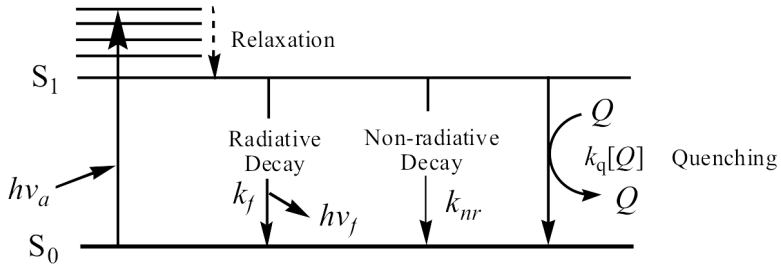

Figure 3.17 Modified Jablonski diagram showing the decay pathways for the quinolinium excited state (figure concept from reference 20)

Jayaraman *et al.*[32] have shown that the log k_q is linearly proportional to the indicated excited state reduction potential of the quinolinium species and the free energy change for charge transfer. In addition, the quenching rate decreases with increasing anion oxidation potential for dynamically quenched systems in water. They conclude therefore that the quenching mechanism is via a dynamic excited state charge transfer process.

Whilst a full scale mechanistic study for compounds **127** and **128** has not been undertaken, insights into the mechanism can be gained via simple experiments. An estimate of the excited state reduction potential (known as the indicated excited state reduction potential) for compound **127** and **128** can be calculated by $E_{red} + E_{0,0}$ where E_{red} is the reduction potential and $E_{0,0}$ is the singlet excitation energy. The $E_{1/2}$ potential may be used for the reduction potential and can be obtained by cyclic voltammetry (see Table 3.2).

The electrochemical behaviour of compound **127** was investigated using cyclic voltammetry in a 0.1 mol dm^{-3} solution of TBA-PF_6 in MeCN (Figure 3.18). The compound has a reduction potential of -0.79 V vs SCE at 100 mV s^{-1}. The compound appears to exhibit an ECE mechanism, whereby an electrochemical reduction occurs, followed by a chemical reaction to another electrochemically active species, which is then oxidised (with an E_{pc} of 0.04 V vs. SCE at 100 mV s^{-1}). No further electrochemical responses are observed.

The -0.79 V redox event appears to be largely irreversible with the $E_{1/2}$ increasing with scan rate. The ΔE is also large at 110 mV and the I_{pa}/I_{pc} is very much less than 1 and is not improved with increased scan rate. The peak at 0.04 V only appears after the compound has been reduced and indicates it is a decay product from the reduction of compound **127**. The peak also increases with scan rate and appears to be irreversible.

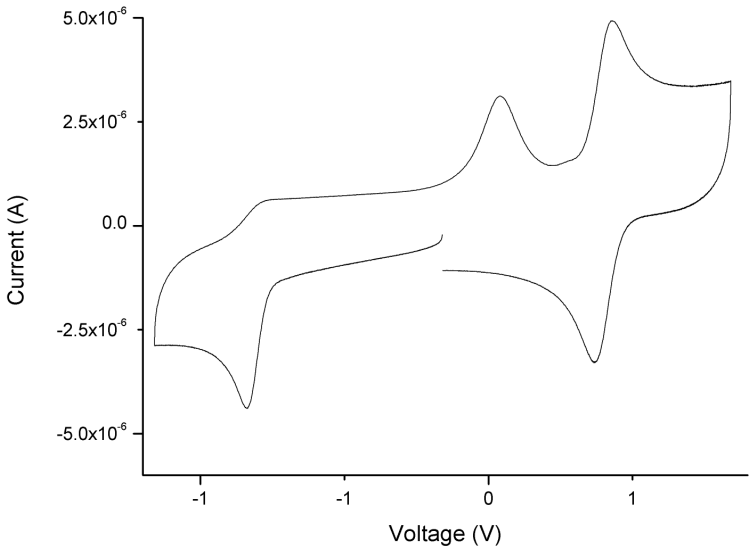

Figure 3.18 Cyclic voltammogram of compound **127** measured at a scan rate of 100 mV s^{-1} in 0.1 mol dm^{-3} TBA-PF_6 in Me CN. Fc/Fc^+ internal reference at 0.4 V

Compound **128** shows identical electrochemical behaviour with a slightly more cathodic $E_{1/2}$ of -0.84 V vs SCE at 100 mV s^{-1}. Again irreversible behaviour is observed. An anodic wave is also observed at 0.1 V vs SCE at 100 mV s^{-1}.

Both compounds **127** and **128** have the same singlet excitation energy of 3.90 eV (the maximum absorbance energy converted to eV) and therefore give an indicated excited state reduction potential of 3.11 V and 3.06 V for compound **127** and **128**, respectively. This is exactly the same as that observed for methyl quinolinium.[32] Given the very similar excited state reduction potentials for compounds **127** and **128** to that of methyl quinolinium, which is known to be quenched by charge transfer processes, it is logical to assume that this mechanism also occurs for compounds **127** and **128**. However further experiments would be required to confirm this.

3.6 Fluorescent Spectroscopic Titrations in Water

An interesting property of the compound **127** is that it is soluble in water. This raises the question of how this compound behaves in water and if it is suitable for biological or environmental applications. Fluorescent spectroscopic titrations were carried out in high purity water titrating with the sodium salts of the appropriate anion. Figure 3.19 shows the spectra obtained for chloride. Whilst there is a decrease in fluorescence intensity, this is almost entirely due to dilution, determined from a control dilution experiment. There is no significant quenching with any anion tested.

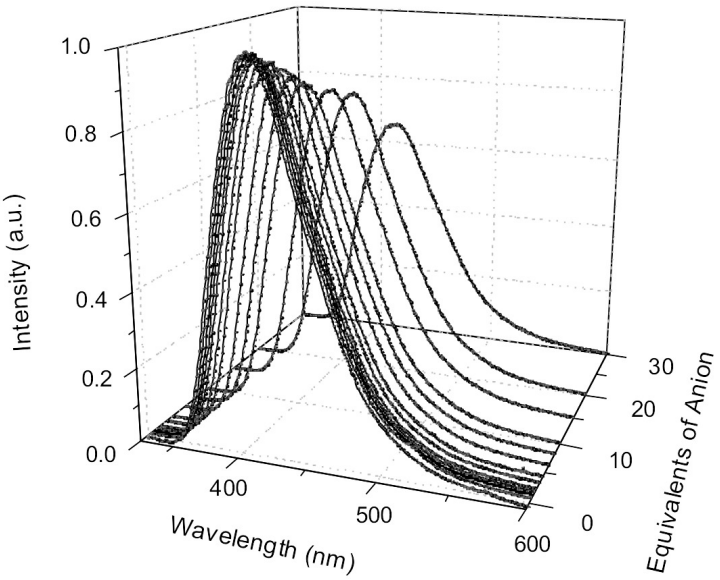

Figure 3.19 Emission spectrum of compound **127** (2.33 x 10^{-6} mol dm^{-3}, λ_{ex} = 317 nm, λ_{em} = 408 nm) in H_2O with increasing amounts of NaCl

It is likely the lack of quenching by anions in water is due to the increase in competition for binding the anion, both from the water and the sodium counter-ion. To prove this hypothesis, the ^{1}H NMR spectrum of compound **127** in D_2O was recorded with different equivalents of NaCl present and shows no significant change in any of the host proton resonances up to the addition of three equivalents of NaCl, although larger chemical shifts may be observed at much higher equivalents of guest. This is in contrast to the large shifts observed in acetonitrile, with no significant shifting above one equivalent. Polar aprotic solvents such as DMSO also proved too competitive for effective anion binding.

3.7 Attempted Synthesis of Quinolinium Based Tripods

In an attempt to further tune the binding properties of quinolinium tripods, several additional binding arms were synthesised and are summarised in Scheme 3.3.

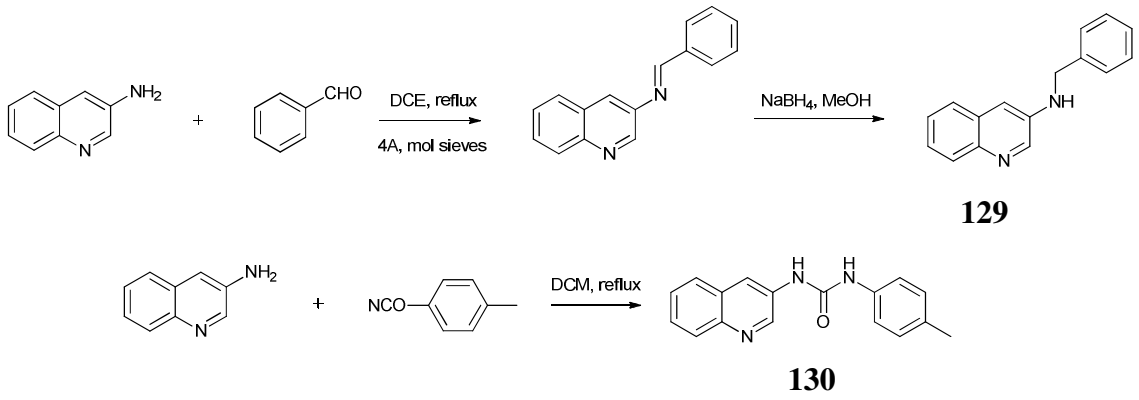

Scheme 3.3 Synthesis of compounds **129** and **130**

Two binding arms, *N*-benzylquinolin-3-amine (**129**) and 1-(quinolin-3-yl)-3-*p*-tolylurea (**130**), both derived from 3-aminoquinoline, have been synthesised. Both designs are based around previously reported compounds.[5, 43] The addition of amine and urea functionality increases the hydrogen bonding capability of the binding arm.

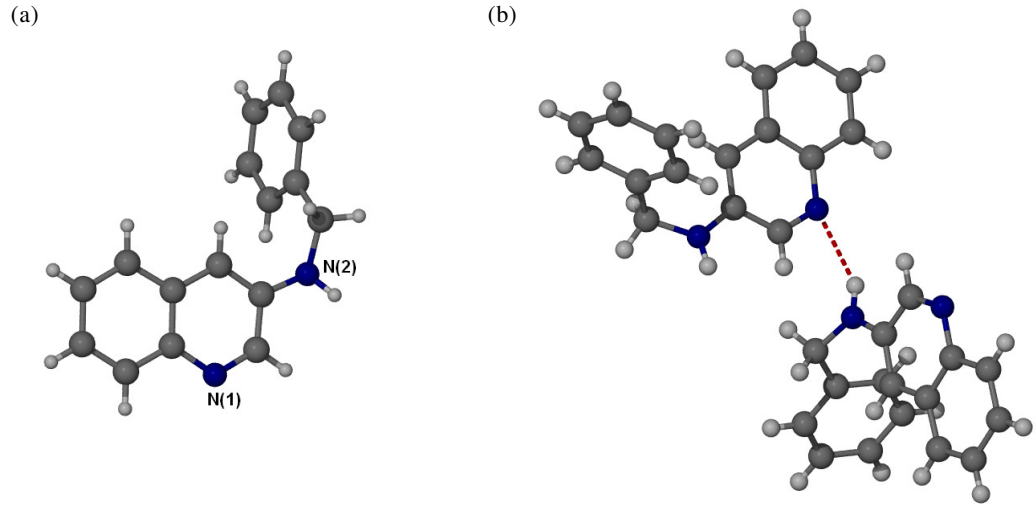

Figure 3.20 (a) Molecular structure of compound **129**, (b) Hydrogen bonding in crystal, the N(1)… N(2) distance is 3.140(5) Å.

The molecular structure of compound **129,** has been obtained and is shown in Figure 3.20. The crystal packing exhibits N(1)...H(2N) hydrogen bonds (see Figure 3.20). The N(2)...N(1) distance is 3.140(5)Å. No π-stacking interactions are apparent.

During the reaction of compound **130** with the 1,3,5-triethyl-2,4,6-(bromomethyl)benzene, an orange crystalline solid precipitated. X-ray crystallographic investigation revealed the crystal structure to be a co-crystal between a protonated quinolinium and a quinoline with a bromide counter ion. The asymmetric unit is shown in the usual colouration, whilst the symmetry generated molecule is shown in an all blue colour (see Figure. 3.21). The protonated quinolinium and the quinoline nitrogen share a hydrogen bond, whilst the respective urea groups hydrogen bond to the bromide counter-ion. The proton was disordered over the N(3) and N(6) atoms and could not be refined, however a proton has been added to Figure 3.21 for clarity.

The proposed mechanism for this reaction involves deprotonation of a methanol solvent molecule, followed by nucleophilic attack of the MeO^- to an Ar-CH_2-Br bond generating Ar-CH_2-OMe and Br^-. Crystallisation can then occur with unreacted **130** and bromide.

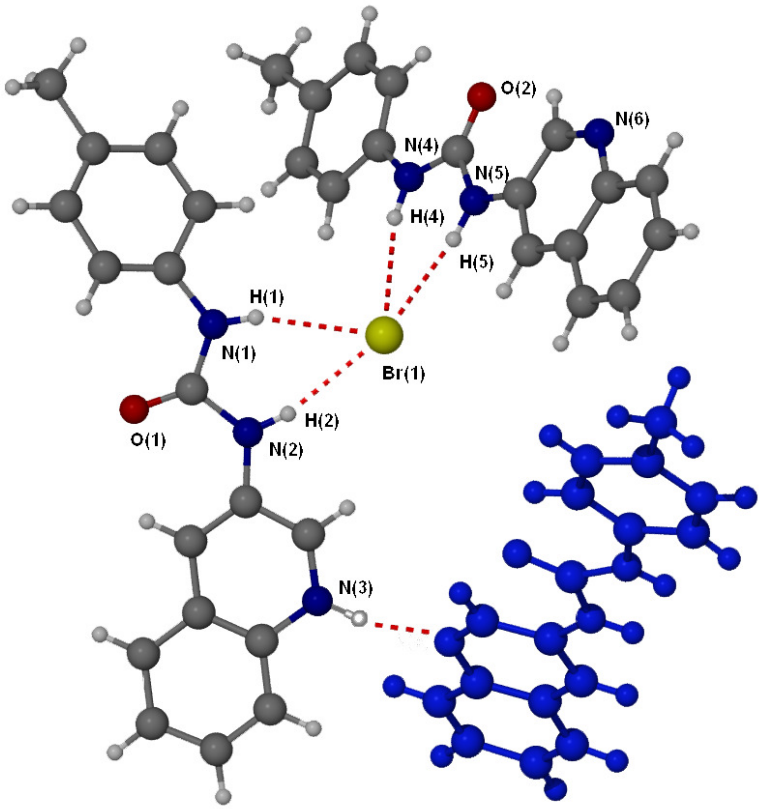

Figure 3.21 Packing diagram from compound **130**. Symmetry generated molecule is shown in blue, *N*-quinolinium hydrogen atom was not located, however it is added into the diagram for clarity

The reaction of compound **129** with the 1,3,5-triethyl-2,4,6-(bromomethyl)benzene was also problematic. Heating at reflux in dichloromethane (DCM) or 1,2-dichloroethane (DCE) for 48 hours did result in a yellow/green compound, which was highly fluorescent under long wave UV light. However, the ^{1}H NMR spectrum was significantly broadened (Figure 3.22). This would indicate that at room temperature the conformational exchange is slow compared to related compounds.[5] In addition MALDI^{+} mass spectrometry revealed the presence of the two armed product, which proved impossible to separate from the three arm product and may explain some of the complexity of the NMR spectrum.

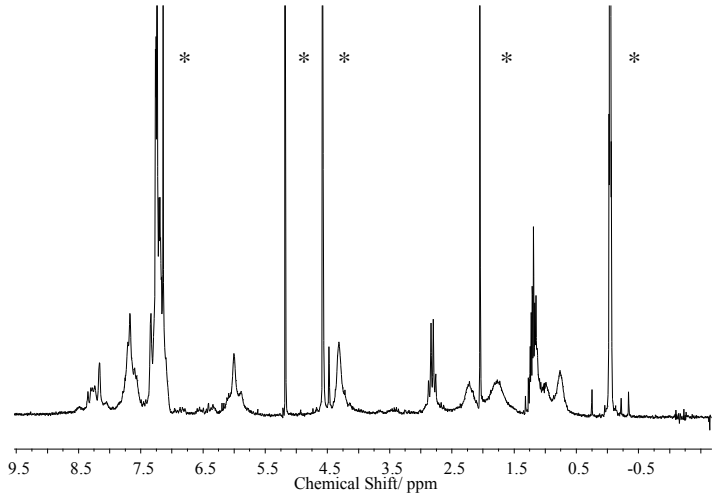

Figure. 3.22 ^{1}H NMR spectra of the crude reaction mixture of the 1,3,5-triethyl-2,4,6-(bromomethyl)benzene and compound **129**. * indicate residual solvent resonances and impurities

In order to simplify the receptor design, 3-aminoquinoline was reacted with the 1,3,5-triethyl-2,4,6-(bromomethyl)benzene. It was hoped that 3-aminoquinoline would not be significantly more sterically demanding than quinoline, but again reflux with DCE for 72 hours, even with catalytic quantities of TBA-I, could not cause the reaction to go to completion and with significant quantities of the partially substituted bis(quinolinium) product. Further investigation into this class of compounds was not completed.

3.8 Conclusions

It has been shown that a tripodal anion receptor (**127**) binds anions via charge assisted hydrogen bonding, with complicated speciation consisting of an unbound host, a host dimer, and both 1:1 and 2:1 host:guest complexes. The fluorescence of the quinolinium groups can be used as an anion sensing reporter, with quenching occurring in the presence of anions. Crucially the preorganised, tripodal receptor **127** exhibits a different quenching selectivity to simple quinolinium derivatives. A mixture of static and dynamic quenching was observed, with selectivity for acetate. In the case of the preorganised compound **127** static quenching dominates, however for compound **128** dynamic quenching dominates. The mechanism of quenching has provisionally been assigned via the formation of a charge transfer complex.

3.9 Experimental

Instrumentation

All NMR spectra were performed on a Varian Mercury-400 (400 MHz for ^{1}H), Varian Inova-500 machine (500 MHz for ^{1}H, 126 Hz for ^{13}C) or a Varian DD-700 (700 MHz for ^{1}H, 176 MHz for ^{13}C) and were referenced to residual solvent. Electrospray (ES) mass spectrometry was recorded on a Thermo-Finnigan LTQ instrument, whilst Matrix Assisted Laser Desorption Ionisation (MALDI) experiments were recorded on an ABI Voyager-DC STR. Fourier transform infrared spectra were recorded with a Perkin Elmer Spectrum 100 ATR instrument (Perkin-Elmer). For each spectrum, 64 scans were conducted over a spectral range of 4000 to 600 cm^{-1} with a resolution of 4 cm^{-1}. The analysis was carried out with the Spectrum Express 1.01 software. Elemental analysis was performed using an Exeter Analytical inc. CE-400 Elemental Analyser. Commercial reagents were used as supplied, without further purification. 1,3,5-Tri(bromomethyl)-2,4,6-triethylbenzene was prepared as previously reported.[44]

General Procedure for ^{1}H NMR Spectroscopic Titrations

All chemical shifts are reported in ppm relative to residual solvent. A solution of the host species of known concentration typically 0.5-1.5mM, was made up in an NMR tube using the appropriate deuterated solvent (0.5 ml). Solutions of the anions, as TBA salts (1 ml) were made ten times the concentration of the host solution. The guest solution was typically added in 10 μl aliquots, representing 0.1 equivalents of the guest with respect to the host. Larger aliquots were used in some cases where no inflection of the trace was evident. Spectra were recorded after each addition and the trace was followed simultaneously. Results were analysed using the curve-fitting program *HypNMR* 2006.[26]

General Procedure for UV-vis Spectroscopic Titrations

UV-vis titrations were carried out using a Perkin-Elmer Lambda 35. A solution of typical concentration 1.0×10^{-4} $moldm^{-3}$ of host was made in a volumetric flask. A 3 ml sample of host solution of concentration of 2.33×10^{-6} mol dm^{-3} for **127** and 1.0×10^{-5} mol dm^{-3} for **128** were prepared by dilution of the stock solution. Guest solutions were

prepared such that 300 μl of guest solution corresponds to 10 equivalents of host. Solutions were prepared using acetonitrile as solvent.

Fluorescence Spectroscopy

Emission and excitation spectra were obtained using a Jobin-Yvon Horiba Fluorolog 3-22 Tau-3 spectrofluorimeter with a right angle illumination method and were corrected for the spectral response of the instrument.

Fluorescence spectroscopic titrations were carried out using the equipment described above. A solution of concentration 1.0 x 10^{-4} mol dm^{-3} of host was made in a volumetric flask. A 3 ml sample of host solution of typical concentration 2.33 x 10^{-6} mol dm^{-3} for **127** and 1.0 x 10^{-5} mol dm^{-3} for **128** was prepared by dilution of the stock solution. Guest solutions were prepared such that 300 μl of guest solution corresponds to 10 equivalents of host. Solutions were prepared using acetonitrile as solvent.

Photoluminescent quantum yields were calculated using a Jobin-Yvon Horiba Fluorolog 3-22 Tau-3 spectrofluorimeter with a right angle illumination method and an intergration sphere, following the intergration sphere method of Beeby *et al.*[30]

Lifetimes were obtained via the time-correlated single-photon counting technique. The method described by Beeby *et al.*[45] was used. Samples were excited using the third harmonic of mode-locked cavity dumped Ti-sapphire laser. The emission was collected at 90° to the source of excitation and the emission wavelength selected by a monochromator (Jobin Yvon Triax 190). Fluorescence detection was obtained using a single photon avalanche diode (ID-Quantique ID-100) that was linked to a time-to-amplitude converter (Ortec 567) and a pulse height analyser, PHA, (E.G. & G. Trump Card and Maestro for Windows v 5.10). Fluorescence decays were recorded to a minimum of 10,000 counts in the peak channel of the PHA with a record length of 1000 channels. The decay and IRF data were transferred to PC for analysis in Microsoft Excel via the method of iterative reconvolution and nonlinear least squares fitting.

General Procedure for Cyclic Voltammetry Experiments

Cyclic voltammetry was carried out on a Chi Instruments Model 420 Electrochemical Analyser with a three electrode cell using two Pt wire counter electrodes and a 2 mm Pt working electrode or a 3 mm glassy carbon working electrode. The ferrocene/ferrocinium redox couple was used as an internal reference. $E_{1/2}$ values are reported vs. SCE (Fc = 0.4 V with TBA-PF_6 in MeCN).[46] A 0.1 mol dm^{-3} solution of TBA-PF_6 in dry MeCN was used as electrolyte. Solutions were degassed by bubbling through N_2 and the cell was kept under positive pressure of N_2 at all times.

Synthesis of 127

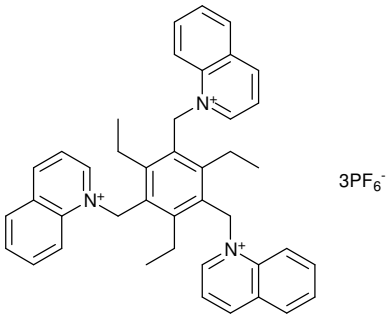

1,3,5-Tri(bromomethyl)-2,4,6-triethylbenzene (0.50 g, 1.1 mmol) and quinoline (0.51 g, 4.0 mmol) were dissolved in dry dichloromethane and heated at reflux for 24 hours. The solvent was evaporated and 50 ml of methanol was added to the residue. Ten equivalents of NH_4PF_6 were added and the product was precipitated as the PF_6^- salt. Yield = 0.28 g, 0.27 mmol, 24 %. m.p. 210 - 222 ^oC; ^1H NMR (CD_3CN, 700 MHz /ppm) δ = 9.18 (3H, d, *J* = 8.7 Hz, ArH), 8.77 (3H, d, *J* = 7.8 Hz, ArH), 8.74 (3H, d, *J* = 6.0 Hz, ArH), 8.47 (3H, d, *J* = 7.8 Hz, ArH), 8.40 (3H, t, *J* = 7.8 Hz, ArH), 8.13 (3H, t, *J* = 7.8 Hz, ArH), 8.1 (3H, dd, *J* = 8.7 and 6.0 Hz, ArH), 6.13 (6H, s, C*H*$_2$-Br), 2.43 (6H, br q, C*H*$_2$CH$_3$), 1.16 (9H, br t, CH$_2$C*H*$_3$); ^{13}C-{^1H} NMR (CD_3CN, 176 MHz /ppm) δ = 151.9, 148.5, 145.8, 139.3, 136.6, 131.3, 130.9, 130.6, 127.9, 122.5, 118.7, 54.0, 24.1, 14.6; ν/cm^{-1} 3096 (C-H), 2972 (C-H), 1625 (Ar C=C), 1591 (Ar C=C), 1524 (Ar C=C), 1377, 1229, 987, 817; Found: C, 45.39; H, 4.44; N, 3.74. Calc. for $C_{42}H_{42}F_{18}N_3P_3.5H_2O$: C, 45.29; H, 4.71; N, 3.77; the presents of water is suggested by NMR and IR spectra. Mass spectrometry could not be obtained for this compound.

Crystal data for compound **127**: $C_{42}H_{42}F_{18}N_3P_3$, M = 1023.70, 0.10 x 0.05 x 0.05 mm^3, monoclinic, space group $P2_1/n$ (No. 14), a = 9.682(5), b = 39.51(2), c = 21.136(12) Å, β = 90.961(7)°, V = 8084(7) Å^3, Z = 8, D_c = 1.682 g/cm^3, F_{000} = 4176, I19, Diamond synchrotron radiation, λ = 0.68890 Å, T = 120(2)K, $2\theta_{max}$ = 42.5º, 47477 reflections collected, 9862 unique (R_{int} = 0.0575). Final *GooF* = 6.197, *R1* = 0.4251, *wR2* = 0.7626, R indices based on 5441 reflections with I >2σ(I) (refinement on F^2), 312 parameters, 24 restraints. Lp and absorption corrections applied, μ = 0.270 mm^{-1}.

Synthesis of 128

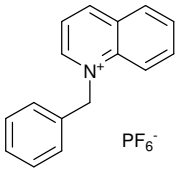

Quinoline (0.50 g, 3.9 mmol) was dissolved in dichloromethane (60 ml). Benzyl bromide was added (3.3 g, 19 mmol) and the solution heated at reflux for 24 hours. The solvent was removed *in vacuo* resulting in a white powder. The powder was washed with diethyl ether then dissolved in methanol. Excess (1.50 g) NH_4PF_6 was added and a white powder precipitated out of solution slowly. The powder was isolated by filtration, washed with diethyl ether and dried under ambient conditions. Yield = 1.16 g, 3.2 mmol, 82%. m.p. 140 - 146 °C; ^{1}H NMR (CD_3CN, 700 MHz /ppm) δ = 9.17 (2H, m, QuinH), 8.39 (1H, d, J = 8.5 Hz, QuinH), 8.34 (1H, d, J = 9.6 Hz, QuinH), 8.16 (1H, m, QuinH), 8.08 (1H, dd, J = 9.0, 6.4 Hz, QuinH), 7.99 (1H, d, J = 7.3 Hz, QuinH), 7.43 (3H, m, ArH), 7.31 (2H, m, ArH), 6.17 (2H, s, CH_2-Br); ^{13}C-{^{1}H} NMR (CD_3CN, 176 MHz /ppm) δ = 150.4, 149.6, 139.4, 137.2, 133.7, 132.0, 131.5, 131.4, 130.4, 130.4, 128.7, 123.2, 119.9, 62.0; *m/z* (ES$^+$) 220.1 [M-PF_6]$^+$; ν/cm^{-1} 3097 (C-H), 1627 (Ar C=C), 1590 (Ar C=C), 1528 (Ar C=C), 1456, 1379, 1361, 1045, 817. Found: C, 51.65; H, 3.85; N, 3.91; Calc. for $C_{16}H_{14}F_6NP.0.3H_2O$: C, 51.85; H, 3.97; N, 3.78; the presence of water is suggested by NMR and IR spectra.

Crystal data for compound **128**: $C_{16}H_{14}F_6NP$, M = 365.25, colourless plate, 0.20 × 0.20 × 0.20 mm^3, monoclinic, space group $P2_1/c$ (No. 14), a = 9.7798(3), b = 11.4208(3), c =

15.9407(5) Å, β = 122.2150(10)°, V = 1506.37(8) Å^3, Z = 4, D_c = 1.611 g/cm^3, F_{000} = 744, MoKα radiation, λ = 0.71073 Å, T = 120(2)K, $2\theta_{max}$ = 58.3º, 25074 reflections collected, 4060 unique (R_{int} = 0.0923). Final *GooF* = 0.995, *R1* = 0.0455, *wR2* = 0.0878, *R* indices based on 2396 reflections with I >2σ(I) (refinement on F^2), 217 parameters, 0 restraints. Lp and absorption corrections applied, μ = 0.247 mm^{-1}.

Synthesis of *N*-Benzylquinolin-3-amine (129)

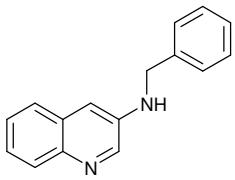

3-Aminoquinoline (1.00 g, 6.3 mmol) and benzaldehyde (0.74 g, 6.9 mmol) were dissolved in 80 ml of 1,2-dichloroethane and heated at reflux for 24 hours in the presence of 4Å molecular sieves. After this time the molecular sieves were filtered off and the solvent removed *in vacuo*. The residue was redissolved in methanol (70 ml) and $NaBH_4$ (1.95 g, 69 mmol) was added slowly. The reaction was stirred at room temperature for 2 hours, after which HCl (37%) was added slowly until the solution was at approximately pH 5. 2M NaOH was the added until a clear solution appeared (approximately pH 9). The aqueous solution was extracted with dichloromethane (3 x 50 ml), the organic extracts combined and dried with $MgSO_4$. The solution was filtered and the solvent removed *in vacuo*. The residue was dissolved in ether and unreacted starting material removed by filtration. The ether was allowed to evaporate leaving colourless plate like crystals. Yield = 1.12 g, 4.8 mmol, 76%. m.p. 60 - 64 ^oC; ^1H NMR ($CDCl_3$, 700 MHz /ppm) δ = 8.48 (1H, d, J = 2.9 Hz, QuinH), 7.94 (1H, dd, J = 6.3 and 3.6 Hz, QuinH), 7.57 (1H, dd, J = 6.3 and 3.6 Hz, QuinH), 7.41-7.35 (6H, m, ArH), 7.30 (1H, t, J = 7.4 Hz, ArH), 7.01 (1H, d, J = 2.9 Hz, QuinH), 4.42 (3H, s, NH+CH_2); ^{13}C-{^1H} NMR ($CDCl_3$, 126 MHz /ppm) δ = 143.2, 142.2, 141.3, 138.2, 129.4, 129.0, 128.8, 127.6, 127.5, 126.9, 126.0, 125.0, 110.4, 47.9; *m/z* (ES^+) 235.2 $[M+H]^+$, 236.3, 239.3; ν/cm^{-1} 3301 (N-H), 3150, 1606 (N-H bend), 1492, 1346, 1288, 1218; Found: C, 81.73; H, 5.95; N, 11.93; Calc. for $C_{16}H_{14}N_2$: C, 82.02; H, 6.02; N, 11.96.

Crystal data for compound **129**: $C_{16}H_{14}N_2$, M = 234.29, 0.30 × 0.20 × 0.10 mm^3, monoclinic, space group $P2_1/n$ (No. 14), a = 12.3367(4), b = 6.0856(2), c = 17.1948(5) Å, β = 103.3820(10)°, V = 1255.87(7) Å^3, Z = 4, D_c = 1.239 g/cm^3, F_{000} = 496, MoKα radiation, λ = 0.71073 Å, T = 120(2)K, $2\theta_{max}$ = 55.0º, 11037 reflections collected, 2887 unique (R_{int} = 0.0319). Final *GooF* = 1.063, *R1* = 0.0697, *wR2* = 0.1866, *R* indices based on 2150 reflections with I >2σ(I) (refinement on F^2), 74 parameters, 0 restraints. Lp and absorption corrections applied, μ = 0.074 mm^{-1}.

Synthesis of 1-(Quinolin-3-yl)-3-p-tolylurea (130)

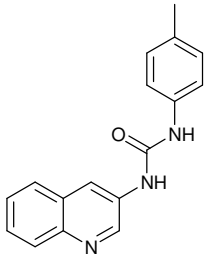

3-Aminoquinoline (1.00 g, 6.3 mmol) and *p*-tolyl isocyanate (0.923 g, 6.9 mmol) were dissolved in 100 ml of dry dichloromethane (DCM) and heated at reflux for 24 hours. The product precipitated from solution, was filtered and washed with DCM and allowed to dry under ambient conditions. Yield = 1.66 g, 5.4 mmol, 86%. m.p. 246 - 256 ^{o}C; ^{1}H NMR (CD_3CN, 500 MHz /ppm) δ = 9.05 (1H, s, NH), 8.79 (1H, d, J = 2.5 Hz, QuinH), 8.76 (1H, s, NH), 8.49 (1H, d, J = 2.5 Hz, QuinH), 7.90 (1H, d, J = 8.2 Hz, QuinH), 7.86 (1H, d, J = 8.2 Hz, QuinH), 7.56 (1H, td, J = 7.6 and 1.5 Hz, QuinH), 7.52 (1H, td, J = 7.6 and 1.1 Hz, QuinH), 7.36 (2H, d, J = 8.3 Hz, ArH), 7.09 (2H, d, J = 8.3 Hz, ArH), 2.23 (3H, s, CH_3); ^{13}C-{^{1}H} NMR (CD_3CN, 126 MHz /ppm) δ = 153.2, 144.7, 144.0, 137.3, 134.1, 131.5, 129.7, 129.0, 128.6, 127.8, 127.5, 127.4, 120.6, 119.0, 20.8; *m/z* (ES$^+$) 278.2 [M+H]$^+$, 279.2, 554.7, 853.5; ν/cm^{-1} 3340 (urea N-H), 3013 (C-H), 2914 (C-H), 1710 (urea C=O), 1591, 1511, 1224, 1190, 899; Found: C, 73.46; H, 5.48; N, 15.18; Calc. for $C_{17}H_{15}N_3O$: C, 73.63: H, 5.45; N, 15.15.

Crystal data for compound 130: $C_{34}H_{31}BrN_6O_2$, M = 635.56, yellow needle, 0.20 × 0.10 × 0.05 mm^3, monoclinic, space group $P2_1/c$ (No. 14), a = 7.3056(17), b = 16.967(4), c = 24.388(5) Å, β = 99.347(10)°, V = 2982.9(12) Å^3, Z = 4, D_c = 1.415 g/cm^3, F_{000} = 1312,

SMART 6K, MoKα radiation, λ = 0.71073 Å, T = 120(2)K, $2\theta_{max}$ = 58.5º, 32510 reflections collected, 8038 unique (R_{int} = 0.2057). Final *GooF* = 1.075, *R1* = 0.1543, *wR2* = 0.4030, *R* indices based on 3566 reflections with I >2σ(I) (refinement on F^2), 390 parameters, 0 restraints. Lp and absorption corrections applied, μ = 1.421 mm^{-1}.

3.10 References

1. J. L. Sessler, P. A. Gale and W.-S. Cho, '*Anion Receptor Chemistry*', Royal Society of Chemistry, Cambridge, 2006.
2. C. Caltagirone and P. A. Gale, *Chem. Soc. Rev.*, 2009, **38**, 520.
3. P. A. Gale, *Coord. Chem. Rev.*, 2006, **250**, 2917 preface to the special issue and subsequent reviews.
4. T. Gunnlaugsson, M. Glynn, G. M. Tocci, P. E. Kruger and F. M. Pfeffer, *Coord. Chem. Rev.*, 2006, **250**, 3094.
5. K. J. Wallace, W. J. Belcher, D. R. Turner, K. F. Syed and J. W. Steed, *J. Am. Chem. Soc.*, 2003, **125**, 9699.
6. D. R. Turner, M. J. Paterson and J. W. Steed, *J. Org. Chem.*, 2006, **71**, 1598.
7. S. J. Dickson, E. V. B. Wallace, A. N. Swinburne, M. J. Paterson, G. O. Lloyd, A. Beeby and J. W. Steed, *New J. Chem.*, 2008, **32**, 786.
8. A. Barnard, S. J. Dickson, M. J. Paterson, A. M. Todd and J. W. Steed, *Org. Biomol. Chem.*, 2008, **7**, 1554.
9. M. H. Filby, S. J. Dickson, N. Zaccheroni, L. Prodi, S. Bonacchi, M. Montalti, C. Chiorboli, M. J. Paterson, T. D. Humphries and J. W. Steed, *J. Am. Chem. Soc.*, 2008, **130**, 4105.
10. V. Amendola, M. Boiocchi, L. Fabbrizzi and A. Palchetti, *Chem.-Eur. J.*, 2005, **11**, 5648.
11. H. Ihm, S. Yun, H. G. Kim, J. K. Kim and K. S. Kim, *Org. Lett.*, 2002, **4**, 2897.
12. Y. Bai, B. G. Zhang, J. Xu, C. Y. Duan, D. B. Dang, D. J. Liu and Q. J. Meng, *New J. Chem.*, 2005, **29**, 777.
13. Y. Bai, B.-G. Zhang, C. Y. Duan, D.-B. Dang and Q.-J. Meng, *New. J. Chem.*, 2006, **30**, 266.
14. J. Zhang, A. M. Bond, J. Belcher, K. J. Wallace and J. W. Steed, *J. Phys. Chem. B*, 2003, **107**, 5777.
15. W. X. Liu and Y. B. Jiang, *Org. Biomol. Chem.*, 2007, **5**, 1771.
16. C. M. G. Dos Santos, T. McCabe and T. Gunnlaugsson, *Tetrahedron Lett.*, 2007, **48**, 3135.
17. R. M. Duke and T. Gunnlaugsson, *Tetrahedron Lett.*, 2007, **48**, 8043.
18. C. M. G. Dos Santos, M. Glynn, T. McCabe, J. S. S. De Melo, H. D. Burrows and T. Gunnlaugsson, *Supramol. Chem.*, 2008, **20**, 407.
19. E. B. Veale, G. M. Tocci, F. M. Pfeffer, P. E. Kruger and T. Gunnlaugsson, *Org. Biomol. Chem.*, 2009, **7**, 3447.
20. C. D. Geddes, *Meas. Sci. Technol.*, 2001, **12**, R53.
21. C. D. Geddes, *J. Photochem. Photobiol. A-Chem.*, 2000, **137**, 145.
22. M. S. Mehata and H. B. Tripathi, *J. Lumines.*, 2002, **99**, 47.
23. O. van den Berg, W. F. Jager and S. J. Picken, *J. Org. Chem.*, 2006, **71**, 2666.

24. L. Baldini, A. Casnati, F. Sansone and R. Ungaro, *Chem. Soc. Rev.*, 2007, **36**, 254.
25. A. K. Yatsimirsky and H.-J Schneider, '*Principles and Methods in Supramolecular Chemistry*', Wiley, New York, 2000.
26. P. Gans, *HypNMR* 2006, University of Leeds, Leeds, 2006.
27. Gaussian 03, Revision D.01 M. J Frisch, G. W. Trucks, H. B Schlegel, G. E Scuseria, M. A. Robb, J. R. Cheeseman, J. A. Montgomery Jr, T. Vreven, K. N. Kudin, J. C. Burant, J. M. Millam, S. S. Iyengar, J. Tomasi, V. Barone, B. Mennucci, M. Cossi, G. Scalmani, N. Rega, G. A. Petersson, H. Nakatsuji, M. Hada, M. Ehara, K. Toyota, R. Fukuda, J. Hasegawa, M. Ishida, T. Nakajima, Y. Honda, O. Kitao, H. Nakai, M. Klene, X. Li, J. E. Knox, H. P. Hratchian, J. B. Cross, C. Adamo, J. Jaramillo, R. Gomperts, R. E. Stratmann, O. Yazyev, A. J. Austin, R. Cammi, C. Pomelli, J. W. Ochterski, P. Y. Ayala, K. Morokuma, G. A. Voth, P. Salvador, J. J. Dannenberg, V. G. Zakrzewski, S. Dapprich, A. D. Daniels, M. C. Strain, O. Farkas, D. K. Malick, A. D. Rabuck, K. Raghavachari, J. B. Foresman, J. V. Ortiz, Q. Cui, A. G. Baboul, S. Clifford, J. Cioslowski, B. B. Stefanov, G. Liu, A. Liashenko, P. Piskorz, I. Komaromi, R. L. Martin, D. J. Fox, T. Keith, M. A. Al-Laham, C. Y. Peng, A. Nanayakkara, M. Challacombe, P. M. W. Gill, B. Johnson, W. Chen, M. W. Wong, C. Gonzalez and J. A. Pople, Gaussian Inc., Pittsburgh (PA), 2003.
28. C. D. Geddes and P. Douglas, *J. Appl. Polym. Sci.*, 2000, **76**, 603
29. R. Krapf, N. P. Illsley, H. C. Tseng and A. S. Verkman, *Biophys. J.*, 1988, **53**, A196.
30. L. Porres, A. Holland, L. O. Palsson, A. P. Monkman, C. Kemp and A. Beeby, *J. Fluorescence*, 2005, **16**, 267.
31. J. R. Lakowicz, *'Principles of Fluorescent Spectroscopy'*, 3rd Ed., Springer, 2006.
32. S. Jayaraman and A. S. Verkman, *Biophys. Chem.*, 2000, **85**, 49.
33. C. D. Geddes, K. Apperson, J. Karolin and D. J. S. Birch, *Dyes and Pigments*, 2001, **48**, 227.
34. C. D. Geddes, K. Apperson and D. J. S. Birch, *Dyes and Pigments*, 2000, **44**, 69.
35. S. G. Schulman, R. M. Threatte, A. C. Capomaccia and W. L. Paul, *J. Pharm. Sci.,* 1974, **63**, 876.
36. D. Pant, H. B. Tripathi and D. D. Pant, *J. Lumines.*, 1992, **51**, 223.
37. J. Najbar and M. Mac, *J. Chem. Soc.-Faraday Trans.*, 1991, **87**, 1523.
38. H. Shizuka, M. Nakamura and T. Morita, *J. Phys. Chem.*, 1980, **84**, 989.
39. H. Shizuka, T. Saito and T. Morita, *Chem. Phys. Lett.*, 1978, **56**, 519.
40. K. A. Abdullah and T. J. Kemp, *J. Photochem.*, 1985, **28**, 61
41. A. R. Watkins, *J. Phys. Chem.*, 1973, **77**, 1207.
42. J. Bendig, S. Helm and D. Kreysig, *Chem. Phys. Lett.*, 1978, **54**, 466.
43. D. R. Turner, B. Smith, A. E. Goeta, I. R. Evans, D. A. Tocher, J. A. K. Howard and J. W. Steed, *CrystEngComm*, 2004, **6**, 633.
44. K. J. Wallace, R. Hanes, E. Anslyn, J. Morey, K. V. Kilway and J. Siegel, *Synthesis-Stuttgart*, 2005, 2080.
45. A. Beeby, S. Fitzgerald and C. F. Stanley, *Photochem. Photobiol.*, 2001, **74**, 566.
46. N. G. Connelly and W. E. Geiger, *Chem. Rev.*, 1996, **96**, 877.

4. Colourimetric Carboxylate Anion Sensors Derived from Viologen Based Receptors

4.1 Introduction

The design of anion receptors capable of selectively sensing an anion is a topical challenge.[1-4] Carboxylate recognition is of particular importance due to the anions' variety of geometries, high basicity and biochemical importance. While carboxylates bind strongly to hydrogen bond donors their basicity can also lead to deprotonation and decomposition.[5-7] The approach of the Steed group[8-10] and others[11-13] is to use an induced-fit binding strategy based upon designing conformationally flexible anion receptors, typically derived from a hexa-substituted triethylbenzene core. As the conformation of the host changes upon anion binding, a fluorescent or electrochemical response is obtained.

A hexa-substituted triethylbenzene core has been used extensively as a scaffold for conformationally flexible receptors. Steric hindrance between adjacent ethyl and binding groups gives a 10 - 15 kcal mol^{-1} preference to a three-up, three-down conformation.[14-16] This arrangement provides a degree of binding cavity preorganisation while still allowing flexibility and hence an induced-fit response. Binding and reporter groups can then be added in a modular approach to receptor design.[14,17]

The viologen moiety is an attractive component as its low lying reduction potential provides a convenient electrochemical reporter group in supramolecular systems.[18-21] The low energy LUMO also allows for charge transfer behaviour which has been extensively studied, while the acidic *ortho*-bipyridinium hydrogen atoms allow for charge assisted hydrogen bonding.[22-23] The viologen group may therefore act as both a binding group and reporter group. A 4,4′-bipyridine derived hexa-substituted benzene receptor (**133**) has previously been reported by the Steed group, functionalised at only one end of the bipyridine.[23] This compound binds ATP, although all other anion binding is weak. Preliminary work carried out by Emma Wallace, Sara Jane Dickson and Kathrin Fisher in the group resulted in the synthesis of viologen derived receptors able to colourimetrically sense anions.[24] This chapter reports a full investigation into

the synthesis, solution state binding and spectroscopic properties of a series of tri- and tetrapodal viologen-based anion receptors based on the hexa-substituted benzene core.

4.2 Synthesis

The synthesis of three tetrapodal viologen derivatives **132**, **125** and **126** was achieved using the intermediate 1,1′-bis(3,5-bis(bromomethyl)-2,4,6-triethylbenzyl-4,4′-bipyridine-1,1′-diium bromide (**131**) which can be synthesised in near quantitative yield via the reaction of excess 1,3,5-triethyl-2,4,6-tribromomethylbenzene with 4,4′-bipyridine. Additional functionalisation can be achieved via reaction with pyridine, 1-pyridin-3-yl-3-*p*-tolyl-urea[25] and *N*-((naphthalen-1-yl)methyl)pyridin-3-amine (Scheme 4.1, synthesis detailed in Chapter 2). These reactions can be performed via traditional solution-state methods (compounds **132** and **134**, below) or alternatively via a mechanochemical reaction (compounds **125** and **126** as described in Chapter 2). Yields vary in the region of 30 – 70%. The bromide salts of the tetrapodal receptors were metathesised to the hexafluorophosphate salt by precipitation of the product from methanol solution with NH_4PF_6.

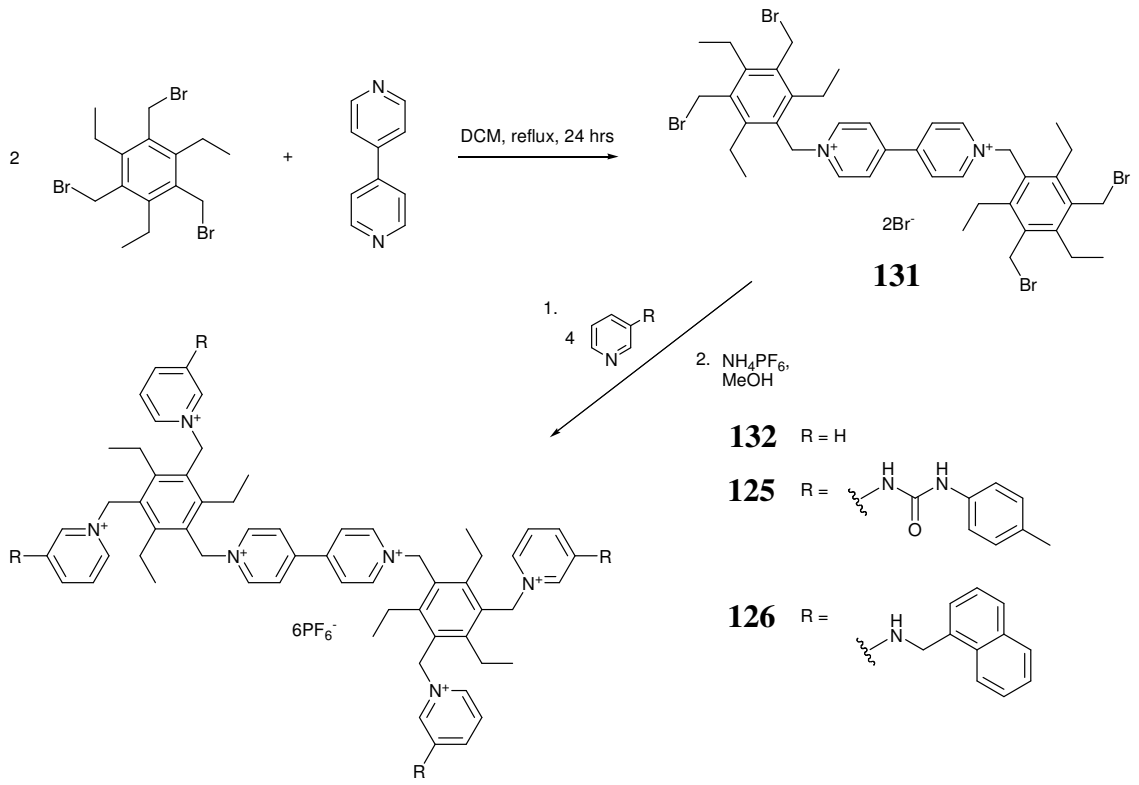

Scheme 4.1 Synthesis of tetrapodal anion receptors

The tripodal tris(bipyridinium) receptor **134** is prepared in high yield from compound **133** by capping the three remaining bipyridyl nitrogen atoms with an excess of benzyl bromide in DMF at 50 °C. Again, anion metathesis to the hexafluorophosphate salt is achieved by the reaction of the bromide salt with NH_4PF_6 (Scheme 4.2).

Several attempts were made to add various capping groups to compound **133**, such as methyl, ethyl, naphthyl and pyrenyl groups, through reaction with the bromomethyl derivatives. However, in all cases except for **134**, no product or only partial capping resulted. The addition of capping groups was also attempted using mechanochemical methods. Unfortunately, a mixture of 1, 2 and 3 capping groups was observed using $MALDI^+$ mass spectrometry.

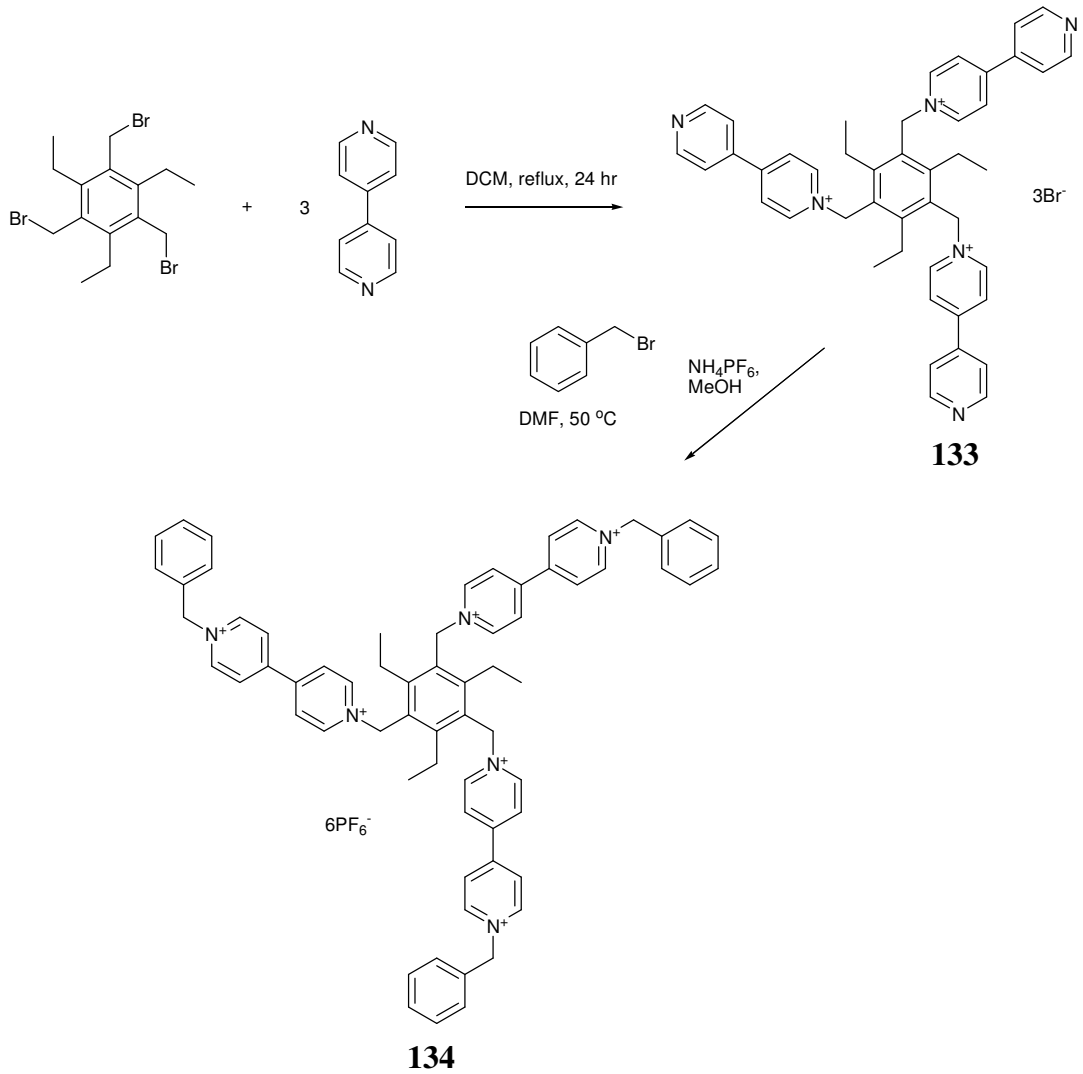

Scheme 4.2 Synthesis of tripodal anion receptor **134**

4.3 Solution-State Binding Properties

The anion binding properties of compounds **132**, **125** and **126** and **134** were investigated using ^{1}H NMR spectroscopy in CD_3CN. All compounds were shown to bind halides strongly. A 1:2 host:guest binding stoichiometry is suggested by ^{1}H NMR spectroscopic titrations for compounds **132**, **125** and **134** and is supported by Job plot analysis. Figure 4.1 shows representative Job plots for the tetrapodal receptor **132** and tripodal receptor **134** with tetra-n-butylammonium (TBA) chloride.

Compound **126** appears to have more complex speciation accompanied by slow guest complexation kinetics or conformational change on the ^{1}H NMR spectroscopic timescale, as evidenced by significant broadening and splitting of several peaks at room temperature. As a result binding constants could not be reliably determined.

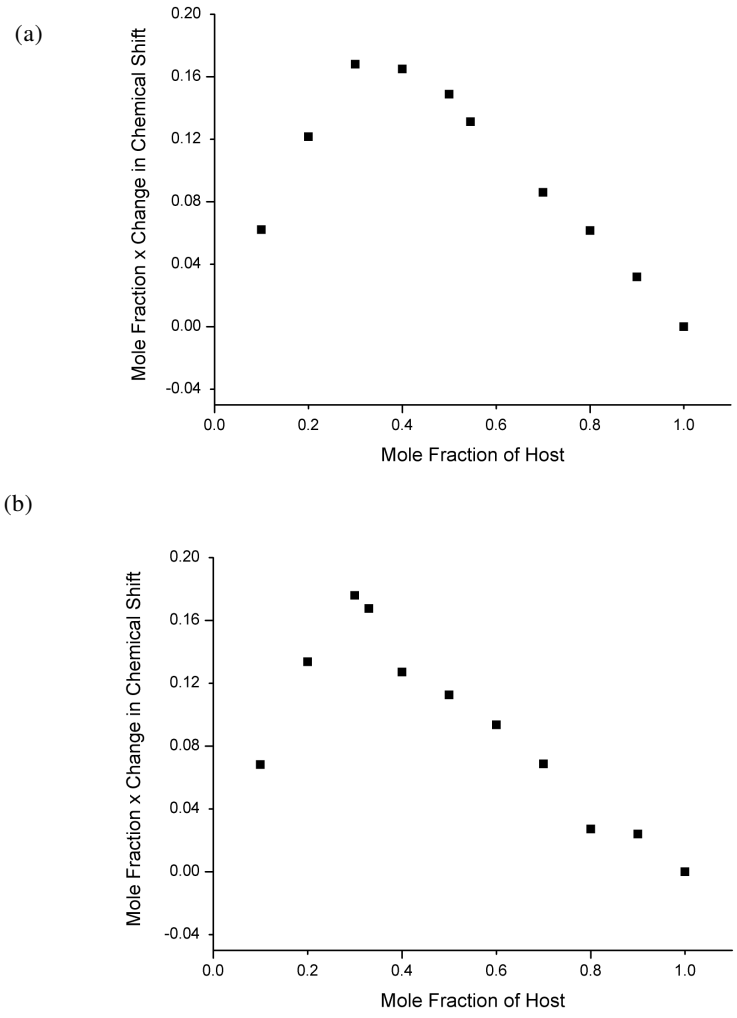

Figure 4.1 Job Plot for (a) compound **132** and (b) compound **134** in CD_3CN with TBA-Cl

The 1:2 binding stoichiometry observed in compounds **132** and **125** can be explained by the existence of two primary binding sites which are essentially tripodal in nature. In the case of compound **132**, anion binding is due to hydrogen bonding from *o*-CH groups of the pyridinium and bipyridinium units to the anion, as indicated by the downfield shift of the respective ^{1}H NMR resonances. This CH...anion interaction has been shown to be important in related systems.[8] An electrostatic contribution to binding is also likely. In the case of **125**, large downfield shifts are observed for the urea NH protons by ^{1}H NMR spectroscopy, as well as smaller changes in the bipyridinium and pyridinium resonances, indicative of hydrogen bonding.

As with **132** and **125**, compound **134** exhibits a 1:2 host:guest binding stoichiometry. Downfield shifts were only observed for the ^{1}H NMR resonances assigned to the *o*-bipyridinium protons upon addition of anions suggesting hydrogen bonding to those protons only. Again an electrostatic contribution to the binding is also likely.

It is difficult to imagine where a second halide anion could bind to compound **134**. One possibility is that the first anion sits low in the binding cavity near the hexa-substituted benzene ring, whilst the second sits high near the three benzyl groups. It could be imagined that hydrogen bonding in this region would be weak as the distance between binding arms is large. This postulate is supported by ^{1}H NMR spectroscopic evidence as no significant chemical shift changes are seen for these 'outer' protons. This model may also explain the low value of the 1:2 host:guest binding constant ($K_{12} = \beta_{12} - \beta_{11}$) in the case of Cl^-. Even though chloride has the highest charge density, its small size means it may not be able to experience the full electrostatic attraction of all three arms. This would favour 1:2 binding for larger halides, as is observed. Table 4.1 contains the binding constants determined for compounds **132**, **125** and **134** by ^{1}H NMR spectroscopic titration using the least-squares curve fitting program *HypNMR* 2006.[26]

Table 4.1 Binding constants determined by ^{1}H NMR spectroscopic titrations for compounds **132**, **125** and **134** in CD_3CN. All anions used a TBA salts. *a* = binding constant could not be refined due to poor fit to the experimental data

	Stoichiometry	**Compound, Log β_{HG}**		
Anion	**HG**	**132**	**125**	**134**
Chloride	1:1	4.30(6)	3.6(1)[24]	4.0(1)
	1:2	7.83(5)	6.94(3)	4.855(2)
Bromide	1:1	3.66(6)	3.8(1)[24]	3.63(4)
	1:2	6.93(5)	5.97(8)	6.0(1)
Iodide	1:1	3.8(1)	3.6(1)	3.3(1)
	1:2	6.9(1)	6.55(7)	5.8(1)
Nitrate	1:1	3.6(2)	2.89(3)	*a*
	1:2	6.64(3)	5.93(9)	
Hydrogen	1:1	Precipitate	Precipitate	Precipitate
Sulfate	1:2			
Dihydrogen	1:1	Precipitate	Precipitate	Precipitate
Phosphate	1:2			

Where species are in the following equilibria:

$$H \overset{K_{11}}{\rightleftharpoons} HG \overset{K_{12}}{\rightleftharpoons} HG_2$$

Binding constants are defined as:

$$K_{11} = \frac{[HG]}{[H][G]} \qquad K_{12} = \frac{[HG_2]}{[HG][G]}$$

$$\text{Log}\,\beta_{11} = \text{Log}\,K_{11} \qquad \text{Log}\,\beta_{12} = \text{Log}\,K_{11} + \text{Log}\,K_{12}$$

H = Host, G = Guest

In the case of compounds **132** and **134** strong chloride binding is observed. Compound **125** exhibits interesting behaviour, in which bromide is bound strongly, with chloride and iodide bound more weakly. Nitrate is the weakest bound. Representative binding isotherms for the tetrapodal receptor **132** and tripodal receptor **134** are shown in Figure 4.2.

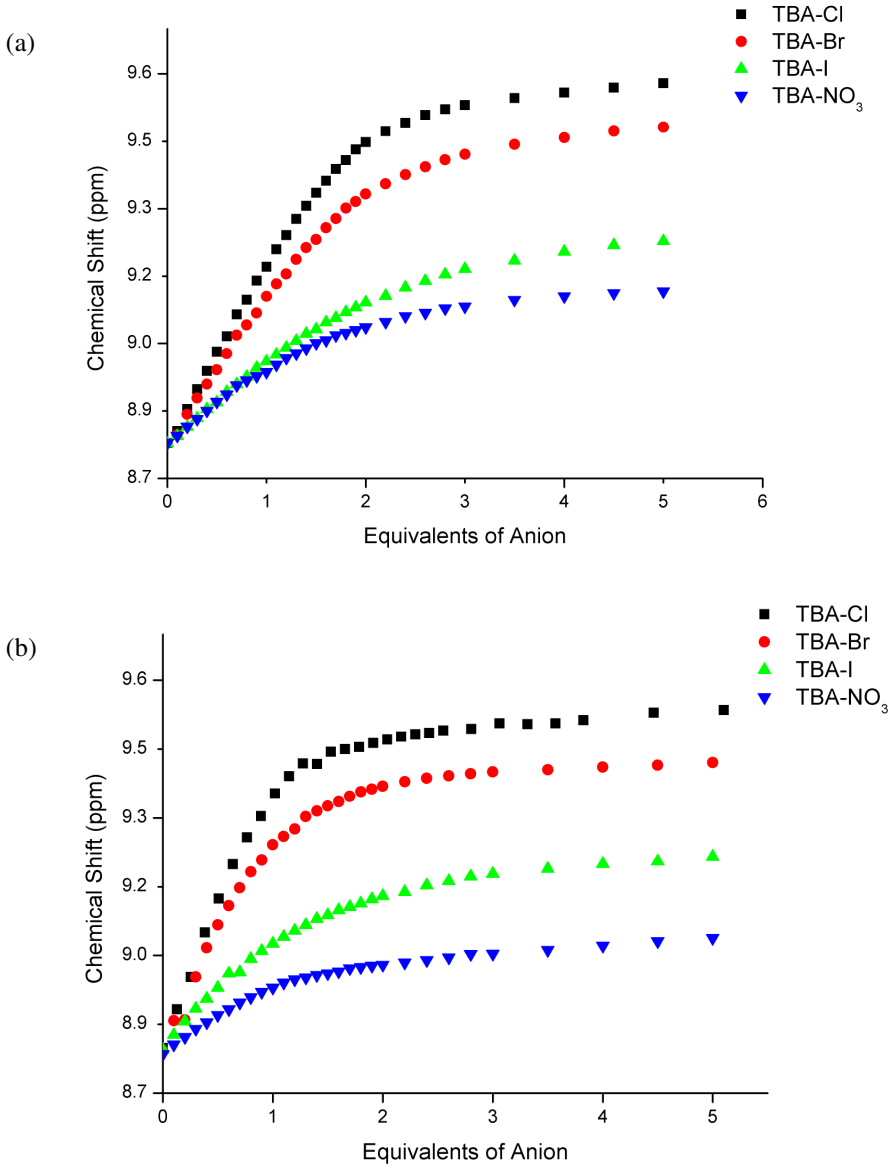

Figure 4.2 Binding isotherms for (a) compound **132** and (b) compound **134** in CD_3CN with various anions

During ^1H NMR spectroscopic titrations with carboxylate anions a colour change from colourless to purple was observed. This colour gradually fades to red and then orange on standing in aerated solutions, but the use of de-gassed solvent gave rise to a long-

lasting purple colouration. ^{1}H NMR spectra in degassed solvent were recorded for compounds **132** and **134** in the presence of acetate. The purple colouration occurs immediately after the addition of acetate to compound **132** and **134** and evidence of decomposition in the form of new peaks in the ^{1}H NMR spectrum are observed at two equivalents or above. This decomposition is likely to arise from oxygen diffusion into the tube during the experiment.

The ^{1}H NMR spectra for compound **132** on addition of acetate shows large shifts for the *o*-pyridinium (0.4 ppm) and *o*-bipyridinium (0.3 ppm) resonances consistent with the observations for halide binding (Figure 4.3). In the case of **125,** large downfield shifts are observed for the resonances assigned to the urea NH protons with only small shifts for the other resonances.[24] Compound **125** does not show decomposition until after two equivalents of acetate are added, suggesting that the decomposition is linked to the observed colour change.

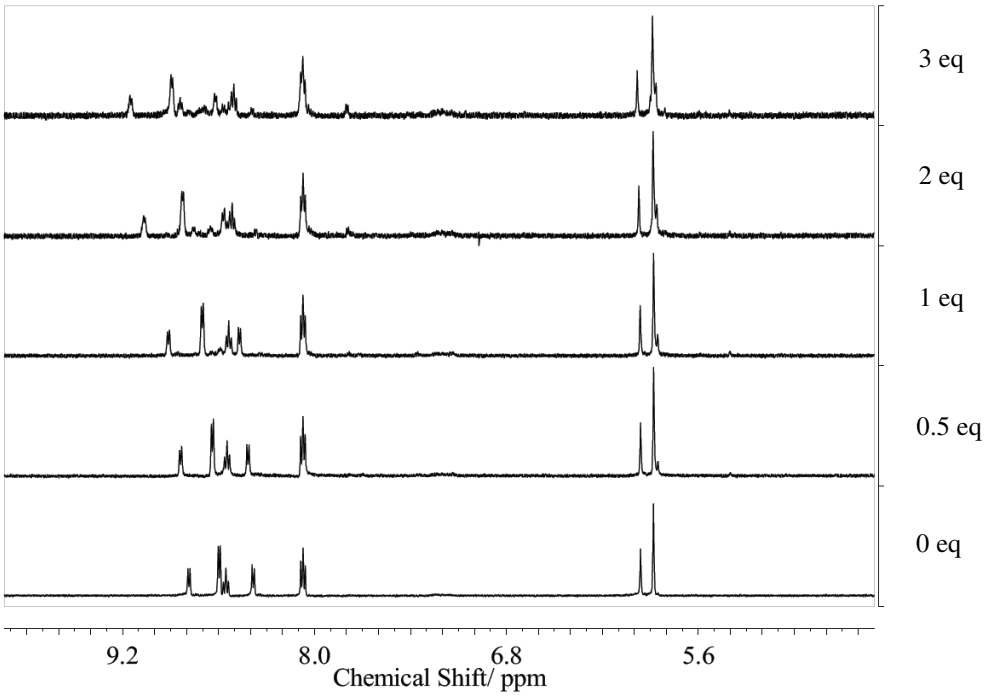

Figure 4.3 Stack plot showing the ^{1}H NMR spectrum of compound **132** in CD_3CN in the presence of TBA-acetate. The ^{1}H NMR assignment can be found in Appendix III

The ^{1}H NMR spectra of **134** upon addition of acetate shows severe broadening of the resonances, with all peaks disappearing before one equivalent. A ^{1}H NMR

spectroscopic titration of compound **134** with TBA-malonate reveals downfield shifts in the bipyridinium resonances suggesting anion binding (Figure 4.4).

Interestingly, in the case of **134**, a colour change is not observed with malonate until higher equivalents of guest, even though NMR spectroscopic evidence suggests anion binding is occurring.

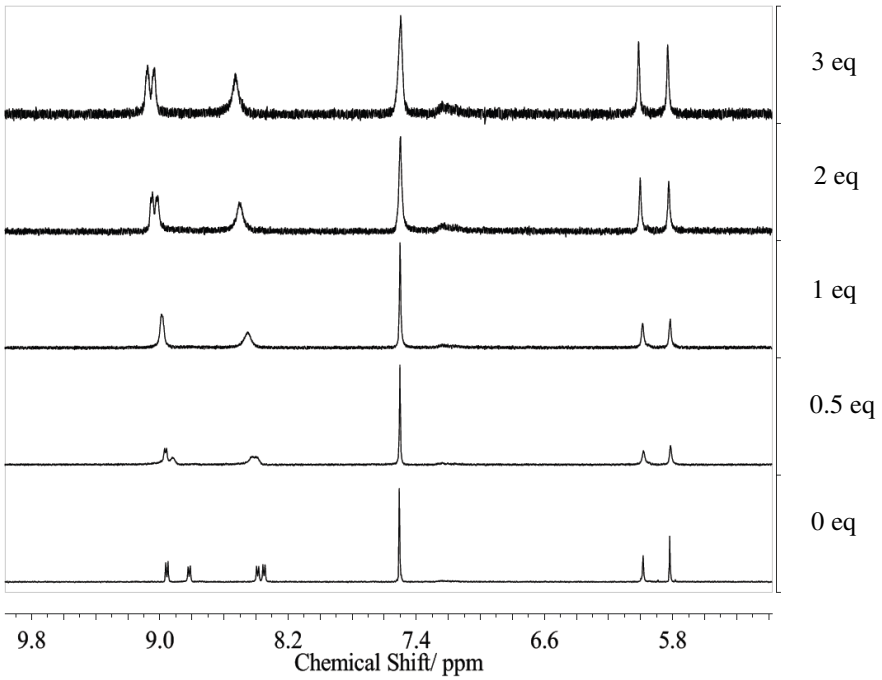

Figure 4.4 Stack plot showing the ^{1}H NMR spectrum of compound **134** in CD_3CN in the presence of 0 – 3 equivalents of TBA-malonate. The ^{1}H NMR assignment can be found in Appendix III

The cause of the decomposition of the carboxylate complexes of **132**, **125** and **134** is unknown. However, the viologen radical cation is known to be oxygen sensitive and the decomposition may be caused by hydroxide generated from dioxygen reduction by the radical cation. Evidence for the presence of the viologen radical cation has been found in the UV-vis spectra of the charge transfer complexes, as well as by Raman and ESR measurements (*vide infra*). The decomposition of the carboxylate complexes means that only qualitative information on carboxylate binding could be obtained by ^{1}H NMR spectroscopy.

An X-ray crystal structure determination of the hexafluorophosphate salt of compound **132** was undertaken. One independent hexacation is observed with PF_6^- counter-ions, with a disordered acetonitrile pocket.

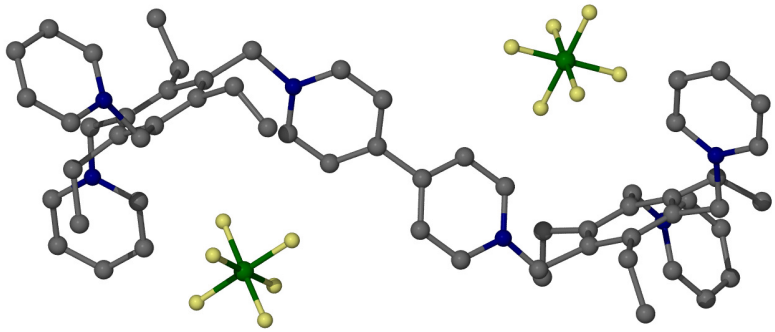

Figure 4.5 Molecular structure of compound **132** determined by X-ray crystallography. Hydrogen atoms removed for clarity[24]

The compound adopts a *transoid* conformation with the hexa-substituted benzene derived unit on alternative sides of bipyridinium. Each tripodal unit adopts a two-up, one-down conformation of the pyridinium groups. Whilst a three-up conformation is expected,[14-16] there is only a small energetic preference for this conformation *ca.* 15 kJ mol^{-1} and the two-up, one-down conformation has been observed in similar systems.[8-9] The molecular structure (Figure 4.5) shows two of the PF_6^- anions within the tripodal binding sites. This is consistent with the solution state anion binding behaviour suggested by ^{1}H NMR spectroscopy. The anions are bound close to the viologen unit, a prerequisite for charge-transfer.

Variable temperature ^{1}H NMR spectroscopic studies were undertaken on compounds **132** and **134** in the presence and absence of chloride. Low temperature ^{1}H NMR spectroscopy in acetone-d_6 was used to help understand the conformations of the compounds. Figure 4.6 shows the ^{1}H NMR spectrum of the hexafluorophosphate salt of host **132** as the temperature is lowered to 183 K. Broadening of the CH_2 (2.85 ppm) and CH_3 (1.12 ppm) resonances is observed. At 203 K the CH_3 groups split from a single peak at 1.12 ppm to two peaks at 0.56 and 1.29 ppm, corresponding to the two-up, one-down and three-up conformations respectively. The up-field shift in the CH_3 resonance is due to shielding of the methyl group by the pyridinium aromatic system

when the methyl substituent is on the same face as the pyridinium ring. There is also additional broadening and peak splitting in the aromatic region suggesting conformational exchange of the bipyridinium protons is occurring.

The addition of one equivalent of TBA-Cl to **132**, results in a downfield shift of the resonances assigned to the *o*-bipyridinium protons (Figure 4.6). There is also increased broadening of the resonances corresponding to the pyridinium and bipyridinium at lower temperatures. Significantly there is still evidence of the two-up, one-down conformer that is observed in the free host, however it has reduced in size. This shows that the compound in the presence of Cl^- guest, adopts a threefold symmetrical ('three-up') conformation at each tripodal unit, however as would be expected only one binding site is populated and therefore the two-up, one-down conformer still persists. The two-up, one-down conformer reduces still further on the addition of further Cl^-. Interestingly there is no evidence for an anion exchange equilibrium characterised by further splitting of the methyl and ethyl resonances which has been observed in a related system.[8]

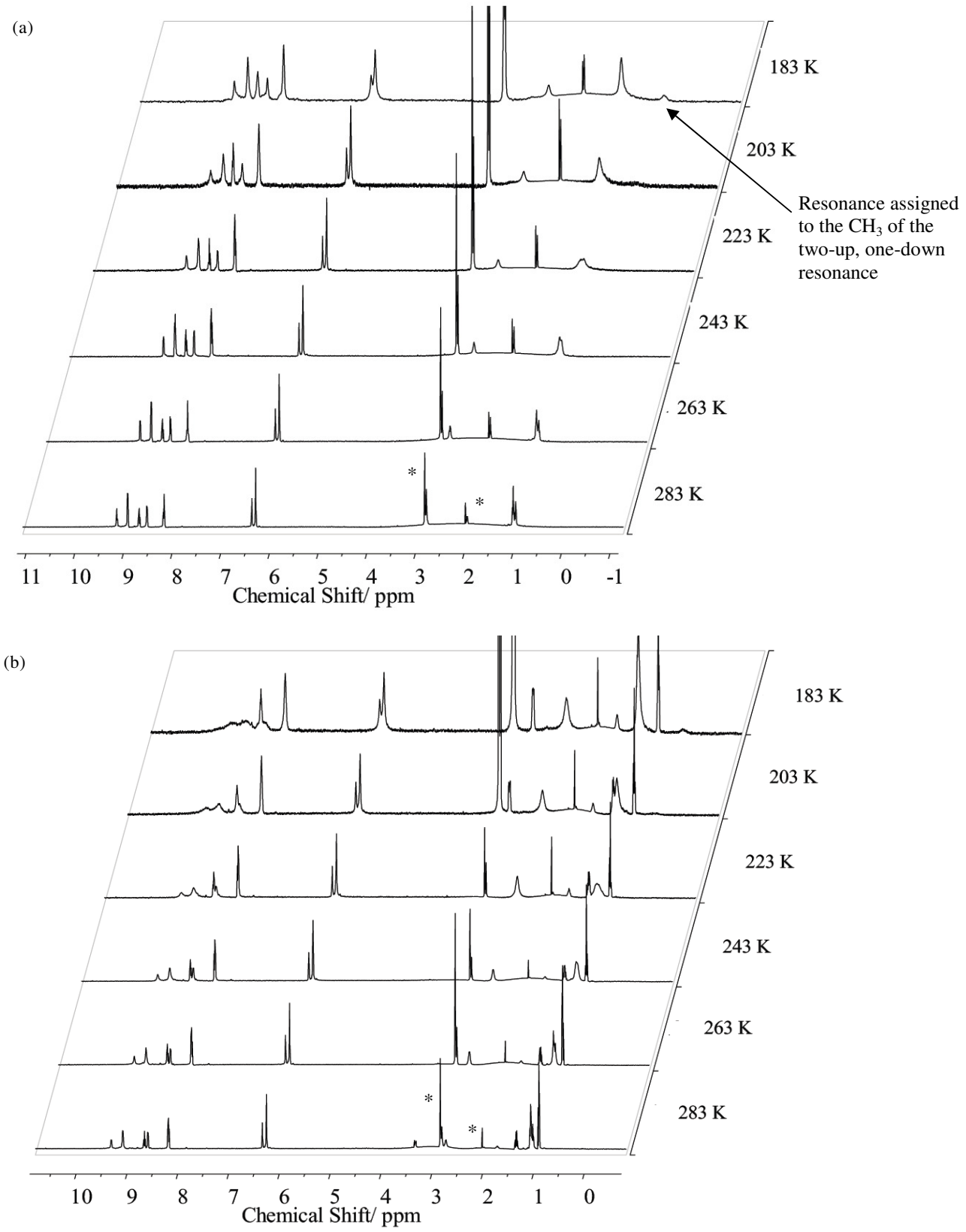

Figure 4.6 Variable temperature ^{1}H NMR spectra of (a) compound **132** in acetone-d_6 and (b) compound **132** in the presence of one equivalent of TBA-Cl. Solvent peaks have been removed for clarity (water at 2.13 ppm and acetone at 2.05 ppm). * indicates residual resonances from solvent impurities. The ^{1}H NMR assignments can be found in Appendix III

The low temperature ^{1}H NMR spectra for compound **134** shows similar behaviour to that of **132** with broadening and eventual splitting of the CH_3 (1.14 ppm) resonances into two peaks at 1.30 and 0.42 ppm, corresponding to the three-up and two-up, one-down conformers respectively (Figure 4.7). The addition of one equivalent of chloride still gives rise to a high field CH_3 resonance assigned to the two-up, one-down conformer, although it is very much reduced. Further addition of chloride reduces the intensity of this resonance as a further equivalent of chloride is bound, again suggesting a conformational change to a pseudo-threefold symmetric form upon anion binding.

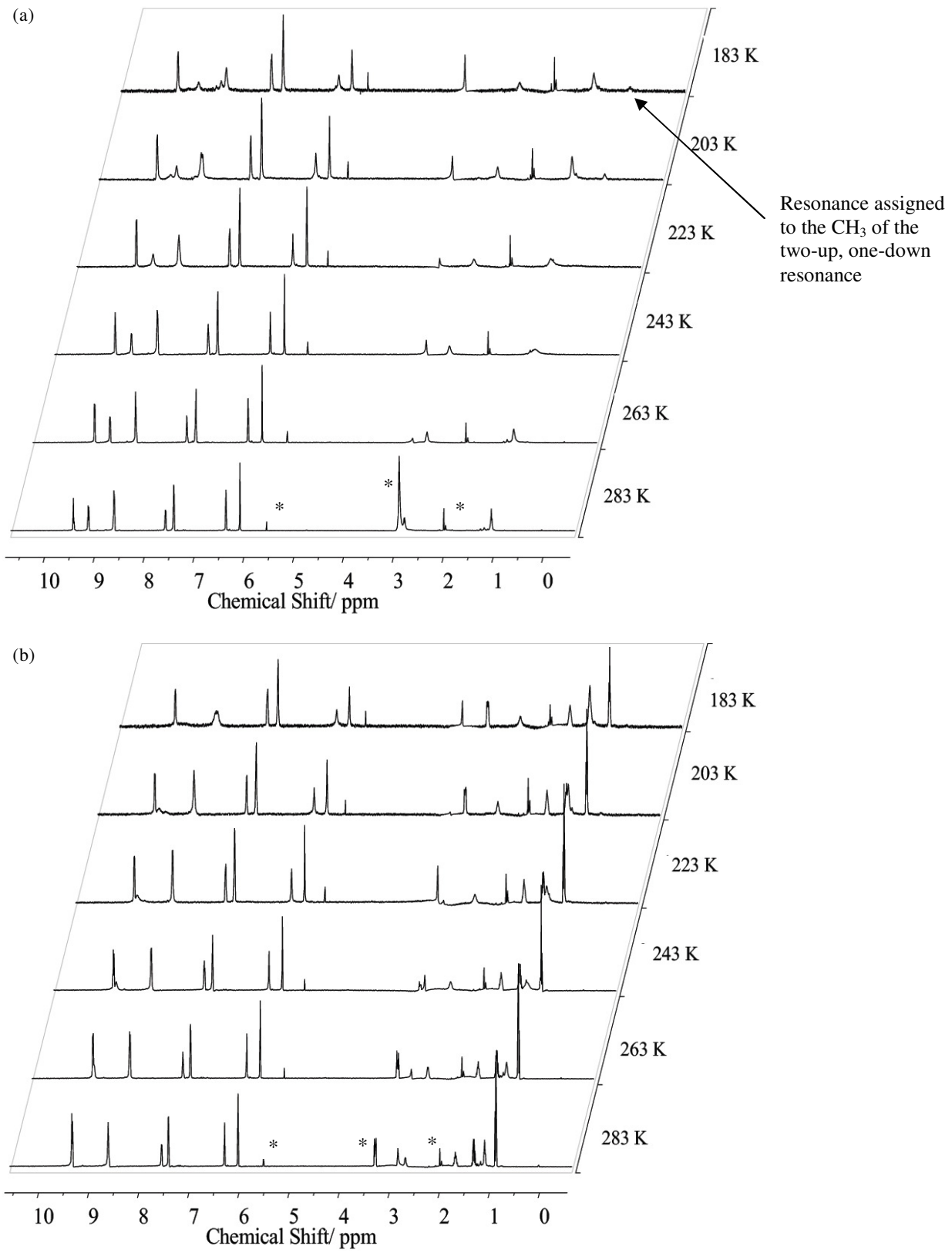

Figure 4.7 Variable temperature ^{1}H NMR spectra for compound **134** in acetone-d_6 with (a) free host and (b) one equivalent of TBA-Cl. Solvent peaks have been removed for clarity (water at 2.13 ppm and acetone at 2.05 ppm). * indicates residual resonances from solvent impurities. The ^{1}H NMR assignment can be found in Appendix III

4.4 Charge Transfer Behaviour

Upon the addition of carboxylates, receptors **132**, **125**, **126**, and **134** all give rise to an intense purple colouration with a band in the UV-vis spectrum centred at approximately 540 nm (Figure 4.8 and 4.9). This absorption is assigned to an anion-viologen charge transfer state. The particularly electron deficient nature of the viologens in these compounds makes them excellent electron acceptors and charge transfer behaviour in viologens is well known. Halides[27-29] (particularly iodide), electron rich arenes[30-31] phenols[32-33], amines[34] and organic acids[32,35] all give rise to charge transfer complexes with viologens.[22]

Figure 4.8 Degassed 1.0 x 10^{-4} mol dm^{-3} solutions of host **132** in MeCN in the presence of one equivalent TBA salts of the following anions (from left to right): succinate, malonate, acetate, chloride, bromide, nitrate, perrhenate

Figure 4.9 Degassed 1.0 x 10^{-4} mol dm^{-3} solutions of hosts **134** in MeCN in the presence of one equivalent TBA salts of the following anions (from left to right): acetate, malonate, chloride, bromide, iodide, nitrate

UV-vis titrations were performed using compounds **132**, **125**, **126**, and **134** with acetate, malonate and succinate (see Figures 4.10-11 for representative examples). Due to the air sensitive nature of the complexes anaerobic conditions were necessary

A series of control experiments showed it was not possible to fully exclude oxygen from the experiment and a certain amount of decomposition occurs. The acetonitrile

used as the solvent in these experiments was degassed by three freeze-pump-thaw cycles and stored in a glove box. All samples used in the experiment were made and stored in a glove box until they were used. A quartz cuvette was used with a B19 quick fit adaptor. Host and guest solutions were sealed in the glove box using suba-seals and parafilm. When adding or removing aliquots of solution to and from a sample, a balloon filled with N_2 was used.

The addition of six equivalents of acetate to a host solution under anaerobic conditions resulted in a long lasting purple colouration; however with time the intensity of the absorbance band decreased and overnight the colour had faded. This shows that either the complex is intrinsically unstable or oxygen leakage into the cuvette causes a reduction in absorbance over time. The addition of six equivalents of guest in a volume of solvent equal to the total volume added in a titration, again produced a purple colour. A further experiment in which six equivalents of acetate were added sequentially, followed by blank solvent up to the total volume of a titration was also performed. Comparison of the maximum absorbance values of the two titrations showed that the second experiment had significantly less intensity due to the unavoidable introduction of oxygen from the repeated addition of solvent. This oxygen leakage is, to an extent, unpredictable and difficult to model. As such it was not possible to determine binding constants using global fitting software and the carboxylate binding can only be discussed qualitatively.

It has been reported that acetate forms a charge transfer complex with methyl viologen (MV), with an intermolecular charge transfer band at 405 nm and emission at 506 nm.[35] However, comparison of the band maxima of the methyl viologen di-acetate complex (denoted $MV.(OAc)_2$) and the acetate complex of compound **132**, shows a large red-shift of 135 nm. Similar shifts are observed for the other viologen based receptors described here. The $MV.(OAc)_2$ complex appears as a yellow/orange solution, whereas the tetrapodal viologen receptors such as **132**, appear purple.

All compounds reach almost the exact same maximum absorbance value with acetate, at a similar number of equivalents. Interestingly, upon addition of acetate to hosts **132**, **125** and **134**, an immediate colour change is observed (Figure 4.10a). However, with host **125**, significant colouration does not appear until more than two equivalents of

acetate are added (Figure 4.10b). This is interpreted as implying binding site competition between the different binding groups present. Compound **125** contains urea as well as *o*-pyridinium binding sites. At low equivalents it is proposed that acetate binds at the urea groups, away from the viologen unit; resulting in no charge transfer. As more equivalents are added and more PF_6^- ions are displaced, acetate is able to bind closer to the viologen and charge transfer is observed. This binding site discrimination allows the tuning of the colourimetric response to the equivalents of guest added.

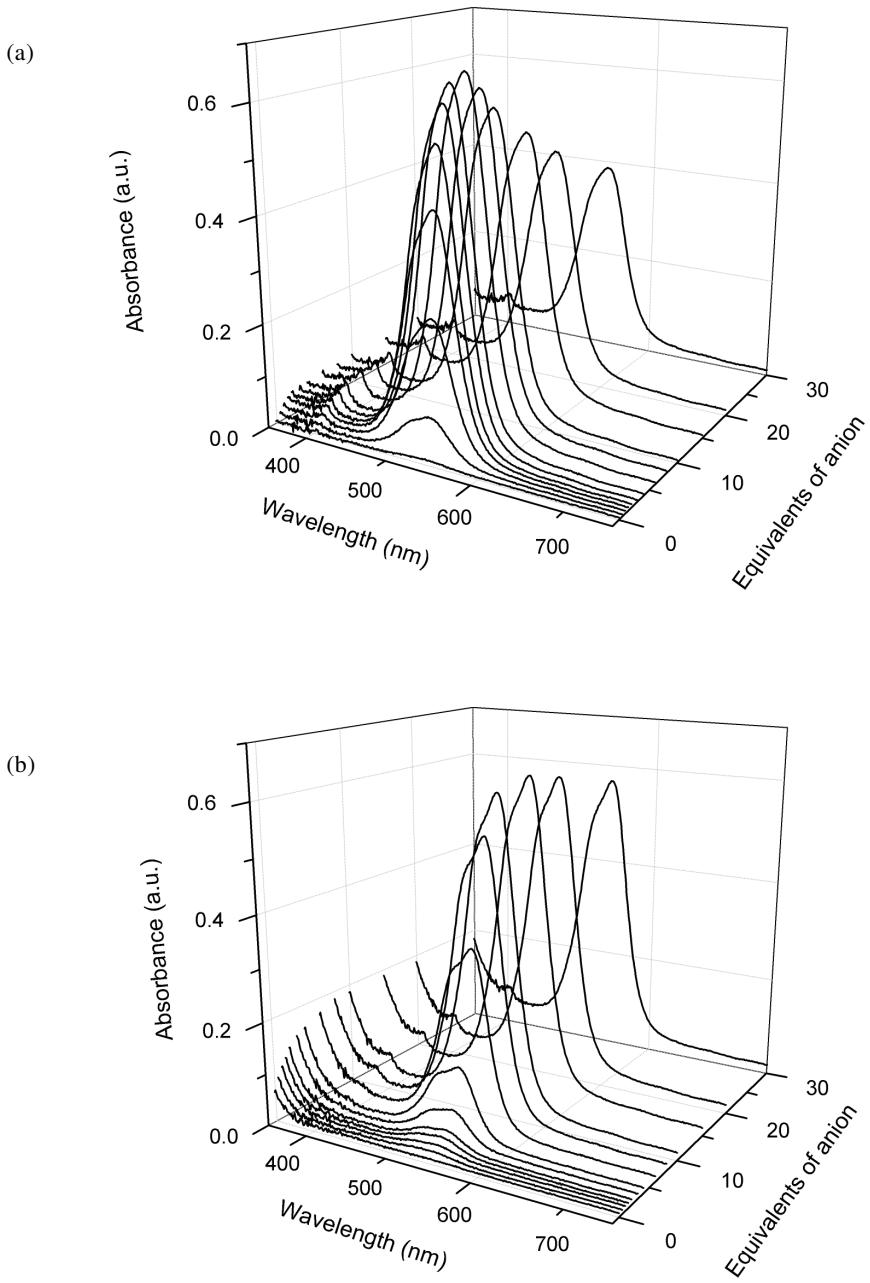

Figure 4.10 UV-vis absorbance spectrum of (a) compound **132** (1.0 x 10^{-4} mol dm^{-1} in MeCN) and (b) compound **125** (1.0 x 10^{-4} mol dm^{-1} in MeCN) upon addition of TBA-acetate

Malonate and succinate also cause a colourimetric response. Succinate causes significant colour changes for all compounds similar to acetate, however for all compounds other than **132**, considerable decomposition was observed, with the host/succinate complex proving to be unstable. Malonate only causes significant colouration with compounds **132** and **125**. Compound **134** requires higher equivalents *ca.* 20 equivalents of malonate for a colour change to be observed. Compound **126** did not show any observable colour change with malonate. A ^{1}H NMR spectroscopic titration of compound **134** with TBA-malonate (Figure 4.4) does suggest anion binding occurs and therefore it appears the lack of charge transfer may be due to an unfavourable conformation of the complex or is of electronic origin.

The UV-vis spectroscopic titration of compound **134** with TBA-acetate results in a broadened band at 540 nm and a very prominent band at 396 nm (Figure 4.11). In contrast in the tetrapodal receptors **132**, **125** and **126**, the band at 396 nm is significantly lower in intensity. The band at 396 nm is consistent with the absorbance profile of the viologen radical cation (bands at 396 and 608 nm)[22,36] and the broadening of the 540 nm band is likely to be due to overlap with the 608 nm band of the radical cation. The band is also observed to a lesser extent for compound **132** and suggests that in addition to the formation of a charge transfer complex, an electron transfer process is also occurring, particularly in **134** (*vide infra*).

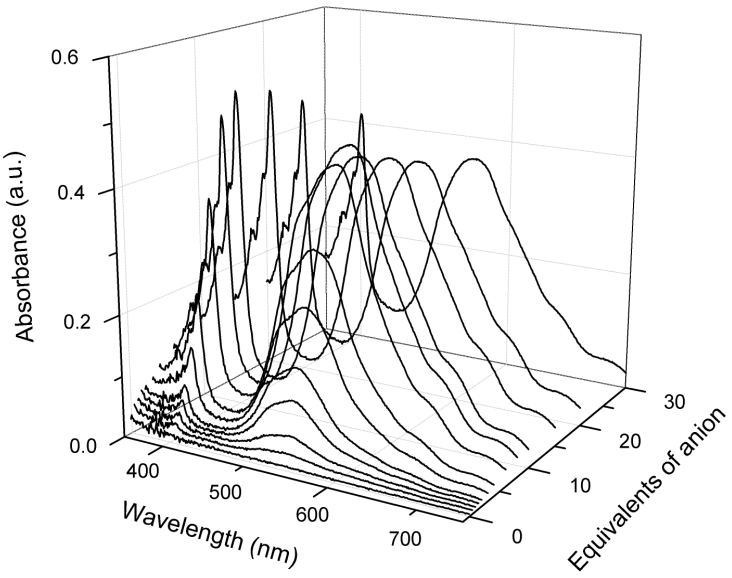

Figure 4.11 UV-vis absorbance spectrum of compound **134** (1.0 x 10^{-4} mol dm^{-3} in MeCN) upon addition of TBA-acetate

4.5 DFT Computational Studies

DFT calculations were undertaken in collaboration with Dr. M. J. Paterson at Heriot Watt University to test the feasibility of the proposed binding model and to interpret the ^{1}H NMR and UV-vis spectroscopic data. Structures were optimised using B3LYP/4-31G on the host, with the hydrogen atoms proximal to the anion augmented with additional s and p diffuse functions and 6-31+G* on the anion. Electronic transitions were calculated using TD-DFT with the B3LYP functional and the 6-31G* basis set on all atoms.[37]

The optimised structure of the receptor **132** with acetate (Figure 4.12) reveals a *transoid* conformation with the acetate bound by pyridinium CH...O hydrogen bonding interactions. Crucially, the structure suggests the acetate is held in close proximity to the viologen core, which would facilitate a charge transfer process.

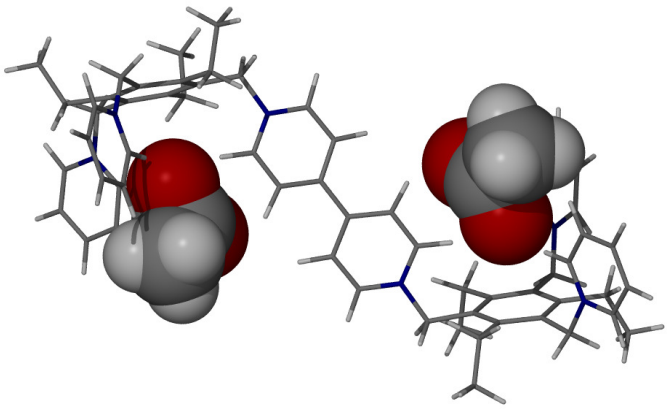

Figure 4.12 Optimised geometry for compound **132** with acetate

The calculated structure of **125** with acetate demonstrates binding of the acetate to the urea functional groups (Figure 4.13), consistent with ^{1}H NMR spectroscopic titrations and are remote from the viologen. TD-DFT calculations do not show a corresponding charge transfer band at 550 nm. This is consistent with the delayed evolution of the purple colouration of the complex.

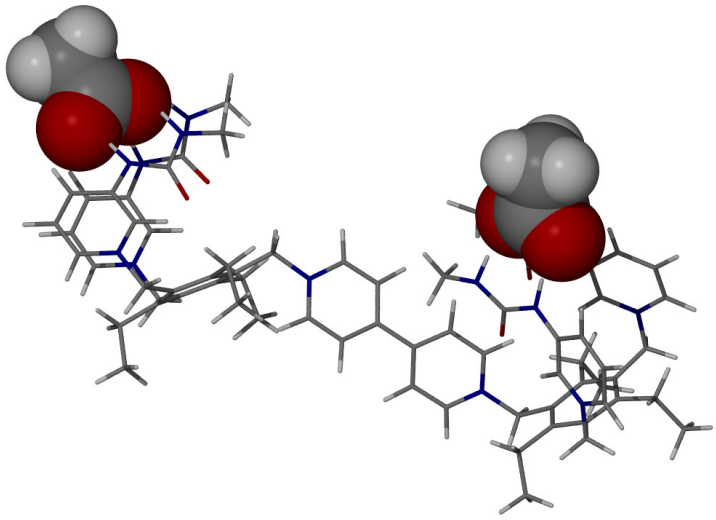

Figure 4.13 Optimised geometry for the **125** with two equivalents of acetate

The optimised structure of **132** with malonate is shown in Figure 4.14a. The flexible nature of the receptor allows the compound to encapsulate the malonate in a *cisoid* manner. The malonate is bound by charge assisted pyridinium CH…O interactions. The anion is situated close to the viologen in a suitable geometry to allow a charge transfer interaction. Time Dependent-DFT (TD-DFT) calculations suggest a transition involving the promotion of an electron in a localised π orbital on the malonate anion to the π* orbital on the bipyridinium moiety (Figure 4.14b). The transition has a large oscillator strength (f = 0.005) and so would be expected to give rise to an intense vibronic band, consistent with observation.

The optimised structure of **134** with acetate, Figure 4.15a, suggests a three-up conformation in which the anion is bound by three charge assisted hydrogen bonds, one of the acetate oxygen atoms is bound by two hydrogen bonds whilst the second is bound by only one. Again, TD-DFT calculations shows a π ← σ transition at 560 nm with an oscillator strength of 0.004 (Figure 4.15b), comparable to **132** with malonate.

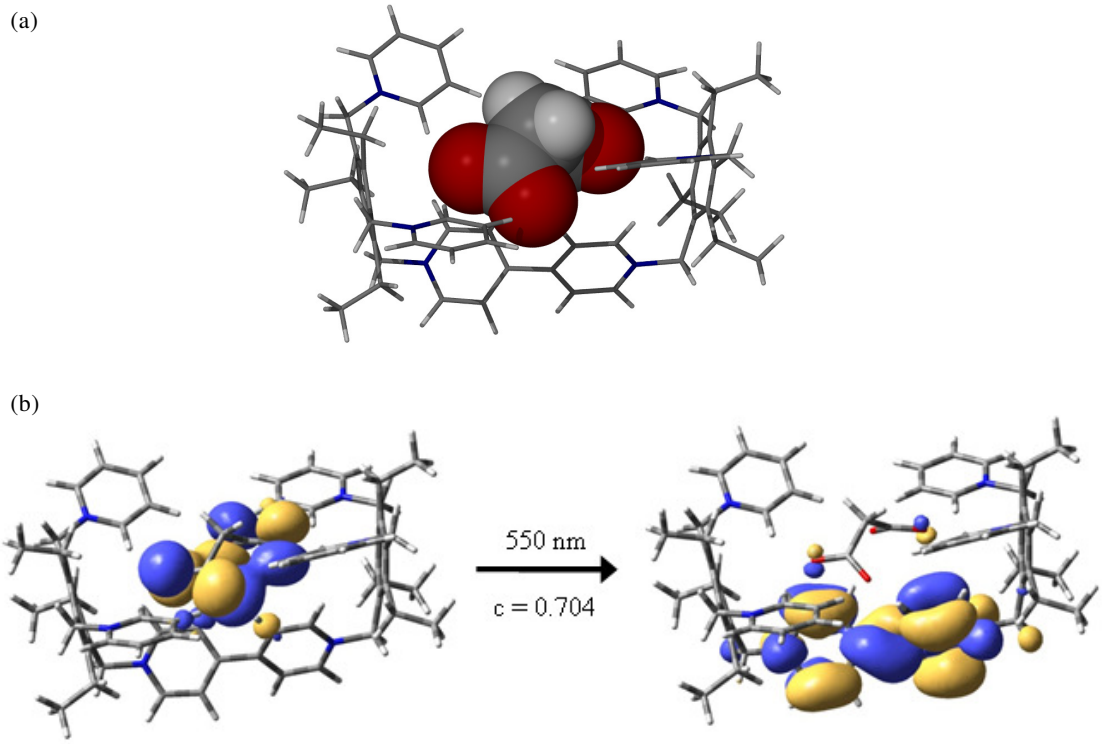

Figure 4.14 (a) Optimised geometry for compound **132** with malonate, (b) calculated electronic transition of **132** with malonate showing charge transfer from the anion to the viologen moiety

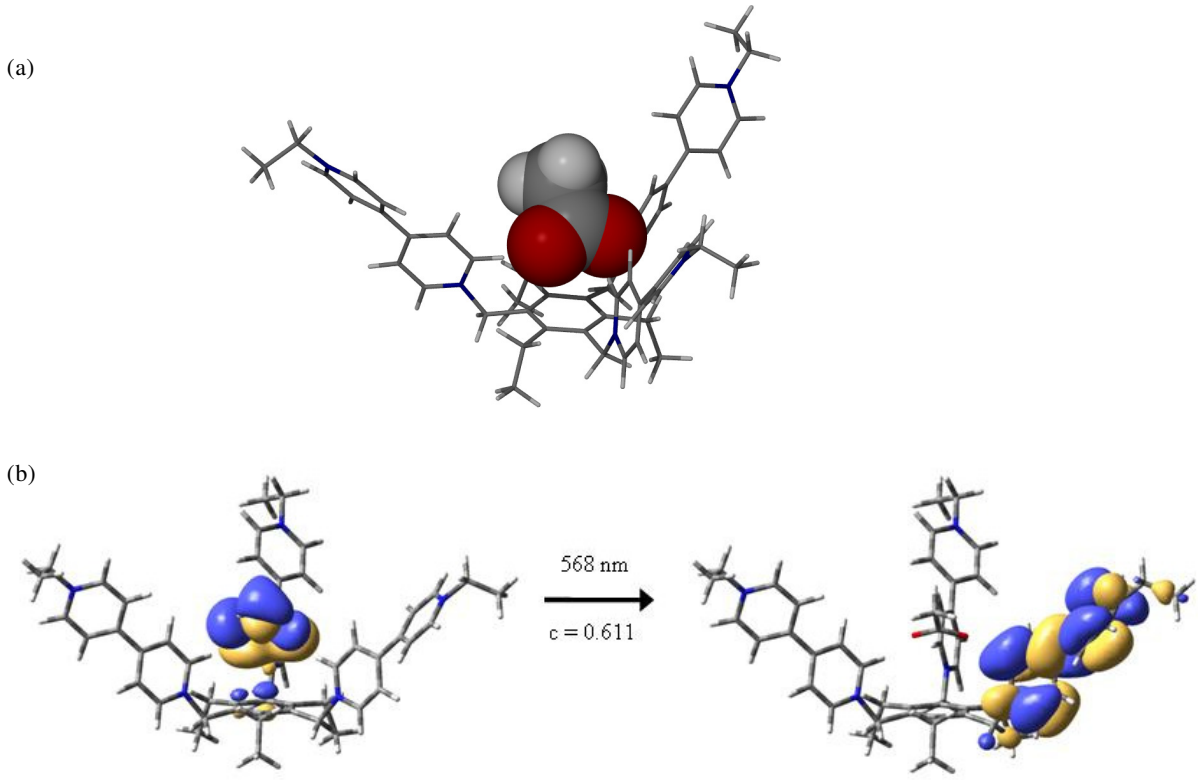

Figure 4.15 (a) Optimised geometry for the **134** with acetate, (b) major component of the calculated electronic absorbance of **134** with acetate showing charge transfer from the anion to the viologen moiety

All the charge transfer complexes described above show unusually low energy charge transfer bands compared to the typical complexes of methyl viologen, suggesting that these polycationic hosts are particularly readily reduced. In order to try and understand this observation, an electrochemical investigation of the hosts was undertaken.

4.6 Electrochemistry

The electrochemistry of viologen derivatives has been extensively investigated.[38] They exhibit two reversible redox couples, the first of which – formation of the radical cation from the dication – is reversible and has an unusually low reduction potential for an organic molecule.

As a control, the reduction potential of methyl viologen di-hexafluorophosphate, (denoted MV.$(PF_6)_2$) was measured in 0.1 mol dm^{-3} TBA-PF_6 in MeCN using a Pt working electrode. The $E_{1/2}$ potentials for the consecutive redox couples were found to be, E_1 = –0.42 and E_2 = –0.83 vs. SCE and are consistent with literature values[36, 38] measured under similar conditions. The peak to peak separation is close to the value expected for a single electron process and shows no significant variation with scan rate. The anode/cathode peak ratio is greater than 0.9 in both waves. A summary of important electrochemical data for compounds **132**, **125**, **126** and **134** is shown in Table 4.2. All viologen derivatives show classic viologen electrochemical behaviour. Two redox couples are observed, however for the tetrapodal derivatives the peak to peak separation is generally higher than for MV.$(PF_6)_2$.

The observed overpotential, particularly with the first redox couple of compounds **125** and **126**, may be due to a conformational change required for the viologen upon accepting an electron at the working electrode. It is also observed that the anode/cathode peak ratio is not as high as with methyl viologen, although good reversibility is still found in most cases. The cyclic voltammogram of compound **132** at a scan rate of 100 mVs^{-1} is shown as a representative example (Figure 4.16a). Compound **134** shows behaviour almost identical to that of MV^{2+}, with good reversibility, except with slight broadening of the radical cation reduction peak (Figure 4.16b).

In all cases, a significantly more cathodic first and second redox potential is found when compared to MV^{2+}, with a cathodic shift of at least 70 mV. A possible explanation may lie with the electron-withdrawing effect of the viologen substituents. For example, for the tetrapodal derivatives, the two quaternarised pyridinium nitrogen atoms give each substituent a formal two plus charge. It has been shown that the reduction potential of viologens obeys a linear free energy relationship (LFER) with the nitrogen substituents, with electron withdrawing groups increasing the reduction potential.[22, 38-39]

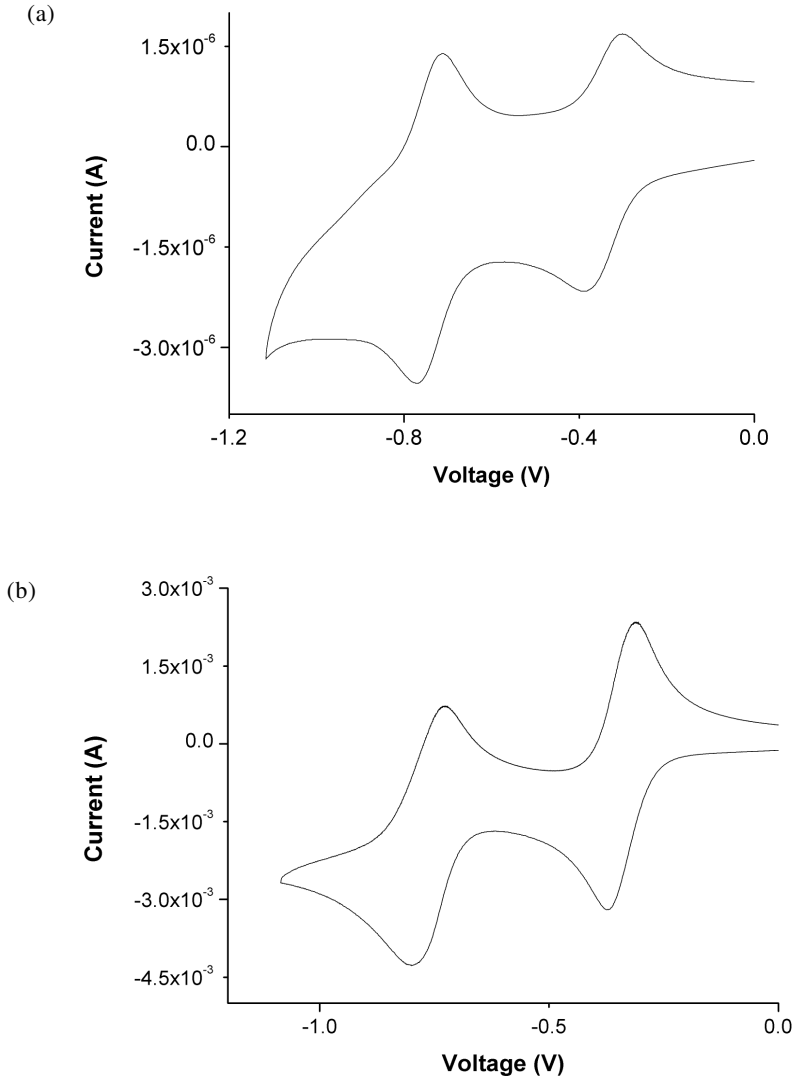

Figure 4.16 Cyclic voltammogram of (a) compound **132** and (b) compound **134**, both recorded at a 100 mV s^{-1} scan rate in 0.1 mol dm^{-3} TBA-PF_6 in MeCN

Table 4.2. Summary of electrochemical data for viologen derivatives, $E_{1/2}$ values reported vs. SCE in 0.1 mol dm^{-3} TBA-PF_6 in MeCN, I_{pa} = anodic peak current, I_{pc} = cathodic peak current

Compound	$E_{1/2}$ /V	ΔE /mV	I_{pa}/I_{pc}
132	E_1 = -0.36	70	0.9
	E_2 = -0.74	70	> 0.9
125	E_1 = -0.31	110	> 0.9
	E_2 = -0.76	90	0.9
126	E_1 = -0.35	100	0.9
	E_2 = -0.74	60	> 0.9
134	E_1 = -0.34	60	> 0.9
	E_2 = -0.76	70	> 0.9

4.7 Electrochemical Titrations

It has been shown that the anion can play a significant role in determining the reduction potential of viologens. In many cases only a small potential shift is found, but this is not always the case.[38] The effect of anions on the redox potential of compounds **132**, **125**, **126** and **134** was investigated. As these receptors are able to bind halides strongly, close to the viologen unit, it was anticipated that significant perturbation of the redox wave would be observed. The ferrocene/ferrocenium couple (Fc/Fc^+) was used as an internal reference. Control titrations with anions and an aqueous Ag/AgCl electrode proved that no significant change in the ferrocene redox wave was observed with added anion. A scan rate of 200 mV s^{-1} was used with the electrochemical cell kept under a constant positive pressure of N_2. Guest solutions were degassed before use (see experimental section).

Almost identical behaviour was seen for compounds **132**, **125** and **126** upon the addition of TBA-Cl. As the number of equivalents is increased, a gradual increase in the peak current is observed with a low to modest cathodic potential shift (e.g. compound **132**, ΔE = 80 mV with 30 equivalents of TBA-Cl). Both the potential shift and current increase were consistent for compounds **132**, **125**, and **126**. A representative stack plot is shown in Figure 4.17. Significantly, smaller intensity gains

and potential shifts were observed for TBA-Br (ΔE = 14 mV). These titrations show that addition of anions does affect the cyclic voltammograms obtained and hence the viologen redox potential.

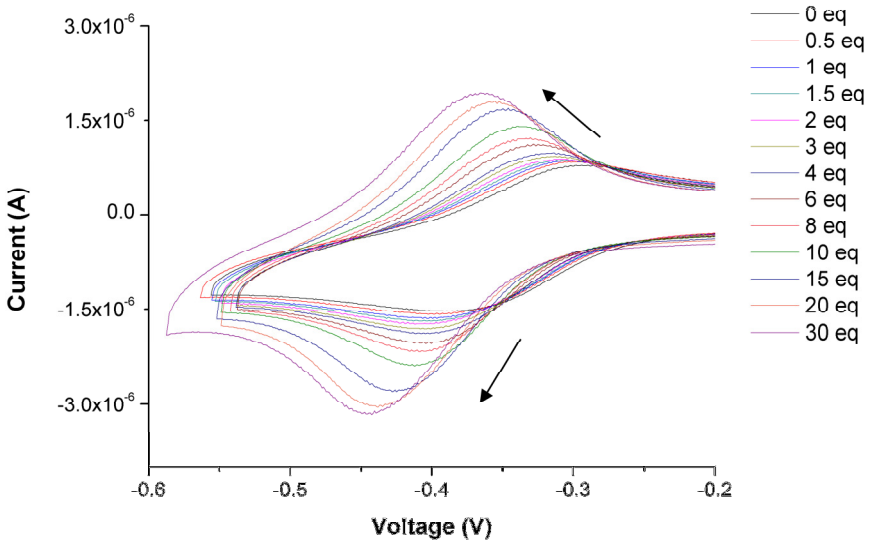

Figure 4.17 Cyclic voltammogram of compound **132** (1.0 x 10^{-4} mol dm^{-3}) with increasing equivalents of TBA-Cl in 0.1 mol dm^{-3} TBA-PF_6 in MeCN

Compound **134** demonstrates a unique property in this series of compounds. At 25 equivalents of TBA-Cl a new reduction wave appears at lower potential on the anodic peak. With addition of further chloride, this shoulder grows and the original peak is reduced (Figure 4.18). The cathodic peak is also reduced. This same effect is also observed to a lesser extent for TBA-Br. Addition of 30 equivalents of TBA-Cl and repeated scanning without further addition of anion also leads to the growth of the shoulder. Thorough cleaning of the electrode surface produced a scan similar to the original scan. This suggests that deposition of the complex on the electrode surface occurs at higher equivalents of halide guest. A similar effect has recently been reported by Gale and co-workers[40] with ferrocene derived phenylenediamine anion receptors. They suggest the effect of electrodeposition may provide a new means of anion sensing.

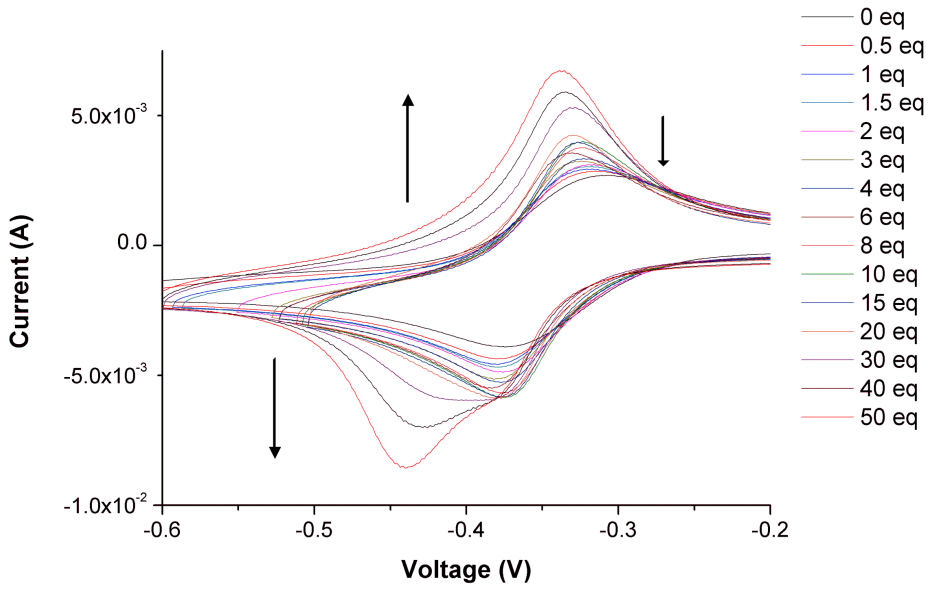

Figure 4.18 Cyclic voltammogram of compound **134** (1.0 x 10^{-4} mol dm^{-3}) with increasing equivalents of TBA-Cl in 0.1 mol dm^{-3} TBA-PF_6 in MeCN

Titrations with carboxylate anions were also undertaken for all compounds. Due to the decomposition of the host/succinate complex during the UV-vis spectroscopic titrations succinate was not investigated in detail. There is a general trend of a gradual decrease in peak current as anion is added in all cases (see Figure 4.19 for a representative example). This is accompanied by a colour change from colourless to purple.

The peak current in cyclic voltammetry is given by the Randles-Sevcik equation with the experimental factors affecting the magnitude being, the concentration of the electroactive species, the scan rate, the area of the electrode and the diffusion coefficient. In the course of the titration experiment only the diffusion coefficient and the concentration of the electroactive species are likely to change. It is unlikely the concentration is the important factor. It has been shown in previous electrochemical titrations, for example of **132** with chloride, that a cathodic shift of *ca*. 80 mV is observed. It would therefore be expected that a shift of similar magnitude would be observed with acetate. This cathodic shift would still be seen within the observation window and therefore the concentration of electroactive species observed should not change. It is therefore likely that the magnitude of the peak current changes due to differences in the diffusion coefficient upon binding of carboxylates. This would be

expected given the changes in both mass and conformational of the electroactive molecule upon anion binding.

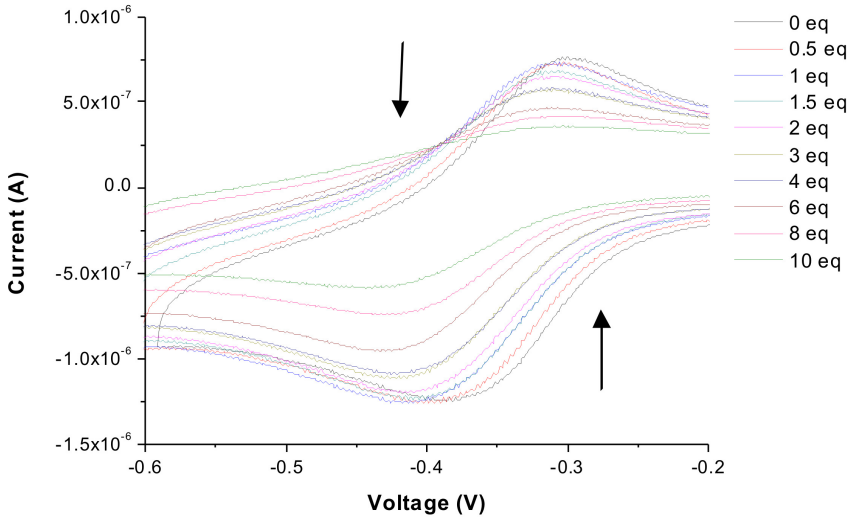

Figure 4.19 Cyclic voltammogram of compound **132** with increasing equivalents of TBA-acetate in 0.1 mol dm^{-3} TBA-PF_6 in MeCN

Given the low reduction potential of the host molecules described above, in principle it should be relatively easy to chemically reduce the viologen unit to the radical cation. Indeed there is evidence for this in the UV-vis spectra of the charge transfer complexes, particularly for compounds **132** and **134** with acetate, which show a significant band at 398 nm and the appearance of a tail on the charge transfer band. These bands are assigned to the formation of a viologen radical cation.

4.8 Investigation into the Radical Cation

The spectroscopy of the viologen radical cation has been extensively studied.[22] The UV-vis spectra of the chemically reduced MV.PF_6, MV.OAc and compound **132** are shown in Figure 4.20. The MV.OAc radical cation is formed upon the addition of TBA-OAc to methyl viologen di-hexafluorophosphate. It appears that the mixing of MV^{2+} and acetate ions in a relatively non-competitive solvent, leads to ion-pairing and electron transfer, with no evidence of a charge transfer band in the UV-vis spectrum.[35] Generation of the radical cation from charge transfer complexes is known and generally

occurs via a photo-electron transfer process.[22,41] However, typically back electron transfer is fast and transient absorption spectroscopy is required to observe the radical.[41] All the spectra shown in Figure 4.20 are essentially identical suggesting the R groups on compound **132** and the change in counter-ion have no effect on the radical's optical transitions and are consistent with the literature values. [22,36]

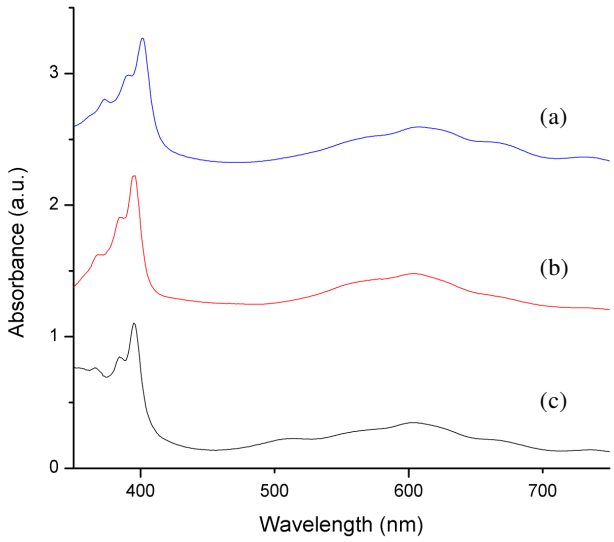

Figure 4.20 UV-vis spectra of the radical cation of viologen derivatives (a) compound **132** radical, (b) MV.OAc radical, (c) MV.PF_6 radical in MeCN

In order to confirm the presence of the cation radical, ESR studies on compounds **132** and **134** were undertaken in acetonitrile at 205 K. Compound **134** does show a weak resonance (Figure 4.21) with a g-factor of 2.0065 - close to the value of a free electron and close to the literature value for methyl viologen.[42] The resonance does not show any hyperfine structure. No ESR resonance was observed for compound **132**, however this is not unexpected. Comparing the UV-vis spectra of the acetate complexes of **132** and **134**, there is significantly less intensity of the 398 nm band for compound **132** indicating a lower concentration of radical and therefore, given the weak signal obtained for **134** (attenuated by the strongly microwave absorbing solvent, acetonitrile), a very weak signal would be expected for **132**.

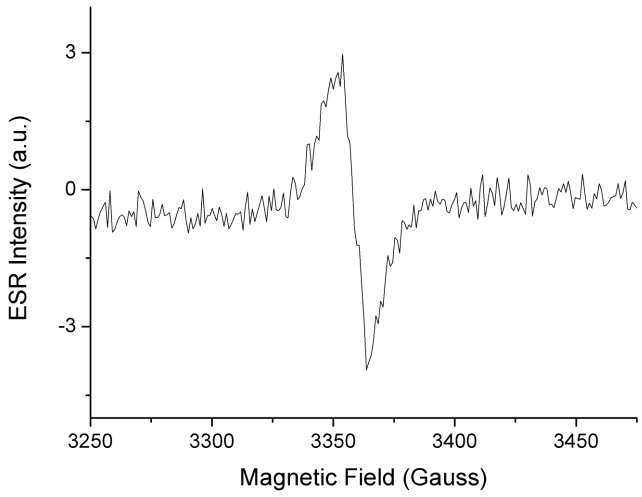

Figure 4.21 ESR spectrum for compound **134** in MeCN at 205 K

The viologen radical cation can also be probed using resonance Raman spectroscopy.[43-46] Figure 4.22a shows the resonance Raman spectrum of the MV.PF_6 radical cation, measured using a 633 nm He-Ne laser. The observed peaks correspond well to the literature.[43] A resonance Raman spectrum was also obtained for the charge transfer complex of **132** with acetate, targeting the charge transfer band using a Nd.YAG laser at 532 nm (Figure 4.22b). Several peaks appear in the spectral region corresponding to bipyridine vibrations, four of which broadly correspond to the radical bands. A resonance Raman spectrum was also obtained for the same complex using the He-Ne laser at 633 nm (Figure 4.22c). The absorbance of the charge transfer band is essentially zero at this wavelength, whilst the absorbance of the radical cation is relatively high. Correspondingly, four prominent bands appear in the spectrum which correspond well with the radical cation. Therefore depending on the wavelength used, both the charge transfer complex and the radical cation or radical cation alone can be targeted.

Interestingly, compound **134** has identical resonance Raman spectra for the charge transfer complex and the radical cation as compound **132**. Given the symmetry differences in the compounds this suggests that the orbitals involved in the radical cation electronic transition are localised almost entirely on the bipyridine unit. The band at 950 cm^{-1} is present in all spectra containing an acetate anion and is tentatively assigned as an acetate vibration.

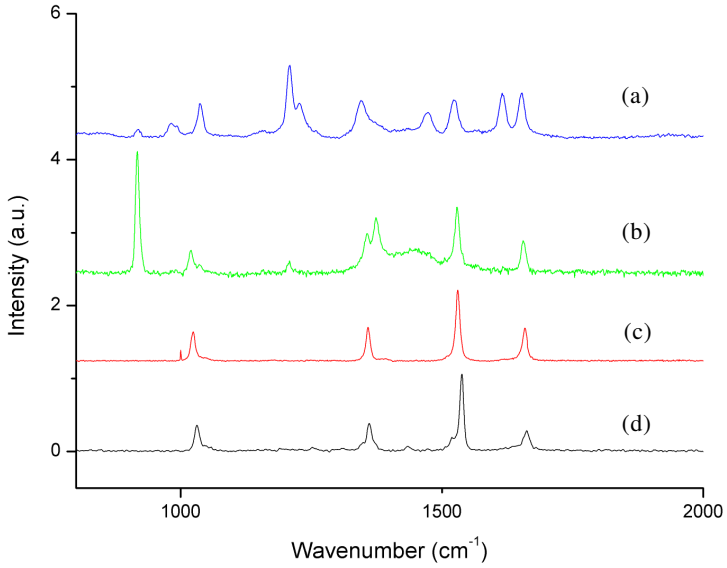

Figure 4.22 Resonance Raman spectra for (a) compound **132** with OAc^-, irradiated with a 532 nm laser, (b) compound **132** with OAc^-, irradiated with a 633 nm laser, compound (c) **132**, chemically reduced, (d) $MV.PF_6$ radical in MeCN

4.9 Conclusions

Four viologen derived anion hosts have been synthesised with either a ditopic, tetrapodal or a monotopic, tripodal design. All compounds bind anions strongly in acetonitrile solution, with a colourimetric response observed upon the addition of only carboxylates. Carboxylates give rise to an absorbance band centred at 540 nm. This is assigned to a charge transfer interaction, an assignment supported by DFT calculations. The band is red-shifted significantly compared to related systems in the literature[22] because of the very low reduction potential of the viologen derivatives synthesised in this work.

Cyclic voltammetric titrations have shown that there are modest cathodic shifts in the reduction potential but significant increase in the peak current. For compound **134**, titrations with chloride gave rise to a cathodically shifted electrodeposition peak. Electrochemical titrations with acetate caused a reduction in the peak current for the viologen redox wave for all compounds and may be due to changes in the diffusion coefficient of the host.

Addition of carboxylates also gives rise to the radical cationic species of the viologen derivatives, particularly for compounds **132** and **134**. The radical cation was characterised by UV-vis, Raman and ESR spectroscopies.

By coupling tripodal anion binding groups to a viologen type reporter it is possible to develop and tune a colourimetric sensor for carboxylate anions. The anion response can be modulated by the presence of other anion binding groups that control access to the chromophore and, in the case of **134** and malonate, appears to depend on the anion binding geometry.

4.10 Experimental

Instrumentation

All NMR spectra were performed on a Varian Mercury-400 (400 MHz for ^{1}H), Varian Inova-500 machine (500 MHz for ^{1}H, 126 Hz for ^{13}C) or a Varian DD-700 (700 MHz for ^{1}H, 176 MHz for ^{13}C) and were referenced to residual solvent. Electrospray (ES) mass spectrometry was recorded on a Thermo-Finnigan LTQ instrument, whilst Matrix Assisted Laser Desorption Ionisation (MALDI) experiments were recorded on an ABI Voyager-DC STR. Elemental analysis was performed using an Exeter Analytical inc. CE-400 Elemental Analyser. All Raman spectra were obtained on a Horiba Jobin-Yvon LabRAM HR equipped with a Nd.YAG (532 nm), He-Ne (633 nm). Spectra were acquired using a 600 g/mm diffraction grating and an Andor CCD detector. Band positions were calibrated against silicon. The software used was Labspec 5. Fourier transform infrared spectra were recorded with a Perkin Elmer Spectrum 100 ATR instrument. For each spectrum, 64 scans were conducted over a spectral range of 4000 to 600 cm^{-1} with a resolution of 4 cm^{-1}. The analysis was carried out with the Spectrum Express 1.01 software. ESR spectra were recorded on a Bruker BioSpin EMX spectrometer at 205 K. All solid state reactions were carried out using a Retsch MM200 ball mill with a 25 ml shaker grinding jar.

General Procedure for ^{1}H NMR Spectroscopy Titrations

^{1}H NMR titration experiments were carried out at room temperature, all chemical shifts are reported in ppm relative to residual solvent. A solution of the host species of known

concentration typically 0.5-1.5 mM, was made up in an NMR tube using the appropriate deuterated solvent (0.5 ml). Solutions of the anions, as TBA salts (1 ml) were made ten times the concentration of the host solution. The guest solution was typically added in 10 µl aliquots, representing 0.1 equivalents of the guest with respect to the host. Larger aliquots were used in some cases where no inflection of the trace was evident. Spectra were recorded after each addition and the trace was followed simultaneously. Results were analysed using the curve-fitting program *HypNMR* 2006.[26]

General Procedure for UV-vis Spectroscopic Titrations

UV-vis titrations were carried out using an ATI-Unicam UV2 UV-vis spectrometer. A solution of concentration 1.0 x 10^{-4} mol dm^{-3} of host was made in a volumetric flask. A 3 ml sample of host solution of concentration 1.0 x 10^{-5} mol dm^{-3} was prepared by dilution of the stock solution. Guest solutions were prepared such that 300 µl of guest solution corresponds to 10 equivalents of host. Solutions were prepared using dry degassed acetonitrile as solvent. All samples were prepared in a glove box and were sealed using suba-seals and parafilm. A nitrogen filled balloon was used to maintain an inert atmosphere during removal or addition of aliquots of solution.

General Procedure for Cyclic Voltammetry Experiments

Cyclic voltammetry was carried out on a Chi Instruments Model 420 Electrochemical Analyser using a three electrode cell with two Pt wire counter electrodes and a 2 mm Pt working electrode or a 3 mm glassy carbon working electrode. The ferrocene/ferrocinium redox couple was used as an internal reference. $E_{1/2}$ values are reported vs. SCE (Fc = 0.40 V with TBA-PF_6 in MeCN[47]). A 0.1 mol dm^{-3} solution of TBA-PF_6 in dry MeCN was used as electrolyte. Solutions were degassed by bubbling through N_2 and the cell was kept under positive pressure of N_2 at all times.

General Procedure for Cyclic Voltammetry Titration Experiments

A host solution of 1.0 x 10^{-4} mol dm^{-3} in 0.1 mol dm^{-3} TBA-PF_6 in MeCN was used. Guest solutions were prepared such that 300 µl of guest solution corresponds to 10 equivalents of host and degassed by bubbling through N_2. A scan rate of 200 mV s^{-1} was used for all scans.

Materials were obtained from standard commercial sources. 1,3,5-Tri(bromomethyl)-2,4,6-triethylbenzene[48] and 1,1'-bis(3,5-bis(bromomethyl)-2,4,6-triethylbenzyl)-4,4'-bipyridine-1,1'-diium bromide[24] were prepared as previously reported.

Synthesis of 132

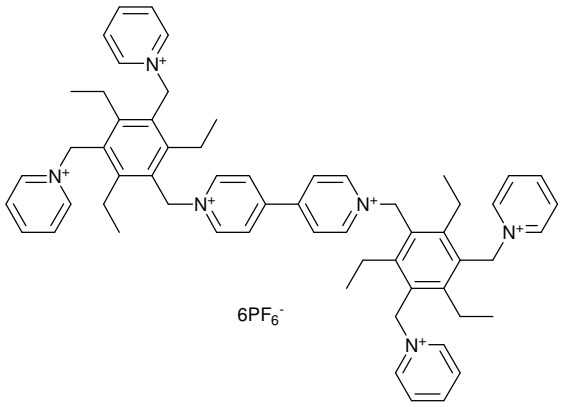

1,1'-bis(3,5-bis(bromomethyl)-2,4,6-triethylbenzyl)-4,4'-bipyridine-1,1'-diium bromide (1.0 g, 0.48 mmol) and pyridine (1.14 g, 1.4 mmol) were dissolved in methanol and stirred at reflux for 18 hours under N_2. The solvent was removed under reduced pressure and a yellow sticky solid was produced (the bromide salt) which could not be characterised fully. The solid was dissolved in 50 ml of methanol and filtered to remove impurities. To the filtrate, excess NH_4PF_6 was added and stirred for 6 hours. The white precipitate was filtered and recrystallised from acetonitrile/diethyl ether to yield the hexafluorophosphate salt. Yield = 0.44 g, 0.28 mmol, 59%. m.p. decomposed by 230 ^oC; ^1H NMR (CD_3CN, 500 MHz /ppm) δ = 8.91 (4H, d, J = 7.5 Hz, PyH), 8.71 (8H, d, J = 6.5 Hz, BpyH), 8.55 (4H, t, J = 7.5 Hz, PyH), 8.41 (8H, d, J = 6.5 Hz, BpyH), 8.09 (4H, t, J = 7.5 Hz, PyH), 5.97 (4H, s, CH_2-Bpy), 5.89 (8H, s, CH_2-Py), 2.54 (12H, br q, CH_2CH$_3$), 1.05 (18H, br t, CH$_3$); ^{13}C-{^1H} NMR (CD_3CN, 126 MHz /ppm) 152.2, 152, 151.3, 147.3 145.8, 144.6, 129.7, 128.6, 128.4, 128.0, 58.9, 58.6, 24.8, 15.3, 15.2; ν/cm^{-1} 3143 (m, Ar C-H), 3104 (m, Ar C-H), 2978 (m, CH$_2$/CH$_3$), 2940 (m, CH$_2$/CH$_3$), 1637 (s, Ar C=C), 1567 (s, Ar C=C), 1503 (s, Ar C=C), 1485, 1448 (m, CH$_2$/CH$_3$ def), 1391 (m, CH$_3$ def) 1219, 1149, 1043, 838, 558; Found: C, 41.31; H, 4.10; N, 4.96; Calc. $C_{60}H_{70}F_{36}N_6P_6$; C, 41.3; H, 4.04; N, 4.82.

Crystal data for **132**: $C_{62}H_{73}F_{36}N_7P_6$, M = 1786.10, colourless plate, 0.42 × 0.26 × 0.14 mm^3, monoclinic, space group $P2_1/c$ (No. 14), a = 27.132(5), b = 9.4203(16), c =

30.586(5) Å, β = 103.680(6)°, V = 7596(2) Å^3, Z = 4, D_c = 1.562 g/cm^3, F_{000} = 3632, Smart 6K, MoKα radiation, λ = 0.71073 Å, T = 120(2)K, $2\theta_{max}$ = 50.0º, 43497 reflections collected, 13381 unique (R_{int} = 0.1288). Final *GooF* = 0.976, *R1* = 0.1144, *wR2* = 0.2870, *R* indices based on 5393 reflections with I >2σ(I) (refinement on F^2), 1056 parameters, 54 restraints. Lp and absorption corrections applied, μ = 0.274 mm^{-1}.

Synthesis of 125

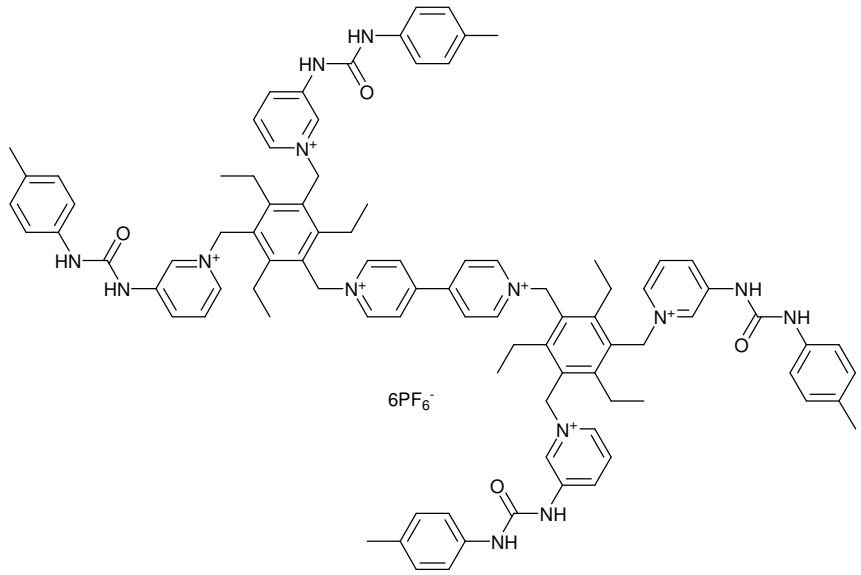

1,1'-bis(3,5-bis(bromomethyl)-2,4,6-triethylbenzyl)-4,4'-bipyridine-1,1'-diium bromide (0.50 g, 0.45 mmol) and 1-pyridin-3-yl-3-*p*-tolyl-urea (0.44 g, 1.9 mmol) were placed in a 25 ml ball mill with 5 drops of acetonitrile and ground for 2 hours at 18 Hz. The residue was dissolved in methanol (50 ml) and any unreacted starting material removed by filtration. Ten equivalents of NH_4PF_6 were added and the solution was stirred for 6 hours at ambient temperature. The solution was filtered and the compound recrystallised from acetonitrile/diethyl ether. Yield = 0.30 g, 0.12 mmol, 27%. m.p. 206 - 213 ^{o}C decomposes in this region; ^{1}H NMR (CD_3CN, 700 MHz /ppm) δ = 9.15 (4H, s, PyH), 8.55 (4H, d, J = 6.2 Hz, BpyH), 8.41 (4H, s, PyH), 7.91 (4H, s, NH), 7.82 (8H, BpyH and PyH), 7.55 (4H, s, PyH), 7.51 (4H, s, NH), 7.15 (8H, d, J = 8.2 Hz, ArH), 7.03 (8H, J = 8.2 Hz, ArH), 5.95 (4H, s, CH_2-Bpy), 5.92 (8H, s, CH_2-Py), 2.80 (8H, q, J = 7.5 Hz, CH_2CH$_3$), 2.54 (16H, q, J = 7.5 Hz, CH_2CH$_3$), 2.16 (12H, s, tolyl-CH$_3$), 1.24 (12H, br s, CH$_2$CH_3), 1.09 (24H, br s, CH$_2$CH_3); ^{13}C-{^{1}H} NMR (CD_3CN, 176 MHz /ppm) δ = 151.9, 151.6, 151.1, 144.3, 140.8, 137.2, 135.3, 133.7, 133.3, 132.1, 129.5, 128.1, 127.0, 126.9, 120.0, 57.8, 24.3, 24.0, 19.8, 15.0, 14.64; ν/cm^{-1}

3413 (s, N-H), 3120 (m, Ar C-H), 2983 (m, CH_2/CH_3), 1714, 1636 (s, Ar C=C), 1593 (s, urea C=O), 1551 (s, Ar C=C), 1503 (s, Ar C=C), 1460, 1443, 1408 (m, CH_2/CH_3 def), 1390 (w, CH_3 def) 1315, 1295, 1243. 840; Found: C, 45.85; H, 4.47; N, 7.97; Calc. for $C_{92}H_{102}N_{14}P_6F_{36}.4H_2O$: C, 45.86; H, 4.60; N, 8.14; the presents of water is suggested by NMR and IR spectra.

Synthesis of 126

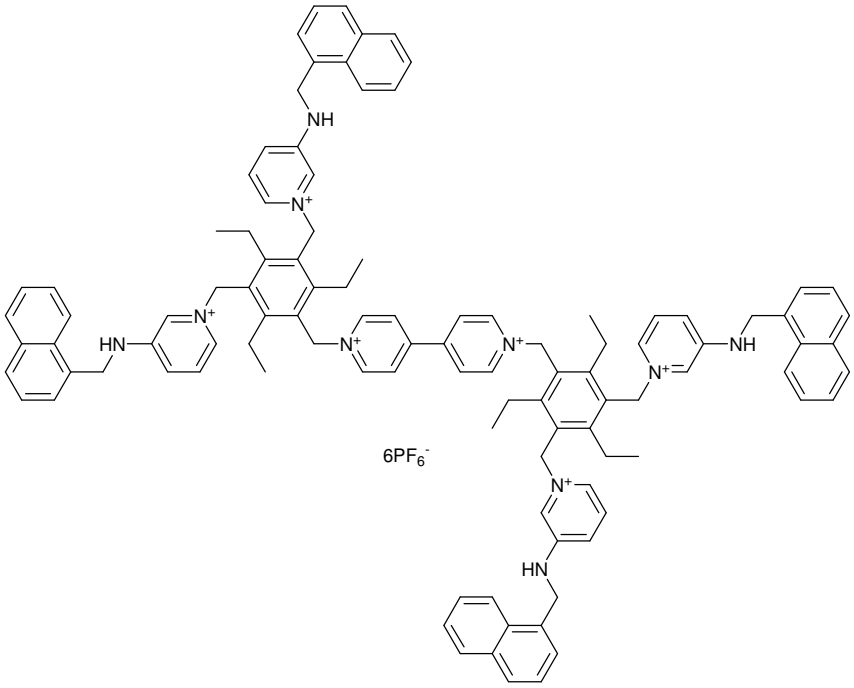

1,1'-bis(3,5-bis(bromomethyl)-2,4,6-triethylbenzyl)-4,4'-bipyridine-1,1'-diium bromide (0.50 g, 0.45 mmol) and *N*-((naphthalene-1-yl)methyl)pyridine-3-amine (0.45 g, 1.9 mmol) were placed in a 25 ml grinding jar with 5 drops of acetonitrile. The reactants were ground at 18 Hz for 60 minutes after which methanol was added and unreacted starting material removed by filtration. Excess (approx. 10 equivalents) NH_4PF_6 was added to the methanol solution and the product precipitated as the PF_6^- salt. The compound was recrystallised from acetonitrile/diethyl ether. Yield = 0.45 g, 0.19 mmol, 39%. m.p. decomposed above 250 ^oC; ^1H NMR (CD_3CN, 700 MHz /ppm) δ = 8.78 (4H, s, ArH), 8.36 (4H, d, *J* = 7.0 Hz, ArH), 8.05 (4H, d, *J* = 8.1 Hz, ArH), 7.97 (4H, d, *J* = 7.6 Hz, ArH), 7.87 (8H, m, ArH), 7.60 (10H, m, ArH), 7.45 (8H, m, ArH), 6.40 (4H, br s, NH), 5.87 (4H, s, CH_2), 5.62 (8H, s, CH_2-Py^+), 4.88 (8H, d, *J* = 5.5 Hz, CH_2CH_3), 2.53 (8H, q, *J* = 7.6 Hz, CH_2CH_3), 2.48 (12H, q, *J* = 7.6 Hz, CH_2CH_3), 0.91 (12H, br s, CH_3), 0.85 (24H, br s, CH_3); ^{13}C-{^1H} NMR (CD_3CN, 176 MHz /ppm) δ =

150.5, 148.2, 144.7, 133.9, 131.6, 131.1, 130.3, 128.8, 128.4, 128.1, 128.1, 127.5, 126.7, 126.5, 126.2, 125.5, 125.0, 123.2, 58.1, 57.5, 44.5, 23.8, 23.7, 14.3, 14.0; ν/cm^{-1} 3431 (w, N-H), 3070 (w, C-H), 2983 (w, CH_2/CH_3), 1636 (m Ar C=C), 1504 (w, Ar C=C), 1446 (m, Ar C=C), 1150. 1041, 823; Found: C, 49.49; H, 4.36; N, 5.55; Calc. for $C_{104}H_{106}N_{10}P_6F_{36}.8H_2O$: C, 49.77; H, 4.90; N, 5.58; the presents of water is suggested by NMR and IR spectra. Reliable mass spectrometry data could not be obtained for this compound.

Synthesis of 133

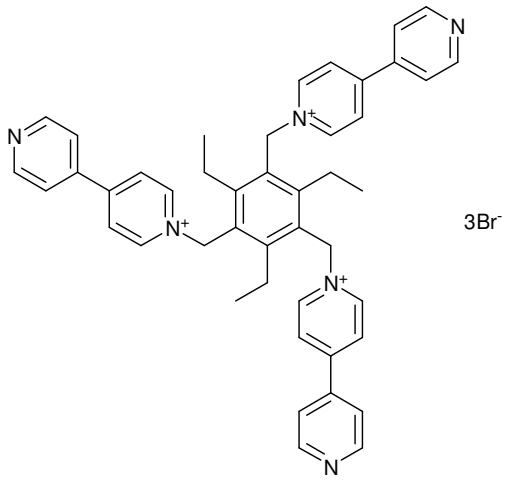

1,3,5-Tri(bromomethyl)-2,4,6-triethylbenzene (0.50 g, 1.1 mmol) and 4,4'-bipyridine (1.77 g, 11 mmol) were dissolved in 150 ml of dry dichloromethane. The resulting solution was stirred at reflux under N_2 for 23 hours. A pale yellow precipitate was produced and isolated by filtration. Yield = 0.97 g, 1.1 mmol, 95 %. Characterisation consistent with published literature.[23]

Synthesis of 134

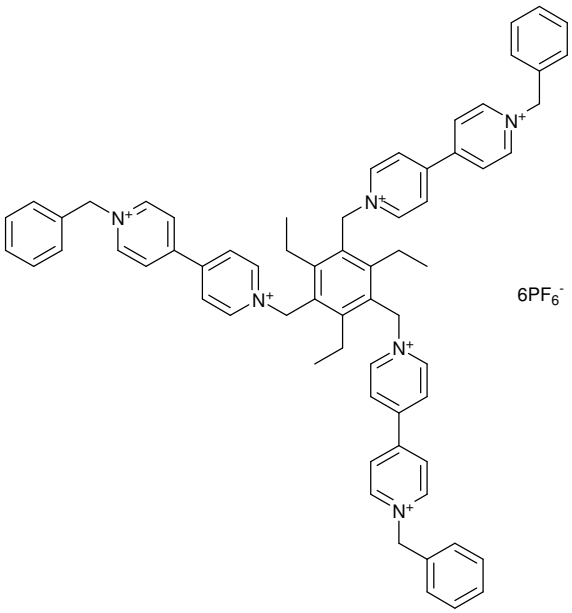

Compound **133** (0.38 g, 0.41 mmol) was dissolved in 5 ml of dry dimethylformamide. Then benzyl bromide (0.52 ml, 4.4 mmol) was added and the yellow mixture was allowed to stir at 70 ^{o}C for 20 hours under N_2. During the reaction a yellow-brownish precipitate occurred. After cooling, the mixture was poured into diethyl ether and a yellow precipitate was observed and isolated by filtration. During drying the product became a sticky brown oil and therefore was metathesised to the PF_6^- salt immediately by dissolving in methanol and adding excess (approx. 10 equivalents) NH_4PF_6 (1.5 g), without characterisation of the bromide salt. Yield = 0.53 g, 0.30 mmol, 71 %. m.p. decomposed above 250 ^{o}C; ^{1}H NMR (CD_3CN, 700 MHz /ppm) δ = 8.96 (8H, d, *J* = 7.0 Hz, BpyH), 8.92 (8H, d, *J* = 7.0 Hz, BpyH), 8.40 (8H, d, *J* = 7.0 Hz, BpyH), 8.36 (8H, d, *J* = 7.0 Hz, BpyH), 7.51 (15H, s, Ph-H), 6.00 (6H, s, C*H*$_2$-Py), 5.82 (6H, s, C*H*$_2$-Bpy), 2.60 (6H, q, *J* = 7.3 Hz, C*H*$_2$CH$_3$), 1.09 ppm (9H, t, *J* = 7.3 Hz, CH_3); ^{13}C–{^{1}H} (CD_3CN, 176 MHz /ppm) δ = 15.5, 25.0, 59.1, 65.8, 128.5, 130.3, 130.6, 131.1, 133.5, 145.8, 146.6, 151.4, 151.5, 152.5; *m/z* (MALDI$^+$) 563.2, 565.2, 647.5, 649.5, 663.5, 1667.3 [M - PF_6]$^+$; ν/cm^{-1} 3131 (w, C-H), 3069 (w, C-H), 1637 (m Ar C=C), 1561 (w, Ar C=C), 1499 (w, Ar C=C), 1447 (m, Ar C=C), 1220. 1144, 1002, 823; Found: C, 41.98; H, 3.62; N, 4.55; Calc. for $C_{66}H_{66}N_6P_6F_{36}.4H_2O$: C, 42.05; H, 3.96; N, 4.46; the presents of water is suggested by NMR and IR spectra.

4.10 References

1. J. L. Sessler, P. A. Gale and W.-S. Cho, '*Anion Receptor Chemistry*', Royal Society of Chemistry, Cambridge, 2006.
2. C. Caltagirone and P. A. Gale, *Chem. Soc. Rev.*, 2009, **38**, 520.
3. P. A. Gale, *Coord. Chem. Rev.*, 2006, **250**, 2917 preface to the special issue and subsequent reviews.
4. T. Gunnlaugsson, M. Glynn, G. M. Tocci, P. E. Kruger and F. M. Pfeffer, *Coord. Chem. Rev.*, 2006, **250**, 3094.
5. M. H. Filby, T. D. Humphries, D. R. Turner, R. Kataky, J. Kruusma and J. W. Steed, *Chem. Commun.*, 2006, 156.
6. M. Boiocchi, L. Del Boca, D. Esteban-Gomez, L. Fabbrizzi, M. Licchelli and E. Monzani, *Chem. - Eur. J.*, 2005, **11**, 3097.
7. V. Amendola, D. Esteban-Gomez, L. Fabbrizzi and M. Licchelli, *Acc. Chem. Res.*, 2006, **39**, 343.
8. K. J. Wallace, W. J. Belcher, D. R. Turner, K. F. Syed and J. W. Steed, *J. Am. Chem. Soc.*, 2003, **125**, 9699.
9. D. R. Turner, M. J. Paterson and J. W. Steed, *J. Org. Chem.*, 2006, **71**, 1598.
10. M. H. Filby, S. J. Dickson, N. Zaccheroni, L. Prodi, S. Bonacchi, M. Montalti, C. Chiorboli, M. J. Paterson, T. D. Humphries and J. W. Steed, *J. Am. Chem. Soc.*, 2008, **130**, 4105.
11. V. Amendola, M. Boiocchi, L. Fabbrizzi and A. Palchetti, *Chem.-Eur. J.*, 2005, **11**, 5648.
12. H. Ihm, S. Yun, H. G. Kim, J. K. Kim and K. S. Kim, *Org. Lett.*, 2002, **4**, 2897.
13. Y. Bai, B.-G. Zhang, C. Y. Duan, D.-B. Dang and Q.-J. Meng, *New. J. Chem.*, 2006, **30**, 266.
14. L. O. Abouderbala, W. J. Belcher, M. G. Boutelle, P. J. Cragg, M. Fabre, J. Dhaliwal, J. W. Steed, D. R. Turner and K. J. Wallace, *Chem. Commun.*, 2002, 358.
15. A. Metzger, V. M. Lynch and E. V. Anslyn, *Angew. Chem., Int. Ed.*, 1997, **36**, 862.
16. G. Hennrich and E. V. Anslyn, *Chem.-Eur. J.*, 2002, **8**, 2218.
17. J. W. Steed, *Chem. Commun.*, 2006, 2637.
18. G. Rogez, B. F. Ribera, A. Credi, R. Ballardini, M. T. Gandolfi, V. Balzani, Y. Liu, B. H. Northrop and J. F. Stoddart, *J. Am. Chem. Soc.*, 2007, **129**, 4633.
19. W. Sliwa, B. Bachowska and T. Girek, *Curr. Org. Chem.*, 2007, **11**, 497.
20. M. Ezoe, S. Yagi, H. Nakazumi, M. Itou, Y. Araki and O. Ito, *Tetrahedron*, 2006, **62**, 2501.
21. S. P. Gromov, A. I. Vedernikov, E. N. Ushakov, N. A. Lobova, A. A. Botsmanova, L. G. Kuz'mina, A. V. Churakov, Y. A. Strelenko, M. V. Alfimov, J. A. K. Howard, D. Johnels and U. G. Edlund, *New J. Chem.*, 2005, **29**, 881.
22. P. M. S. Monk, '*The Viologens: Physicochemical Properties Synthesis and Applications of the Salts of 4,4'-Bipyridine*', Wiley, New York, 1998
23. W. J. Belcher, M. Fabre, T. Farhan and J. W. Steed, *Org. Biomol. Chem.*, 2006, **4**, 781.
24. S. J. Dickson, E. V. B. Wallace, A. N. Swinburne, M. J. Paterson, G. O. Lloyd, A. Beeby and J. W. Steed, *New J. Chem.*, 2008, **32**, 786.
25. D. R. Turner, E. C. Spencer, J. A. K. Howard, D. A. Tocher and J. W. Steed, *Chem. Commun.*, 2004, 1352.

26. P. Gans, *HypNMR* 2006, University of Leeds, Leeds, 2006.
27. P. M. S. Monk and N. M. Hodgkinson, *Electrochim. Acta*, 1998, **43**, 245.
28. P. M. S. Monk, N. M. Hodgkinson and R. D. Partridge, *Dyes and Pigments*, 1999, **43**, 241.
29. S. G. Bertolotti, J. J. Cosa, H. E. Gsponer and C. M. Previtali, *Can. J. Chem.-Rev. Can. Chim.*, 1987, **65**, 2425.
30. S. M. Hubig and J. K. Kochi, *J. Phys. Chem.*, 1995, **99**, 17578.
31. G. Briegleb and J. Czekalla, *Zeitschrift Fur Elektrochemie*, 1959, **63**, 6.
32. B. G. White, *Transactions of the Faraday Society*, 1969, **65**, 2000.
33. A. Ledwith and H. J. Woods, *J. Chem. Soc. C-Organic*, 1970, 1422.
34. A. S. N. Murthy and A. P. Bhardwaj, *Spectroc. Acta Pt. A-Molec. Biomolec. Spectr.*, 1982, **38**, 207.
35. J. P. Kuczynski, B. H. Milosavljevic, A. G. Lappin and J. K. Thomas, *Chem. Phys. Lett.*, 1984, **104**, 149.
36. T. M. Bockman and J. K. Kochi, *J. Org. Chem.*, 1990, **55**, 4127.
37. Gaussian 03, Revision D.01 M. J Frisch, G. W. Trucks, H. B Schlegel, G. E Scuseria, M. A. Robb, J. R. Cheeseman, J. A. Montgomery Jr, T. Vreven, K. N. Kudin, J. C. Burant, J. M. Millam, S. S. Iyengar, J. Tomasi, V. Barone, B. Mennucci, M. Cossi, G. Scalmani, N. Rega, G. A. Petersson, H. Nakatsuji, M. Hada, M. Ehara, K. Toyota, R. Fukuda, J. Hasegawa, M. Ishida, T. Nakajima, Y. Honda, O. Kitao, H. Nakai, M. Klene, X. Li, J. E. Knox, H. P. Hratchian, J. B. Cross, C. Adamo, J. Jaramillo, R. Gomperts, R. E. Stratmann, O. Yazyev, A. J. Austin, R. Cammi, C. Pomelli, J. W. Ochterski, P. Y. Ayala, K. Morokuma, G. A. Voth, P. Salvador, J. J. Dannenberg, V. G. Zakrzewski, S. Dapprich, A. D. Daniels, M. C. Strain, O. Farkas, D. K. Malick, A. D. Rabuck, K. Raghavachari, J. B. Foresman, J. V. Ortiz, Q. Cui, A. G. Baboul, S. Clifford, J. Cioslowski, B. B. Stefanov, G. Liu, A. Liashenko, P. Piskorz, I. Komaromi, R. L. Martin, D. J. Fox, T. Keith, M. A. Al-Laham, C. Y. Peng, A. Nanayakkara, M. Challacombe, P. M. W. Gill, B. Johnson, W. Chen, M. W. Wong, C. Gonzalez and J. A. Pople, Gaussian Inc., Pittsburgh (PA), 2003.
38. C. L. Bird and A. T. Kuhn, *Chem. Soc. Rev.*, 1981, 49.
39. S. Hunig and W. Schenk, *Liebigs Annalen Der Chemie*, 1979, 1523.
40. M. Arroyo, P. R. Birkin, P. A. Gale, S. E. Garcia-Garrido and M. E. Light, *New J. Chem.*, 2008, **32**, 1221.
41. F. Ito and T. Nagamura, *J. Photochem. Photobiol. C-Photochem. Rev.*, 2007, **8**, 174.
42. C. S. Johnson and H. S. Gutowsky, *J. Chem. Phys.*, 1963, **39**, 58.
43. M. Forster, R. B. Girling and R. E. Hester, *J. Raman Spectrosc.*, 1982, **12**, 36.
44. C. A. Melendres, P. C. Lee and D. Meisel, *J. Electrochem. Soc.*, 1983, **130**, 1523.
45. D. J. Barker, R. P. Cooney and L. A. Summers, *J. Raman Spectrosc.*, 1987, **18**, 443.
46. Y. X. Huang and J. B. Hopkins, *J. Phys. Chem.*, 1996, **100**, 9585.
47. N. G. Connelly and W. E. Geiger, *Chem. Rev.*, 1996, **96**, 877.
48. K. J. Wallace, R. Hanes, E. Anslyn, J. Morey, K. V. Kilway and J. Siegel, *Synthesis-Stuttgart*, 2005, 2080.

5. Fluorescent Anion Sensors Derived from Diphenyl-acetylene Based Molecular Clips

5.1 Introduction

Rigidly preorganised receptors for anionic, cationic and molecular guests exhibit high binding constants and high selectivity. Such characteristics are desirable in the design of high specificity molecular sensors. However, because there is no change in conformation between free and bound host, any change in observable characteristics, such as fluorescence emission, must result from the electronic effects of the bound guest.[1-3] In contrast flexible systems allow the possibility of induced fit[4] sensing in which the binding event brings sensing moieties into close mutual proximity, for example binding-induced conformational change can lead to the close mutual proximity of fluorophores resulting in excimer formation,[5-10] or may change the degree of twist in a conjugated aromatic system, altering its photophysical properties.[11,12] Similarly, conformational changes may result in changes to the electrochemical properties of redox-active sensing units.[13-15] However, flexible receptors are often less selective and exhibit lower overall affinities compared to their more rigid analogues.[16-19] With careful molecular design it should be possible to reduce the number of conformational degrees of freedom of a receptor such that binding of a specific anion results in a well defined induced-fit process. This involves only a single bond rotation, thus combining the benefits of rigid preorganisation and induced-fit sensing. The aim of this chapter is to design receptors which fulfill these criteria using neutral, rigid acetylene based anion receptors.[20-23]

The diphenylacetylene (DPA) moiety was chosen as the core unit for the receptors as the relatively rigid conjugated aromatic groups can provide a degree of preorganisation, whilst allowing rotation around the acetylene group and induced-fit recognition. Diphenylacetylene, its derivatives and longer congeners have interesting and complicated photophysical properties. DPA and diphenylbutadiyne exhibit low quantum yields of fluorescence due to the presence of a non-emissive $^1A_{1u}$ state (a $\pi_y^* \leftarrow \pi_x$ transition) which lies close in energy to the emissive $^1B_{1u}$ state ($\pi_x^* \leftarrow \pi_x$ transition). Excited state population transfer to the non-emissive $^1A_{1u}$ state, from the

emissive $^1B_{1u}$ state results in low emission and is an activated process, i.e. an activation barrier is present.[24-25] Tethered DPA derivatives, in which the conformation is restricted to a more planar geometry, show red-shifted UV-vis spectra and greater conjugation, combined with an increase in the barrier to internal conversion and importantly enhanced fluorescent emission.[26-28] DPA derivatives therefore seem ideally suited to induced-fit sensing and the functionalisation of DPA and its congeners with anion binding groups could lead to new anion sensors.

A series of acetylene based anion receptors has been synthesised by varying the conjugation length and the configuration of the DPA core (see Figure 5.1). It is hoped that this will provide a range of both cavity sizes and binding geometries, as well as photophysical behaviour. The key design feature of all compounds is the ability to have rotation around the acetylene group. The urea moiety was chosen as the binding motif as the synthesis of amine derived DPA derivatives is facile (*vida infra*) and the conversion of secondary amines to urea groups is generally high yielding.

5.2 Synthesis

Compound **135** was synthesised in high yield from the homo-coupling of 2-ethynylaniline via an Eglington reaction, to give the intermediate diyne **140** (Scheme 5.1).[29-30] The reaction of the intermediate amine, **140** with *p*-tolyl isocyanate gives the final product **135**. Compounds **136** – **139** were synthesised using Sonogashira methodology (Scheme 5.1).[31-32] Compound **136** was synthesised by the coupling of 2-ethynylaniline and 4-iodoaniline to give **141**, followed by reaction with *p*-tolyl isocyanate (39%). **137** – **139** were synthesised by a similar procedure to **136** and were obtained in high yield. The intermediate amine derivatives, **140** – **143**, Scheme 5.1 proved to have low nucleophilicity, for example aliphatic isocyanates proved highly unreactive towards the amines. The *p*-tolyl derivates (as well as other phenyl derivatives, *vida infra*) proved the most facile to synthesise, however they proved to have low solubility which requires DMSO solvent mixtures in order to study anion binding. Whilst a solvent mixture is not ideal, this solvent system was chosen as it was not possible to successfully synthesise long chain aliphatic derivatives which would have increased the solubility in organic solvents.

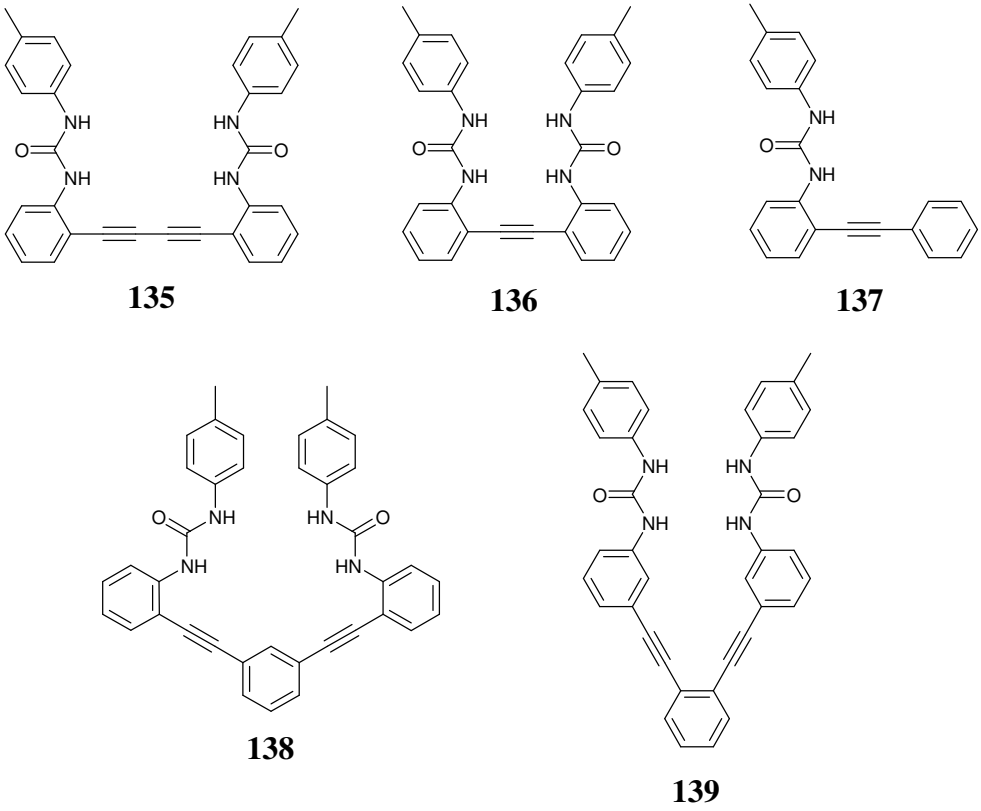

Figure 5.1 Fluorescent receptors **135** – **139**

All compounds were successfully synthesised and characterised, with details given in the experimental section. It proved particularly difficult to purify compound **139** due to the presence of a mono-urea product which could be identified in the ^{1}H NMR and by mass spectrometry. Integrating the size of the final product and impurity resonances suggests a purity of *ca.* 90%. All experimental data is reported with the 10% impurity present.

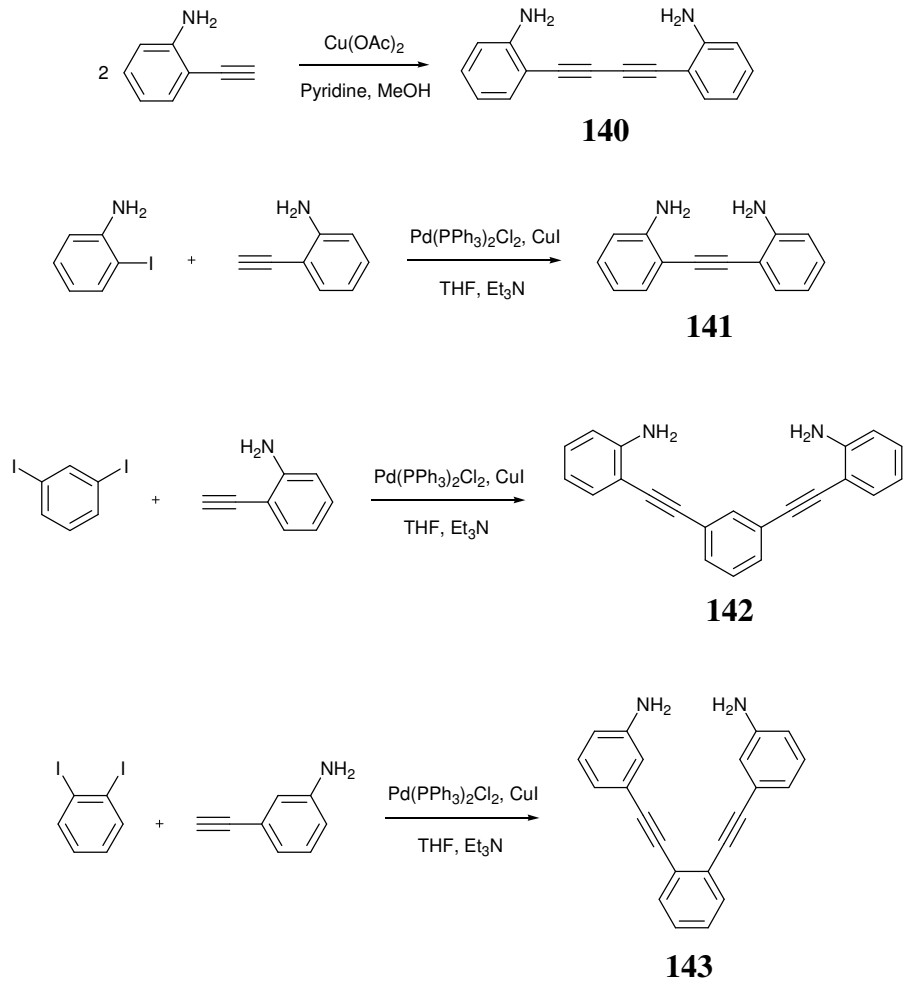

Scheme 5.1 Synthesis of compounds **140** - **143**

5.3 Anion Binding and Sensing by Linear Mono- and Dialkynes

The anion binding of **135** – **139** was investigated using ^{1}H NMR spectroscopic titrations in $CDCl_3$/DMSO-d_6 (*v/v* 70/30). Table 5.1 shows the binding constants determined using the non-linear least squares fitting program *HypNMR* 2006[33] for anions covering a range of basicities and geometries. Compounds **138 – 139** will be discussed in detail in this section.

Table 5.1 Binding constants for compound **135** – **139** using ^{1}H NMR spectroscopic titrations in $CDCl_3$/DMSO-d_6 (*v/v* 70/30). All anions used as TBA salts

	Receptor, Log β				
Anion	**135**	**136**	**137**	**138**	**139**
Fluoride	Log β_{11} 4.01(6) Log β_{12} 5.58(6)	Log β_{11} 4.09(6) Log β_{12} 6.58(5)	Log β_{11} 2.45(3) Log β_{21} 5.21(9)	Log β_{11} 3.328(2) Log β_{12} 4.150(2)	Log β_{11} 4.245(2) Log β_{12} 5.94(4)
Chloride	2.557(5)	1.831(7)	< 1	1.57(1)	2.292(6)
Bromide	1.56(1)	< 1	< 1	< 1	1.752(8)
Iodide	< 1	< 1	< 1	< 1	< 1
Nitrate	< 1	< 1	< 1	< 1	< 1
Acetate	3.61(1)	2.993(6)	Log β_{11} 2.41(4) Log β_{21} 5.11(9)	3.09(1)	2.48(1)
Dihydrogen phosphate	4.29(5)	3.29(1)	Log β_{11} 2.01(2) Log β_{21} 4.60(4)	3.46(2)	3.55(3)
Hydrogen sulfate	1.61(1)	1.2888(1)	< 1	1.56(3)	1.96(2)

Where species are in the following equilibria:

$$H \overset{K_{11}}{\rightleftharpoons} HG \overset{K_{12}}{\rightleftharpoons} HG_2$$

$$H \overset{K_{11}}{\rightleftharpoons} HG \overset{K_{21}}{\rightleftharpoons} H_2G$$

Binding constants are defined as:

$$K_{11} = \frac{[HG]}{[H][G]} \qquad K_{12} = \frac{[HG_2]}{[HG][G]} \qquad K_{21} = \frac{[H_2G]}{[H][HG]}$$

$$\text{Log}\,\beta_{11} = \text{Log}\,K_{11} \qquad \text{Log}\,\beta_{12} = \text{Log}\,K_{11} + \text{Log}\,K_{12}$$

$$\text{Log}\,\beta_{21} = \text{Log}\,K_{11} + \text{Log}\,K_{21}$$

H = Host, G = Guest

All hosts bind basic anions such as fluoride, dihydrogen phosphate and acetate strongly. For all hosts the urea NH protons show significant shifting in the ^{1}H NMR spectrum and confirm the urea groups as the primary site for anion binding. Figure 5.2 shows a representative binding isotherm for an NH proton of **135**. Job plot analysis suggests a 1:1 host:guest stoichiometry for the majority of anions (for example Figure 5.2b). However, in the case of fluoride, binding is strong enough to lead to a 1:2 host:guest binding mode in all cases. Job plot analysis could not be obtained for TBA-F as a degree of broadening is observed in the urea NH protons on addition of F^- (splitting of the peaks is not observed). This makes it difficult to accurately determine the peak position at some of the concentrations used for the Job plot analysis. However non-linear least squares regression using both ^{1}H NMR and UV-vis and fluorescence spectroscopic titrations suggest 1:1 and 1:2 host:guest binding. This is likely to be attributable to the ability of fluoride to form particularly strong hydrogen bonds, as well as the poor size match between fluoride and the binding cavity with some hosts. Compound **137** shows 2:1 host:guest binding, behaviour unique for this series of compounds and is due to the absence of a second binding arm which prevents intramolecular cooperative binding. This anion-induced dimer formation is known in self assembled metal based ion-pair systems[34-35] as well as with organic urea derivatives.[36]

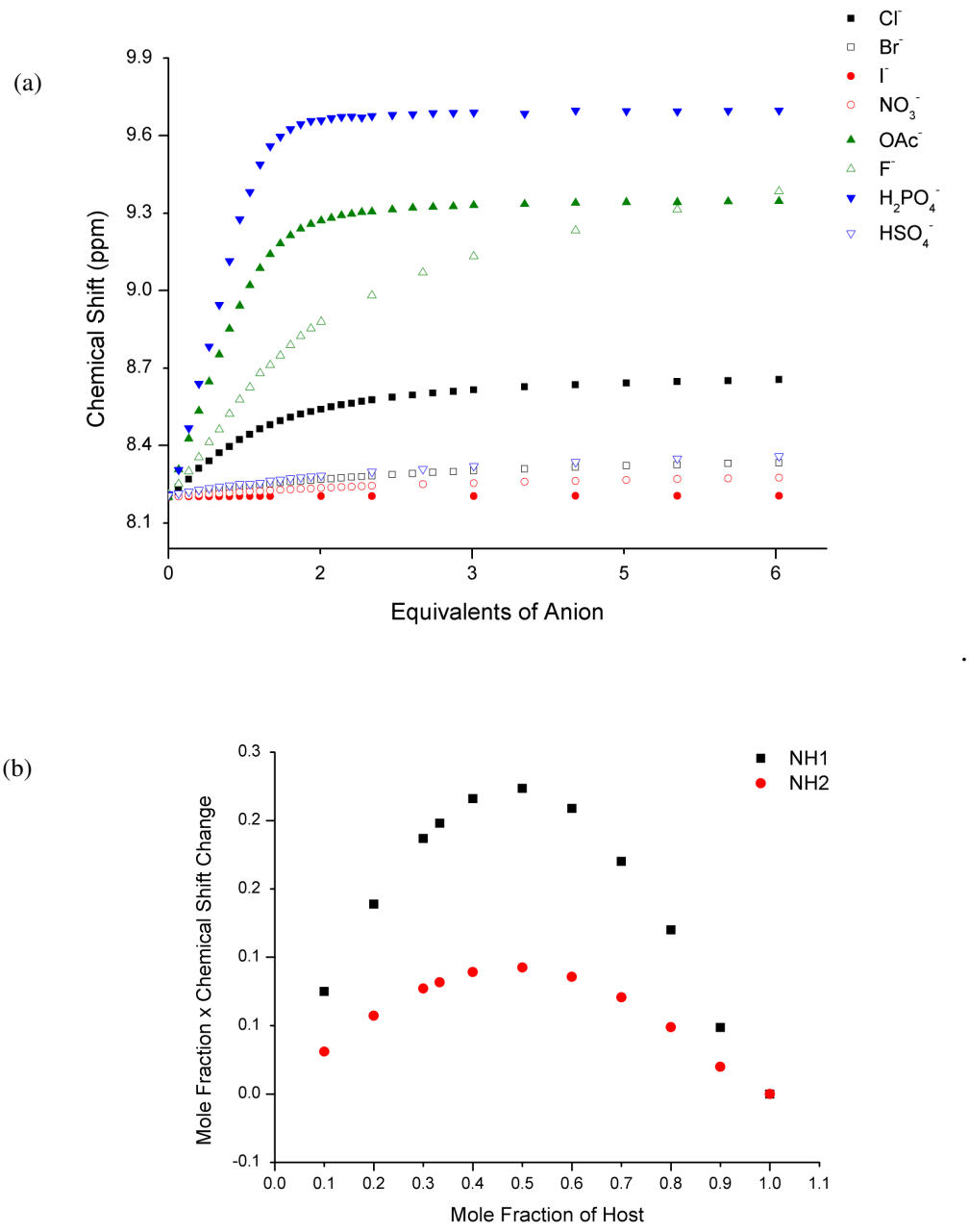

Figure 5.2 (a) Binding isotherms for **135** with a range of anions, observed using ^{1}H NMR spectroscopy in $CDCl_3$/DMSO-d_6 (*v/v* 70/30), anions used as TBA salts, (b) Job plot of **135** with TBA-Cl in $CDCl_3$/DMSO-d_6 (*v/v* 70/30)

A high degree of size selectivity is observed in these systems. For example, **135** has a larger binding cavity than **136** due to the extra alkyne group. Compound **135** therefore shows significantly higher binding to chloride than **136** (log β of 2.56 for **135** vs. 1.83 for **136**). Conversely, the large size of bromide prevents significant binding in **136** but it is bound relatively strongly in **135**. Similarly, the larger cavity of **135** allows for stronger dihydrogen phosphate binding than **136**.

In order to understand the conformations of the free and bound receptors, DFT calculations (B3LYP/6-311G(d,p)), were undertaken in collaboration with Dr. Martin Paterson at Herriot-Watt University.[37] The calculations suggest that for compound **135** in the gas phase, a twisted geometry in which the urea groups are well separated, is more stable than an eclipsed structure, by approximately 3 kJ mol^{-1} (Figure 5.3). An exceptionally low rotational barrier between the two conformers (determined by DFT calculations) was found and is consistent with related systems.[38-40] Interestingly the calculations also suggest a degree of preorganisation arising from intramolecular CH···O and NH···π(alkyne) interactions that favour the positioning of the urea NH groups over the central alkyne unit. This conformational feature is also observed in the X-ray crystal structure of the DMSO disolvate of the receptor. Crystals of **135**.2DMSO were obtained from a DMSO/water solution and the crystal data is given in the experimental section. The X-ray structure shows a planar *transoid* geometry with NH···O hydrogen bonding interactions to the DMSO guest molecules which are therefore positioned adjacent to the alkyne moieties (Figure 5.3c). NOESY NMR studies on the unbound host **135** also suggest there is no close contact between the NH and any proton on the diphenylbutadiyne phenyl ring and provides further experimental evidence to the positioning of the NH group over the alkyne unit in solution, consistent with the calculated geometry.

The 1:1 host:guest binding can readily be explained by the binding of the guest in-between the two urea groups in a *cisoid* manner and is supported by DFT optimisations indicating this to be the lowest energy conformation with chloride, showing good complementarity to the host cavity size (Figure 5.3b). The lowest energy conformation of **136** is also twisted (Figure 5.4a), however unlike with compound **135**, in the presence of chloride, compound **136** has two low energy conformations, *cisoid* and *transoid* (Figures 5.4b and c). The *cisoid* conformation is significantly twisted compared to the equivalent compound **135** complex, highlighting the smaller cavity size. As such a low energy *transoid* conformation is also found, in which binding to one urea group is predicted, with an anion...CH interaction with the second phenyl ring. The chloride binding constant for **136** is significantly higher than that of **137** and suggests that co-operative binding between the two arms is found and the *cisoid* conformation is dominant.

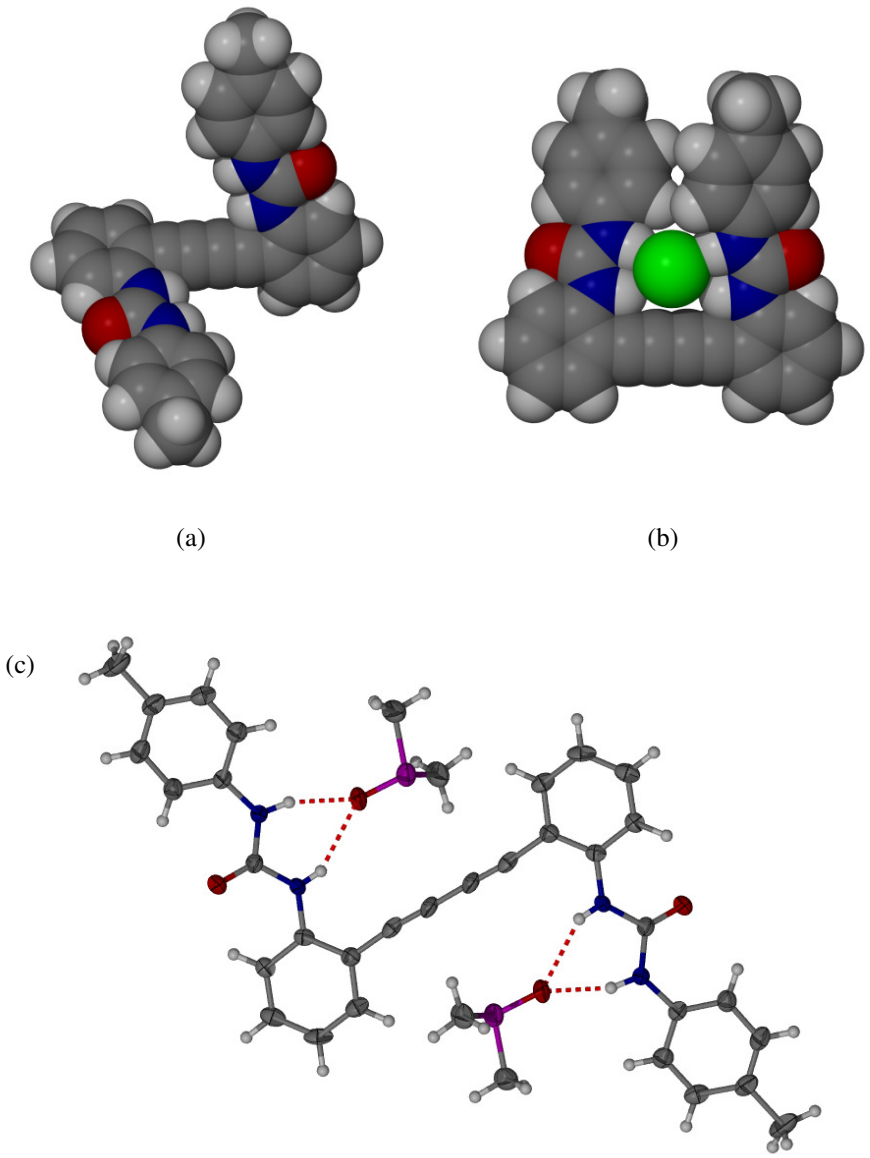

Figure 5.3 DFT optimised geometries for (a) unbound **135**, (b) **135**.Cl⁻ and (c) X-ray crystal structure of **135**·2DMSO. Hydrogen bond lengths are 2.792(5) and 2.942(5) Å

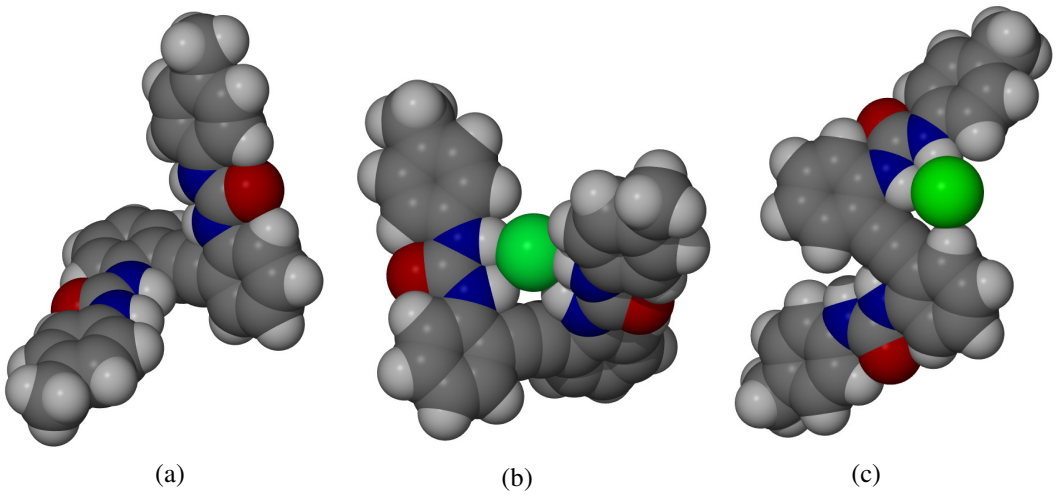

Figure 5.4 DFT optimised geometries for (a) unbound **136** and (b) *cisoid* **136**.Cl^- and (c) *transoid* **136**.Cl^-

The absorbance, emission and excitation spectra for compound **135** are shown in Figure 5.5. The fluorescent properties of compounds **135** – **139** are summarised in Table 5.2 with analogous plots to Figure 5.5 shown in Appendix IV. Experimental methods are described in the experimental section.

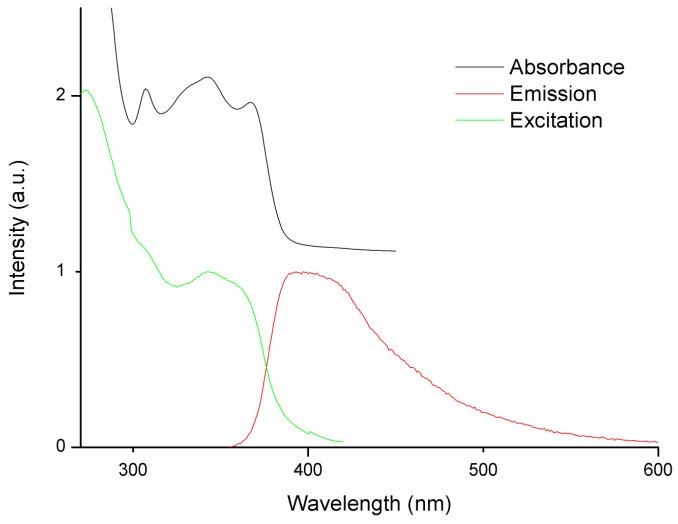

Figure 5.5 Fluorescence emission, excitation and absorbance spectra for compound **135** (λ_{ex} = 340 nm, λ_{em} = 395 nm, in $CHCl_3$/DMSO *v/v* 95/5)

Table 5.2 Photophysical properties of compounds **135** – **139** in $CDCl_3$/DMSO-d_6 (*v/v* 95/5)

Compound	Absorbance λ_{max} (nm)	Excitation λ_{max} (nm)	Emission λ_{max} (nm)	ε (at λ_{max}) (mol^{-1} dm^3 cm^{-1})	PLQY	Lifetime (ns)
135	344	340	395	28200 ± 70	0.0063	1.97 0.49
136	320	320	375	10600 ± 30	0.057	1.74 0.54
137	320	320	370	17100 ± 90	0.078	0.45
138	325	325	380	21700 ± 200	0.26	1.64 0.86
139	310	304	374	21200 ± 300	0.25	3.20 0.98

Compound **135** has the lowest energy λ_{max}, consistent with the greatest conjugation. It is interesting to note that compound **135** shows a significantly different excitation spectrum to its absorbance spectrum. This is not observed for the related compound **136** or any other receptor and will be discussed in more detail later in this section. Compounds **136** and **137** have identical absorbance maxima consistent with their DPA core. The photoluminescent quantum yield (PLQY) of **135** is low, consistent with that of diphenylbutadiyne. As the conjugation length is decreased *c.f.* **136** and **137**, the PLQY increases as the energy of the dark $^1A_{1u}$ state increases.[25]

The sensing abilities of compounds **135** – **137** were investigated using fluorescence and UV-vis spectroscopic titrations in $CHCl_3$/DMSO (*v/v* 95/5). Upon addition of strongly bound anions such as chloride, acetate and fluoride, red-shifts were observed in the UV-vis spectrum of compounds **135** of *ca.* 5 nm, consistent with increased conjugation through planarisation (Figure 5.6a). Upon addition of anions to compound **136** the growth of a shoulder is observed at 345 nm for strongly bound anions (Figure 5.6b). Compound **137** shows very little change in the UV-vis spectrum on the addition of any anion.

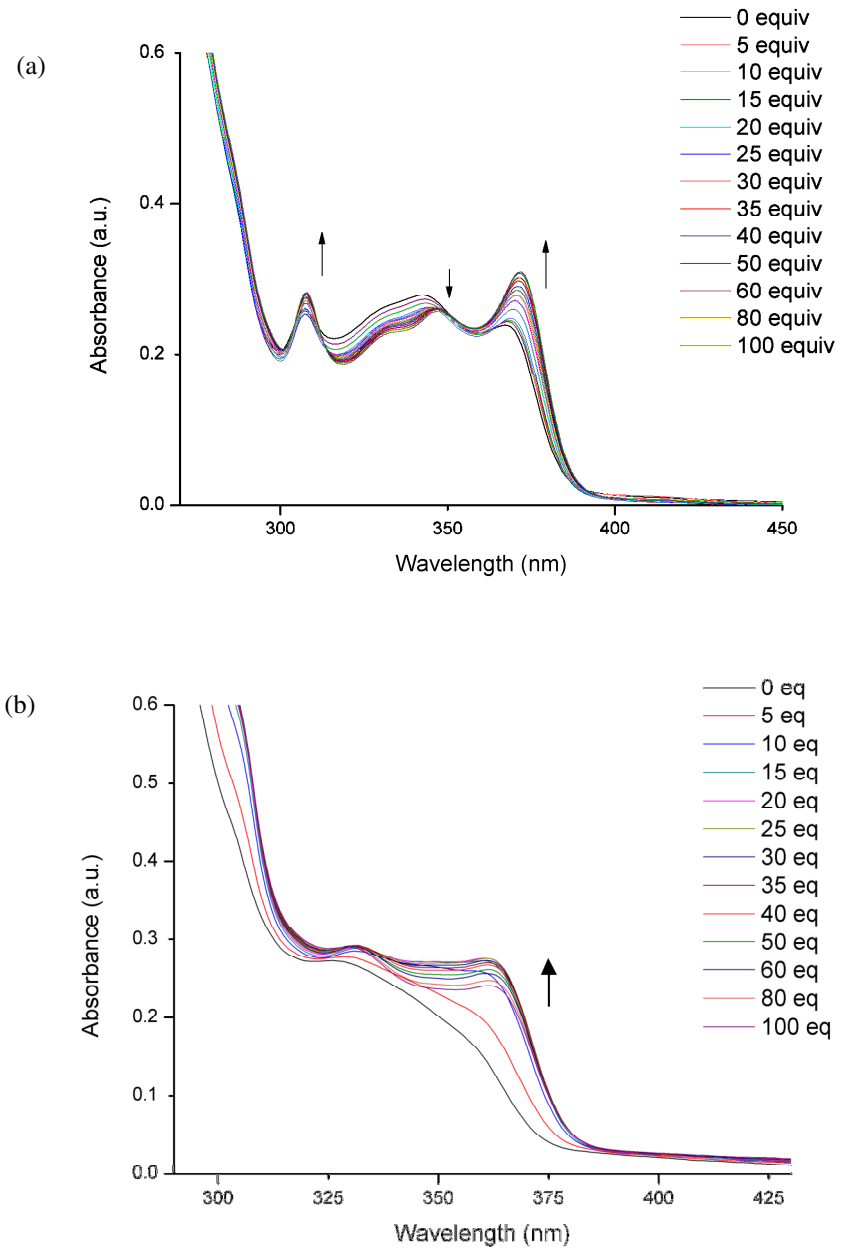

Figure 5.6 UV-vis spectroscopic titration of (a) **135** (1.0 x 10^{-5} mol dm^{-3}) with TBA-Cl and (b) **136** (2.5 x 10^{-5} mol dm^{-3}) with TBA-H_2PO_4 in $CDCl_3$/DMSO-d_6 (*v/v* 95/5)

Fluorescence spectroscopic titrations were used to investigate the hosts change in luminescence with anions. In the case of **135**, the addition of anions leads to a 'turn-on' response from the host. The degree of fluorescence enhancement varies considerably (Figure 5.7). For example, iodide shows almost no enhancement whilst chloride shows the greatest. The trend of increasing turn-on response can largely be matched to the

binding affinities of the anions. However, the strongly bound anions fluoride, dihydrogen phosphate and acetate (as measured using ^{1}H NMR spectroscopic titrations) show a smaller turn-on response than chloride even though chloride is bound at least an order of magnitude less in all cases. This suggests that binding geometry, specifically planarity, is important, not the binding strength.

(a)

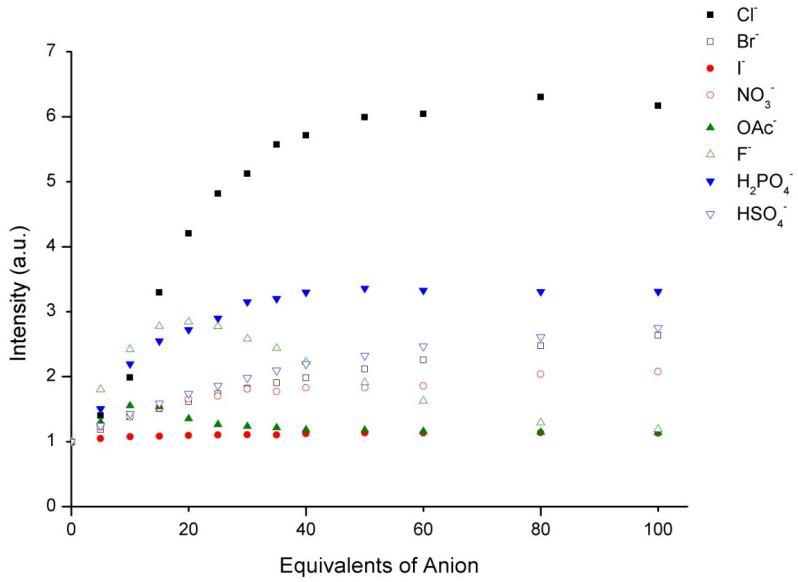

(b)

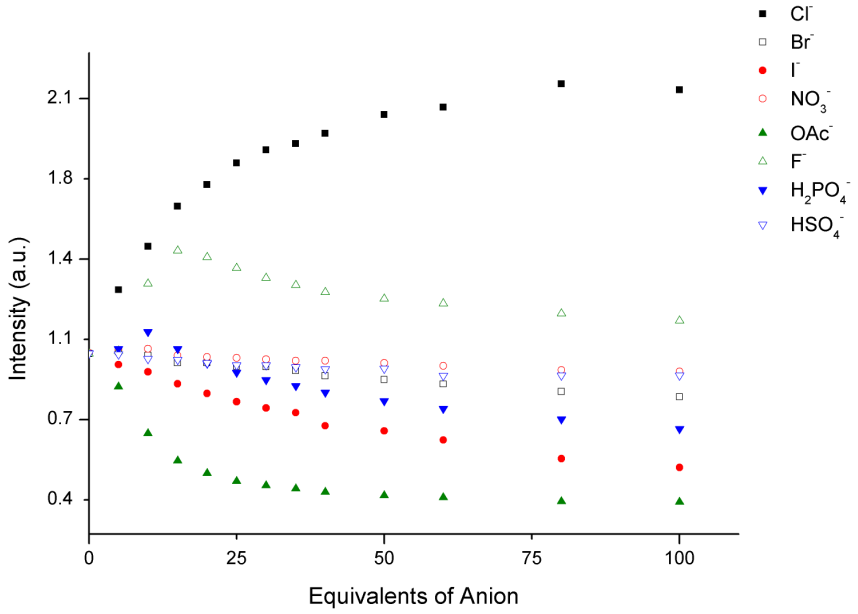

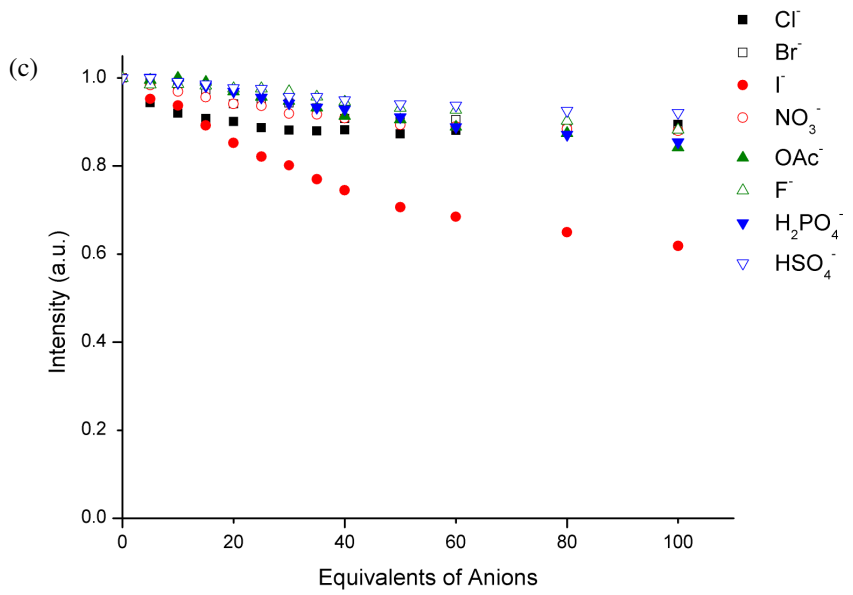

Figure 5.7 Fluorescence spectroscopic titrations of (a) **135** (λ_{ex} = 340 nm, λ_{em} = 395 nm, 1.0 x 10^{-5} mol dm^{-3}), (b) **136** (λ_{ex} = 320 nm, λ_{em} = 375 nm, 2.5 x 10^{-5} mol dm^{-3}), (c) **137** (λ_{ex} = 320 nm, λ_{em} = 370 nm, 2.0 x 10^{-5} mol dm^{-3}) in $CHCl_3$/DMSO (*v/v* 95/5) solution. Anions used a TBA-salts

Chloride and fluoride also lead to a turn-on response with **136**, with the degree of enhancement being smaller in both cases (Figure 5.7b). It is likely this is due to the induced conformation of the host. DFT optimisations of the **136**.Cl^- complex (Figure 5.4) suggest a twisted geometry compared to that of the almost planar geometry of the **135**.Cl^- complex, suggesting a lower activation barrier to internal conversion for compound **136**. Fluoride shows an interesting turn-on-turn-off effect with **135** and **136**. ^{1}H NMR spectroscopic titrations imply a 1:2 host:guest stoichiometry is present for both hosts. This is consistent with the initial binding of a fluoride as a 1:1 complex leading to planarisation. Further fluoride binding leads to a twisted 1:2 complex, analogous in conformation to the optimised free host. In the case of **135**, acetate also leads to a turn-on-turn-off effect, but to a lesser extent than fluoride. Job plot analysis suggests a 1:1 host:guest binding stoichiometry and the DFT optimised geometry of the **135**.OAc^- complex shows a planar conformation (Figure 5.8) which would be expected to give a turn-on response. It is likely that in the less competitive environment of the fluorescence titrations ($CHCl_3$/DMSO *v/v* 95/5 vs. $CDCl_3$/DMSO-d_6 *v/v* 70/30), a 1:2 host:guest stoichiometry may be possible and would lead to a turn-off response analogous to fluoride.

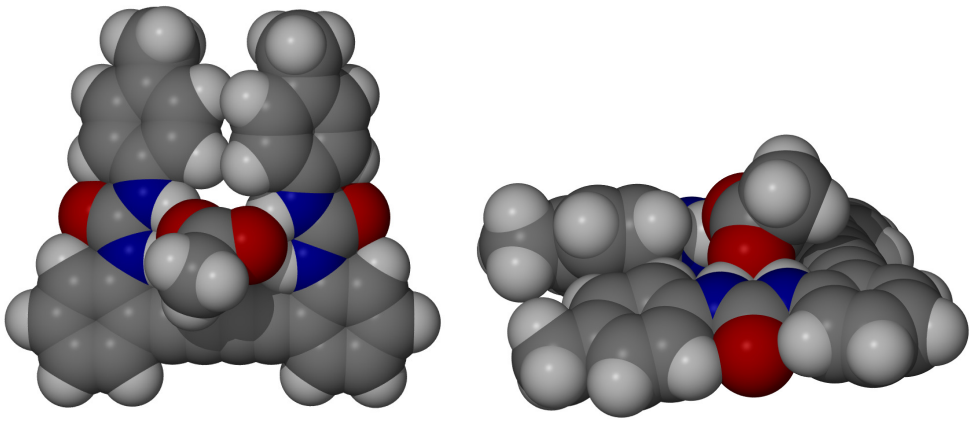

(a) (b)

Figure 5.8 Optimised geometry for the **135**.OAc^- complex (a) front view, (b) side view

The intensity of emission in tethered DPA derivatives has been shown to increase as the conformation is restricted to a more planar geometry.[28] This change is due to the increased activation energy of the $^1A_{1u}$-$^1B_{1u}$ internal conversion for the planar conformation. This increased activation energy results in a larger k_f (rate of fluorescence) value observed for conformationally restricted derivatives and a lower k_{nr} (rate of non-radiative excitation transfer). The emission from compound **135** shows a bi-exponential decay (lifetimes of 1.97 and 0.49 ns). Both of these values reduce upon addition of chloride (*cf.* 1.01 and 0.15 ns). This behaviour is also observed with **136** (1.74 and 0.54 reducing to 1.22 and 0.52 ns). Given the increase in quantum yield of fluorescence upon addition of chloride, this suggests an increase in k_f and a decrease in k_{nr}, consistent with the planarisation of the chromophore and an increase in the activation energy of internal conversion. The turn-on response in **136** is less than that for **135** as the small cavity size results in twisted binding conformations and a higher barrier to internal conversion.

Lifetime measurements were recorded using the time-correlated single photon counting (TCSPC) method[41] (see experimental section). However, measurements proved difficult as it was observed that the measured lifetimes increased in value after prolonged exposure to laser irradiation. In all cases the lifetime proved inhomogeneous over the emission profile. An emission spectrum was recorded before laser irradiation and after 5 minutes of irradiation. Representative spectra for compound **136** are shown in Figure 5.9. Two emission profiles are clearly visible, with a new band appearing at

lower energy compared to the emission of the host. This is suggestive of decomposition of the receptor. In order to minimise the effect of decomposition, all lifetimes were recorded as quickly as possible to limit exposure to the laser. The data was measured at the lowest wavelength possible to avoid overlap with the decomposed products emission. In addition, perturbation of the fluorescence lifetime with anions is markedly reduced after prolonged exposure to laser irradiation, indicating the decomposition product is not anion sensitive, suggesting all anion induced changes in the lifetime measured are due to the host (*vide infra*).

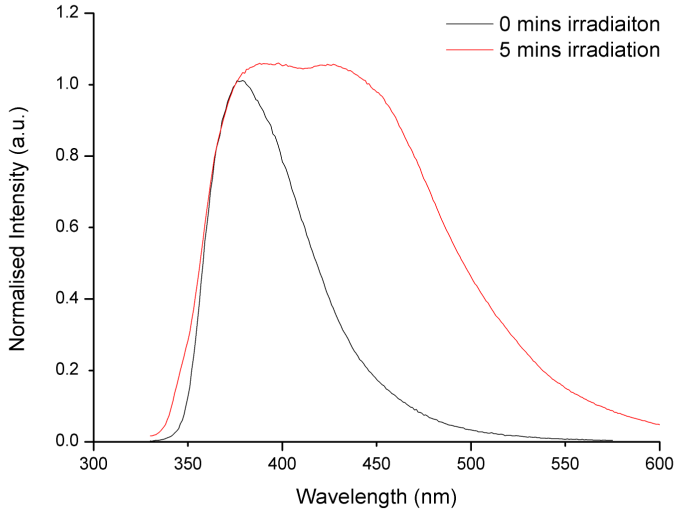

Figure 5.9 Emission spectrum of compound **136** before and after prolonged laser irradiation (300 nm) in $CDCl_3$/DMSO-d_6 (*v/v* 70/30)

In order to further understand the origins of the turn-on behaviour, a series of time dependent DFT calculations were undertaken using the recently developed Coulomb attenuated extension of the B3LYP functional, CAM-B3LYP.[42] The 6-311G(d,p) basis was used on all atoms for **135**, and augmented for the **135**.Cl^- complex with the 6-311+G(d) on Cl, and an additional diffuse set of s, p and d functions added to each peripheral hydrogen atom. In the case of free **135** the $S_1 \leftarrow S_0$ transition is strongly allowed (a $\pi_x^* \leftarrow \pi_x$) and would appear to be responsible for the observed emission in the free host. There is a low-lying accessible dark state (a $\pi_y^* \leftarrow \pi_x$) which crosses with the populated $\pi_x^* \leftarrow \pi_x$ state at twisted geometries. For example at the *transoid* conformation the bright S_1 state is only 0.03 eV lower than the dark $\pi_y^* \leftarrow \pi_x$ state, (Figure 5.10a). This excited surface crossing is further confirmed by complete active-space self-consistent field (CASSCF) calculations on diphenylbutadiyne, which show

that the $\pi_x^* \leftarrow \pi_x$, and $\pi_y^* \leftarrow \pi_x$ electronic states form the components of a degenerate state at fully twisted (D_{2d}) geometries. Thus there exists a Jahn-Teller conical intersection ($E \otimes (b, \oplus b,)$) that facilitates very efficient radiationless population transfer between such states. Therefore in **135** excitation drives the system towards a region of surface crossing and the optically dark state becomes populated. In contrast, in the **135**.Cl^- complex, the binding-enforced planarity of the chloride complex means the two states are ~0.5 eV apart and population transfer cannot readily occur, Figure 5.10b.

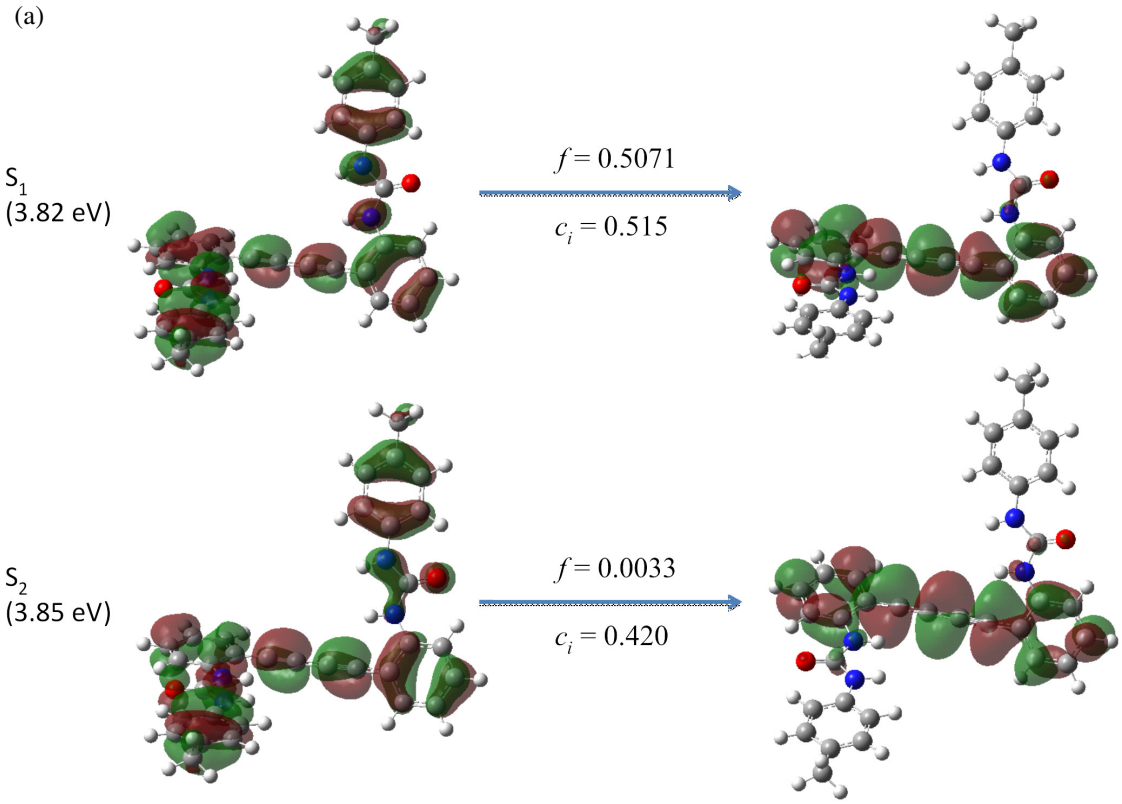

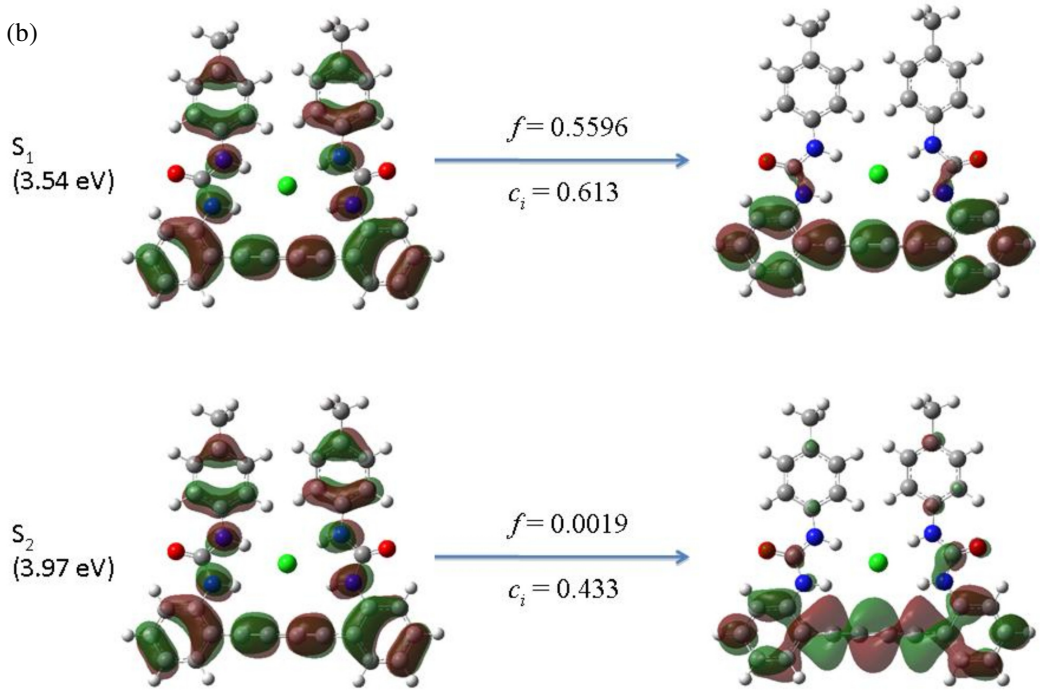

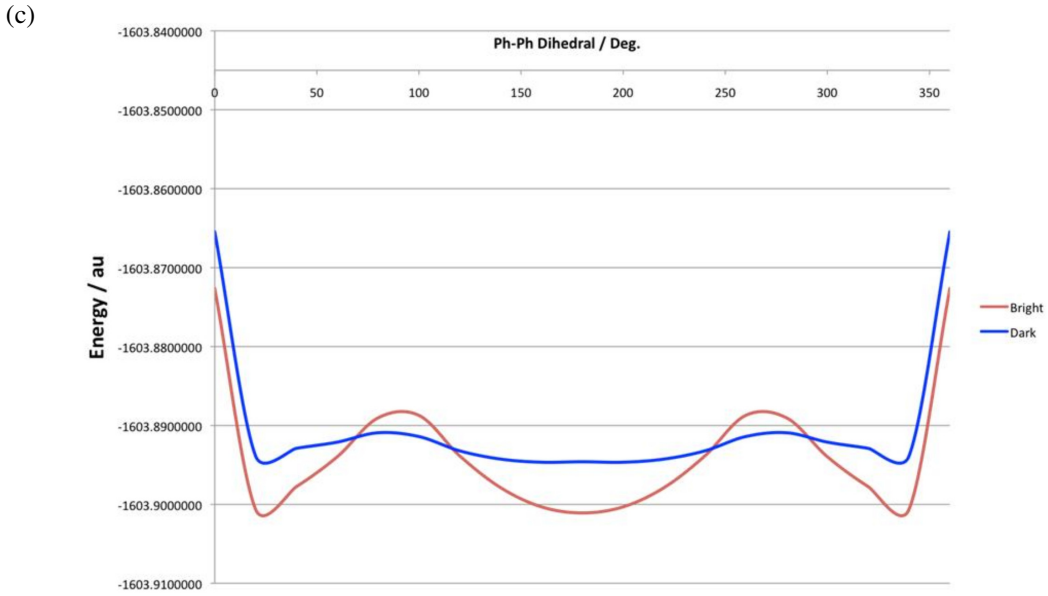

Figure 5.10 Principal components of relevant low-lying electronic states giving rise to the fluorescence (S_1) and non-radiative decay (S_2) as obtained from TD-DFT computations (*f*– oscillator strength of transition, c_i coefficent of orbital transition in response eigenvector) for (a) free host in cisoid geometry and (b) optimised **135**.Cl^- complex. (c) unrelaxed scan across the alkyne dihedral angle for the bright and dark states.

Interestingly compound **136** shows either a turn-on or turn-off response depending on the anion, allowing increased discrimination between anions. For example, chloride results in fluorescence enhancement, whilst acetate causes quenching. Iodide, bromide, nitrate and hydrogen sulfate results in a small decrease in the emission, however, dihydrogen phosphate and acetate cause a large quenching response. In addition, the quenching response with iodide is linear with a small decrease observed in the fluorescence lifetime, suggestive of dynamic quenching. Dihydrogen phosphate and acetate show very non-linear quenching behaviour which is consistent with static quenching.[43] Compound **137** shows only modest fluorescent quenching for all anions, with linear behaviour, suggesting dynamic quenching dominates.

Lifetime measurements can also give insights into the turn-on-turn-off behaviour observed with fluoride and acetate for compounds **135** and **136**. There is a decrease in the lifetime of compound **135** in the presence of ten equivalents of TBA-F (1.75, 0.22 ns) consistent with planarisation of the fluorophore. One hundred equivalents of TBA-F leads to a lengthening of the lifetime (2.8, 0.69 ns) and is consistent with a twisted geometry. This behaviour is also observed to an extent with TBA-OAc (1.97, 0.36 ns for 10 equivalents and 2.94, 0.81 ns for 100 equivalents), as well as with **136** with TBA-F (1.54, 0.60 ns for 10 equivalents and 1.86, 0.75 with 100 equivalents). However, measurements at 100 equivalents of anion with **135** gave values with consistently large χ^2 values (*ca.* 4) but in each case there is an obvious increase in the gradient of the decay curve as the anion concentration increases. The general trend of an increase in lifetime is consistent with different anions and receptors. It is therefore likely that this is a true effect being observed.

The excitation profile of **135** in the absence of anions is significantly different to the absorbance profile. However with the addition of chloride the excitation spectrum matches that of the absorbance spectrum well (Figure 5.11). It is likely that this behaviour is linked to the non-radiative energy transfer processes involving the $^1A_{1u}$ and $^1B_{1u}$ states. Planarisation of the compound by chloride reduces the non-radiative decay and therefore the absorbance and excitation spectra match.

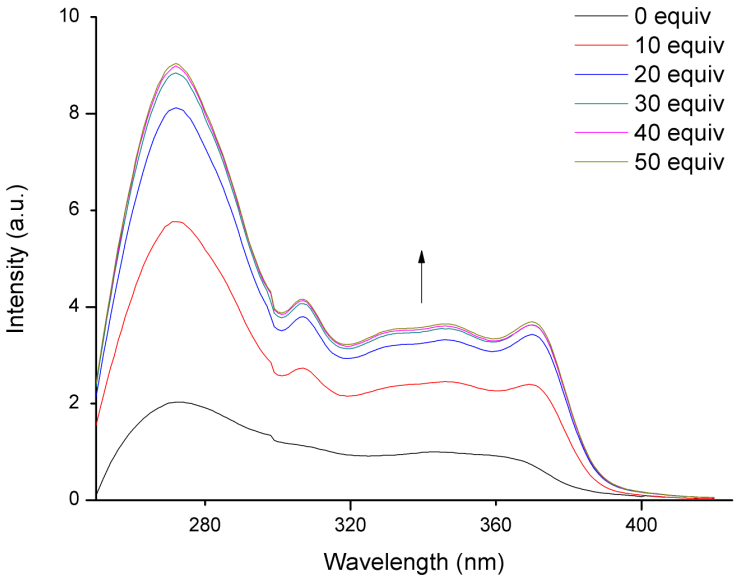

Figure 5.11 Excitation spectrum of **135** (1 x 10^{-5} mol dm^{-3} in $CHCl_3$/DMSO *v/v* 95/5, λ_{em} = 395 nm) with the addition of TBA-Cl

5.4 Anion Binding and Sensing in Extended Alkynes

The anion binding of compounds **138** and **139** was also investigated by ^{1}H NMR spectroscopic titrations in $CHCl_3$/DMSO (*v/v* 70/30). The binding constants determined are summarised in Table 5.1. Compound **139** shows binding strengths similar to those of compound **135**. These are considerably higher than **136** for all anions. Given that the overall cavity size should be similar between compound **136** and **139**, this suggests that there is a greater degree of flexibility in **139**, allowing a variable cavity size and stronger anion binding. Compound **138** shows surprisingly low affinity to anions e.g. it binds chloride more weakly than any other host. Small downfield shifts in the ^{1}H NMR spectrum on addition of anions are also observed in the proton attached to the aromatic ring between the two alkyne substituents. This suggests a small degree of additional hydrogen bonding and the positioning of the anion within the binding cavity, as shown in Figure 5.12. This binding conformation may be sterically hindered and may explain the lower binding affinity compared with its congener **139**. However, basic anions such as acetate and dihydrogen phosphate are bound strongly.

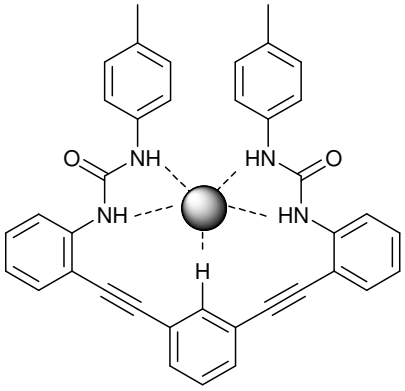

Figure 5.12 Anion binding mode for **138** suggested by ^{1}H NMR spectroscopic titrations

The photophysical properties of compound **138** and **139** are summarised in Table 5.2. Compounds **137** and **139** show identical absorbance band profiles, however **139** is red-shifted by 5 nm. This is due to the *meta* configuration of the binding arms in **138**, which prevents full conjugation across the molecule and results in a conjugation length similar to that of **137**.[44] Compound **139** has a broad absorbance spectrum, with a λ_{max} of 310 nm. However the band extends to 350 nm, consistent with the greater conjugation in the *ortho* configuration and the red-shifted λ_{max} compared to **138**. Interestingly, the extinction coefficient and the quantum yield of compounds **138** and **139** are very similar, which is unexpected given the different configurations and absorbance profiles (see Appendix IV) of the two receptors.

The fluorescence and UV-vis responses of compounds **138** and **139** on the addition of anions were also investigated. As with compounds **137**, compounds **138** and **139** show only very small changes in the UV-vis spectrum on titrating with anions. However, the emission spectra of **138** and **139** show fluorescence quenching upon addition of anions (Figure 5.13). Bromide, nitrate and iodide all show linear Stern-Volmer behaviour for both compounds, consistent with dynamic quenching and the low binding constants measured by NMR experiments. The Stern-Volmer constants for the compounds and anions which show linear trends are summarised in Table 5.3. Dihydrogen phosphate, acetate and fluoride all cause non-linear quenching and may suggest significant static quenching. Compound **139** in particular shows very high quenching with emission at *ca.* 2% of its original intensity at 100 equivalents of acetate, fluoride and dihydrogen phosphate. Lifetime measurements were used to try and confirm the assignment of

predominantly static quenching for acetate, fluoride and dihydrogen phosphate for **138** and **139** and dynamic quenching for the halides (except chloride) and nitrate for **138** and **139**. Compound **138** in the presence of TBA-OAc showed a slight increase in the lifetime. As there is no decrease in the lifetime, this is suggestive of largely static quenching. Additionally, the presence of TBA-Br leads to a reduction in the lifetime of the receptor, consistent with dynamic quenching, indicated by fluorescence spectroscopic titrations. The addition of TBA-Br to receptor **139** leads to analogous results. In contrast, however, TBA-OAc with **139**, results in a decrease in the lifetime, suggesting that a dynamic quenching component also contributes to the quenching for this receptor.[45]

Table 5.3 Calculated Stern-Volmer constants in $CDCl_3$/DMSO-d_6 (*v/v* 70/30),. Anion used as TBA salts. - = not applicable for that compound

	K_{sv} /M^{-1}			
Anion	**136**	**137**	**138**	**139**
Bromide	106 ± 4	-	190 ± 10	670 ± 20
Iodide	429 ± 8	330 ± 20	580 ± 40	1540 ± 30
Nitrate	-	-	153 ± 9	570 ± 20

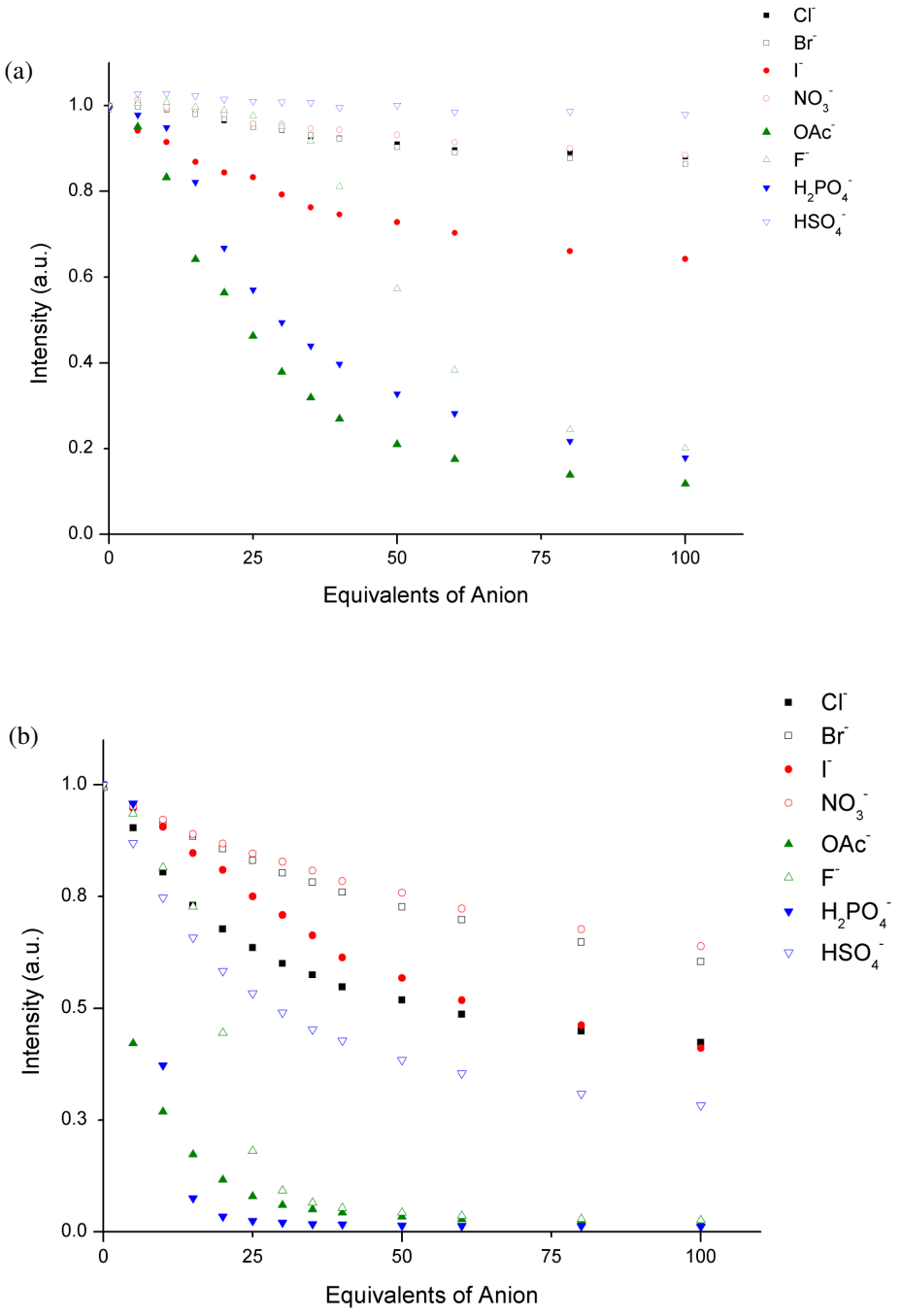

Figure 5.13 Fluorescence spectroscopic titrations of (a) **138** (λ_{ex} = 325 nm, λ_{em} = 380 nm, 1.0 x 10^{-5} mol dm^{-3}), and (b) **139** (λ_{ex} = 310 nm, λ_{em} = 374 nm, 1.0 x 10^{-5} mol dm^{-3}) in $CHCl_3$/DMSO (*v/v* 95/5) solution. Anions used as TBA-salts

The mechanism of quenching in **138** and **139**, as well as **136** and **137**, is unknown. However the dynamic nature of the quenching with halides suggests that a conformational change is not the cause in all cases, as essentially no binding is

observed. It is likely that a photo-induced electron transfer (PET) process or heavy atom effect is responsible.[46-47] A PET process could account for the observed quenching with harder anions such as acetate, where the low mass means heavy atom quenching is unlikely. It may also be expected that even though the oxidation potential of acetate is high, the static nature of the acetate quenching would lead to greater quenching than for the collisional quenching of iodide. In fact, with **137**, no significant binding interactions are apparent at the concentrations used for UV-vis and fluorescence spectroscopic titrations and the strongest quenching observed is with iodide, not acetate. Of the determined Stern-Volmer constants summarised in Table 5.3, iodide consistently shows the strongest quenching. This could be accounted for by the heavy atom effect. However the low oxidation potential of I^- means a PET process cannot be ruled out. The $I^- > Br^- > NO_3^-$ order of quenching seen in Table 5.3 also follows the increasing oxidation potential of the anions. Compound **135** does not show any fluorescent quenching with any anion. The increased conjugation in compound **135** will increase the HOMO energy. It is possible that in compound **135** the HOMO energy is higher than that of the anion and so PET cannot occur, therefore quenching is not observed.

Interestingly, compound **139** shows a significant red-shift of *ca.* 30 nm with the addition of TBA-Cl and F (see Figure 5.14), accompanied by a significant decrease in emission intensity. This behaviour is observed to a lesser extent with **138** and TBA-F. It is likely that this shifting is due to a conformational change in the molecule upon anion binding which is less emissive than the free host. In the case of the fluoride complexes of **138** and **139**, the ^{1}H NMR spectroscopic titration suggests a 1:1 and 1:2 host:guest stoichiometry. The fluorescence isotherms also show a sigmoidal curvature which would be consistent with multiple binding stoichiometries (Figure 5.13). The binding of the first fluoride may cause little conformational change, however the second fluoride changes the conformation of the host in such a way as to red-shift the emission and reduce the intensity. A 1:1 stoichiometry is observed with chloride and it is likely its larger size distorts the conformation of the host sufficiently to account for the observed changes in emission.

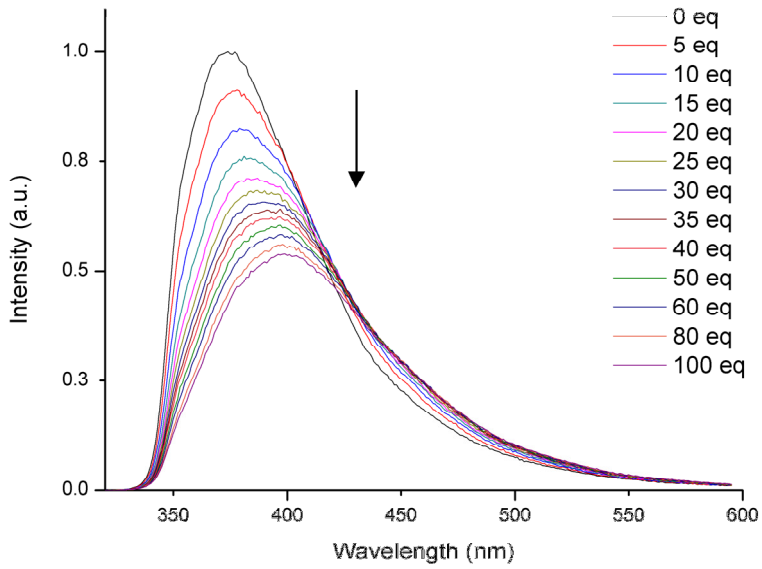

Figure 5.14 Fluorescence emission spectrum of **139** (λ_{ex} = 310 nm, λ_{em} = 374 nm, 1.0 x 10^{-5} mol dm^{-3} in $CHCl_3$/DMSO *v/v* 95/5) with increasing equivalents of TBA-Cl

5.5 Application of Molecular Clip Based Sensors

The recognition and sensing properties of compounds **135** – **139** have so far, only been investigated in a relatively uncompetitive solvent of $CHCl_3$/DMSO (*v/v* 95/5). In order to test the feasibility using these sensors in real world applications such as biological, environmental and array applications, investigations in more competitive media were undertaken, including aqueous systems.

5.5.1 Discrimination of Anions Using an Array Sensing System

The concept of a sensing array was introduced in Chapter 1 in discussing the work of Anslyn.[48-49] In this type of system, an array of several receptors, typically with small structural modifications are exposed to anions and the emission or absorbance spectrum recorded. Each receptor has a subtly different peak anion selectivity or reporter response and the use of pattern recognition software can be used to deconvolute each receptors individual emission/absorbance spectrum. An advantage of this system is that whilst the ability of each different type of receptor to discriminate a particular anion may be small, when used as part of an array where each receptor has a different selectivity, the system can discriminate between anions.

The wide range of responses to anions observed between the receptors synthesised in this work, ranging from purely turn-on responses to mixed fluorescence enhancement and quenching, through to purely quenching, has the ability to discriminate between a range of different anions, by a simple traffic-light turn-on, turn-off response. Quantitative analysis using pattern recognition may allow for even more accurate identification of the anion. Taking as examples receptors **135**, **136** and **139** with 50 equivalents of anion, chloride gives rise to fluorescence enhancement with **135** and **136** but quenching with **139**. Alternatively, dihydrogen phosphate leads to enhancement with **135** but quenching with **136** and **137**, whilst acetate results in little or no enhancement with **135** and quenching with **136** and **139**. Table 5.4 collates the responses of receptors with the anion studied and how they can be discriminated. In difficult cases such as distinguishing bromide and iodide, receptor **137** can be used as bromide gives rise to virtually no quenching whereas iodide is quenched significantly. Further investigation into the applicability of using these sensors in this way is still required; of particular importance for real world applications is the ability of the receptors to sense anions in more competitive solvents, ideally water, therefore the binding and sensing properties of this class of receptor were investigated in more competitive solvents.

Table 5.4 Fluorescence response of each receptors **135**, **136** and **139** with 50 equivalents of anion

	Receptor		
Anion	**135**	**136**	**139**
Fluoride	On	On	Off
Chloride	On	On	Off
Bromide	On	Off	No change
Iodide	On	Off	Off
Acetate	No change	Off	Off
Dihydrogen Phosphate	On	Off	Off
Hydrogen Sulfate	On	No change	Off

5.5.2 DMSO Solvent Systems

Compound **135** was chosen for a preliminary investigation of its sensing abilities in more competitive solvents. Compound **135** has the largest anion binding constants and is therefore most likely to bind anions well in competitive media. Ideally, aqueous systems would be used as any biological and environmental application would require the sensor to function in water. However, all receptors studied are insoluble in water. As an alternative a DMSO/H_2O solvent system was used, with a ratio of DMSO/H_2O (*v/v* 80/20) as a compromise allowing significant water content whilst reducing the overall competitiveness of the solvent system by using DMSO. Unfortunately, even low water ratios resulted in precipitation of the receptor. In order to solubilise the product, γ-cyclodextrin was used. The receptor was soluble in a wide range of cyclodextrin:receptor ratios, however a 1:1 ratio was chosen.

Fluorescence spectroscopic titrations of **135** in DMSO/H_2O (*v/v* 80/20) with one equivalent of γ-cyclodextrin were investigated using TBA-Cl and TBA-H_2PO_4. In both cases no significant change in the fluorescence emission spectrum was observed (Figure 5.15). In addition, no change in the UV-vis spectrum of the receptor was observed suggesting very low anion binding and that the solvent system or the solubilising cyclodextrin, or both, are competing for binding the anion and the host.

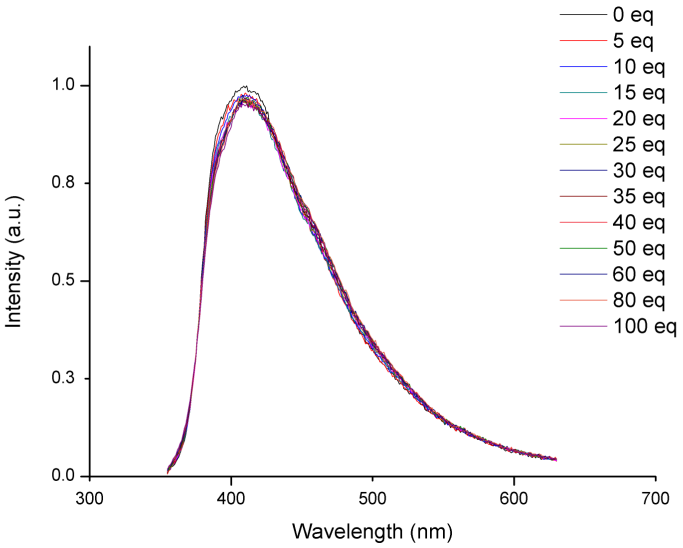

Figure 5.15 Fluorescence spectroscopic titration of **135** (λ_{ex} = 340 nm, λ_{em} = 395 nm, 1.0 x 10^{-4} mol dm^{-3}) with TBA-H_2PO_4 in DMSO/H_2O (*v/v* 80/20) with one equivalent of γ-cyclodextrin

^{1}H NMR, UV-vis and fluorescence spectroscopic titrations were also undertaken with **135** in DMSO. ^{1}H NMR spectroscopic titrations show significant downfield shifts in the urea NH protons, consistent with anion binding and of a similar magnitude to those observed in $CDCl_3$/DMSO-d_6 (*v/v* 70/30). UV-vis spectroscopic titrations also suggest anion binding, with similar spectral changes observed with $CDCl_3$/DMSO-d_6 (*v/v* 95/5). However larger equivalents of anion are required to create the same changes (*ca.* 400 equivalents, Figure 5.16a), consistent with a more competitive solvent. Fluorescence spectroscopic titrations show a 2.4-fold enhancement in intensity at 395 nm for chloride (Figure 5.16b). This is consistent with $CDCl_3$/DMSO-d_6 (*v/v* 95/5), although the absolute value of enhancement is lower. Interestingly, dihydrogen phosphate also shows UV-vis spectral changes consistent with that observed in $CDCl_3$/DMSO-d_6 (*v/v* 95/5), however no significant changes are observed in the fluorescence emission spectrum which may suggest an alternative binding mode. In general, the observations in DMSO are consistent with those in $CDCl_3$/DMSO-d_6 (*v/v* 95/5), given the greater competitive medium.

A ^{1}H NMR spectroscopic titration of **135** with γ-cyclodextrin in DMSO-d_6 showed no significant shifts in proton resonances for either **135** or the cyclodextrin, suggesting little interaction in solution. Titrating TBA-Cl into a solution of **135** with one equivalent of γ-cyclodextrin showed downfield shifts (up to 1 ppm) in the urea resonances of **135** (Figure 5.17). Importantly splitting of the resonances was also observed indicating multiple environments for the urea NH groups in slow exchange. This is not observed with **135** and chloride alone and implies the possible formation of a slow exchange **135**-chloride-γ-cyclodextrin complex. The addition of γ-cyclodextrin to a solution of **135** in DMSO with one equivalent of Cl, results in upfield shifting of the urea protons, indicative of reduced anion binding due to competition with the cyclodextrin.

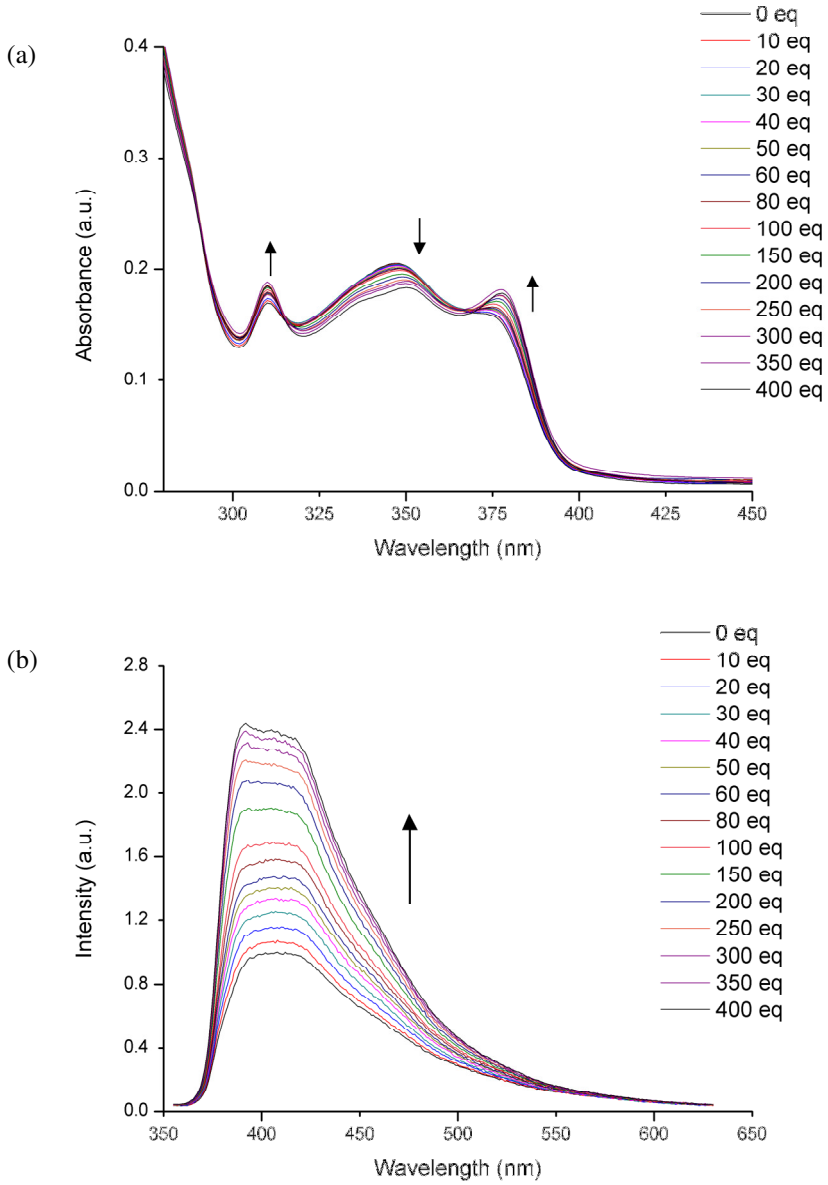

Figure 5.16 (a) UV-vis spectroscopic titration of **135** (1.0 x 10^{-5} mol dm^{-3}) with TBA-Cl in DMSO and (b) fluorescence spectroscopic titration of **135** (λ_{ex} = 340 nm, λ_{em} = 395 nm, 1.0 x 10^{-5} mol dm^{-3}) with TBA-Cl in DMSO

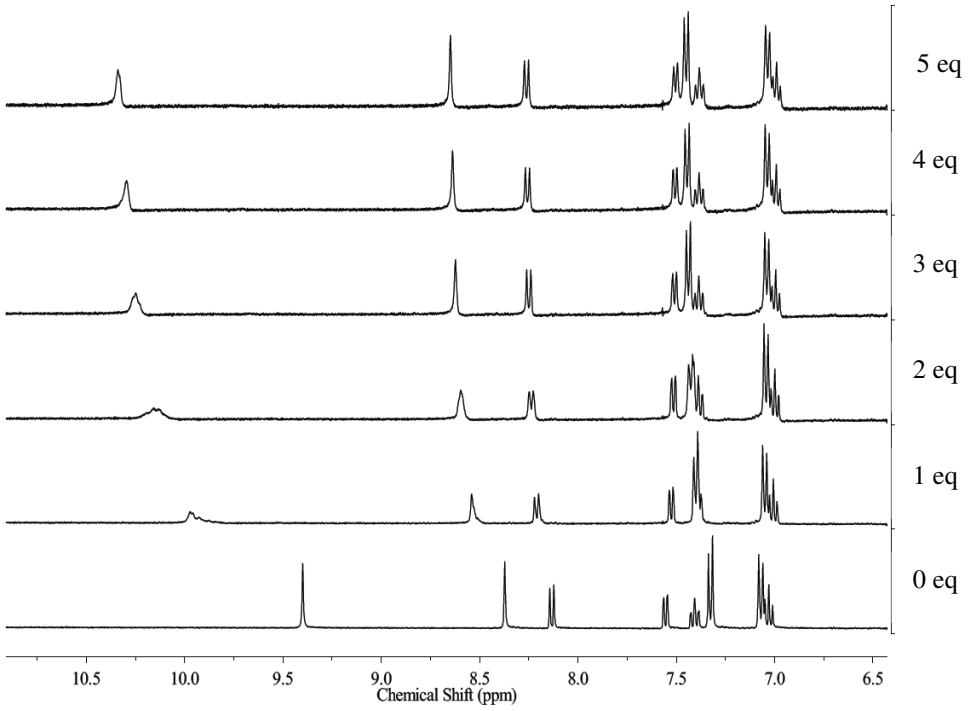

Figure 5.17 ^{1}H NMR spectra of **135** in DMSO-d_6 with one equivalent of γ-cyclodextin on increasing equivalents of TBA-Cl. The ^{1}H NMR assignment can be found in Appendix IV

The above experiments suggest that γ-cyclodextrin is capable of competing with **135** to bind chloride, either by direct binding of the anion (or more likely the TBA group and chloride as an ion pair) or the formation of a **135**-chloride-γ-cyclodextrin complex. In solvent systems such as DMSO/H_2O (*v/v* 80/20) it is likely that the increased competition from the H_2O and cyclodextrin results in a significant reduction in anion binding to **135** and as such, little change is seen in the fluorescence response.

5.5.3 An Aqueous System Incorporating a Surfactant

As an alternative to cyclodextrin, surfactants can be used to solubilise organic molecules in water and have been used successfully in anion sensors.[50,51] The surfactant Triton-X 100 was chosen as it is non-ionic and would not lead to attraction, repulsion or ion pairing of the anion and the surfactant. Solubilisation of **135** was achieved in a 1%vol of Triton-X 100 in high purity water. This is a concentration above the critical micelle concentration (CMC) of the surfactant.[52] Unfortunately, both UV-vis and fluorescent spectroscopic titrations with TBA-Cl and TBA-H_2PO_4 in H_2O

showed no significant changes in the spectra (see Figure 5.18). This suggests anion binding is not occurring.

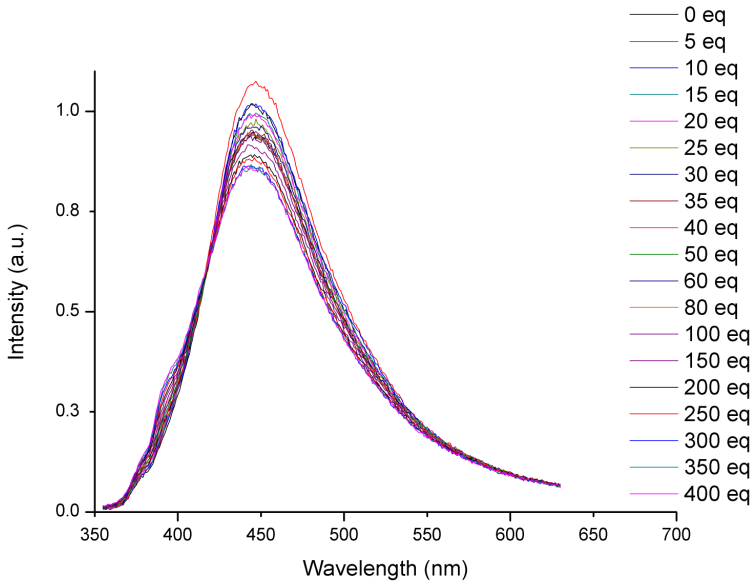

Figure 5.18 Fluorescence spectroscopic titration of **135** (λ_{ex} = 340 nm, λ_{em} = 395 nm, 1.0 x 10^{-5} mol dm^{-3}) with TBA-Cl in water with 1%vol Triton-X 100

5.5.4 Incorporation of an Alkyne Based Sensor into a Dipstick

The use of a dipstick as a device to detect chloride using fluorescence emission and a colourimetric response has recently been published using a squarane-based rotaxane receptor.[53] The system shows an 18-fold increase in emission intensity, greater than that seen in solution, after dipping in TBA-Cl solution. This method of device formation was investigated for compound **135**.

C18 reverse phase silica gel TLC plates were impregnated with compound **135** by dipping the TLC plate in a solution of **135** (1.0 x 10^3 M^{-1} in $CHCl_3$/DMSO *v/v* 70/30) for two seconds and allowed to dry, forming a homogenous covering (studied under UV light). For this system, the reverse phase silica gel TLC plates provide a hydrophobic environment for the receptor. Here the insolubility of the receptor in water becomes an advantage as the compound can be dipped without leaching away. Similarly, it may be possible to wash away any bound anion using distilled water, with minimal loss of the host or damage to the dipstick and hence could allow for its reuse.

The integrated fluorescence emission intensity of a coated silica plate was measured using a fluorescence microscope (see experimental section). The plate was then dipped in a solution of TBA-Cl (0.3 mol dm^{-3}) in H_2O for two seconds and allowed to dry in the air. The integrated emission intensity was then remeasured. Unfortunately, no significant change was seen over several observations. As with the previous systems it is likely that the binding constant for **135** with chloride is too low to effectively extract chloride out of water. To test this, a newly coated silica plate was dipped in a 1 mol dm^{-3} solution of TBA-Cl in acetonitrile; a less competitive solvent but one in which the host is also largely insoluble. In this case a 100% increase in the average emission intensity was observed after dipping (Figure 5.19).

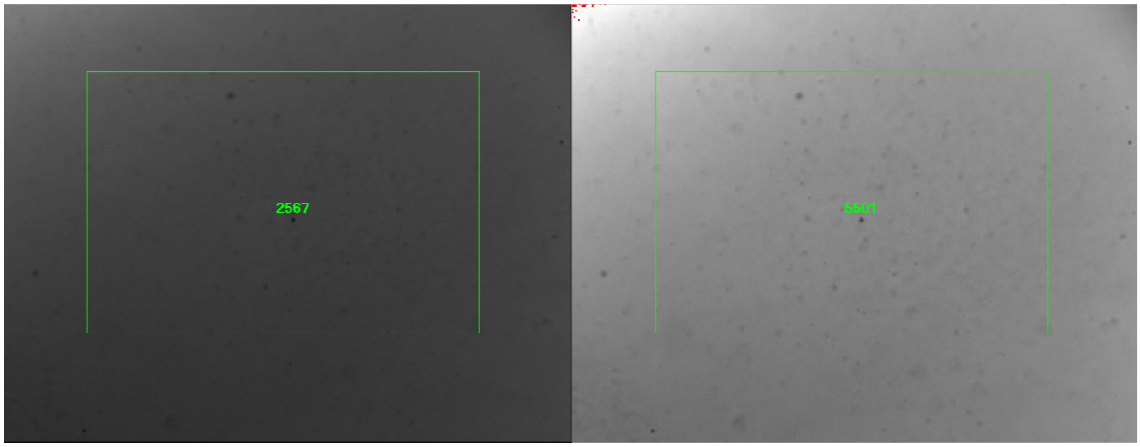

Figure 5.19 (a) Image of immobilized **135** on dipstick without exposure to chloride (integrated emission intensity = 2567), (b) image of immobilized **135** on dipstick after dipping in 1 mol dm^{-3} TBA-Cl in MeCN for 2 seconds (integrated emission intensity = 5501). The measured average integrated emission intensity is also shown in the marked area

5.5.5 Synthesis of 2nd Generation Sensors

Compound **135** shows limited sensing in competitive solvents due to weak anion binding. In order to increase the binding constant, electron-withdrawing groups were incorporated into the receptor to increase the acidity of the urea NH groups. Nitro and trifluoromethyl moieties were used by reaction of the intermediate, **140** with the 3-nitrophenyl isocyanate or 4-trifluoromethylphenyl isocyanate, to give compounds **144** and **145** (Figure 5.20).

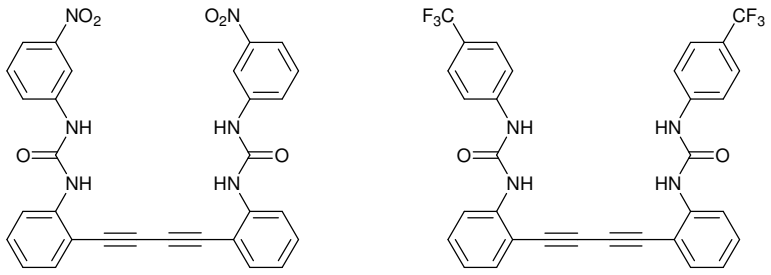

144 **145**

Figure 5.20 Compounds **144** and **145**

^{1}H NMR spectroscopic titrations of **144** and **145** in $CDCl_3$/DMSO-d_6 (*v*/v 70/30) were undertaken with TBA-Cl. Both compounds show increased binding constants over compound **135**, with **144** showing the largest binding constant of log β 3.36(3). However the receptor did not show any fluorescence emission. Compound **145** has a lower chloride binding constant of log β 3.10(1), however it is fluorescent.

Compound **145** shows interesting fluorescence emission, with a shoulder at approximately 500 nm which became more pronounced at higher concentrations (Figure 5.21a) and may indicate excimer/aggregrate emission. The absorbance spectrum of compound **145** is identical to that to that of compound **135** and is unaffected by concentration, however the excitation spectrum measured at an emission wavelength of 400 nm shows a red-shift of approximately 5 nm. In addition, the excitation spectrum measured at an emission wavelength of 500 nm shows a change in relative intensities of the bands compared to the excitation spectrum measured at 400 nm (Figure 5.21b). This also supports the hypothesis that a dynamic excimer process may be occurring and further investigation into the photophysical properties of this compound is required.[54]

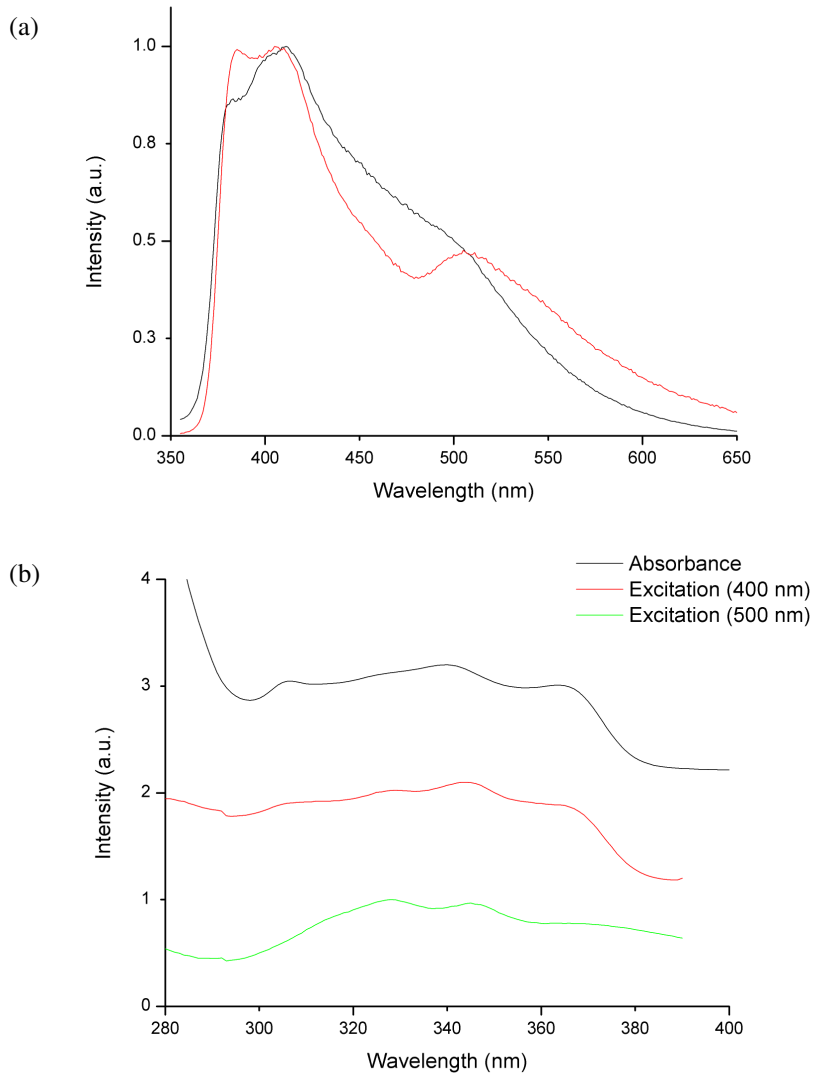

Figure 5.21 Comparison plots of (a) fluorescence emission spectrum of **145** at 1.0 x 10^{-5} mol dm^{-3} in $CHCl_3$/DMSO (*v/v* 95/5) , λ_{ex} = 340 nm (black line) and 1.0 x 10^{-4} mol dm^3, λ_{ex} = 340 nm (red line), (b) absorbance and excitation spectra of compound **145** in $CHCl_3$/DMSO (*v/v* 95/5) with emission wavelength given in parenthesis in the legend

UV-vis and fluorescence spectroscopic titrations of compound **145** with TBA-Cl were undertaken. The UV-vis spectrum shows behaviour consistent with that of compound **135**. If compound **145** does indeed emit both monomeric (400 nm) and excimer emission (500 nm), it may function as a ratiometric sensor. The band at 400 nm increases in intensity upon addition of chloride (Figure 5.22a) with little change in the intensity at 500 nm. A plot of the ratio of band intensities (I_{400}/I_{500}) against equivalents of chloride (Figure 5.22b) shows an initial increase in the band ratio; however this

decreases at higher equivalents through an as yet unknown mechanism. There is also poor correlation of the data.

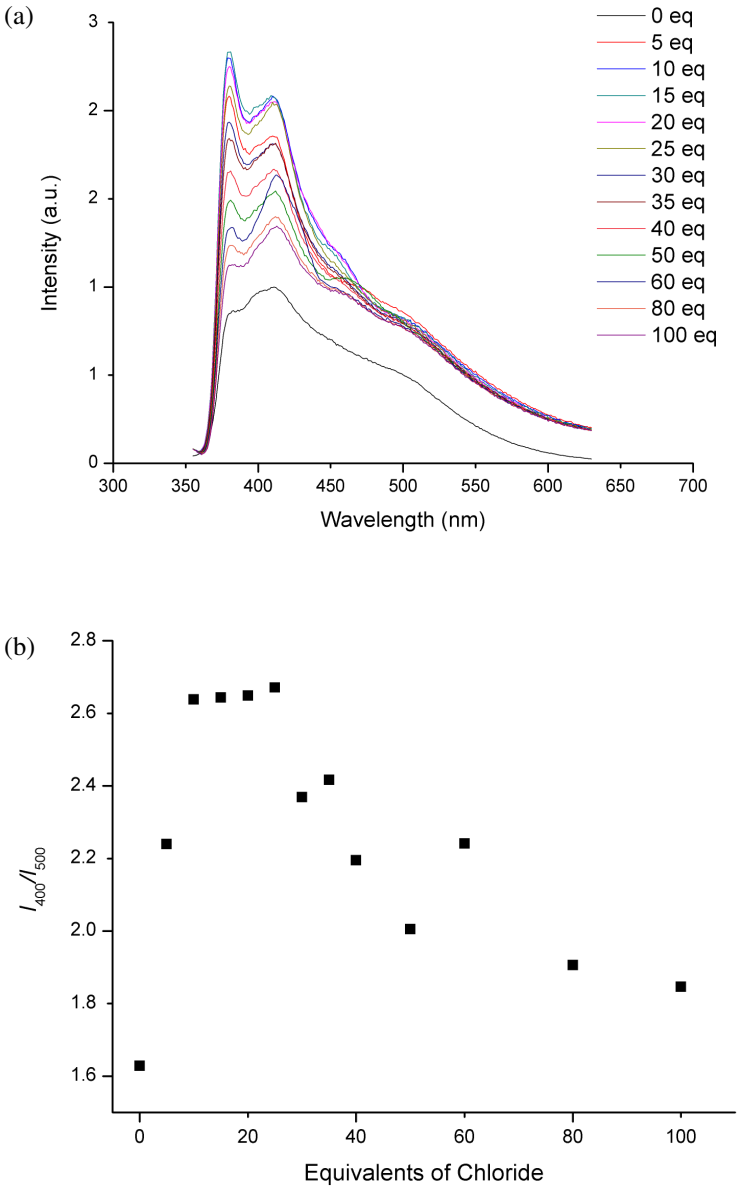

Figure 5.22 (a) Fluorescence emission spectrum of compound **145** (λ_{ex} = 340 nm, 1.0 x 10^{-5} mol dm^{-3} in $CHCl_3$/DMSO (*v/v* 95/5) with increasing equivalents of chloride (used as TBA salt), (b) Ratio of emission band intensities (400 nm and 500 nm) of compound **145** with increasing concentration of chloride (used as TBA salt)

5.6 Conclusions

In conclusion, a series of anion receptors in which the strength of anion binding can be tuned through modification of the cavity size and flexibility of the molecule have been synthesised. The progressive modification of the receptor design also gives rise to a turn-on response to anions observed with compound **135** only, a turn-on or turn-off response observed with **136** only and turn-off response for **138** and **139**. Higher order binding stoichiometries for fluoride give rise to a turn-on-turn-off response with anions for **135** and **136** as the conformation changes with the number of fluoride bound.

In the case of **135** and **136** the turn-on response is due to the planarisation of the chromophore increasing the barrier to non-radiative decay, resulting in increased fluorescence emission. In the case of **136**, **138** and **139** a mixture of static and dynamic quenching is observed depending on the binding strength of the anion. The mechanism is likely to be a PET process, however, in the case of **138** with TBA-F and **139** with TBA-Cl and F there is evidence a conformational change may cause the change in fluorescence. When used in array with each other these sensors can discriminate between anions using a simple traffic-light turn-on, turn-off system.

5.7 Experimental

Instrumentation

All NMR spectra were performed on a Varian Mercury-400 (400 MHz for ^{1}H), Varian Inova-500 machine (500 MHz for ^{1}H, 126 Hz for ^{13}C) or a Varian DD-700 (700 MHz for ^{1}H, 176 MHz for ^{13}C and 698 MHz for ^{19}F) and were referenced to residual solvent. Electrospray (ES) mass spectrometry was recorded on a Thermo-Finnigan LTQ instrument. Fourier transform infrared spectra were recorded with a Perkin Elmer Spectrum 100 ATR instrument. For each spectrum, 16 scans were conducted over a spectral range of 4000 to 600 cm^{-1} with a resolution of 4 cm^{-1}. The analysis was carried out with the Spectrum Express 1.01 software. Elemental analysis was performed using an Exeter Analytical inc. CE-400 Elemental Analyser. Commercial reagents were used as supplied, without further purification.

General Procedure for ^{1}H NMR spectroscopy experiments

A solution of the host species of known concentration typically 0.5-1.5 mM, was made up in an NMR tube using the appropriate deuterated solvent (0.5 ml $CDCl_3$/DMSO-d_6 (*v/v* 70/30)). Solutions of the anions, as TBA salts (1 ml) were made ten times the concentration of the host solution. The guest solution was typically added in 10 μl aliquots, representing 0.1 equivalents of the guest with respect to the host. Larger aliquots were used in some cases where no inflection of the trace was evident. Spectra were recorded after each addition and the trace was followed simultaneously. Results were analysed using the curve-fitting program *HypNMR* 2006.[33]

General Procedure for UV-vis Spectroscopic Titrations

UV-vis spectroscopic titrations were carried out using a Perkin-Elmer Lambda 35 spectrometer. A solution of typical concentration 1.0 x 10^{-4} mol dm^{-3} of host was made in a volumetric flask. A 3 ml sample of host solution of concentration of 1.0 x 10^{-5} mol dm^{-3} for **135**, **138**, **139** and **145**, 2.5 x 10^{-5} mol dm^{-3} for **136** and 2.0 x 10^{-5} mol dm^{-3} for **137** were prepared by dilution of the stock solution. Guest solutions were prepared such that 100 μl of guest solution corresponds to 100 equivalents of host. Solutions were prepared using $CHCl_3$/DMSO (*v/v* 95/5) as solvent.

Photophysical Measurements

Emission and excitation spectra were obtained using a Jobin-Yvon Horiba Fluorolog 3-22 Tau-3 spectrofluorimeter with a right angle illumination method and were corrected for the spectral response of the instrument.

Fluorescence spectroscopic titrations were carried out using the equipment described above. A solution of concentration 1.0 x 10^{-4} mol dm^{-3} of host was made in a volumetric flask. A 3 ml sample of host solution of typical concentration of 1.0 x 10^{-5} mol dm^{-3} for **135**, **138** and **139**, 2.5 x 10^{-5} mol dm^{-3} for **136** and 2.0 x 10^{-5} mol dm^{-3} for **137** were prepared by dilution of the stock solution. Guest solutions were prepared such that 100 μl of guest solution corresponds to 100 equivalents of host. Solutions were prepared using $CHCl_3$/DMSO (*v/v* 95/5) as solvent.

Photoluminescent quantum yields were calculated using a Jobin-Yvon Horiba Fluorolog 3-22 Tau-3 spectrofluorimeter with a right angle illumination method following the method of Williams *et al*.[55] for compound **135**. The fluorescent standard used was quinine sulfate in 0.1 M H_2SO_4 (aq), quantum yield = 0.54.[56] Measurements were taken over a range of five different concentrations, all with an absorbance below 0.1. A refractive index of 1.4465 was used for $CHCl_3$/DMSO (*v/v* 95/5).[57] The intergration sphere methodology of Beeby *et al.* was used to obtain quantum yields for compounds **136** – **139**.[58]

Lifetimes were obtained via the time-correlated single-photon counting (TCSPC) technique. The method described by Beeby *et al*. was used.[41] Samples were excited using the third harmonic of mode-locked cavity dumped Ti-sapphire laser. The emission was collected at 90° to the source of excitation and the emission wavelength selected by a monochromator (Jobin Yvon Triax 190). Fluorescence detection was obtained using a single photon avalanche diode (ID-Quantique ID-100) that was linked to a time-to-amplitude converter (Ortec 567) and a pulse height analyser, PHA, (E.G. & G. Trump Card and Maestro for Windows v 5.10). Fluorescence decays were recorded to a minimum of 10,000 counts in the peak channel of the PHA with a record length of 1000 channels. The decay and IRF data were transferred to PC for analysis in Microsoft Excel via the method of iterative reconvolution and nonlinear least squares fitting.

Fluorescence Microscopy

The design of the dipstick follows the method of Smith *et al.*[53] Time-resolved microscopy was performed based upon time-gated detection as follows. The excitation source was a Q-switched Nd:YAG laser (UV FQ, Elforlight LtD) and its output is optical pulses at 355 nm through internal third harmonic generation with a temporal width of ~5 ns (FWHM). The microscope was a Leica 135 axiovert epi fluorescence microscope. The laser excitation pulses were fed into the microscope through a beam expander and focused onto the sample using long working distances objective lenses (Zeiss LD plan neofluar, 10x, 40x or 63x). The PL was detected using a combination of dichroic mirrors and bandpass or long pass filters. The PL was signal was collected using a time-gated CCD camera (752 by 582 pixels), (Imagex nanoCCD, Photonics

Research Systems). In the excitation-detection sequence the CCD camera control unit triggers the laser with TTL pulse and the PL signals are acquired with a suitable delay and time gate combination. The CCD camera system has 16 different time banks.

Computational Details

Geometries were optimized using density functional theory (DFT) as implemented in the Gaussian 09 program suite.[37] The B3LYP functional was used in conjunction with the 6-311G(d,p) for **135**, while for **135**.Cl^- this was augmented with an additional diffuse set of s, p and d functionals added to each peripheral hydrogen atom. Optimised critical points were confirmed as minima by observing that the Hessian matrix was positive definite. The time-dependent DFT computations used the CAM-B3LYP functional.

CASSCF calculations were performed on a model system of diphenylbutadiyne with D_{2d} symmetry. The CASSCF wavefunctions were constructed from the natural orbitals of an unrestricted Hartree-Fock calculation. Eight electrons were distributed in eight orbitals, selected on the basis of the natural orbital occupation, to generate 1764 singlet configuration state functions. The CASSCF wavefunctions were optimised by the state-averaging equally over the 2nd and 3rd lowest roots, which were found to be degenerate. Upon inspection of the orbitals, and the configuration interaction coefficients, these two states (S_1 and S_2) were identified as the $\pi_x^* \leftarrow \pi_x$ and $\pi_y^* \leftarrow \pi_x$ states.

2-[(2-Aminophenyl)ethynyl]phenylamine, 2-[4-(2-aminophenyl)-1,3-butadiynyl]phenyl amine and 2-(phenylethynyl)aniline were synthesised according to literature procedures.[32]

Synthesis of 135:

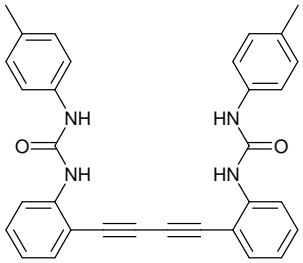

2-[4-(2-aminophenyl)-1,3-butadiynyl]phenylamine (0.25 g, 1.1 mmol) was dissolved in 20 ml of dry dichloromethane. *p*-Tolyl isocyanate (0.35 g, 2.6 mmol) was added and the solution heated to reflux under N_2 for 48 hours. The solution was filtered and the solid isolated and washed with diethyl ether and dried under ambient conditions. Yield = 0.32 g, 0.65 mmol, 59%. m.p. decomposed above 154 ^{o}C; ^{1}H NMR (700 MHz, DMSO-d_6 /ppm) δ = 9.41 (2H, s, NH), 8.39 (2H, s, NH), 8.16 (2H, d, J = 8.5 Hz, ArH), 7.58 (2H, dd, J = 1.4, 7.7 Hz, ArH), 7.43 (2H, td, J = 1.4, 8.5 Hz, ArH), 7.35 (4H, d, J = 8.3 Hz, ArH), 7.09 (4H, d, J = 8.3 Hz, ArH), 7.05 (2H, td, J = 0.8, 7.7 Hz, ArH), 2.25 (6H, s, CH_3); ^{13}C-{^{1}H} NMR (176 MHz, DMSO-d_6 /ppm) δ = 152.1, 142.0, 136.7, 133.4, 131.1, 130.7, 129.2, 122.2, 119.7, 118.5, 109.5, 79.7, 79.5, 20.3; m/z (ES$^-$) 364.4, 497.2 [M-H]$^-$, 533.3 [M+Cl]$^-$, 543.1, 572.9, 994.8 [2M]$^-$, 1030.2 [2M+Cl]$^-$; ν/cm^{-1} 3286 (s, urea NH), 3030 (w, CH), 2918 (w, CH), 1646 (s, C=O), 1600, 1577, 1539 (s, Ar C=C), 1511 (s, Ar C=C), 1472, 1446, 1406, 1293, 1236, 1206, 1106, 1020, 944, 817, 750, 644; Found: C, 74.94; H, 5.14; N, 10.71; Calc for $C_{32}H_{26}N_4O_2.0.75H_2O$: C, 75.05; H, 5.41; N, 10.94; the presence of water is suggested by NMR and IR spectra.

Crystal data for **135**: $C_{36}H_{38}N_4O_4S_2$, M = 654.82, yellow plate, 0.15 × 0.10 × 0.02 mm^3, monoclinic, space group $P2_1/c$ (No. 14), a = 15.6775(11), b = 6.1785(5), c = 17.4171(12) Å, β = 96.985(2)°, V = 1674.6(2) Å^3, Z = 2, D_c = 1.299 g/cm^3, F_{000} = 692, SMART 6K, MoKα radiation, λ = 0.71073 Å, T = 120(2)K, $2\theta_{max}$ = 50.0º, 19711 reflections collected, 2948 unique (R_{int} = 0.1772). Final *GooF* = 0.982, *R1* = 0.0610, *wR2* = 0.1334, R indices based on 1483 reflections with I >2σ(I) (refinement on F^2), 212 parameters, 0 restraints. Lp and absorption corrections applied, μ = 0.204 mm^{-1}.

Synthesis of 136:

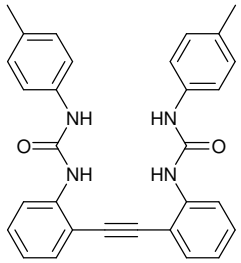

2-[(2-Aminophenyl)ethynyl]phenylamine (0.20 g, 1.0 mmol) was dissolved in 20 ml of dry dichloromethane. *p*-Tolyl isocyanate (0.24 g, 2.4 mmol) was added and the solution heated to reflux under N_2 for 48 hours. The solution was filtered and the solid isolated and washed with diethyl ether and dried under ambient conditions. Yield = 0.16 g, 0.39 mmol, 39%. m.p. 154 - 155 ^{o}C; ^{1}H NMR (700 MHz, DMSO-d_6 /ppm) δ = 9.36 (2H, s, NH), 8.25 (2H, s, NH), 8.16 (2H, d, *J* = 8.4 Hz ArH), 7.62 (2H, dd, *J* = 1.5, 7.7 Hz, ArH), 7.39 (2H, td, *J* = 1.5 and 7.7 ArH), 7.28 (4H, d, *J* = 8.3 Hz, ArH), 7.06 (2H, td, *J* = 1.0, 7.7 Hz, ArH), 7.03 (4H, d, *J* = 8.3 Hz, ArH), 2.22 (6H, s, CH_3); ^{13}C-{^{1}H} NMR (176 MHz, DMSO-d_6 /ppm) δ = 152.3, 140.4, 136.7, 132.7, 130.9, 129.6, 129.1, 121.8, 119.5, 118.6, 111.4, 90.9, 20.3; *m/z* (ES^-) 473.2 $[M-H]^-$, 509.3 $[M+Cl]^-$, 519.0, 946.6 $[2M]^-$, 982.3 $[2M+Cl]^-$; ν/cm^{-1} 3298 (s, urea NH), 3031 (w, CH), 2922 (w, CH), 1645 (s, C=O), 1610, 1579, 1539 (s, Ar C=C), 1511 (s, Ar C=C), 1485, 1465, 1405, 1305, 1293, 1257, 1219, 1110, 1049, 1020, 942, 908, 754, 743, 647; Found: C, 75.09; H, 5.48; N, 11.69; Calc. for $C_{30}H_{26}N_4O_2.0.25H_2O$: C, 75.21; H, 5.58; N, 11.70; the presence of water is suggested by NMR and IR spectra.

Synthesis of 137:

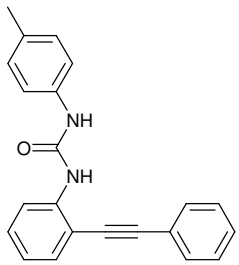

2-(phenylethynyl)aniline (0.18 g, 1.0 mmol) was dissolved in 20 ml of dry dichloromethane. *p*-Tolyl isocyanate (0.17 g, 1.4 mmol) was added and the solution

heated to reflux under N_2 for 48 hours. The solvent was removed *in vacuo* and 20 ml diethyl ether added. The solution was filtered and the solid isolated and washed with ether and dried in a vacuum desiccator. Yield = 0.21 g, 0.63 mmol, 63%. m.p. 205 - 211 ^{o}C; ^{1}H NMR (500 MHz, DMSO-d_6 /ppm) δ = 9.45 (1H s, NH), 8.21 (1H, s, NH), 8.12 (1H, d, *J* = 8.5, ArH), 7.69 – 7.63 (2H, m, ArH), 7.52 (1H, dd, *J* = 1.3, 7.6 Hz, ArH), 7.49 – 7.42 (4H, m, ArH), 7.36 (2H, d, *J* = 8.2, ArH), 7.10 (2H, d, *J* = 8.2, ArH), 7.04 (1H, td, *J* = 1.3, 7.6 Hz, ArH), 2.25 (3H, s, CH_3); ^{13}C-{^{1}H} NMR (126 MHz, DMSO-d_6 /ppm) δ = 152.2, 140.2, 136.9, 132.3, 131.7, 131.0, 129.5, 129.3, 129.0, 128.7, 122.3, 122.1, 119.6, 118.6, 111.4, 95.3, 85.2, 79.2, 20.4; *m/z* (ES$^-$) 325.3 [M-H]$^-$, 571.0, 650.6 [2M]$^-$, 686.5 [2M+Cl]$^-$; ν/cm^{-1} 3308 (s, urea NH), 3030 (w, CH), 2924 (w, CH), 1645 (s, C=O), 1608, 1577, 1546 (s, Ar C=C), 1512 (s, Ar C=C), 1494, 1474, 1405, 1306, 1259, 1163, 1259, 1219, 1049, 1020, 941, 914, 753, 688, 642; Found: C, 78.94; H, 5.45; N, 8.13; Calc. for $C_{22}H_{28}N_4O_2.0.5H_2O$: C, 78.78; H, 5.71; N, 8.35; the presence of water is suggested by NMR and IR spectra.

Synthesis of 2-(2-(3-(2-(2-aminophenyl)ethynyl)phenyl)ethynyl)benzenamine (142):

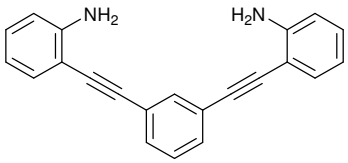

1,2-Diiodobenzene (1.0 g, 3.0 mmol) and 2-ethynylaniline (0.78 g, 6.7 mmol) were added to a Schlenk tube and placed under a N_2 atmosphere. Dry tetrahydrofuran (20 ml) and dry triethylamine (2 ml) were added and the solvent degassed by the freeze, pump, thaw method (three cycles). $Pd(PPh_3)_2Cl_2$ (106 mg, 0.15 mmol, 5 mol%) and CuI (28 mg, 0.15 mmol, 5 mol%) were added and the solution stirred under N_2 for 24 hours. Diethyl ether was added and the solution filtered through celite with further diethyl ether. The solvent was removed from the filtrate *in vacuo* and water (50 ml) added. The water was extracted with dichloromethane, the organic washings were combined and dried with $MgSO_4$. The solid was removed by filtration and the solvent removed *in vacuo*. The crude product was purified by column chromatography (60:40 diethyl ether:hexane). Yield = 0.34 g, 1.1 mmol, 36%. m.p. 120 - 122 ^{o}C; ^{1}H NMR

(700 MHz, $CDCl_3$ /ppm) δ = 7.68 (1H, s, ArH), 7.46 (2H, dd, *J* = 1.5 and 7.7 Hz, ArH), 7.35 (2H, d, *J* = 7.7 Hz, ArH), 7.32 (1H, t, *J* = 7.7 Hz, ArH), 7.14 (2H, td, *J* = 1.5, 7.7, ArH), 6.71 (4H, m, ArH), 4.26 (4H, s, NH_2); ^{13}C-{^1H} NMR (126 MHz, $CDCl_3$/ ppm) δ = 148.1, 134.4, 132.4, 131.2, 130.2, 128.8, 123.9, 118.2, 114.6, 107.8, 94.1, 86.9; *m/z* (ES^+) Found 309.1403; Calc. Mass 309.1392; ν/cm^{-1} 3459 (s, N-H), 3370 (s, N-H), 3072 (w, C-H), 2199 (m, C≡C), 1607, 1493, 1453, 1314, 1255, 1151.

Synthesis of 3-(2-(2-(2-(3-aminophenyl)ethynyl)phenyl)ethynyl)benzenamine (143):

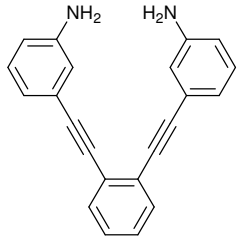

1,3-Diiodobenzene (1.0 g, 3.0 mmol) and 3-ethynylaniline (0.78 g, 6.7 mmol) were added to a Schlenk tube and placed under a nitrogen atmosphere. Dry tetrahydrofuran (20 ml) and dry triethylamine (2 ml) were added and the solvent degassed by the freeze, pump, thaw method (three cycles). $Pd(PPh_3)_2Cl_2$ (106 mg, 0.15 mmol, 5 mol%) and CuI (28 mg, 0.15 mmol, 5 mol%) were added and the solution stirred under N_2 for 24 hours. Diethyl ether was added and the solution filtered through celite with further diethyl ether. The solvent was removed from the filtrate *in vacuo* and water (50 ml) added. The water was extracted with dichloromethane, the organic washings were combined and dried with $MgSO_4$. The solid was removed by filtration and the solvent removed *in vacuo*. The crude product was purified by column chromatography (diethyl ether). Yield = 0.52 g, 1.7 mmol, 56%. m.p. 126 - 128 ^oC; ^1H NMR (700 MHz, $CDCl_3$ /ppm) δ = 7.51 (2H, dd, *J* = 3.3 and 5.8, ArH), 7.27 (2H, dd, *J* = 3.3 and 5.8 Hz), 7.11 (2H, t, *J* = 7.8 Hz, ArH), 6.97 (2H, d, *J* = 7.8 Hz), 6.90 (2H, s, ArH), 6.64 (2H, dd, *J* = 1.6 and 7.8 Hz, ArH), 3.65 (4H, s, NH_2); ^{13}C-{^1H} NMR (126 MHz, $CDCl_3$ /ppm) δ = 146.5, 131.7, 129.5, 128.1, 126.3, 124.2, 122.2, 118.4, 115.7, 94.2, 88.1; *m/z* (ES^+) Found 309.1384; Calc. Mass 309.1392; *ν*/cm^{-1} 3405 (w, N-H), 3353 (w, N-H), 1601, 1494, 1447, 1219, 882.

Synthesis of 138:

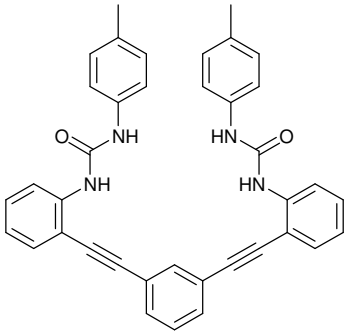

142 (0.15 g, 0.48 mmol) was dissolved in 20 ml of dry dichloromethane. *p*-Tolyl isocyanate (0.14 g, 1.1 mmol) was added and the solution heated to reflux under N_2 for 48 hours. The solvent was removed *in vacuo* and 20 ml diethyl ether added. The solution was filtered and the solid isolated and washed with diethyl ether and dried under ambient conditions. Yield = 0.19 g, 0.33 mmol, 69%. m.p. decomposition upon melting, 240 - 246 ^{o}C. ^{1}H NMR (500 MHz, DMSO-d_6 /ppm) δ = 9.40 (2H, s, NH), 8.22 (2H, s, NH), 8.13 (2H, d, *J* = 8.4 Hz, ArH), 7.95 (1H, s, ArH), 7.73 (2H, dd, *J* = 1.5 and 7.7 Hz, ArH), 7.61 – 7.48 (3H, m, ArH), 7.44 – 7.31 (6H, m, ArH), 7.14 – 6.99 (6H, m, ArH), 2.23 (6H, s, CH_3); ^{13}C-{^{1}H} NMR (126 MHz, DMSO-d_6 /ppm) δ = 152.3, 140.5, 136.9, 134.3, 132.5, 132.1, 131.1, 129.8, 129.3, 129.3, 122.9, 122.2, 119.9, 118.7, 111.3, 94.3, 86.3, 20.4; *m/z* (ES$^+$) 575.2 $[M+H]^+$, 597.2 $[M+Na]^+$, 613.2; ν/cm^{-1} 3279 (s, urea NH), 3048 (w, CH), 3026 (w, CH), 2912 (w, CH), 1645 (s, C=O), 1605, 1578, 1542 (s, Ar C=C), 1511 (s, Ar C=C), 1480, 1449, 1405, 1305, 1290, 1241, 1227, 1102, 1038, 817, 782, 751, 644; Found: C, 79.06; H, 5.24; N, 9.65; Calc. for $C_{28}H_{30}N_4O_2$: C, 79.42: H, 5.26; N, 9.75; the presence of water is suggested by NMR and IR spectra.

Synthesis of 139:

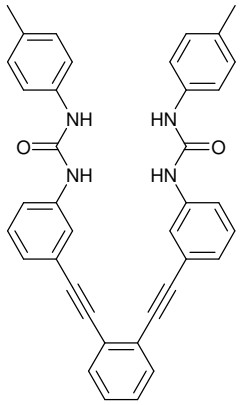

143 (0.20 g, 0.65 mmol) was dissolved in 20 ml of dry dichloromethane. *p*-Tolyl isocyanate (0.19 g, 1.4 mmol) was added and the solution heated to reflux under N_2 for 48 hours. The solvent was removed *in vacuo* and 20 ml diethyl ether added. The solution was filtered and the solid isolated and washed with diethyl ether and dried under ambient conditions. Yield = 0.23 g, 0.39 mmol, 60%. m.p. decomposition upon melting, 230 - 236 ^{o}C; ^{1}H NMR (500 MHz, DMSO-d_6 /ppm) δ = 8.77 (2H, s, NH), 8.61 (2H, s, NH), 7.87 (2H, s, ArH), 7.68 (2H, dd, *J* = 3.3 and 5.8 Hz, ArH), 7.47 (2H, dd, *J* = 3.3 and 5.8 Hz,), 7.40 – 7.27 (8H, m, ArH), 7.22 (2H, d, *J* = 7.3 Hz, ArH), 7.09 (4H, d, *J* = 8.4 Hz, ArH), 2.24 (6H, s, CH_3); ^{13}C-{^{1}H} NMR (126 MHz, DMSO-d_6 /ppm) δ = 152.5, 140.2, 136.9, 132.0, 130.8, 129.4, 129.3, 124.9, 124.6, 122.4, 120.5, 118.9, 118.4, 93.7, 87.6, 20.4; *m/z* (ES)$^+$ 575.2 [M+H]$^+$, 597.2 [M+Na]$^+$, 613.2; ν/cm^{-1} 3281 (s, urea NH), 3025 (w, CH), 2915 (w, CH), 1636 (s, C=O), 1585, 1549 (s, Ar C=C), 1488, 1422, 1308, 1285, 1224, 876, 817, 790, 750, 682, 644; Found: C, 77.14; H, 5.24; N, 9.66; Calc. for $0.9C_{38}H_{30}N_4O_2.0.1C_{30}H_{23}N_3O.H_2O$: C, 77.12; H, 5.45; N, 9.43; presence of impurity and water was confirmed by NMR and IR spectroscopy.

Synthesis of 144:

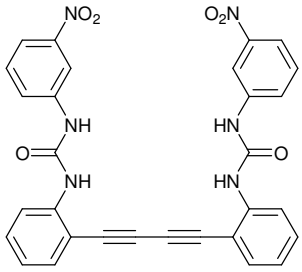

2-[4-(2-aminophenyl)-1,3-butadiynyl]phenylamine (0.20 g, 0.86 mmol) was dissolved in 50 ml of dry chloroform. 3-nitrophenyl isocyanate (0.31 g, 1.9 mmol) was added and the solution heated to reflux under N_2 for 24 hours. The solvent was removed *in vacuo* and 20 ml diethyl ether added. The solution was filtered and the solid isolated and washed with diethyl ether and dried under ambient conditions. Yield = 0.27 g, 0.47 mmol, 55%. m.p. 214 - 222 ^{o}C; ^{1}H NMR (700 MHz, DMSO-d_6 /ppm) δ = 10.01 (2H, s, NH), 8.56 (2H, t, J = 2.2 Hz, ArH), 8.53 (2H, s, NH), 8.17 (2H, d, J = 8.2 Hz, ArH), 7.83 (2H, ddd, J = 0.8, 2.3 and 8.2 Hz, ArH), 7.69 (2H, dd, J = 1.3 and 7.6 Hz. ArH), 7.61 (2H, dd, J = 1.4 and 7.6 Hz, ArH), 7.56 (2H, t, J = 8.2 Hz, ArH), 7.47 (2H, t, J = 7.6 Hz, ArH), 7.11 (2H, td, J = 1.0 and 7.6 Hz, ArH); ^{13}C-{^{1}H} NMR (176 MHz, DMSO-d_6 /ppm) δ = 206.4, 152.0, 148.1, 141.4, 140.6, 133.4, 130.9, 130.1, 124.2, 120.12, 116.6, 112.1, 110.0, 79.7, 79.4; *m/z* (ES^{+}) 151.2, 192.2, 242.4 281.3, 561.1 [M+H]$^{+}$, 583.3 [M+Na]$^{+}$, ν/cm^{-1} 3326 (m, N-H), 1658 (s, C=O), 1549 (m, Ar C=C), 1519 (s, NO_2) 1347 (s, NO_2), 1353, 1306, 1243, 733; Found: C, 63.72; H, 3.58; N, 14.66; Calc. for $C_{30}H_{20}N_6O_6$; C; 64.28, H; 3.60; N, 14.66.

Synthesis of 145:

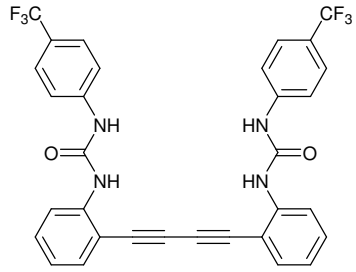

2-[4-(2-aminophenyl)-1,3-butadiynyl]phenylamine (0.20 g, 0.86 mmol) was dissolved in 50 ml of dry chloroform. *p*-Trifluoromethylphenyl isocyanate (0.35 g, 1.9 mmol) was added and the solution heated to reflux under N_2 for 24 hours. The solvent was removed *in vacuo* and 20 ml diethyl ether added. The solution was filtered and the solid isolated and washed with diethyl ether and dried under ambient conditions. Yield = 0.32 g, 0.52 mmol, 60%. m.p. decomposed above 230 ^{o}C; ^{1}H NMR (700 MHz, DMSO-d_6 /ppm) δ = 9.89 (2H, s, NH), 8.54 (2H, s, NH), 8.15 (2H, d, *J* = 8.4 Hz, ArH), 7.74 – 7.54 (10H, m, ArH), 7.46 (2H, t, *J* = 7.6 Hz, ArH), 7.10 (2H, t, *J* = 7.6 Hz); ^{13}C-{^{1}H} NMR (176 MHz, DMSO-d_6 /ppm) δ = 151.9, 143.0, 141.5, 133.5, 130.8, 126.1, 125.2, 123.6, 122.7, 120.0, 118.0, 109.9, 79.6, 79.4; ^{19}F NMR (698 MHz, DMSO-d_6 /ppm) δ = -60.15; *m/z* (ES^{+}) 242.3, 607.2 [M+H]$^{+}$; ν/cm^{-1} 3349 (s, N-H), 3306 (m, N-H), 1662 (s, C=O), 1549 (m, Ar C=C), 1336, 1110 (s, CF_3), 1105 (s, CF_3), 852, 761; Found: C, 62.71; H, 3.30; N, 9.00; Calc. for $C_{32}H_{20}F_6N_4O_2$; C; 63.37, H; 3.32; N, 9.24.

5.8 References

1. T. Gunnlaugsson, M. Glynn, G. M. Tocci, P. E. Kruger and F. M. Pfeffer, *Coord. Chem. Rev.*, 2006, **250**, 3094.
2. L. Fabbrizzi, M. Licchelli, G. Rabaioli and A. Taglietti, *Coord. Chem. Rev.*, 2000, **205**, 85.
3. A. P. de Silva, D. B. Fox, T. S. Moody and S. M. Weir, *Pure Appl. Chem.*, 2001, **73**, 503.
4. D. E. Koshland, *Angew. Chem., Int. Ed.*, 1995, **33**, 2375.
5. K. J. Wallace, W. J. Belcher, D. R. Turner, K. F. Syed and J. W. Steed, *J. Am. Chem. Soc.*, 2003, **125**, 9699.
6. M. H. Filby, S. J. Dickson, N. Zaccheroni, L. Prodi, S. Bonacchi, M. Montalti, C. Chiorboli, M. J. Paterson, T. D. Humphries and J. W. Steed, *J. Am. Chem. Soc.*, 2008, **130**, 4105.
7. B. Schazmann, N. Alhashimy and D. Diamond, *J. Am. Chem. Soc.*, 2006, **128**, 8607.
8. Y. Bai, B. G. Zhang, J. Xu, C. Y. Duan, D. B. Dang, D. J. Liu and Q. J. Meng, *New J. Chem.*, 2005, **29**, 777.

9. A. Pramanik and G. Das, *Tetrahedron*, 2009, **65**, 2196.
10. S. K. Kim, J. H. Bok, R. A. Bartsch, J. Y. Lee and J. S. Kim, *Org. Lett.*, 2005, **7**, 4839.
11. D. H. Lee, J. H. Im, J. H. Lee and J. I. Hong, *Tetrahedron Lett.*, 2002, **43**, 9637.
12. S. Kondo and M. Sato, *Tetrahedron*, 2006, **62**, 4844.
13. P. D. Beer, *Acc. Chem. Res.*, 1998, **31**, 71.
14. Y. Bai, B.-G. Zhang, C. Y. Duan, D.-B. Dang and Q.-J. Meng, *New. J. Chem.*, 2006, **30**, 266.
15. J. Zhang, A. M. Bond, J. Belcher, K. J. Wallace and J. W. Steed, *J. Phys. Chem. B*, 2003, **107**, 5777.
16. J. W. Steed and K. J. Wallace, in '*Advances in Supramolecular Chemistry*', ed. G. W. Gokel, Cerberus, New York, 2003.
17. D. J. Cram, *Angew. Chem., Int. Ed.*, 1986, **25**, 1039.
18. F. Hettche, P. Reiß and R. W. Hoffmann, *Chem. -Eur. J.*, 2002, **8**, 4946.
19. J. W. Steed and J. L. Atwood, '*Supramolecular Chemistry*', J. Wiley & Sons, Chichester, 2009.
20. C. Caltagirone and P. A. Gale, *Chem. Soc. Rev.*, 2009, **38**, 520.
21. J. L. Sessler, P. A. Gale and W.-S. Cho, '*Anion Receptor Chemistry*', Royal Society of Chemistry, Cambridge, 2006.
22. C. N. Carroll, O. B. Berryman, C. A. Johnson, L. N. Zakharov, M. M. Haley and D. W. Johnson, *Chem. Commun.*, 2009, 2520.
23. P. D. Jones and T. E. Glass, *Tetrahedron*, 2004, **60**, 11057.
24. Y. Nagano, T. Ikoma, K. Akiyama and S. Tero-Kubota, *J. Am. Chem. Soc.*, 2003, **125**, 14103.
25. Y. Hirata, T. Okada and T. Nomoto, *Chem. Phys. Lett.*, 1998, **293**, 371.
26. G. T. Crisp and T. P. Bubner, *Tetrahedron*, 1997, **53**, 11881.
27. G. Brizius, K. Billingsley, M. D. Smith and U. H. F. Bunz, *Org. Lett.*, 2003, **5**, 3951.
28. S. A. McFarland and N. S. Finney, *J. Am. Chem. Soc.*, 2002, **124**, 1178.
29. G. Eglinton and A. R. Galbraith, *Chem. Ind.*, 1956, 737.
30. P. Siemsen, R. C. Livingston and F. Diederich, *Angew. Chem., Int. Ed.*, 2000, **39**, 2633.
31. K. Sonogashira, *J. Organomet. Chem.,* **2001**, *653*, 46.
32. C. Koradin, W. Dohle, A. L. Rodriguez, B. Schmid and P. Knochel, *Tetrahedron*, 2003, **59**, 1571.
33. P. Gans, *HypNMR* 2006, University of Leeds, Leeds, 2006.
34. D. R. Turner, E. C. Spencer, J. A. K. Howard, D. A. Tocher and J. W. Steed, *Chem. Commun.*, 2004, 1352.
35. M. Barboiu, G. Vaughan and A. van der Lee, *Org. Lett.*, 2003, **5**, 3073.
36. P. Byrne, D. R. Turner, G. O. Lloyd, N. Clarke and J. W. Steed, *Cryst. Growth Des.*, 2008, **8**, 3335.
37. Gaussian 09, Revision **A.2**, M. J. Frisch, G. W. Trucks, H. B. Schlegel, G. E. Scuseria, M. A. Robb, J. R. Cheeseman, G. Scalmani, V. Barone, B. Mennucci, G. A. Petersson, H. Nakatsuji, M. Caricato, X. Li, H. P. Hratchian, A. F. Izmaylov, J. Bloino, G. Zheng, J. L. Sonnenberg, M. Hada, M. Ehara, K. Toyota, R. Fukuda, J. Hasegawa, M. Ishida, T. Nakajima, Y. Honda, O. Kitao, H. Nakai, T. Vreven, J. A. Montgomery, Jr., J. E. Peralta, F. Ogliaro, M. Bearpark, J. J. Heyd, E. Brothers, K. N. Kudin, V. N. Staroverov, R. Kobayashi, J. Normand, K. Raghavachari, A. Rendell, J. C. Burant, S. S. Iyengar, J. Tomasi, M. Cossi, N. Rega, J. M. Millam, M. Klene, J. E. Knox, J. B. Cross, V. Bakken, C. Adamo, J. Jaramillo, R. Gomperts, R. E. Stratmann, O. Yazyev, A. J. Austin, R. Cammi,

C. Pomelli, J. W. Ochterski, R. L. Martin, K. Morokuma, V. G. Zakrzewski, G. A. Voth, P. Salvador, J. J. Dannenberg, S. Dapprich, A. D. Daniels, O. Farkas, J. B. Foresman, J. V. Ortiz, J. Cioslowski, and D. J. Fox, Gaussian, Inc., Wallingford CT, 2009.

38. K. Okuyama, T. Hasegawa, M. Ito and N. Mikami, *J. Phys. Chem.*, 1984, **88**, 1711.
39. S. J. Greaves, E. L. Flynn, E. L. Futcher, E. Wrede, D. P. Lydon, P. J. Low, S. R. Rutter and A. Beeby, *J. Phys. Chem. A*, 2006, **110**, 2114.
40. S. Toyota, *Chem. Rev.*, 2010, **110**, 5398.
41. A. Beeby, S. Fitzgerald and C. F. Stanley, *Photochem. Photobiol.*, 2001, **74**, 566.
42. T. Yanai, D. P. Tew and N. C. Handy, *Chem. Phys. Lett.*, 2004, **393**, 51.
43. C. M. G. Dos Santos, T. McCabe and T. Gunnlaugsson, *Tetrahedron Lett.*, 2007, **48**, 3135.
44. J. S. Melinger, Y. C. Pan, V. D. Kleiman, Z. H. Peng, B. L. Davis, D. McMorrow and M. Lu, *J. Am. Chem. Soc.*, 2002, **124**, 12002.
45. C. D. Geddes, *Meas. Sci. Technol.*, 2001, **12**, R53.
46. R. Martinez-Manez and F. Sancenon, *Chem. Rev.*, 2003, **103**, 4419.
47. J. R. Lakowicz, *'Principles of Fluorescent Spectroscopy'*, 3rd Ed., Springer, 2006.
48. A. Goodey, J. J. Lavigne, S. M. Savoy, M. D. Rodriguez, T. Curey, A. Tsao, G. Simmons, J. Wright, S. J. Yoo, Y. Sohn, E. V. Anslyn, J. B. Shear, D. P. Neikirk and J. T. McDevitt, *J. Am. Chem. Soc.*, 2001, **123**, 2559.
49. S. C. McCleskey, M. J. Griffin, S. E. Schneider, J. T. McDevitt and E. V. Anslyn, *J. Am. Chem. Soc.*, 2003, **125**, 1114.
50. T. Abalos, S. Royo, R. Martinez-Manez, F. Sancenon, J. Soto, A. M. Costero, S. Gil and M. Parra, *New J. Chem.*, 2009, **33**, 1641.
51. K. Niikura and E. V. Anslyn, *J. Org. Chem.*, 2003, **68**, 10156.
52. G. E. Tiller, T. J. Mueller, M. E. Dockter, W. G. Struve, *Anal. Biochem*., 1984, **141**, 262.
53. J. J. Gassensmith, S. Matthys, J. J. Lee, A. Wojcik, P. V. Kamat and B. D. Smith, *Chem.-Eur. J.*, 2010, **16**, 2916.
54. F. M. Winnik, *Chem. Rev.*, 1993, **93**, 587.
55. A. T. R. Williams, S. A. Winfield and J. N. Miller, *Analyst*, 1983, **108**, 1067.
56. W. H. Melhuish, *J. Phys. Chem.*, 1961, **65**, 229.
57. P. M. Mancini, A. D. Perez and L. R. Vottero, *J. Solut. Chem.*, 2001, **30**, 695.
58. L. Porres, A. Holland, L. O. Palsson, A. P. Monkman, C. Kemp and A. Beeby, *J. Fluorescence*, 2005, **16**, 267.

Publications Arising From This Work

Sara Jane Dickson, Emma V. B. Wallace, Adam N. Swinburne, Martin J. Paterson, Gareth O. Lloyd, Andrew Beeby, Warwick J. Belcher and Jonathan W. Steed, "Intramolecular binding site competition as a means of tuning the response of a colourimetric anion sensor", *New. J. Chem.*, 2008, **32**, 786

Adam N. Swinburne and Jonathan W. Steed, "The Mechanochemical Synthesis of Tripodal Anion Receptors", *CrystEngComm.*, 2009, **11**, 433

Adam N. Swinburne, Martin J. Paterson, Kathrin H. Fischer, Sara Jane Dickson, Emma V. B. Wallace, Warwick J. Belcher, Andrew Beeby and Jonathan W. Steed, "Colourimetric Carboxylate Anion Sensors Derived from Viologen Based Receptors", *Chem. -Eur. J.*, 2010, **16**, 1480

Adam N. Swinburne, Martin J. Paterson, Andrew Beeby, Jonathan W. Steed, "A quinolinium-derived turn-off fluorescence anion sensor", *Org. Biomol. Chem.,* 2010, **8**, 1010

Adam N. Swinburne, Martin J. Paterson, Andrew Beeby, Jonathan W. Steed, "*Fluorescent* 'Twist-on' Sensing by Induced-Fit Anion Stabilisation of a Planar Chromophore", *Chem. -Eur. J.*, 2010, **16**, 2714

Appendix I – Supplementary Information Relating to Chapter 2

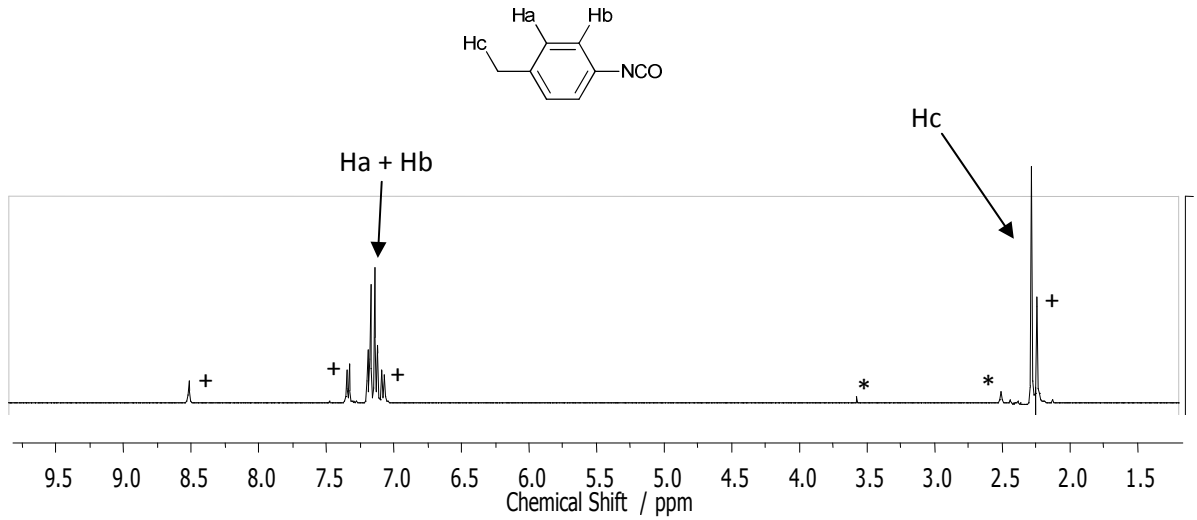

AI.1 ^{1}H NMR assignment for *p*-tolyl isocyanate in DMSO-d_6. * indicates residual solvent resonances (DMSO and water)

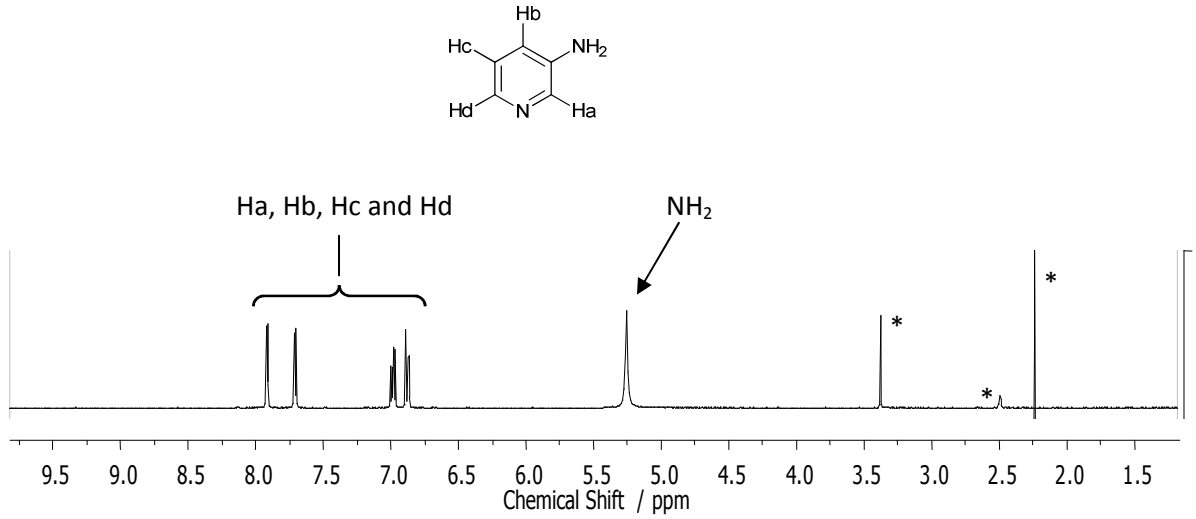

AI.2 ^{1}H NMR assignment for pyridine in DMSO-d_6. * indicates residual solvent resonances (DMSO and water) and impurities

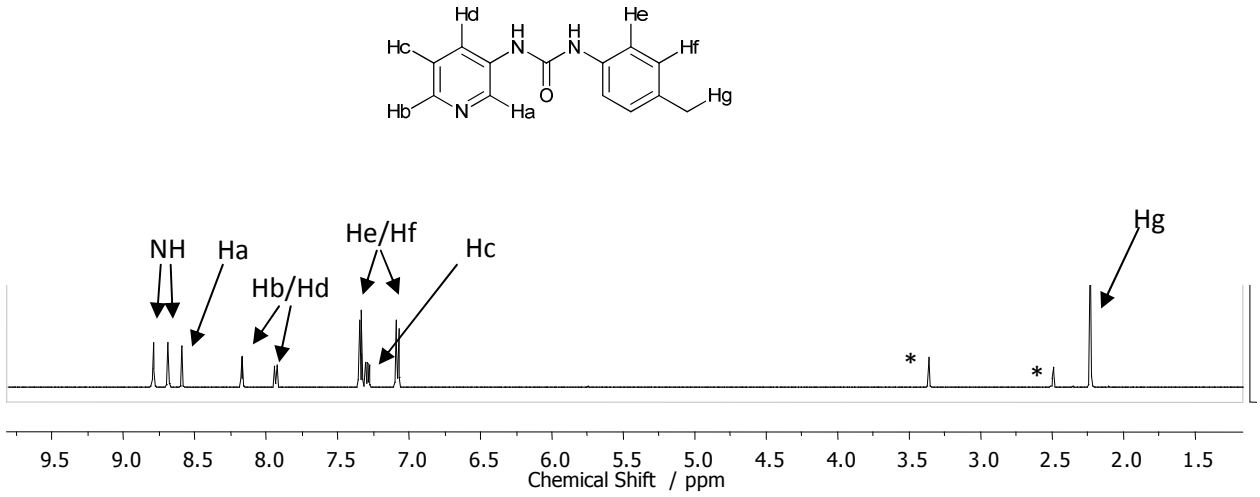

AI.3 [1]H NMR assignment of **118** in DMSO-d_6. * indicates residual solvent resonances (DMSO and water)

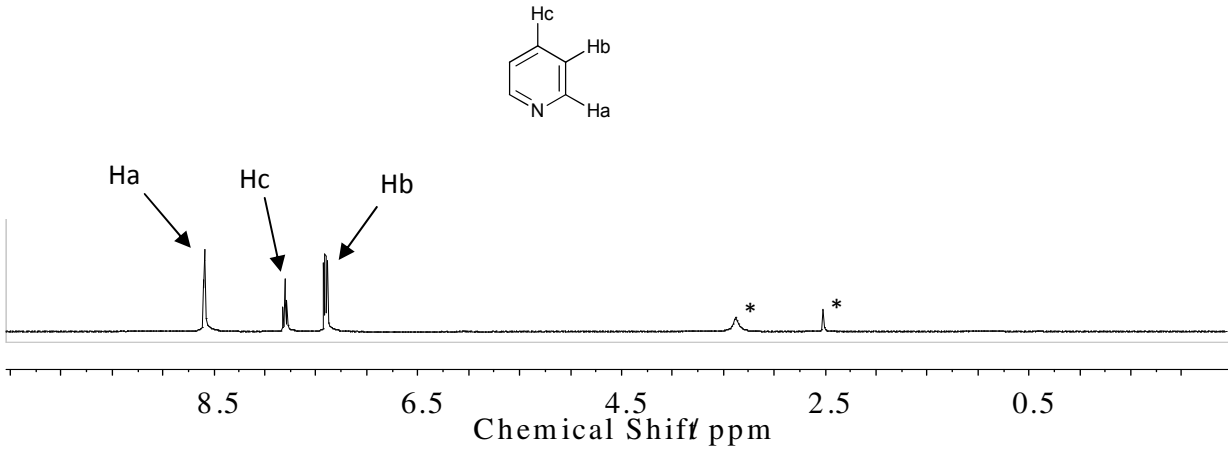

AI.4 [1]H NMR assignment of pyridine in DMSO-d_6. * indicates residual solvent resonances (DMSO and water)

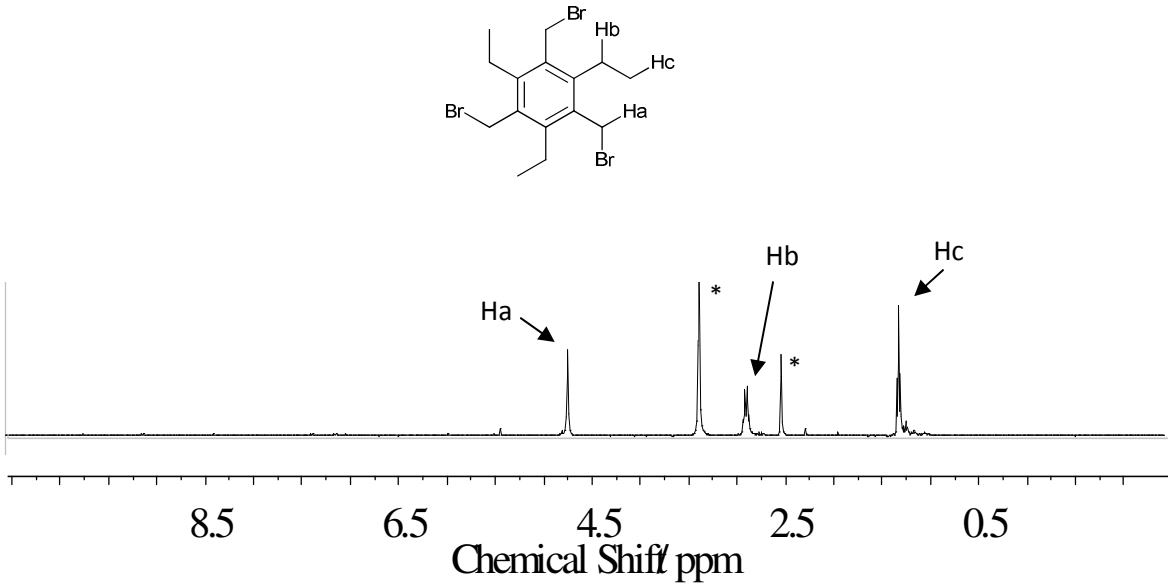

AI.5 ^{1}H NMR assignment for 1,3,5-triethylbenzene in DMSO-d_6. * indicates residual solvent resonances (DMSO and water)

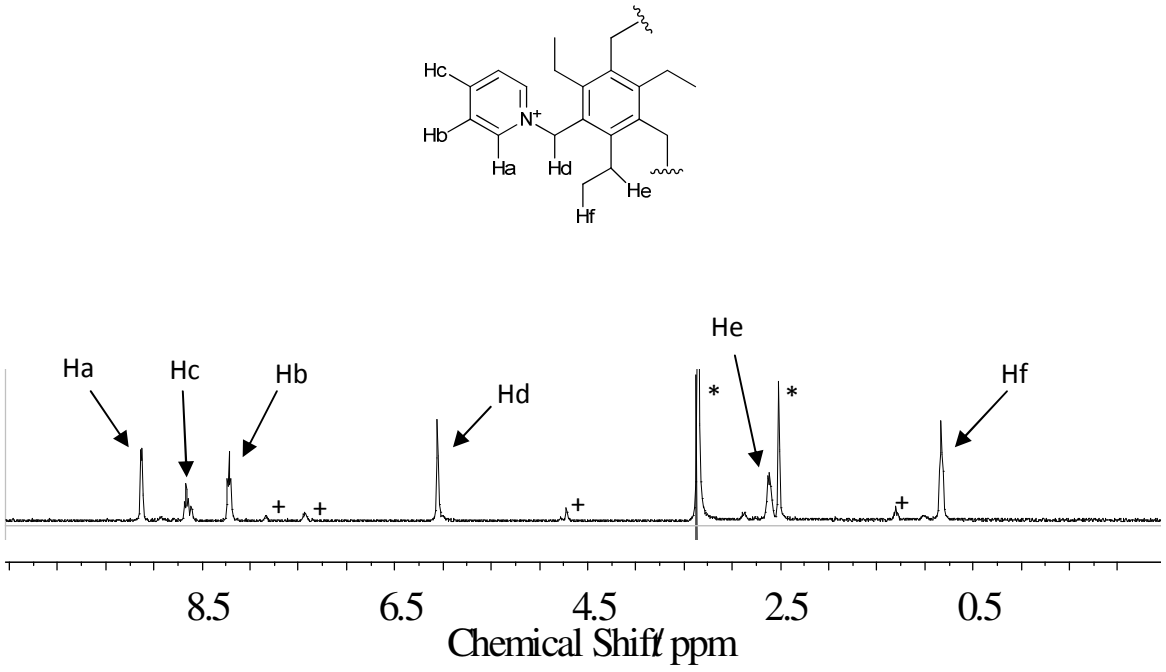

AI.6 ^{1}H NMR assignment for **119** in DMSO-d_6. * indicates residual solvent resonances (DMSO and water), + indicates starting material impurities

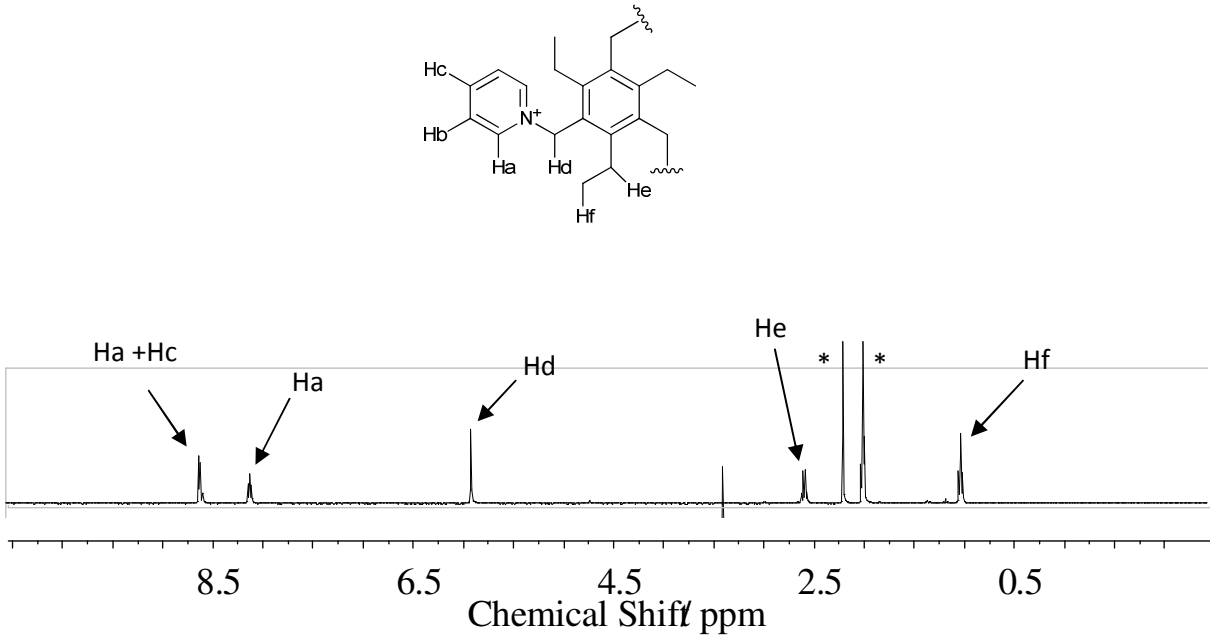

AI.7 ^{1}H NMR assignment of **120** in CD_3CN. * indicates residual solvent resonances (acetonitrile and water)

Appendix II – Supplementary Information Relating to Chapter 3

(a)

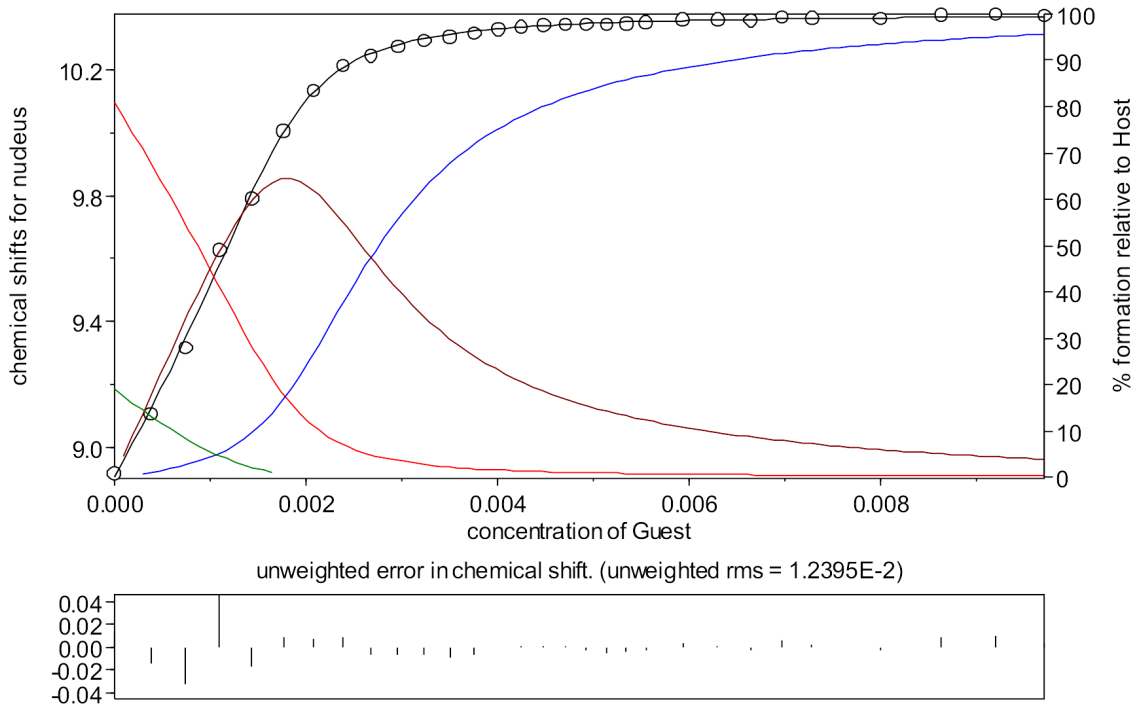

(b)

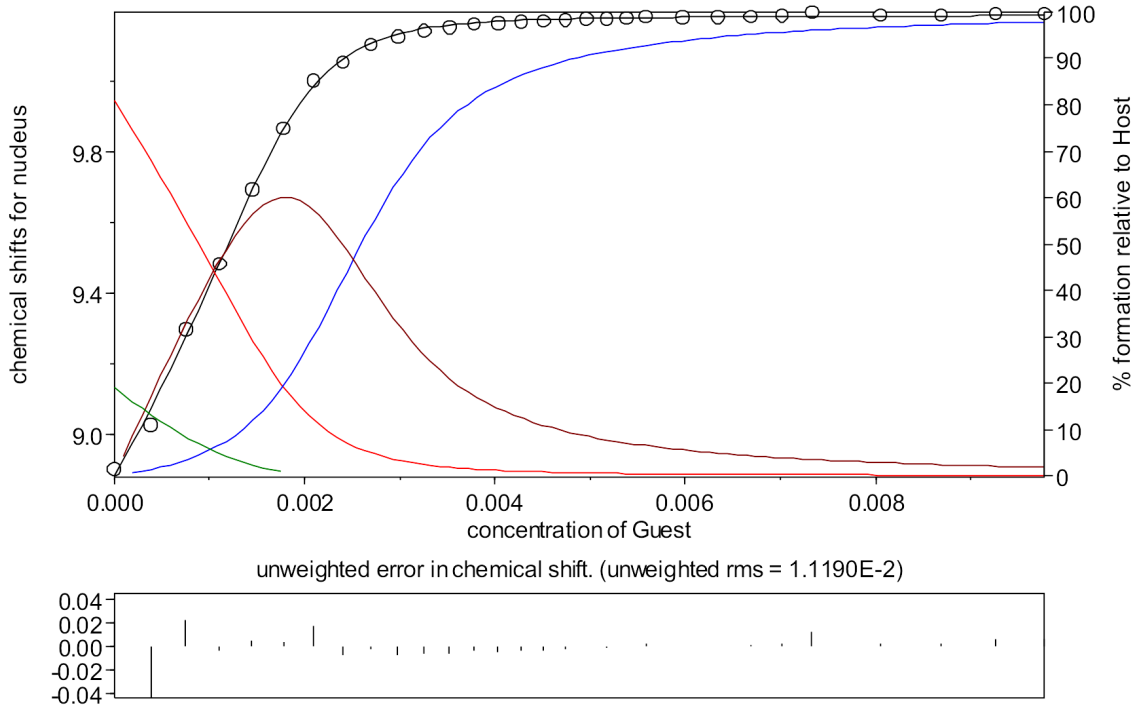

(c)

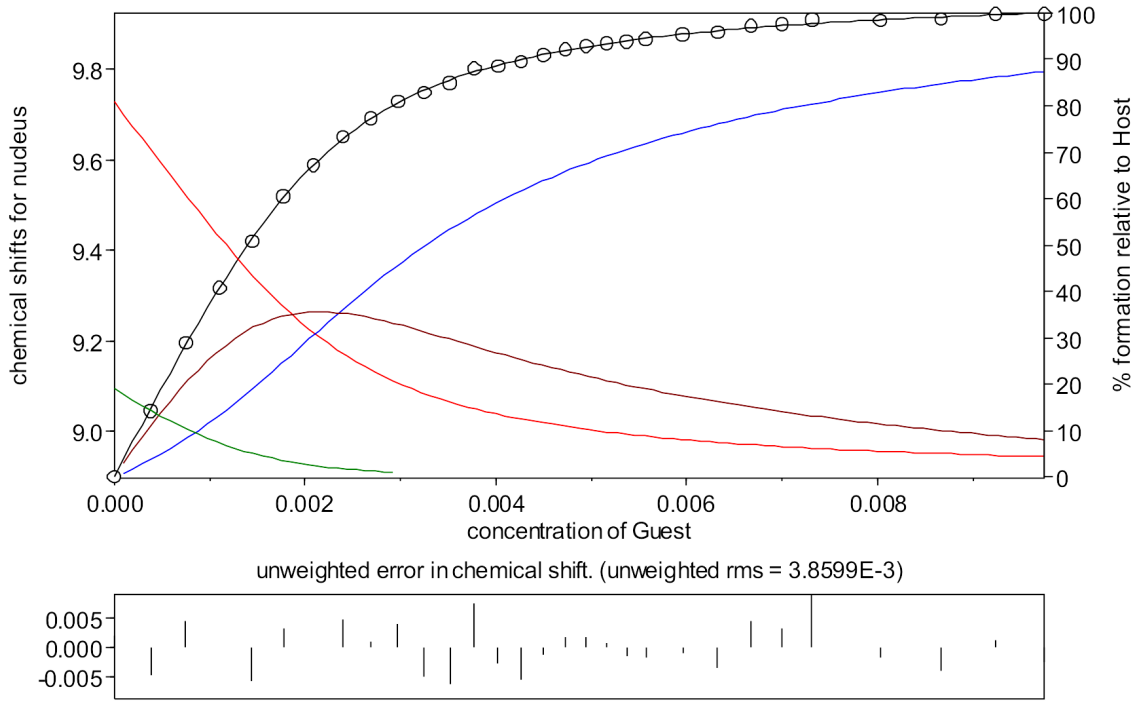

(d)

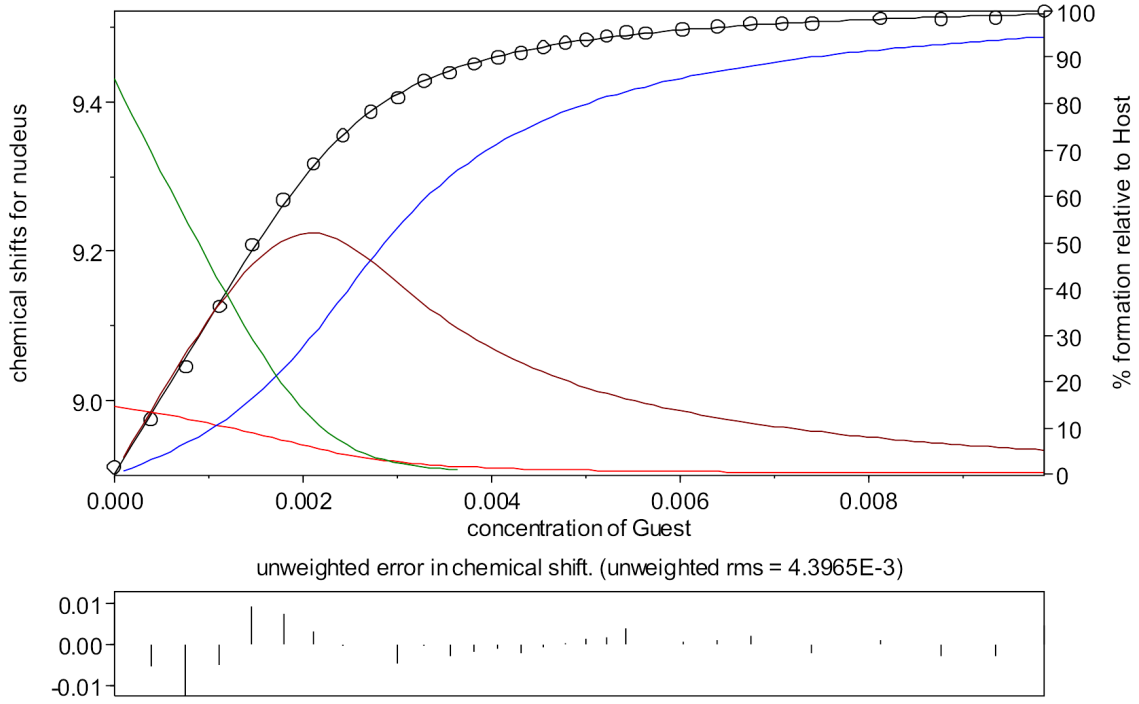

AII.1 Speciation plot showing experimental data from ^{1}H NMR spectroscopic titrations on compound **128** in CD_3CN and the fit for the calculated binding constants for (a) chloride, (b) bromide, (c) iodide and (d) nitrate

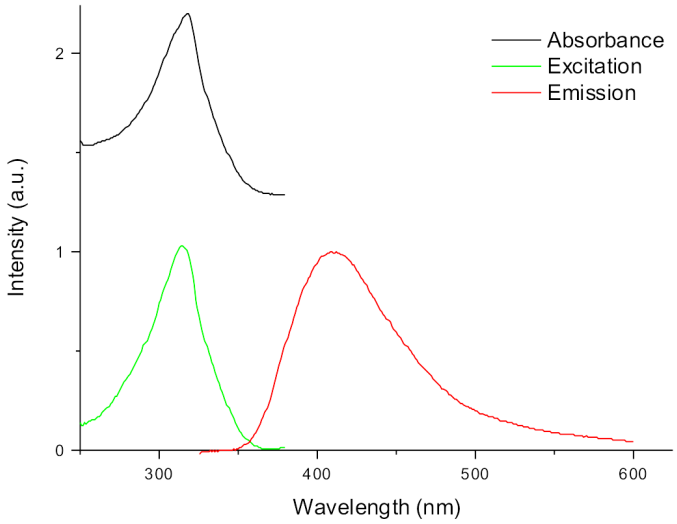

AII.2 Absorbance, excitation and emission spectra of compound **128**. λ_{ex} = 317 nm, λ_{em} = 408 nm, 1.0 x 10^{-5} mol dm^{-3} in MeCN.

(a)

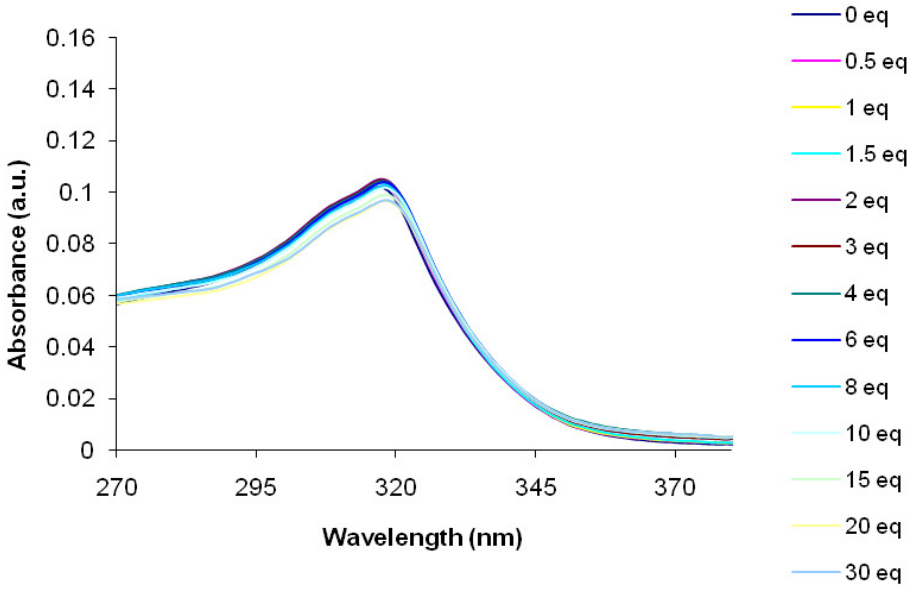

(b)

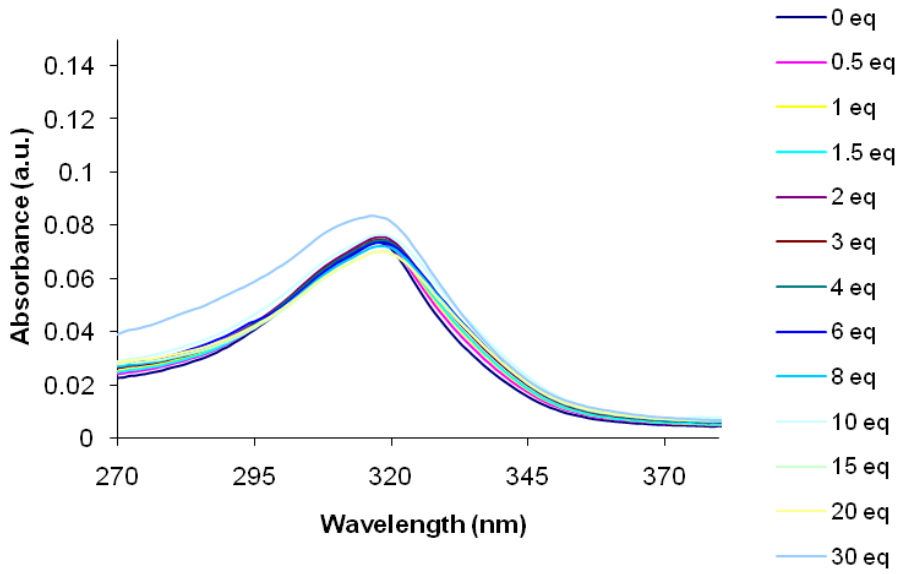
Absorbance (a.u.)
0.14
0.12
0.1
0.08
0.06
0.04
0.02
0
270
295
320
345
370
Wavelength (nm)
0 eq
0.5 eq
1 eq
1.5 eq
2 eq
3 eq
4 eq
6 eq
8 eq
10 eq
15 eq
20 eq
30 eq

(c)

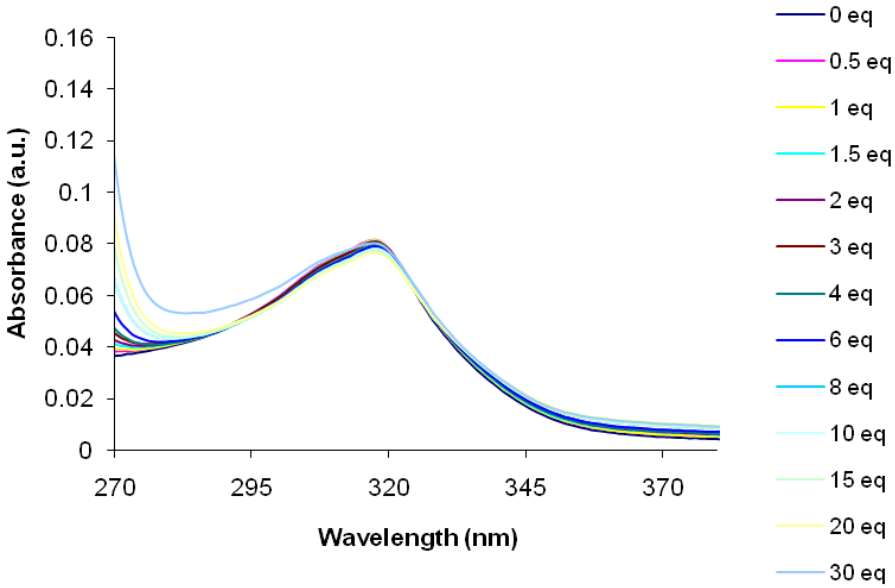
Absorbance (a.u.)
0.16
0.14
0.12
0.1
0.08
0.06
0.04
0.02
0
270
295
320
345
370
Wavelength (nm)
0 eq
0.5 eq
1 eq
1.5 eq
2 eq
3 eq
4 eq
6 eq
8 eq
10 eq
15 eq
20 eq
30 eq

(d)

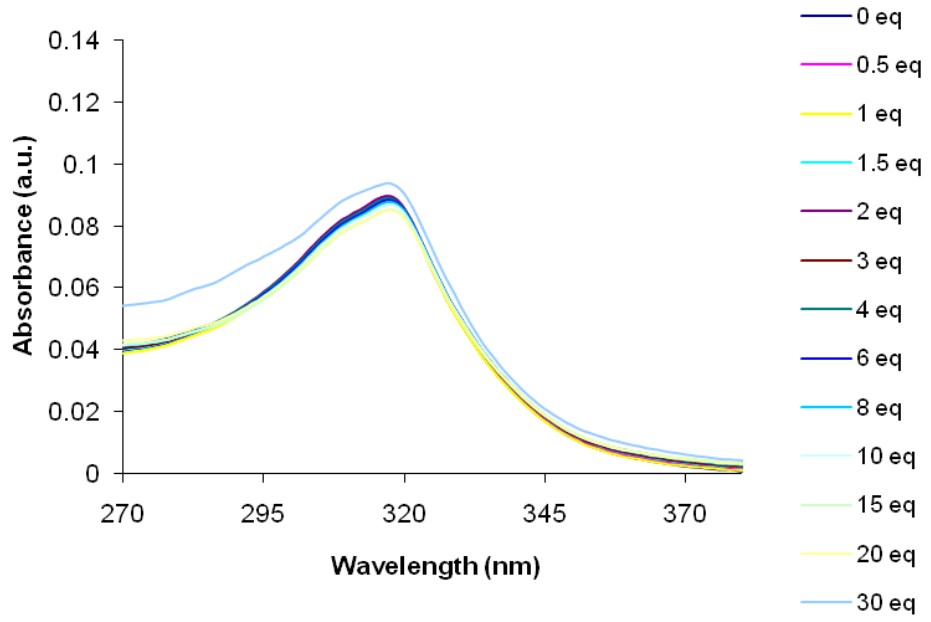
0.14
0.12
0.1
0.08
0.06
0.04
0.02
0
Absorbance (a.u.)
270
295
320
345
370
Wavelength (nm)
0 eq
0.5 eq
1 eq
1.5 eq
2 eq
3 eq
4 eq
6 eq
8 eq
10 eq
15 eq
20 eq
30 eq

(e)

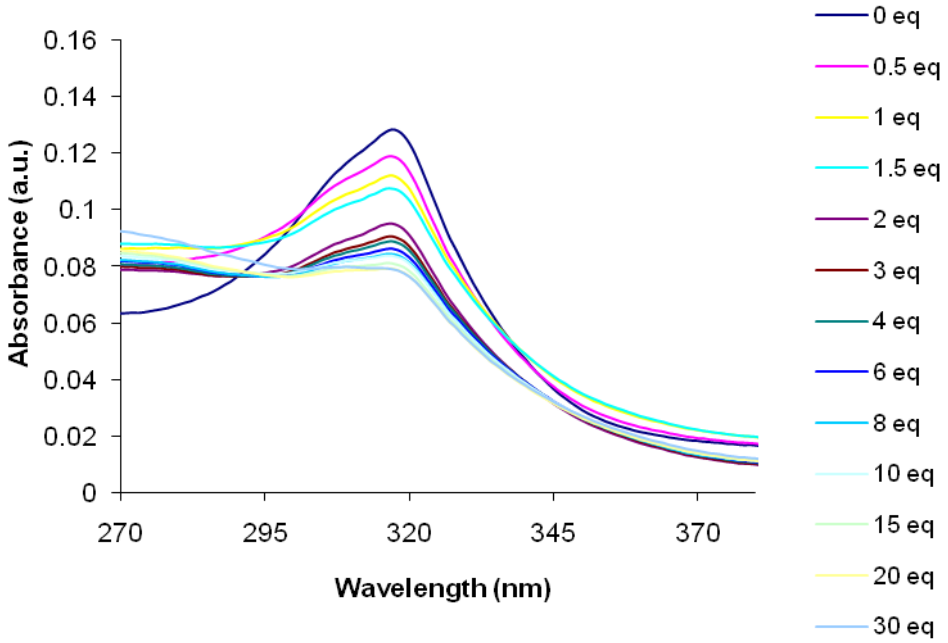
0.16
0.14
0.12
0.1
0.08
0.06
0.04
0.02
0
Absorbance (a.u.)
270
295
320
345
370
Wavelength (nm)
0 eq
0.5 eq
1 eq
1.5 eq
2 eq
3 eq
4 eq
6 eq
8 eq
10 eq
15 eq
20 eq
30 eq

(f)

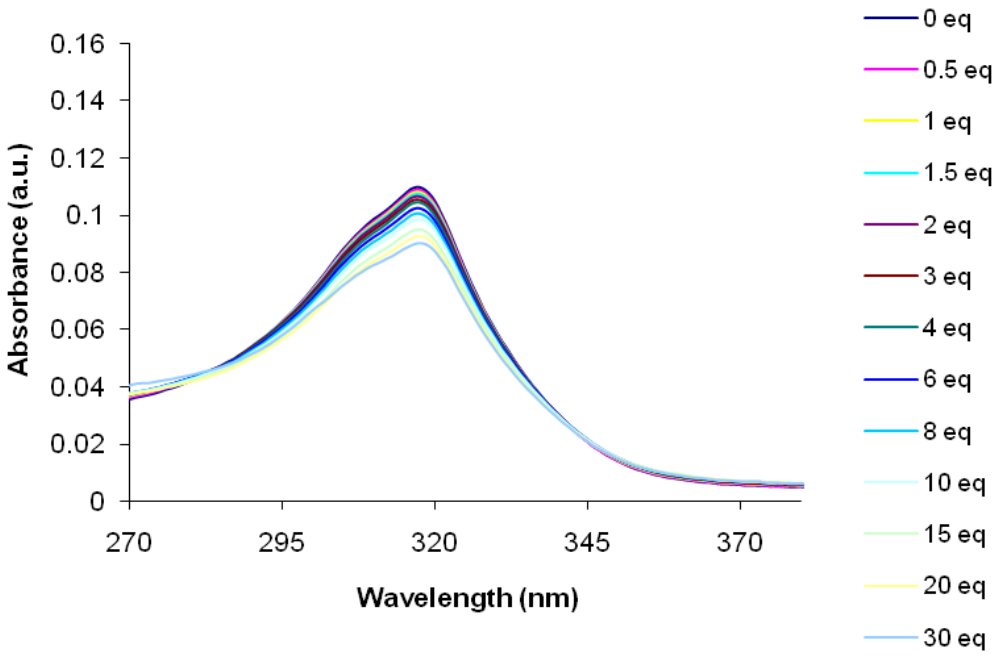

AII.3 UV-Vis spectroscopic titrations of compound **127** (2.33 x 10^{-6} mol dm^{-3} in MeCN) with (a) chloride, (b) bromide (c) iodide, (d) nitrate, (e) acetate, (f) dilution study

(a)

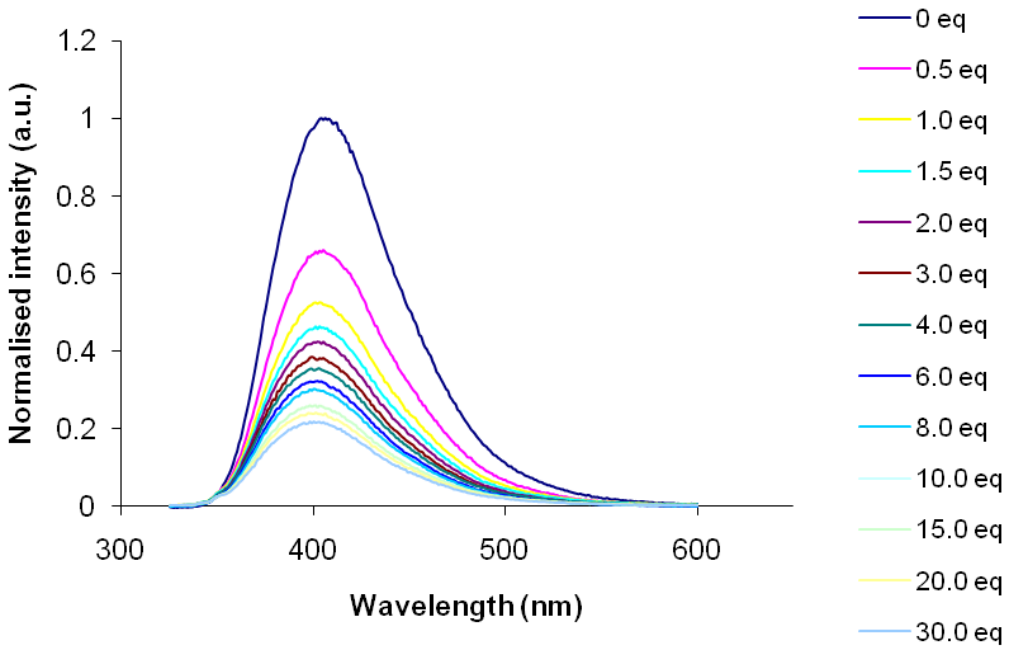

(b)

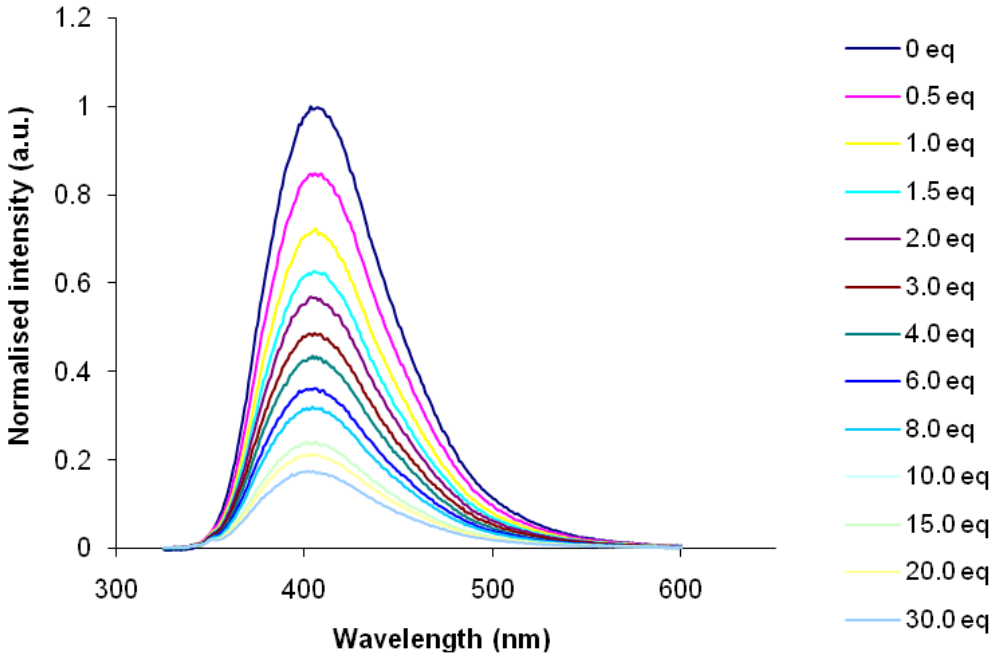
Normalised intensity (a.u.)
1.2
1
0.8
0.6
0.4
0.2
0
300
400
500
600
Wavelength (nm)
0 eq
0.5 eq
1.0 eq
1.5 eq
2.0 eq
3.0 eq
4.0 eq
6.0 eq
8.0 eq
10.0 eq
15.0 eq
20.0 eq
30.0 eq

(c)

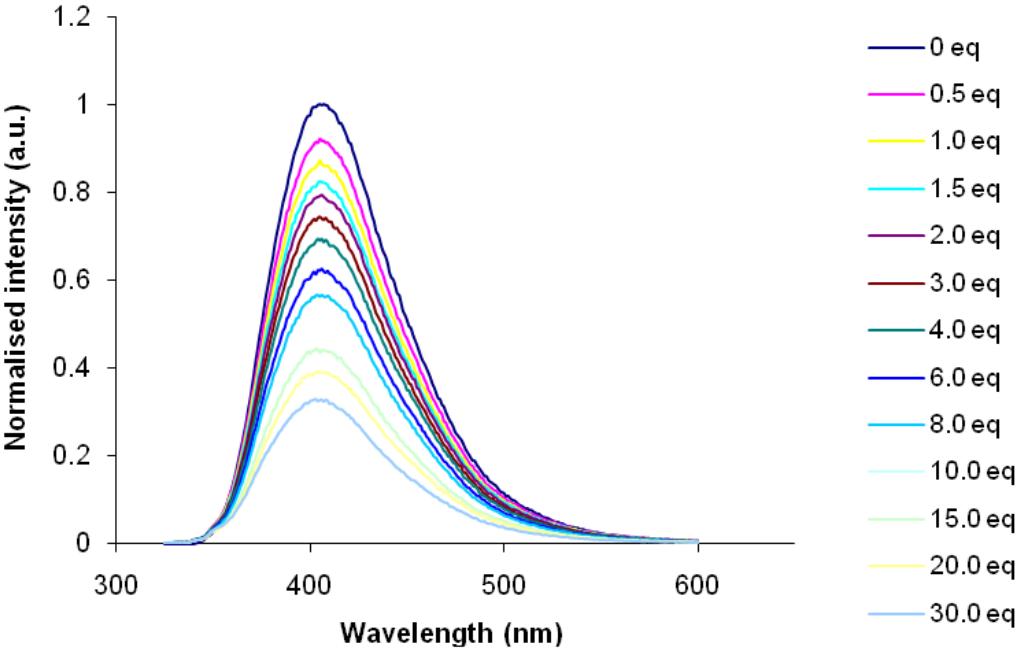
Normalised intensity (a.u.)
1.2
1
0.8
0.6
0.4
0.2
0
300
400
500
600
Wavelength (nm)
0 eq
0.5 eq
1.0 eq
1.5 eq
2.0 eq
3.0 eq
4.0 eq
6.0 eq
8.0 eq
10.0 eq
15.0 eq
20.0 eq
30.0 eq

(d)

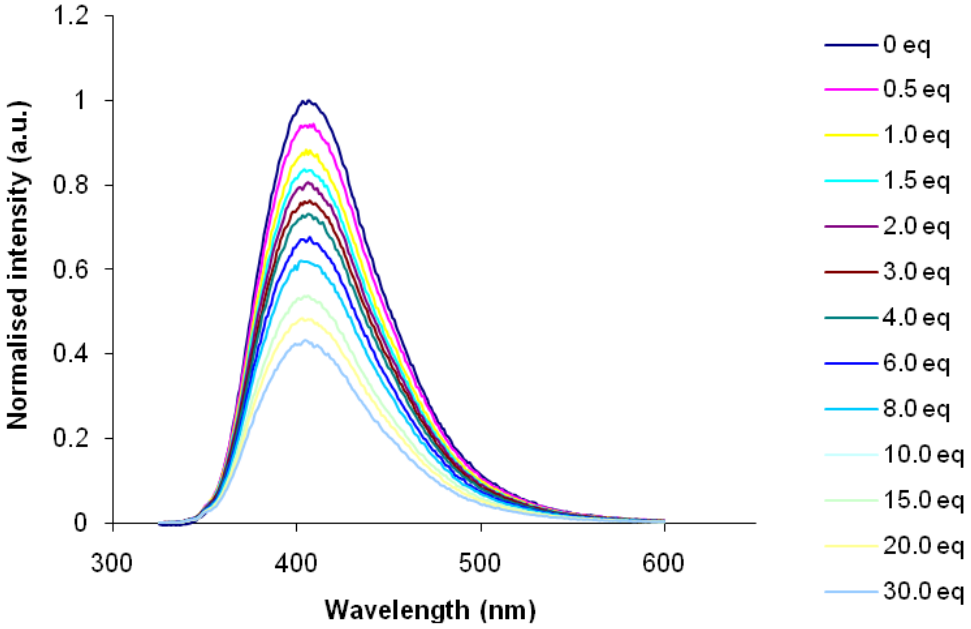
1.2
1
0.8
0.6
0.4
0.2
0
Normalised intensity (a.u.)
300
400
500
600
Wavelength (nm)
0 eq
0.5 eq
1.0 eq
1.5 eq
2.0 eq
3.0 eq
4.0 eq
6.0 eq
8.0 eq
10.0 eq
15.0 eq
20.0 eq
30.0 eq

(e)

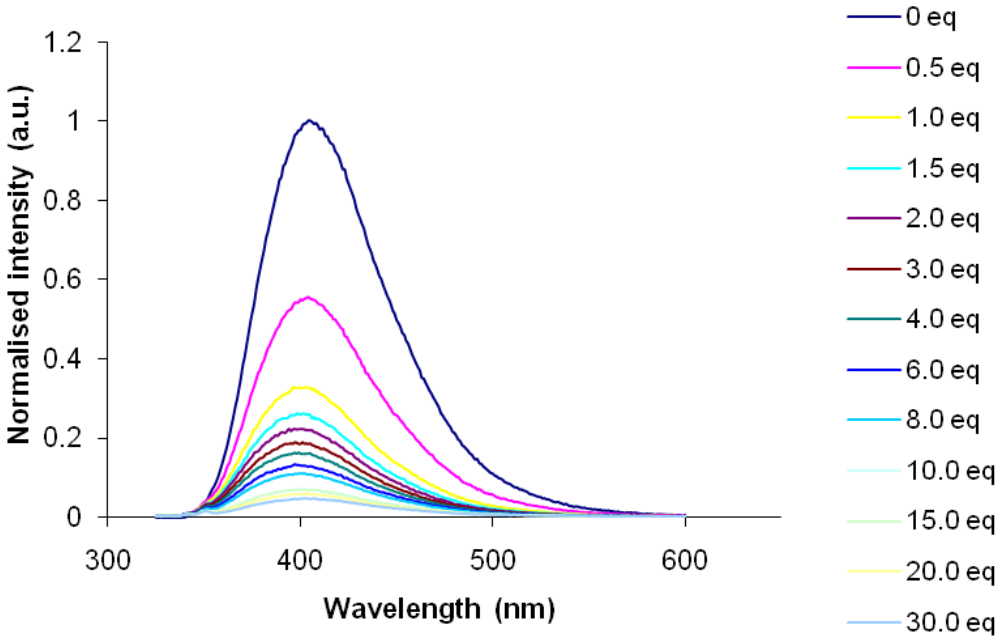
1.2
1
0.8
0.6
0.4
0.2
0
Normalised intensity (a.u.)
300
400
500
600
Wavelength (nm)
0 eq
0.5 eq
1.0 eq
1.5 eq
2.0 eq
3.0 eq
4.0 eq
6.0 eq
8.0 eq
10.0 eq
15.0 eq
20.0 eq
30.0 eq

(f)

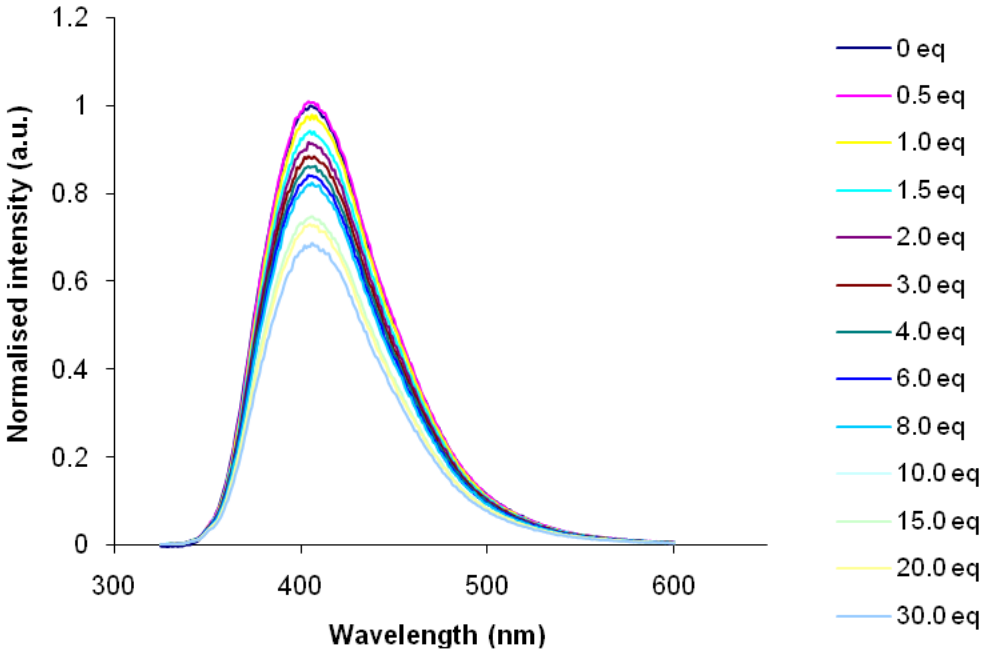

AII.4 Fluorescence emission spectroscopic titrations of compound **127** (λ_{ex} = 317 nm, 2.33 x 10^{-6} mol dm^{-3} in MeCN) with (a) chloride, (b) bromide (c) iodide, (d) nitrate, (e) acetate, (f) dilution study

(a)

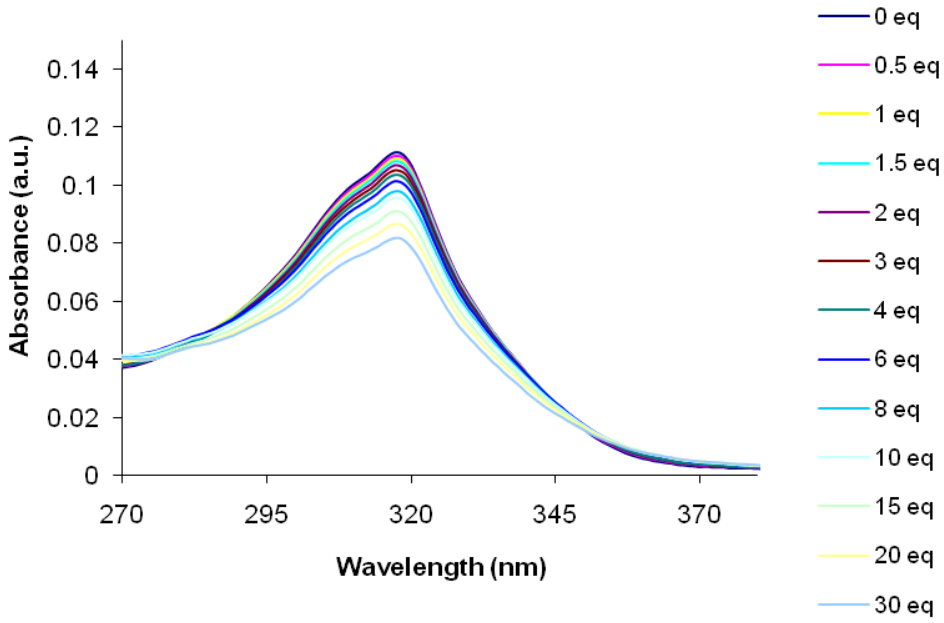

(b)

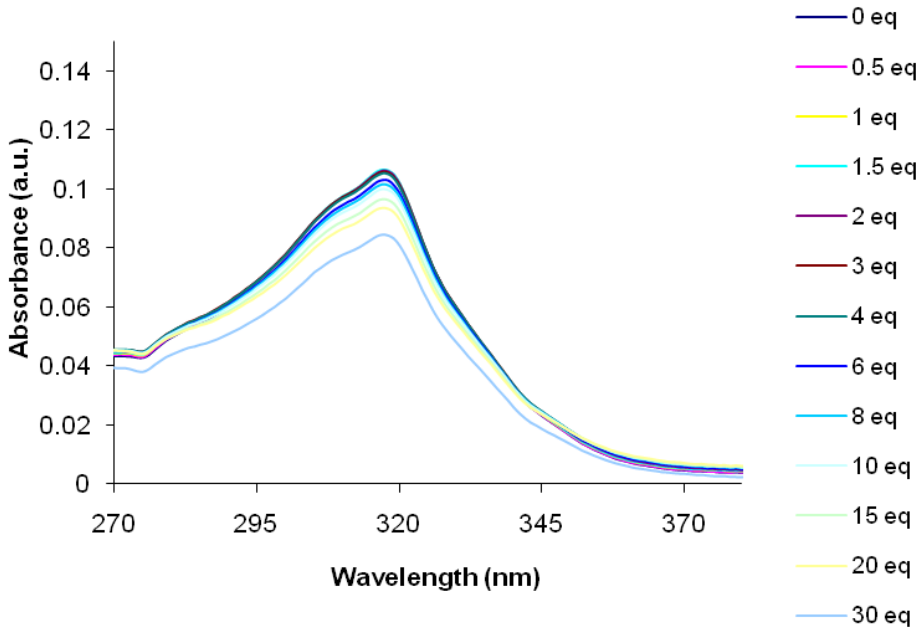
Absorbance (a.u.)
0.14
0.12
0.1
0.08
0.06
0.04
0.02
0
270
295
320
345
370
Wavelength (nm)
0 eq
0.5 eq
1 eq
1.5 eq
2 eq
3 eq
4 eq
6 eq
8 eq
10 eq
15 eq
20 eq
30 eq

(c)

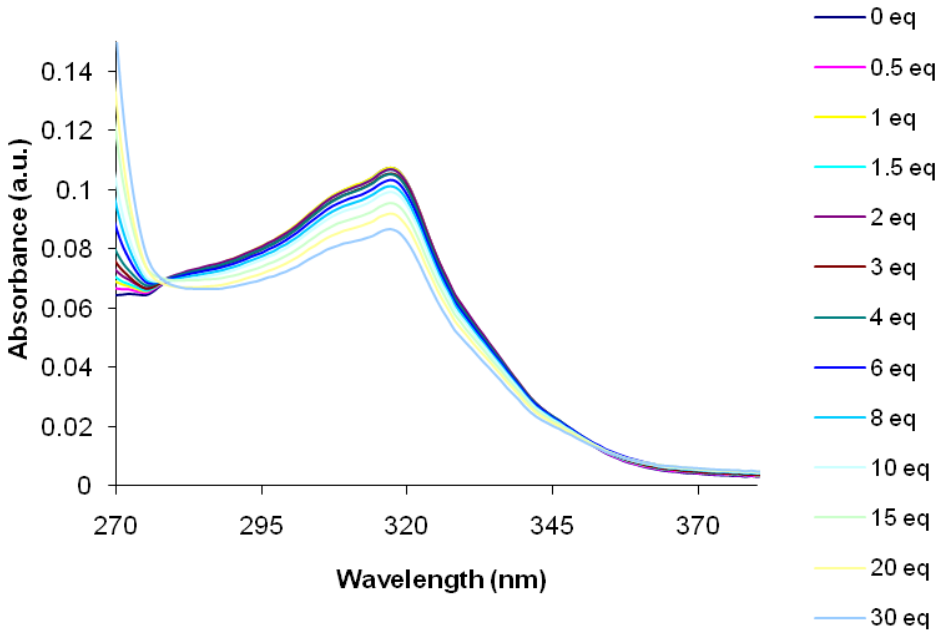
Absorbance (a.u.)
0.14
0.12
0.1
0.08
0.06
0.04
0.02
0
270
295
320
345
370
Wavelength (nm)
0 eq
0.5 eq
1 eq
1.5 eq
2 eq
3 eq
4 eq
6 eq
8 eq
10 eq
15 eq
20 eq
30 eq

(d)

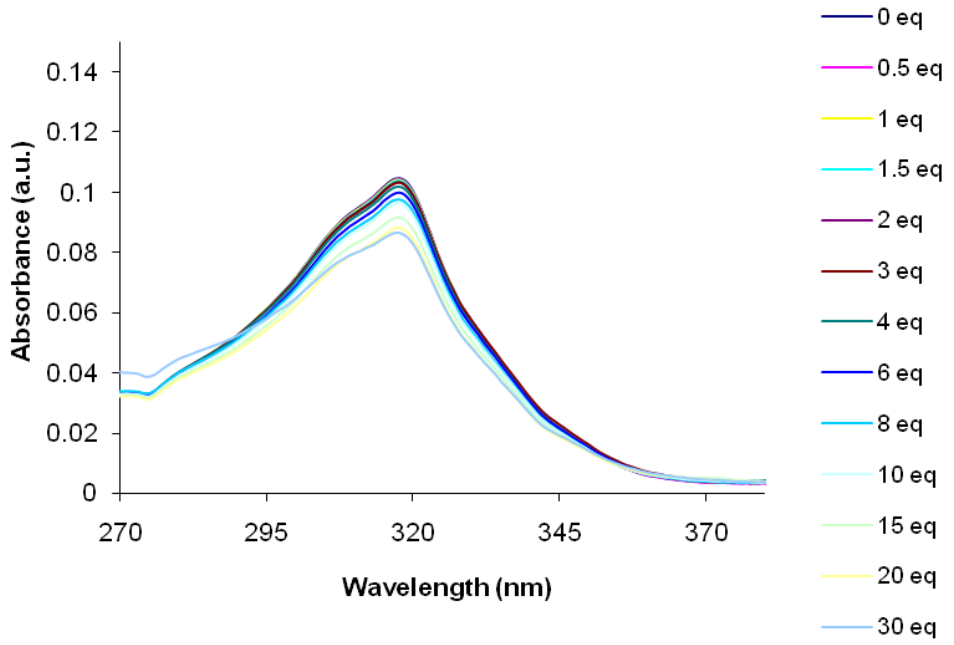
Absorbance (a.u.)
0.14
0.12
0.1
0.08
0.06
0.04
0.02
0
270
295
320
345
370
Wavelength (nm)
0 eq
0.5 eq
1 eq
1.5 eq
2 eq
3 eq
4 eq
6 eq
8 eq
10 eq
15 eq
20 eq
30 eq

(e)

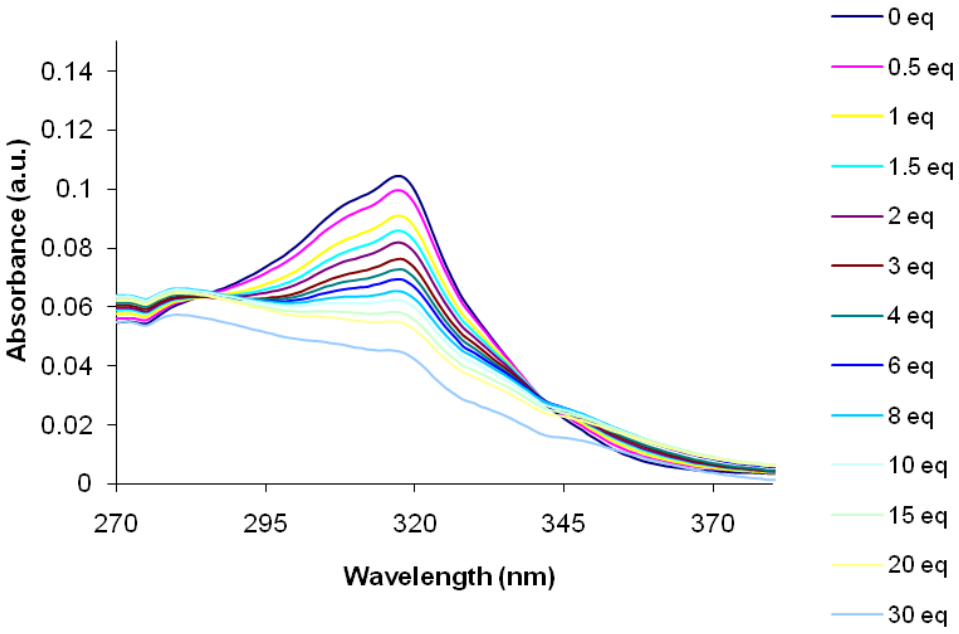
Absorbance (a.u.)
0.14
0.12
0.1
0.08
0.06
0.04
0.02
0
270
295
320
345
370
Wavelength (nm)
0 eq
0.5 eq
1 eq
1.5 eq
2 eq
3 eq
4 eq
6 eq
8 eq
10 eq
15 eq
20 eq
30 eq

(f)

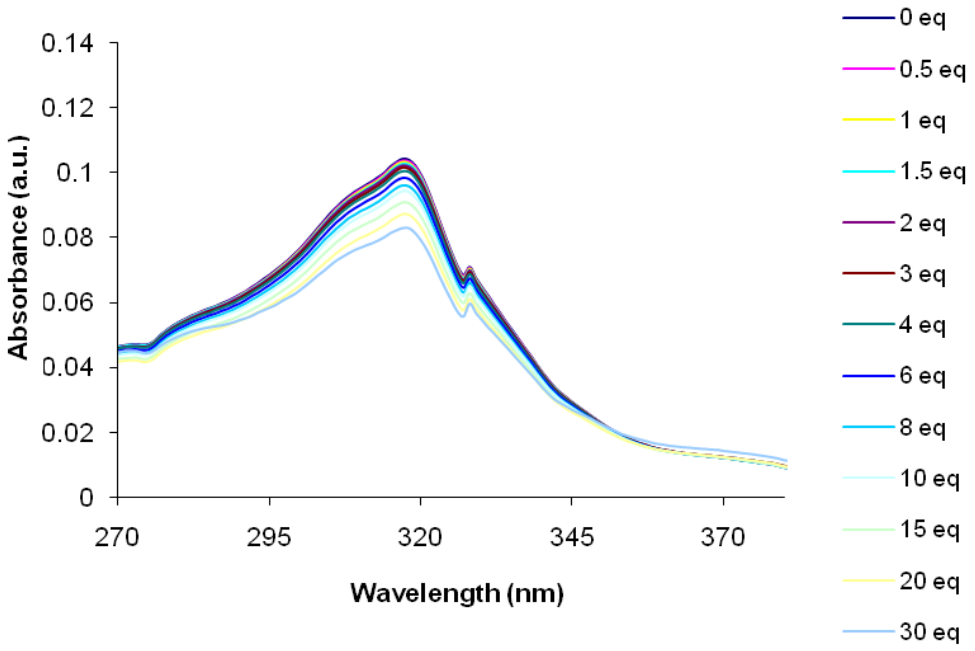

AII.5 UV-Vis spectroscopic titrations of compound **128** (1 x 10^{-5} mol dm^{-3} in MeCN) with (a) chloride, (b) bromide (c) iodide, (d) nitrate, (e) acetate, (f) dilution study

(a)

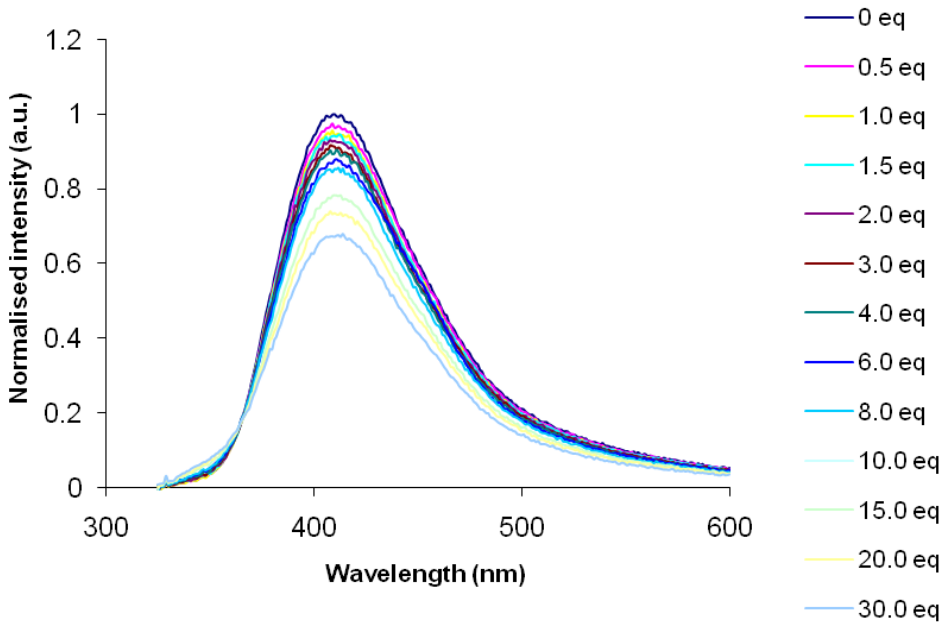

(b)

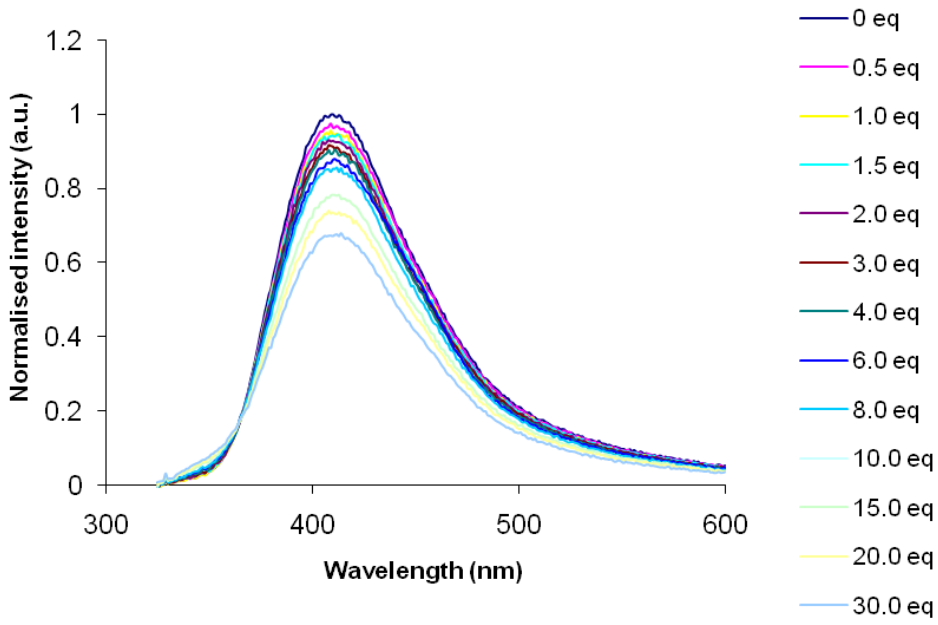
Normalised intensity (a.u.)
1.2
1
0.8
0.6
0.4
0.2
0
300
400
500
600
Wavelength (nm)
0 eq
0.5 eq
1.0 eq
1.5 eq
2.0 eq
3.0 eq
4.0 eq
6.0 eq
8.0 eq
10.0 eq
15.0 eq
20.0 eq
30.0 eq

(c)

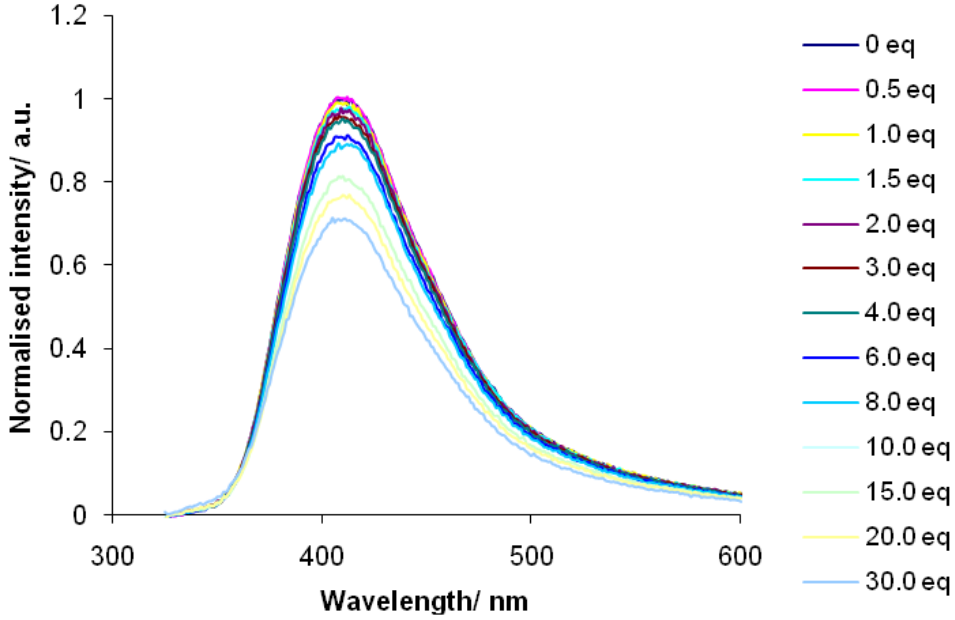
Normalised intensity/ a.u.
1.2
1
0.8
0.6
0.4
0.2
0
300
400
500
600
Wavelength/ nm
0 eq
0.5 eq
1.0 eq
1.5 eq
2.0 eq
3.0 eq
4.0 eq
6.0 eq
8.0 eq
10.0 eq
15.0 eq
20.0 eq
30.0 eq

(d)

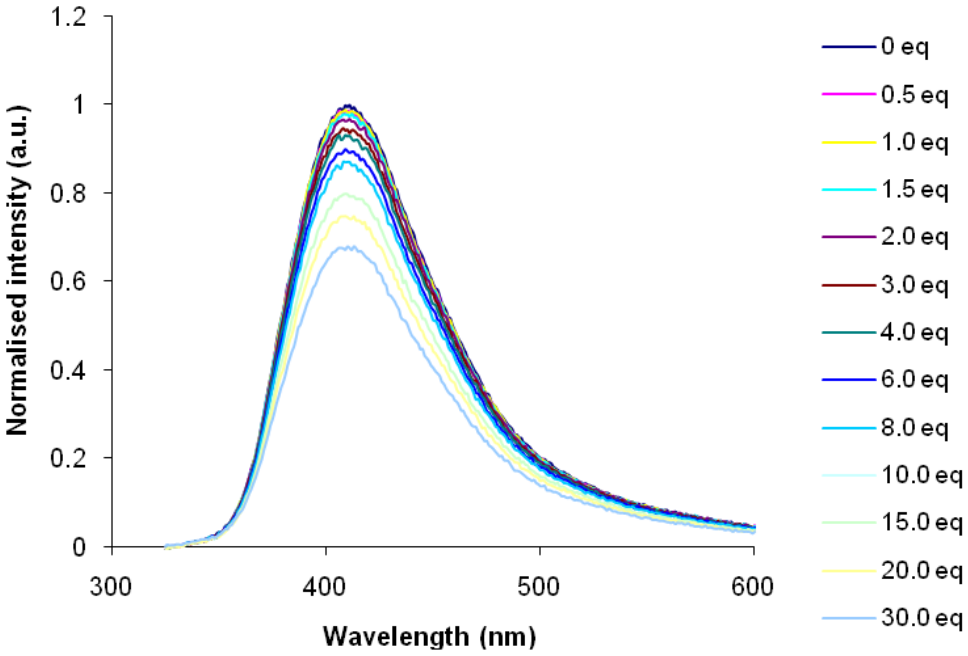
1.2
1
0.8
0.6
0.4
0.2
0
Normalised intensity (a.u.)
300
400
500
600
Wavelength (nm)
0 eq
0.5 eq
1.0 eq
1.5 eq
2.0 eq
3.0 eq
4.0 eq
6.0 eq
8.0 eq
10.0 eq
15.0 eq
20.0 eq
30.0 eq

(e)

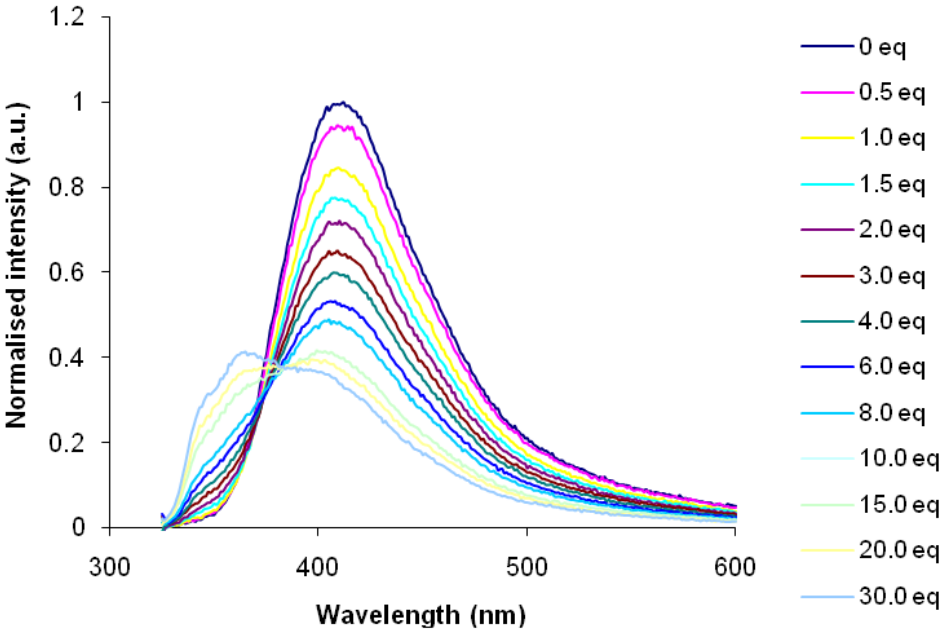
1.2
1
0.8
0.6
0.4
0.2
0
Normalised intensity (a.u.)
300
400
500
600
Wavelength (nm)
0 eq
0.5 eq
1.0 eq
1.5 eq
2.0 eq
3.0 eq
4.0 eq
6.0 eq
8.0 eq
10.0 eq
15.0 eq
20.0 eq
30.0 eq

(f)

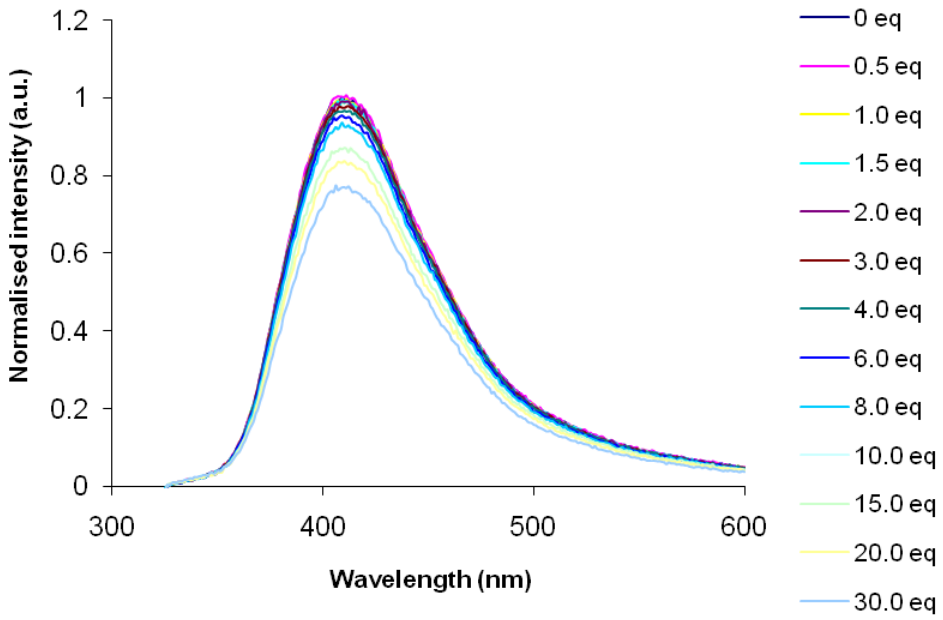

AII.6 Fluorescence emission spectroscopic titrations of compound **128** (λ_{ex} = 317 nm, 1 x 10^{-5} mol dm^{-3} in MeCN) with (a) chloride, (b) bromide (c) iodide, (d) nitrate, (e) acetate, (f) dilution study

Appendix III – Supplementary Information Relating to Chapter 4

(a)

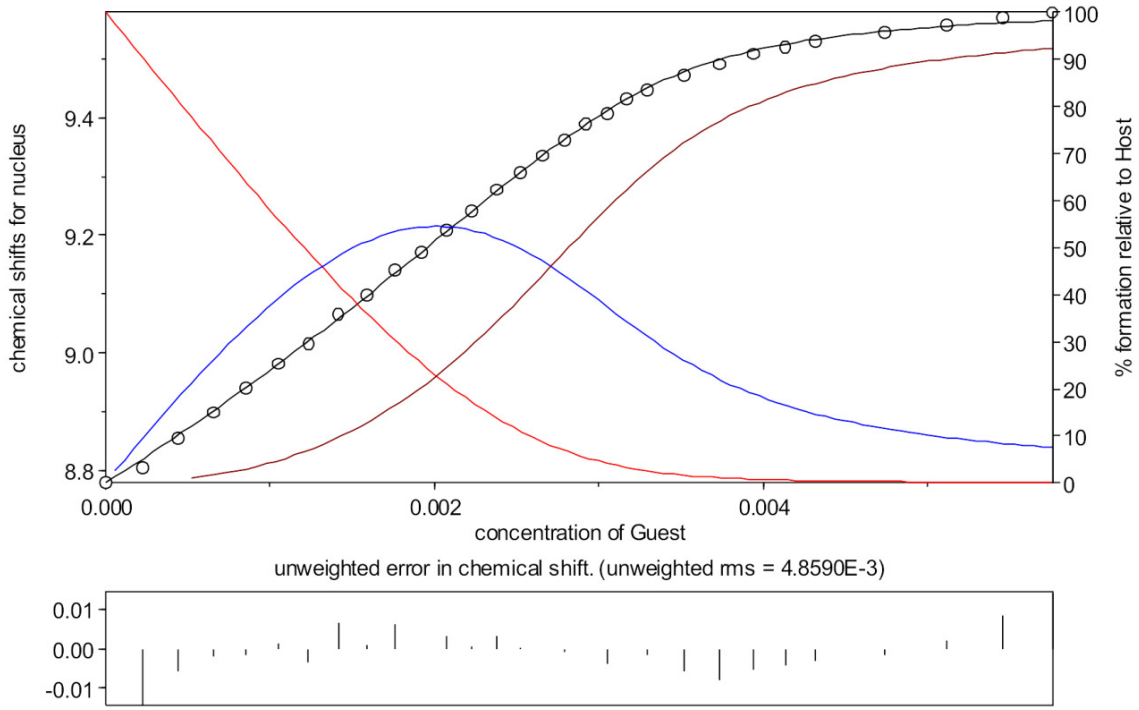

(b)

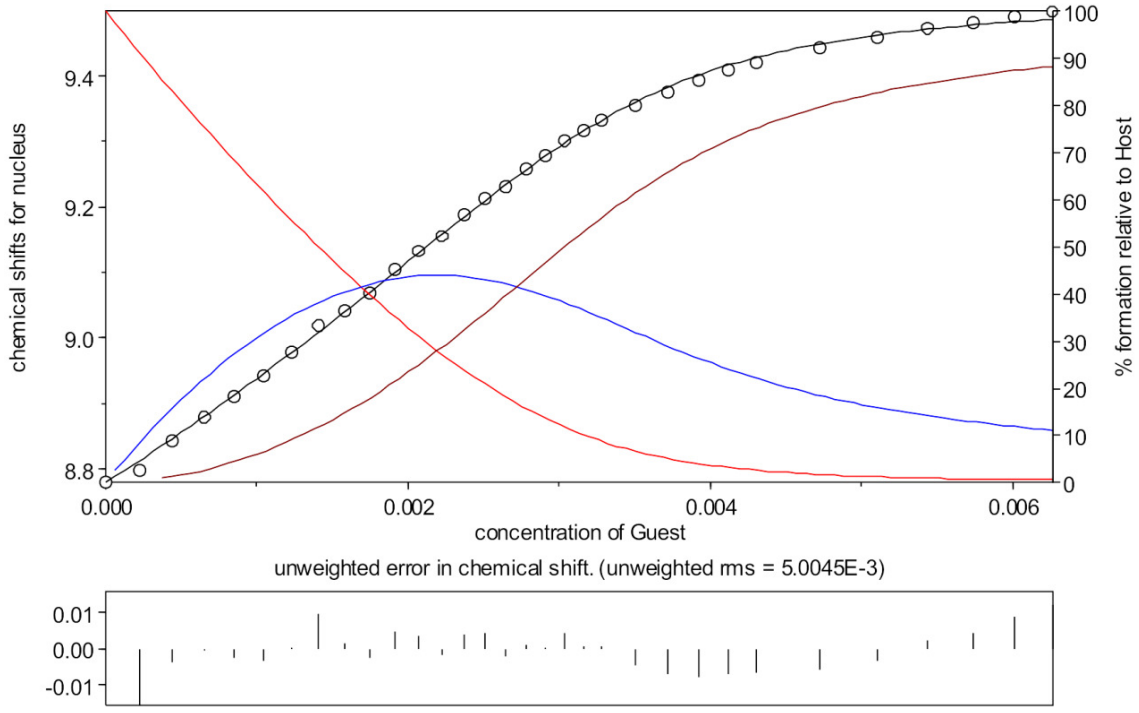

(c)

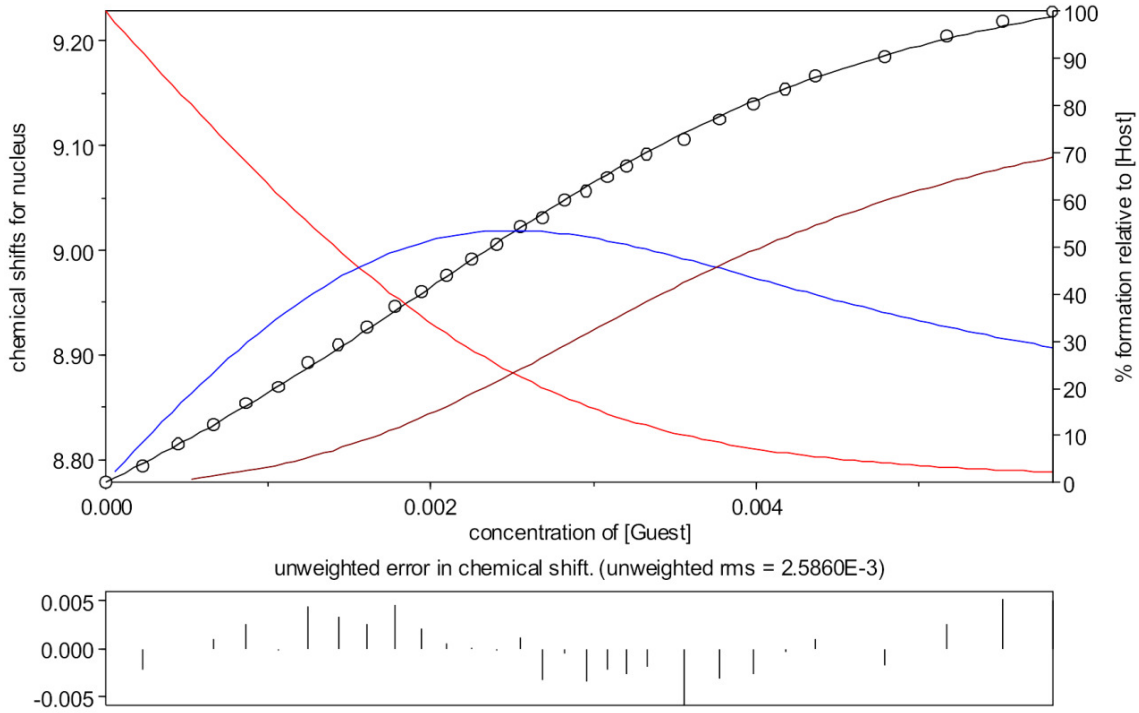

(d)

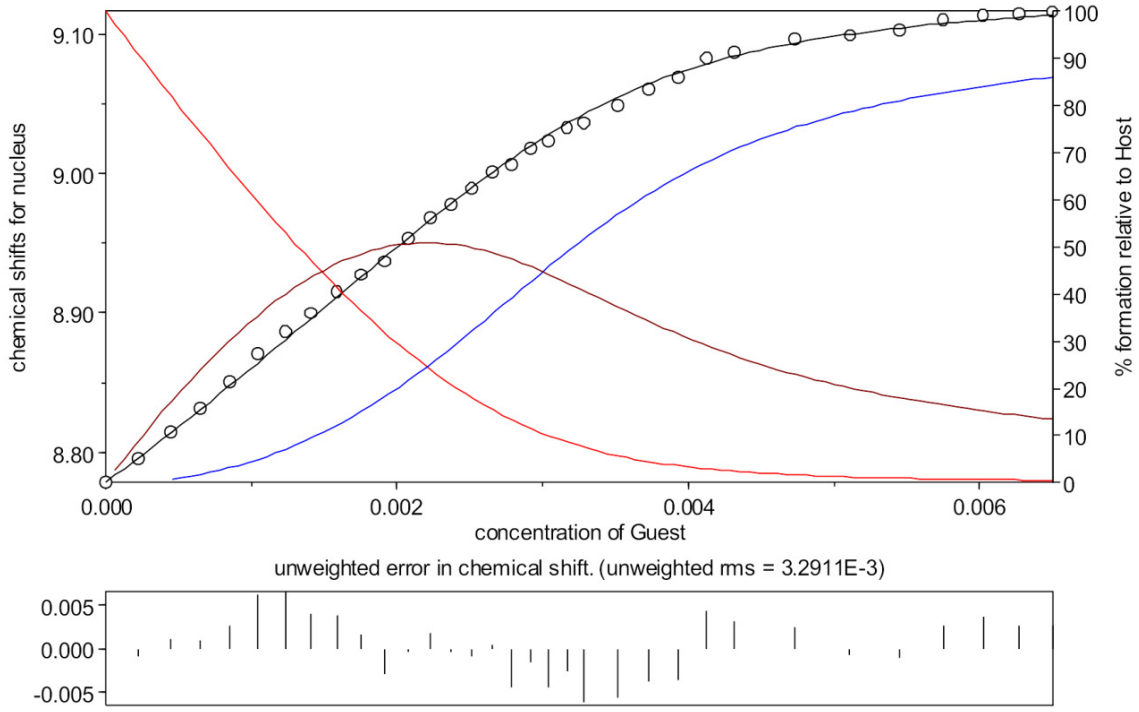

AIII.1 Speciation plot showing experimental data from ^{1}H NMR spectroscopic titrations on compound **132** in CD_3CN and the fit for the calculated binding constants for (a) chloride, (b) bromide, (c) iodide and (d) nitrate

(a)

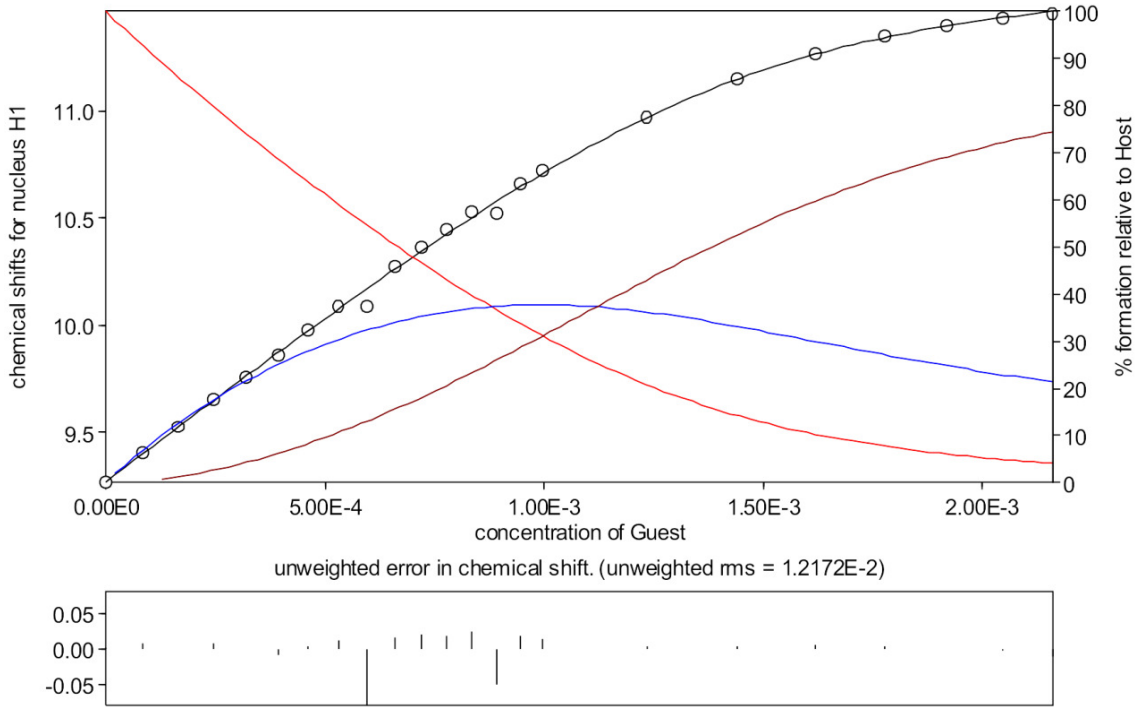
chemical shifts for nucleus H1
% formation relative to Host
concentration of Guest
unweighted error in chemical shift. (unweighted rms = 1.2172E-2)

(b)

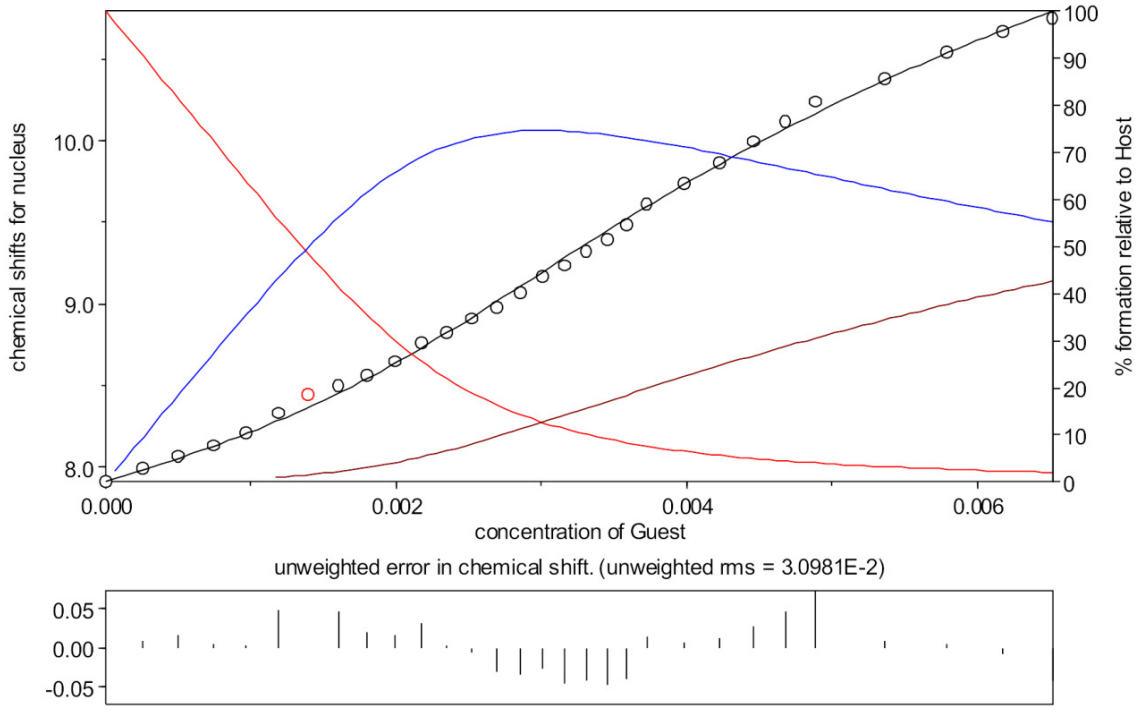
chemical shifts for nucleus
% formation relative to Host
concentration of Guest
unweighted error in chemical shift. (unweighted rms = 3.0981E-2)

(c)

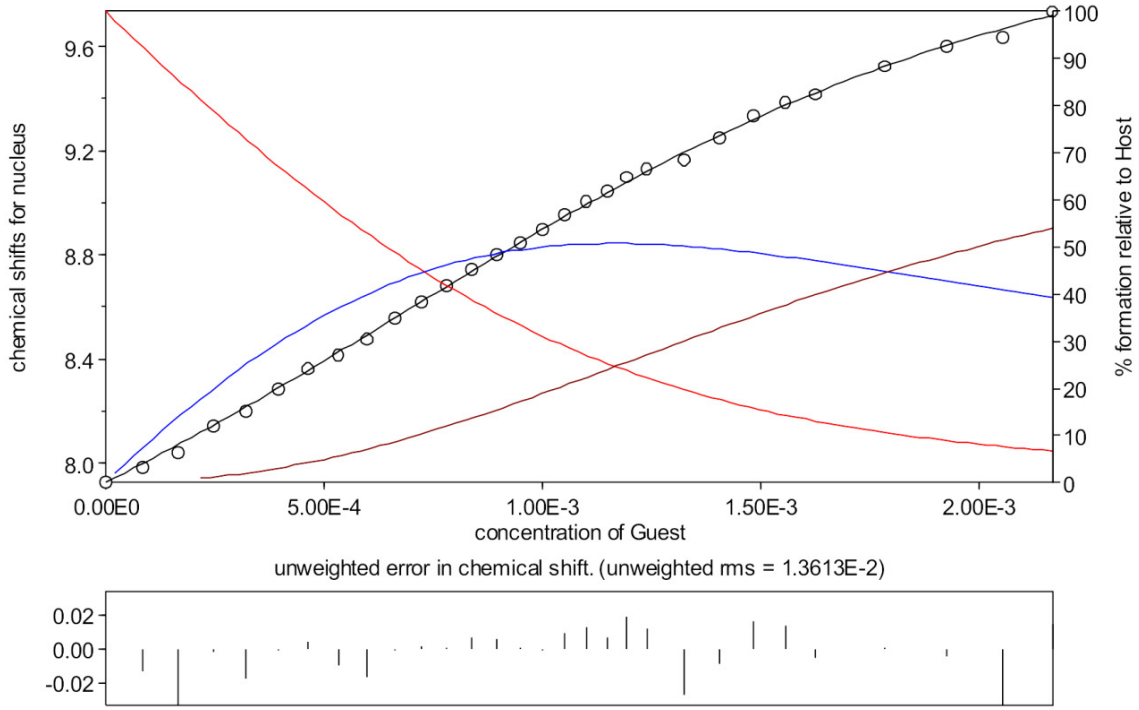

(d)

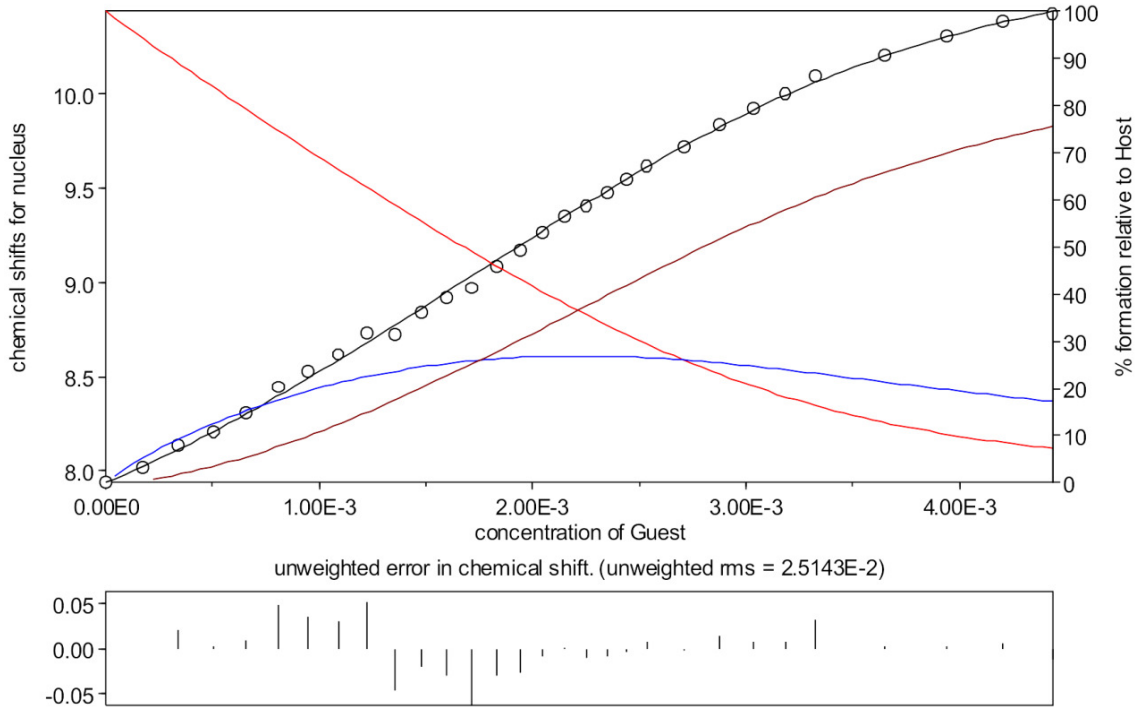

AIII.2 Speciation plot showing experimental data from ^{1}H NMR spectroscopic titrations on compound **125** in CD_3CN and the fit for the calculated binding constants for (a) chloride, (b) bromide, (c) iodide and (d) nitrate

(a)

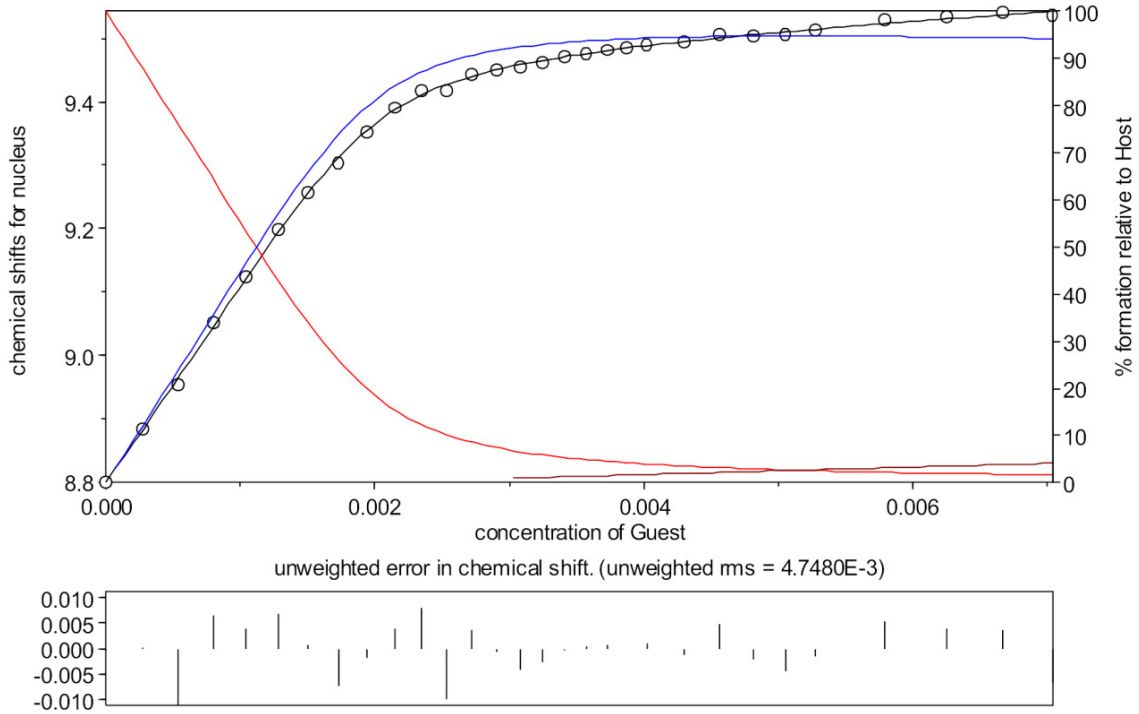
chemical shifts for nucleus
% formation relative to Host
concentration of Guest
unweighted error in chemical shift. (unweighted rms = 4.7480E-3)

(b)

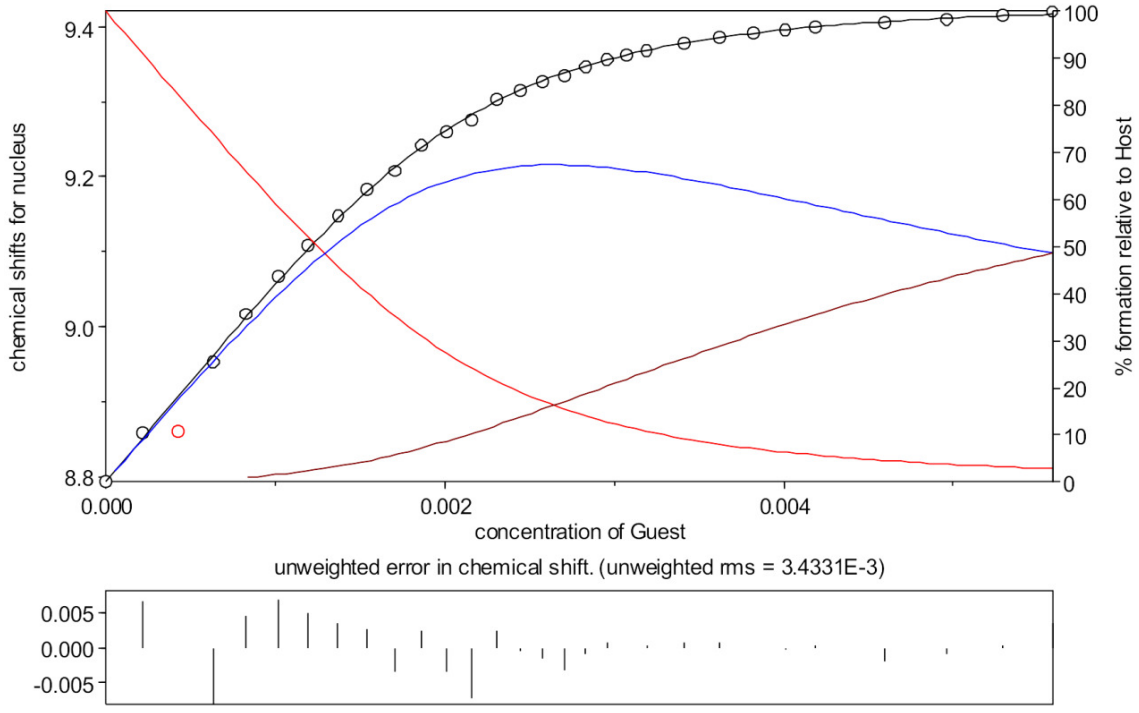
chemical shifts for nucleus
% formation relative to Host
concentration of Guest
unweighted error in chemical shift. (unweighted rms = 3.4331E-3)

(c)

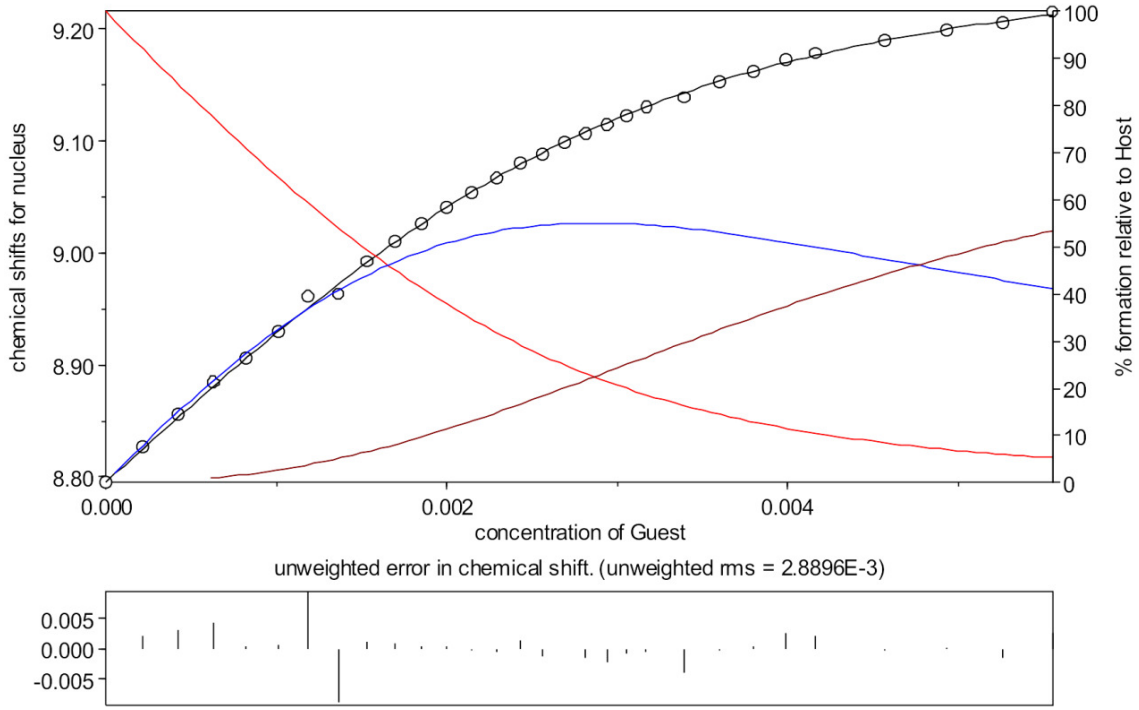

AIII.3 Speciation plot showing experimental data from ^{1}H NMR spectroscopic titrations on compound **134** in CD_3CN and the fit for the calculated binding constants for (a) chloride, (b) bromide and (c) iodide

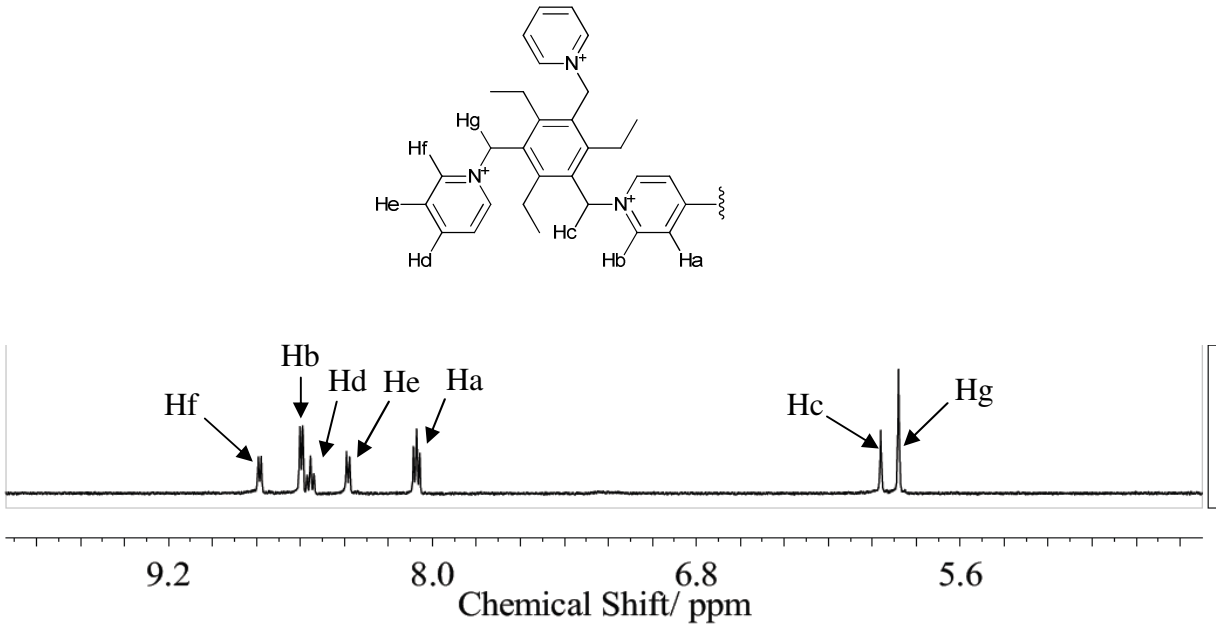

AIII.4 ^{1}H NMR assignment for **132** in CD_3CN

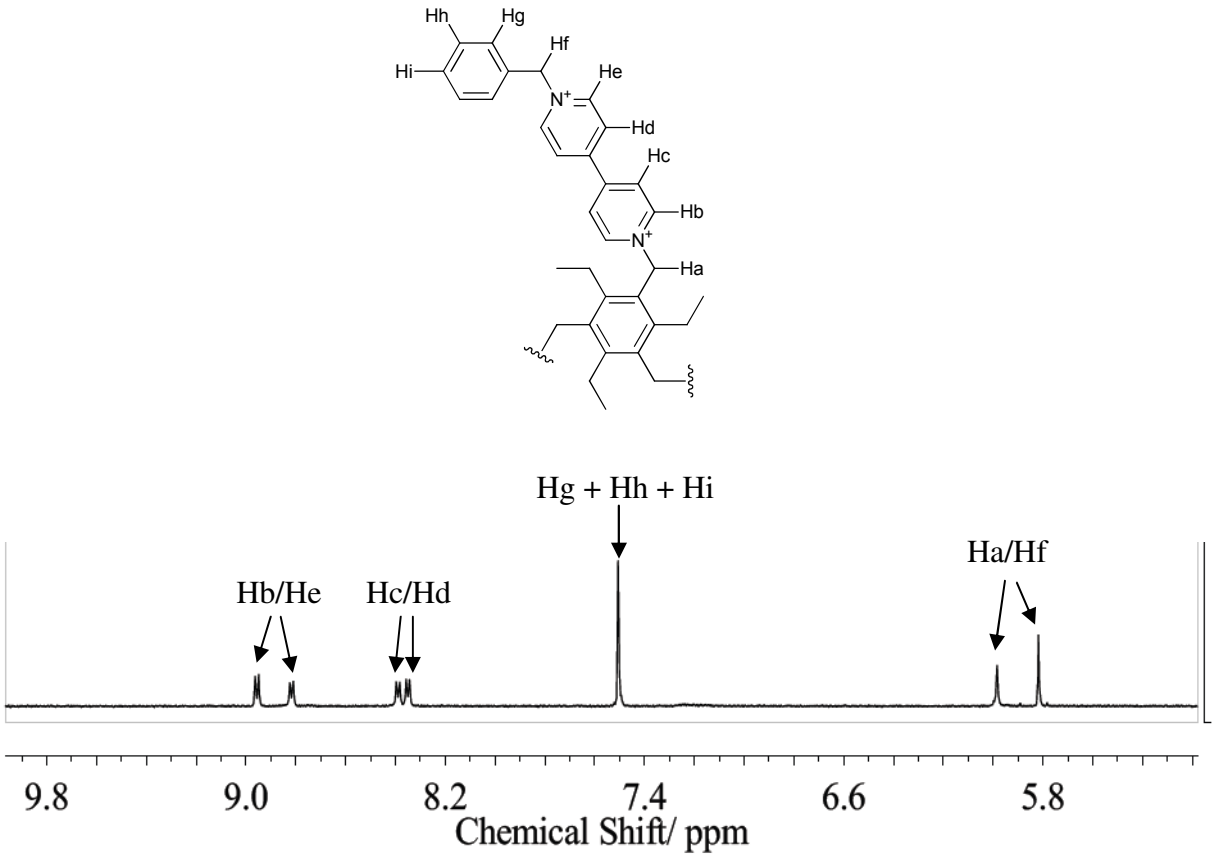

AIII.5 ^{1}H NMR assignment for compound **134** in CD_3CN

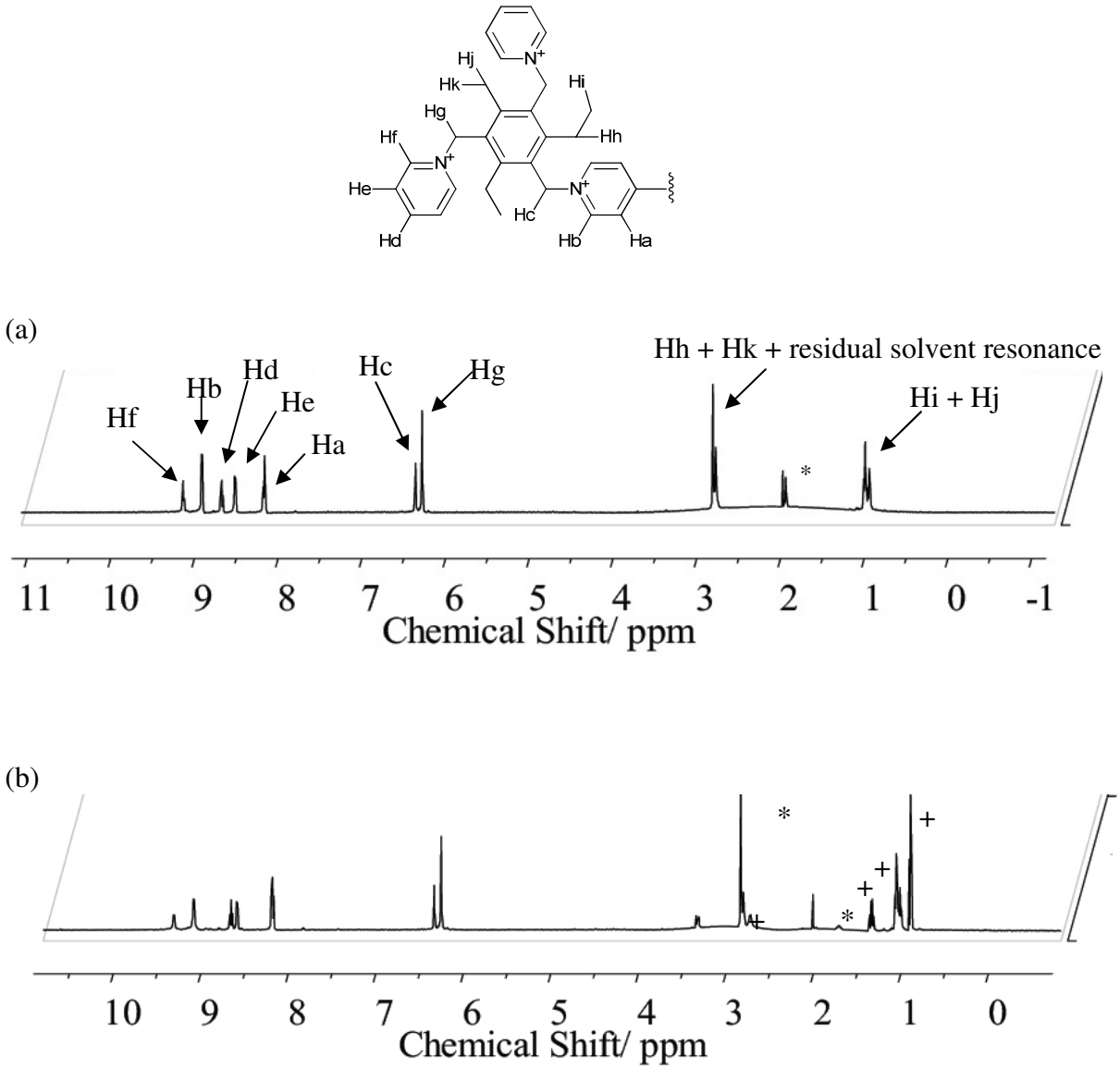

AIII.6 ^{1}H NMR resonances for (a) **132** and (b) **132** with 1 equivalent of TBA-Cl (the assignment is as with (a), tetrabutylammonium resonances indicated by + and * indicates residual solvent resonances

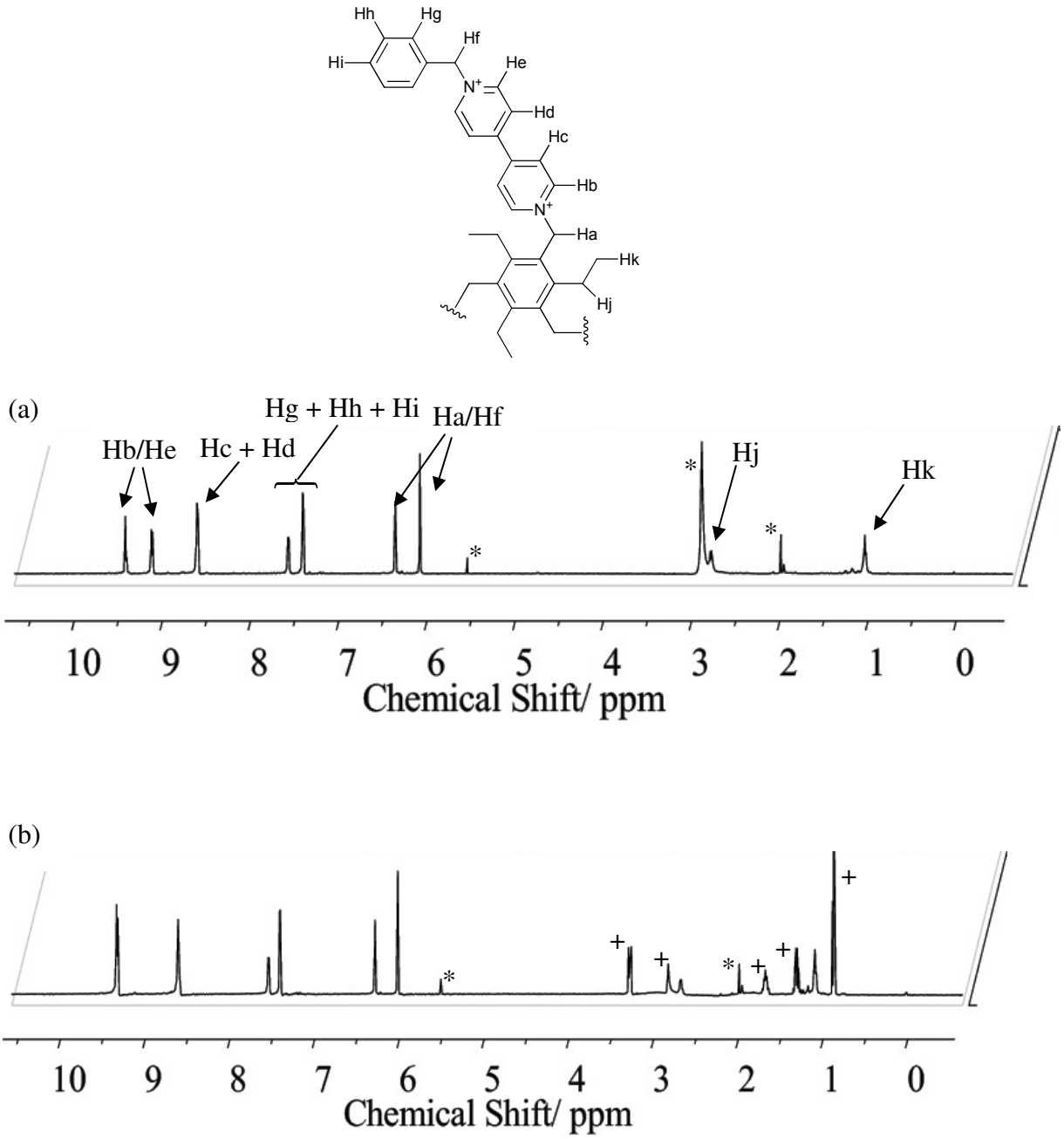

AIII.7 ^{1}H NMR resonances for (a) **134** and (b) **134** with 1 equivalent of TBA-Cl (the assignment is as with (a), tetrabutylammonium resonances indicated by + and * indicates residual solvent resonances

(a)

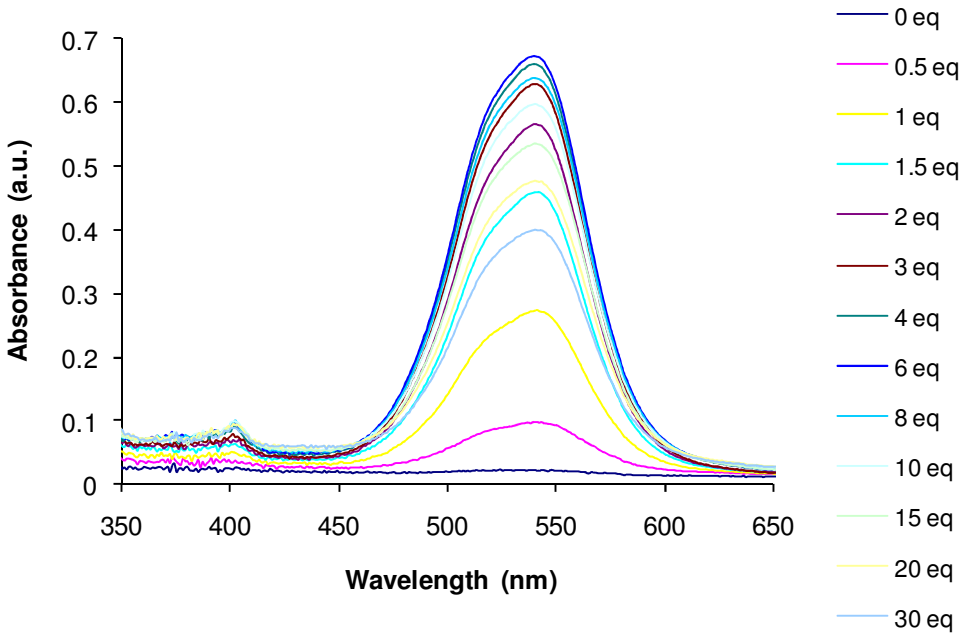
Absorbance (a.u.)
0.7
0.6
0.5
0.4
0.3
0.2
0.1
0
350
400
450
500
550
600
650
Wavelength (nm)
0 eq
0.5 eq
1 eq
1.5 eq
2 eq
3 eq
4 eq
6 eq
8 eq
10 eq
15 eq
20 eq
30 eq

(b)

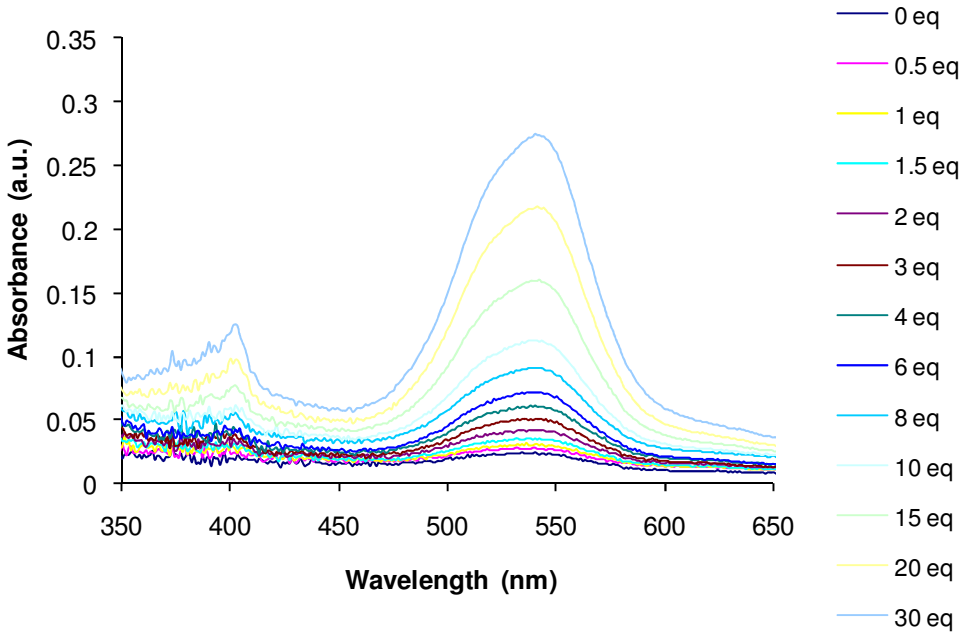
Absorbance (a.u.)
0.35
0.3
0.25
0.2
0.15
0.1
0.05
0
350
400
450
500
550
600
650
Wavelength (nm)
0 eq
0.5 eq
1 eq
1.5 eq
2 eq
3 eq
4 eq
6 eq
8 eq
10 eq
15 eq
20 eq
30 eq

(c)

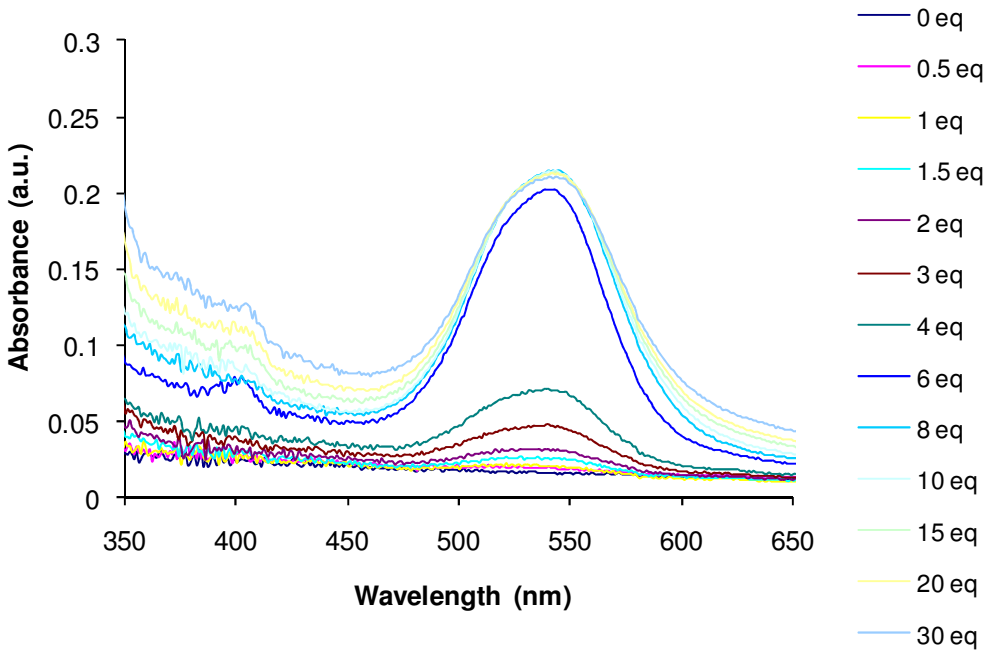

AIII.8 UV-vis spectroscopic titrations of **132** (1.0×10^{-4} mol dm^{-3} in MeCN) with (a) acetate, (b) malonate, (c) succinate used as TBA salts

(a)

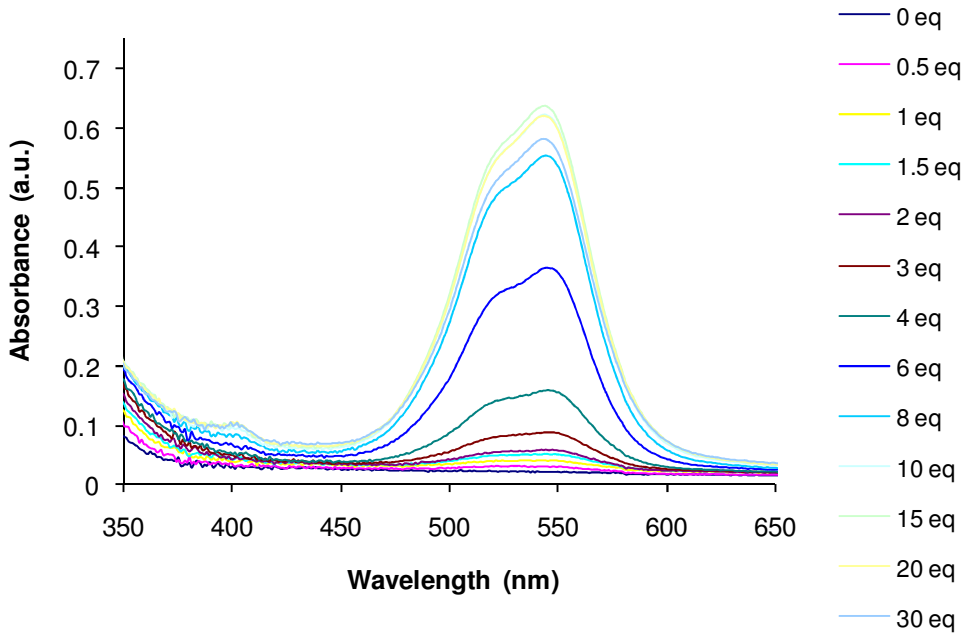

(b)

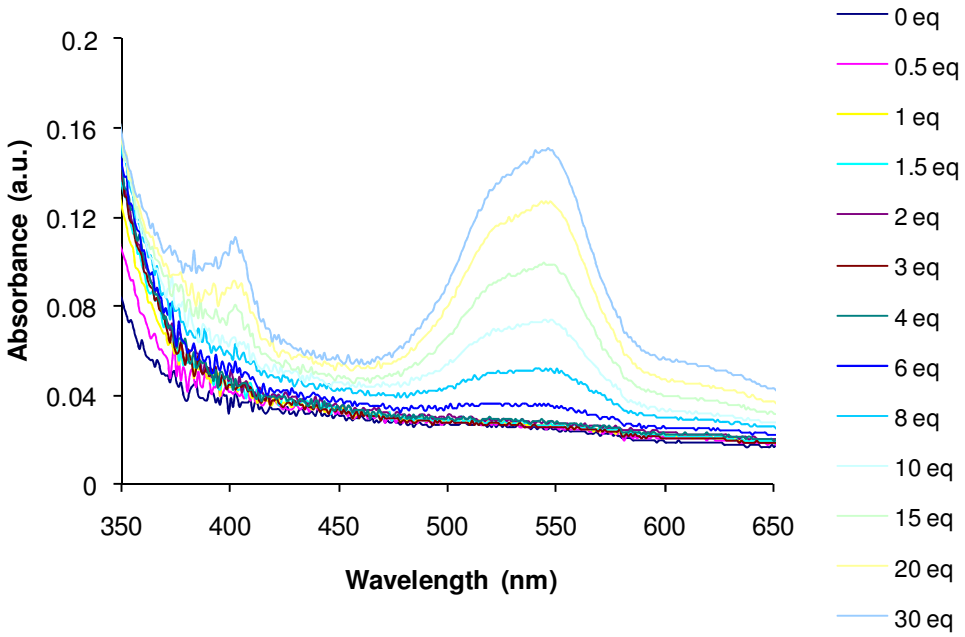

(c)

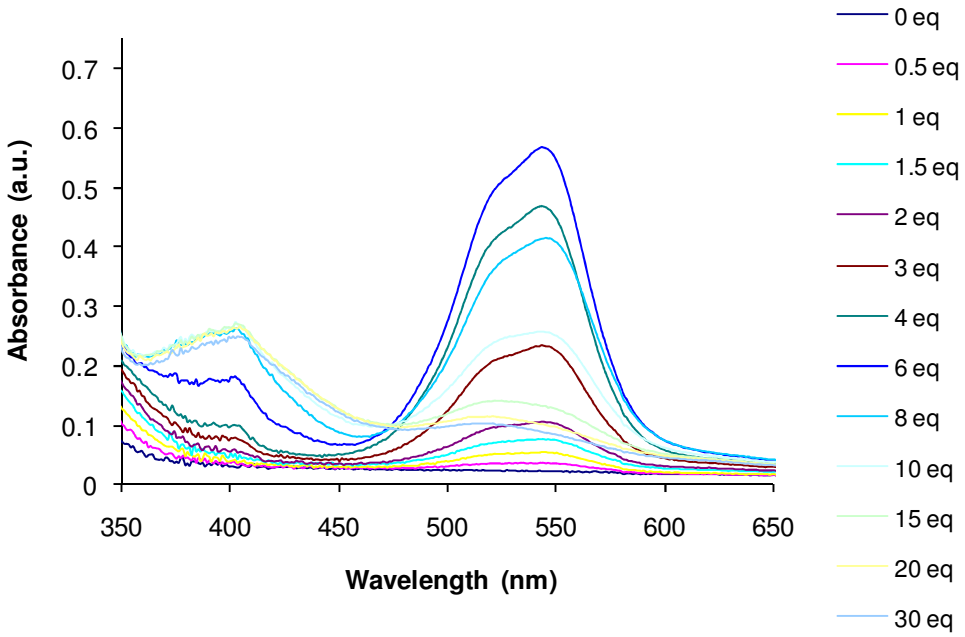

AIII.9 UV-vis spectroscopic titrations of **125** (1.0×10^{-4} mol dm^{-3} in MeCN) with (a) acetate, (b) malonate, (c) succinate used as TBA salts.

(a)

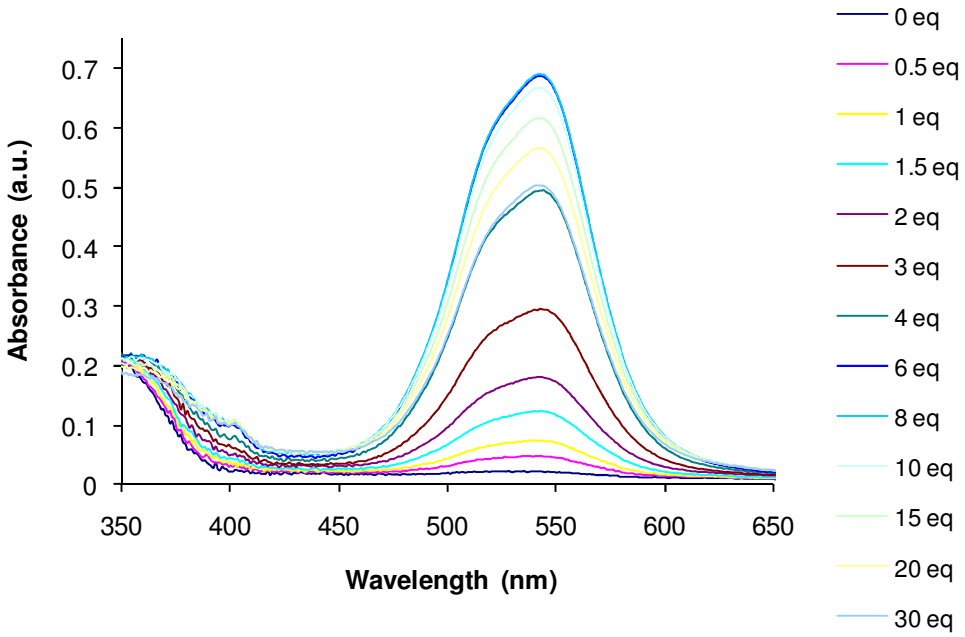
Absorbance (a.u.)
0.7
0.6
0.5
0.4
0.3
0.2
0.1
0
350
400
450
500
550
600
650
Wavelength (nm)
0 eq
0.5 eq
1 eq
1.5 eq
2 eq
3 eq
4 eq
6 eq
8 eq
10 eq
15 eq
20 eq
30 eq

(b)

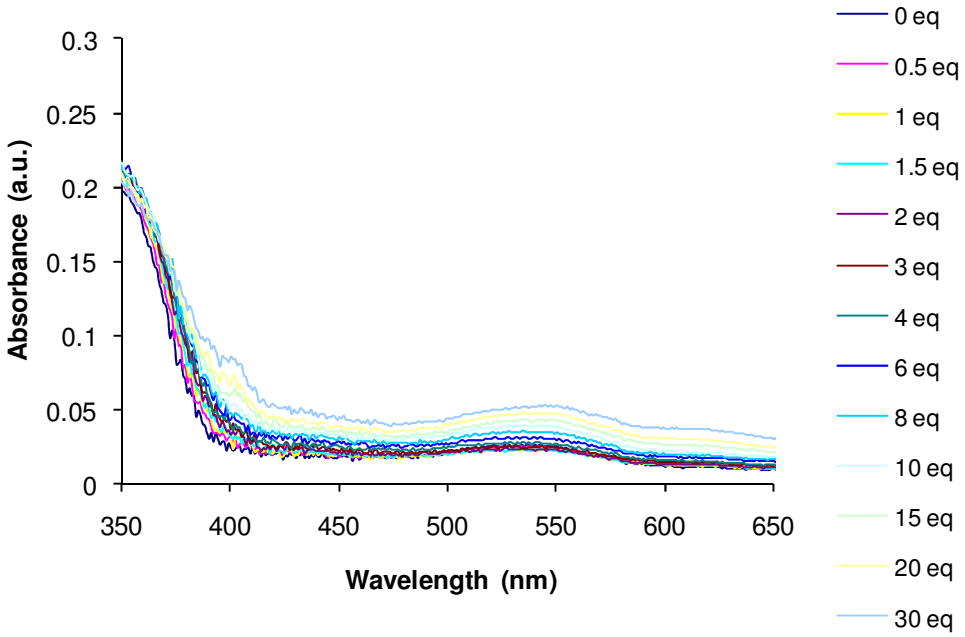
Absorbance (a.u.)
0.3
0.25
0.2
0.15
0.1
0.05
0
350
400
450
500
550
600
650
Wavelength (nm)
0 eq
0.5 eq
1 eq
1.5 eq
2 eq
3 eq
4 eq
6 eq
8 eq
10 eq
15 eq
20 eq
30 eq

(c)

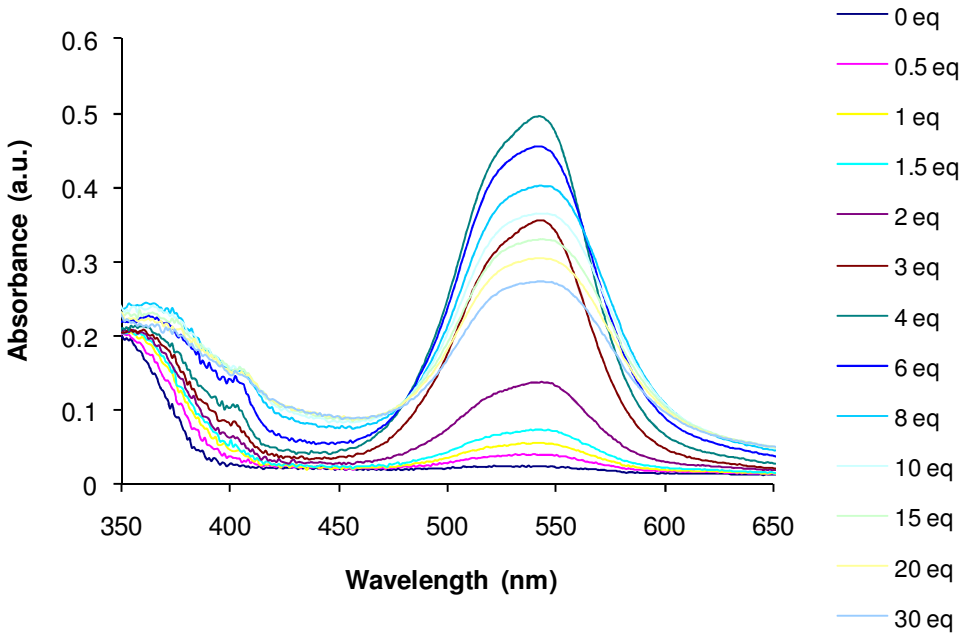

AIII.10 UV-vis spectroscopic titrations of **126** (1.0 x 10^{-4} mol dm^{-3} in MeCN) with (a) acetate, (b) malonate, (c) succinate used as TBA salts.

(a)

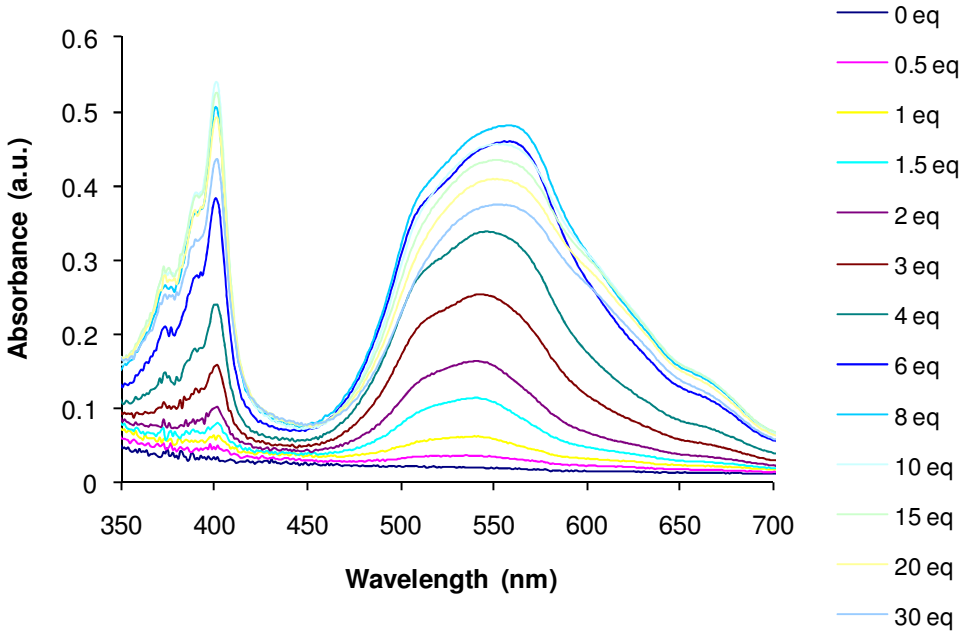

(b)

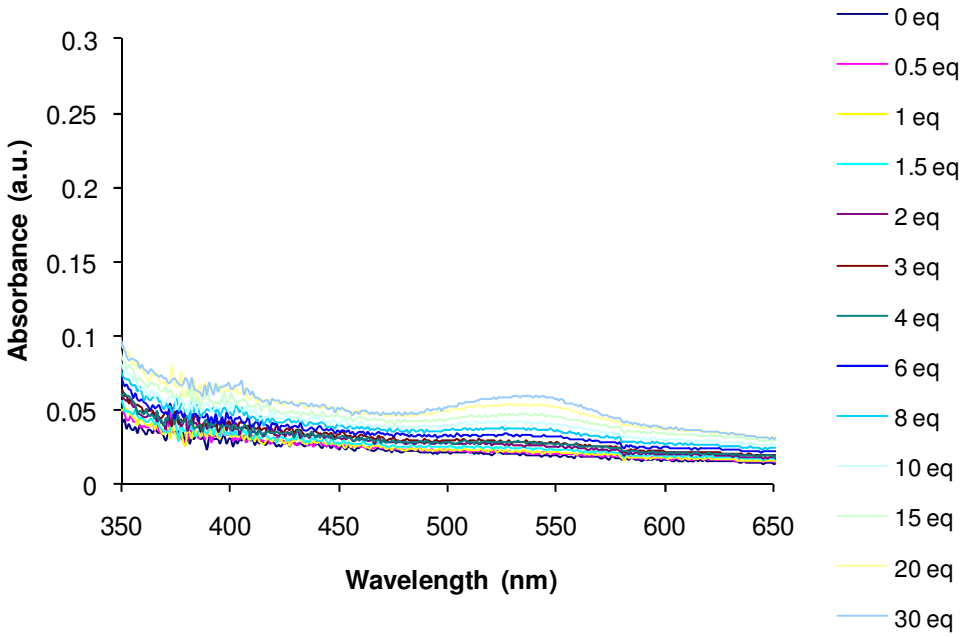

(c)

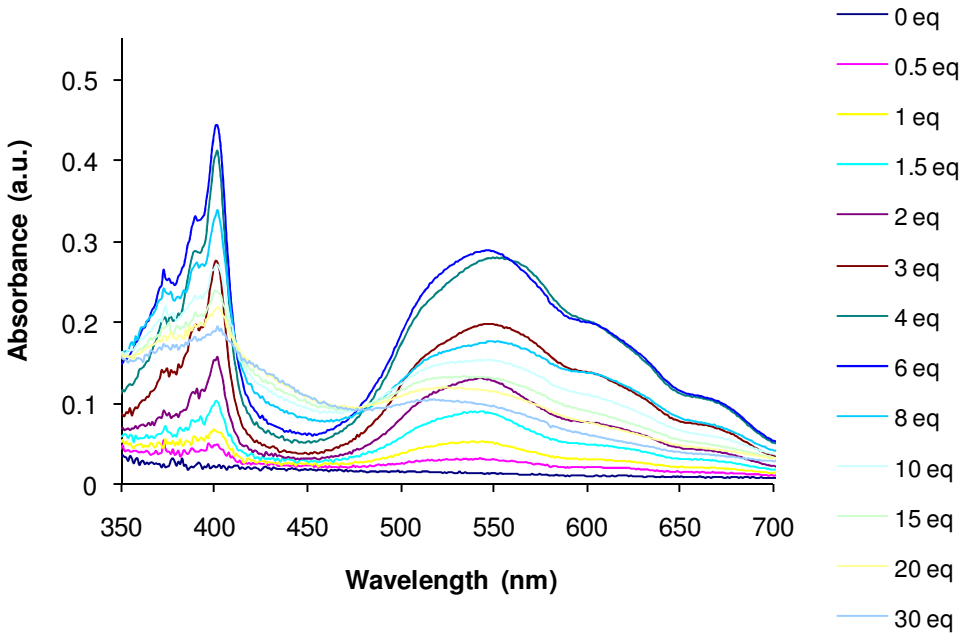

AIII.11 UV-vis spectroscopic titrations of **134** (1.0×10^{-4} mol dm^{-3} in MeCN) with (a) acetate, (b) malonate, (c) succinate used as TBA salts.

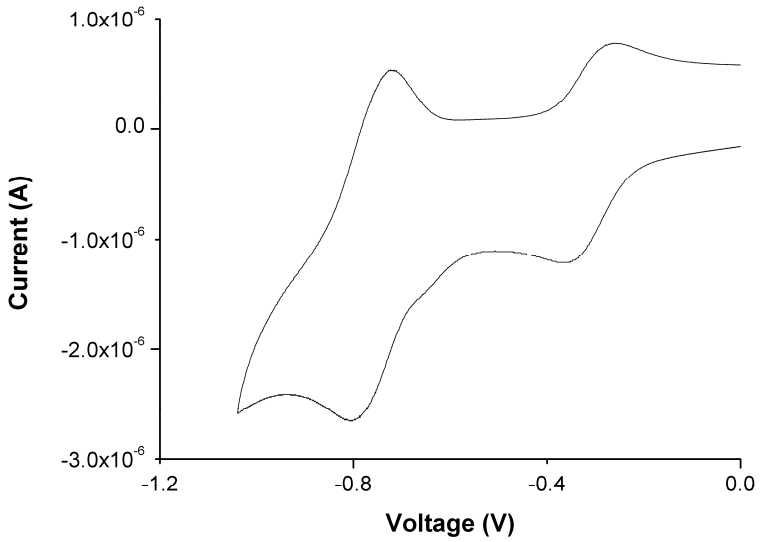

AIII.12 Cyclic voltammogram of compound **125** at a scan rate of 100 mV s^{-1} in 0.1 mol dm^{-1} in MeCN

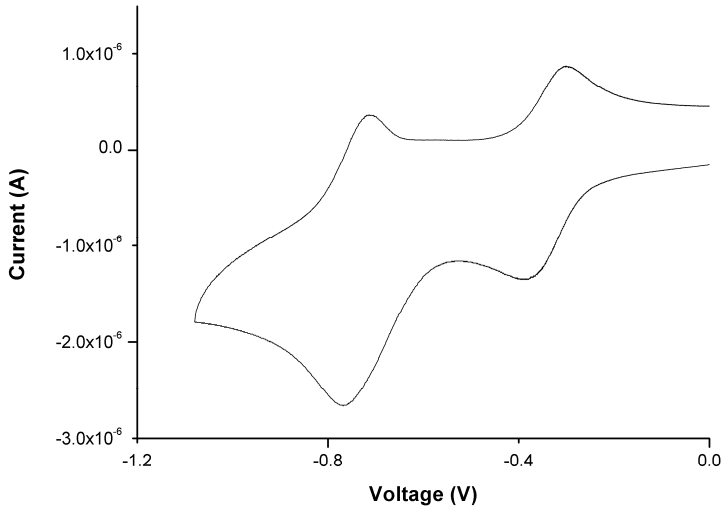

AIII.13 Cyclic voltammogram of compound **126** at a scan rate of 100 mV s^{-1} in 0.1 mol dm^{-1} in MeCN

(a)

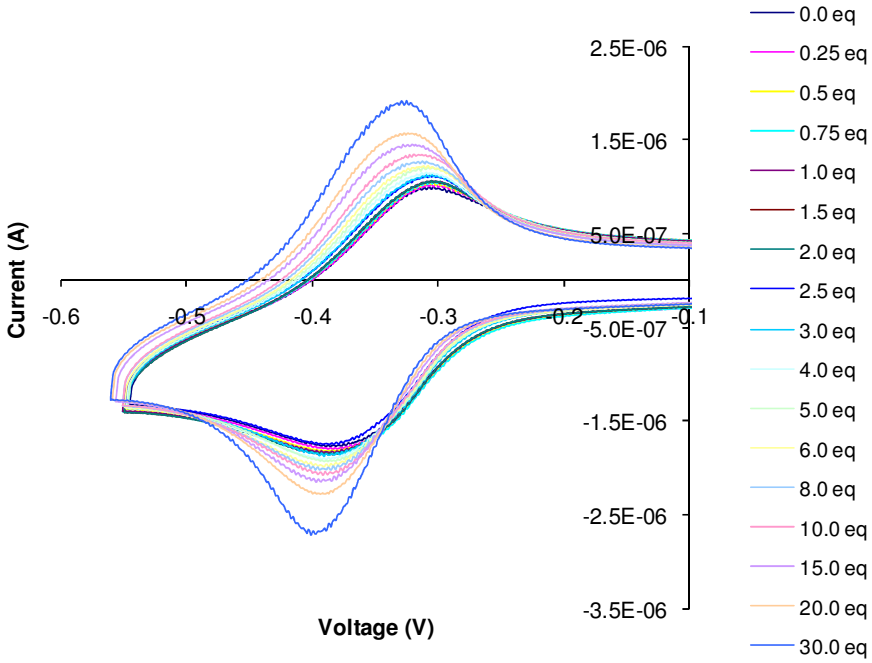

(b)

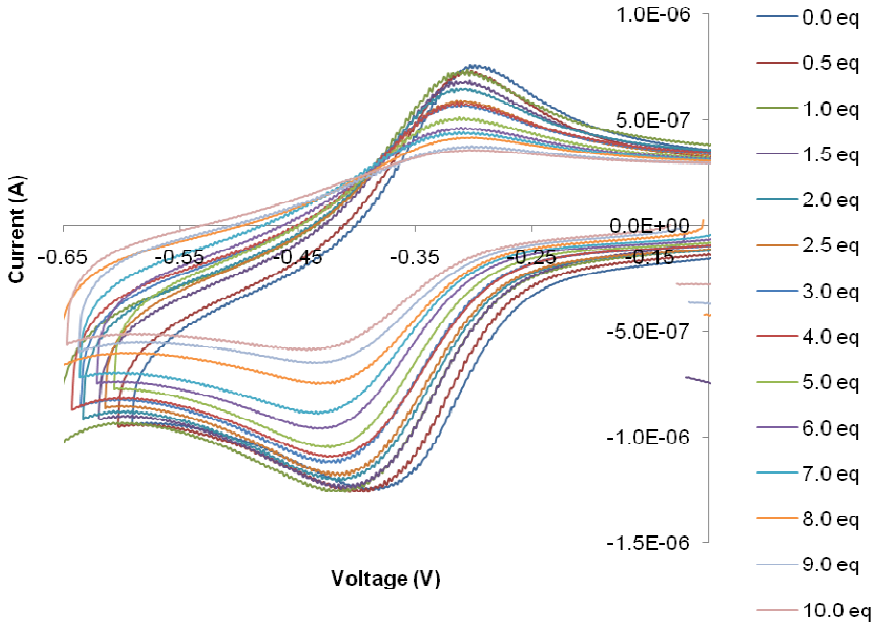

AIII.14 Cyclic voltammetric titration of **132** (1.0×10^{-4} mol dm^{-3} in 0.1 mol dm^{-3} TBA-PF_6 in MeCN) with (a) bromide, (b) malonate, used as TBA salts

(a)

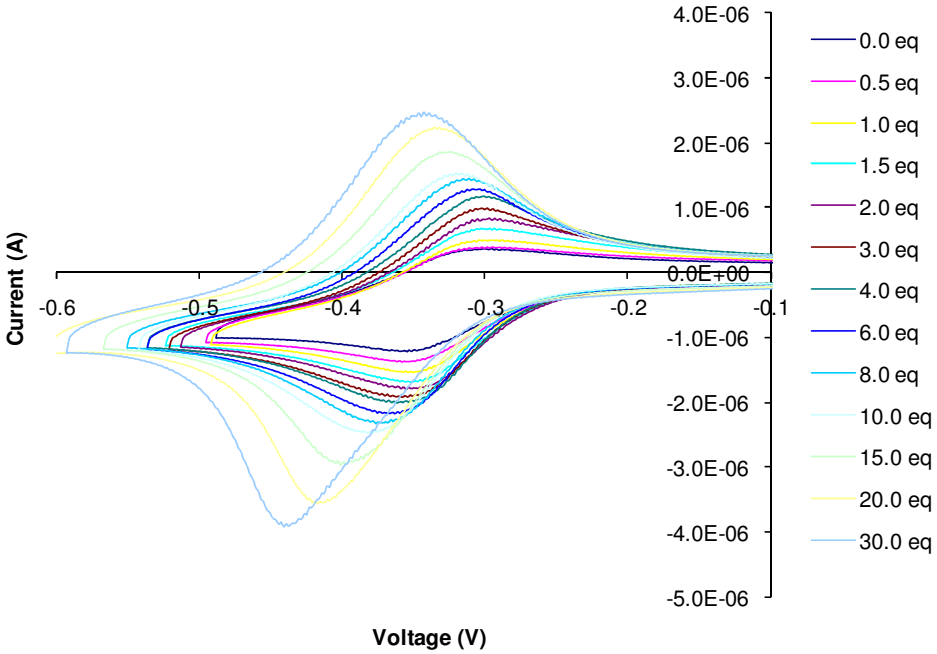
4.0E-06
3.0E-06
2.0E-06
1.0E-06
0.0E+00
-1.0E-06
-2.0E-06
-3.0E-06
-4.0E-06
-5.0E-06
-0.6
-0.5
-0.4
-0.3
-0.2
-0.1
Current (A)
Voltage (V)
0.0 eq
0.5 eq
1.0 eq
1.5 eq
2.0 eq
3.0 eq
4.0 eq
6.0 eq
8.0 eq
10.0 eq
15.0 eq
20.0 eq
30.0 eq

(b)

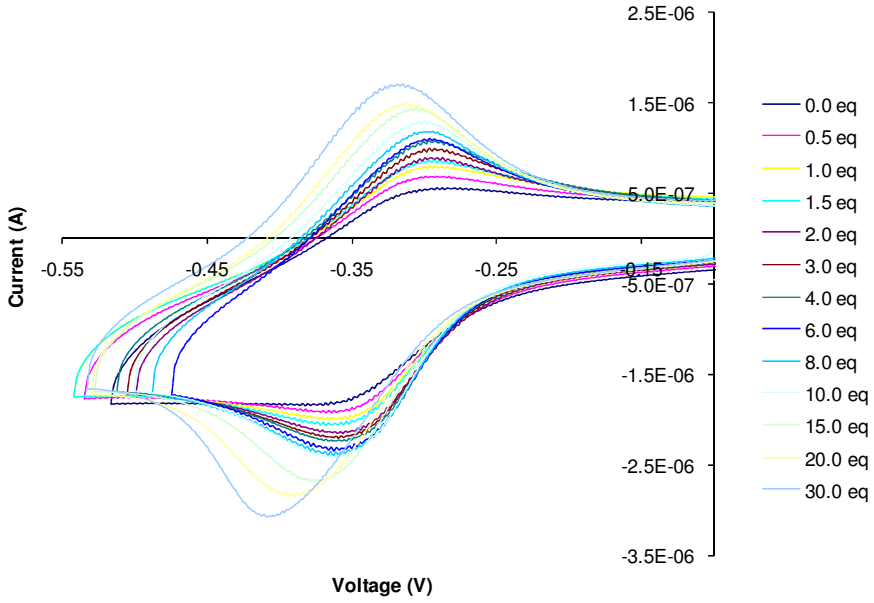
2.5E-06
1.5E-06
5.0E-07
-5.0E-07
-1.5E-06
-2.5E-06
-3.5E-06
-0.55
-0.45
-0.35
-0.25
-0.15
Current (A)
Voltage (V)
0.0 eq
0.5 eq
1.0 eq
1.5 eq
2.0 eq
3.0 eq
4.0 eq
6.0 eq
8.0 eq
10.0 eq
15.0 eq
20.0 eq
30.0 eq

(c)

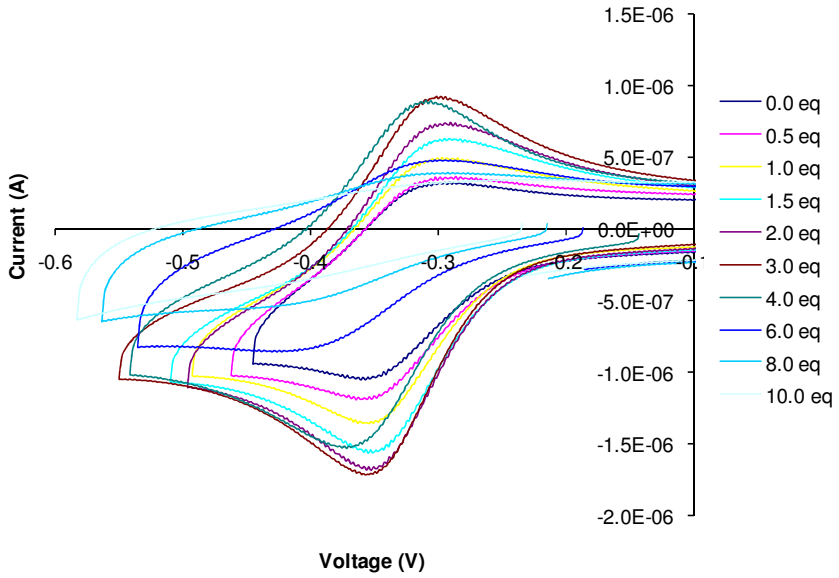

AIII.15 Cyclic voltammetric titration of **125** (1.0 x 10^{-4} mol dm^{-3} in 0.1 mol dm^{-3} TBA-PF_6 in MeCN) with (a) chloride, (b) bromide, (c) acetate, used as TBA salts

(a)

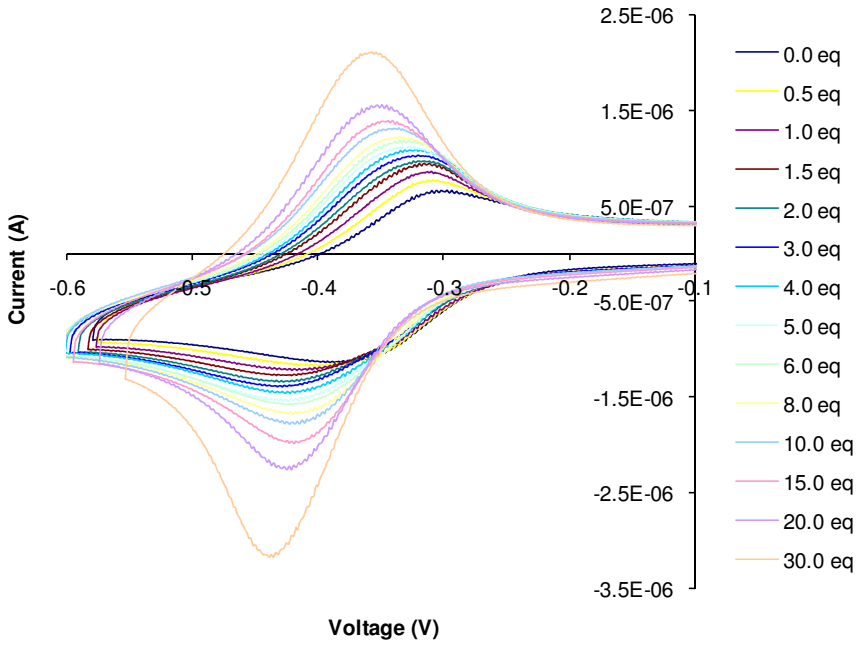

(b)

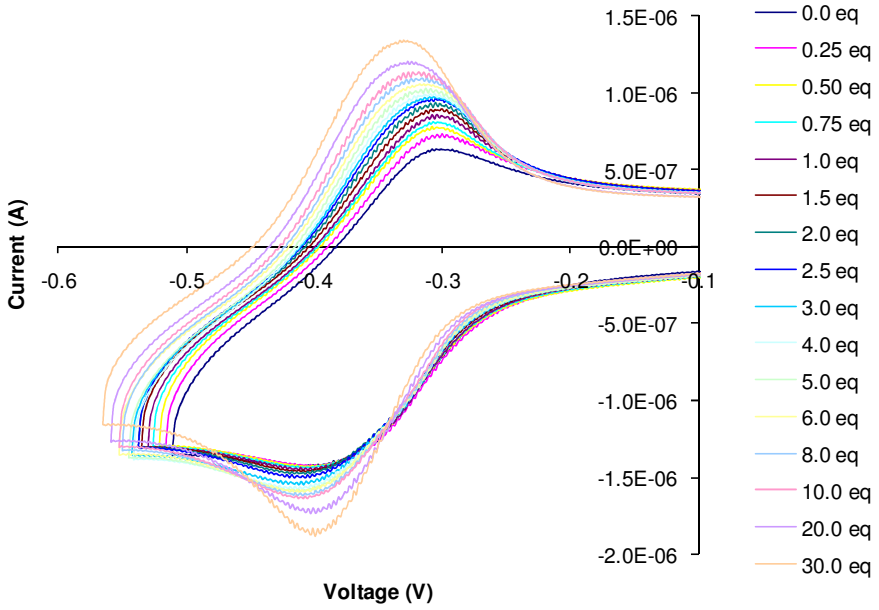
1.5E-06
1.0E-06
5.0E-07
0.0E+00
-5.0E-07
-1.0E-06
-1.5E-06
-2.0E-06
-0.6
-0.5
-0.4
-0.3
-0.2
-0.1
Current (A)
Voltage (V)
0.0 eq
0.25 eq
0.50 eq
0.75 eq
1.0 eq
1.5 eq
2.0 eq
2.5 eq
3.0 eq
4.0 eq
5.0 eq
6.0 eq
8.0 eq
10.0 eq
20.0 eq
30.0 eq

(c)

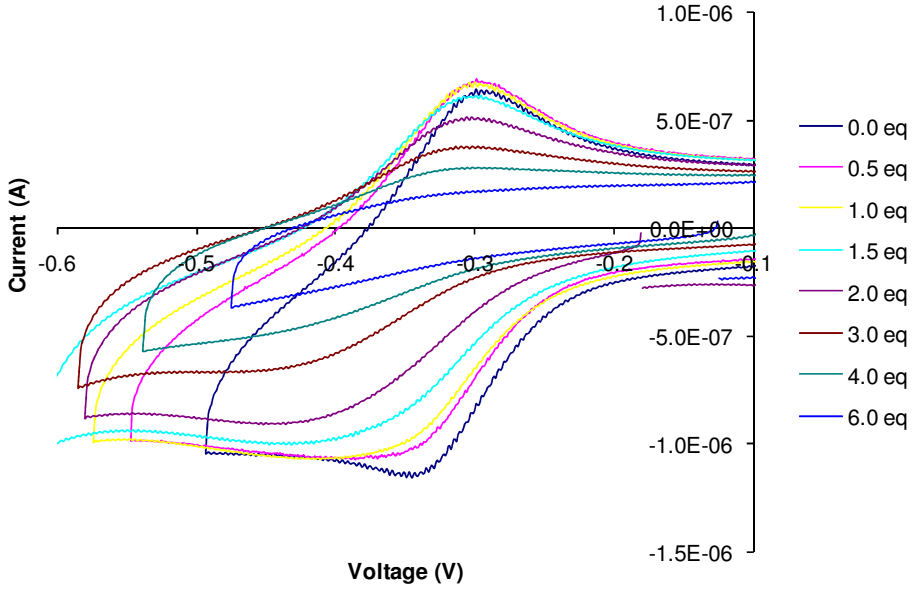
1.0E-06
5.0E-07
0.0E+00
-5.0E-07
-1.0E-06
-1.5E-06
-0.6
-0.5
-0.4
-0.3
-0.2
-0.1
Current (A)
Voltage (V)
0.0 eq
0.5 eq
1.0 eq
1.5 eq
2.0 eq
3.0 eq
4.0 eq
6.0 eq

(d)

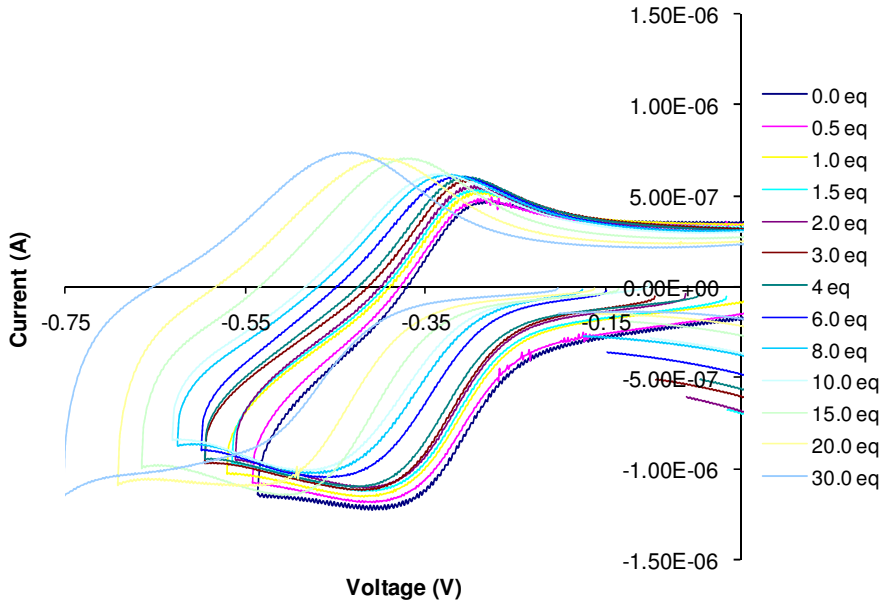

AIII.16 Cyclic voltammetric titration of **126** (1.0 x 10^{-4} mol dm^{-3} in 0.1 mol dm^{-3} TBA-PF_6 in MeCN) with (a) chloride, (b) bromide, (c) acetate (d) malonate, used as TBA salts

(a)

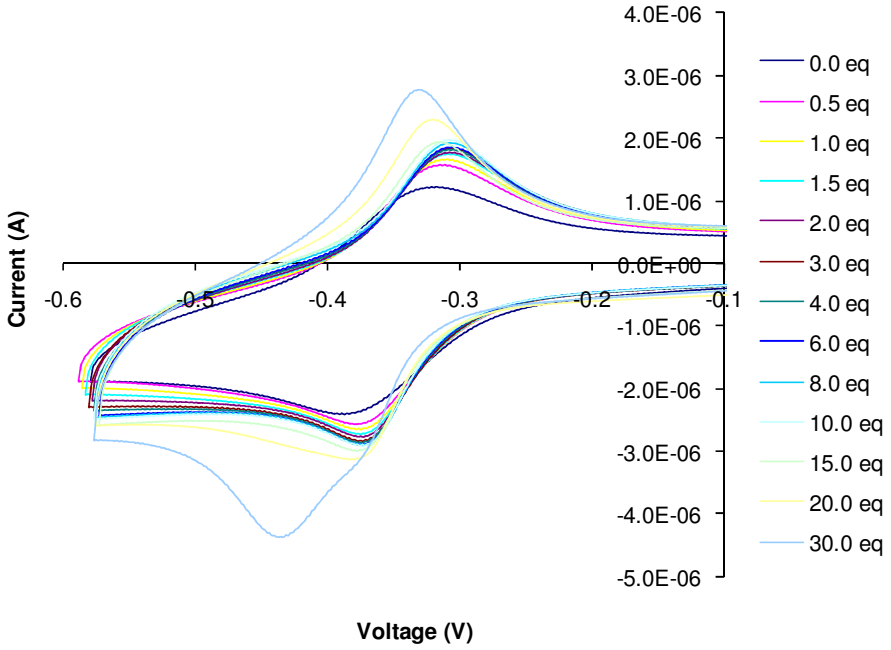

(b)

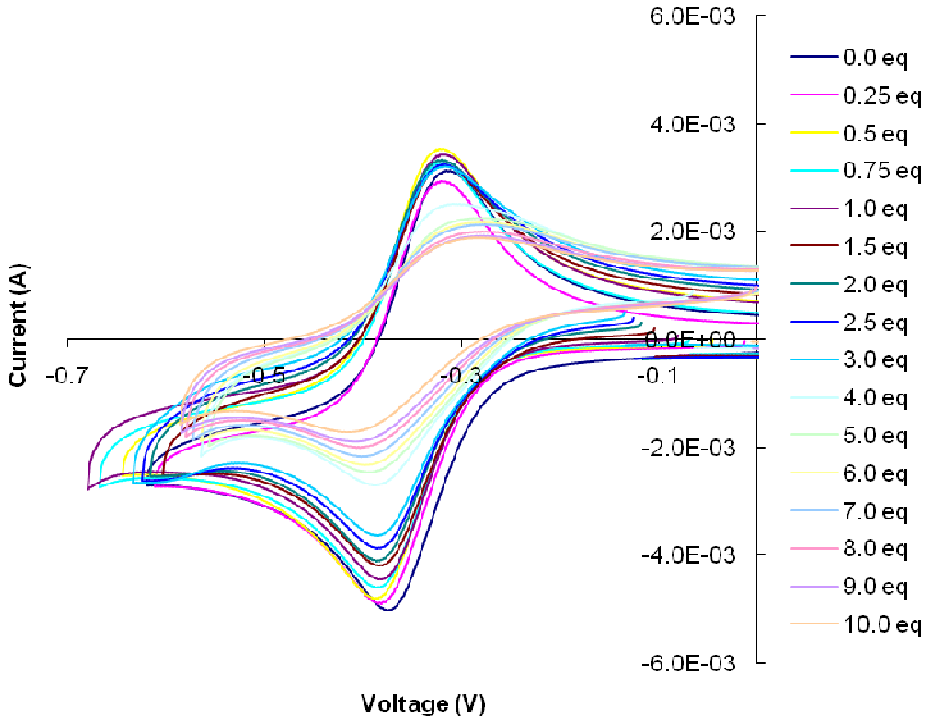

(c)

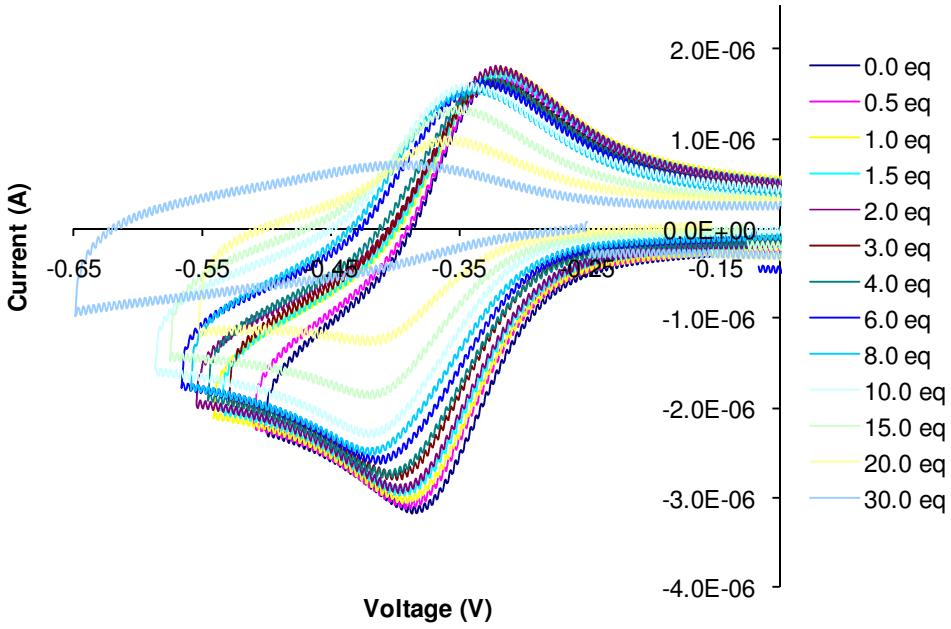

AIII.17 Cyclic voltammetric titration of **134** (1.0×10^{-4} mol dm^{-3} in 0.1 mol dm^{-3} TBA-PF_6 in MeCN) with (a) bromide, (b) acetate, (c) malonate, used as TBA salts

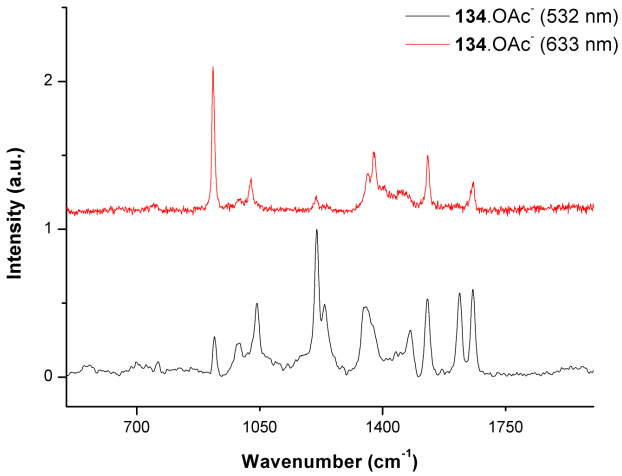

AIII.18 Resonance Raman spectra of **134** with OAc^- in MeCN measured using 532 and 633 nm laser light

Appendix IV – Supplementary Information Relating to Chapter 5

(a)

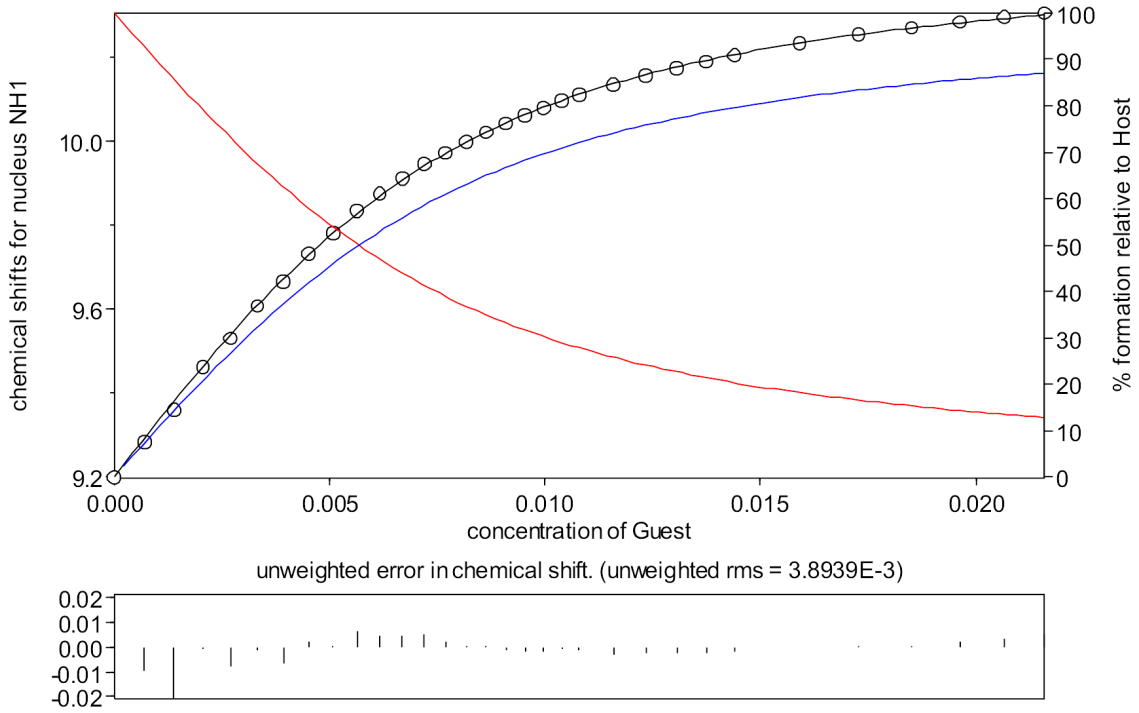

(b)

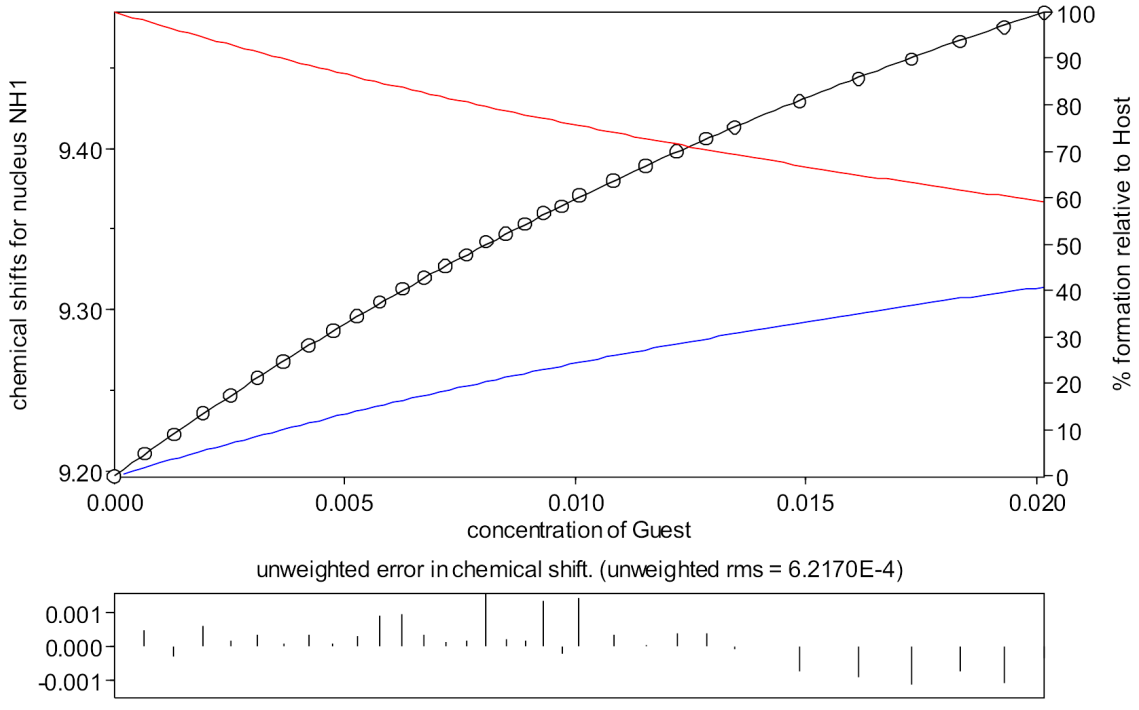

(c)

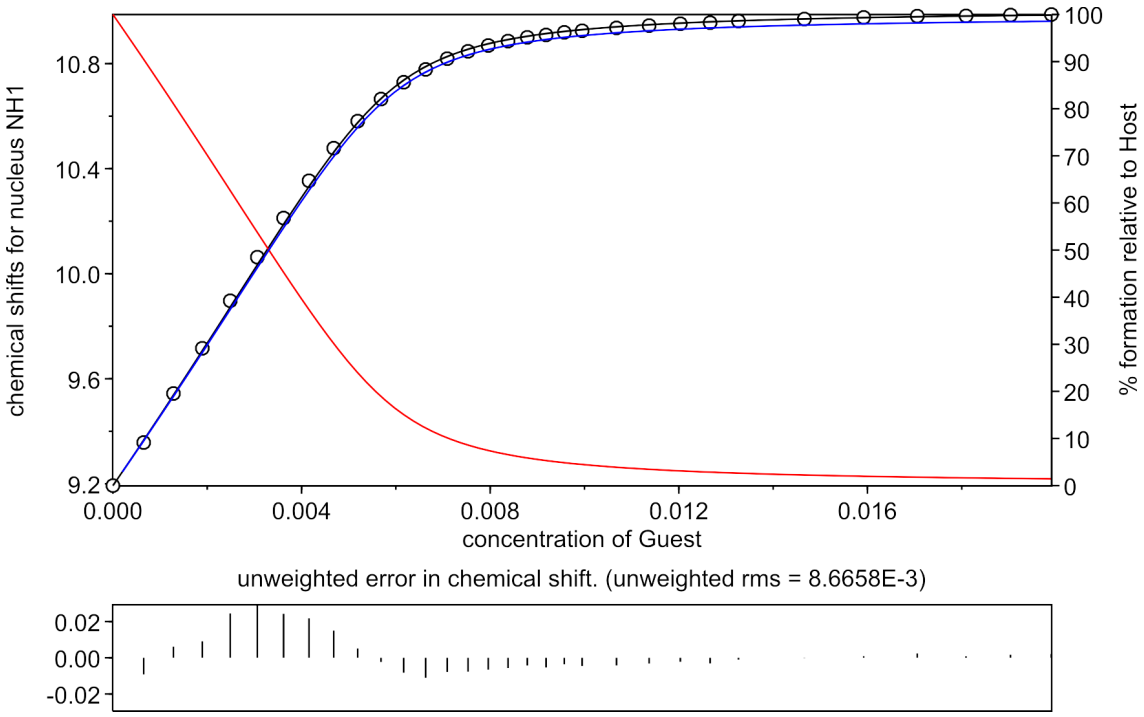
chemical shifts for nucleus NH1
10.8
10.4
10.0
9.6
9.2
0.000
0.004
0.008
0.012
0.016
concentration of Guest
100
90
80
70
60
50
40
30
20
10
0
% formation relative to Host
unweighted error in chemical shift. (unweighted rms = 8.6658E-3)
0.02
0.00
-0.02

(d)

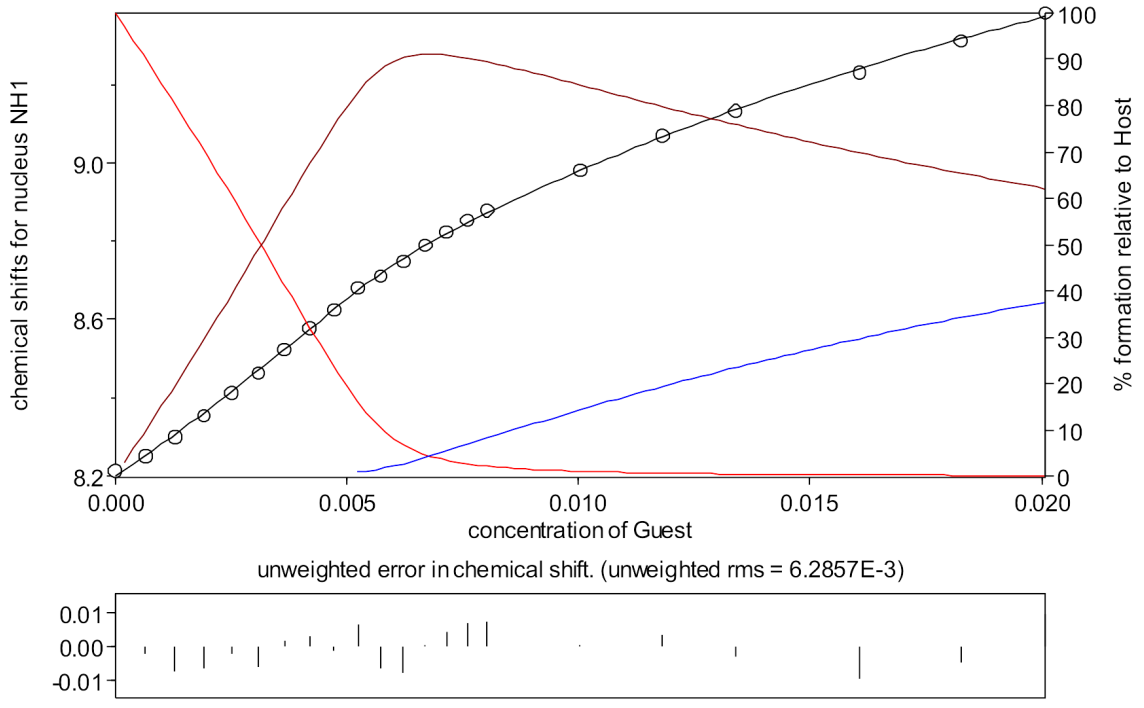
chemical shifts for nucleus NH1
9.0
8.6
8.2
0.000
0.005
0.010
0.015
0.020
concentration of Guest
100
90
80
70
60
50
40
30
20
10
0
% formation relative to Host
unweighted error in chemical shift. (unweighted rms = 6.2857E-3)
0.01
0.00
-0.01

(e)

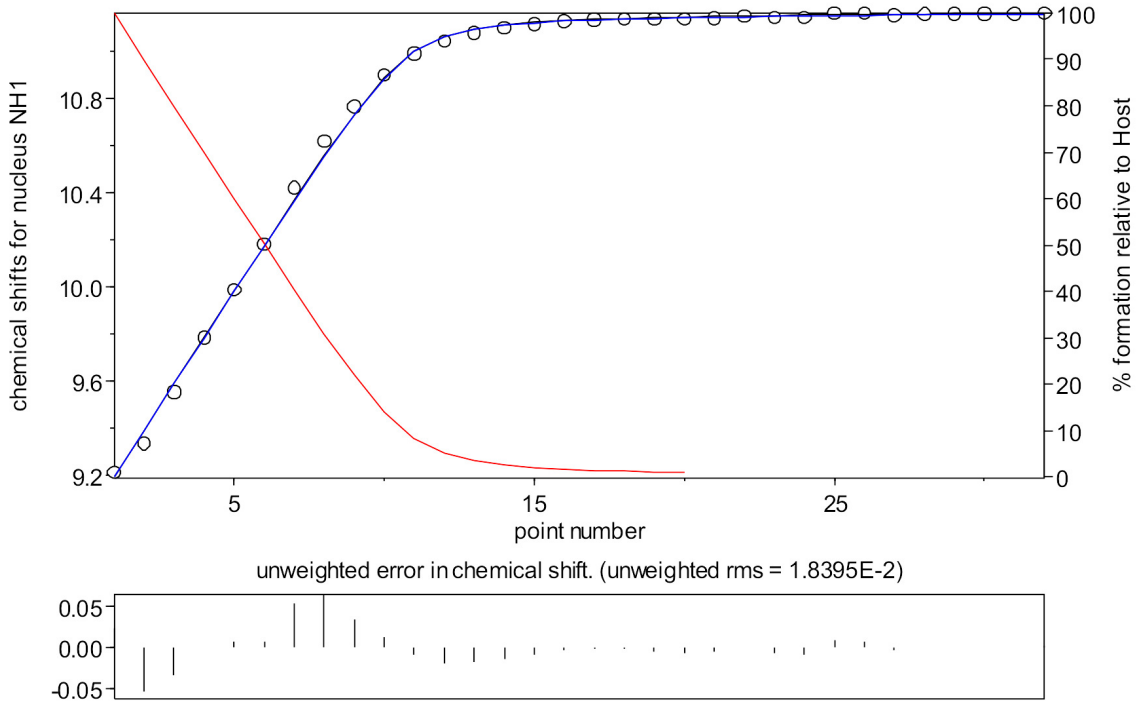

(f)

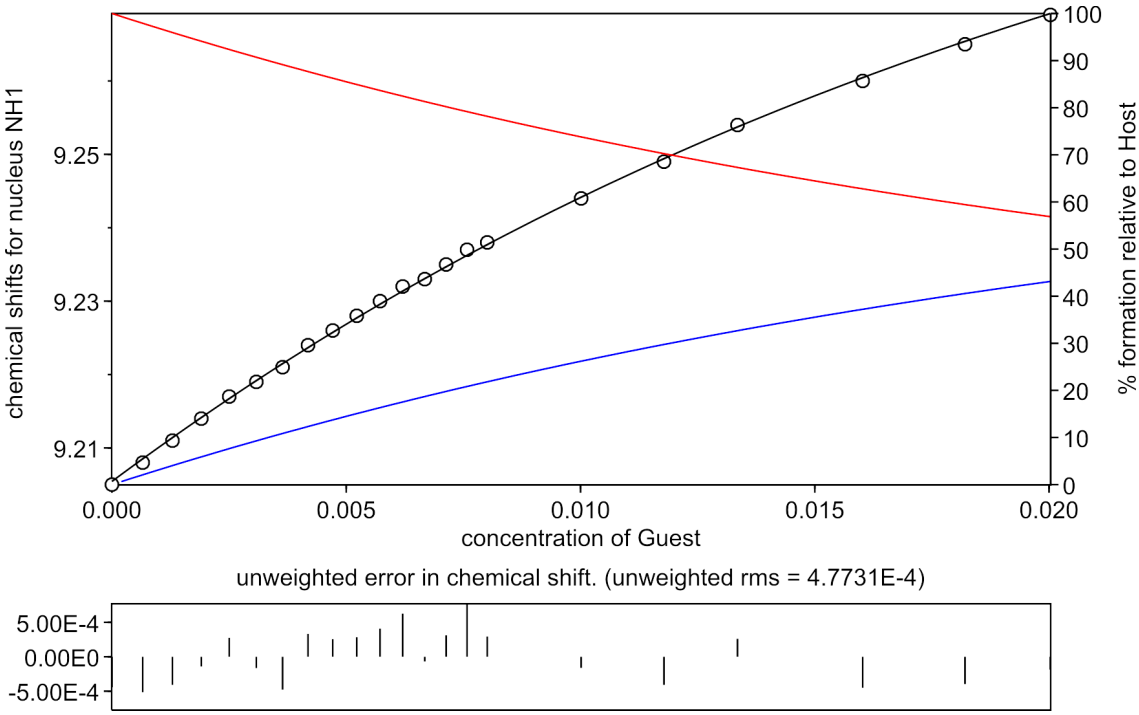

AIV.1 Speciation plot showing experimental data from ^{1}H NMR spectroscopic titrations on compound **135** in $CDCl_3$/DMSO-d_6 (*v/v* 70/30) and the fit for the calculated binding constants for (a) chloride, (b) bromide (c) acetate, (d) fluoride, (e) dihydrogen phosphate and (f) hydrogen sulfate

(a)

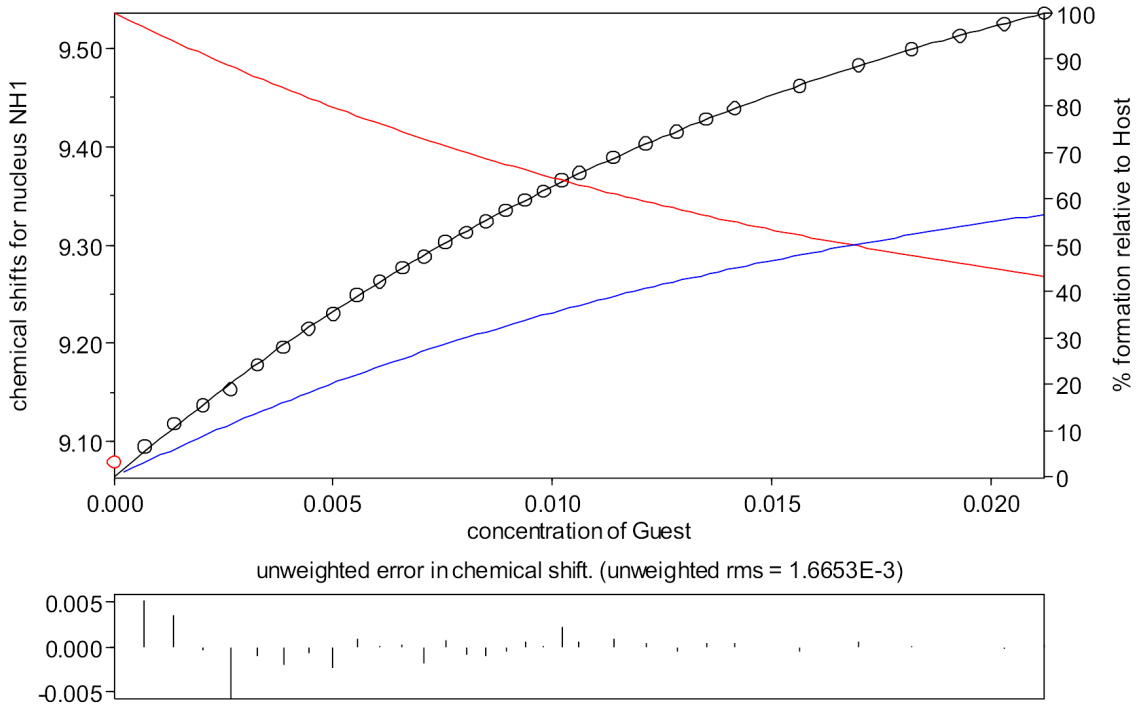
chemical shifts for nucleus NH1
9.50
9.40
9.30
9.20
9.10
0.000
0.005
0.010
0.015
0.020
concentration of Guest
% formation relative to Host
100
90
80
70
60
50
40
30
20
10
0
unweighted error in chemical shift. (unweighted rms = 1.6653E-3)
0.005
0.000
-0.005

(b)

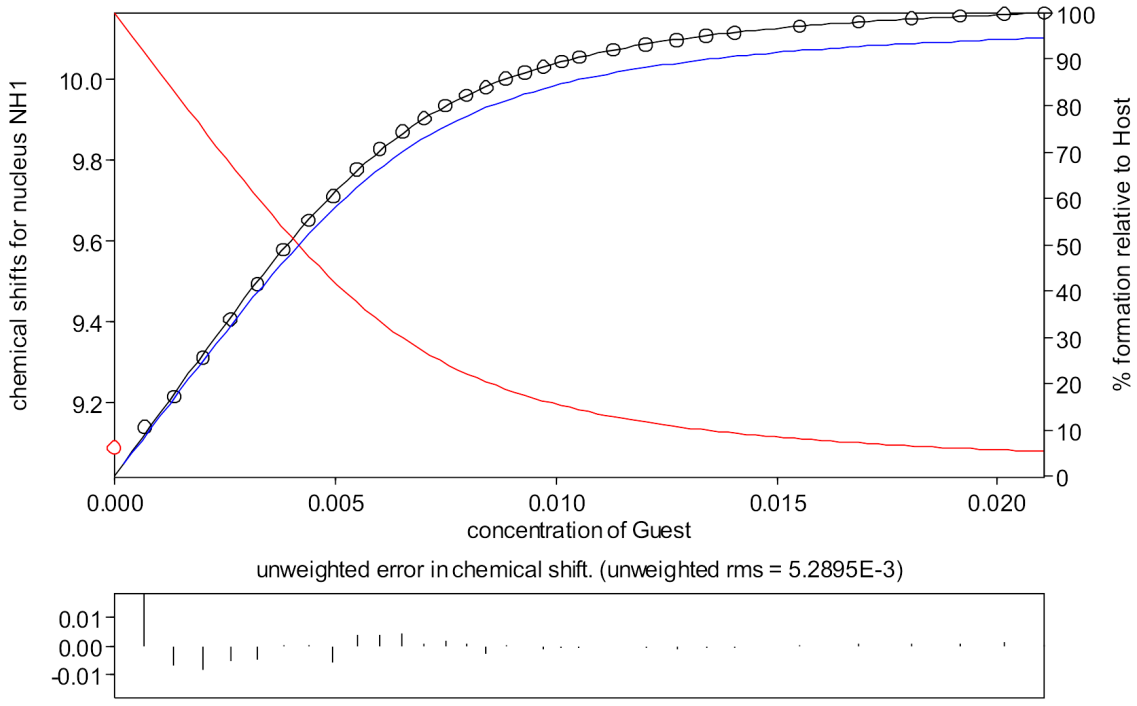
chemical shifts for nucleus NH1
10.0
9.8
9.6
9.4
9.2
0.000
0.005
0.010
0.015
0.020
concentration of Guest
% formation relative to Host
100
90
80
70
60
50
40
30
20
10
0
unweighted error in chemical shift. (unweighted rms = 5.2895E-3)
0.01
0.00
-0.01

(c)

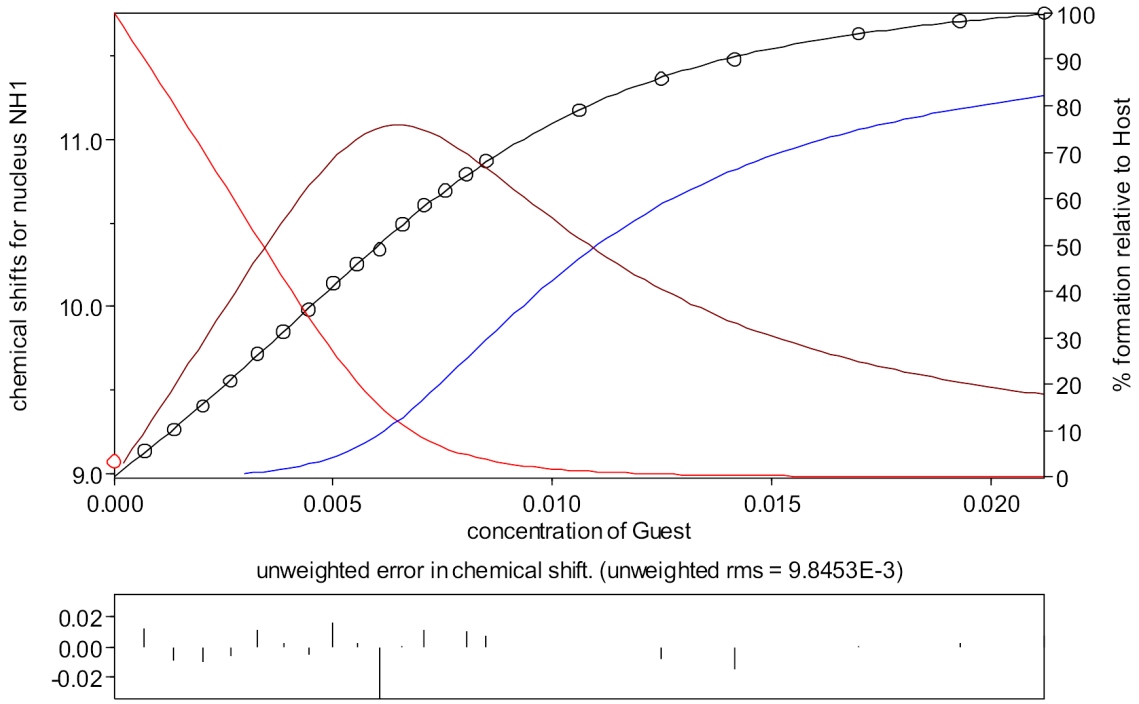
chemical shifts for nucleus NH1
11.0
10.0
9.0
0.000
0.005
0.010
0.015
0.020
concentration of Guest
% formation relative to Host
100
90
80
70
60
50
40
30
20
10
0
unweighted error in chemical shift. (unweighted rms = 9.8453E-3)
0.02
0.00
-0.02

(d)

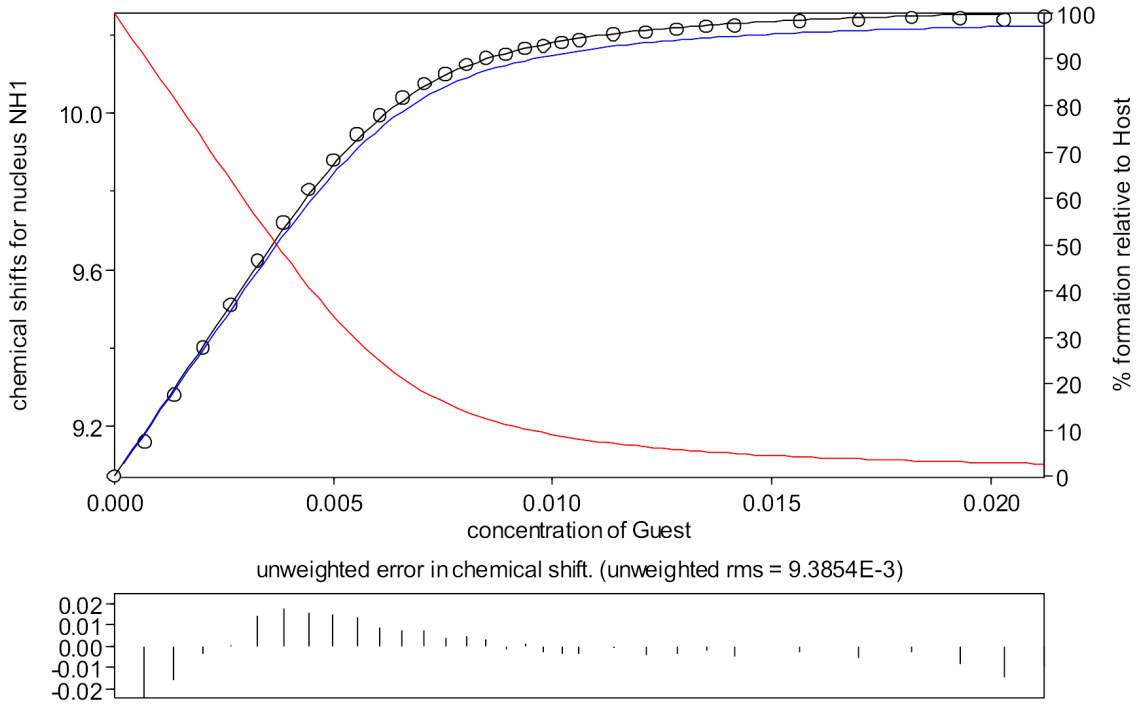
chemical shifts for nucleus NH1
10.0
9.6
9.2
0.000
0.005
0.010
0.015
0.020
concentration of Guest
% formation relative to Host
100
90
80
70
60
50
40
30
20
10
0
unweighted error in chemical shift. (unweighted rms = 9.3854E-3)
0.02
0.01
0.00
-0.01
-0.02

(e)

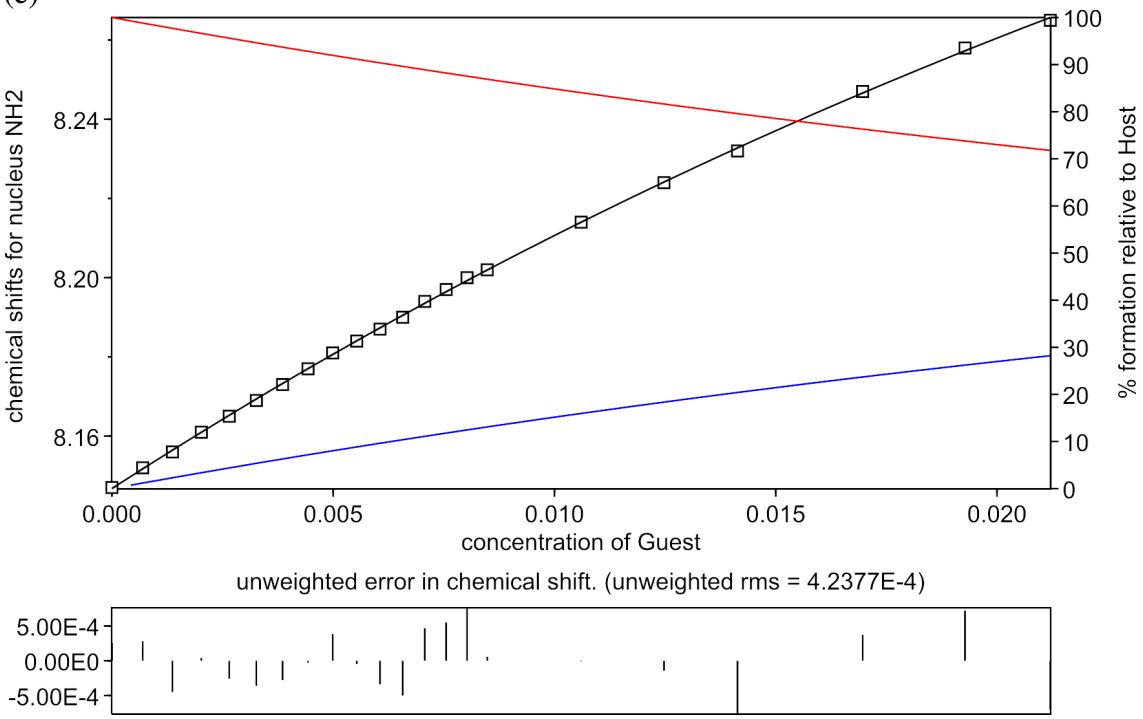

AIV.2 Speciation plot showing experimental data from ^{1}H NMR spectroscopic titrations on compound **136** in $CDCl_3$/DMSO-d_6 (*v/v* 70/30) and the fit for the calculated binding constants for (a) chloride, (b) acetate, (c) fluoride, (d) dihydrogen phosphate and (e) hydrogen sulphate.

(a)

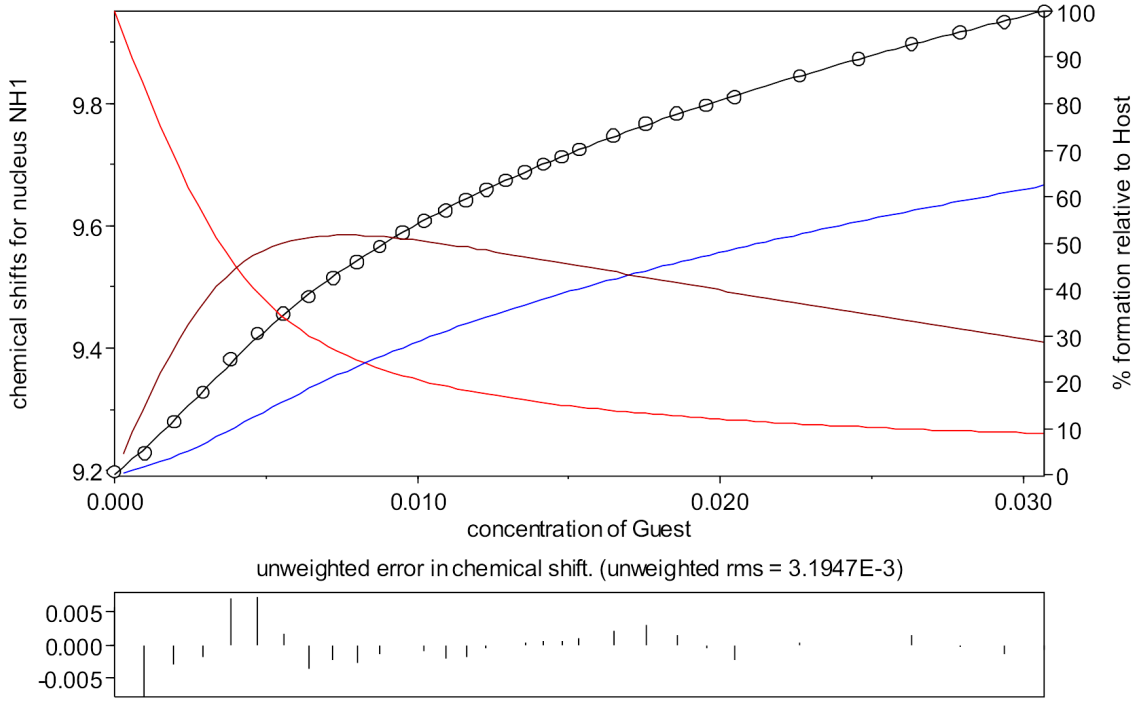

(b)

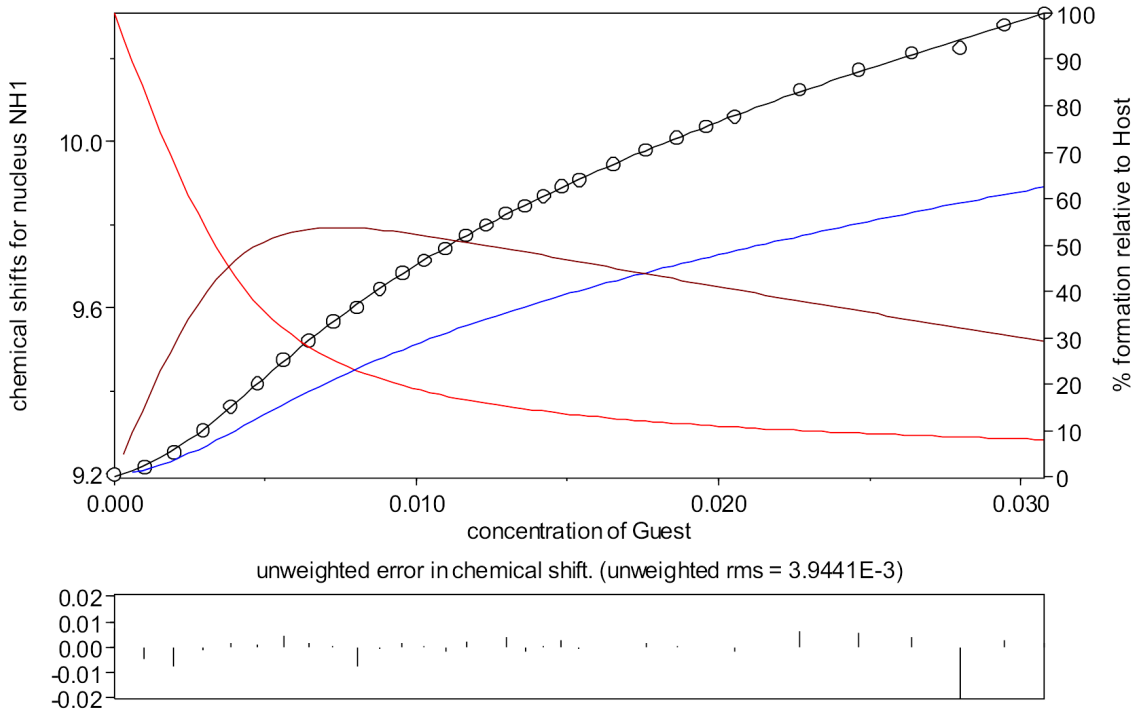

(c)

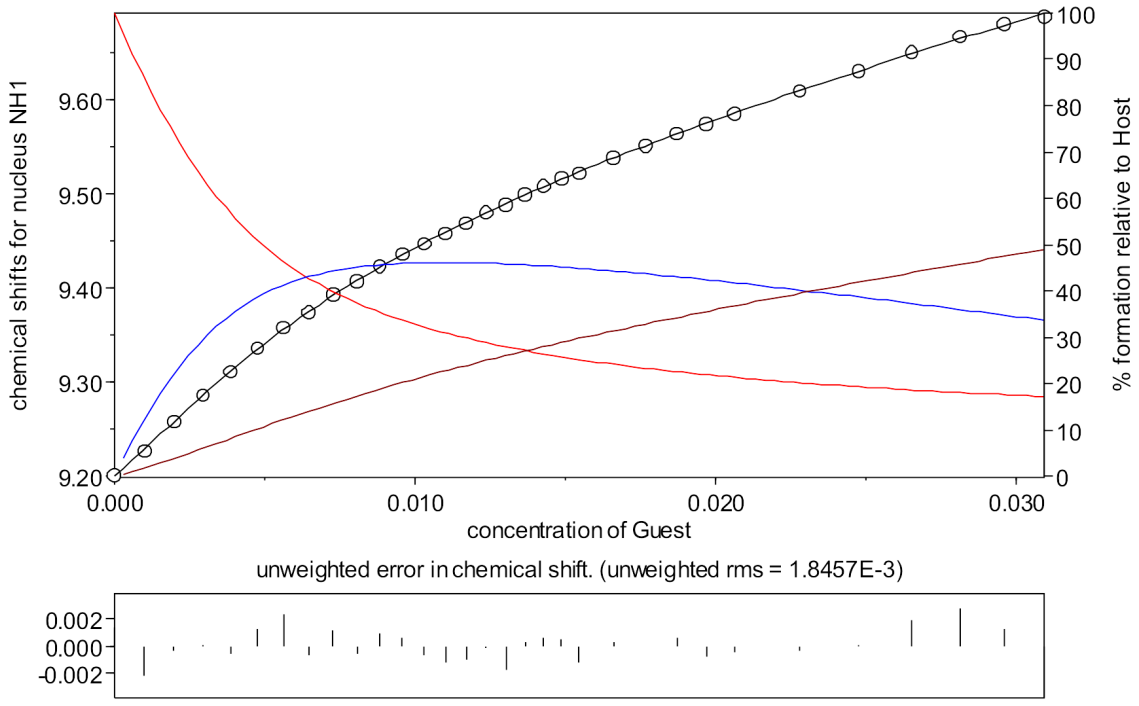

AIV.3 Speciation plot showing experimental data from ^{1}H NMR spectroscopic titrations on compound **137** in $CDCl_3$/DMSO-d_6 (*v/v* 70/30) and the fit for the calculated binding constants for (a) acetate, (b) fluoride, (c) dihydrogen phosphate

(a)

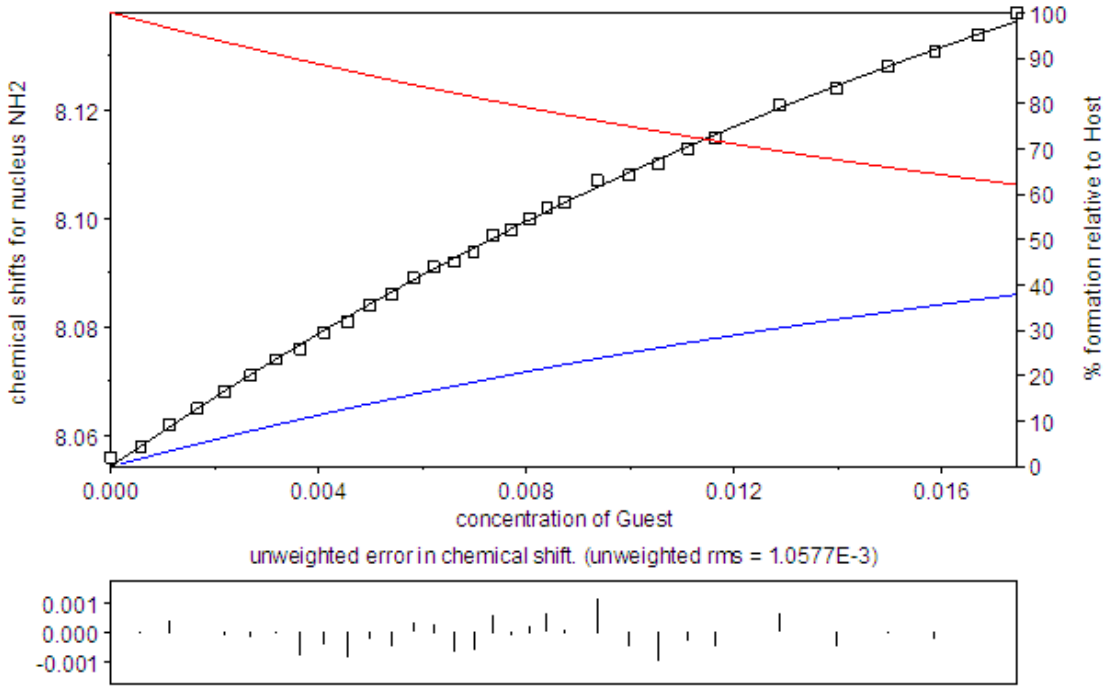
chemical shifts for nucleus NH2
8.12
8.10
8.08
8.06
0.000
0.004
0.008
0.012
0.016
concentration of Guest
% formation relative to Host
100
90
80
70
60
50
40
30
20
10
0
unweighted error in chemical shift. (unweighted rms = 1.0577E-3)
0.001
0.000
-0.001

(b)

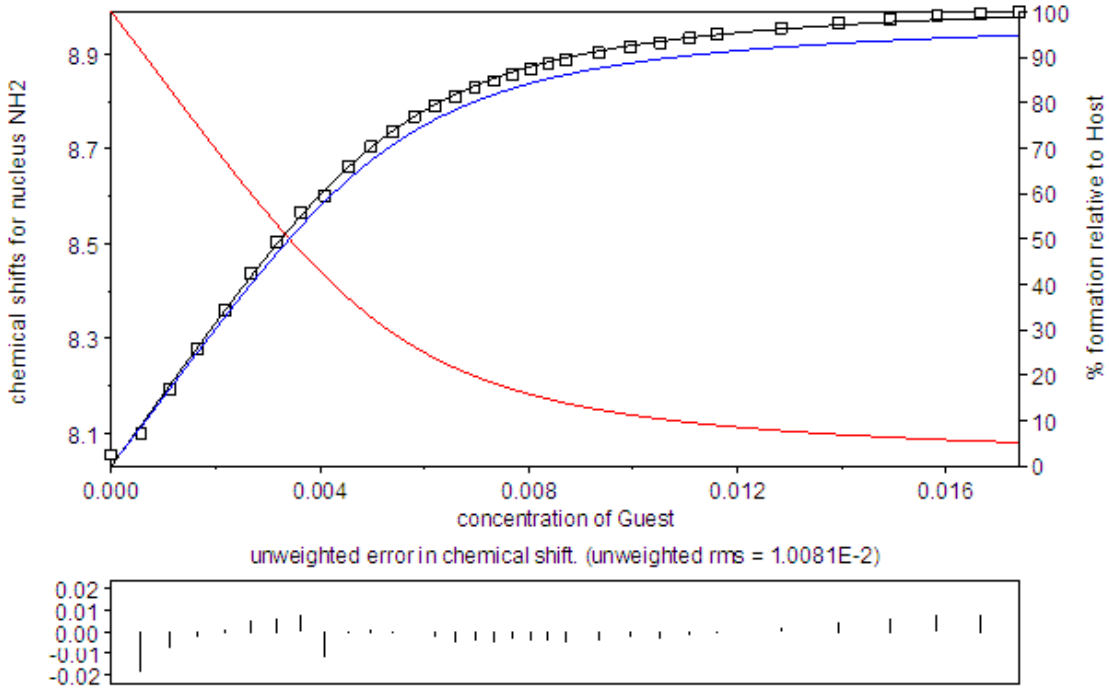
chemical shifts for nucleus NH2
8.9
8.7
8.5
8.3
8.1
0.000
0.004
0.008
0.012
0.016
concentration of Guest
% formation relative to Host
100
90
80
70
60
50
40
30
20
10
0
unweighted error in chemical shift. (unweighted rms = 1.0081E-2)
0.02
0.01
0.00
-0.01
-0.02

(c)

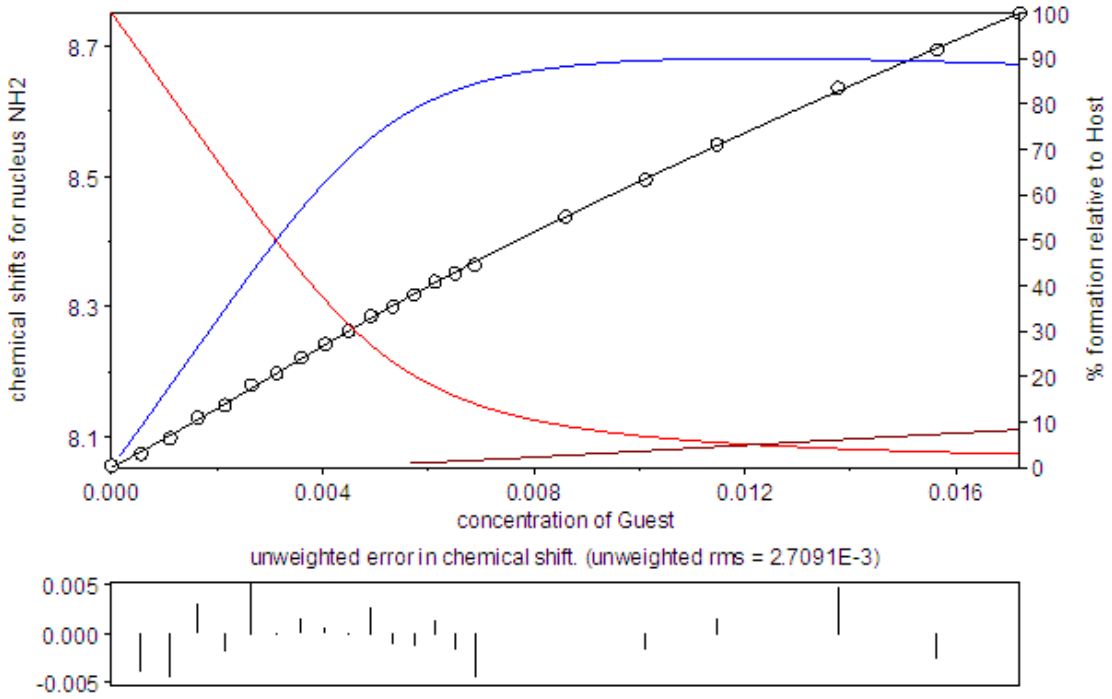
chemical shifts for nucleus NH2
% formation relative to Host
concentration of Guest
8.7
8.5
8.3
8.1
0.000
0.004
0.008
0.012
0.016
100
90
80
70
60
50
40
30
20
10
0
unweighted error in chemical shift. (unweighted rms = 2.7091E-3)
0.005
0.000
-0.005

(d)

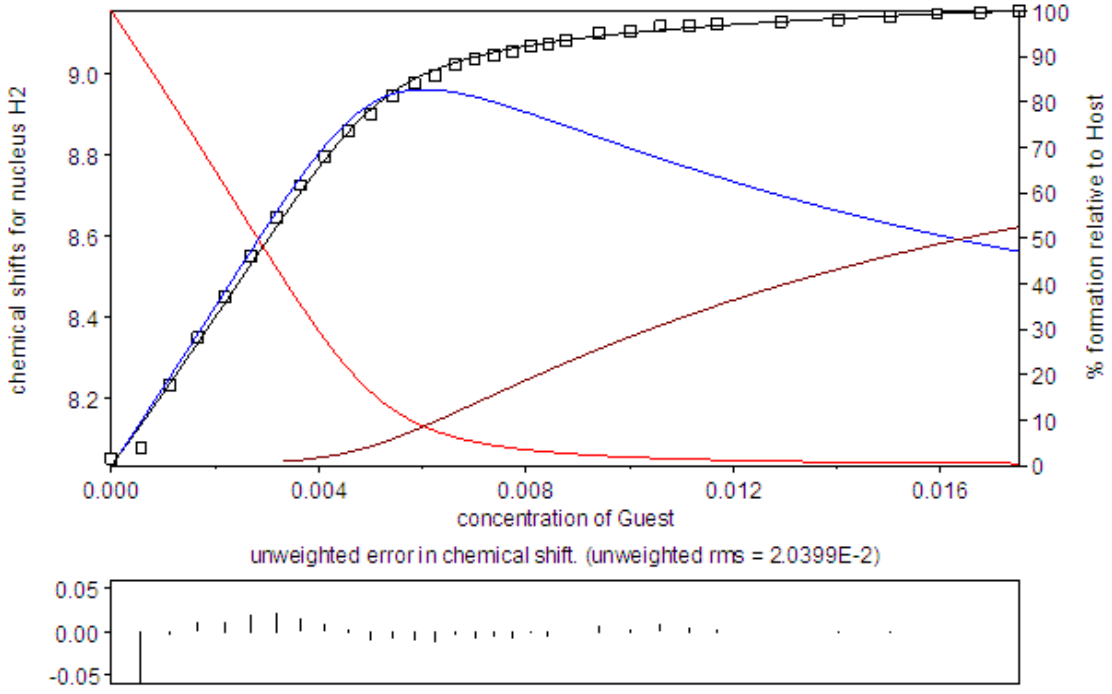
chemical shifts for nucleus H2
% formation relative to Host
concentration of Guest
9.0
8.8
8.6
8.4
8.2
0.000
0.004
0.008
0.012
0.016
100
90
80
70
60
50
40
30
20
10
0
unweighted error in chemical shift. (unweighted rms = 2.0399E-2)
0.05
0.00
-0.05

(e)

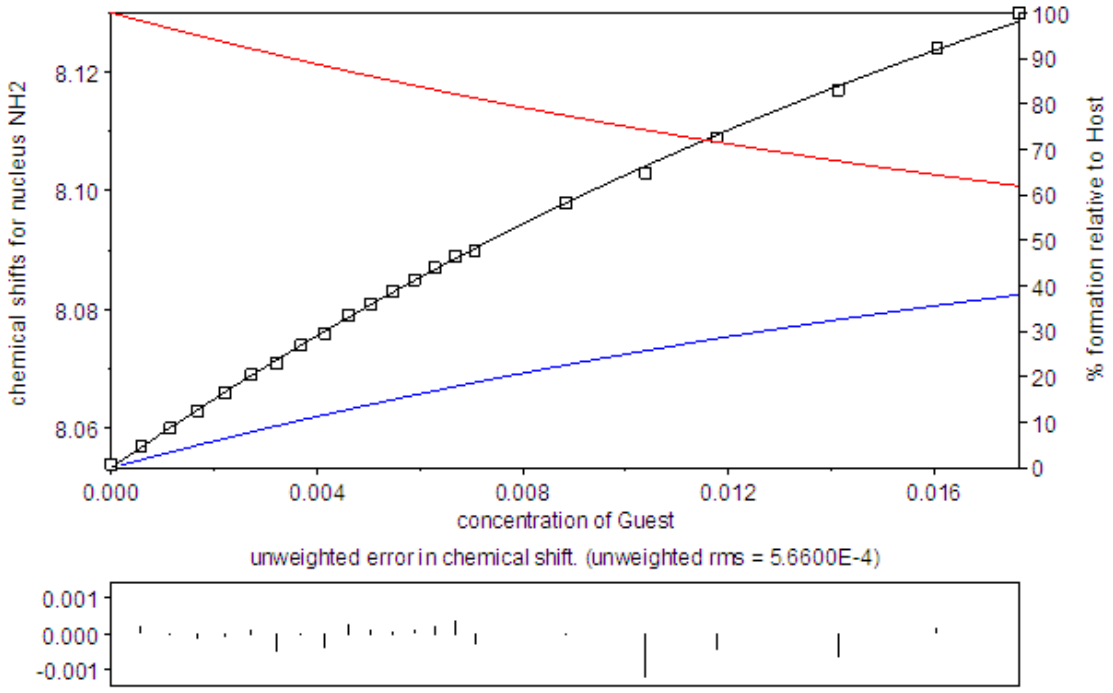

AIV.4 Speciation plot showing experimental data from ^{1}H NMR spectroscopic titrations on compound **138** in $CDCl_3$/DMSO-d_6 (*v/v* 70/30) and the fit for the calculated binding constants for (a) chloride, (b) acetate, (c) fluoride, (d) dihydrogen phosphate and (e) hydrogen sulfate

(a)

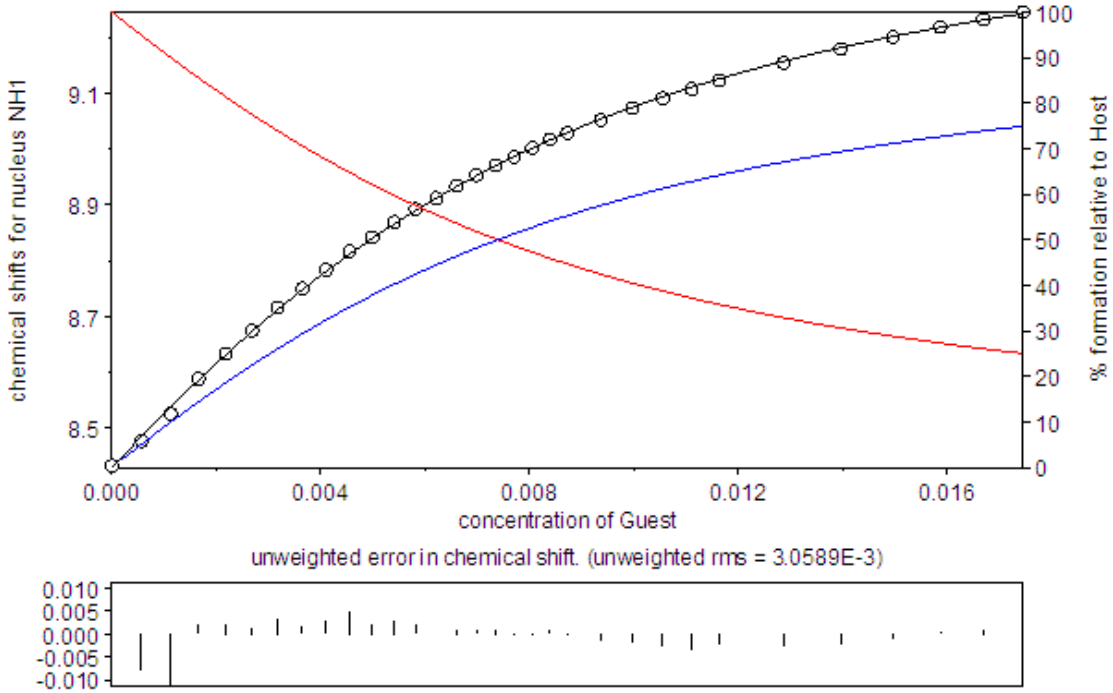

(b)

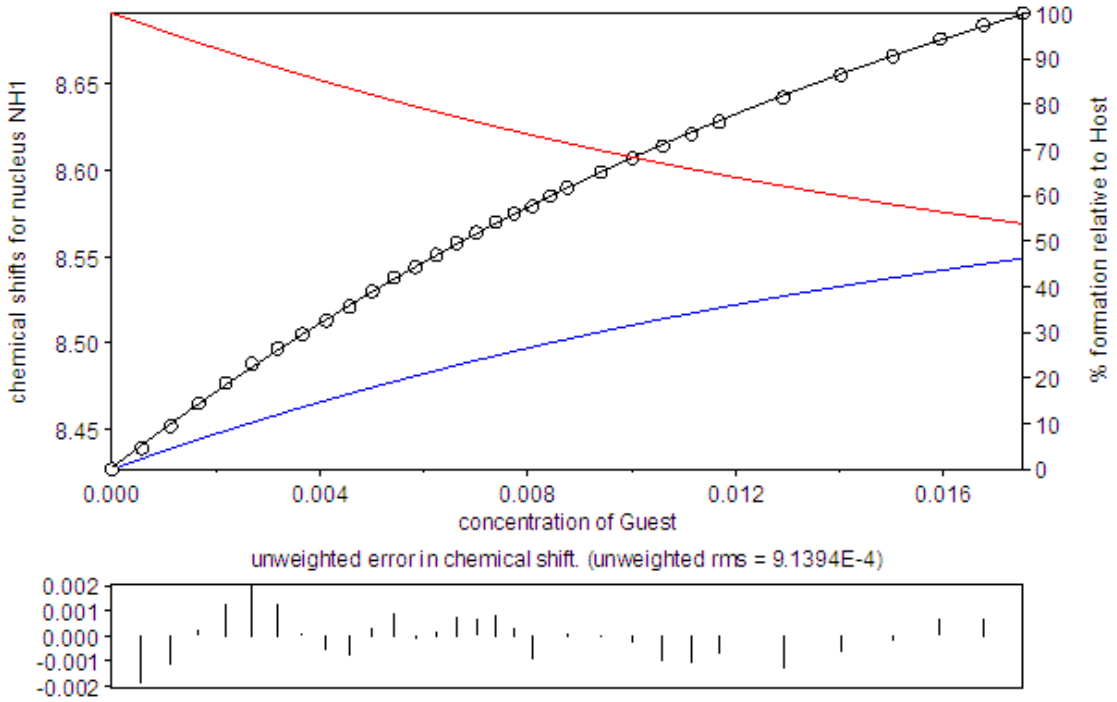
chemical shifts for nucleus NH1
8.65
8.60
8.55
8.50
8.45
0.000
0.004
0.008
0.012
0.016
concentration of Guest
100
90
80
70
60
50
40
30
20
10
0
% formation relative to Host
unweighted error in chemical shift. (unweighted rms = 9.1394E-4)
0.002
0.001
0.000
-0.001
-0.002

(c)

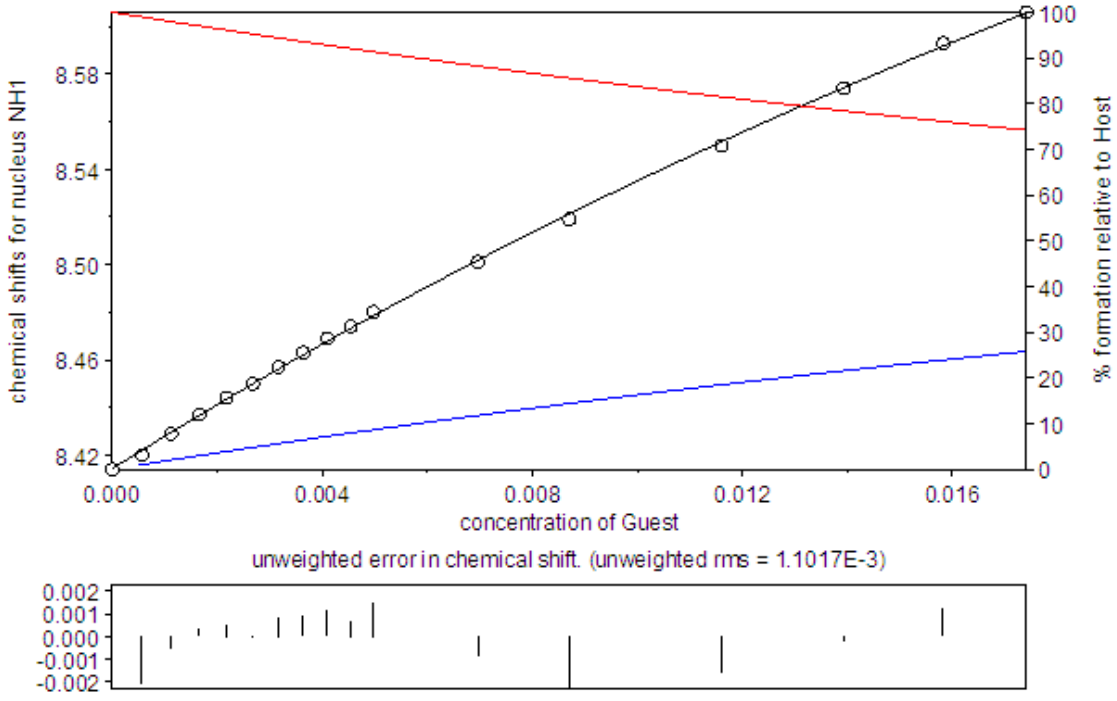
chemical shifts for nucleus NH1
8.58
8.54
8.50
8.46
8.42
0.000
0.004
0.008
0.012
0.016
concentration of Guest
100
90
80
70
60
50
40
30
20
10
0
% formation relative to Host
unweighted error in chemical shift. (unweighted rms = 1.1017E-3)
0.002
0.001
0.000
-0.001
-0.002

(d)

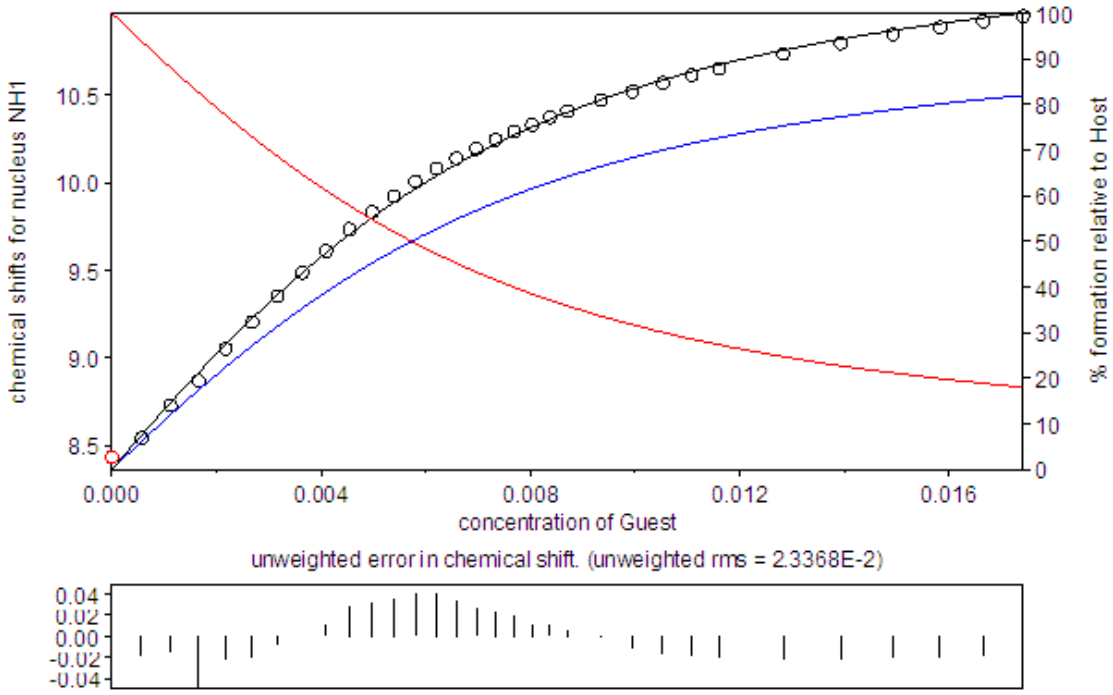
chemical shifts for nucleus NH1
% formation relative to Host
concentration of Guest
unweighted error in chemical shift. (unweighted rms = 2.3368E-2)

(e)

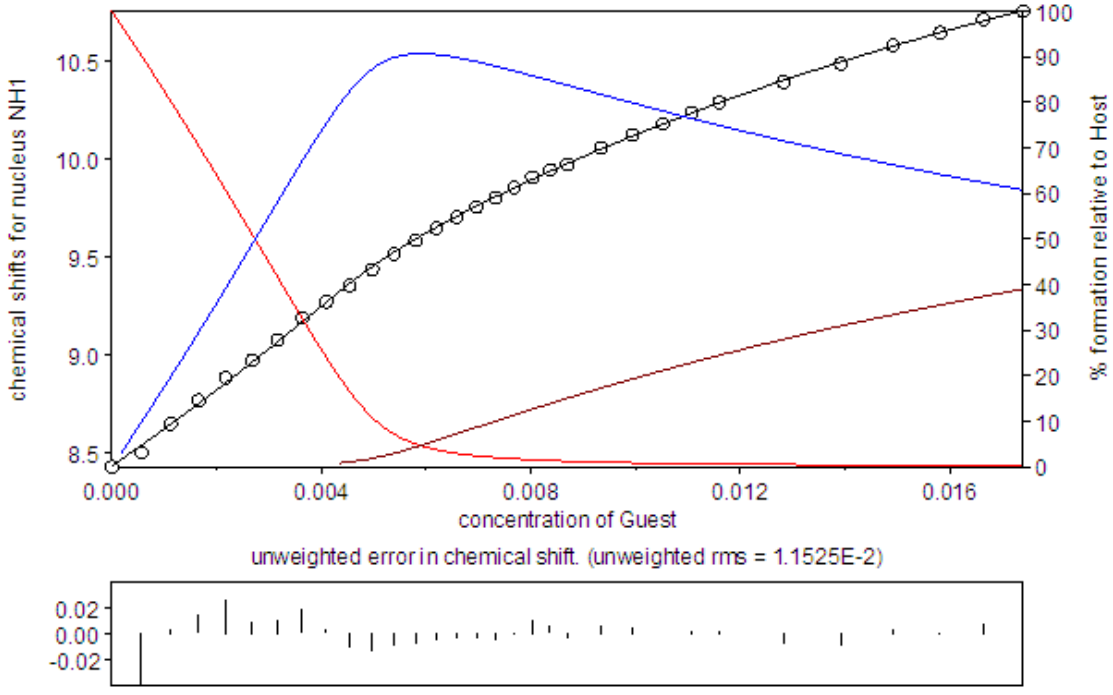
chemical shifts for nucleus NH1
% formation relative to Host
concentration of Guest
unweighted error in chemical shift. (unweighted rms = 1.1525E-2)

(f)

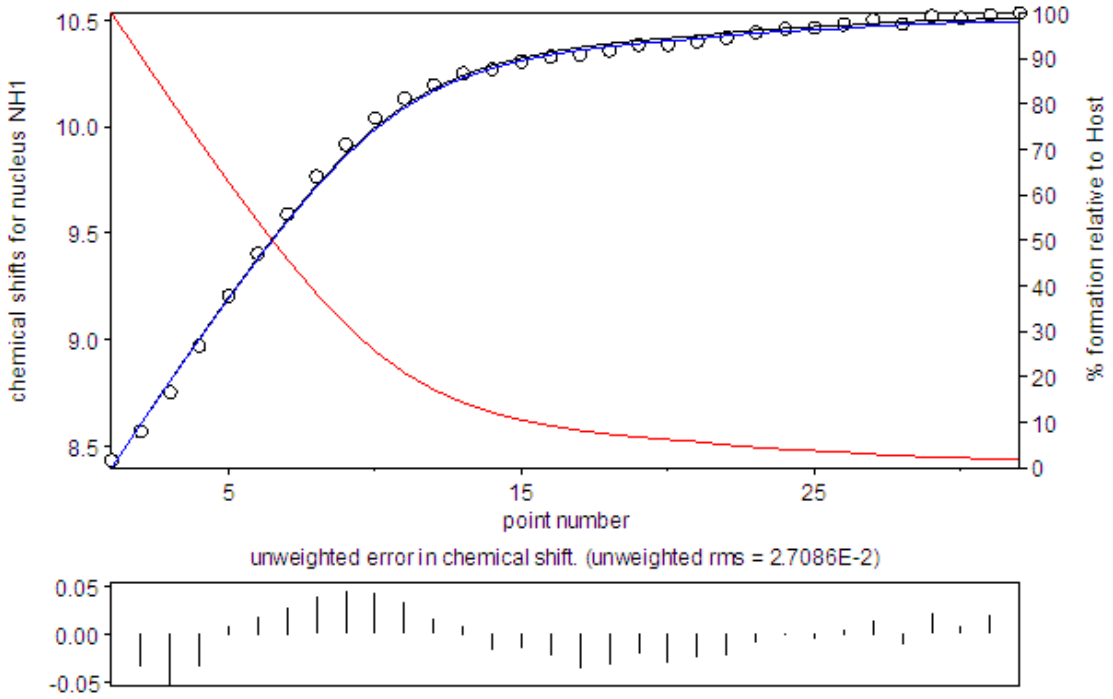

(g)

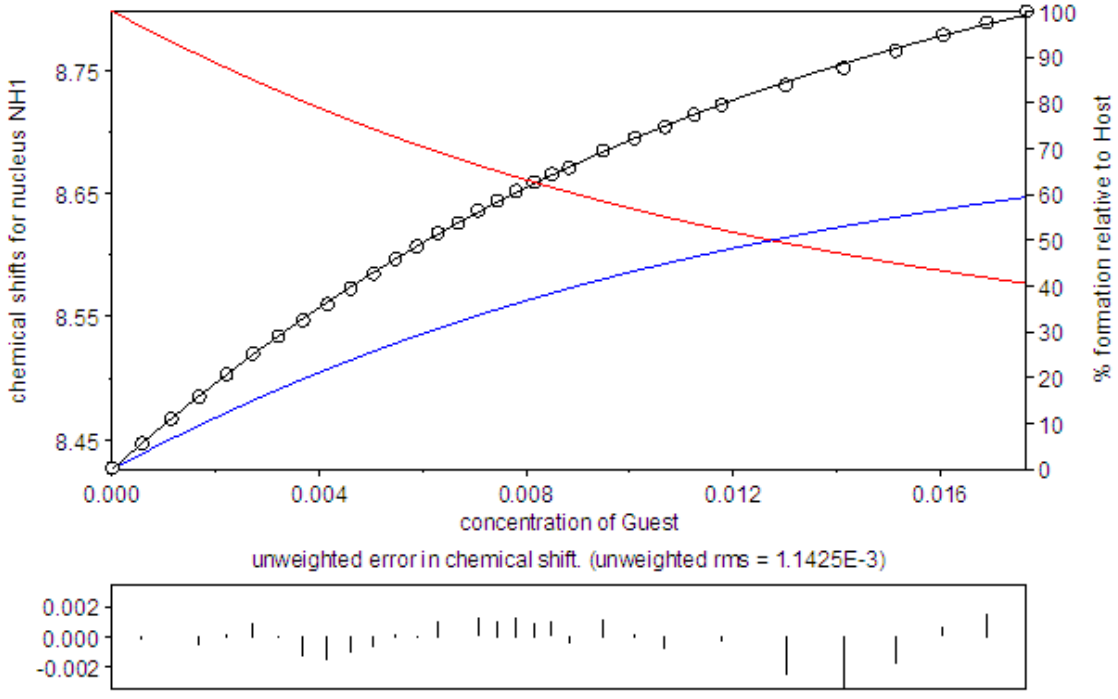

AIV.5 Speciation plot showing experimental data from ^{1}H NMR spectroscopic titrations on compound **139** in $CDCl_3$/DMSO-d_6 (*v/v* 70/30) and the fit for the calculated binding constants for (a) chloride, (b) bromide, (c) nitrate, (d) acetate, (e) fluoride, (f) dihydrogen phosphate and (g) hydrogen sulfate

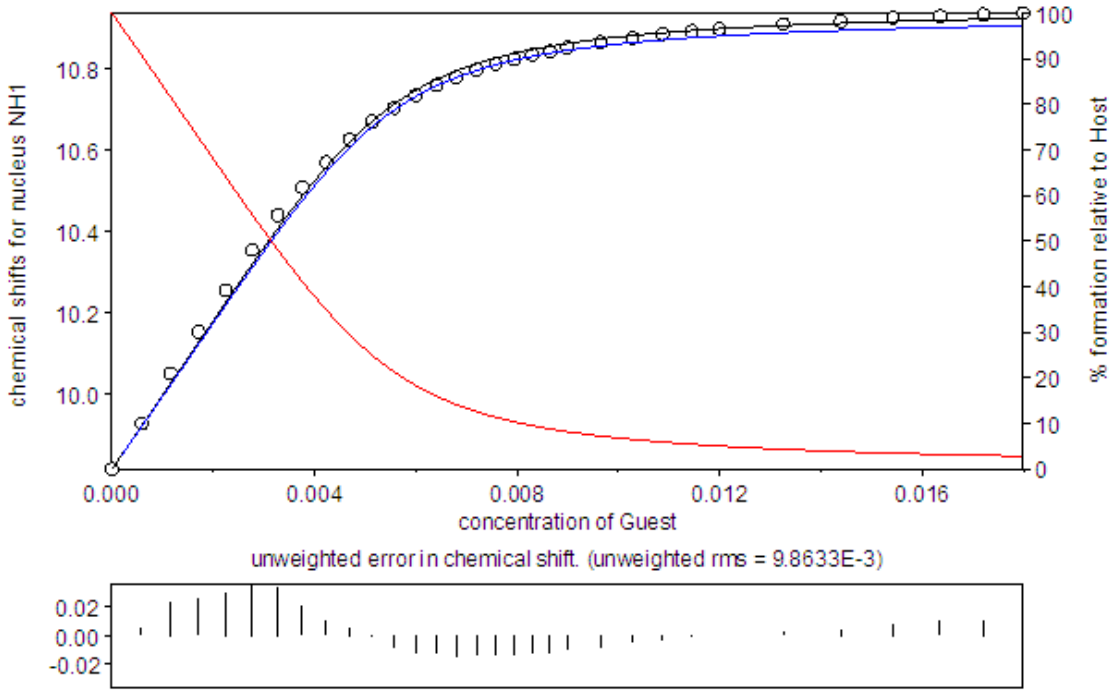

AIV.6 Speciation plot showing experimental data from ^{1}H NMR spectroscopic titrations on compound **144** in $CDCl_3$/DMSO-d_6 (*v/v* 70/30) and the fit for the calculated binding constants for chloride

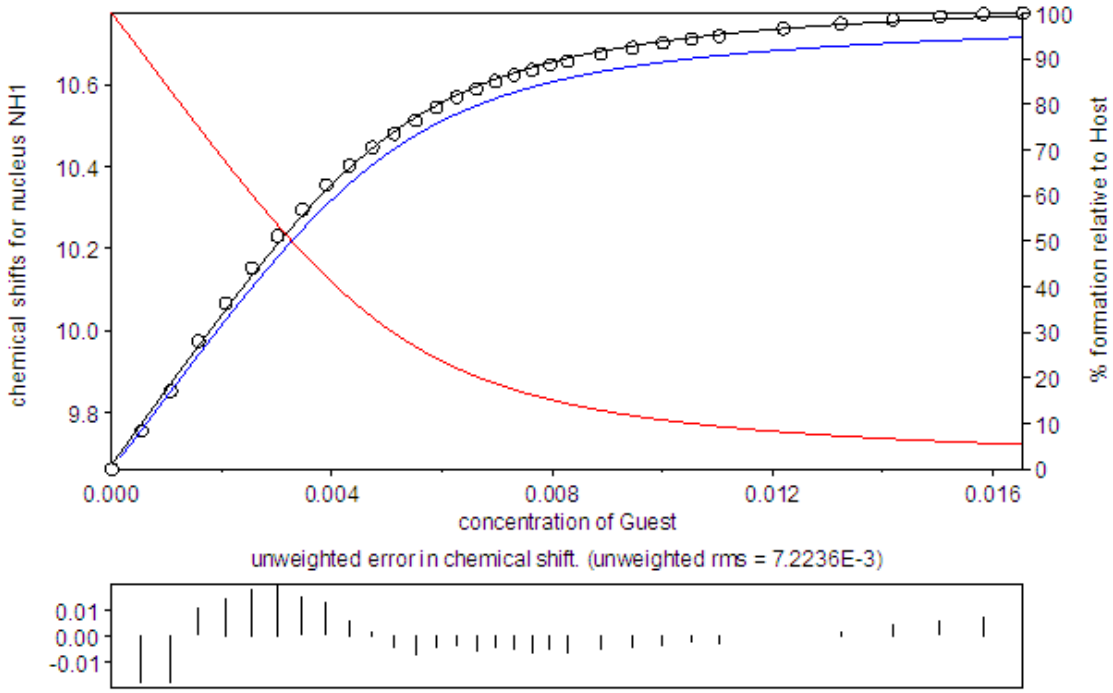

AIV.7 Speciation plot showing experimental data from ^{1}H NMR spectroscopic titrations on compound **145** in $CDCl_3$/DMSO-d_6 (*v/v* 70/30) and the fit for the calculated binding constants for chloride

(a)

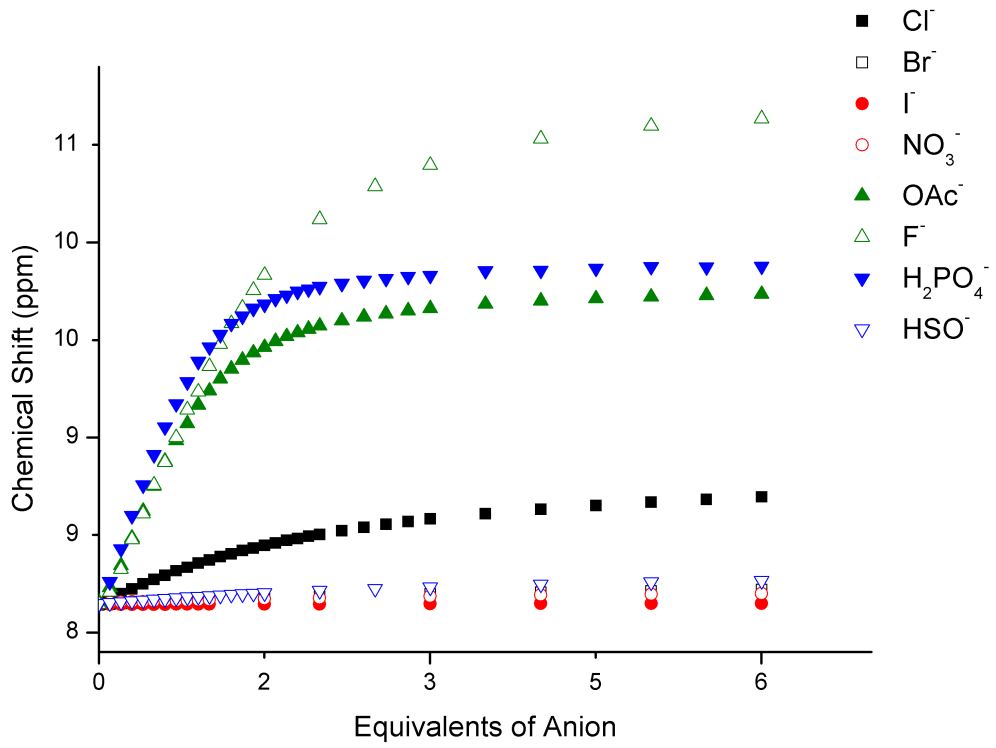
Chemical Shift (ppm)
Equivalents of Anion
Cl-
Br-
I-
NO3-
OAc-
F-
H2PO4-
HSO4-

(b)

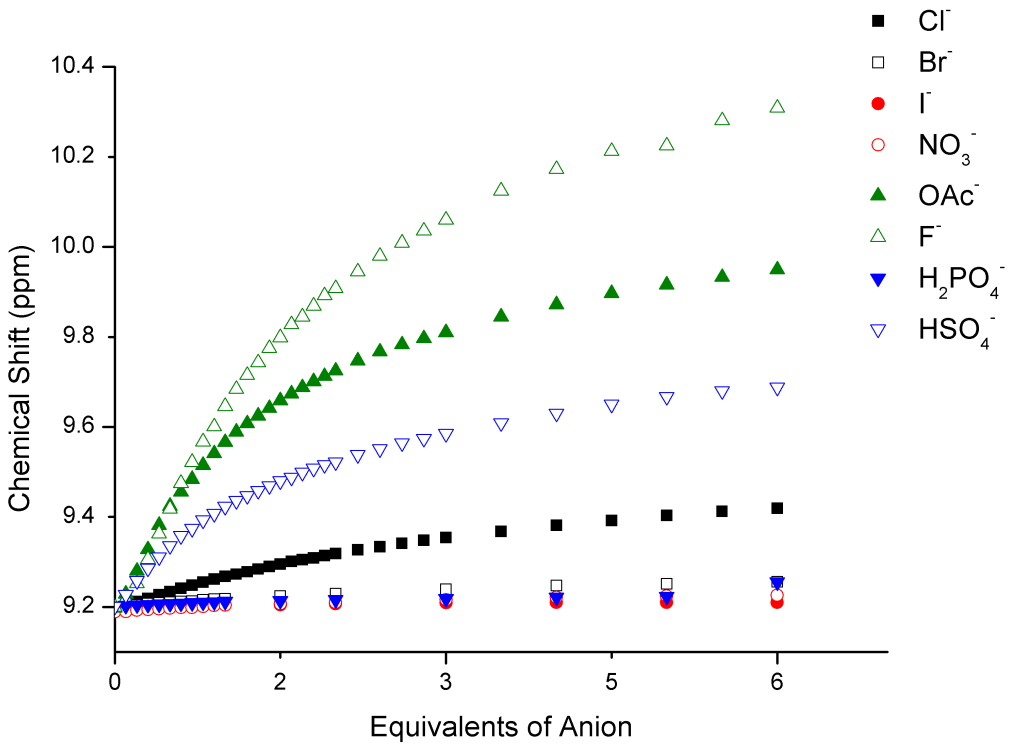
Chemical Shift (ppm)
Equivalents of Anion
Cl-
Br-
I-
NO3-
OAc-
F-
H2PO4-
HSO4-

(c)

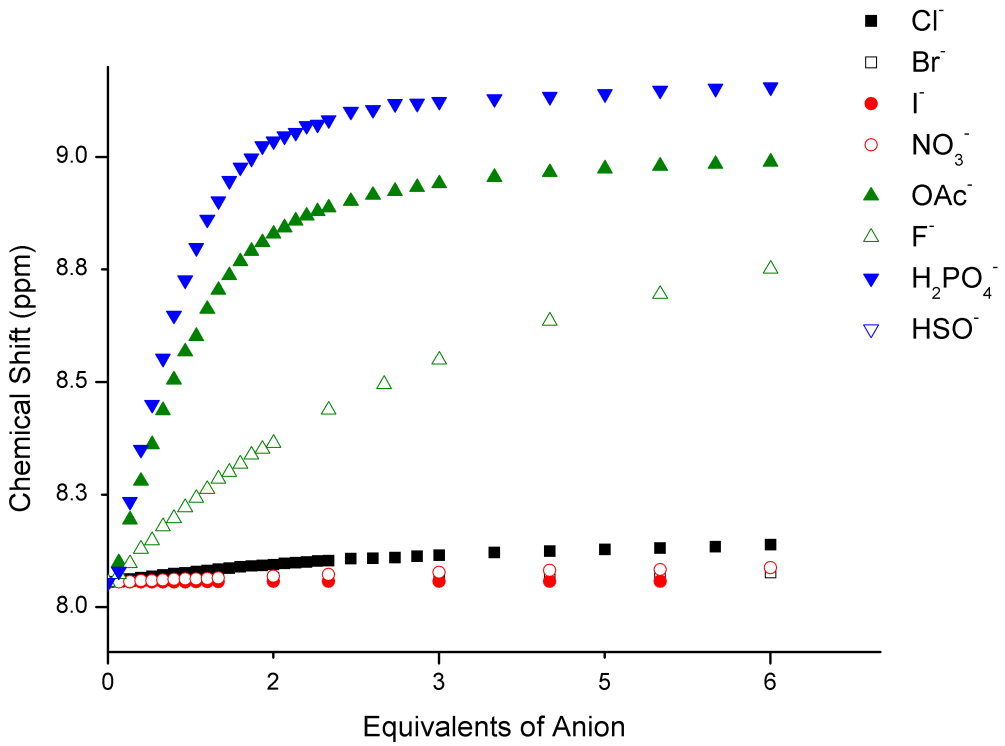

(d)

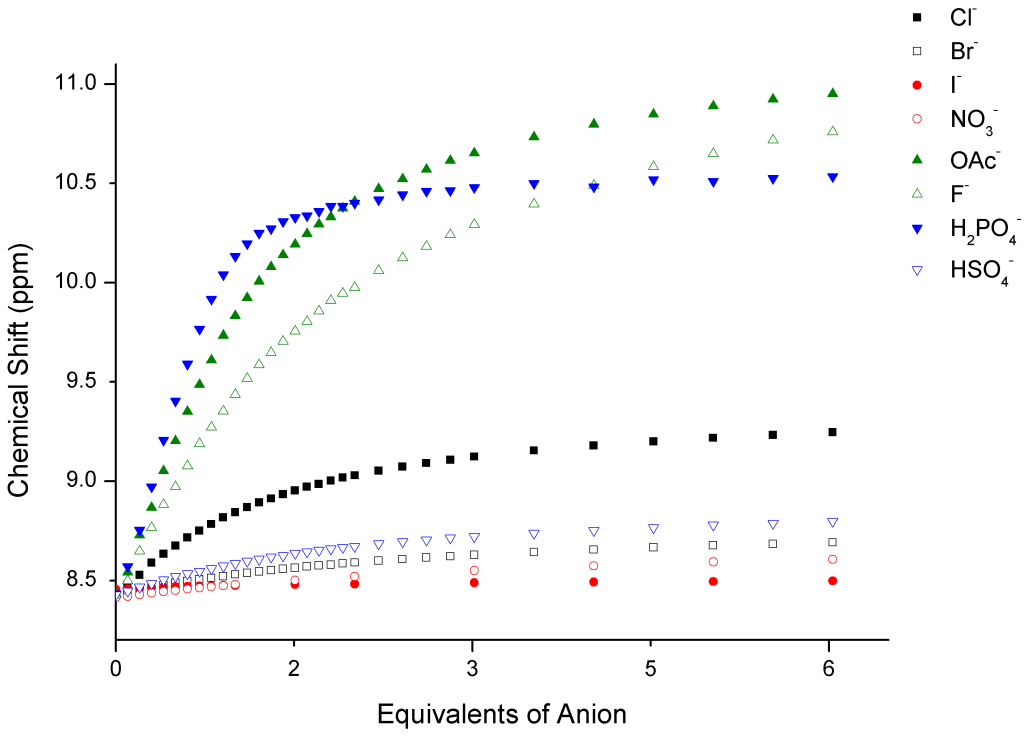

AIV.8 Binding isotherms with a range of anions, observed using ^{1}H NMR spectroscopy in $CDCl_3$/DMSO-d_6 (*v/v* 70/30) for (a) **136**, (b) **137**, (c) **138**, (d) **139**

(a)

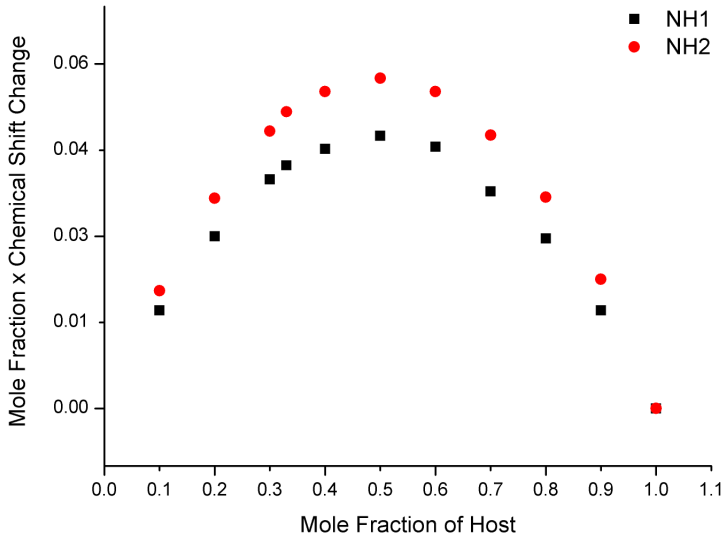
NH1
NH2
Mole Fraction x Chemical Shift Change
0.00
0.01
0.03
0.04
0.06
0.0
0.1
0.2
0.3
0.4
0.5
0.6
0.7
0.8
0.9
1.0
1.1
Mole Fraction of Host

(b)

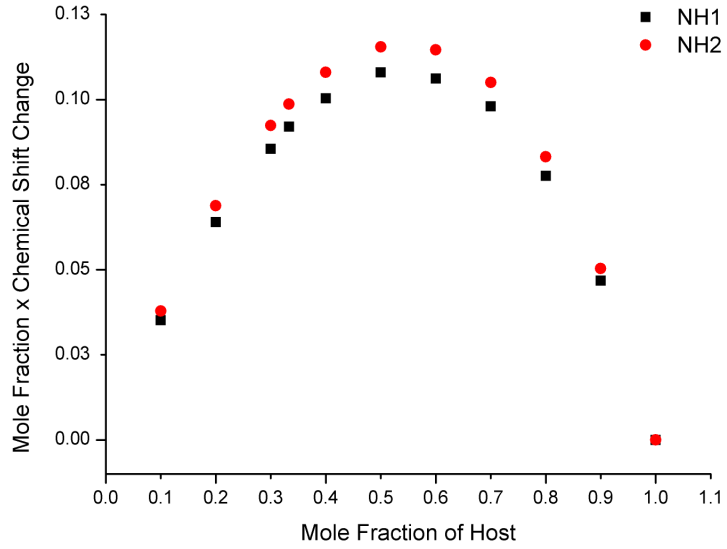
NH1
NH2
Mole Fraction x Chemical Shift Change
0.00
0.03
0.05
0.08
0.10
0.13
0.0
0.1
0.2
0.3
0.4
0.5
0.6
0.7
0.8
0.9
1.0
1.1
Mole Fraction of Host

(c)

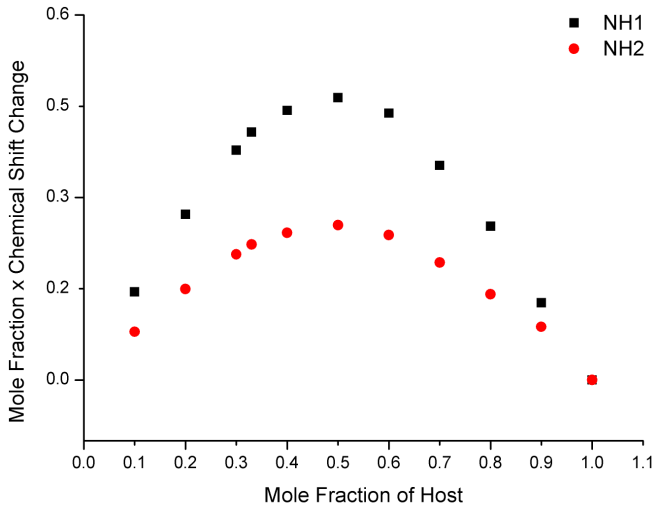

(d)

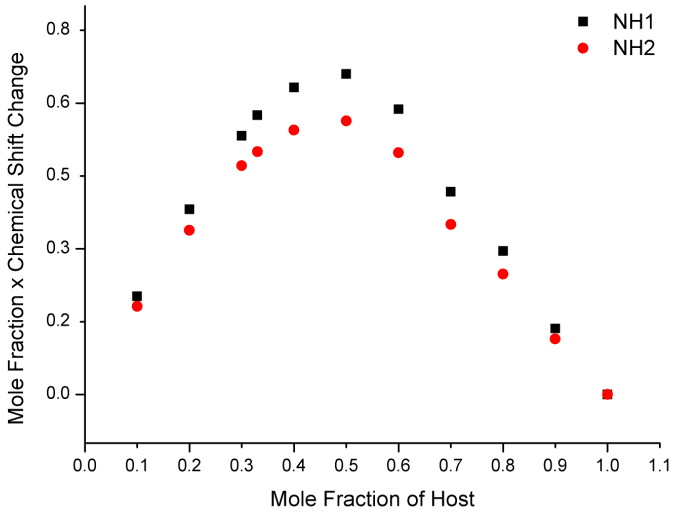

AIV.9 Job Plot in $CDCl_3$/DMSO-d_6 (*v/v* 70/30) for (a) **136** with TBA-Cl, (b) **137** with TBA-OAc, (c) **138** with TBA-OAc and (d) **139** with TBA-OAc

(a)

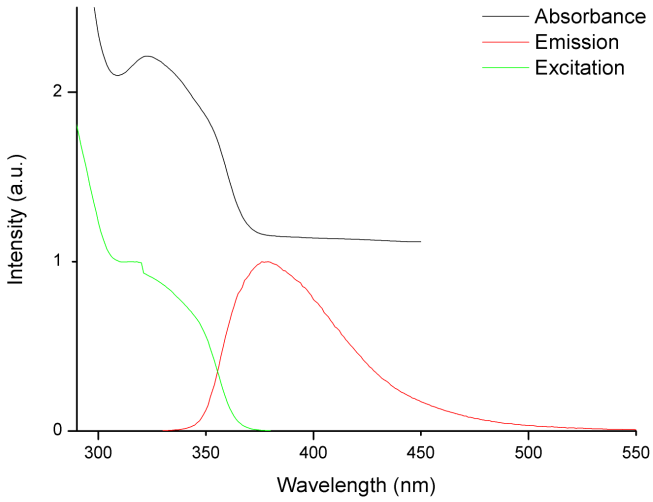
Absorbance
Emission
Excitation
Intensity (a.u.)
0
1
2
300
350
400
450
500
550
Wavelength (nm)

(b)

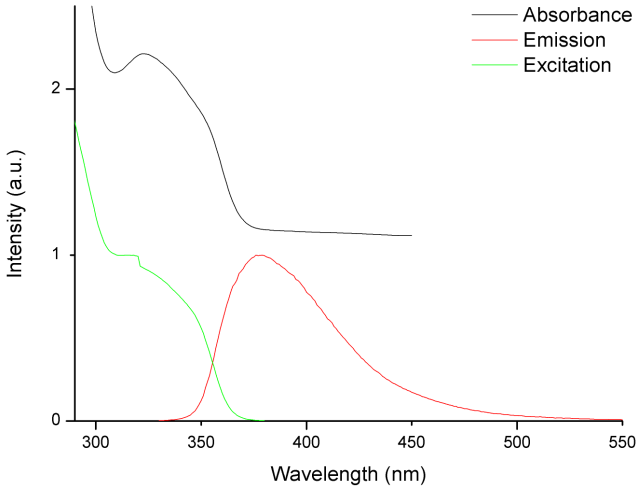
Absorbance
Emission
Excitation
Intensity (a.u.)
0
1
2
300
350
400
450
500
550
Wavelength (nm)

(c)

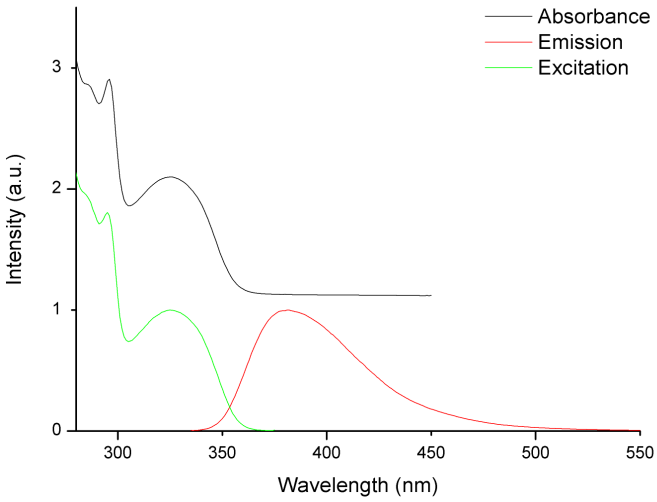

(d)

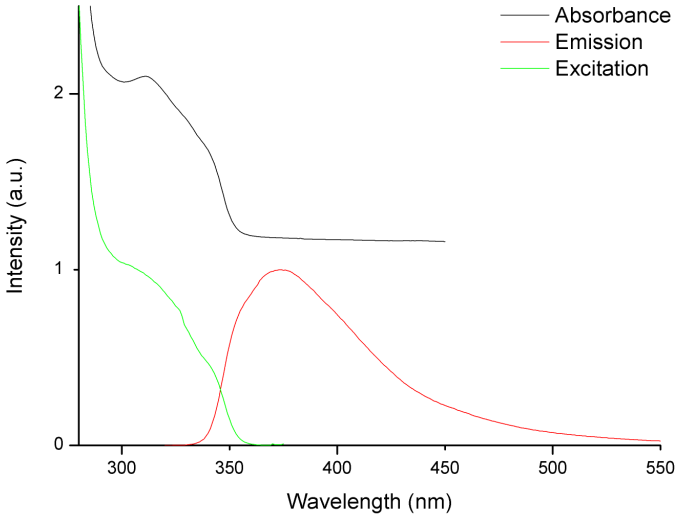

AIV.10 Absorbance, excitation and emission spectra for (a) **136** (λ_{ex} = 320 nm, λ_{em} = 375 nm), (b) **137** (λ_{ex} = 320 nm, λ_{em} = 370 nm), (c) **138** (λ_{ex} = 325 nm, λ_{em} = 380 nm) and (d) **139** (λ_{ex} = 310 nm, λ_{em} = 374 nm) in $CDCl_3$/DMSO-d_6 (*v/v* 95/5)

(a)

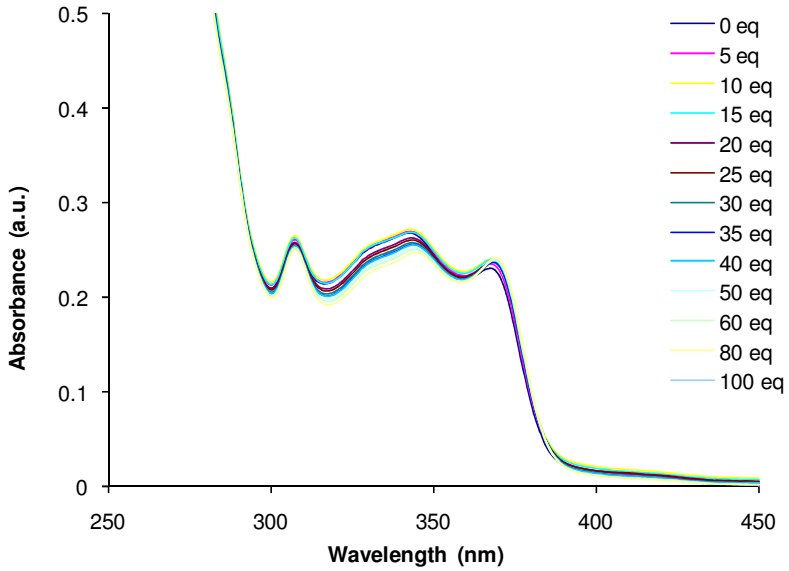
0.5
0.4
0.3
0.2
0.1
0
Absorbance (a.u.)
250
300
350
400
450
Wavelength (nm)
0 eq
5 eq
10 eq
15 eq
20 eq
25 eq
30 eq
35 eq
40 eq
50 eq
60 eq
80 eq
100 eq

(b)

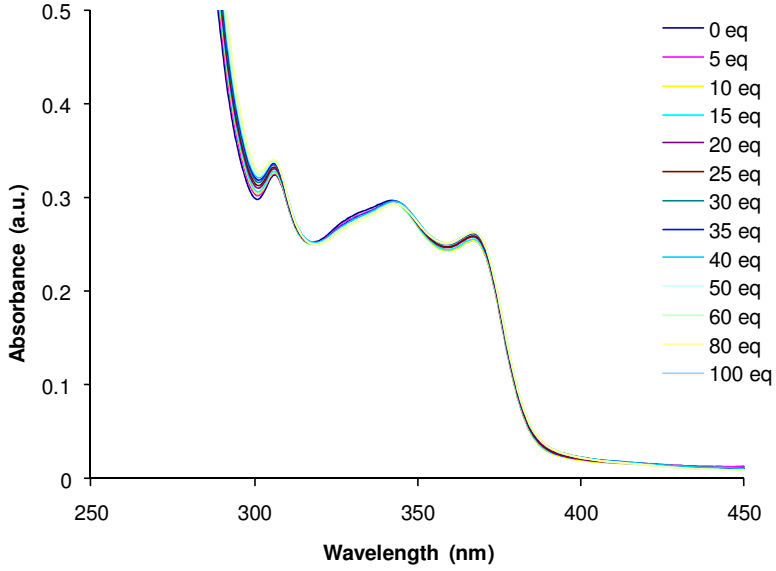
0.5
0.4
0.3
0.2
0.1
0
Absorbance (a.u.)
250
300
350
400
450
Wavelength (nm)
0 eq
5 eq
10 eq
15 eq
20 eq
25 eq
30 eq
35 eq
40 eq
50 eq
60 eq
80 eq
100 eq

(c)

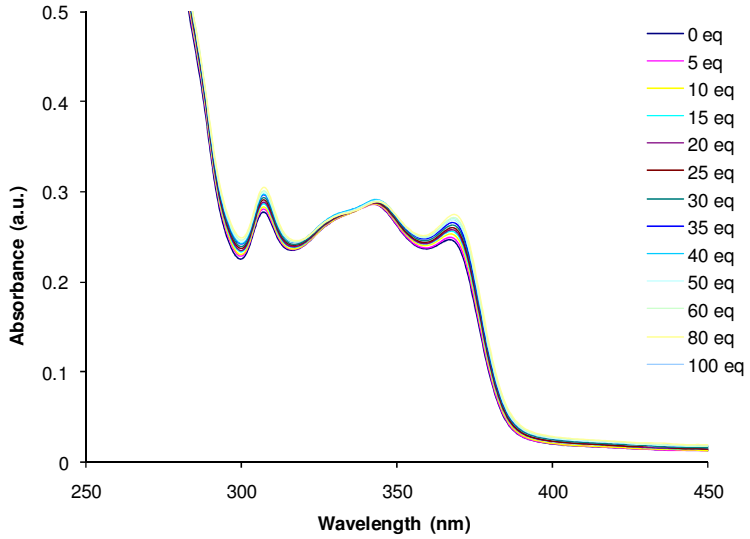
0.5
0.4
0.3
0.2
0.1
0
Absorbance (a.u.)
250
300
350
400
450
Wavelength (nm)
0 eq
5 eq
10 eq
15 eq
20 eq
25 eq
30 eq
35 eq
40 eq
50 eq
60 eq
80 eq
100 eq

(d)

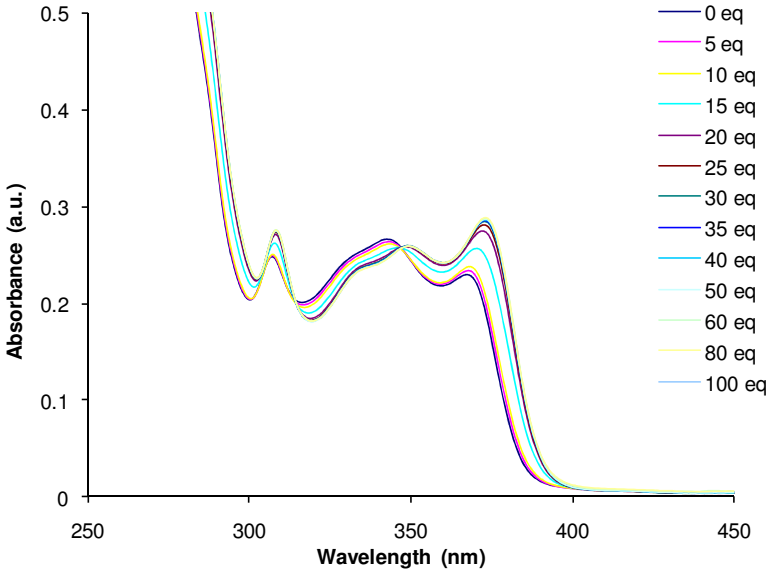
0.5
0.4
0.3
0.2
0.1
0
Absorbance (a.u.)
250
300
350
400
450
Wavelength (nm)
0 eq
5 eq
10 eq
15 eq
20 eq
25 eq
30 eq
35 eq
40 eq
50 eq
60 eq
80 eq
100 eq

(e)

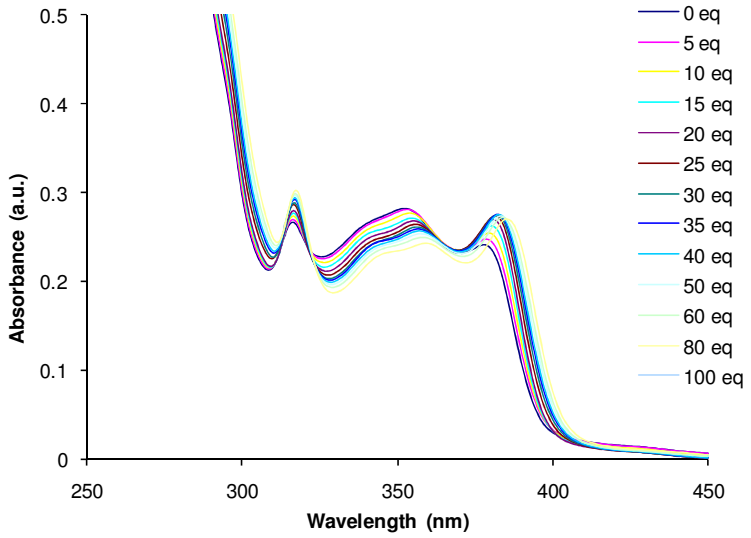
0.5
0.4
0.3
0.2
0.1
0
Absorbance (a.u.)
250
300
350
400
450
Wavelength (nm)
0 eq
5 eq
10 eq
15 eq
20 eq
25 eq
30 eq
35 eq
40 eq
50 eq
60 eq
80 eq
100 eq

(f)

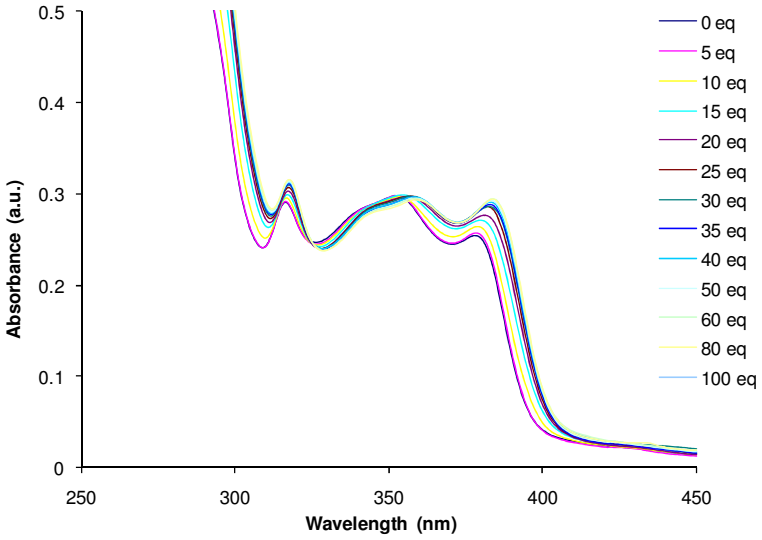
0.5
0.4
0.3
0.2
0.1
0
Absorbance (a.u.)
250
300
350
400
450
Wavelength (nm)
0 eq
5 eq
10 eq
15 eq
20 eq
25 eq
30 eq
35 eq
40 eq
50 eq
60 eq
80 eq
100 eq

(g)

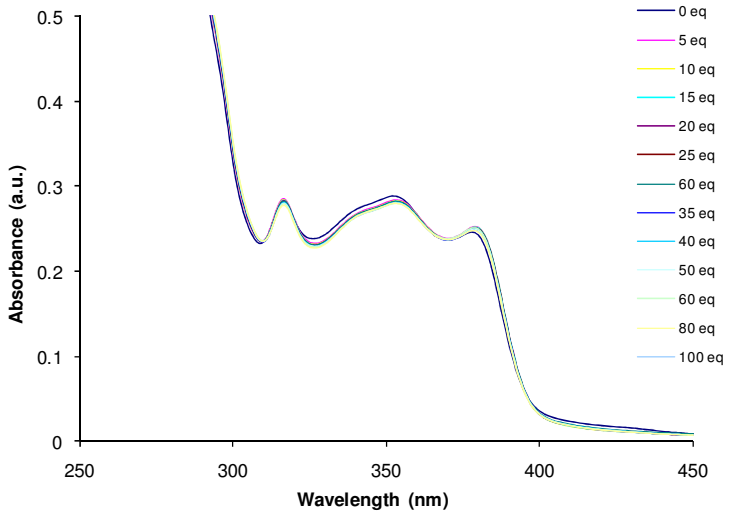

AIV.11 UV-vis spectroscopic titrations of **135** (1.0×10^{-5} mol dm^{-3} in $CDCl_3$/DMSO-d_6 *v/v* 95/5) with (a) bromide, (b) iodide, (c) nitrate, (d) acetate (e) fluoride, (f) dihydrogen phosphate and (g) hydrogen sulfate used as TBA salts

(a)

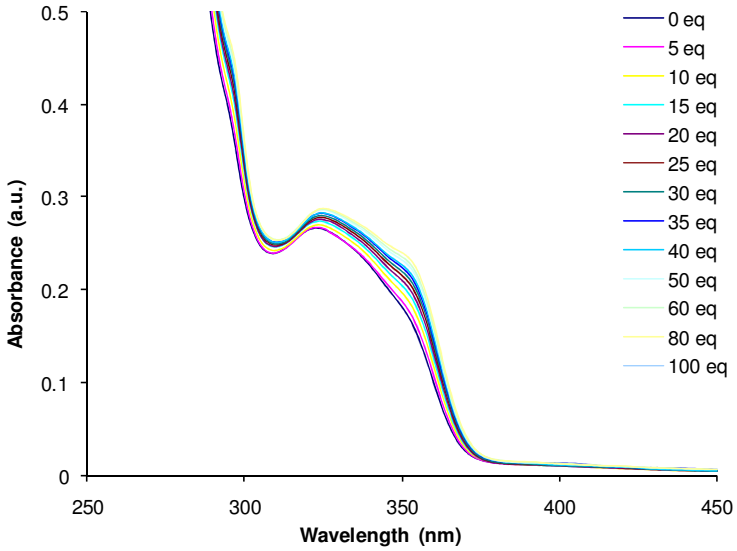

(b)

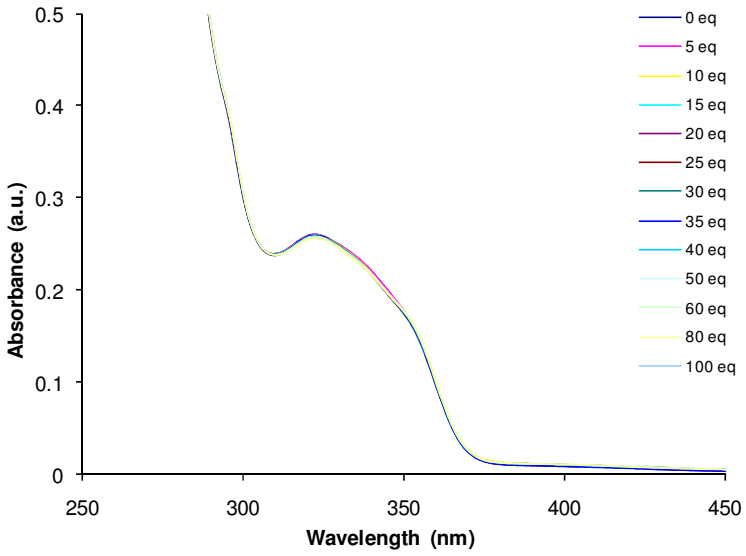
0.5
0.4
0.3
0.2
0.1
0
Absorbance (a.u.)
250
300
350
400
450
Wavelength (nm)
0 eq
5 eq
10 eq
15 eq
20 eq
25 eq
30 eq
35 eq
40 eq
50 eq
60 eq
80 eq
100 eq

(c)

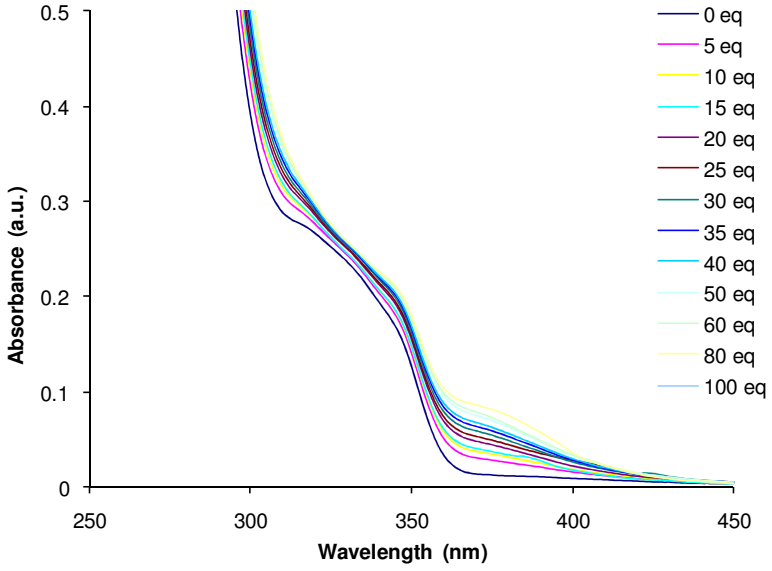
0.5
0.4
0.3
0.2
0.1
0
Absorbance (a.u.)
250
300
350
400
450
Wavelength (nm)
0 eq
5 eq
10 eq
15 eq
20 eq
25 eq
30 eq
35 eq
40 eq
50 eq
60 eq
80 eq
100 eq

(d)

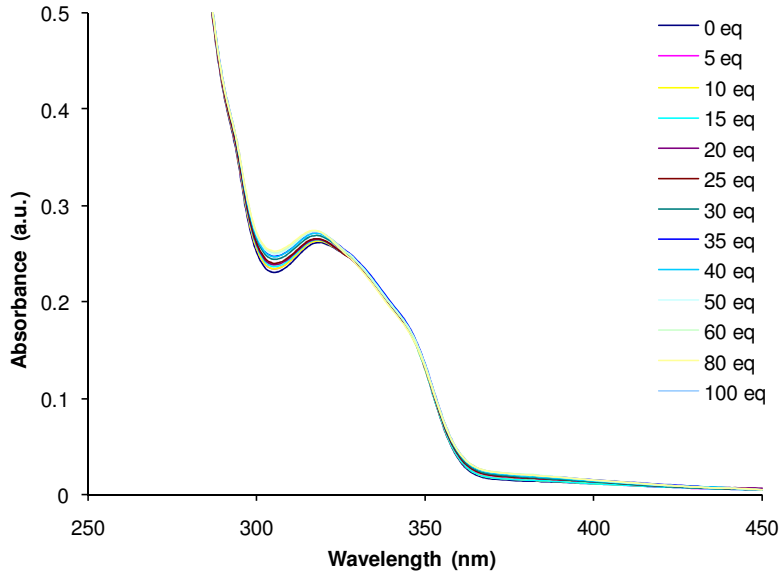
0.5
0.4
0.3
0.2
0.1
0
Absorbance (a.u.)
250
300
350
400
450
Wavelength (nm)
0 eq
5 eq
10 eq
15 eq
20 eq
25 eq
30 eq
35 eq
40 eq
50 eq
60 eq
80 eq
100 eq

(e)

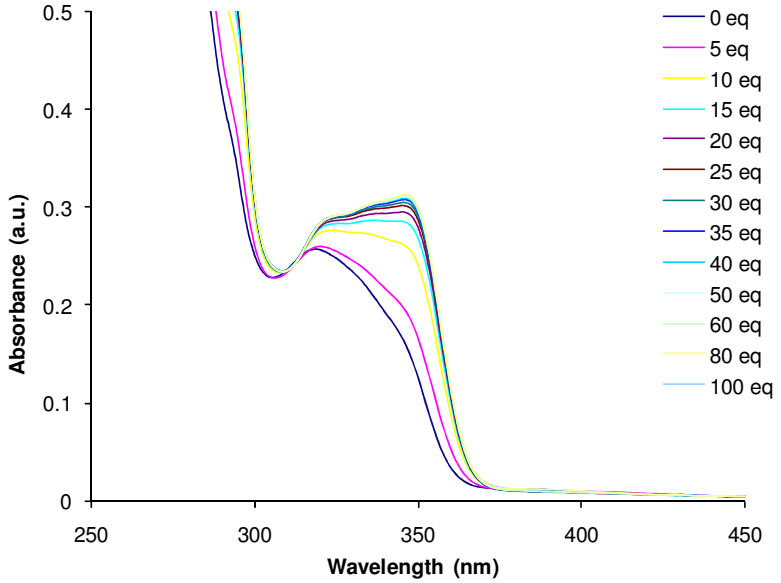
0.5
0.4
0.3
0.2
0.1
0
Absorbance (a.u.)
250
300
350
400
450
Wavelength (nm)
0 eq
5 eq
10 eq
15 eq
20 eq
25 eq
30 eq
35 eq
40 eq
50 eq
60 eq
80 eq
100 eq

(f)

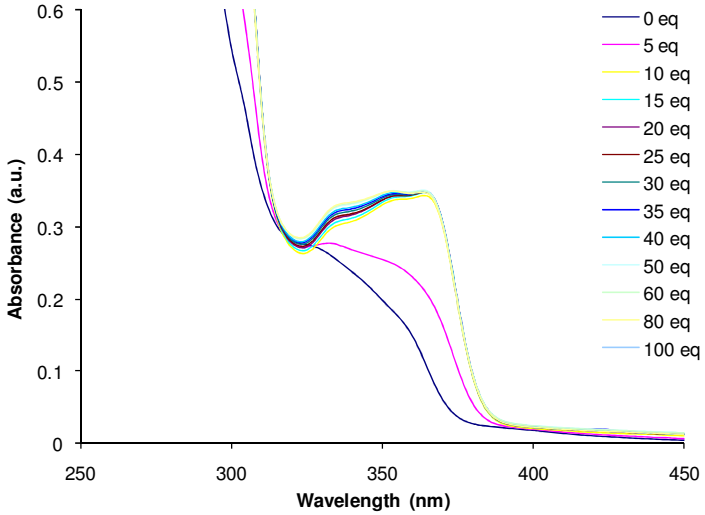

(g)

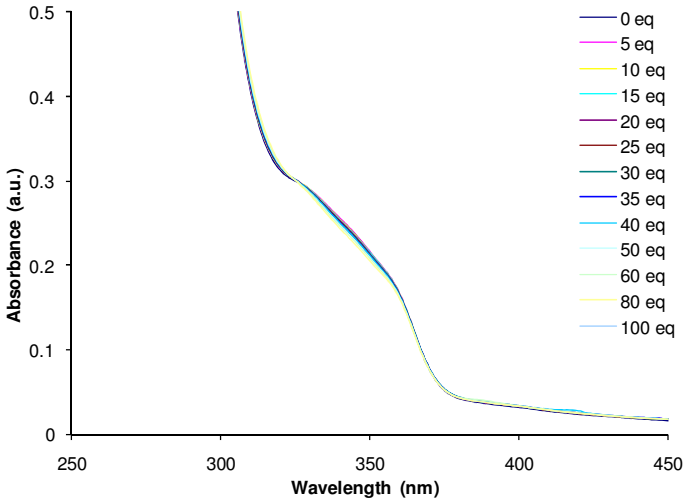

AIV.12 UV-vis spectroscopic titrations of **136** (2.5 x 10^{-5} mol dm^{-3} in $CDCl_3$/DMSO-d_6 *v/v* 95/5) with (a) chloride, (b) bromide, (c) iodide, (d) nitrate, (e) acetate, (f) fluoride and (g) hydrogen sulfate used as TBA salts

(a)

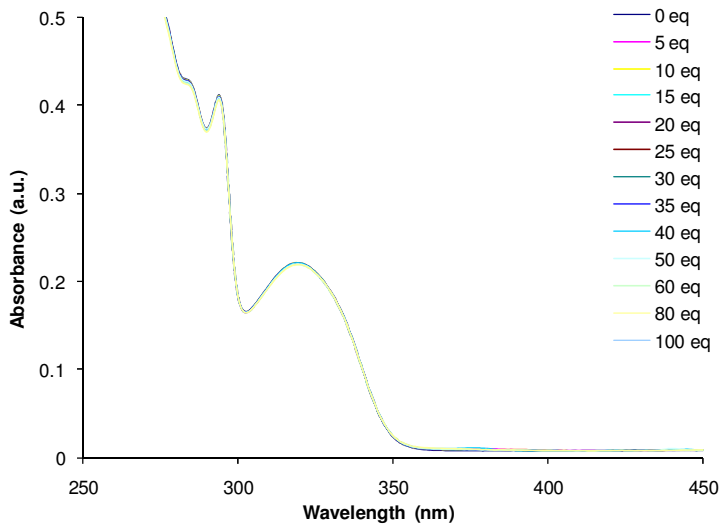
0.5
0.4
0.3
0.2
0.1
0
Absorbance (a.u.)
250
300
350
400
450
Wavelength (nm)
0 eq
5 eq
10 eq
15 eq
20 eq
25 eq
30 eq
35 eq
40 eq
50 eq
60 eq
80 eq
100 eq

(b)

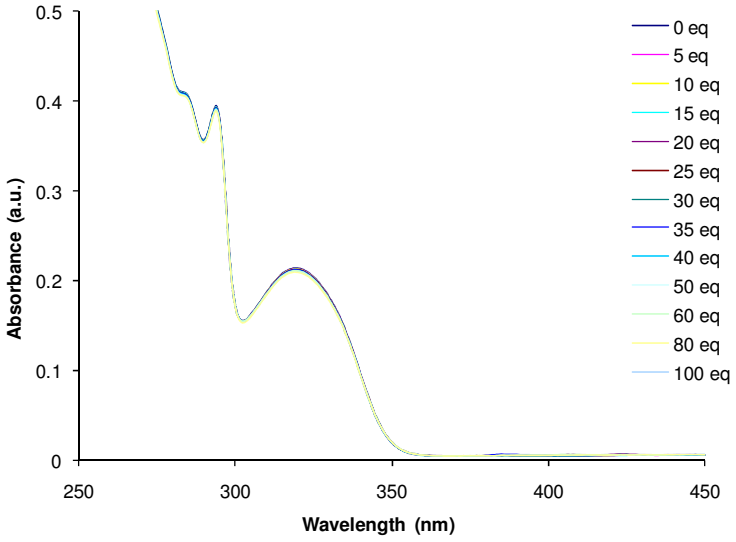
0.5
0.4
0.3
0.2
0.1
0
Absorbance (a.u.)
250
300
350
400
450
Wavelength (nm)
0 eq
5 eq
10 eq
15 eq
20 eq
25 eq
30 eq
35 eq
40 eq
50 eq
60 eq
80 eq
100 eq

(c)

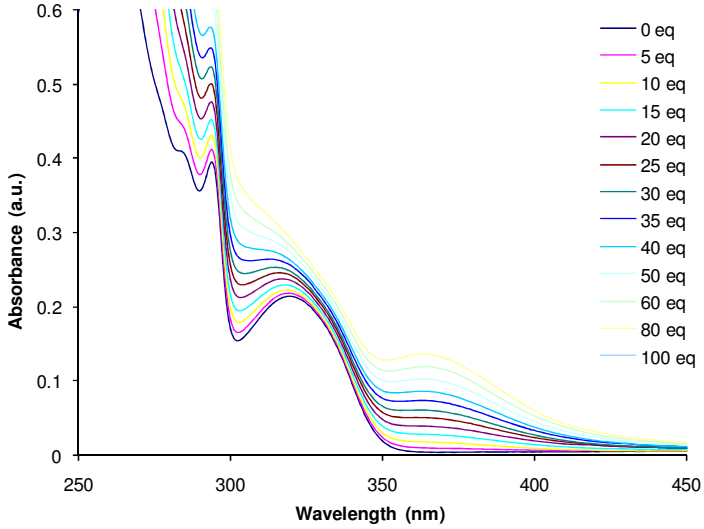
0.6
0.5
0.4
0.3
0.2
0.1
0
Absorbance (a.u.)
250
300
350
400
450
Wavelength (nm)
0 eq
5 eq
10 eq
15 eq
20 eq
25 eq
30 eq
35 eq
40 eq
50 eq
60 eq
80 eq
100 eq

(d)

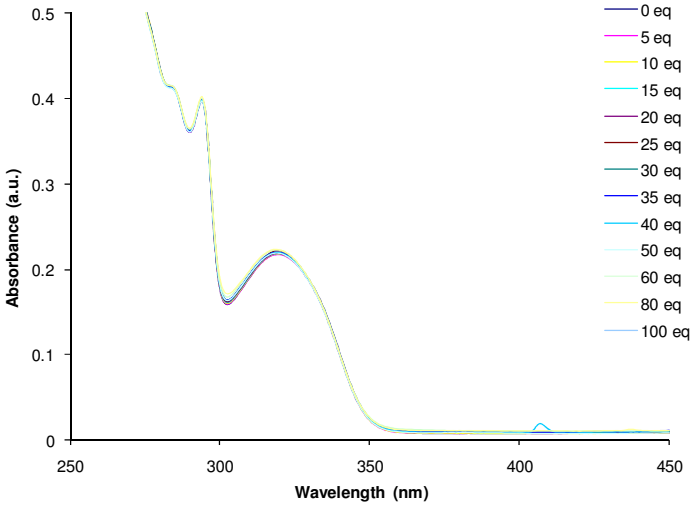
0.5
0.4
0.3
0.2
0.1
0
Absorbance (a.u.)
250
300
350
400
450
Wavelength (nm)
0 eq
5 eq
10 eq
15 eq
20 eq
25 eq
30 eq
35 eq
40 eq
50 eq
60 eq
80 eq
100 eq

(e)

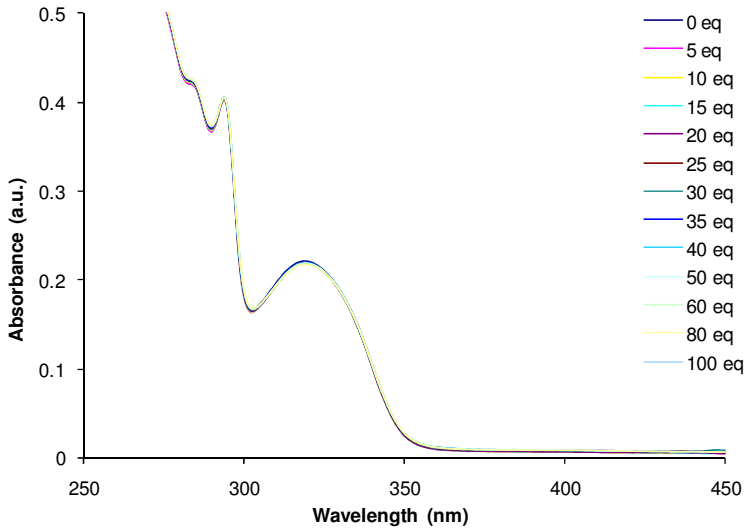
0.5
0.4
0.3
0.2
0.1
0
Absorbance (a.u.)
250
300
350
400
450
Wavelength (nm)
0 eq
5 eq
10 eq
15 eq
20 eq
25 eq
30 eq
35 eq
40 eq
50 eq
60 eq
80 eq
100 eq

(f)

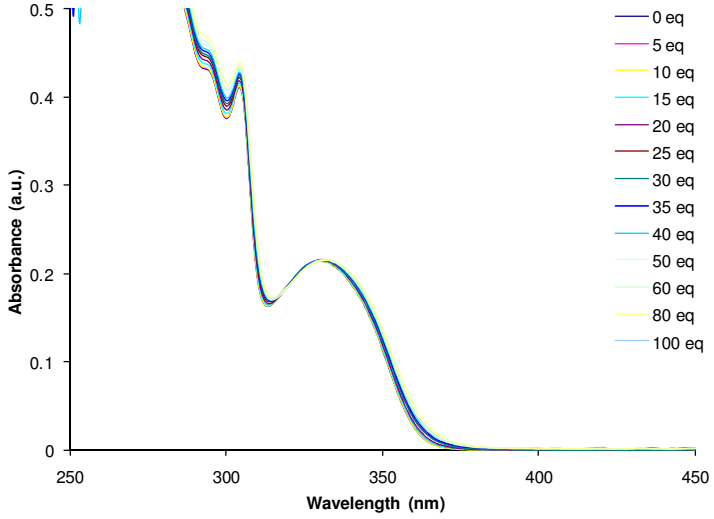
0.5
0.4
0.3
0.2
0.1
0
Absorbance (a.u.)
250
300
350
400
450
Wavelength (nm)
0 eq
5 eq
10 eq
15 eq
20 eq
25 eq
30 eq
35 eq
40 eq
50 eq
60 eq
80 eq
100 eq

(g)

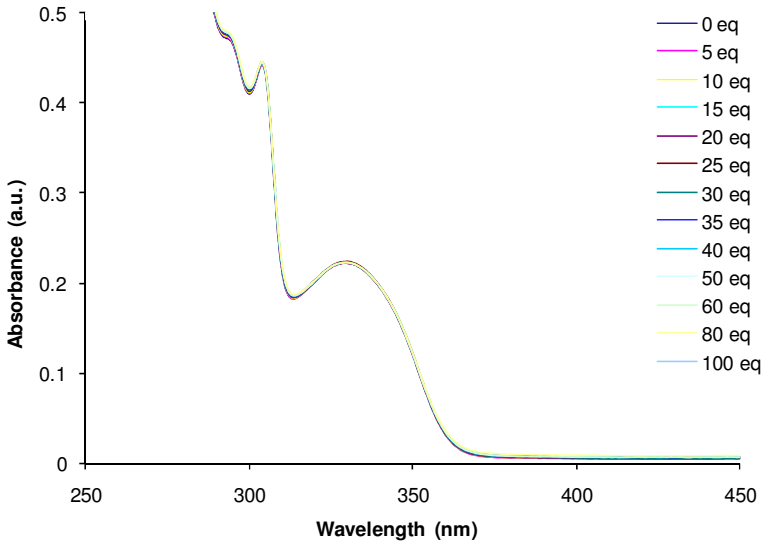

(h)

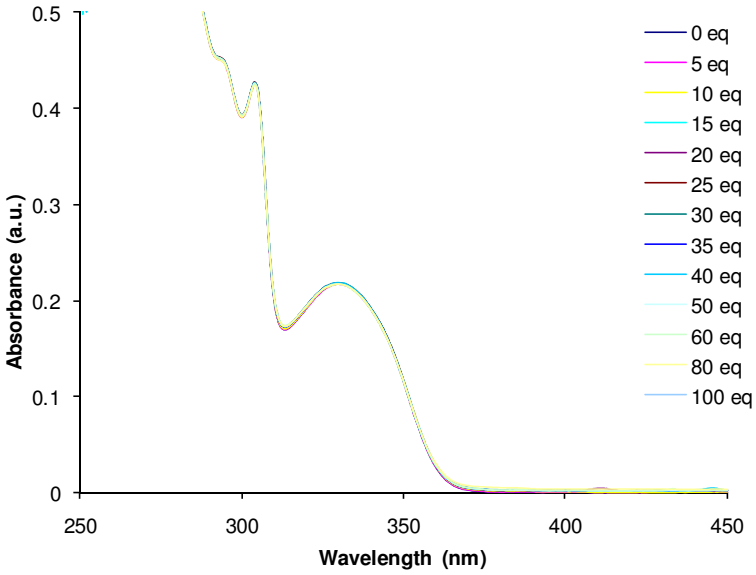

AIV.13 UV-vis spectroscopic titrations of **137** (2.0×10^{-5} mol dm^{-3} in $CDCl_3$/DMSO-d_6 *v/v* 95/5) with (a) chloride, (b) bromide, (c) iodide, (d) nitrate, (e) acetate, (f) fluoride, (g) dihydrogen phosphate and (h) hydrogen sulfate used as TBA salts

(a)

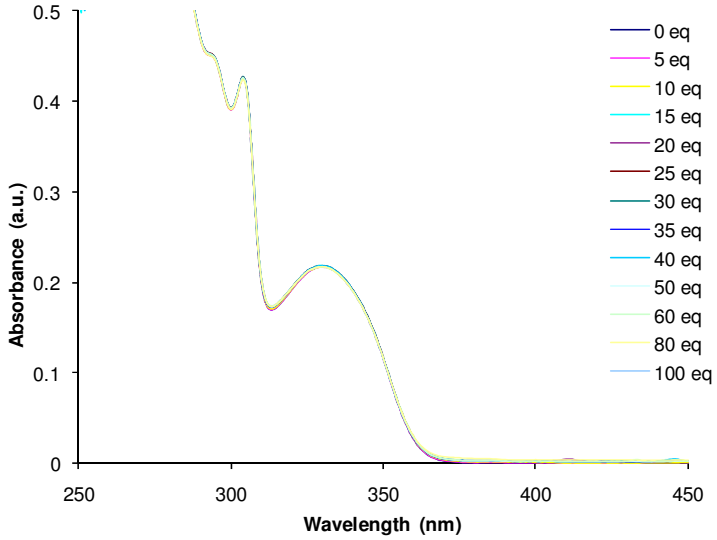
0.5
0.4
0.3
0.2
0.1
0
Absorbance (a.u.)
250
300
350
400
450
Wavelength (nm)
0 eq
5 eq
10 eq
15 eq
20 eq
25 eq
30 eq
35 eq
40 eq
50 eq
60 eq
80 eq
100 eq

(b)

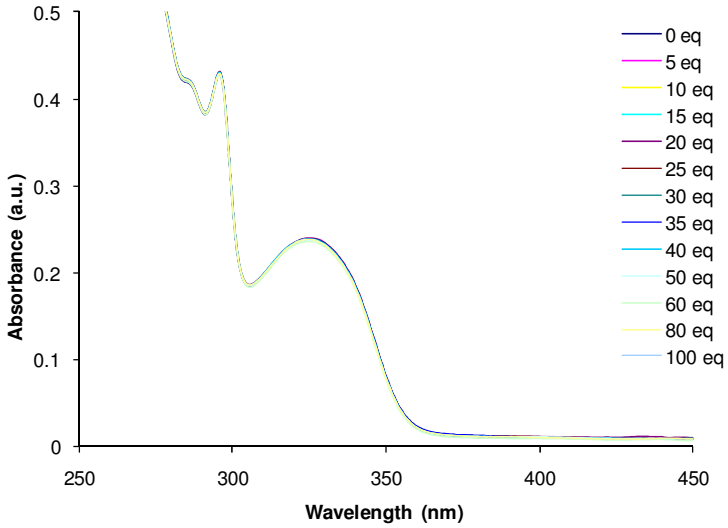
0.5
0.4
0.3
0.2
0.1
0
Absorbance (a.u.)
250
300
350
400
450
Wavelength (nm)
0 eq
5 eq
10 eq
15 eq
20 eq
25 eq
30 eq
35 eq
40 eq
50 eq
60 eq
80 eq
100 eq

(c)

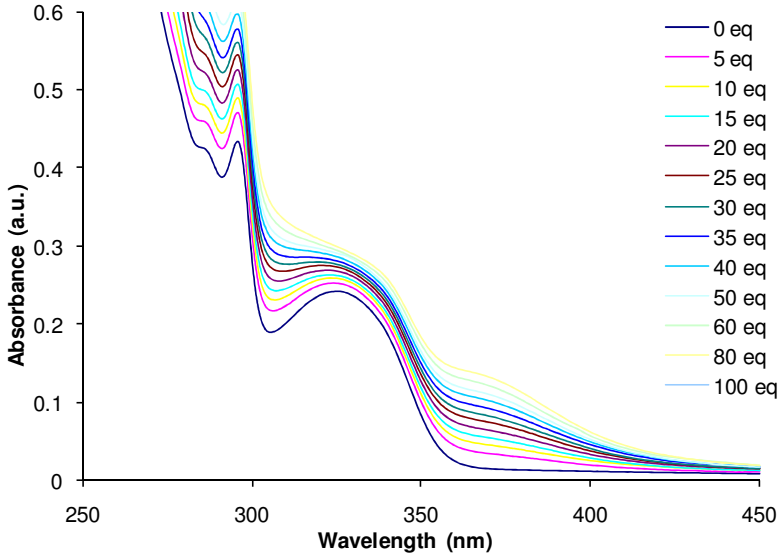
0.6
0.5
0.4
0.3
0.2
0.1
0
Absorbance (a.u.)
250
300
350
400
450
Wavelength (nm)
0 eq
5 eq
10 eq
15 eq
20 eq
25 eq
30 eq
35 eq
40 eq
50 eq
60 eq
80 eq
100 eq

(d)

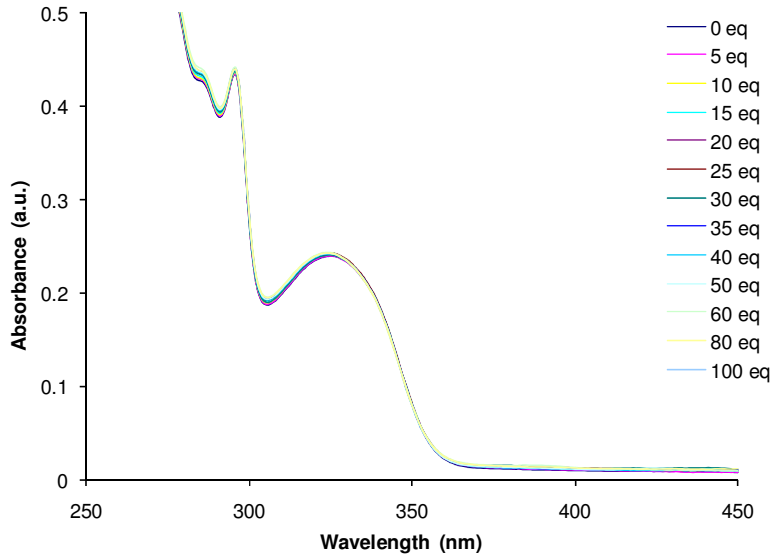
0.5
0.4
0.3
0.2
0.1
0
Absorbance (a.u.)
250
300
350
400
450
Wavelength (nm)
0 eq
5 eq
10 eq
15 eq
20 eq
25 eq
30 eq
35 eq
40 eq
50 eq
60 eq
80 eq
100 eq

(e)

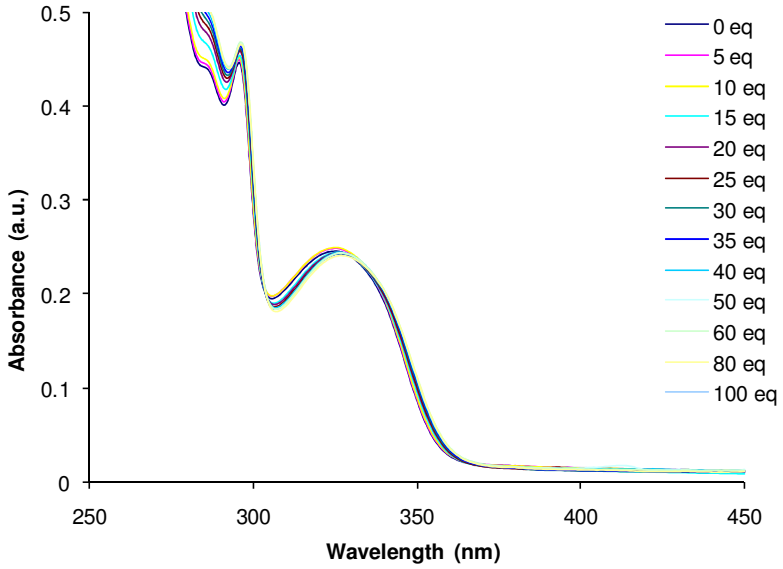
0.5
0.4
0.3
0.2
0.1
0
Absorbance (a.u.)
250
300
350
400
450
Wavelength (nm)
0 eq
5 eq
10 eq
15 eq
20 eq
25 eq
30 eq
35 eq
40 eq
50 eq
60 eq
80 eq
100 eq

(f)

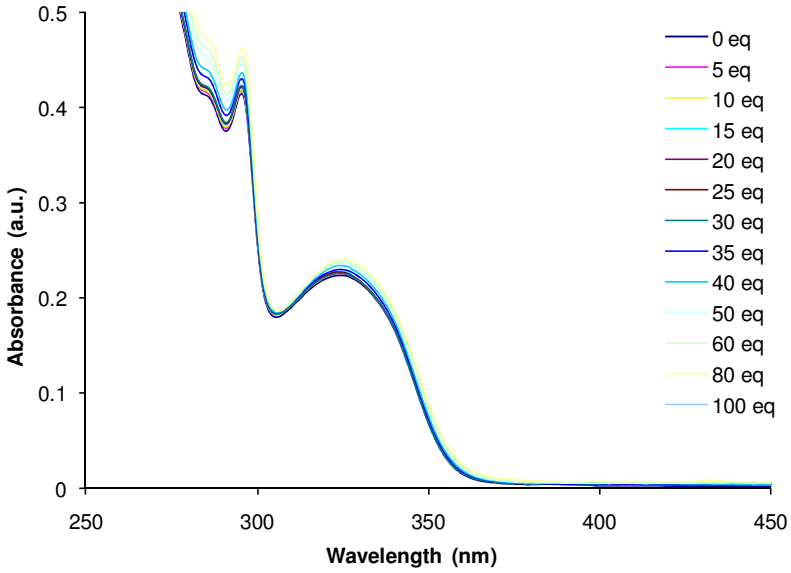
0.5
0.4
0.3
0.2
0.1
0
Absorbance (a.u.)
250
300
350
400
450
Wavelength (nm)
0 eq
5 eq
10 eq
15 eq
20 eq
25 eq
30 eq
35 eq
40 eq
50 eq
60 eq
80 eq
100 eq

(g)

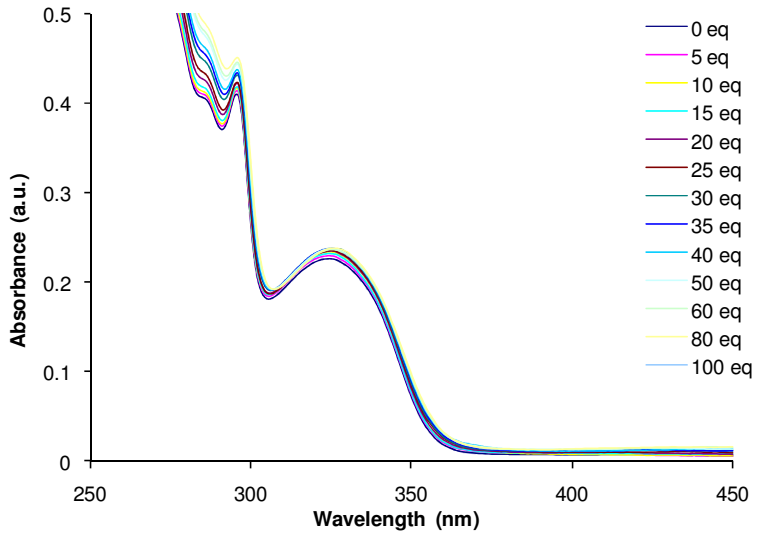

(h)

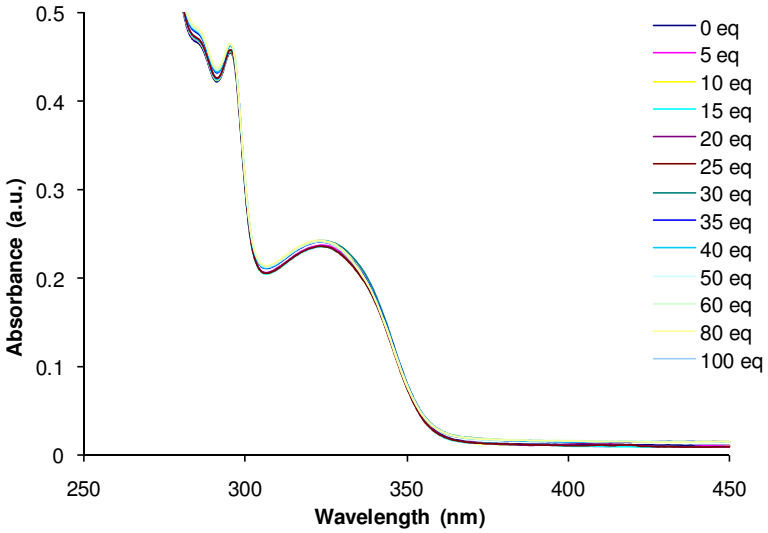

AIV.14 UV-vis spectroscopic titrations of **138** (1.0 x 10^{-5} mol dm^{-3} in $CDCl_3$/DMSO-d_6 *v/v* 95/5) with (a) bromide, (b) iodide, (c) nitrate, (d) acetate, (e) fluoride, (f) dihydrogen phosphate and (g) hydrogen sulfate used as TBA salts

(a)

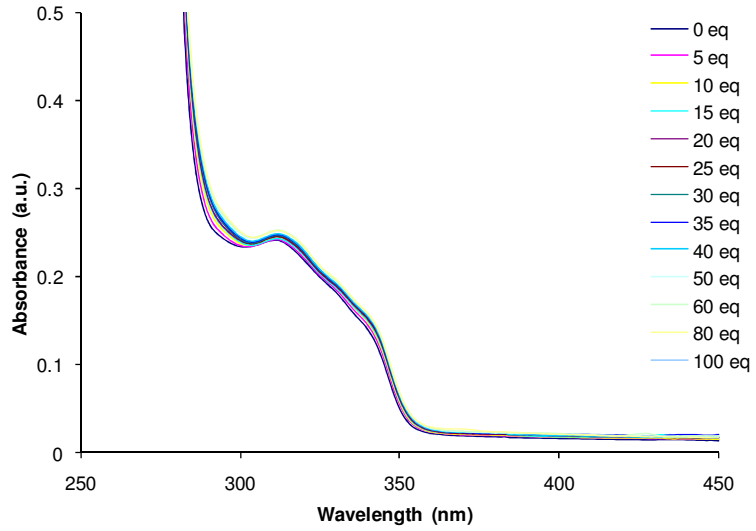
0.5
0.4
0.3
0.2
0.1
0
Absorbance (a.u.)
250
300
350
400
450
Wavelength (nm)
0 eq
5 eq
10 eq
15 eq
20 eq
25 eq
30 eq
35 eq
40 eq
50 eq
60 eq
80 eq
100 eq

(b)

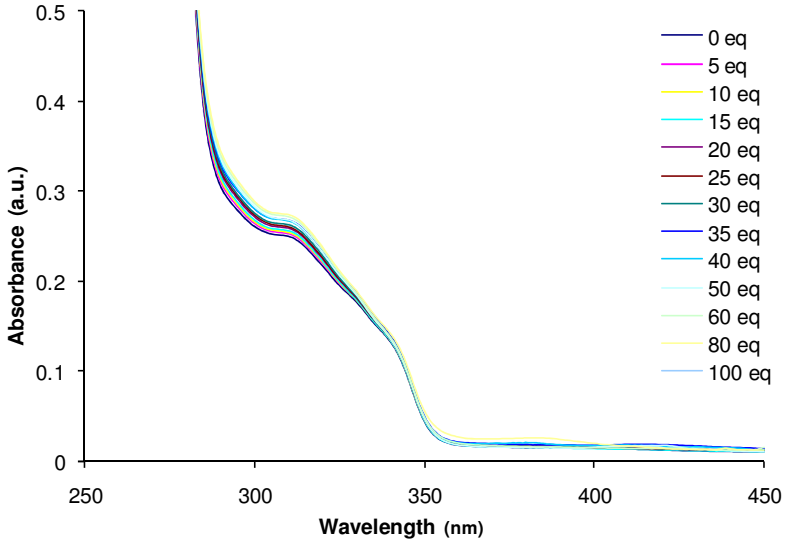
0.5
0.4
0.3
0.2
0.1
0
Absorbance (a.u.)
250
300
350
400
450
Wavelength (nm)
0 eq
5 eq
10 eq
15 eq
20 eq
25 eq
30 eq
35 eq
40 eq
50 eq
60 eq
80 eq
100 eq

(c)

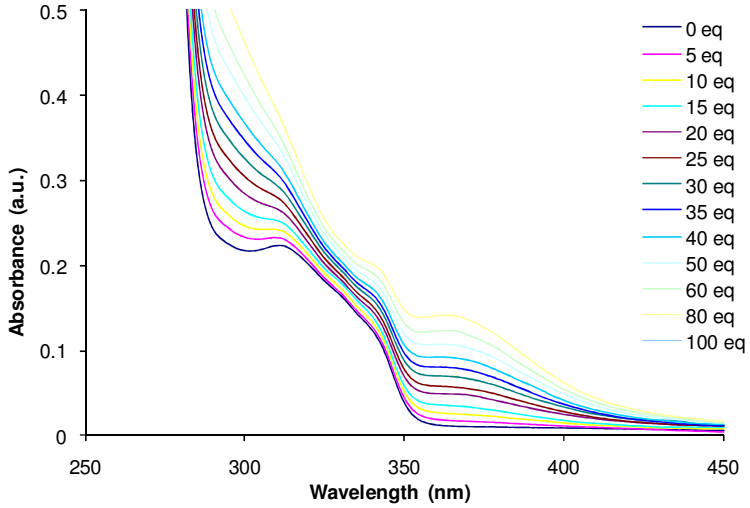
0.5
0.4
0.3
0.2
0.1
0
Absorbance (a.u.)
250
300
350
400
450
Wavelength (nm)
0 eq
5 eq
10 eq
15 eq
20 eq
25 eq
30 eq
35 eq
40 eq
50 eq
60 eq
80 eq
100 eq

(d)

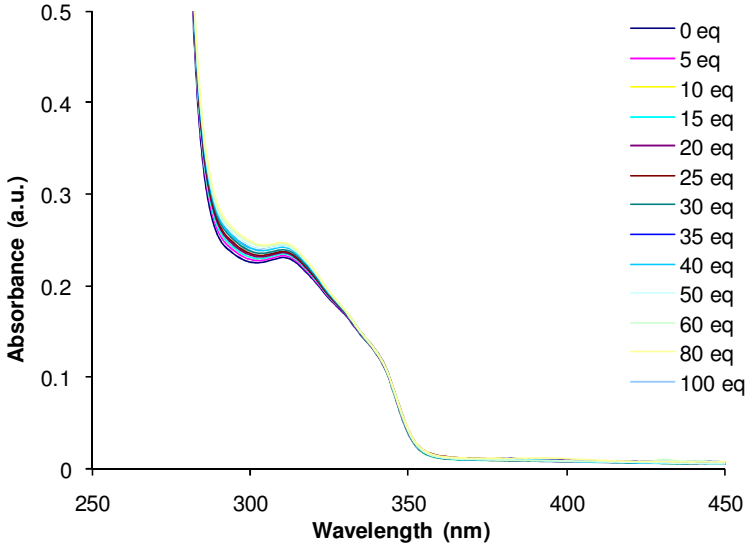
0.5
0.4
0.3
0.2
0.1
0
Absorbance (a.u.)
250
300
350
400
450
Wavelength (nm)
0 eq
5 eq
10 eq
15 eq
20 eq
25 eq
30 eq
35 eq
40 eq
50 eq
60 eq
80 eq
100 eq

(e)

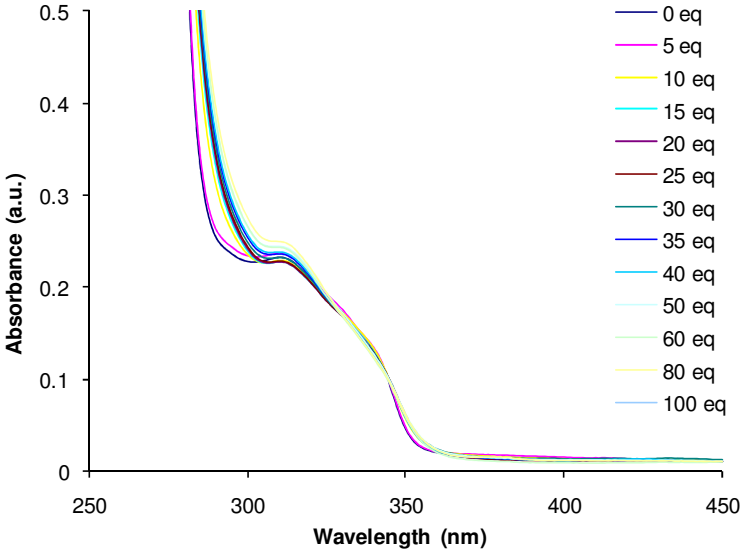
0.5
0.4
0.3
0.2
0.1
0
Absorbance (a.u.)
250
300
350
400
450
Wavelength (nm)
0 eq
5 eq
10 eq
15 eq
20 eq
25 eq
30 eq
35 eq
40 eq
50 eq
60 eq
80 eq
100 eq

(f)

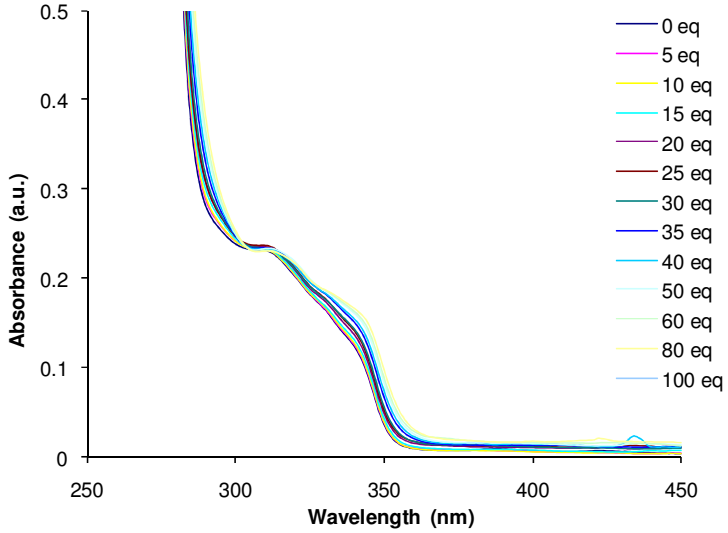
0.5
0.4
0.3
0.2
0.1
0
Absorbance (a.u.)
250
300
350
400
450
Wavelength (nm)
0 eq
5 eq
10 eq
15 eq
20 eq
25 eq
30 eq
35 eq
40 eq
50 eq
60 eq
80 eq
100 eq

(g)

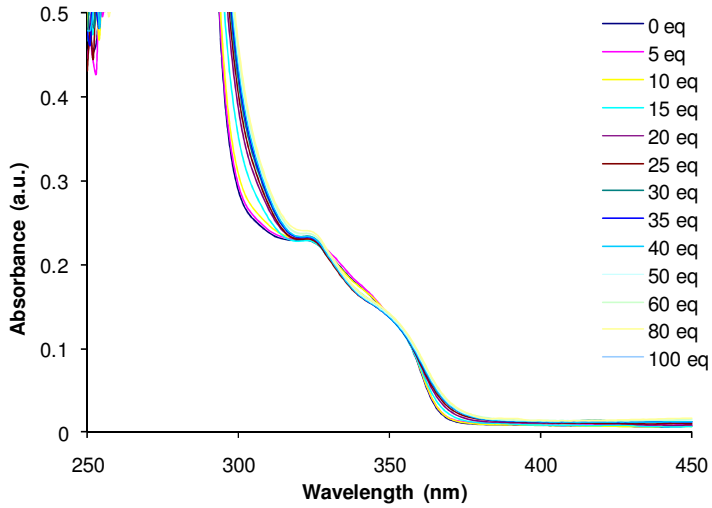

(h)

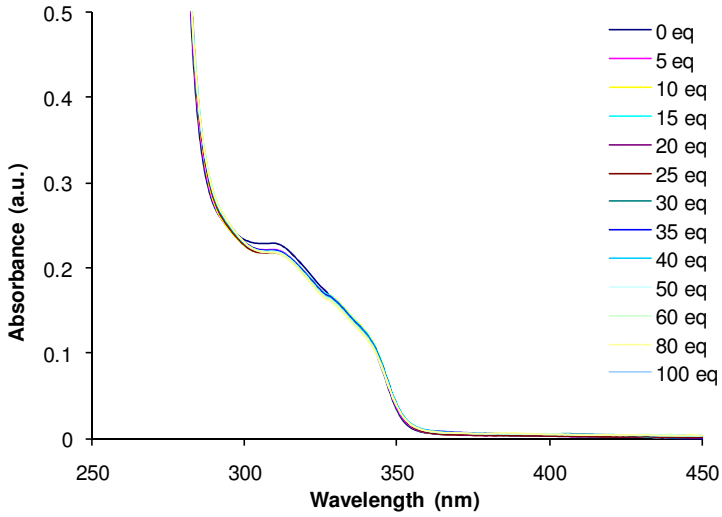

AIV.15 UV-vis spectroscopic titrations of **139** (1.0×10^{-5} mol dm^{-3} in $CDCl_3$/DMSO-d_6 *v/v* 95/5) with (a) bromide, (b) iodide, (c) nitrate, (d) acetate, (e) fluoride, (f) dihydrogen phosphate and (g) hydrogen sulfate used as TBA salts

(a)

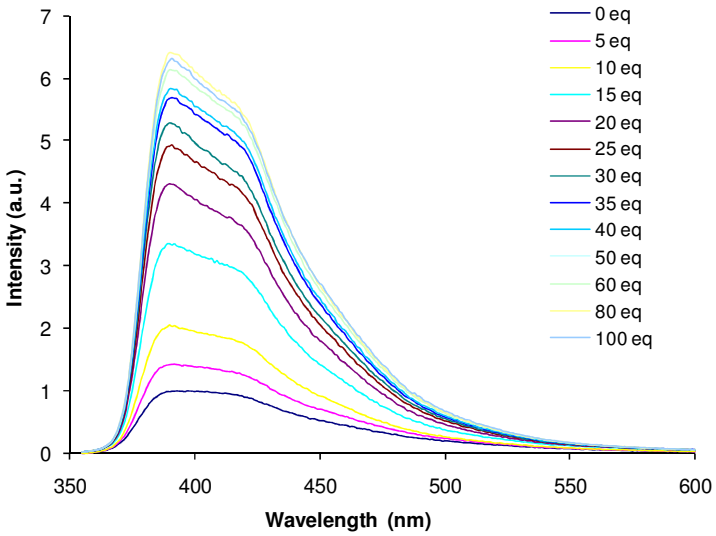
Intensity (a.u.)
Wavelength (nm)
0 eq
5 eq
10 eq
15 eq
20 eq
25 eq
30 eq
35 eq
40 eq
50 eq
60 eq
80 eq
100 eq

(b)

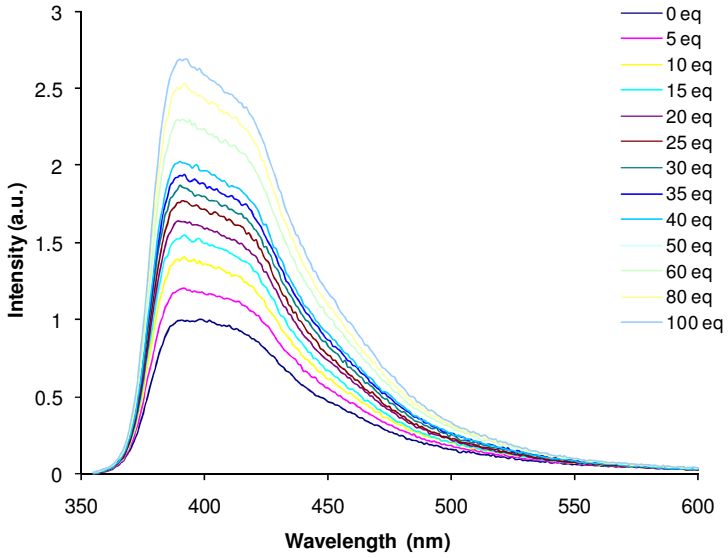
Intensity (a.u.)
Wavelength (nm)
0 eq
5 eq
10 eq
15 eq
20 eq
25 eq
30 eq
35 eq
40 eq
50 eq
60 eq
80 eq
100 eq

(c)

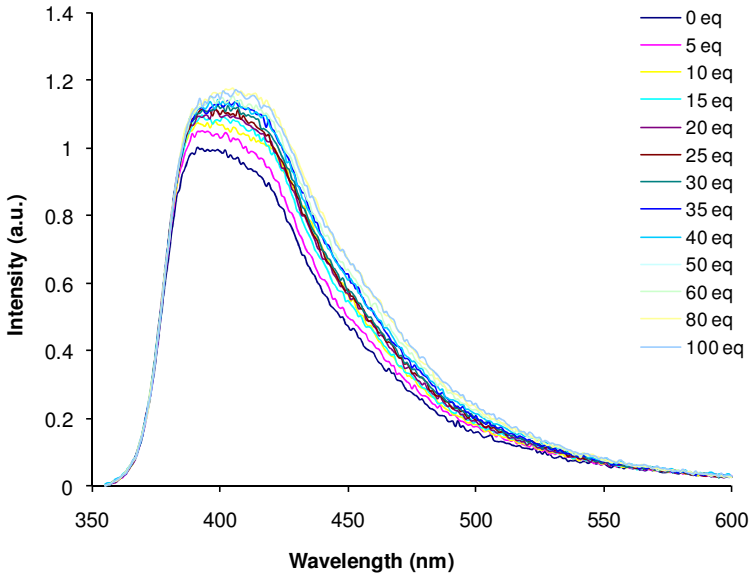
1.4
1.2
1
0.8
0.6
0.4
0.2
0
Intensity (a.u.)
350
400
450
500
550
600
Wavelength (nm)
0 eq
5 eq
10 eq
15 eq
20 eq
25 eq
30 eq
35 eq
40 eq
50 eq
60 eq
80 eq
100 eq

(d)

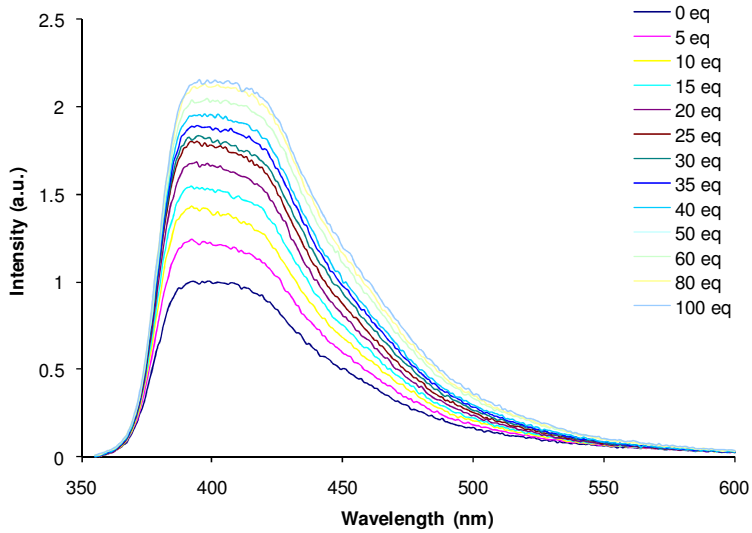
2.5
2
1.5
1
0.5
0
Intensity (a.u.)
350
400
450
500
550
600
Wavelength (nm)
0 eq
5 eq
10 eq
15 eq
20 eq
25 eq
30 eq
35 eq
40 eq
50 eq
60 eq
80 eq
100 eq

(e)

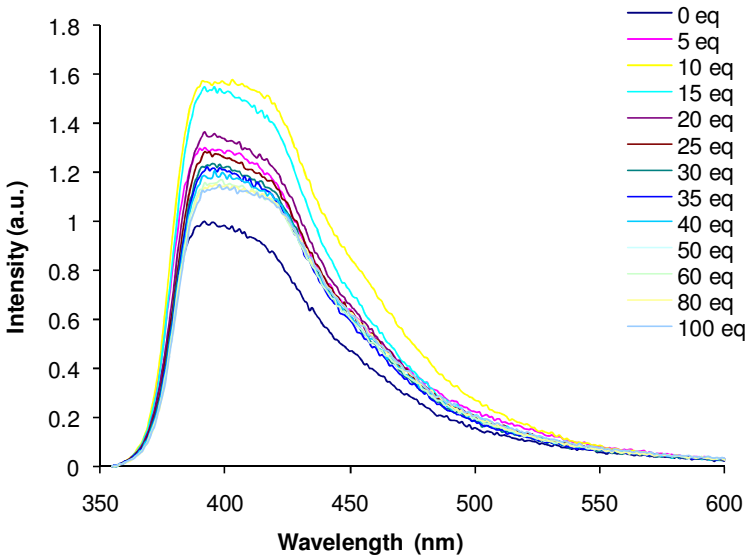
Intensity (a.u.)
Wavelength (nm)
0 eq
5 eq
10 eq
15 eq
20 eq
25 eq
30 eq
35 eq
40 eq
50 eq
60 eq
80 eq
100 eq

(f)

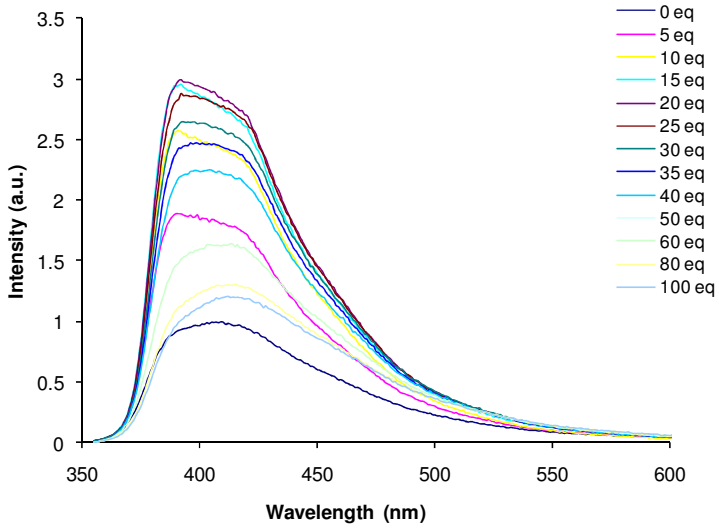
Intensity (a.u.)
Wavelength (nm)
0 eq
5 eq
10 eq
15 eq
20 eq
25 eq
30 eq
35 eq
40 eq
50 eq
60 eq
80 eq
100 eq

(g)

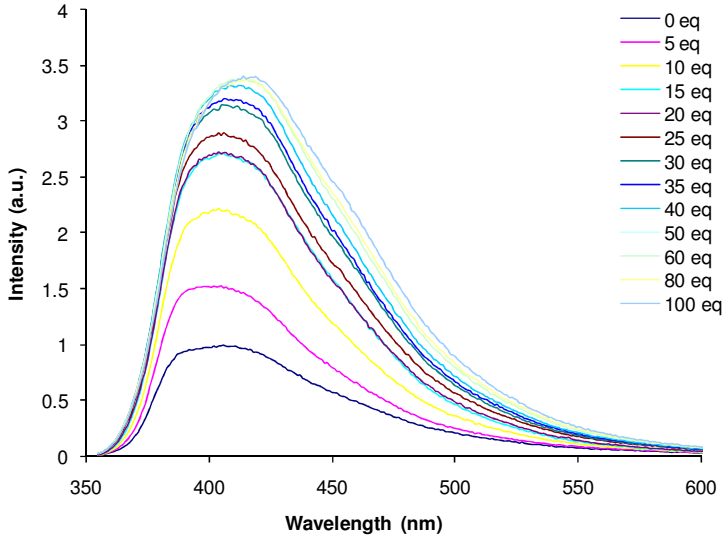

(h)

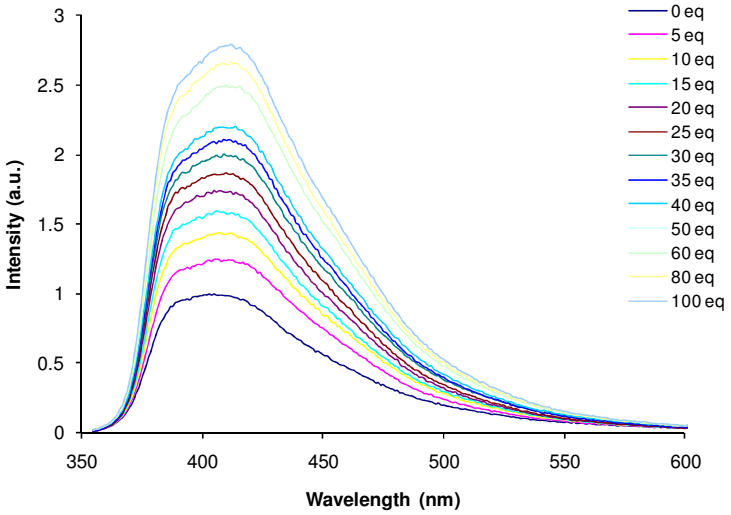

AIV.16 Fluorescence spectroscopic titrations of **135** (λ_{ex} = 340 nm, 1.0 x 10^{-5} mol dm^{-3} in $CDCl_3$/DMSO-d_6 *v/v* 95/5) with (a) chloride, (b) bromide, (c) iodide, (d) nitrate, (e) acetate, (f) fluoride, (g) dihydrogen phosphate and (h) hydrogen sulfate used as TBA salts

(a)

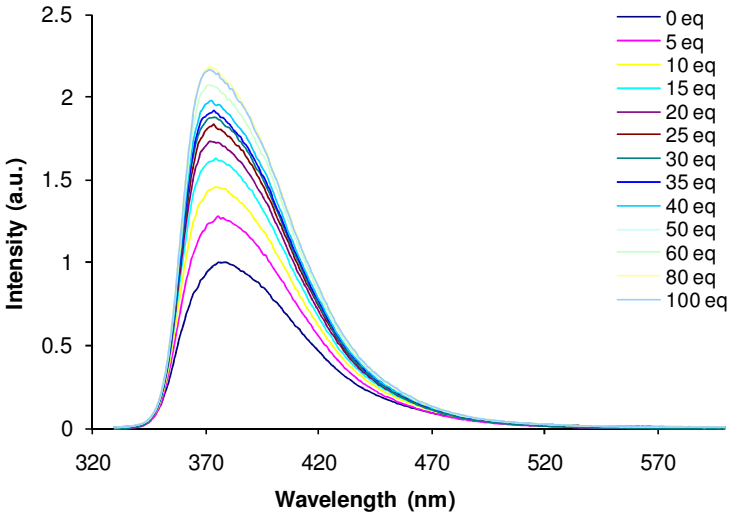
2.5
2
1.5
1
0.5
0
Intensity (a.u.)
320
370
420
470
520
570
Wavelength (nm)
0 eq
5 eq
10 eq
15 eq
20 eq
25 eq
30 eq
35 eq
40 eq
50 eq
60 eq
80 eq
100 eq

(b)

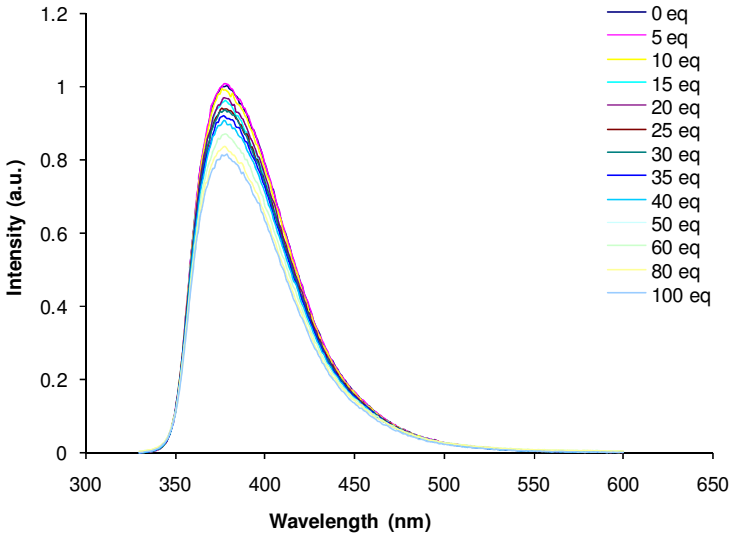
1.2
1
0.8
0.6
0.4
0.2
0
Intensity (a.u.)
300
350
400
450
500
550
600
650
Wavelength (nm)
0 eq
5 eq
10 eq
15 eq
20 eq
25 eq
30 eq
35 eq
40 eq
50 eq
60 eq
80 eq
100 eq

(c)

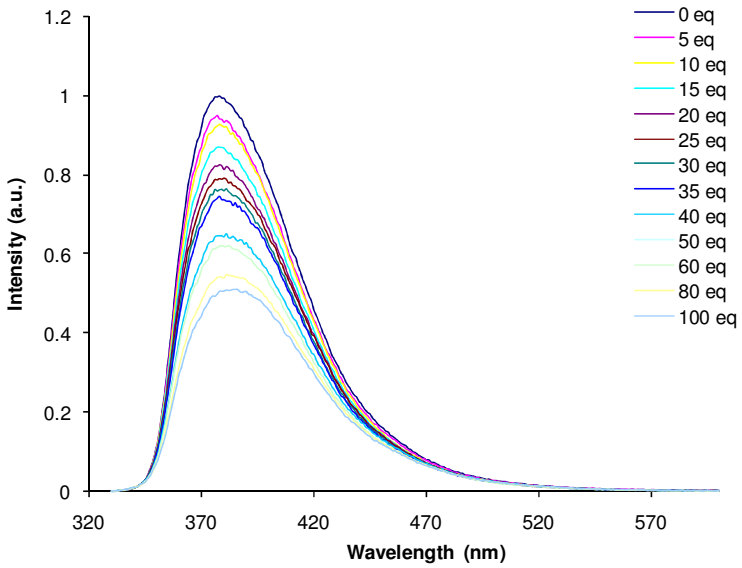
1.2
1
0.8
0.6
0.4
0.2
0
Intensity (a.u.)
320
370
420
470
520
570
Wavelength (nm)
0 eq
5 eq
10 eq
15 eq
20 eq
25 eq
30 eq
35 eq
40 eq
50 eq
60 eq
80 eq
100 eq

(d)

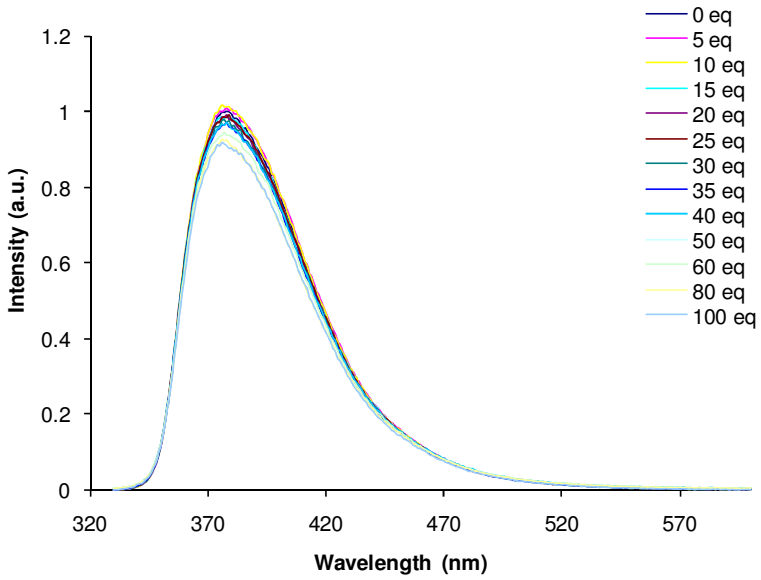
1.2
1
0.8
0.6
0.4
0.2
0
Intensity (a.u.)
320
370
420
470
520
570
Wavelength (nm)
0 eq
5 eq
10 eq
15 eq
20 eq
25 eq
30 eq
35 eq
40 eq
50 eq
60 eq
80 eq
100 eq

(e)

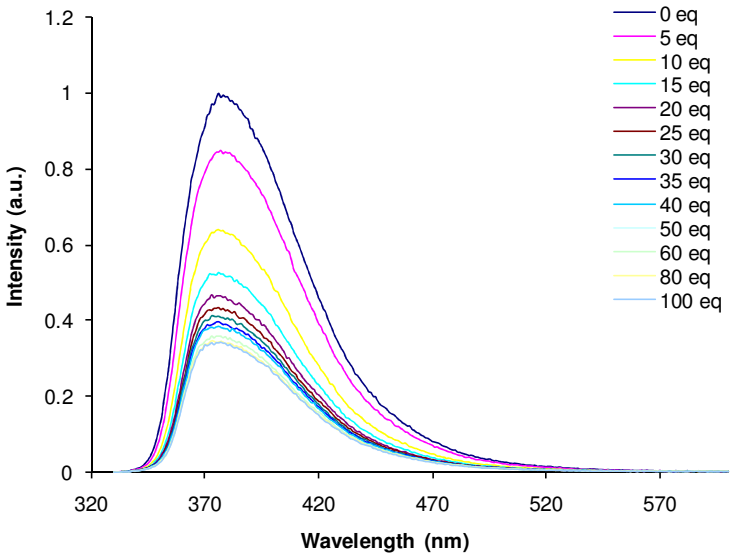
1.2
1
0.8
0.6
0.4
0.2
0
Intensity (a.u.)
320
370
420
470
520
570
Wavelength (nm)
0 eq
5 eq
10 eq
15 eq
20 eq
25 eq
30 eq
35 eq
40 eq
50 eq
60 eq
80 eq
100 eq

(f)

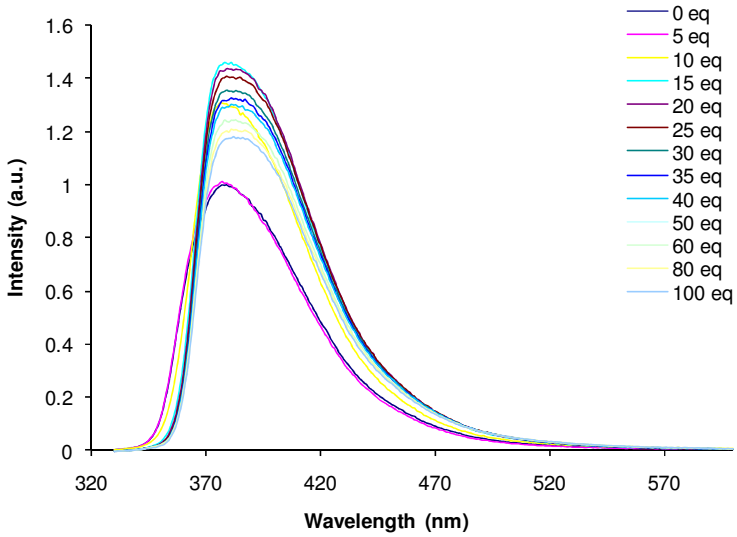
1.6
1.4
1.2
1
0.8
0.6
0.4
0.2
0
Intensity (a.u.)
320
370
420
470
520
570
Wavelength (nm)
0 eq
5 eq
10 eq
15 eq
20 eq
25 eq
30 eq
35 eq
40 eq
50 eq
60 eq
80 eq
100 eq

(g)

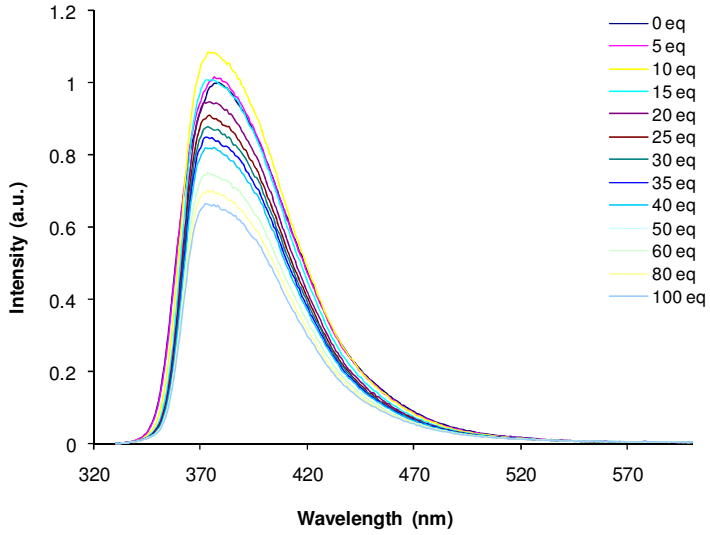

(h)

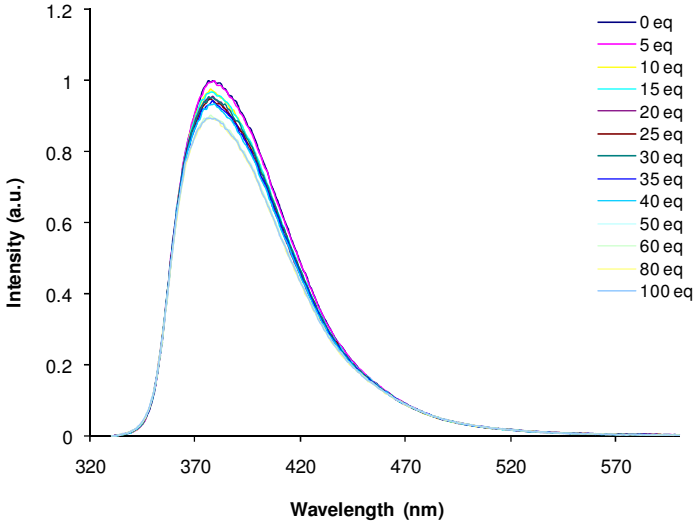

AIV.17 Fluorescence spectroscopic titrations of **136** (λ_{ex} = 320 nm, 1.0 x 10^{-5} mol dm^{-3} in $CDCl_3$/DMSO-d_6 *v/v* 95/5) with (a) chloride, (b) bromide, (c) iodide, (d) nitrate, (e) acetate, (f) fluoride, (g) dihydrogen phosphate and (h) hydrogen sulfate used as TBA salts

(a)

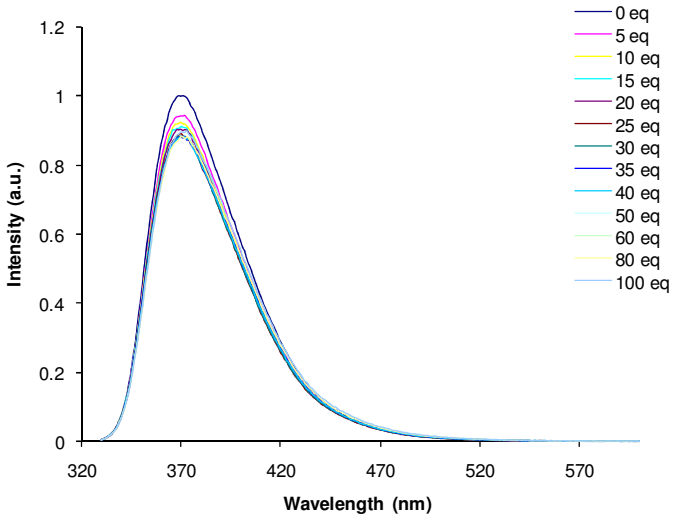
1.2
1
0.8
0.6
0.4
0.2
0
Intensity (a.u.)
320
370
420
470
520
570
Wavelength (nm)
0 eq
5 eq
10 eq
15 eq
20 eq
25 eq
30 eq
35 eq
40 eq
50 eq
60 eq
80 eq
100 eq

(b)

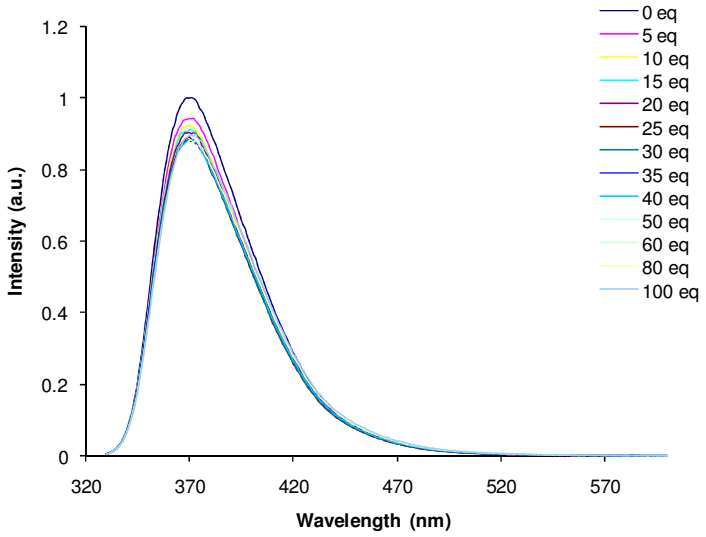
1.2
1
0.8
0.6
0.4
0.2
0
Intensity (a.u.)
320
370
420
470
520
570
Wavelength (nm)
0 eq
5 eq
10 eq
15 eq
20 eq
25 eq
30 eq
35 eq
40 eq
50 eq
60 eq
80 eq
100 eq

(c)

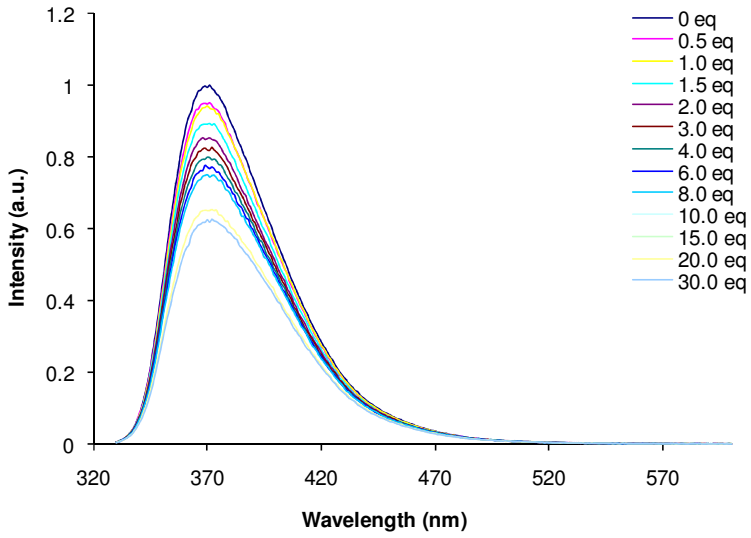
1.2
1
0.8
0.6
0.4
0.2
0
Intensity (a.u.)
320
370
420
470
520
570
Wavelength (nm)
0 eq
0.5 eq
1.0 eq
1.5 eq
2.0 eq
3.0 eq
4.0 eq
6.0 eq
8.0 eq
10.0 eq
15.0 eq
20.0 eq
30.0 eq

(d)

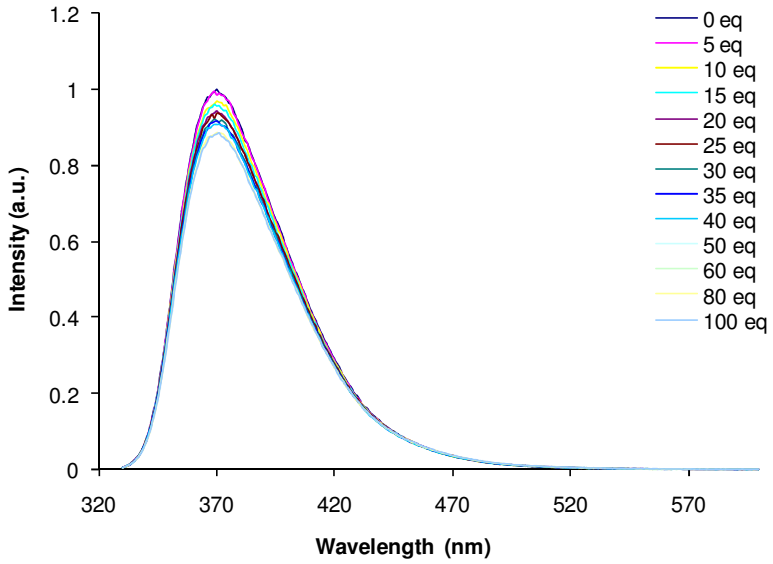
1.2
1
0.8
0.6
0.4
0.2
0
Intensity (a.u.)
320
370
420
470
520
570
Wavelength (nm)
0 eq
5 eq
10 eq
15 eq
20 eq
25 eq
30 eq
35 eq
40 eq
50 eq
60 eq
80 eq
100 eq

(e)

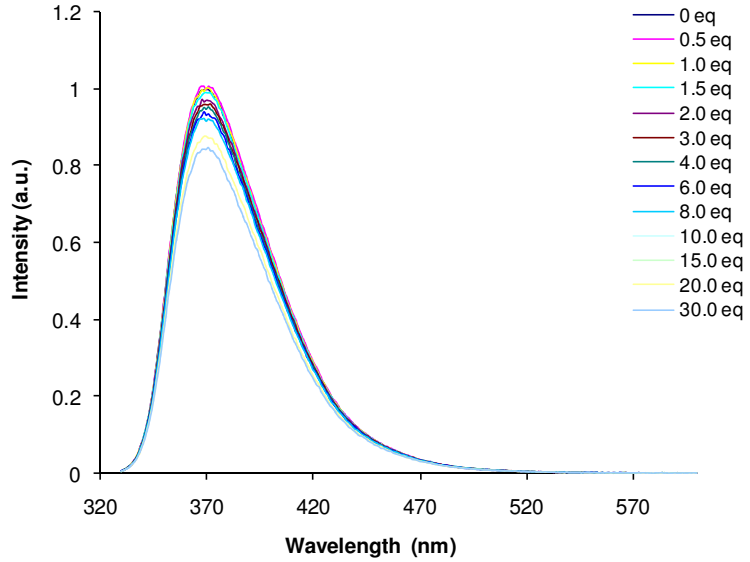
1.2
1
0.8
0.6
0.4
0.2
0
Intensity (a.u.)
320
370
420
470
520
570
Wavelength (nm)
0 eq
0.5 eq
1.0 eq
1.5 eq
2.0 eq
3.0 eq
4.0 eq
6.0 eq
8.0 eq
10.0 eq
15.0 eq
20.0 eq
30.0 eq

(f)

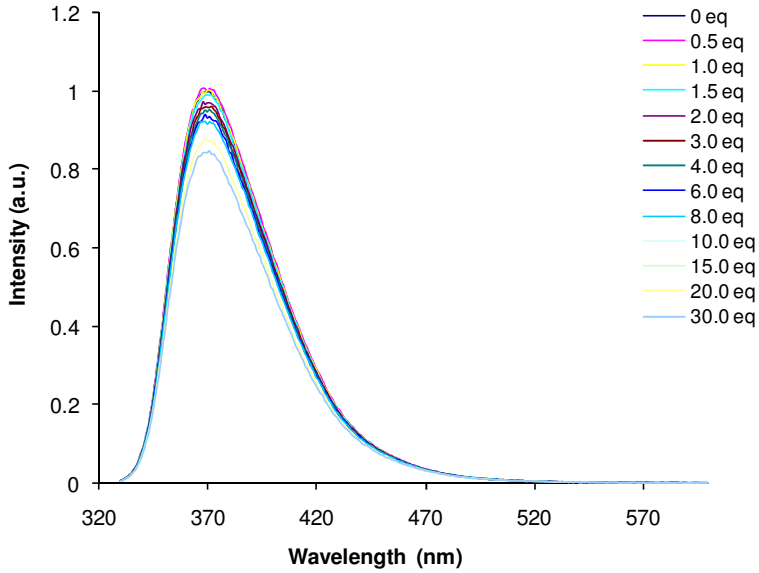
1.2
1
0.8
0.6
0.4
0.2
0
Intensity (a.u.)
320
370
420
470
520
570
Wavelength (nm)
0 eq
0.5 eq
1.0 eq
1.5 eq
2.0 eq
3.0 eq
4.0 eq
6.0 eq
8.0 eq
10.0 eq
15.0 eq
20.0 eq
30.0 eq

(g)

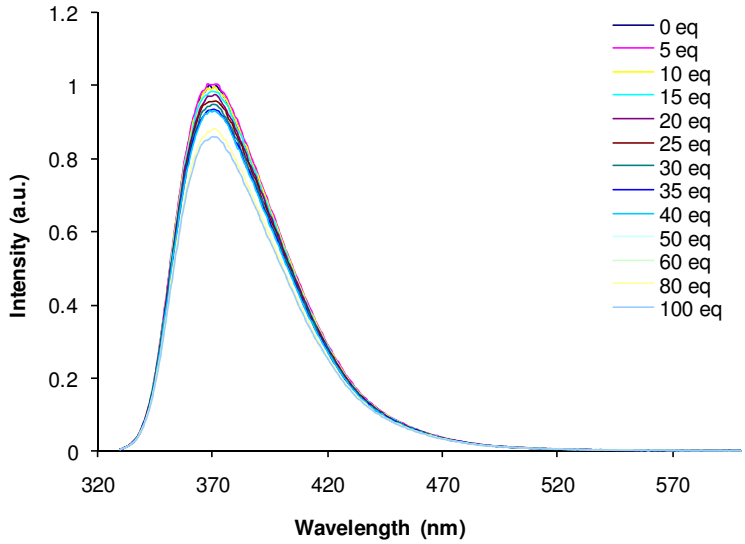

(h)

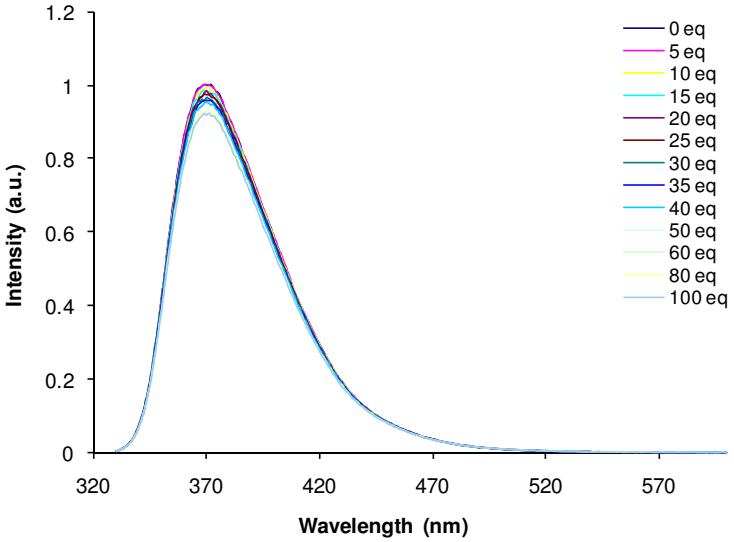

AIV.18 Fluorescence spectroscopic titrations of **137** (λ_{ex} = 320 nm, 2.0 x 10^{-5} mol dm^{-3} in $CDCl_3$/DMSO-d_6 *v/v* 95/5) with (a) chloride, (b) bromide, (c) iodide, (d) nitrate, (e) acetate, (f) fluoride, (g) dihydrogen phosphate and (h) hydrogen sulfate used as TBA salts

(a)

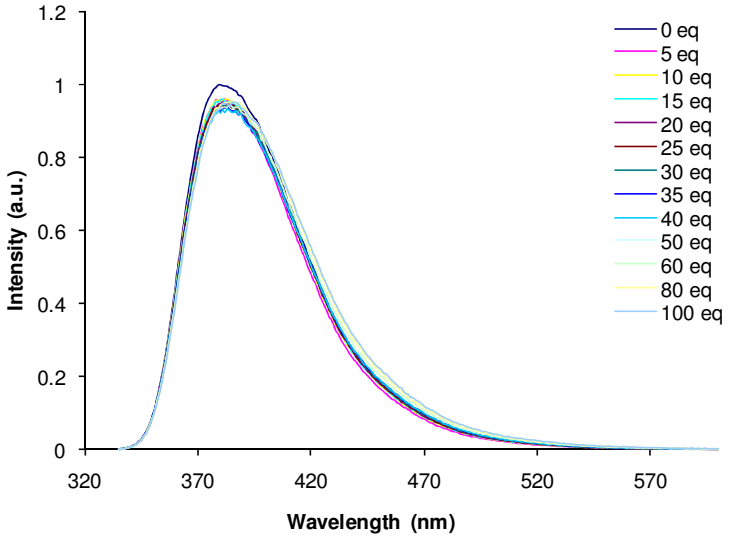
1.2
1
0.8
0.6
0.4
0.2
0
Intensity (a.u.)
320
370
420
470
520
570
Wavelength (nm)
0 eq
5 eq
10 eq
15 eq
20 eq
25 eq
30 eq
35 eq
40 eq
50 eq
60 eq
80 eq
100 eq

(b)

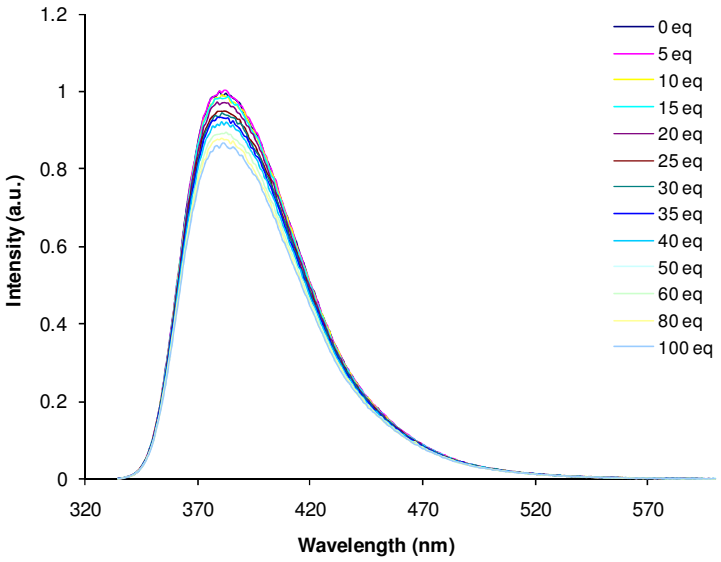
1.2
1
0.8
0.6
0.4
0.2
0
Intensity (a.u.)
320
370
420
470
520
570
Wavelength (nm)
0 eq
5 eq
10 eq
15 eq
20 eq
25 eq
30 eq
35 eq
40 eq
50 eq
60 eq
80 eq
100 eq

(c)

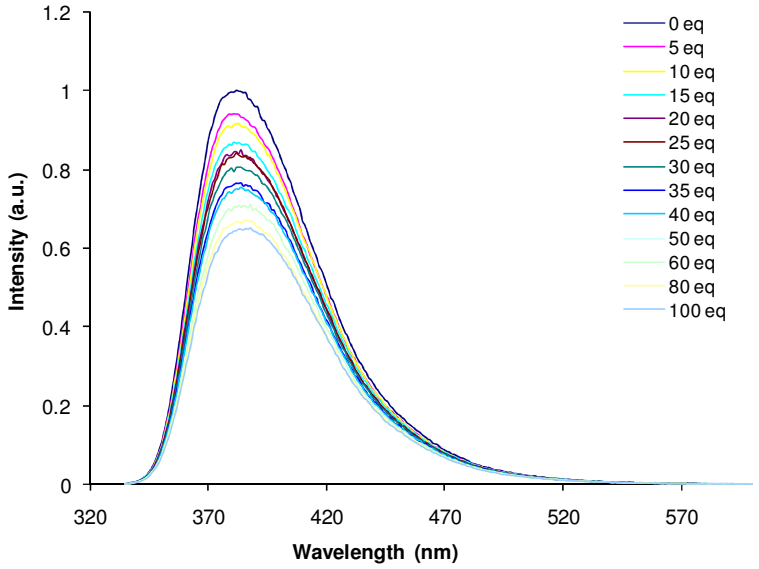
1.2
1
0.8
0.6
0.4
0.2
0
Intensity (a.u.)
320
370
420
470
520
570
Wavelength (nm)
0 eq
5 eq
10 eq
15 eq
20 eq
25 eq
30 eq
35 eq
40 eq
50 eq
60 eq
80 eq
100 eq

(d)

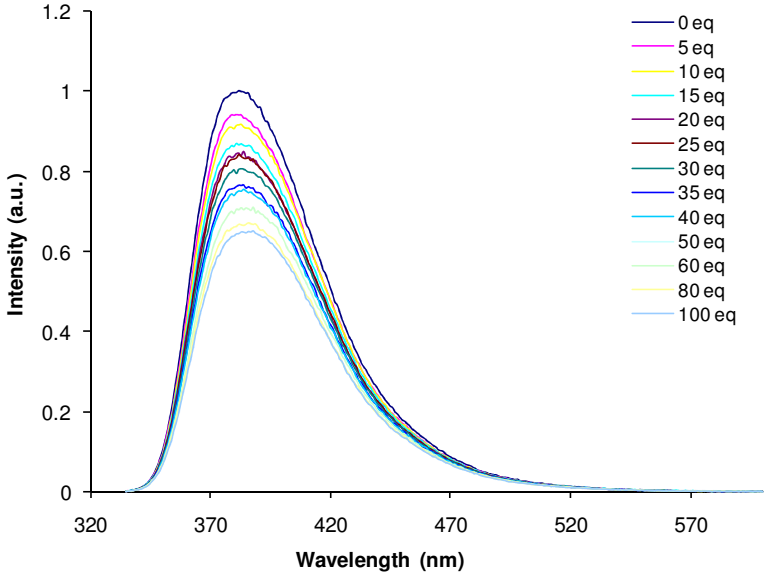
1.2
1
0.8
0.6
0.4
0.2
0
Intensity (a.u.)
320
370
420
470
520
570
Wavelength (nm)
0 eq
5 eq
10 eq
15 eq
20 eq
25 eq
30 eq
35 eq
40 eq
50 eq
60 eq
80 eq
100 eq

(e)

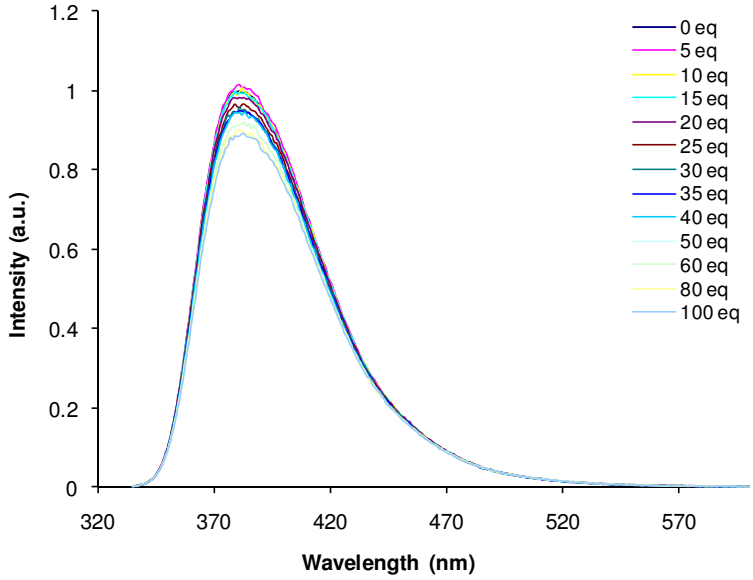
1.2
1
0.8
0.6
0.4
0.2
0
Intensity (a.u.)
320
370
420
470
520
570
Wavelength (nm)
0 eq
5 eq
10 eq
15 eq
20 eq
25 eq
30 eq
35 eq
40 eq
50 eq
60 eq
80 eq
100 eq

(f)

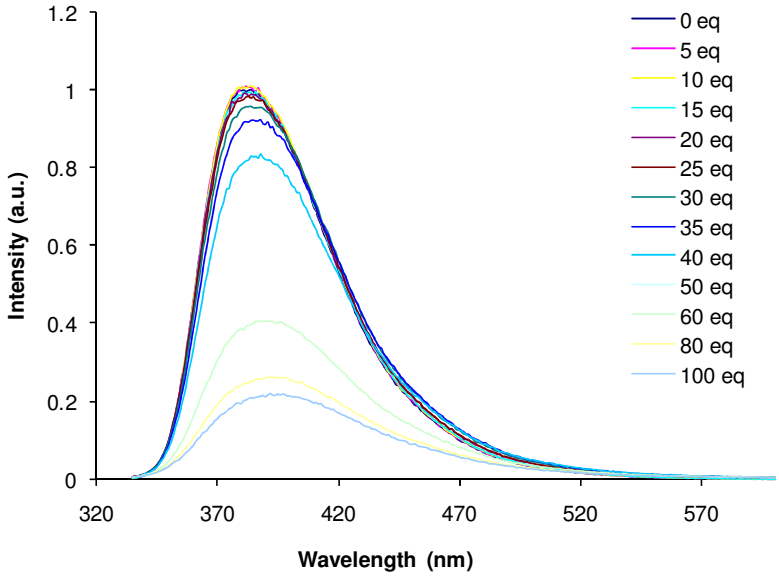
1.2
1
0.8
0.6
0.4
0.2
0
Intensity (a.u.)
320
370
420
470
520
570
Wavelength (nm)
0 eq
5 eq
10 eq
15 eq
20 eq
25 eq
30 eq
35 eq
40 eq
50 eq
60 eq
80 eq
100 eq

(g)

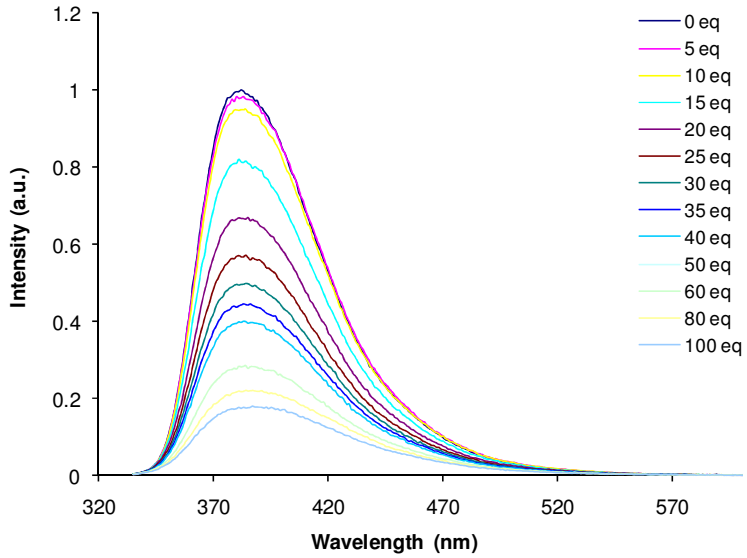

(h)

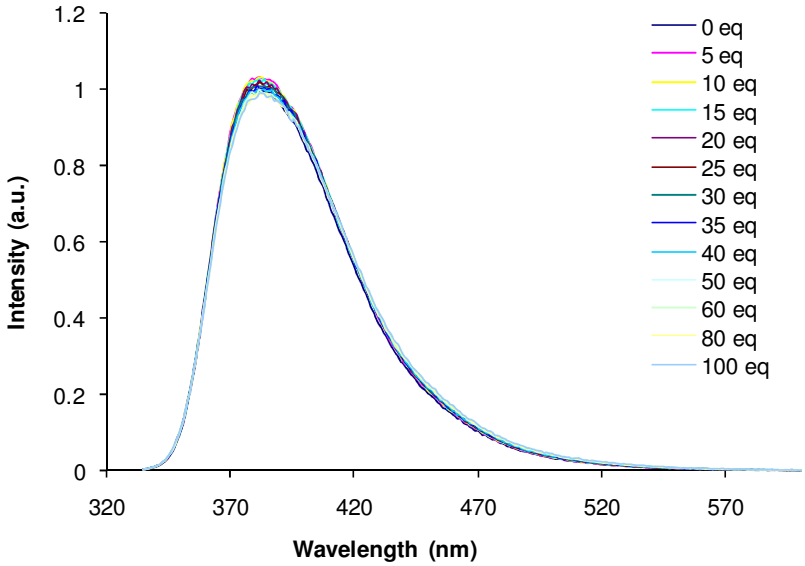

AIV.19 Fluorescence spectroscopic titrations of **138** (λ_{ex} = 325 nm, 1.0 x 10^{-5} mol dm^{-3} in $CDCl_3$/DMSO-d_6 *v/v* 95/5) with (a) chloride, (b) bromide, (c) iodide, (d) nitrate, (e) acetate, (f) fluoride, (g) dihydrogen phosphate and (h) hydrogen sulfate used as TBA salts

(a)

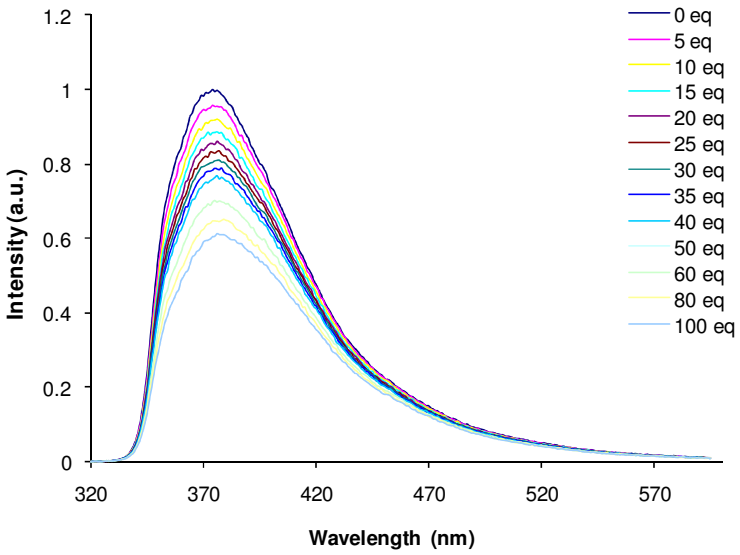
1.2
1
0.8
0.6
0.4
0.2
0
Intensity (a.u.)
320
370
420
470
520
570
Wavelength (nm)
0 eq
5 eq
10 eq
15 eq
20 eq
25 eq
30 eq
35 eq
40 eq
50 eq
60 eq
80 eq
100 eq

(b)

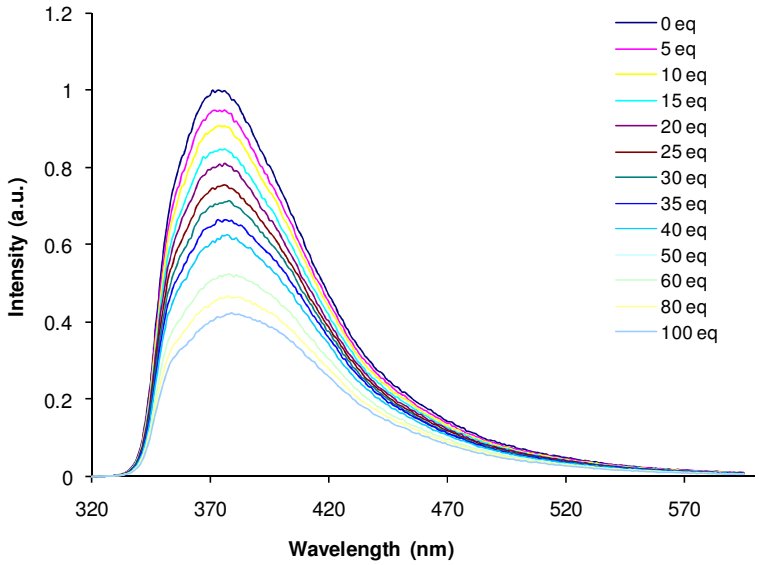
1.2
1
0.8
0.6
0.4
0.2
0
Intensity (a.u.)
320
370
420
470
520
570
Wavelength (nm)
0 eq
5 eq
10 eq
15 eq
20 eq
25 eq
30 eq
35 eq
40 eq
50 eq
60 eq
80 eq
100 eq

(c)

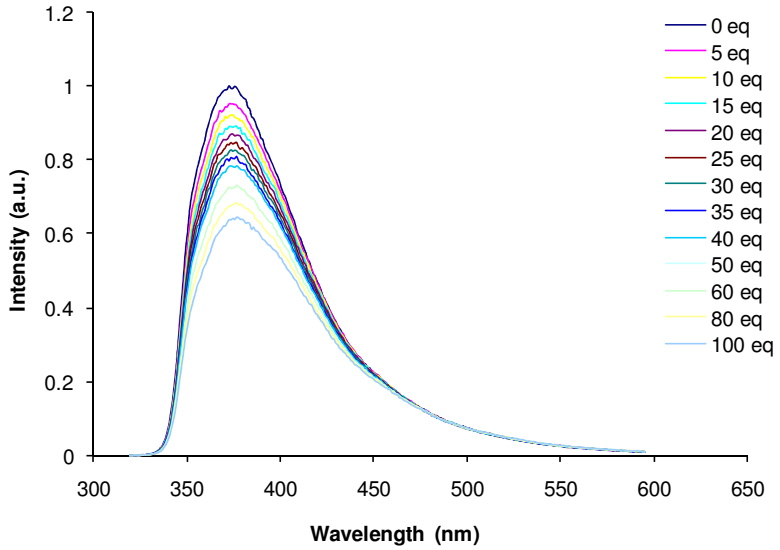
1.2
1
0.8
0.6
0.4
0.2
0
Intensity (a.u.)
300
350
400
450
500
550
600
650
Wavelength (nm)
0 eq
5 eq
10 eq
15 eq
20 eq
25 eq
30 eq
35 eq
40 eq
50 eq
60 eq
80 eq
100 eq

(d)

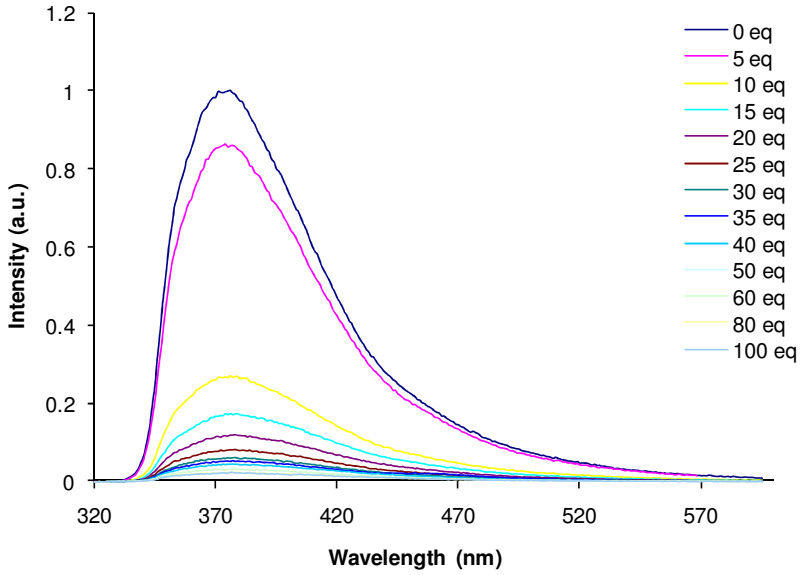
1.2
1
0.8
0.6
0.4
0.2
0
Intensity (a.u.)
320
370
420
470
520
570
Wavelength (nm)
0 eq
5 eq
10 eq
15 eq
20 eq
25 eq
30 eq
35 eq
40 eq
50 eq
60 eq
80 eq
100 eq

(e)

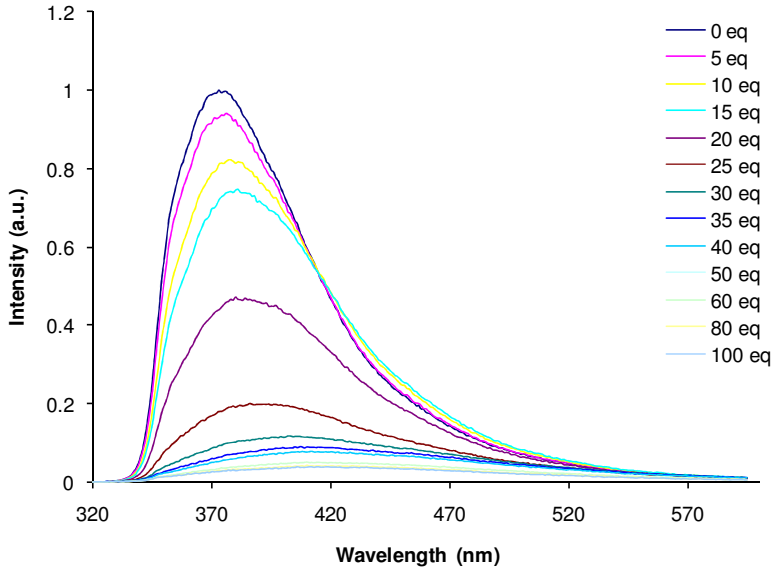
1.2
1
0.8
0.6
0.4
0.2
0
Intensity (a.u.)
320
370
420
470
520
570
Wavelength (nm)
0 eq
5 eq
10 eq
15 eq
20 eq
25 eq
30 eq
35 eq
40 eq
50 eq
60 eq
80 eq
100 eq

(f)

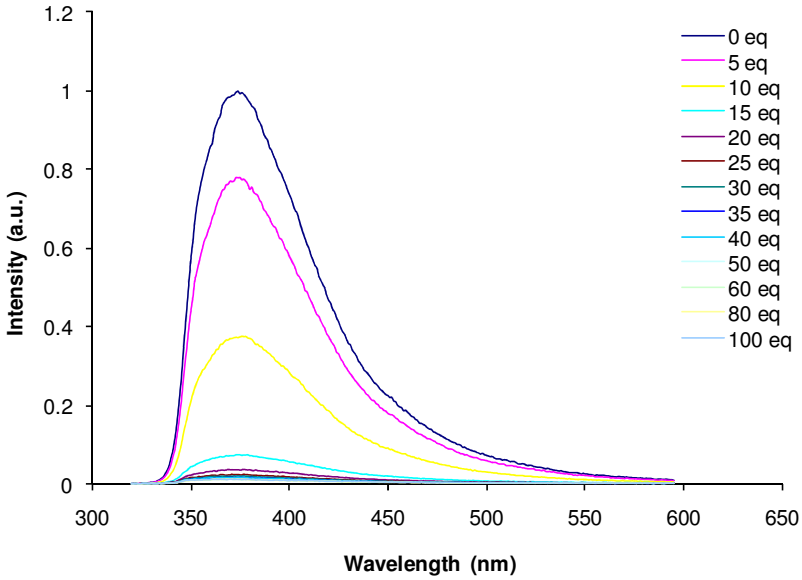
1.2
1
0.8
0.6
0.4
0.2
0
Intensity (a.u.)
300
350
400
450
500
550
600
650
Wavelength (nm)
0 eq
5 eq
10 eq
15 eq
20 eq
25 eq
30 eq
35 eq
40 eq
50 eq
60 eq
80 eq
100 eq

(g)

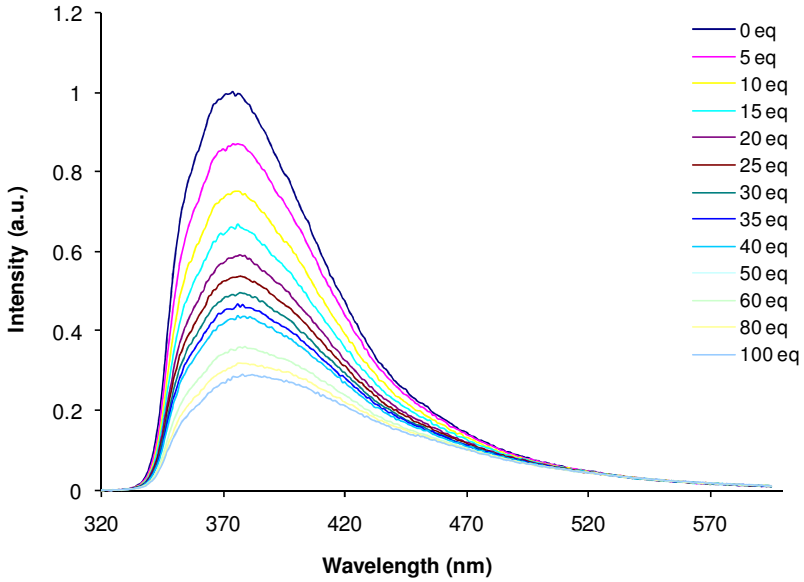

AIV.20 Fluorescence spectroscopic titrations of **139** (λ_{ex} = 320 nm, 1.0 x 10^{-5} mol dm^{-3} in $CDCl_3$/DMSO-d_6 *v/v* 95/5) with (A) bromide, (b) iodide, (c) nitrate, (d) acetate, (e) fluoride, (f) dihydrogen phosphate and (g) hydrogen sulfate used as TBA salts

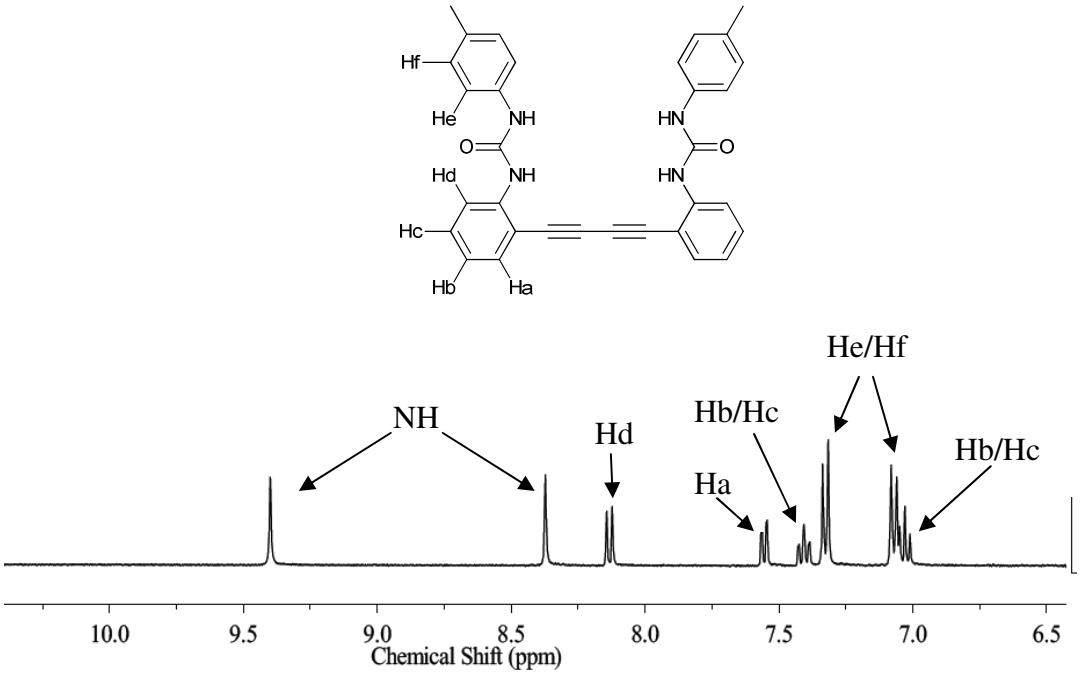

AIV.21 ^{1}H NMR assignment for compound **135** in DMSO-d_6